



# Toward battery electric and hydrogen fuel cell military vehicles for land, air, and sea



Scott M. Katalenich<sup>\*</sup>, Mark Z. Jacobson

Stanford University, Department of Civil & Environmental Engineering, Atmosphere/Energy Program, Stanford, CA, USA

## ARTICLE INFO

### Article history:

Received 11 October 2021

Received in revised form

30 April 2022

Accepted 21 May 2022

Available online 24 May 2022

### Keywords:

Military vehicles

Battery electric

Hydrogen fuel cell

Clean renewable energy

## ABSTRACT

A long-term solution to the climate and air pollution crises facing the world today includes electrification of almost all energy and obtaining that electricity from clean, renewable sources. Whereas electric alternatives exist for nearly all energy sectors, they do not exist for long-distance, heavy passenger aircraft, freight locomotives, or ships. Of particular note, solutions do not currently exist for military combat vehicles, such as armored tanks, oceangoing vessels, and rotary- and fixed-wing aircraft. Some have claimed such transport cannot be transitioned. This study evaluates whether such land, air, and sea vehicles can be replaced with battery electric and/or hydrogen fuel cell equivalents while maintaining vehicle range, mass, volume, and power- or thrust-to-weight ratio characteristics, more parameters than previously evaluated. Here we show that armored tanks, freight trains, boats, oceangoing vessels, helicopters, prop planes, and jumbo jets have potential to transition using identified technological advancements and solutions suggested achievable within literature. Furthermore, we provide an example of the impact to sustainability by showing that transitioning energy for United States Army vehicles could have the equivalent environmental improvement of taking nearly 700,000 passenger cars off the road today.

Published by Elsevier Ltd.

## 1. Introduction

Military vehicles operating on land, in the air, and at sea represent some of the most challenging vehicle types to transition to run on clean, renewable energy. However, transitioning to zero emissions by using battery electric (BE) or hydrogen fuel cell (HFC) systems is critically important. Beyond supporting the similar transition of civilian vehicles, transitioning military vehicles could overcome the inefficiencies and risks of using fossil fuels (FF) in military operations. A U.S. Marine Corps study found that, for every gallon of fuel used in Afghanistan, seven gallons were needed to transport it there [1]. Attacks on resupply operations have resulted in thousands wounded or killed in action [2,3]. Since wind and/or solar power produced directly at contingency bases could recharge batteries or power electrolyzers to produce hydrogen, transitioning military vehicles to BE or HFC systems could potentially save lives. Furthermore, fully-electric military vehicles could significantly reduce greenhouse gas emissions. Still, no study to date has

considered the feasibility of transitioning entire military fleets to either BE or HFC vehicles.

Some research suggests that transitioning heavy and/or long-distance vehicles is infeasible [4]. However, such assessments compare just the specific energy and energy density of onboard energy storage instead of considering the whole system. Other studies have enlarged the parameter space by comparing overall system efficiencies of FF burning, internal combustion engine (ICE) systems with BE systems or by benchmarking vehicles in terms of acceleration, gradeability, and speed characteristics [5,6]. This paper goes further and applies a design approach that optimizes efficiency of the whole vehicle system [7].

This study identifies and evaluates four major vehicle characteristics to assess the feasibility of transitioning: mass, volume, range, and either power-to-weight ratio (PWR) or thrust-to-weight ratio (TWR). Furthermore, the study investigates seven critical technologies: electric motor PWR, battery pack specific energy and energy density, hydrogen storage system specific energy and energy density, and HFC stack specific power and power density.

<sup>\*</sup> Corresponding author.

E-mail addresses: [katalenich@alumni.stanford.edu](mailto:katalenich@alumni.stanford.edu) (S.M. Katalenich), [jacobson@stanford.edu](mailto:jacobson@stanford.edu) (M.Z. Jacobson).

## Nomenclature

### Abbreviations

AC	Alternating Current	DOE	Department Of Energy
BE	Battery Electric	FF	Fossil Fuel
BOP	Balance Of Plant	GWP	Global Warming Potential
cc fb	climate-carbon feedback	HFC	Hydrogen Fuel Cell
CcH2	Cryogenic-compressed Hydrogen	ICE	Internal Combustion Engine
CGH2	Compressed Gas Hydrogen	JP-8	Jet Propellant 8
CH <sub>4</sub>	Methane	LH2	Liquid Hydrogen
CO <sub>2</sub>	Carbon Dioxide	NASA	National Aeronautics and Space Administration
CO <sub>2</sub> e	Carbon Dioxide Equivalent	N <sub>2</sub> O	Nitrous Oxide
DC	Direct Current	PEMFC	Proton-Exchange Membrane Fuel Cell
		PWR	Power-to-Weight Ratio
		RPM	Revolutions Per Minute
		TWR	Thrust-to-Weight Ratio
		U.S.	United States

### 1.1. Review of military vehicle fleets and performance characteristics

Military vehicles operate across land, air, and sea. For example, the U.S. Army fleet has approximately 300,000 ground vehicles, 4000 aircraft, and 500 watercraft [8]. However, most are variants of just a few vehicle platforms. By selecting specific platforms, this study provides coverage of ~75% of all land-based vehicles, ~67% of all helicopters, ~78% of all airplanes, and ~73% of all watercraft across the U.S. Army's inventory. Additionally, although not a part of the U.S. Army fleet, this study investigates freight locomotives and both medium- and long-haul jet airliners typical of civilian assets used to transport military materiel and personnel to a theater of operations.

There are four major characteristics that should be either met or improved when transitioning vehicles to ensure desired capabilities: mass, volume, range, and either overall vehicle PWR or TWR. Mass and volume are important because vehicles must be capable of crossing combat bridges, being recovered by wreckers, and being transported themselves by rail, ship, or air. Range is important because it affects the ability to conduct sustained combat operations and logistics required for resupply. The PWR (or TWR) is a key indicator of vehicle performance, impacting ability to accelerate or, in the case of airplanes, to take off and climb to cruising altitude. The common definition for PWR is the maximum engine power (kilowatts) divided by vehicle curb mass (kilograms). However, with military vehicles, the primary concern is performance while transporting payload at maximum mass. Consequently, this study uses vehicle gross mass for both mass and PWR calculations. For turboprop airplanes, it is thrust force, not power, that defines capability. Takeoff thrust significantly exceeds the thrust required to maintain cruise at altitude, so this study adopts the common definition of TWR as the static thrust force at sea-level (Newtons) divided by maximum gross takeoff weight (Newtons).

## 2. Methods

This study considers nine vehicle categories: tracked and wheeled combat vehicles, locomotives, helicopters, prop planes, medium- and long-haul turboprop airliners, waterjet boats, and cargo ships. Results are generalized using averaged values for the vehicles studied within each category. Thus, individual vehicles within each category may have results above or below the averaged results. For a rigorous explanation of the methodology and all equation derivations, please see the Supplementary Material.

### 2.1. Concept

The methodology envisions taking an existing ICE vehicle platform and stripping away its major FF-based components (fuel, fuel tank(s), combustion engine(s), transmission(s), oil, and fluids) to establish mass and volume budgets for a new, all-electric system using either BE or HFC architecture. Calculations use the most inclusive definitions for the seven critical technologies considered, meaning values for each system include all balance of plant (BOP) components. For example, pack-level battery values include the mass and volume of control units, sensors, and battery management systems, which in turn include the mass and volume of power electronics. Thermal management architecture is part of pack-level values for batteries, "Integrated Transportation Fuel Cell Power System" values for fuel cells, and PWR values for electric motors. One exception is future feasible values for liquid hydrogen (LH2) storage, where researchers cite values that do not include BOP components and argue they are either not necessary in certain applications or can be integrated into other components of future vehicle designs [9,10].

### 2.2. Establishing the baseline

The first step is to record baseline characteristics of existing ICE vehicles, to include mass (curb, gross, and payload), volume, fuel (density, tank volume, mass and volume of fuel, storage tank efficiency, mass and volume of tank material), engine (type, number, size, volume, dry mass, power, and torque), oil (type, volume, and mass), antifreeze (type, volume, and mass), and transmission (type, size, volume, dry mass, and fluids). Engines and transmissions contain fluids, so those fluids count toward the FF system's mass but not its volume. Vehicle performance characteristics are also quantified, to include the chemical energy content of onboard fuel, onboard useful energy, maximum range, fuel economy, velocity at cruise, max torque and power, and PWR at curb and gross weight.

The model requires an objective means of comparing range between existing ICE vehicles and possible BE and HFC variants. To accomplish this, the model considers the force that each vehicle must overcome to produce movement and the onboard useful energy that each vehicle carries. This stems from the principles that energy is the capacity to do work and work is a force times distance. The onboard useful energy is equal to the force a vehicle must overcome to produce movement times the distance (or range) of movement. The ratio of onboard useful energy to force needed for movement can thereby be a proxy for comparing range between vehicle variants under the same environmental conditions. For

ground vehicles, the model calculates a road load using a simplified drive cycle and the road load components of grade resistance, air resistance, and rolling resistance. This leads to a ratio of onboard useful energy to road load. For locomotives, the analysis considers required friction and adhesion with the rail and determines a ratio of onboard useful energy to tractive effort. For helicopters, the model uses the ratio of onboard useful energy to lift required for hovering. For prop planes, the model uses lift-to-drag ratio, power specific fuel consumption, fuel flow, and fuel weight in the Breguet range equation. The same applies for turbofan airliners, except for the substitution of thrust specific fuel consumption for power specific fuel consumption. The model uses estimates of takeoff power required and thrust provided by just the ducted fans in turbofan engines to meet the original turbofan's static thrust (from its combined jet core and ducted fan components). The model calculates total hull resistance for boats and ships as the summation of friction resistance, residual resistance (wave plus eddy resistance), and air resistance, which requires dimensions of the wetted hull, draft, and displacement.

### 2.3. Overall system efficiency

Calculating onboard useful energy requires calculating overall system efficiency, the ratio of useful work produced to energy input required from fueling (or charging) to movement, for each vehicle type and variant (see Fig. 1). The overall system efficiency is the product of all sub-system efficiencies; e.g., engine, driveline, brakes, and accessories in ground vehicles; diesel engine, alternator, ancillaries, rectifier, electric motors, transmission, and traction auxiliaries in locomotives; turboshaft engines, transmissions, and rotor figure of merit in helicopters; turboprop engine thermal and propulsion efficiencies in prop planes; turbofan thermal and propulsion efficiencies in jet airliners; engine, hull, jet, and pump efficiencies for waterjet boats; and marine diesel engine, shaft, hull, propeller, and relative rotative efficiencies in cargo ships.

### 2.4. Electric motors and gearboxes

The continuous and peak power, volume, and mass of electric motors (both commercial and projected) are parameters for calculating electric motor power density and power-to-weight ratio. An analysis of gearboxes paired with electric motors provides scaling factors for the total mass and volume of electric motors, gearboxes, and oil used per dry weight (mass) of electric motors needed for an application. Not all applications require gearboxes.

### 2.5. Batteries

The specific energy and energy density (at the pack-level) for batteries is quantified. The overall BE system efficiency for each vehicle type is determined by replacing ICE vehicle sub-component efficiencies with sub-efficiencies for battery charging, discharging, the direct current-to-alternating current (DC-to-AC) inverter, control systems, power electronics, electric motors, gearboxes, and ducted fans, as appropriate per vehicle type.

### 2.6. Hydrogen fuel cells and storage

HFC options require quantifying the specific energy and energy density of hydrogen storage system options, such as 700 bar Compressed Gas Hydrogen (CGH<sub>2</sub>), Cryogenic-compressed Hydrogen (CCH<sub>2</sub>), and LH<sub>2</sub>, as well as the specific power and power density of fuel cell stacks. The overall HFC system efficiency for each vehicle category is determined by replacing ICE vehicle sub-component efficiencies with HFC system sub-efficiencies, e.g., the

efficiency of a fuel cell stack.

System component efficiencies shown in gray are the same as in existing FF/ICE vehicles while those in blue are needed for electric/BE variants and those in purple are specific to HFC variants. Blanks correspond to system components not needed by a variant and are shown for clarity in comparisons.

### 2.7. Comparing energy carrying capacity

Direct comparisons of onboard raw energy between ICE, BE, and HFC variants that do not consider the entire vehicle system's efficiency are commonplace yet inadequate.

#### 2.7.1. Onboard raw energy comparison

To illustrate, the model first compares equivalent raw energy content between variants based on the mass and volume of FF from a full ICE vehicle's fuel tank. Dividing the raw chemical energy content of FF by the battery pack-level specific energy and energy density yields the mass and volume, respectively, of batteries required for the same amount of energy. The same process for HFC vehicles yields the amount of hydrogen required. Dividing mass and volume values for batteries and hydrogen by mass and volume values of FF yields mass and volume battery: fuel and hydrogen: fuel ratios. Batteries must be much heavier and larger than FF with the same raw energy content, while hydrogen weighs much less but requires much more volume.

#### 2.7.2. Onboard useful energy comparison

Taking this comparison a step further, the model compares the overall system efficiencies for ICE, BE, and HFC vehicles. Since BE and HFC vehicles are more efficient in using their onboard energy, the battery: fuel and hydrogen: fuel ratios improve significantly.

### 2.8. Whole-system design solutions

From here, a whole-system design approach analyzes potential solution spaces for vehicles while simultaneously ensuring that the four vehicle characteristics of mass, volume, range, and PWR/TWR are either met or improved when transitioning to BE or HFC variants using both commercial and future feasible technology values, as illustrated by Fig. 2. Linear equations depend upon just two variables for each vehicle characteristic: either electric motor mass and battery pack mass for BE vehicles or electric motor mass and hydrogen storage system mass for HFC vehicles. (Full derivations for these equations are in the Supplementary Material, to include explanations for how all other parameters depend upon these variables.) This allows plotting, in two-dimensions, lines for each of the four vehicle characteristics, like those shown in Fig. 3(a) and Fig. 4(a). As in optimization problems, the solution space is within the boundaries of the intersecting lines, if such a space exists. Sometimes, a solution does not exist where all four characteristics can be either met or improved; for example, when a solution only meets or improves upon three characteristics and sacrifices the fourth. This is where designers must consider whether such a sacrifice is acceptable to the vehicle's purpose and is compatible with the transportation infrastructure that supports it. This model calculates the six possible intersections between these four lines as well as the vehicle variant ratios for each of the four characteristics. Results less than or equal to 100% are good for mass and volume whereas results greater than or equal to 100% are good for PWR/TWR and range. Plotted, these results provide the first four of the eight graphs per vehicle type shown in the Supplementary Material, indicating what is possible now and in the future for both BE and HFC variants (see Fig. S.23 through Fig. S.94).

Solid bars represent commercial technology: electric motor

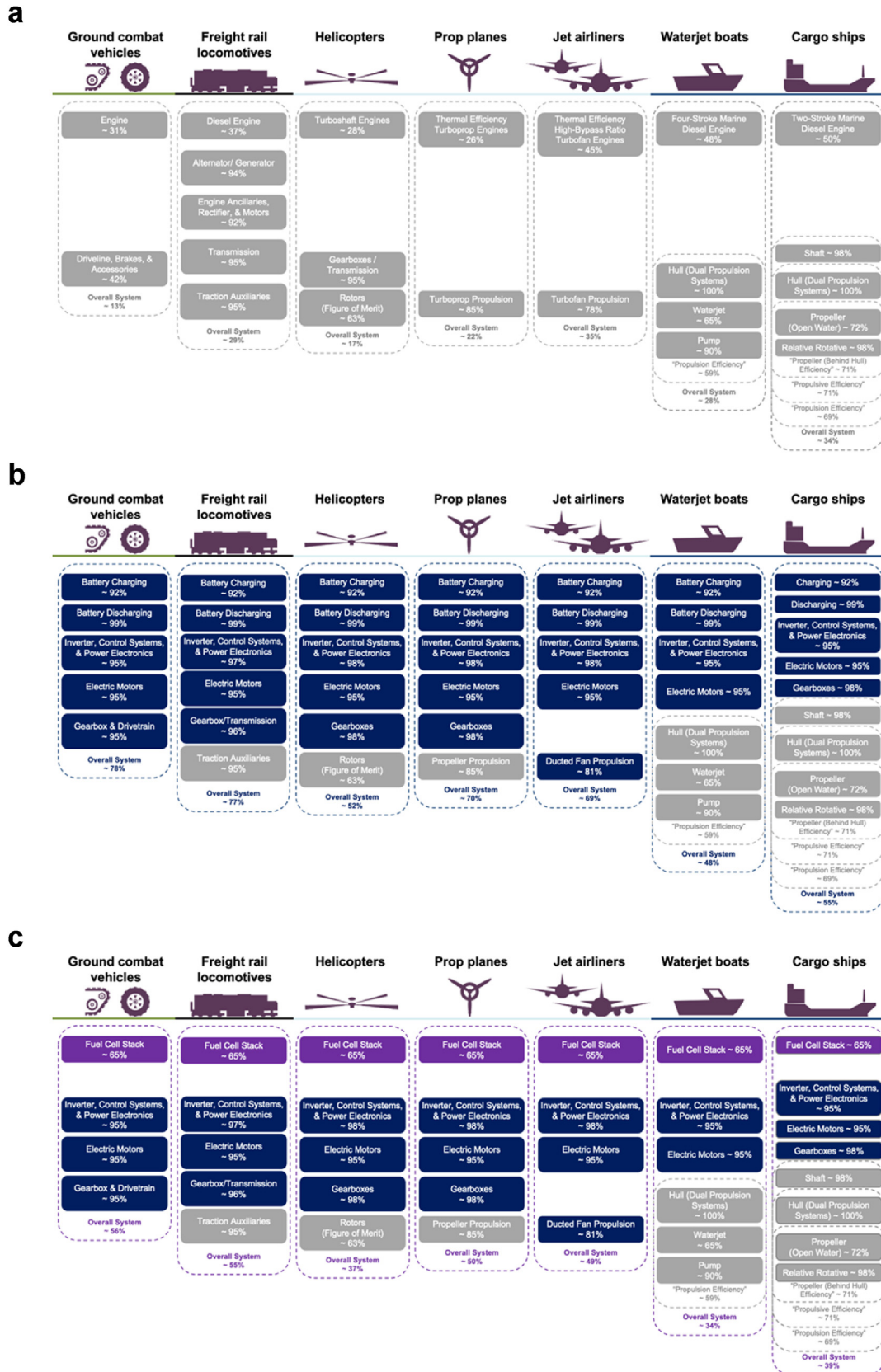


Fig. 1. Overall system efficiency for fossil fuel/internal combustion engine (a), battery electric (b), and hydrogen fuel cell (c) variants of vehicle platforms.

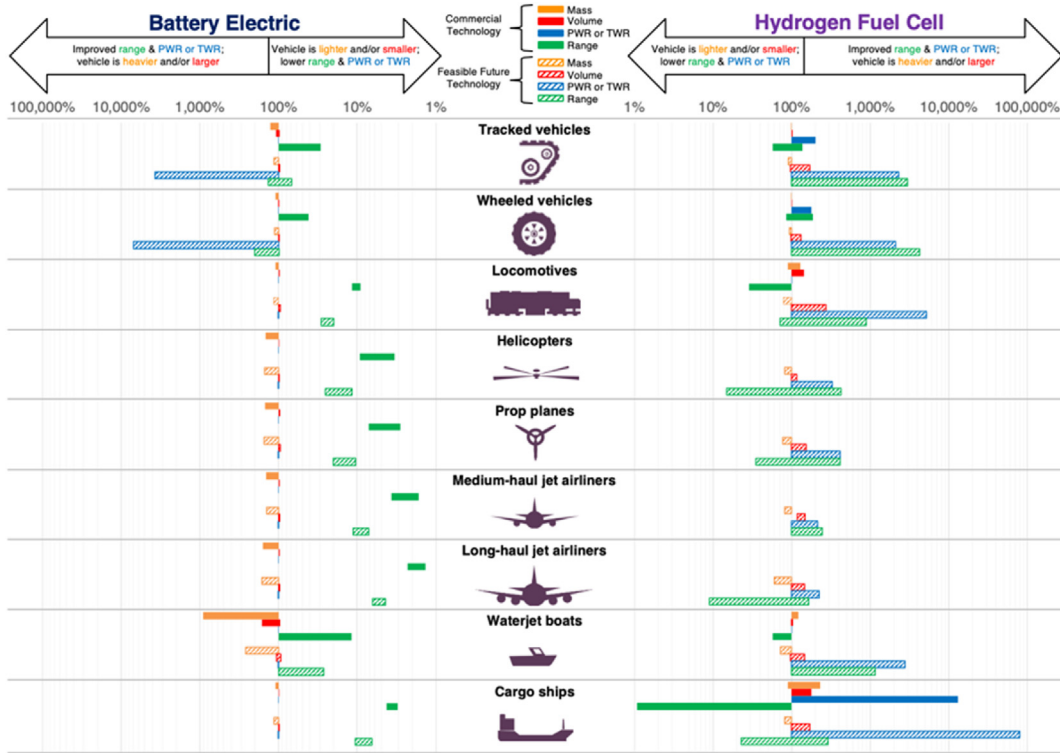


Fig. 2. Feasible characteristics of BE (left) and HFC (right) variants as compared to existing ICE vehicles upon conversion with equal or improved overall vehicle PWR (or TWR).

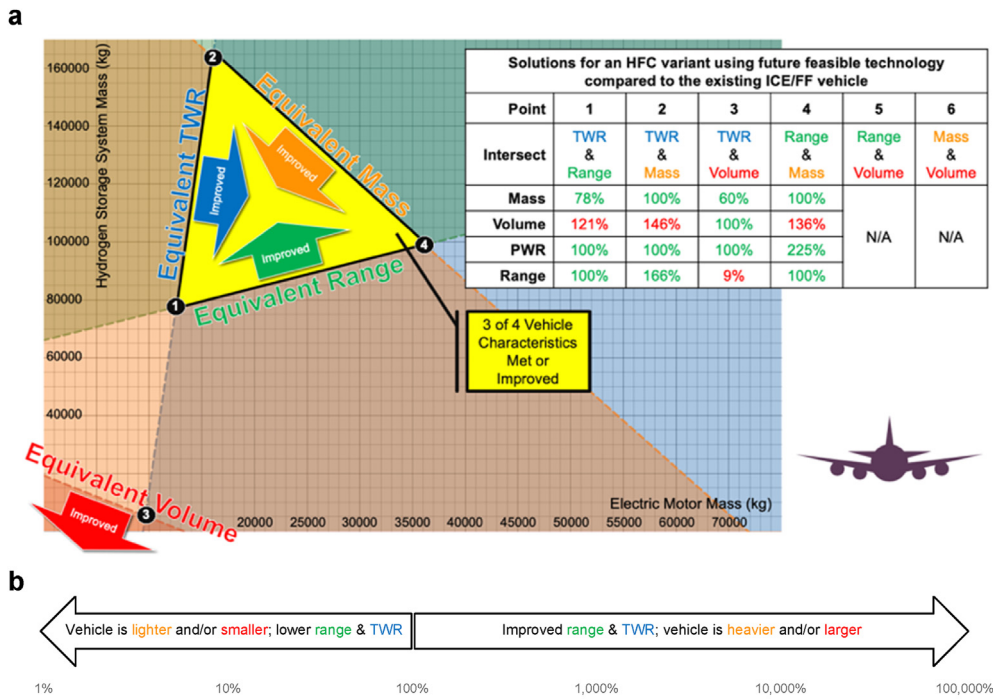


Fig. 3. Example of solutions for a long-haul jet airliner using future feasible technology.

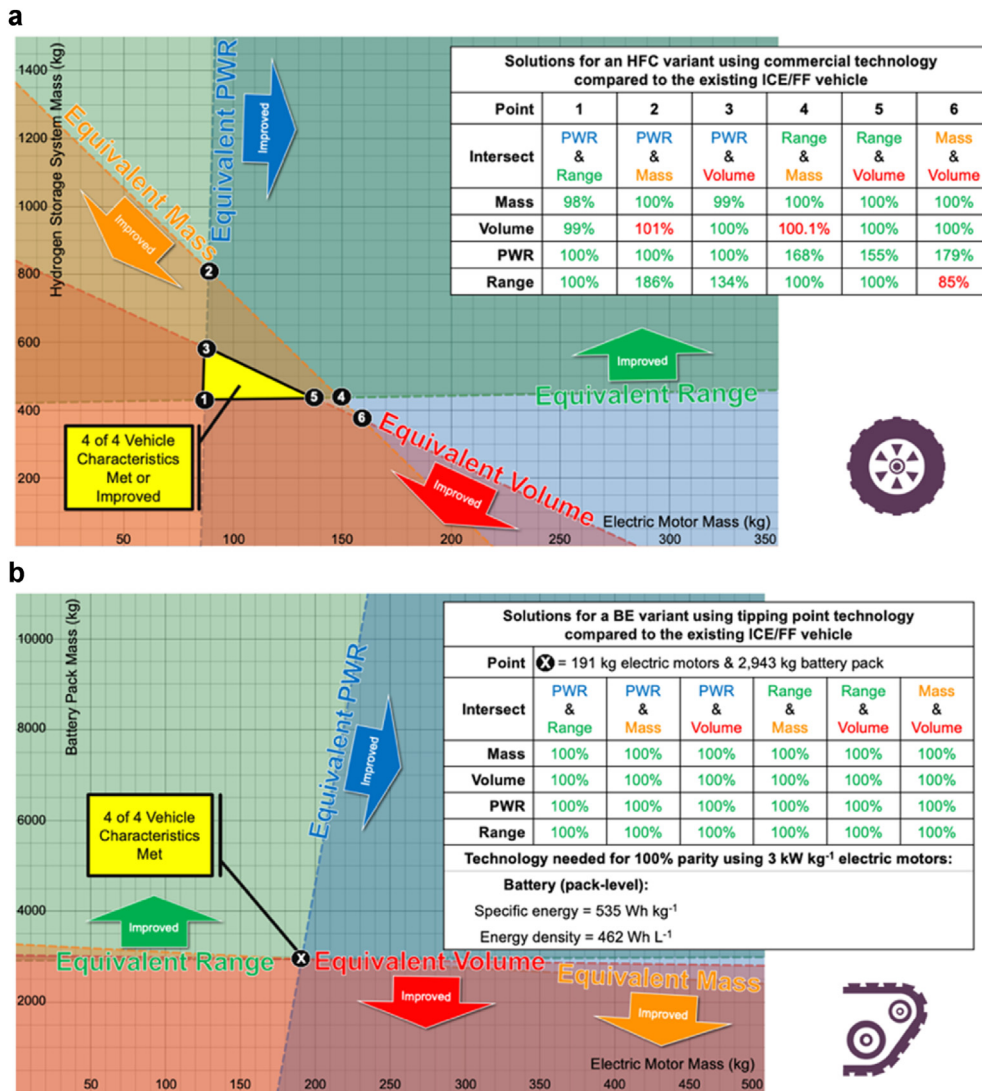


Fig. 4. Example of solutions for an HFC wheeled vehicle using commercial technology (a) and a tracked vehicle using tipping point technology (b).

PWR: 3 kW kg<sup>-1</sup>; battery pack-level specific energy: 157 Wh kg<sup>-1</sup> and energy density: 260 Wh L<sup>-1</sup>; hydrogen storage system specific energy: 1465 Wh kg<sup>-1</sup> and energy density: 833 Wh L<sup>-1</sup>; fuel cell stack specific power: 659 W kg<sup>-1</sup> and power density: 640 W L<sup>-1</sup> [11–15]. Hatched bars represent future feasible technology suggested by the literature: electric motor PWR: 15 kW kg<sup>-1</sup>; battery pack-level specific energy: 335 Wh kg<sup>-1</sup> and energy density: 670 Wh L<sup>-1</sup> (using claimed lithium metal battery achievements and an assumed 33% decrease in energy per unit mass or volume from the battery cell to battery pack levels); hydrogen storage system specific energy: 21 kWh kg<sup>-1</sup> and energy density: 1.7 kWh L<sup>-1</sup>; fuel cell stack specific power: 8 kW kg<sup>-1</sup> and power density: 850 W L<sup>-1</sup> [9,10,13,16–20]. Bars represent ranges of potential values, as further explained in Fig. 3.

Lines in (a) denote combinations of design variables for electric motor mass and hydrogen storage system mass that result in HFC variant characteristics equivalent to the existing aircraft. Shaded regions indicate solutions that result in improved characteristics in the HFC variant. Note that only three of four characteristics have overlapping shaded regions. This demonstrates that solutions exist that meet or exceed the characteristics of mass, TWR, and range, but the fourth characteristic, volume, cannot simultaneously be

equivalent to the existing aircraft using the specified technology. Should designers use the parameters for Point 1, an HFC variant would need to be at least 21% larger in volume. The black lines within each bar in (b) illustrate how an individual solution, using Point 1 in (a) as an example, might appear within the data shown in Fig. 2. Point 1 describes a solution where an HFC variant using future feasible technology has 100% of the range and TWR, has 22% less mass, but is 21% larger than the existing long-haul jet airliner.

Lines denote the combination of design variables for electric motor mass and either hydrogen storage system mass (a) or battery pack mass (b) that result in characteristics equivalent to the average existing ICE vehicle. Shaded regions indicate values that would result in improved characteristics. A feasible region exists in (a) where solutions simultaneously meet and/or exceed all four characteristics for an HFC wheeled vehicle using 3 kW kg<sup>-1</sup> electric motors, hydrogen storage system specific energy and energy density of 1465 Wh kg<sup>-1</sup> and 833 Wh L<sup>-1</sup>, and fuel cell stack system specific power and power density of 659 W kg<sup>-1</sup> and 640 W L<sup>-1</sup>. A single point, as in (b) for a BE tracked vehicle, illustrates the technological tipping points required for all four characteristics to equal to those of the average existing ICE vehicle.

### 2.9. Technological tipping point solutions

Lastly, the model determines technological tipping points required for BE and HFC vehicles to meet today's ICE vehicle characteristics, e.g., Fig. 4(b). Each comparison begins with a baseline set of values for the seven critical technologies. Some technologies are "locked," while others are left "unlocked" and made variables in order to investigate technological tipping points. These results provide the last four of the eight graphs per vehicle type shown in the Supplementary Material (see Fig. S.23 through Fig. S.94).

Fig. 5 details BE vehicles. Fig. 5(a) uses an electric motor PWR and a range of pack-level battery specific energy values in order to calculate the battery pack mass and electric motor mass required using the intersection of the PWR and range lines, which shows equivalency in these two characteristics between the existing ICE and theoretical BE variants. This leads to calculating the mass of a BE variant and the resulting BE:ICE mass ratio. Fig. 5(a) is useful because it shows not just the 1:1 solution for a BE:ICE mass ratio but also solutions for other mass ratios; e.g., if designers believe a 20% increase in vehicle mass is acceptable, then lower battery pack-level specific energy technologies become acceptable and can be determined from the figure. Using spreadsheet software with a built-in optimization solver function, the model solves for the pack-

level battery specific energy required to achieve a 1:1 BE:ICE mass ratio.

Calculations require BE variants to have the same PWR (or TWR) and range as existing ICE vehicles and use claimed  $15 \text{ kW kg}^{-1}$  electric motors [16]. Commercial battery technology is shown by the vertical green dashed line for specific energy (a) and energy density (b) [12]. The horizontal red dashed line shows a 1:1 ratio between BE and ICE vehicles for overall vehicle mass (a) and volume (b). The intersection with a vertical line drawn will indicate the percent increase or decrease in overall vehicle mass or volume achieved upon conversion at that battery technology. The point at which each vehicle's line crosses the red dashed line indicates the technological tipping point where the BE variant will have the same mass or volume as the existing ICE vehicle. Each vehicle type's battery specific energy tipping point from (a) is used in the calculations to determine energy density tipping points in (b).

Similarly, Fig. 5(b) uses the specified electric motor PWR, pack-level battery specific energy, and a range of pack-level battery energy density values. The battery pack mass and electric motor mass required does not change, but the volume of the resulting BE variant does. The model calculates the BE variant volume along with the BE:ICE volume ratio. If done using the adopted value for pack-level battery specific energy, the model can optimize the

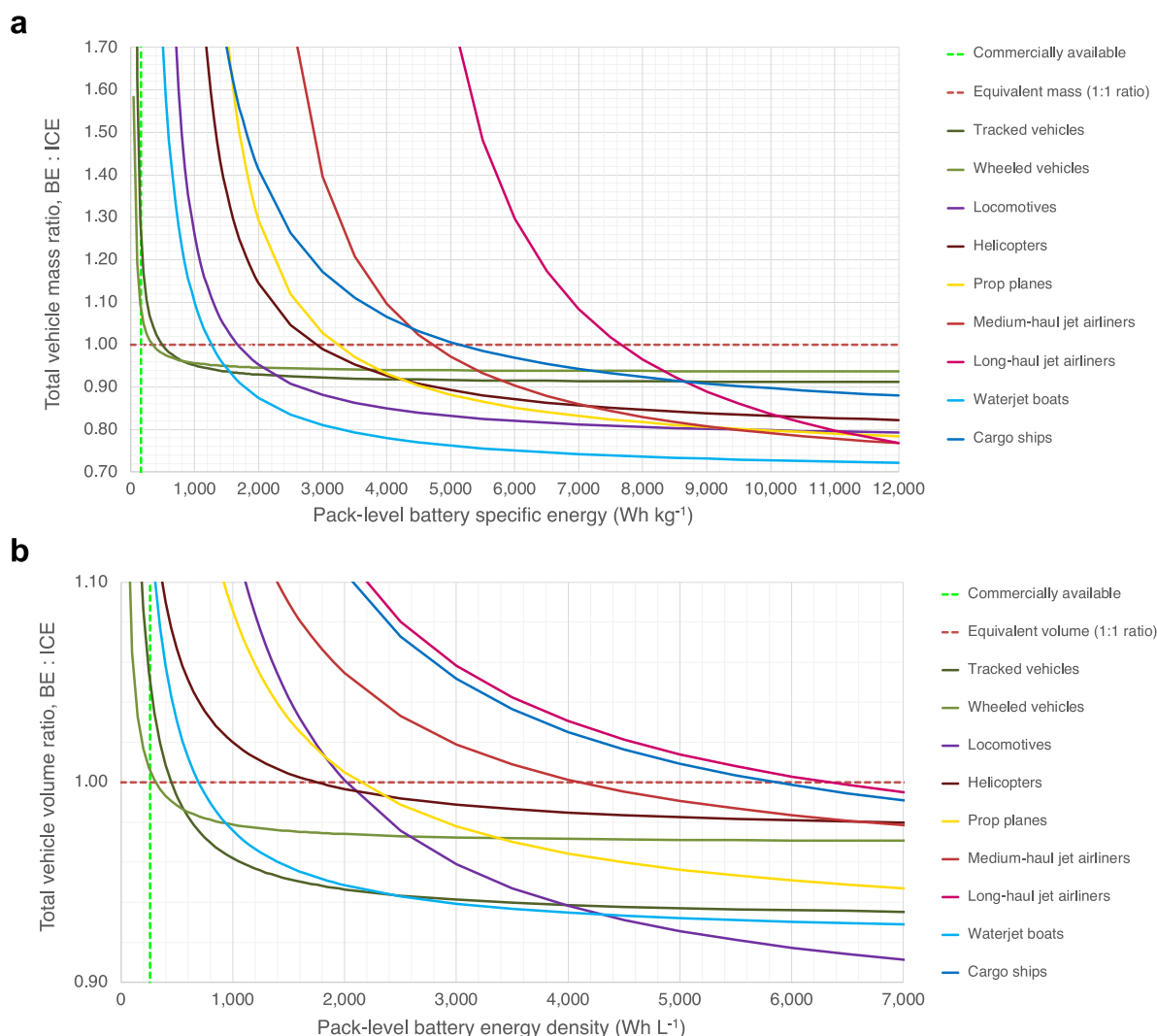


Fig. 5. Impact of pack-level battery specific energy on total vehicle mass (a) and energy density on total vehicle volume (b).

result for volume without necessarily first meeting the mass characteristic. This is useful if designers were concerned about volume but not mass in a new BE variant. However, one can also repeat the process using an electric motor PWR and the pack-level battery specific energy solution from the 1:1 BE:ICE mass ratio. In this instance, the model first meets the PWR and range characteristics, then the mass characteristic, and then finds a volume solution such that all four characteristics are simultaneously satisfied. In both cases, the solver function and Fig. 5(b) can be helpful in finding the 1:1 BE:ICE volume ratio or to investigate other acceptable designs.

HFC variants are more difficult to analyze because of the competition between hydrogen storage and fuel cell stacks for both mass and volume budgets. The first step is to make a range of possible hydrogen storage system specific energy values and values for the electric motor PWR and fuel cell stack specific power. Again, the model first meets both vehicle PWR and range characteristics before calculating the hydrogen storage system mass and electric motor mass required. This facilitates calculating the mass of the HFC variant and the resulting HFC:ICE mass ratio. A solver function finds the optimal solution for hydrogen storage system specific energy to achieve a 1:1 HFC:ICE mass ratio. The model follows a similar process using a range of possible hydrogen storage system energy density values along with values for electric motor PWR, hydrogen storage system specific energy, and fuel cell stack specific power and power density. The solver function then finds the desired technological tipping point for hydrogen storage system energy density.

After investigating the hydrogen storage system, the model considers fuel cell stacks using the same baseline assumptions along with a range for fuel cell stack specific power and locked values for the electric motor PWR and hydrogen storage system specific energy. The intersection of the PWR and range vehicle characteristic lines identifies a solution for the hydrogen storage system mass and electric motor mass required, and the model uses this to calculate the resulting mass of the HFC variant and the HFC:ICE mass ratio. The solver function finds the optimal fuel cell stack specific power to achieve a 1:1 HFC:ICE mass ratio under these assumptions.

Next, the model uses values for the electric motor PWR, the hydrogen storage system specific energy and energy density, and the fuel cell stack specific power along with a range of possible values for the fuel cell stack power density. The intersection of the PWR and range vehicle characteristic lines identifies a solution for the hydrogen storage system mass and electric motor mass required, followed by the resulting volume of the HFC variant and the HFC:ICE volume ratio. The solver function determines optimal fuel cell stack power density to achieve a 1:1 HFC:ICE mass ratio under these assumptions.

Finally, Fig. 6 shows the interdependency between hydrogen storage system and fuel cell stack mass and volume. This requires working backwards by assuming that 1:1 HFC:ICE mass, PWR, and range ratios are met, which permits using the fuel cell stack specific power and hydrogen storage system specific energy parameters as variables. A range of possible fuel cell stack specific power values allows for the calculation of resulting hydrogen storage system specific energy values required for Fig. 6(a). One can also apply a "mass scaling factor." For example, a 1.05 scaling factor reflects the resulting hydrogen storage system specific energy values if a 5% increase in mass is acceptable. Increases in acceptable mass, in effect, shift the curves shown in Fig. 6(a) down and to the left, meaning that lower technology levels can facilitate acceptable solutions. To investigate the interdependency between fuel cell stack power density and hydrogen storage system energy density, the model uses a volume scaling factor of 1.0. The model establishes

several cases for investigation using values for the fuel cell stack specific power and their resulting required hydrogen storage system specific energy. A range of values for the fuel cell stack power density permits the calculation of a range of resulting hydrogen storage system energy density values. The values graphed in Fig. 6(b) reflect the case where fuel cell stacks have achieved  $8 \text{ kW kg}^{-1}$  specific power.

Shown are values that can achieve a 1:1 HFC:ICE mass ratio (a) and volume ratio (b) for each vehicle platform. Calculations require HFC variants to have the same PWR (or TWR) and range as existing ICE vehicles and use  $15 \text{ kW kg}^{-1}$  electric motors and  $8 \text{ kW kg}^{-1}$  fuel cell stacks [10,16]. Values for commercially-available and future feasible fuel cell stack systems are shown by the vertical green and amber dotted lines, respectively [10,14]. In (a), specific energy values for commercially-available 700-bar hydrogen storage systems, future feasible LH2 storage tanks (no BOP components), and hydrogen alone (no tank or BOP components) are shown by the horizontal green, amber, and red dashed lines, respectively [9,13]. In (a), points A and B show two possible examples of technology levels that would enable all HFC variants to have equivalent or improved characteristics for PWR (or TWR), range, and mass. In (b), energy density values for commercially-available 700-bar hydrogen storage systems, the DOE's ultimate target for light-duty vehicle hydrogen storage, and LH2 alone (no tank or components) are shown by the horizontal green, amber, and red dashed lines, respectively [13]. Vehicles with lines above the red dashed line require other design changes to create more volume budget for energy storage.

## 2.10. Environmental improvements

To demonstrate an example of potential environmental improvements from transitioning energy sources in this unique transportation sector, this paper calculates U.S. Army vehicle "tailpipe" greenhouse gas emissions. The authors use published data from the U.S. Department of Defense and the U.S. General Services Administration's Federal Fleet Reports, along with emissions factors published by the U.S. Environmental Protection Agency and The Climate Registry. Emissions calculations use annual data for operational fuel consumption with estimated proportions to tactical vehicles as well as worldwide vehicle miles recorded for non-tactical vehicles. Tailpipe emissions from both tactical and non-tactical vehicles are combined to find the annual, total U.S. Army vehicle emissions, which is then converted to carbon dioxide equivalent ( $\text{CO}_2\text{e}$ ), Global Warming Potential (GWP), and the number of passenger cars on the road producing equivalent greenhouse gas pollution.

## 2.11. Additional functionality

Additionally, two optimization solvers for BE vehicles and three for HFC vehicles allow for investigating design options with different technologies.

## 2.12. Uncertainty

Uncertainty is acknowledged throughout by using low, middle, and high values in calculations for each parameter. The middle value reflects a known value or the mean of high and low estimates. The model performs calculations such that low and high estimates compound to produce an all-inclusive range of results. For graphing/reporting purposes, results use middle values.



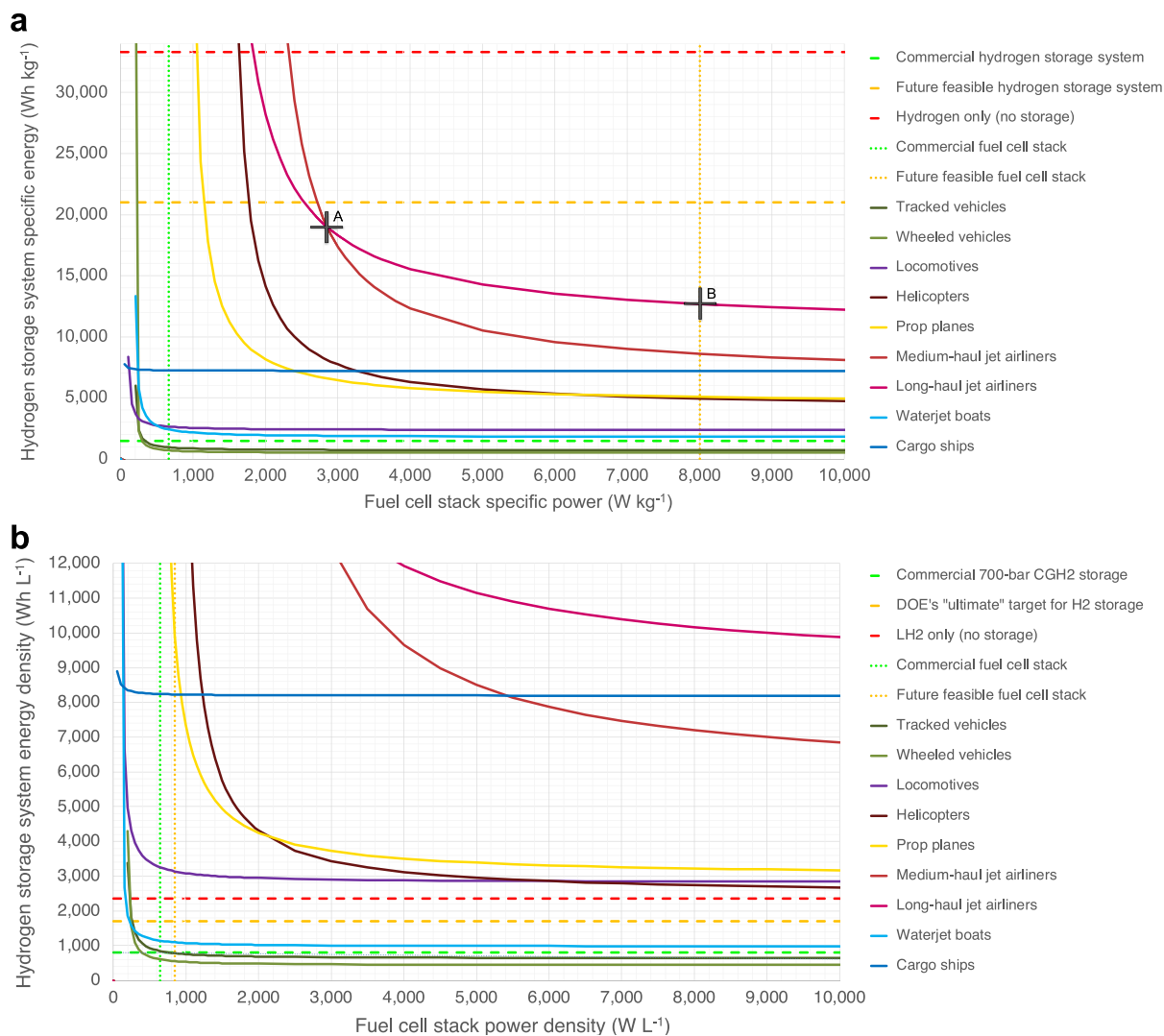


Fig. 6. Competition between hydrogen storage system and fuel cell stack requirements to achieve equivalent mass (a) and volume (b) between HFC and ICE variants.

### 3. Results

If all U.S. Army vehicles are transitioned to either BE or HFC platforms and electricity comes from clean, renewable sources, then current tailpipe and upstream greenhouse gas emissions will decrease to zero – a significant benefit from an air pollution, climate, and sustainability point of view. Using recent data, total tailpipe greenhouse gas emissions of carbon dioxide (CO<sub>2</sub>); methane (CH<sub>4</sub>); and nitrous oxide (N<sub>2</sub>O) for all U.S. Army vehicles are estimated on an annual basis [21–24]. Emissions are combined with 20- and 100-yr GWPs, both with and without climate-carbon feedback (cc fb), to obtain CO<sub>2</sub>e emission units [25]. Finally, to put these values into perspective, total tailpipe emissions are related to the equivalent number of passenger cars on the road today [26]. As shown in Table 1, transitioning all U.S. Army vehicles could decrease tailpipe emissions by over 3 megatonne-CO<sub>2</sub>e/yr, equivalent to taking 690,000 passenger cars off the road each year. Additional upstream savings of CO<sub>2</sub>e emissions will also occur upon transitioning these vehicles due to producing electricity from clean, renewable sources versus mining, transporting, and refining oil to gasoline or diesel and then transporting those products around the world for use.

Beyond environmental improvements, our results indicate that

some vehicles have the potential to transition using technology that is either commercially available or possibly will be soon, whereas other vehicles will require significant design changes and/or large improvements in technology. Fig. 2 summarizes results for each vehicle platform with regard to commercial and future feasible technologies. Many vehicles have the potential to improve capabilities, while others cannot simultaneously realize equivalency in all four vehicle characteristics using just calculated budgets for mass and volume. In such cases, vehicles must be either larger or heavier. For example, no feasible solution exists for aircraft platforms using commercial HFC technology because such technology cannot achieve the necessary PWR (or TWR), and the aircraft would likely be unable to take off. Fig. 3 illustrates that a long-haul jet airliner using future feasible technology is capable of realizing equivalent or improved mass, range, and TWR characteristics at the cost of increasing volume by ~21%. Fig. 4 illustrates ground combat vehicles capable of equivalent or improved characteristics using either commercial HFC technology or tipping point BE technologies. Table 2 summarizes the tipping point technologies required for both BE and HFC variants of each vehicle type, which can aid decision-makers in assessing what transitions may be possible, when they might occur, and where to place emphasis on research and development. Figs. 5 and 6 illustrate how achievements in the

**Table 1**  
Total U.S. Army vehicle tailpipe greenhouse gas emissions by year.

Year	CO <sub>2</sub> (tonne)	CH <sub>4</sub> (tonne)	N <sub>2</sub> O (tonne)	20-yr GWP (megatonne CO <sub>2</sub> e)		100-yr GWP (megatonne CO <sub>2</sub> e)		Approximate equivalence to number of passenger cars [26]
				No cc fb	With cc fb	No cc fb	With cc fb	
2019	3,150,000	75.5	90.4	3.18	3.18	3.17	3.18	690,000
2018	3,210,000	77.4	92.2	3.24	3.24	3.24	3.24	705,000
2017	2,690,000	64.4	76.9	2.72	2.72	2.71	2.72	591,000
2016	2,560,000	60.9	72.5	2.59	2.59	2.58	2.58	562,000
2015	2,620,000	62.3	73.9	2.65	2.65	2.64	2.65	576,000
2014	3,510,000	84.6	101	3.55	3.55	3.54	3.54	771,000
2013	4,370,000	105	126	4.41	4.41	4.40	4.41	958,000
2012	5,460,000	132	159	5.51	5.51	5.50	5.51	1,200,000
2011	6,840,000	165	198	6.90	6.90	6.89	6.90	1,500,000

Note that annual emissions are highly dependent upon the level of wartime or peacetime conditions, among other factors, that the U.S. Army is operating under. GWP = Global Warming Potential; cc fb = climate-carbon feedback.

**Table 2**  
Combinations required, by platform and electric motor PWR, of pack-level battery technology (a) and hydrogen storage + fuel cell stack system technologies (b) to ensure all four vehicle characteristics of mass, volume, range, and vehicle PWR (or TWR) are equivalent to today's ICE vehicles.

<b>(a)</b>												
Variant	Battery electric											
Electric motor power-to-weight ratio	3 kW kg <sup>-1</sup>					15 kW kg <sup>-1</sup>						
Technology parameter	Battery pack					Battery pack						
	Specific energy (Wh kg <sup>-1</sup> )		Energy density (Wh L <sup>-1</sup> )			Specific energy (Wh kg <sup>-1</sup> )		Energy density (Wh L <sup>-1</sup> )				
<b>Vehicle platform</b>												
Tracked vehicles	535		462			491		451				
Wheeled vehicles	377		319			342		311				
Locomotives	1731		2037			1673		2012				
Helicopters	4692		1855			2889		1747				
Prop planes	5520		2329			3214		2130				
Medium-haul jet airliners	9435		4605			4707		4099				
Long-haul jet airliners	11,488		6801			7652		6328				
Waterjet boats	1325		700			1263		695				
Cargo ships	5149		5850			5140		5846				
<b>(b)</b>												
Variant	Hydrogen fuel cell											
Electric motor power-to-weight ratio	3 kW kg <sup>-1</sup>					15 kW kg <sup>-1</sup>						
Technology parameter	Hydrogen storage		Fuel cell stack		Percent change required		Hydrogen storage		Fuel cell stack		Percent change required	
	Specific energy (Wh kg <sup>-1</sup> )	Energy density (Wh L <sup>-1</sup> )	Specific power (W kg <sup>-1</sup> )	Power density (W L <sup>-1</sup> )	Mass	Volume	Specific energy (Wh kg <sup>-1</sup> )	Energy density (Wh L <sup>-1</sup> )	Specific power (W kg <sup>-1</sup> )	Power density (W L <sup>-1</sup> )	Mass	Volume
<b>Vehicle platform</b>												
Tracked vehicles	1317	1021	448	454	N/A	N/A	1209	997	411	443	N/A	N/A
Wheeled vehicles	1034	775	445	436	N/A	N/A	938	755	404	425	N/A	N/A
Locomotives	21,000	1700	8000	850	-20%	5%	21,000	1700	8000	850	-21%	5%
Helicopters	21,000	1700	8000	850	-7%	4%	21,000	1700	8000	850	-15%	3%
Prop planes	21,000	1700	8000	850	-9%	10%	21,000	1700	8000	850	-20%	7%
Medium-haul jet airliners	21,000	1700	8000	850	2%	23%	21,000	1700	8000	850	-18%	17%
Long-haul jet airliners	21,000	1700	8000	850	0%	29%	21,000	1700	8000	850	-22%	21%
Waterjet boats	2723	1330	572	365	N/A	N/A	2596	1322	545	363	N/A	N/A
Cargo ships	21,000	1700	8000	850	-14%	19%	21,000	1700	8000	850	-14%	19%

Battery technology in (a) is not capped, and results show what would be required for all four vehicle characteristics to be met. HFC technology in (b) is capped at literature-cited future feasible values for hydrogen storage (21,000 Wh kg<sup>-1</sup> and 1700 Wh L<sup>-1</sup>) and fuel cell stacks (8000 W kg<sup>-1</sup> and 850 W L<sup>-1</sup>). If using these capped values still do not result in simultaneously meeting all four vehicle characteristics, then the model first meets both vehicle PWR (or TWR) and range, and then calculates the resulting change in mass and/or volume as compared to today's ICE variants. For example, a future HFC long-haul jet airliner could have the same range, TWR, and mass as today's ICE long-haul jet airliner, but it would need to be 29% larger. A future HFC medium-haul jet airliner would require an increase in both mass (2%) and volume (23%) in order to have the same range and TWR as today's ICE medium-haul jet airliner. A future HFC cargo ship could have 14% less mass than today's ICE cargo ship, but it would have to be 19% larger to maintain range and PWR. Any HFC solution using a storage specific energy of 21,000 Wh kg<sup>-1</sup> does not include all BOP components and would likely necessitate further design changes based on intended vehicle use (see section 4.3. Hydrogen storage)

seven critical technologies identified affect each vehicle's potential to transition. For complete results by vehicle category, please see the Supplementary Material.

### 3.1. Ground vehicles

Ground vehicles can transition to BE with the same vehicle mass, volume, PWR, and range as existing ICE vehicles if pack-level battery specific energy technology reaches 342 to 377 Wh kg<sup>-1</sup> for the average wheeled vehicle and 491 to 535 Wh kg<sup>-1</sup> for the average tracked vehicle (Table 2), with the highest values corresponding to commercial electric motors and the lowest values corresponding to a 5× improvement in electric motor PWR. Improving battery specific energy will always improve range, but since onboard energy storage is only one component of a vehicle's mass, improvements beyond 800 Wh kg<sup>-1</sup> offer diminishing benefits to meeting gross weight targets (Fig. 5(a)). HFC variants can most often meet all four characteristics of the existing ICE vehicles while simultaneously improving their range. Using commercial HFC technology, the average wheeled vehicle can realize 134% of its existing range, while the average tracked vehicle can realize 98%. Future feasible HFC technology could result in 328% (wheeled) and of 241% (tracked) of existing range, but, again, future feasible HFC technology does not include all BOP components, like insulation, for LH2 tanks. Therefore, further work is required to determine if such tanks could be used for specific missions like non-stop, long-distance movements. Without insulation, boil-off and venting requirements would significantly reduce results.

### 3.2. Freight locomotives

For equivalent characteristics, a BE locomotive would require pack-level battery specific energy of 1673 to 1731 Wh kg<sup>-1</sup> depending upon electric motors used. HFC locomotives would likely require LH2, but they still would not meet the established volume budget. Railway infrastructure like tunnels, trestles, bridges, and the rail itself places limits on overall locomotive mass and volume. Locomotives are as heavy as allowable (~196,000 kg) to increase track adhesion. However, lightweighting or reducing non-power system components (which there was little incentive to do before) could increase budgets for onboard energy storage. Another solution is to pull an additional railcar with batteries or hydrogen. Alternatively, recharging zones can charge batteries via a third rail or catenary while the locomotive is underway to extend range. Although results indicate the need for technology improvements, design options suggest transitioning locomotives is possible.

### 3.3. Rotary-wing aircraft

BE helicopters would require pack-level battery specific energy values between 2889 Wh kg<sup>-1</sup> (15 kW kg<sup>-1</sup> motors) and 4692 Wh kg<sup>-1</sup> (3 kW kg<sup>-1</sup> motors). HFC helicopters would need to be ~3%–4% larger than today's variants (Table 2), although this considers LH2 tanks without insulation. Rotor thrust to produce lift, which counters a helicopter's weight, is the major requirement for both hovering and forward flight, but adding heavy batteries or fuel cell stacks with hydrogen storage systems quickly consumes mass and volume budgets. Improvements to fuel cell stack specific power will significantly reduce improvements needed for hydrogen storage (Fig. 6(a)). New helicopter designs could potentially incorporate design changes or trade payload mass and volume for HFC system components.

### 3.4. Fixed-wing aircraft

HFC airplanes using future feasible technologies are theoretically achievable with an overall volume increase of ~7%–21%, depending upon airplane type (Table 2), but this requires the assumption that insulation is either unnecessary or can be reduced due to constant extraction of hydrogen, sufficient to avoid boil-off and venting, during all phases of flight [9,10]. Fig. 3 uses a long-haul jet airliner to illustrate HFC designs solutions that meet, or improve upon, targets for mass, volume, TWR, and range, although not all four simultaneously. BE airplanes require pack-level battery specific energy values of 3214 to 11,488 Wh kg<sup>-1</sup> depending upon airplane type and the PWR of electric motors used, which represents technology improvements that may be theoretically possible but are beyond the foreseeable future. Fig. 2 illustrates these results where none of the range bars for a medium- or long-haul jet airliner exceed ~10% of existing capabilities. Transitioning aircraft is challenging. Planes generally carry jet fuel in “wet-wings” where the structure of the wings themselves form the fuel tank, but storing batteries or hydrogen requires more complex solutions. Increasing an airplane's overall volume will result in increased drag, but other design changes may be possible to maintain a favorable lift-to-drag ratio, e.g., existing super transporter airplanes designed to carry outsized cargo.

### 3.5. Watercraft

Depending upon the electric motor PWR used, waterjet boats require pack-level battery specific energy values of 1263 to 1325 Wh kg<sup>-1</sup> while cargo ships require 5140 to 5149 Wh kg<sup>-1</sup> in order to meet all four characteristics (Table 2). Waterjet boats can meet all targets today using commercial HFC technology. Cargo ships using future feasible HFC technology would need to be ~19% larger, but, as stated previously, this does not include all BOP components. The challenge for cargo ships is the onboard energy storage necessary to sustain long-durations between ports of call.

## 4. Discussion: technology for transitions

### 4.1. Electric motors and gearboxes

Electric motors are much smaller and lighter than their ICE counterparts. The 2016 BMW i3 radial flux motor has a peak PWR of 3 kW kg<sup>-1</sup>, but new axial flux motors claim peak PWRs up to 15 kW kg<sup>-1</sup> [11,27]. Electric motors produce maximum torque starting from zero revolutions per minute (RPM) and useable torque across a wide RPM range, so it is possible to use a direct-drive gear (1:1 ratio between motor RPM and wheel RPM). Some electric vehicle manufacturers design for an appropriate single-speed (constant gear ratio) while others use two-speed gearboxes for increased torque in first gear to climb hills and increased speed in second gear for traveling at highway speeds [28]. This study uses manufacturers' data to estimate mass and volume of appropriately-sized gearboxes paired with electric motors to replace transmissions as appropriate [29,30].

### 4.2. Batteries

Although various battery chemistries exist, overall specific energy and energy density are of primary concern. Values are often cited using different boundaries with increasing inactive components at the material-, electrode-, cell-, module-, to system/pack-levels. For example, the module-level includes cells, a container, control units, and sensors, while the pack-level contains modules plus a battery management system and cooling architecture.

Calculations here use the most inclusive, pack-level values. Published goals for 2020 were 350 Wh kg<sup>-1</sup> and 750 Wh L<sup>-1</sup> at the cell-level and 235 Wh kg<sup>-1</sup> and 500 Wh L<sup>-1</sup> at the pack-level [17,18]. This reflects a ~33% decrease when moving from the cell-to pack-level in both parameters due to the mass and volume of inactive components.

Although liquid electrolyte lithium-ion batteries may be reaching their limits, other types of batteries may eventually achieve published goals [31]. Recent claims for cell-level solid state batteries include values as high as 700 Wh kg<sup>-1</sup> and 1200 Wh L<sup>-1</sup> [32,33]. Additionally, post-lithium-ion technologies like lithium-sulfur and lithium-oxygen batteries have reported theoretical specific energy values of 2600 Wh kg<sup>-1</sup> and 11,400 Wh kg<sup>-1</sup>, respectively, while the theoretical energy density of iron-air batteries is 9700 Wh L<sup>-1</sup> [34–36]. Of course, any inactive components within the pack-level boundary will further reduce such values. To estimate future feasible BE technology, this study takes the lower-end of recently reported claims, i.e., 500 Wh kg<sup>-1</sup> and 1000 Wh L<sup>-1</sup> [20], and further applies a 33% reduction to obtain 335 Wh kg<sup>-1</sup> and 670 Wh L<sup>-1</sup>, which is consistent with the decrease in performance moving from cell-to pack-levels as reflected by current lithium-ion battery goals for electric vehicles [18]. Achieving these levels would make transitioning wheeled and tracked vehicles more likely, especially with some additional design changes to create more budget. Transitioning other vehicles requires further technological advancements.

#### 4.3. Hydrogen storage

The volumetric energy density of hydrogen is a challenge for long-distance transport, as illustrated by Fig. 6(b). In terms of mass, hydrogen has nearly three times the energy content of jet propellant 8 (JP-8), the fuel used in many military vehicles, with 33.3 kWh kg<sup>-1</sup> compared to 12 kWh kg<sup>-1</sup>. In terms of volume, however, the relationship reverses with JP-8 at 10 kWh L<sup>-1</sup> and hydrogen at 1.37 kWh L<sup>-1</sup> (at 700-bar pressure) or 2.36 kWh L<sup>-1</sup> (as a liquid at -253 °C). Hydrogen must be either compressed or cooled to a low temperature and insulated to store sufficient quantities on-board vehicles. Published “projected” performance is 1400 Wh kg<sup>-1</sup> and 800 Wh L<sup>-1</sup> for 700-bar CGH2 systems and 2300 Wh kg<sup>-1</sup> and 1400 Wh L<sup>-1</sup> for Cch2 systems, where all values include BOP components and exclude the unusable energy resulting from maintaining minimum fuel cell pressure, flow, and temperature requirements [13,37]. Nevertheless, a 2017 commercial example shows that these metrics have been met [13]. Published “ultimate” targets for hydrogen storage specific energy and energy density are 2200 Wh kg<sup>-1</sup> and 1700 Wh L<sup>-1</sup> [13]. Researchers have determined that exemplary cylindrical tanks can achieve a storage density of 64% hydrogen by mass (a hydrogen storage specific energy of 21 kWh kg<sup>-1</sup>), but this does not include insulation or other tank periphery [9]. Thus, such tanks may only be suitable for specific applications, like non-stop vehicle movement between ports with constant hydrogen extraction sufficient to overcome boil-off and venting requirements [10]. Regarding economies of scale, a survey of commercial data shows that 700-bar and LH2 storage systems exhibit similar performance up to ~5 kg hydrogen stored but, beyond that, LH2 systems occupy significantly less mass and volume [38].

#### 4.4. Fuel cells

Fuel cells produce an electric current from hydrogen. Most fuel cells in transportation applications are Proton-Exchange Membrane Fuel Cells (PEMFCs), which can be stacked to provide required power output [39]. The 2018 Toyota Mirai’s fuel cell stack

has a specific power of 2000 W kg<sup>-1</sup> and an output power density of 3100 W L<sup>-1</sup>, but the U.S. Department of Energy (DOE) published targets of 650 W kg<sup>-1</sup> and 850 W L<sup>-1</sup> and an achieved status of 659 W kg<sup>-1</sup> and 640 W L<sup>-1</sup> [19,40]. DOE targets are lower than Toyota’s achieved values because the DOE reports values in terms of an “Integrated Transportation Fuel Cell Power System” to include all BOP components and a thermal management system. Still, literature suggests a reasonable estimate for future development of PEMFC specific power of 8 kW kg<sup>-1</sup> and even toward >10 kW kg<sup>-1</sup> due to improvements in both active and passive components of the fuel cell, specifically new electrocatalysts in the membrane electrode assembly, metal bipolar plates with corrosion resistance coatings, and reductions to end plates and screws [10]. Such room for improvement exists because PEMFCs have been mostly used for automotive applications where targets have already been reached and ultra-lightweight applications have not yet been strongly pursued. Further improvements to PEMFCs are still important, as illustrated in Fig. 6. As fuel cells become lighter and smaller, more budget exists for hydrogen storage.

## 5. Conclusion

This analysis demonstrates that there is potential to transition even the most energy-demanding vehicles; however, without significant technology advancements or design changes, not all vehicles can transition to either BE or HFC systems. Nevertheless, pursuing the technology to facilitate such transitions will provide significant benefits, ranging from significant reductions in greenhouse gas emissions to increased vehicle performance. Strategically, the military could improve its energy security and resilience by using a diverse set of renewables to produce its own energy. Operationally, the military could recharge batteries or make hydrogen using electrolyzers at contingency bases, which would reduce round-the-world resupply logistics and casualties. Batteries could be made swappable across vehicles, allowing for the cross-leveling of energy on the battlefield. Additionally, as technology improves, simply replacing old batteries could increase vehicle range without having to remove vehicles from the fleet for upgrades. Tactically, combat vehicles without internal combustion engines are quieter and cooler, which improves stealth and frustrates thermal vision devices and weapons systems that rely on heat signatures. Replacing internal combustion engines with multiple, long-lasting electric motors can improve resilience and reduce maintenance requirements. The potential to transition military vehicles to either battery electric or hydrogen fuel cell systems and capitalize upon environmental sustainability improvements reinforces the need for further research and development.

## Disclaimer

The views expressed in this paper are those of the authors and do not reflect the official policy or position of the Department of the Army, the Department of Defense, or the United States Government. Reference to any specific commercial product, process, or service by trade name, trademark, manufacturer, or otherwise neither constitutes nor implies endorsement, recommendation, or favor.

## Funding

S.M.K. received support under the U.S. Army’s Advanced Civil Schooling program.

## Credit author statement

**Scott Katalenich:** Conceptualization, Methodology, Software, Validation, Formal analysis, Investigation, Resources, Data curation, Writing – original draft, Writing – review & editing, Visualization, Funding acquisition, **Mark Jacobson:** Conceptualization, Methodology, Writing – review & editing, Supervision, Project administration

## Declaration of competing interest

The authors declare that they have no known competing financial interests or personal relationships that could have appeared to influence the work reported in this paper.

## Acknowledgements

The authors thank S. Billington, D. Gragg, and S. Onori of Stanford University, J. Dabiri of the California Institute of Technology, and J. Eichman of the National Renewable Energy Laboratory for their helpful discussions.

## Appendix A. Supplementary data

Supplementary data to this article can be found online at <https://doi.org/10.1016/j.energy.2022.124355>.

## References

- Vavrin J. *Power and energy considerations at forward operating bases (FOBs)*. Champaign, IL: USACE, ERDC, CERL; 2010.
- Nicholson M, Stepp M. Lean, mean, and clean II: assessing DOD investments in clean energy innovation 2012.
- Jones-Bonbrest N. Army to deliver fuel-efficient generators to Afghanistan. *US Army*; 2012. [https://www.army.mil/article/81578/army\\_to\\_deliver\\_fuel\\_efficient\\_generators\\_to\\_afghanistan](https://www.army.mil/article/81578/army_to_deliver_fuel_efficient_generators_to_afghanistan). [Accessed 20 August 2018].
- Davis SJ, Lewis NS, Shaner M, Aggarwal S, Arent D, Azevedo IL, et al. Net-zero emissions energy systems. *Science* 2018;(80):360. <https://doi.org/10.1126/science.aas9793>.
- Earl T, Mathieu L, Cornelis S, Kenny S, Ambel CC, Nix J. Analysis of long haul battery electric trucks in EU. In: Amended paper (August 2018) originally presented at the 8th Commercial Vehicle Workshop, Graz, 17–18 May 2018. *Eur Fed Transp Environ*; 2018. Available at: [https://www.transportenvironment.org/wp-content/uploads/2021/07/20180725\\_T&E\\_Battery\\_Electric\\_Trucks\\_EU\\_FINAL.pdf](https://www.transportenvironment.org/wp-content/uploads/2021/07/20180725_T&E_Battery_Electric_Trucks_EU_FINAL.pdf).
- Marcinkoski J, Vijayagopal R, Kast J, Duran A. Driving an industry: medium and heavy duty fuel cell electric truck component sizing. *World Electr Veh J* 2016;8:78–89.
- Lovins AB, Lovins LH, Hawken P. *A road map for natural capitalism*. *Harv Bus Rev*; 1999 [May–June].
- Gerth R. US Army sustainability needs. In: NCMS sustainability conference; 2012. *Ann Arbor, MI*.
- Winnefeld C, Kadyk T, Bensmann B, Krewer U, Hanke-Rauschenbach R. Modelling and designing cryogenic hydrogen tanks for future aircraft applications. *Energies* 2018;11:1–23. <https://doi.org/10.3390/en11010105>.
- Kadyk T, Winnefeld C, Hanke-Rauschenbach R, Krewer U. Analysis and design of fuel cell systems for aviation. *Energies* 2018;11:375. <https://doi.org/10.3390/en11020375>.
- Ozpineci B. *Annual progress report for the electric drive technologies program*. 2016. Oak Ridge, TN.
- Proterra. Proterra to power North America's first electric double deck transit bus. 2018. <https://www.proterra.com/press-release/global-double-deck-bus-market-leader-alexander-dennis-selects-proterra-to-power-north-americas-first-electric-double-deck-transit-bus/>. [Accessed 23 August 2018].
- Department of Energy. *US DRIVE hydrogen storage technical team roadmap*. 2017.
- Department of Energy. *US DRIVE fuel cell technical team roadmap*. 2017.
- Department of Energy. *US DRIVE fuel cell technical team roadmap*. 2013.
- Moreels D, Leijnen P. *High efficiency axial flux machines*. 2018.
- Department of Energy. *US drive - electrochemical energy storage technical team roadmap*. 2017.
- United States Advanced Battery Consortium. *Goals for advanced high-performance batteries for electric vehicle (EV) applications*. USCAR Website Energy Storage System Goals 2018. [http://www.uscar.org/commands/files\\_download.php?files\\_id=364](http://www.uscar.org/commands/files_download.php?files_id=364). [Accessed 23 August 2018].
- Department of Energy. *Technical targets for fuel cell systems and stacks for transportation applications 2019*. <https://www.energy.gov/eere/fuelcells/doe-technical-targets-fuel-cell-systems-and-stacks-transportation-applications>. [Accessed 3 May 2019].
- Kane M. *Sion power – production of breakthrough 500 Wh/kg cell starts this year*. *InsideEVs* 2018 (accessed, <https://insideevs.com/news/336329/sion-power-production-of-breakthrough-500-wh-kg-cell-starts-this-year/>). [Accessed 18 April 2019].
- Environmental Protection Agency. *Emission factors for greenhouse gas inventories*. 2020.
- Environmental Protection Agency. *Greenhouse gas inventory guidance: direct emissions from mobile combustion sources*. 2016.
- Department of Defense. *Annual operational energy reports*. Off Assist Sec Def Sustain; 2020. [https://www.acq.osd.mil/eie/OE/OE\\_library.html](https://www.acq.osd.mil/eie/OE/OE_library.html). [Accessed 28 February 2021].
- General Services Administration. *Vehicle management library*. Fed fleet reports. 2019. <https://www.gsa.gov/policy-regulations/policy/vehicle-management-policy/vehicle-management-library>. [Accessed 28 February 2021].
- Myhre G, Shindell D, Bréon F-M, Collins W, Fuglestedt J, Huang J, et al. Anthropogenic and natural radiative forcing. In: Stocker TF, Qin D, Plattner G-K, Tignor M, Allen SK, Boschung J, et al., editors. *Clim. Chang. 2013 phys. Sci. Basis contrib. Work. Gr. I to fifth assess. Rep. Intergov. Panel clim. Chang*. Cambridge, UK: Cambridge University Press; 2013.
- Environmental Protection Agency. *Greenhouse gas emissions from a typical passenger vehicle*. 2018. <https://www.epa.gov/greenvehicles/greenhouse-gas-emissions-typical-passenger-vehicle>. [Accessed 28 February 2021].
- Breakthrough Magnax. *Motor technology for electric vehicles*. 2019. <https://www.magnax.com>. [Accessed 1 May 2019].
- Faid S. *A highly efficient two speed transmission for electric vehicles*. In: 28th International Electric Vehicle Symposium and Exhibition 2015 (EVS28) at Goyang, Korea, 3–6 May 2015, Vol. 1(3); 2015. p. 129–39. ISBN: 978-1-5108-0926-0.
- Chavdar B. *Multi-speed transmission for commercial delivery medium duty plug-in electric drive vehicles*. Eaton Corporation; 2016.
- Eaton. *Electric vehicle 2-speed transmission* 2016.
- Janek J, Zeier WG. *A solid future for battery development*. *Nat Energy* 2016;1:16141. <https://doi.org/10.1038/nenergy.2016.141>.
- SolidEnergy. *Hermes™ high energy rechargeable metal cells for space*. 2017. [http://assets.solidenergysystems.com/wp-content/uploads/2017/09/08171937/Hermes\\_Spec\\_Sheet1.pdf](http://assets.solidenergysystems.com/wp-content/uploads/2017/09/08171937/Hermes_Spec_Sheet1.pdf). [Accessed 18 April 2019].
- Solid Power. *The promise and challenge of scaling lithium metal batteries*. 2019. <http://solidpowerbattery.com/solid-state-101/CONTACT>. [Accessed 18 April 2019].
- Fan Y, Chen X, Legut D, Zhang Q. *Modeling and theoretical design of next-generation lithium metal batteries*. *Energy Storage Mater* 2019;16:169–93. <https://doi.org/10.1016/j.ensm.2018.05.007>.
- Weinrich H, Come J, Tempel H, Kungl H, Eichel R, Balke N. *Nano energy understanding the nanoscale redox-behavior of iron-anodes for rechargeable iron-air batteries*. *Nano Energy* 2017;41:706–16. <https://doi.org/10.1016/j.nanoen.2017.10.023>.
- Julich F. *Iron-air batteries promise higher energy density than lithium-ion batteries*. *SciTechDaily* 2019. <https://scitechdaily.com/iron-air-batteries-promise-higher-energy-density-than-lithium-ion-batteries/>. [Accessed 6 February 2019].
- Department of Energy. *US drive - target explanation document: onboard hydrogen storage for light-duty fuel cell vehicles*. 2017.
- Thirkell A, Chen R, Harrington I. *A fuel cell system sizing tool based on current production aircraft*. In: SAE aerop congr exhib 2017; 2017. <https://doi.org/10.4271/2017-01-2135>.
- National Fuel Cell Research Center. *Hybrid fuel cell/gas turbine systems Proton exchange membrane fuel cell (PEMFC)*. 2004.
- Toyota. *2018 Mirai*. 2018. [https://ssl.toyota.com/mirai/assets/modules/carpaghowitworks/Docs/MY18\\_Mirai\\_eBrochure\\_FuelCellTech.pdf](https://ssl.toyota.com/mirai/assets/modules/carpaghowitworks/Docs/MY18_Mirai_eBrochure_FuelCellTech.pdf). [Accessed 13 September 2018].

# *Supplementary Material*

## **Toward battery electric and hydrogen fuel cell military vehicles for land, air, and sea**

**Scott M. Katalenich<sup>a\*</sup> and Mark Z. Jacobson<sup>a</sup>**

---

<sup>a</sup> Stanford University, Department of Civil & Environmental Engineering, Atmosphere/Energy Program, Stanford, CA, USA.

\* Corresponding author. Stanford University, Department of Civil & Environmental Engineering, Atmosphere/Energy Program, Stanford, CA, USA.

E-mail addresses: [smk58963@alumni.stanford.edu](mailto:smk58963@alumni.stanford.edu) (S. Katalenich),  
[jacobson@stanford.edu](mailto:jacobson@stanford.edu) (M. Jacobson).

**The views expressed in this report are those of the authors and do not reflect the official policy or position of the Department of the Army, the Department of Defense, or the U.S. Government. Reference to any specific commercial product, process, or service by trade name, trademark, manufacturer, or otherwise neither constitutes nor implies endorsement, recommendation, or favor.**

# NOMENCLATURE

## Acronyms and abbreviations

AAR = American Association of Railroads  
ABYC = American Boat & Yacht Council  
AC = Alternating Current  
AMRDEC = Aviation and Missile Research, Development, and Engineering Center  
APC = Armored Personnel Carrier  
ATAAC = Air To Air After Cooled  
BE = Battery Electric  
BII = Basic Issue Items  
BOP = Balance Of Plant  
BWC = Bridge Weight Classification  
CCDC = Combat Capabilities Development Command  
CcH2 = Cryogenic-Compressed Hydrogen  
CGH2 = Compressed Gas Hydrogen  
CH = Cargo Helicopter  
CID = Commercial Item Description  
CID = Cubic Inch Displacement  
CNG = Compressed Natural Gas  
CO<sub>2</sub> = Carbon Dioxide  
COTS = Commercially-available Off-The-Shelf  
CTW = Charge-To-Wheels  
DA = Department of the Army  
DC = Direct Current  
DF-1 = Diesel Fuel (Oil) # 1 (also 1-D)  
DF-2 = Diesel Fuel (Oil) # 2 (also 2-D)  
DF-A = Diesel Fuel, Arctic Grade  
DLA = Defense Logistics Agency  
DOD = Department of Defense  
DOE = Department of Energy  
DWT = Deadweight Tonnage  
EPA = Environmental Protection Agency  
EV = Electric Vehicle  
FCEV = Fuel Cell Electric Vehicle  
FCS = Fuel Cell Stack  
FED = Fuel Efficient Demonstrator  
FF = Fossil Fuel  
FSP = Fragment Simulating Projectile  
FY = Fiscal Year  
FOB = Forward Operating Base  
GE = General Electric  
GCWR = Gross Combined Weight Rating  
GM-EMD = General Motors Electro-Motive Division  
GVSC = Ground Vehicle Systems Center  
GVW = Gross Vehicle Weight

H<sub>2</sub> = Hydrogen  
HAL = Heavy Axle Load  
HB = High Benefit Scenario  
HDPE = High-Density Polyethylene  
HEUI = Hydraulically-actuated Electronically-controlled Unit Injector  
HFO = Heavy Fuel Oil  
ICE = Internal Combustion Engine  
IEA = International Energy Agency  
IED = Improvised Explosive Device  
ISA = International Standard Atmosphere  
KTAS = Knots True Air Speed  
LH<sub>2</sub> = Liquid Hydrogen  
LIB = Lithium Ion Battery  
HBR = High Bypass Ratio  
HFC = Hydrogen Fuel Cell  
HTS = High-Temperature Super-conducting  
JP-4 = Jet Propellant 4  
JP-8 = Jet Propellant 8 (also NATO Code F-34)  
LB = Low Benefit Scenario  
LO = Lubrication Order  
LPG = Liquified Petroleum Gas  
MDF = Marine Diesel Fuel  
MDRW = Maximum Design Ramp Weight  
MDTW = Maximum Design Taxi Weight  
MGTO = Maximum Gross Takeoff Weight  
MIL-DTL-# = Military Detail Specification  
MIL-L-# = Military Lubricant Specification  
MIL-PRF-# = Military Performance Specification  
MK = Medial or Known Value  
MLC = Military Load Classification  
MOGAS = Motor Gasoline  
MPG = Miles Per Gallon  
MRAP = Mine-Resistant Ambush Protected  
MSDS = Material Safety Data Sheet  
MTOW = Maximum Takeoff Weight  
MZFW = Maximum design Zero Fuel Weight  
NASA = National Aeronautics and Space Administration  
NATO = North Atlantic Treaty Organization  
NEMA = National Electrical Manufacturers Association  
NG = Next Generation  
NTV = Non-Tactical Vehicle  
OE = Operational Energy  
OEW = Operating Empty Weight  
PEMFC = Proton-Exchange (or Polymer-Electrolyte) Membrane Fuel Cell  
PHEV = Plug-in Hybrid Electric Vehicle  
PWR = Power-to-Weight Ratio



RDECOM = Research, Development and Engineering Command  
RE = Renewable Energy  
RE100 = 100% Renewable Energy  
RPM = Revolutions Per Minute  
SAE = Society of Automotive Engineers  
SEP = System Enhancement Package  
SI = International System of Units  
TARDEC = Tank Automotive Research Development and Engineering Center  
TOP = Test Operating Procedure  
TTW = Tank-To-Wheels  
TWR = Thrust-to-Weight Ratio  
UH = Utility Helicopter  
ULSD = Ultra Low Sulfur Diesel  
UNFCCC = United Nations Framework Convention on Climate Change  
USACE = United States Army Corps of Engineers  
USAF = United States Air Force  
US DRIVE = United States Driving Research and Innovation for Vehicle efficiency and Energy sustainability  
USMC = United States Marine Corps  
U.S.C. = United States Code  
WTW = Well-To-Wheels  
ZEV = Zero-Emission Vehicle

## Symbols and subscripts

$\%R_{FF}$  [%] = percent range of the fossil fuel variant maintained by a battery electric or hydrogen fuel cell variant

$a$  [%] = adhesion level

$a$   $\left[\frac{m}{s^2}\right]$  = acceleration

$A$  [ $m^2$ ] = area

$A_{air}$  [ $m^2$ ] = front cross-sectional area of boat/ship above the water line

$A_f$  [ $m^2$ ] = front cross-sectional area of vehicle

$A_s$  [ $m^2$ ] = boat/ship hull wetted surface area

$A_{s,light}$  [ $m^2$ ] = boat/ship hull wetted surface area (below waterline) at curb weight

$A_{s,loaded}$  [ $m^2$ ] = boat/ship hull wetted surface area (below waterline) at gross weight

$b_1, c$  [ $kg$ ] = y-intercept of line 1 (power-to-weight ratio or thrust-to-weight ratio) for the curb weight scenario

$b_1, g$  [ $kg$ ] = y-intercept of line 1 (power-to-weight ratio or thrust-to-weight ratio) for the gross weight scenario

$b_2, c$  [ $kg$ ] = y-intercept of line 2 (ratio of onboard useful energy to force required or cruising range) for the curb weight scenario

$b_2, g$  [ $kg$ ] = y-intercept of line 2 (ratio of onboard useful energy to force required or cruising range) for the gross weight scenario

$BPR$  [-] = bypass ratio of turbofan engine

$c_1, c; c_1, g$   $\left[\frac{Wh}{N}\right]$  = non-linear graphing constant (#1) used in line 2 (ratio of onboard useful energy to force required or cruising range) for the curb; gross weight scenarios

$c_2, c; c_2, g$   $\left[\frac{Wh}{kg}\right]$  = non-linear graphing constant (#2) used in line 2 (ratio of onboard useful energy to force required or cruising range) for the curb; gross weight scenarios

$c_3, c; c_3, g$  [-] = non-linear graphing constant (#3) used in line 2 (ratio of onboard useful energy to force required or cruising range) for the curb; gross weight scenarios

$c_4, c; c_4, g$   $\left[\frac{kg}{m \cdot s^2}\right]$  = non-linear graphing constant (#4) used in line 2 (ratio of onboard useful energy to force required or cruising range) for the curb; gross weight scenarios

$c_5, c; c_5, g$  [ $m$ ] = non-linear graphing constant (#5) used in line 2 (ratio of onboard useful energy to force required or cruising range) for the curb; gross weight scenarios

$c_6, c; c_6, g$  [ $m$ ] = non-linear graphing constant (#6) used in line 2 (ratio of onboard useful energy to force required or cruising range) for the curb; gross weight scenarios

$c_7, c; c_7, g$  [ $m$ ] = non-linear graphing constant (#7) used in line 2 (ratio of onboard useful energy to force required or cruising range) for the curb; gross weight scenarios

$c_b$  [ $kg$ ] = y-intercept constant in the propulsor component mass-fan power at takeoff line

$c_m$   $\left[\frac{kg}{W}\right]$  = slope constant in the propulsor component mass-fan power at takeoff line

$C_{A,light}$  [-] = coefficient of air resistance at boat/ship curb weight

$C_{A,loaded}$  [-] = coefficient of air resistance at boat/ship gross weight

$C_B$  [-] = block coefficient

$C_{B-B}$  [-] = Brier-Bragg coefficient

$C_d$  [-] = coefficient of aerodynamic drag

$C_f$  [-] = coefficient of friction

$C_{rr}$  [-] = coefficient of rolling resistance  
 $C_R$  [-] = coefficient of residual resistance  
 $C_T$  [-] = coefficient of total hull towing resistance  
 $CP$  [W] = engine cruise power  
 $CR_{BE,c}$  [m] = maximum cruising range of battery electric variant in the curb weight scenario  
 $CR_{BE,g}$  [m] = maximum cruising range of battery electric variant in the gross weight scenario  
 $CR_{FF}$  [m] = maximum cruising range of fossil fuel variant  
 $CR_{HFC,c}$  [m] = maximum cruising range of hydrogen fuel cell variant in the curb weight scenario  
 $CR_{HFC,g}$  [m] = maximum cruising range of hydrogen fuel cell variant in the gross weight scenario  
 $d_c$  [m] = diameter of cabin  
 $d_e$  [m] = diameter of fossil fuel engine  
 $d_{m,i}$  [m] = diameter of individual electric motor  
 $D$  [m] = watercraft draft  
 $D_{light}$  [m] = watercraft draft at curb weight  
 $D_{loaded}$  [m] = watercraft draft at gross weight  
 $E_{c,FF}$  [Wh] = chemical energy content of onboard fossil fuel (less latent heat of vaporization)  
 $ED_B$   $\left[\frac{Wh}{L}\right]$  = system (pack)-level volumetric battery energy density  
 $ED_{B,C}$   $\left[\frac{Wh}{L}\right]$  = cell-level volumetric battery energy density  
 $ED_{B,COTS}$   $\left[\frac{Wh}{L}\right]$  = commercially-available off the shelf system (pack)-level volumetric battery energy density  
 $ED_{B,DV}$   $\left[\frac{Wh}{L}\right]$  = decision variable for system (pack)-level volumetric battery energy density  
 $ED_{B,F}$   $\left[\frac{Wh}{L}\right]$  = future feasible system (pack)-level volumetric battery energy density  
 $ED_{H_2storage}$   $\left[\frac{Wh}{L}\right]$  = volumetric energy density of hydrogen storage system  
 $ED_{H_2storage,COTS}$   $\left[\frac{Wh}{L}\right]$  = commercially-available off the shelf volumetric energy density of hydrogen storage system  
 $ED_{H_2storage,DV}$   $\left[\frac{Wh}{L}\right]$  = decision variable for volumetric energy density of hydrogen storage system  
 $ED_{H_2storage,F}$   $\left[\frac{Wh}{L}\right]$  = future feasible volumetric energy density of hydrogen storage system  
 $ED_{H_2storage,300}$   $\left[\frac{Wh}{L}\right]$  = volumetric energy density of hydrogen storage system at 300 bar  
 $ED_{H_2storage,700}$   $\left[\frac{Wh}{L}\right]$  = volumetric energy density of hydrogen storage system at 700 bar  
 $ED_{H_2storage,LH_2}$   $\left[\frac{Wh}{L}\right]$  = volumetric energy density of liquid hydrogen storage system  
 $ED_{H_2}$   $\left[\frac{Wh}{kg}\right]$  = volumetric energy density of hydrogen  
 $ED_{H_2,300}$   $\left[\frac{Wh}{kg}\right]$  = volumetric energy density of hydrogen at 300 bar  
 $ED_{H_2,700}$   $\left[\frac{Wh}{kg}\right]$  = volumetric energy density of hydrogen at 700 bar  
 $ED_{LH_2}$   $\left[\frac{Wh}{kg}\right]$  = volumetric energy density of liquid hydrogen

$F$  [N] = force  
 $F_a$  [%] = locomotive adhesion factor  
 $F_{m_{GB},m_m}$  [%] = scaling factor, dry weight (mass) of gearbox used per dry weight (mass) of electric motor  
 $F_{m_{m+GB+o},m_m}$  [%] = scaling factor, total mass of electric motor, gearbox, and oil used per dry weight (mass) of electric motors  
 $F_{m,s}$  [%] = scaling factor, overall vehicle mass  
 $F_R$  [%] = reduction factor used to estimate volume within a rectangular cuboid defined by published maximum height, width, and length dimensions or area within a rectangle defined by height and width  
 $F_{T,DF,TF}$  [%] = scaling factor, fraction of thrust produced by the ducted fan component of a turbofan engine  
 $F_{V_{GB},V_m}$  [%] = scaling factor, volume of gearbox used per volume of electric motor  
 $F_{V,m}$  [%] = scaling factor, total volume of electric motor and gearbox used per dry weight (mass) of electric motor  
 $F_{V_o,GB,V_{GB}}$  [%] = scaling factor, volume of gearbox oil used per volume of gearbox  
 $F_{V,s}$  [%] = scaling factor, overall vehicle volume  
 $Fr$  [–] = Froude Number  
 $FE_{FF}$   $\left[\frac{km}{L}\right]$  = fuel economy of fossil fuel variant  
 $FF$   $\left[\frac{kg}{s}\right]$  = fuel flow (consumption rate)  
 $FN_f$  [N] = normal force on front wheels  
 $FN_r$  [N] = normal force on rear wheels  
 $g$   $\left[\frac{m}{s^2}\right]$  = universal gravitational constant  
 $h$  [m] = height  
 $h_e$  [m] = height of fossil fuel engine  
 $h_r$  [m] = height of rudder  
 $h_s$  [m] = height of stabilizer  
 $h_T$  [m] = height of transmission (gearbox)  
 $h_v$  [m] = maximum height of vehicle platform  
 $h_w$  [m] = height of wing  
 $K_{light}$  [N] = reference force at boat/ship curb weight  
 $K_{loaded}$  [N] = reference force at boat/ship gross weight  
 $l_e$  [m] = length of fossil fuel engine  
 $l_{fuselage}$  [m] = length of fuselage  
 $l_{m,i}$  [m] = length of individual electric motor  
 $l_r$  [m] = length of rudder  
 $l_s$  [m] = length of stabilizer  
 $l_T$  [m] = length of transmission (gearbox)  
 $l_v$  [m] = maximum length of vehicle platform  
 $l_w$  [m] = length of wing  
 $L_B$  [m] = boat/ship beam  
 $L_{BE,c}$  [N] = lift force for the battery electric helicopter variant in the curb weight scenario  
 $L_{BE,g}$  [N] = lift force for the battery electric helicopter variant in the gross weight scenario

$L_{FF,c}$  [N] = lift force required for a fossil fuel helicopter to maintain equilibrium at hover and at curb weight  
 $L_{FF,g}$  [N] = lift force required for a fossil fuel helicopter to maintain equilibrium at hover and at gross weight  
 $L_{HFC,c}$  [N] = lift force for the hydrogen fuel cell helicopter variant in the curb weight scenario  
 $L_{HFC,g}$  [N] = lift force for the hydrogen fuel cell helicopter variant in the gross weight scenario  
 $L_{OA}$  [m] = overall length of a boat/ship  
 $L_{PP}$  [m] = length between perpendiculars on a boat/ship hull  
 $L_{WL}$  [m] = length at the waterline on a boat/ship hull  
 $LDR$   $\left[\frac{N}{N}\right]$  = lift-to-drag ratio of aircraft (also L/D ratio)  
 $LHV_{FF}$   $\left[\frac{MJ}{L}\right]$  = lower heating value (net heat of combustion) of fossil fuel  
 $LHV_{H_2}$   $\left[\frac{Wh}{kg}\right]$  = lower heating value (net calorific value) of hydrogen  
 $m$  [kg] = mass  
 $m_{1,c}$  [-] = slope of line 1 (power-to-weight ratio or thrust-to-weight ratio) for the curb weight scenario  
 $m_{1,g}$  [-] = slope of line 1 (power-to-weight ratio or thrust-to-weight ratio) for the gross weight scenario  
 $m_{2,c}$  [-] = slope of line 2 (ratio of onboard useful energy to force required or cruising range) for the curb weight scenario  
 $m_{2,g}$  [-] = slope of line 2 (ratio of onboard useful energy to force required or cruising range) for the gross weight scenario  
 $m_{af,e}$  [kg] = mass of antifreeze (or coolant fluid) used in fossil fuel engine  
 $m_{ATF}$  [kg] = mass of automatic transmission fluid (or transmission oil)  
 $m_B$  [kg] = mass of battery pack  
 $m_{B,avail}$  [kg] = mass available for battery pack  
 $m_{B,DV}$  [kg] = decision variable for mass of battery pack  
 $m_{BE,c}$  [kg] = mass of the battery electric variant in the curb weight scenario  
 $m_{BE,g}$  [kg] = mass of the battery electric variant in the gross weight scenario  
 $m_{c,FF}$  [kg] = curb vehicular mass of the fossil fuel variant  
 $m_{c,strippedFF}$  [kg] = curb mass of vehicle stripped of all fossil fuel system components  
 $m_{DF,PC}$  [kg] = mass of ducted fan, propulsor components from turbofan engines  
 $m_e$   $\left[\frac{kg}{engine}\right]$  = mass of fossil fuel engine  
 $m_f$  [kg] = mass of onboard fossil fuel (fuel only) when tank is topped-off  
 $m_{f+t}$  [kg] = combined total mass of fossil fuel and tank  
 $m_{FCS}$  [kg] = mass of fuel cell stack  
 $m_{FCS,avail}$  [kg] = mass available for fuel cell stack  
 $m_{g,FF}$  [kg] = gross vehicular mass of the fossil fuel variant  
 $m_{g,strippedFF}$  [kg] = gross mass of vehicle stripped of all fossil fuel system components  
 $m_{GB}$  [kg] = mass of gearbox  
 $m_{H_2}$  [kg] = mass of stored hydrogen  
 $m_{H_2storage}$  [kg] = mass of hydrogen storage system  
 $m_{H_2storage,avail}$  [kg] = mass available for hydrogen storage system

$m_{H_2storage,DV} [kg]$  = decision variable for mass of hydrogen storage system  
 $m_{HFC,c} [kg]$  = mass of the hydrogen fuel cell variant in the curb weight scenario  
 $m_{HFC,g} [kg]$  = mass of the hydrogen fuel cell variant in the gross weight scenario  
 $m_m [kg]$  = mass of electric motor(s)  
 $m_{m,DV} [kg]$  = decision variable for mass of electric motor(s)  
 $m_{m+GB+o} [kg]$  = combined mass of electric motor, gearbox, and oil  
 $m_{m,i} [kg]$  = mass of individual electric motor  
 $m_{o,e} [kg]$  = mass of fossil fuel engine oil  
 $m_{o,GB} [kg]$  = mass of gearbox oil  
 $m_{p,FF} [kg]$  = payload mass of the fossil fuel variant  
 $m_{PC} [kg]$  = mass of propulsor components in a turbofan engine  
 $m_{sys,FF} [kg]$  = combined mass of fossil fuel system components  
 $m_T [kg]$  = mass of transmission (gearbox)  
 $m_{t,FF} [kg]$  = mass of the fossil fuel tank (tank material only; empty)  
 $m_{total,e} [kg]$  = total mass of fossil fuel engine(s) to include all engines, lubricating oil, and antifreeze coolant  
 $m_{total,GB} [kg]$  = total electric gearbox mass to include all gearboxes and lubricating oil  
 $m_{total,T} [kg]$  = total transmission (gearbox) mass to include all transmissions and automatic transmission fluid (or transmission oil)  
 $\dot{m} \left[ \frac{kg}{s} \right]$  = mass flow rate  
 $\dot{m}_0 \left[ \frac{kg}{s} \right]$  = total mass flow rate of air through turbofan at takeoff  
 $\dot{m}_c \left[ \frac{kg}{s} \right]$  = mass flow rate of air intake into the turbofan jet core  
 $\dot{m}_e \left[ \frac{kg}{s} \right]$  = mass flow rate of air exhaust from the turbofan jet core  
 $\dot{m}_f \left[ \frac{kg}{s} \right]$  = mass flow rate of air bypassed around the turbofan jet core  
 $n_e [engines]$  = number of fossil fuel engines used  
 $n_m [motors]$  = number of electric motors used  
 $n_s [stabilizers]$  = number of stabilizer wings  
 $n_T [transmissions]$  = number of transmissions (gearboxes) used  
 $n_w [wings]$  = number of wings  
 $OUE_{BE,c} [Wh]$  = onboard useful energy of battery electric variant (includes overall system efficiency) in the curb weight scenario  
 $OUE_{BE,g} [Wh]$  = onboard useful energy of battery electric variant (includes overall system efficiency) in the gross weight scenario  
 $OUE_{FF} [Wh]$  = onboard useful energy of fossil fuel variant (includes overall system efficiency)  
 $OUE_{HFC,c} [Wh]$  = onboard useful energy of hydrogen fuel cell variant (includes overall system efficiency) in the curb weight scenario  
 $OUE_{HFC,g} [Wh]$  = onboard useful energy of hydrogen fuel cell variant (includes overall system efficiency) in the gross weight scenario  
 $OUE_{max,BE,m_{B,avail}} [Wh]$  = maximum onboard useful energy available in the battery electric variant based upon the mass available for a battery pack

$OUE_{max, BE, V_{B, avail}}$  [Wh] = maximum onboard useful energy available in the battery electric variant based upon the volume available for a battery pack  
 $p$  [Pa] = pressure  
 $P$  [W] = power  
 $P_{BE, c}$  [W] = maximum power of battery electric variant in the curb weight scenario  
 $P_{BE, g}$  [W] = maximum power of battery electric variant in the gross weight scenario  
 $P_F$  [W] = power of ducted fan  
 $P_{F, TO}$  [W] = power of ducted fan at takeoff  
 $P_{F, TO, FF}$  [W] = power of ducted fan only as a component of the takeoff power of the FF variant  
 $P_{FF}$  [W] = maximum power of fossil fuel variant  
 $P_h$  [W] = power required by a helicopter at hover  
 $P_{HFC, c}$  [W] = maximum power of hydrogen fuel cell variant in the curb weight scenario  
 $P_{HFC, g}$  [W] = maximum power of hydrogen fuel cell variant in the gross weight scenario  
 $P_{m, c}$  [W] = continuous power output of combined electric motors  
 $P_{m, c, i} \left[ \frac{W}{motor} \right]$  = continuous power output of individual electric motor  
 $P_{m, p, i} \left[ \frac{W}{motor} \right]$  = peak power output of individual electric motor  
 $P_{max, e}$  [W] = maximum power of fossil fuel engine  
 $PD_{FCS} \left[ \frac{W}{kg} \right]$  = power density of proton-exchange membrane fuel cell stack  
 $PD_{FCS, COTS} \left[ \frac{W}{kg} \right]$  = commercially-available off the shelf power density of proton-exchange membrane fuel cell stack  
 $PD_{FCS, DV} \left[ \frac{W}{kg} \right]$  = decision variable for power density of proton-exchange membrane fuel cell stack  
 $PD_{FCS, F} \left[ \frac{W}{kg} \right]$  = future feasible power density of proton-exchange membrane fuel cell stack  
 $PD_m \left[ \frac{W}{L} \right]$  = power density of electric motor(s)  
 $PL \left[ \frac{N}{W} \right]$  = power loading of helicopter rotor at hover  
 $PSFC \left[ \frac{s^2}{m^2} \right]$  = power specific fuel consumption  
 $PWR_{BE, c} \left[ \frac{kW}{kg} \right]$  = maximum power-to-weight ratio of battery electric variant in curb weight scenario  
 $PWR_{BE, g} \left[ \frac{kW}{kg} \right]$  = maximum power-to-weight ratio of battery electric variant in gross weight scenario  
 $PWR_{FF, c} \left[ \frac{kW}{kg} \right]$  = maximum power-to-weight ratio of fossil fuel variant at curb weight  
 $PWR_{FF, g} \left[ \frac{kW}{kg} \right]$  = maximum power-to-weight ratio of fossil fuel variant at gross weight  
 $PWR_{HFC, c} \left[ \frac{kW}{kg} \right]$  = maximum power-to-weight ratio of hydrogen fuel cell variant in curb weight scenario  
 $PWR_{HFC, g} \left[ \frac{kW}{kg} \right]$  = maximum power-to-weight ratio of hydrogen fuel cell variant in gross weight scenario

$PWR_{m,c} \left[ \frac{kW}{kg} \right]$  = power-to-weight ratio (continuous) of electric motor(s)  
 $PWR_{m,p} \left[ \frac{kW}{kg} \right]$  = power-to-weight ratio (peak) of electric motor(s)  
 $R [m]$  = range  
 $R_A [N]$  = air resistance  
 $R_{DFP\_TFT} \left[ \frac{W}{N} \right]$  = ratio of ducted fan power to turbofan thrust (as a component of FF turbofan thrust)  
 $R_{DFTOP\_TOT} \left[ \frac{W}{N} \right]$  = ratio of electric ducted fan takeoff power to takeoff thrust  
 $R_{ED} \left[ \frac{kg H_2}{L H_2 storage system} \right]$  = ratio of usable hydrogen energy density (net useful energy) to maximum hydrogen storage system volume  
 $R_{F,c} [N]$  = boat/ship hull friction resistance at curb vehicle weight  
 $R_{F,g} [N]$  = boat/ship hull friction resistance at gross vehicle weight  
 $R_{max,FF} [m]$  = maximum range of the fossil fuel variant  
 $R_{R,c} [N]$  = boat/ship hull residual (wave + eddy) resistance at curb weight  
 $R_{R,g} [N]$  = boat/ship hull residual (wave + eddy) resistance at gross weight  
 $R_{SE} \left[ \frac{kg H_2}{kg H_2 storage system} \right]$  = ratio of usable hydrogen specific energy (net useful energy) to maximum hydrogen storage system mass  
 $R_{T,BE,c} [N]$  = total hull resistance of boat/ship battery electric variant in the curb weight scenario  
 $R_{T,BE,g} [N]$  = total hull resistance of boat/ship battery electric variant in the gross weight scenario  
 $R_{T,FF,c} [N]$  = total hull resistance of boat/ship fossil fuel variant at curb weight  
 $R_{T,FF,g} [N]$  = total hull resistance of boat/ship fossil fuel variant at gross weight  
 $R_{T,HFC,c} [N]$  = total hull resistance of boat/ship hydrogen fuel cell variant in the curb weight scenario  
 $R_{T,HFC,g} [N]$  = total hull resistance of boat/ship hydrogen fuel cell variant in the gross weight scenario  
 $R_{V_{m+GB\_m_m}} \left[ \frac{m^3}{kg} \right]$  = ratio of total volume of electric motor and gearbox used per dry weight (mass) of electric motors  
 $Re [-]$  = Reynolds number  
 $RL_{BE,c} [N]$  = road load force for the battery electric variant in the curb weight scenario  
 $RL_{BE,g} [N]$  = road load force for the battery electric variant in the gross weight scenario  
 $RL_{FF,c} [N]$  = road load force for the fossil fuel variant at curb weight  
 $RL_{FF,g} [N]$  = road load force for the fossil fuel variant at gross weight  
 $RL_{HFC,c} [N]$  = road load force for the hydrogen fuel cell variant in the curb weight scenario  
 $RL_{HFC,g} [N]$  = road load force for the hydrogen fuel cell variant in the gross weight scenario  
 $SE_B \left[ \frac{Wh}{kg} \right]$  = system (pack)-level gravimetric battery energy density (specific energy)  
 $SE_{B,C} \left[ \frac{Wh}{kg} \right]$  = cell-level gravimetric battery energy density (specific energy)  
 $SE_{B,COTS} \left[ \frac{Wh}{kg} \right]$  = commercially-available off the shelf system (pack)-level gravimetric battery energy density (specific energy)



$SE_{B,DV} \left[ \frac{Wh}{kg} \right]$  = decision variable for system (pack)-level gravimetric battery energy density (specific energy)  
 $SE_{B,F} \left[ \frac{Wh}{kg} \right]$  = future feasible system (pack)-level gravimetric battery energy density (specific energy)  
 $SE_{H_2} \left[ \frac{Wh}{kg} \right]$  = gravimetric energy density (specific energy) of hydrogen  
 $SE_{H_2storage} \left[ \frac{Wh}{kg} \right]$  = gravimetric energy density (specific energy) of hydrogen storage  
 $SE_{H_2storage,COTS} \left[ \frac{Wh}{kg} \right]$  = commercially-available off the shelf gravimetric energy density (specific energy) of hydrogen storage  
 $SE_{H_2storage,DV} \left[ \frac{Wh}{kg} \right]$  = decision variable for gravimetric energy density (specific energy) of hydrogen storage  
 $SE_{H_2storage,F} \left[ \frac{Wh}{kg} \right]$  = future feasible gravimetric energy density (specific energy) of hydrogen storage  
 $SE_{H_2storage,300} \left[ \frac{Wh}{kg} \right]$  = gravimetric energy density (specific energy) of hydrogen storage at 300 bar  
 $SE_{H_2storage,700} \left[ \frac{Wh}{kg} \right]$  = gravimetric energy density (specific energy) of hydrogen storage at 700 bar  
 $SE_{H_2storage,LH_2} \left[ \frac{Wh}{kg} \right]$  = gravimetric energy density (specific energy) of liquid hydrogen storage system  
 $SFC \left[ \frac{kg}{Wh} \right]$  = specific fuel consumption  
 $SP_{FCS} \left[ \frac{W}{kg} \right]$  = specific power of proton-exchange membrane fuel cell stack  
 $SP_{FCS,COTS} \left[ \frac{W}{kg} \right]$  = commercially-available off the shelf specific power of proton-exchange membrane fuel cell stack  
 $SP_{FCS,DV} \left[ \frac{W}{kg} \right]$  = decision variable for specific power of proton-exchange membrane fuel cell stack  
 $SP_{FCS,F} \left[ \frac{W}{kg} \right]$  = future feasible specific power of proton-exchange membrane fuel cell stack  
 $T [N]$  = thrust  
 $T_F [N]$  = thrust force from ducted fan component of turbofan engine  
 $T_{JC} [N]$  = thrust force from jet core component of turbojet engine  
 $T_{TF} [N]$  = total thrust force from turbofan engine  
 $T_{TJ} [N]$  = thrust force from turbojet engine  
 $T_{TO,BE,c} [N]$  = thrust at takeoff for the battery electric variant in the curb weight scenario  
 $T_{TO,BE,g} [N]$  = thrust at takeoff for the battery electric variant in the gross weight scenario  
 $T_{TO,FF,i} [N]$  = thrust at takeoff for the fossil fuel variant from an individual engine  
 $T_{TO,FF,Fonly} [N]$  = thrust from fan component of turbofan engine at takeoff for the fossil fuel variant  
 $T_{TO,FF,tot} [N]$  = total thrust at takeoff for the fossil fuel variant from all engines

$T_{TO,HFC,c}$  [N] = thrust at takeoff for the hydrogen fuel cell variant in the curb weight scenario  
 $T_{TO,HFC,g}$  [N] = thrust at takeoff for the hydrogen fuel cell variant in the gross weight scenario  
 $TE$  [N] = locomotive tractive effort  
 $TE_A$  [N] = locomotive tractive effort required to overcome acceleration  
 $TE_{BE,c}$  [N] = locomotive battery electric variant continuous tractive effort in the curb weight scenario  
 $TE_{BE,g}$  [N] = locomotive battery electric variant continuous tractive effort in the gross weight scenario  
 $TE_C$  [N] = locomotive tractive effort required to overcome curvature  
 $TE_{cont}$  [N] = locomotive continuous tractive effort at 13.7 miles per hour  
 $TE_G$  [N] = locomotive tractive effort required to overcome grade  
 $TE_{HFC,c}$  [N] = locomotive hydrogen fuel cell variant continuous tractive effort in the curb weight scenario  
 $TE_{HFC,g}$  [N] = locomotive hydrogen fuel cell variant continuous tractive effort in the gross weight scenario  
 $TE_{req}$  [N] = locomotive tractive effort required  
 $TE_{RR}$  [N] = locomotive tractive effort required to overcome rolling resistance  
 $TE_{start}$  [N] = locomotive starting tractive effort (from zero velocity) at 35% engine power  
 $TF_f$  [N] = tractive force at front wheels  
 $TF_r$  [N] = tractive force at rear wheels  
 $TMR_{DF}$   $\left[\frac{N}{kg}\right]$  = thrust-to-mass ratio of ducted fan, excluding electric motors  
 $TP_{ED,B}$   $\left[\frac{Wh}{L}\right]$  = tipping point for system (pack)-level volumetric battery energy density  
 $TP_{ED,H_2storage}$   $\left[\frac{Wh}{L}\right]$  = tipping point for volumetric energy density of hydrogen storage system  
 $TP_{PD,FCS}$   $\left[\frac{W}{L}\right]$  = tipping point for power density of proton-exchange membrane fuel cell stack  
 $TP_{SE,B}$   $\left[\frac{Wh}{kg}\right]$  = tipping point for system (pack)-level gravimetric battery energy density (specific energy)  
 $TP_{SE,H_2storage}$   $\left[\frac{Wh}{kg}\right]$  = tipping point for gravimetric energy density (specific energy) of hydrogen storage  
 $TP_{SP,FCS}$   $\left[\frac{W}{kg}\right]$  = tipping point for specific power of proton-exchange membrane fuel cell stack  
 $TSFC$   $\left[\frac{kg}{N \cdot s}\right]$  = thrust specific fuel consumption  
 $TWR_{TO,BE,c}$   $\left[\frac{N}{N}\right]$  = takeoff thrust-to-weight ratio of battery electric variant in the curb weight scenario  
 $TWR_{TO,BE,g}$   $\left[\frac{N}{N}\right]$  = takeoff thrust-to-weight ratio of battery electric variant in the gross weight scenario  
 $TWR_{TO,FF,c}$   $\left[\frac{N}{N}\right]$  = thrust-to-weight ratio of fossil fuel variant at curb weight  
 $TWR_{TO,FF,g}$   $\left[\frac{N}{N}\right]$  = thrust-to-weight ratio of fossil fuel variant at gross weight

$TWR_{TO,HFC,c} \left[ \frac{N}{N} \right]$  = takeoff thrust-to-weight ratio of hydrogen fuel cell variant in the curb weight scenario

$TWR_{TO,HFC,g} \left[ \frac{N}{N} \right]$  = takeoff thrust-to-weight ratio of hydrogen fuel cell variant in the gross weight scenario

$v \left[ \frac{m}{s} \right]$  = velocity

$v_0 \left[ \frac{m}{s} \right]$  = total turbofan intake air velocity

$v_e \left[ \frac{m}{s} \right]$  = turbofan jet core exhaust air velocity

$v_f \left[ \frac{m}{s} \right]$  = velocity of air bypassed around the turbofan jet core

$V_{af,e} [m^3]$  = volume of antifreeze (or coolant fluid) used in fossil fuel engine

$V_{ATF} [L]$  = volume of automatic transmission fluid (or transmission oil)

$V_B [m^3]$  = volume of battery pack

$V_{B,avail} [m^3]$  = volume available for battery pack

$V_{BE,c} [m^3]$  = volume of the battery electric variant in the curb weight scenario

$V_{BE,g} [m^3]$  = volume of the battery electric variant in the gross weight scenario

$V_e [m^3]$  = volume of fossil fuel engine

$V_f [m^3]$  = volume of onboard fossil fuel (fuel only) when tank is topped-off

$V_{f+t} [m^3]$  = combined total volume of fossil fuel and tank

$V_{fuselage} [m^3]$  = volume of fuselage

$V_{FCS} [m^3]$  = volume of fuel cell stack

$V_{FCS,avail} [m^3]$  = volume of fuel cell stack

$V_{FF} [m^3]$  = volume of the fossil fuel variant

$V_{GB} [m^3]$  = volume of gearbox

$V_{H_2} [m^3]$  = volume of stored hydrogen

$V_{H_2storage} [m^3]$  = volume of hydrogen storage system

$V_{H_2storage,avail} [m^3]$  = volume available for hydrogen storage system

$V_{HFC,c} [m^3]$  = volume of the hydrogen fuel cell variant in the curb weight scenario

$V_{HFC,g} [m^3]$  = volume of the hydrogen fuel cell variant in the gross weight scenario

$V_m [m^3]$  = volume of electric motor(s)

$V_{m+GB} [m^3]$  = combined volume of electric motor and gearbox

$V_{m,i} \left[ \frac{m^3}{motor} \right]$  = volume of individual electric motor

$V_{o,e} [m^3]$  = volume of oil used in fossil fuel engine

$V_{o,GB} [m^3]$  = volume of oil used in gearbox

$V_{strippedFF} [m^3]$  = volume of vehicle stripped of all fossil fuel system components

$V_{sys,FF} [m^3]$  = combined volume of fossil fuel system components

$V_t [L]$  = volume of fossil fuel tank (maximum fuel capacity)

$V_{t,FF} [m^3]$  = volume of the fossil fuel tank (tank material only)

$V_{ta} [m^3]$  = volume of tail assembly

$V_{total,e} [m^3]$  = total volume of fossil fuel engine(s) to include all engines

$V_{total,T} [m^3]$  = total transmission (gearbox) volume to include all transmissions

$V_w [m^3]$  = volume of wings

$w_e [m]$  = width of fossil fuel engine  
 $w_r [m]$  = width of rudder  
 $w_s [m]$  = width of stabilizer  
 $w_T [m]$  = width of transmission (gearbox)  
 $w_v [m]$  = maximum width of vehicle platform  
 $w [m]$  = width of wing  
 $W [N]$  = weight of vehicle  
 $W_{BE,c} [N]$  = weight of the battery electric variant in the curb weight scenario  
 $W_{BE,g} [N]$  = weight of the battery electric variant in the gross weight scenario  
 $W_f [N]$  = final weight of vehicle  
 $W_{HFC,c} [N]$  = weight of the hydrogen fuel cell variant in the curb weight scenario  
 $W_{HFC,g} [N]$  = weight of the hydrogen fuel cell variant in the gross weight scenario  
 $W_i [N]$  = initial weight of vehicle

$\Delta [kg]$  = boat/ship displacement mass  
 $\nabla [m^3]$  = boat/ship displacement volume  
 $\nabla_{BE,c} [m^3]$  = battery electric variant boat/ship displacement volume in the curb weight scenario  
 $\nabla_{BE,g} [m^3]$  = battery electric variant boat/ship displacement volume in the gross weight scenario  
 $\nabla_{HFC,c} [m^3]$  = battery electric variant boat/ship displacement volume in the curb weight scenario  
 $\nabla_{HFC,g} [m^3]$  = battery electric variant boat/ship displacement volume in the gross weight scenario

$\Delta_{light} [kg]$  = boat/ship displacement mass at curb weight  
 $\Delta_{loaded} [kg]$  = boat/ship displacement mass at gross weight  
 $\nabla_{light} [m^3]$  = boat/ship displacement volume at curb weight  
 $\nabla_{loaded} [m^3]$  = boat/ship displacement volume at gross weight  
 $\eta_B [-]$  = efficiency of battery discharging  
 $\eta_C [-]$  = efficiency of battery charging  
 $\eta_{DF} [-]$  = efficiency of ducted fan  
 $\eta_{DFA,BE} [-]$  = overall ducted fan airplane battery electric system efficiency  
 $\eta_{DFA,HFC} [-]$  = overall ducted fan airplane hydrogen fuel cell system efficiency  
 $\eta_{FCS} [-]$  = efficiency of fuel cell stack  
 $\eta_{GB} [-]$  = efficiency of gearbox/transmission  
 $\eta_{H,BE} [-]$  = overall helicopter battery electric system efficiency  
 $\eta_{H,e} [-]$  = efficiency of helicopter turboshaft engine  
 $\eta_{H,FF} [-]$  = overall helicopter fossil fuel system efficiency  
 $\eta_{H,HFC} [-]$  = overall helicopter hydrogen fuel cell system efficiency  
 $\eta_{H,r} [-]$  = efficiency of helicopter rotors (“figure of merit”)  
 $\eta_{H,T} [-]$  = efficiency of helicopter transmissions (gearboxes)  
 $\eta_I [-]$  = combined efficiency of DC-to-AC inverter, control systems, and power electronics  
 $\eta_{L,alt} [-]$  = efficiency of freight locomotive alternator/generator  
 $\eta_{L,anc} [-]$  = combined efficiency of freight locomotive engine ancillaries, rectifier, and electric motors  
 $\eta_{L,BE} [-]$  = overall freight locomotive battery electric system efficiency  
 $\eta_{L,e} [-]$  = efficiency of freight locomotive diesel engine

$\eta_{L,FF}$  [-] = overall freight locomotive fossil fuel system efficiency  
 $\eta_{L,HFC}$  [-] = overall freight locomotive hydrogen fuel cell system efficiency  
 $\eta_{L,T}$  [-] = efficiency of freight locomotive transmission  
 $\eta_{L,trac}$  [-] = efficiency of freight locomotive traction auxiliaries  
 $\eta_m$  [-] = efficiency of electric motor  
 $\eta_{PA,BE}$  [-] = overall prop airplane battery electric system efficiency  
 $\eta_{PA,HFC}$  [-] = overall prop airplane hydrogen fuel cell system efficiency  
 $\eta_{PS,bh}$  [-] = behind hull efficiency of propeller ship  
 $\eta_{PS,BE}$  [-] = overall propeller ship battery electric system efficiency  
 $\eta_{PS,e}$  [-] = efficiency of propeller ship marine diesel engine  
 $\eta_{PS,FF}$  [-] = overall propeller ship fossil fuel system efficiency  
 $\eta_{PS,h}$  [-] = efficiency of propeller ship hull  
 $\eta_{PS,HFC}$  [-] = overall propeller ship hydrogen fuel cell system efficiency  
 $\eta_{PS,ow}$  [-] = open water efficiency of propeller ship  
 $\eta_{PS,p}$  [-] = propulsive efficiency of propeller ship  
 $\eta_{PS,P}$  [-] = propulsion efficiency of propeller ship  
 $\eta_{PS,rr}$  [-] = relative rotative efficiency of propeller ship  
 $\eta_{PS,s}$  [-] = efficiency of propeller ship shaft  
 $\eta_{SEB}$  [-] = efficiency of system (pack)-level gravimetric battery energy density  
 $\eta_{t,FF}$  [-] = efficiency of storage density for the fossil fuel tank  
 $\eta_{TF,e}$  [-] = efficiency of high bypass ratio turbofan engine (thermal efficiency)  
 $\eta_{TF,FF}$  [-] = overall turbofan airplane fossil fuel system efficiency  
 $\eta_{TF,P}$  [-] = efficiency of high bypass ratio turbofan airplane (propulsion efficiency)  
 $\eta_{TP,e}$  [-] = efficiency of turboprop engine (thermal efficiency)  
 $\eta_{TP,FF}$  [-] = overall turboprop airplane fossil fuel system efficiency  
 $\eta_{TP,P}$  [-] = efficiency of turboprop airplane (propulsion efficiency)  
 $\eta_{TV,BE}$  [-] = overall tactical vehicle battery electric system efficiency  
 $\eta_{TV,dl}$  [-] = combined efficiency of tactical vehicle driveline, brakes, and accessories  
 $\eta_{TV,e}$  [-] = efficiency of tactical vehicle fossil fuel engine  
 $\eta_{TV,FF}$  [-] = overall tactical vehicle fossil fuel system efficiency  
 $\eta_{TV,HFC}$  [-] = overall tactical vehicle hydrogen fuel cell system efficiency  
 $\eta_{WJB,BE}$  [-] = overall waterjet boat battery electric system efficiency  
 $\eta_{WJB,e}$  [-] = efficiency of waterjet marine diesel engine  
 $\eta_{WJB,FF}$  [-] = overall waterjet boat fossil fuel system efficiency  
 $\eta_{WJB,h}$  [-] = efficiency of waterjet boat hull  
 $\eta_{WJB,HFC}$  [-] = overall waterjet boat hydrogen fuel cell system efficiency  
 $\eta_{WJB,j}$  [-] = efficiency of waterjet jet  
 $\eta_{WJB,p}$  [-] = efficiency of waterjet pump  
 $\eta_{WJB,P}$  [-] = efficiency of waterjet propulsion  
 $\nu \left[ \frac{m^2}{s} \right]$  = kinematic viscosity of water  
 $\rho_{af} \left[ \frac{kg}{L} \right]$  = antifreeze (or coolant fluid) density

$\rho_{air,SL} \left[ \frac{kg}{m^3} \right]$  = density of air at sea level  
 $\rho_{air,37000ft} \left[ \frac{kg}{m^3} \right]$  = density of air at 37,000 ft altitude  
 $\rho_{ATF} \left[ \frac{kg}{L} \right]$  = density of automatic transmission fluid (or transmission oil)  
 $\rho_{B,sys} \left[ \frac{kg}{m^3} \right]$  = physical density of battery pack system  
 $\rho_{FF} \left[ \frac{kg}{L} \right]$  = density of fossil fuel  
 $\rho_{H_2} \left[ \frac{kg}{m^3} \right]$  = density of hydrogen  
 $\rho_{H_2,300} \left[ \frac{kg}{m^3} \right]$  = density of hydrogen at 300 bar  
 $\rho_{H_2,700} \left[ \frac{kg}{m^3} \right]$  = density of hydrogen at 700 bar  
 $\rho_{H_2,sys} \left[ \frac{kg}{m^3} \right]$  = physical density of hydrogen storage system  
 $\rho_{LH_2} \left[ \frac{kg}{m^3} \right]$  = density of liquid hydrogen  
 $\rho_o \left[ \frac{kg}{L} \right]$  = density of lubricating oil  
 $\rho_{t,FF} \left[ \frac{kg}{m^3} \right]$  = density of fossil fuel tank (tank material only)  
 $\rho_{water,sea} \left[ \frac{kg}{m^3} \right]$  = density of sea water at 15°C  
 $\rho_{water,fresh} \left[ \frac{kg}{m^3} \right]$  = density of fresh water at 15°C  
 $\tau_{FF} [N \cdot m]$  = maximum torque of fossil fuel variant  
 $\tau_{m,i} \left[ \frac{N \cdot m}{motor} \right]$  = torque output from individual electric motor  
 $\tau_{max,e} [N \cdot m]$  = maximum torque of fossil fuel engine  
 $\tau_{rr,f} [N \cdot m]$  = torque due to rolling resistance at front wheels  
 $\tau_{rr,r} [N \cdot m]$  = torque due to rolling resistance at rear wheels  
 $\theta [rad]$  = road grade

## **1. SUPPLEMENTARY METHODS, DERIVATIONS, AND EQUATIONS**

This section provides detailed calculations and explanations of necessary assumptions such that a reader can replicate the results presented within the main manuscript. This section explains, step-by-step, all parts of the model. The order of presentation follows the Methods section from main text.

### **1.A. Experimental design and background**

#### **1.A.1. Objective**

Our objective in conducting this research is to examine the options available for electrifying military and civilian vehicles required to transport military personnel and materiel to a theater of operations.

#### **1.A.2. Purpose**

Our purpose in conducting this research is to inform researchers, industry, and key decision-makers of the benefits and challenges of electrifying military and related vehicles.

#### **1.A.3. Approach**

We consider only specific, existing vehicles and their capabilities and develop a method of examining the options, benefits, and challenges of transitioning them from fossil fuel (FF) vehicles with internal combustion engines (ICEs) to either 100% battery electric (BE) or 100% hydrogen fuel cell (HFC) vehicles.

#### **1.A.4. Background**

This study is motivated by the fact that many countries, states, cities, and companies are committing to 100% clean, renewable energy in multiple energy sectors, including transportation [41–43]. Sixty-one countries have committed to 100% renewables in the electric power sector and one (Denmark) in all energy sectors [41]. At least twelve bills and resolutions in the US Congress call for 100% renewables in the electric power and, in some cases, all energy sectors [44–52].

The question of whether or not it is feasible to transition the transportation sector has been largely answered by commercial production of BE or HFC light-duty passenger cars and trucks, class-8 semis, short-distance locomotives, small and short-distance aircraft, vertical takeoff and landing (VTOL) air taxis, speedboats, and ferries. For example, Honda, Hyundai, Mercedes, and Toyota have all commercially produced HFC cars, while Addax, Audi, BMW, BYD, Chevrolet, Citroen, Fiat, Ford, Honda, Hyundai, Kia, Jaguar, Mercedes-Benz, Mini, Mitsubishi, Nissan, Renault, Tesla, Toyota, and Volkswagen have all commercially produced BE cars. Freightliner, Kenworth, Renault, Tesla, Toyota, and Volvo are all working on all-electric semis. A HFC locomotive already exists, and GE is building a BE locomotive. Pipistrel is selling battery electric airplanes, while Airbus, Ampaire, Eviation, Lilium, and Wright Electric are working on developing everything from small, VTOL air taxis to medium-range electric airliners. Torqeedo and Cigarette-AMG make battery electric boats and speedboats while electric ferries are already in use in Norway. Nevertheless, the question remains: is it feasible to design large and heavy all-electric tanks, airplanes, helicopters, boats, and ships that are equally capable with what we have today?

This feasibility question has yet to be addressed in-depth or specifically by scientific research articles. For example, one assessment suggested that the “physical constraints of gravimetric and volumetric energy density likely preclude battery- or hydrogen-powered aircraft for long-distance cargo or passenger service” [4]. But this assessment only compares the specific energy and energy density of onboard energy storage itself, i.e., the fuel and a fuel tank in a FF/ICE vehicle, a battery pack in a BE vehicle, or a hydrogen storage system in an HFC vehicle.

To answer the question posed, a whole-system design approach is necessary. Whole-system design focuses on optimizing efficiency of the complete system by recognizing that a change to one sub-part will affect the requirements (and efficiencies) of other sub-parts [7]. Thus, the question needs to be addressed by enlarging the parameter set analyzed.

Some studies have enlarged the parameter space over that offered in [4]. One study estimated overall system efficiencies of FF/ICE and BE semi-trucks [5]. In lieu of analyzing real-world speed and inclination profiles from specified drive cycles, the authors analytically examined the road load force opposing forward motion and calculated the energy required to overcome that force. That study concluded that BE semi-trucks in the EU were indeed technically feasible [5]. Another study sought to establish the feasibility of medium- and heavy-duty hydrogen fuel cell trucks. In that study, the authors benchmarked existing FF/ICE vehicles in terms of their characteristics: acceleration, grade, and speed. They conducted a comparison of overall vehicular mass between FF/ICE and HFC vehicles, ensuring that the payload remained constant and adding/subtracting the mass of components required by each vehicle type. They then used drive cycle data and a computational model called “Autonomie” to conclude that “there are no major technical hurdles to meet performance requirements for [class 2b – class 8] trucks with hydrogen and fuel cell systems” [6]. Numerous other articles conclude that certain electric locomotives [53], helicopters [54], airplanes [9,10,55–57], boats and ships [58,59] may be feasible. Still, no study to date has considered the types of civilian and military vehicles needed to deploy and conduct military missions.

The most important characteristics of military vehicles are their mass, volume, range, and power-to-weight ratio (PWR) or thrust-to-weight ratio (TWR). A vehicle’s overall mass and volume places limits on what other vehicles can transport it (e.g., loading a 68-ton M1 Abrams tank onto a C17 airplane and flying it to a military theater of operations). A vehicle’s range places limits on its operational capabilities and dictates logistical requirements for fuel (or energy) resupply. A vehicle’s PWR or TWR defines its ability to accelerate to a top speed.

Whereas previous studies consider some of these vehicle characteristics, none consider all of them together in a whole-system approach or specifically for military vehicles. This study considers all four vehicle characteristics simultaneously for both BE and HFC variants and compares results to known capabilities of existing FF/ICE vehicles. We do not attribute engineering data specific to any military vehicle. Instead, we group military vehicles into categories (ground combat vehicles – tracked and wheeled, rotary-wing aircraft, prop planes, waterjet boats, and cargo ships) and use averaged input data to produce results indicative of each vehicle category itself.

## **1.B. Orientation to the model**

These Supplementary Methods contain a detailed description of the data and calculations presented in the model. Calculations include, where appropriate, a range of values to cover












scenarios from low benefit (LB) to high benefit (HB) with either known or medial values averaged in-between.

The term “benefit” refers to each parameter’s numerical effect on the resulting technological potential of converting an existing FF vehicle to an all-electric (either BE or HFC) variant. It does not directly refer to any post-conversion effects such as lower cost from energy saved or reduction in greenhouse gases. The LB scenario corresponds to the lightest, smallest, and most efficient FF vehicle as well as to the heaviest, largest, and least efficient BE or HFC variant. Similarly, the HB scenario corresponds to the heaviest, largest, and least efficient FF vehicle as well as the lightest, smallest, and most efficient BE or HFC variant. By combining estimates in this manner, we are confident that actual results lie somewhere within the range of combinations presented. Unless otherwise stated, we calculate the results shown in graphs and tables using the medial/known (MK) values in order to provide clarity and simplicity in presentation.

We investigated multiple vehicle platforms, which we grouped into categories as shown in Table S.1. The table shows how the terms “domain,” “type,” “platform,” and “variant” apply.

**Table S.1. Vehicle platforms studied and associated terminology.**

“Domain”	“Type”	“Platform”		“Variant”
Land	Ground combat vehicles	Tracked		FF/ICE  BE HFC
		Wheeled		
	Freight rail	Locomotives		
Air	Rotary-wing aircraft	Helicopters		
	Fixed-wing aircraft	Prop planes		
		Medium-haul jet airliners		
		Long-haul jet airliners		
Sea	Watercraft	Waterjet boats		
		Cargo ships		

### 1.C. Input data and preparatory calculations

This first section of the “Analysis” worksheet organizes all of the relevant data for each vehicle platform, as well as baseline information for FF, BE, and HFC systems as they apply to each vehicle type. We organize this section with four major parts described in detail below: characteristics of baseline fossil fuel vehicle platforms (Section 1.C.1); characteristics of electric

motors and gearboxes applicable to both BE and HFC variants (Section 1.C.3); characteristics of BE variants (Section 1.C.4); and characteristics of HFC variants (Section 1.C.5).

### **1.C.1. Characteristics of baseline fossil fuel vehicle platforms**

This framework relies upon the known characteristics of the existing FF vehicle platform, specifically the mass and volume of FF system components that could be “stripped” away, thereby leaving room for replacement by all-electric components.

#### **1.C.1.A. Platform mass**

For each vehicle platform, we are particularly concerned with three aspects of mass: curb, gross, and payload.

##### **1.C.1.A.1. Curb vehicular mass of the fossil fuel variant**

$(m_{c,FF})$

###### **1.C.1.A.1.A. Ground combat vehicles**

The curb weight, or “empty” weight, is defined as the total weight of the operational vehicle to include all fuel, system fluids, and vehicle basic issue items (BII) [60]. Note that the curb weight does not include crew weight. We recorded the curb weight (in terms of mass) from manuals or other documents as appropriate [60].

Sometimes, manuals do not publish a curb weight for a platform type. In these instances, we calculate an estimate using the published gross mass and subtracting the combined mass of crewmembers with individual weapons, body armor, ammunition, and gear; additional mission gear; applicable combat systems; and defined combat loads of ammunition for weapon systems. In other cases, sources publish different terminology or metrics for certain platforms, generally with regards to the North Atlantic Treaty Organization’s (NATO’s) Military Load Classification (MLC) system of standards, which classifies routes based upon vehicle weight in short tons. Throughout this analysis, whenever we encounter conflicting values, we use the heaviest values.

###### **1.C.1.A.1.B. Freight rail**

For freight locomotives, the curb weight equals the gross weight; there is no “payload” onboard the actual locomotive itself [61].

###### **1.C.1.A.1.C. Rotary-wing aircraft**

Helicopters use slightly different terminology, to include “basic weight” and “operating weight.” The basic weight of a helicopter includes all hydraulic and oil systems with fluids, unusable fuel, and fixed equipment. Operating weight includes the basic weight plus the weights of aircrew, aircrew baggage, and emergency equipment. It does not include the weight of fuel, ammunition, cargo, passengers, or external auxiliary fuel tanks [60].

###### **1.C.1.A.1.D. Fixed-wing aircraft**

The US Army defines “basic empty weight” as “the aircraft weight with fixed ballast, unusable fuel, engine oil, engine coolant, hydraulic fluid, and in other respects as required by

applicable regulatory standards” [60]. Whenever manuals do not report a value, we use a curb weight based upon the empty weight of civilian versions of the same airframes.

The jet airliners use slightly different terminology, to include operating empty weight (OEW), which is defined as the weight of the aircraft, crew, and gear only [62,63].

#### **1.C.1.A.1.E. Watercraft**

The displacement of a watercraft is the volume of water it displaces, which is equivalent to its mass including all of its contents. Sometimes, manuals do not report the empty weight of boats but do report a “shipping weight.” In these instances, we adopt the shipping weight as equivalent to the empty weight. For cargo ships, manuals often use the terminology of “light” and “loaded” configurations and describe performance characteristics such as speed, range, and draft in terms of both. In these instances, we use reported values for “light displacement” to calculate the “curb weight.”

#### **1.C.1.A.2. Gross vehicular mass of the fossil fuel variant**

$(m_{g,FF})$

##### **1.C.1.A.2.A. Ground combat vehicles**

The gross weight, or “loaded,” “combat,” or “operational” weight as termed in various documents, is the curb weight plus ammunition, crew, and any other additional payload that may be attached to or contained within the vehicle [60]. We recorded the gross weights published in each platform’s specific manual [60]. Note that the gross vehicle weight (GVW) is different from the gross combination weight rating (GCWR), which includes trailer towing capacity.

##### **1.C.1.A.2.B. Freight rail**

Locomotive design depends upon weight requirements in order to achieve maximum tractive effort, which is limited by wheel adhesion to the track as well as railway infrastructure capabilities [64]. The ET44AC has a maximum mass of 195,952 kg (432,000 lb.) [61]. Given that the locomotive has 6 axles, this equates to 36 tons per axle. Not without coincidence, 36-ton axle loads were found to be most cost effective in the American Association of Railroads’ (AAR’s) Heavy Axle Load (HAL) research program in the 1990s [65]. Although heavier axle loads may be acceptable in some areas, the HAL program found that 36 tons was the best compromise for axle load in order to maximize adhesion while minimizing rail fatigue, turnout and bridge deterioration, and other railway infrastructure maintenance requirements. This relationship between locomotive mass and its supporting infrastructure plays an important role in determining possible solutions for all-electric variants.

##### **1.C.1.A.2.C. Rotary-wing aircraft**

We recorded the maximum gross weight for each aircraft in the “slick configuration,” meaning the helicopter is configured for troop and cargo carrying and does not include external add-ons such as fuel tanks or weapons [60].

##### **1.C.1.A.2.D. Fixed-wing aircraft**

Airplanes use maximum takeoff weight (MTOW) or maximum gross takeoff weight (MGTOW) for the maximum takeoff weight and maximum design taxi weight (MDTW) or

maximum design ramp weight (MDRW) for the maximum taxi weight. The MDTW is the OEW plus trip fuel, reserve fuel, taxi fuel, and payload. The difference between MDTW and MTOW is taxi fuel used prior to takeoff. We use reported values of MDRW for prop planes and MDTW for long-haul jet airliners, which are 0.3% to 0.7% larger than their respective MTOW values [60,63]. We use a published MTOW for the Boeing 737-700 NG under medium-haul jet airliners [66,67].

#### **1.C.1.A.2.E. Watercraft**

We use data plate GVW values for waterjet boats and the design draft for cargo ships [60].

#### **1.C.1.A.3. Payload mass of the fossil fuel variant**

$(m_{p,FF})$

In this analysis, we calculate the total payload as the difference between the gross mass and the curb mass (Eq. (S.1)) in accordance with general terminology found in the manuals [60]. The only variations from this method were for the medium-haul jet airliners, where the reported value for “Maximum Structural Payload” is used, for long-haul jet airliners, where the payload is specifically calculated as the difference between the maximum zero fuel weight (MZFW) and the OEW, for some waterjet boats, where the payload is taken as the reported “maximum carrying capacity,” and for some cargo ships, where the payload is taken as the reported maximum cargo load, in order to be consistent with industry terminology and values [60,63,67].

**Eq. (S.1)**

$$m_{p,FF}[kg] = m_{g,FF}[kg] - m_{c,FF}[kg]$$

#### **1.C.1.B. Platform volume**

##### **1.C.1.B.1. Reduction factor used to estimate volume within a rectangular cuboid defined by published maximum height, width, and length dimensions**

$(F_R)$

Published values for the overall volume of vehicle platforms are unavailable, so we derive approximate values for this analysis. Since there are some published values for overall dimensions (such as maximum length, width, and height), we can calculate the volume of a rectangular cuboid and then estimate an appropriate reduction factor for each platform to account for unused space within that volume. The reduction factor takes into account multiple aspects (e.g., ground clearance). For aircraft, which do not fit within a rectangular cuboid as closely as other vehicle platforms, we estimate the size of individual airframe components and find the summation, as illustrated in Section 1.C.1.B.2.

### 1.C.1.B.2. Volume of the fossil fuel variant

( $V_{FF}$ )

#### 1.C.1.B.2.A. Ground combat vehicles, freight rail, and watercraft

We calculate an approximate volume for each platform using length, height, and width data and then multiply by the estimated reduction factor to account for unused space within the calculated rectangular cuboid (Eq. (S.2)). When we encountered both maximum and reduced values for dimensions (often used for shipping vehicles when components like side-view mirrors can be folded in or other components removed), we averaged these values [60,68].

Eq. (S.2)

$$V_{FF}[m^3] = l_v[m] \cdot w_v[m] \cdot h_v[m] \cdot F_R[-]$$

#### 1.C.1.B.2.B. Rotary-wing aircraft

We are unable to readily find values for the overall volume of helicopters, so we estimate them using values for dimensions that are available [60].

#### 1.C.1.B.2.C. Fixed-wing aircraft

To calculate airplane overall volume, we break each platform down into four major components: engines, wings, tail assembly, and fuselage. We estimate the volume of the engines as cylinders with an average length and diameter (Eq. (S.3)). We estimate the volume of the wings as rectangular cuboids with an applied reduction factor to account for their angle and taper (Eq. (S.4)). We find the tail assembly volume (consisting of the rudder along with two horizontal stabilizers and elevators) by a series of tapered rectangular cuboids (Eq. (S.5)). Finally, we estimate the fuselage volume as a cylinder using the cabin diameter and fuselage length with an applied reduction factor to take into account the tapering at the nose and tail (Eq. (S.6)). The overall volume of each airplane is found by the summation of the results of Eq. (S.3) through Eq. (S.6), as shown in Eq. (S.7).

Eq. (S.3)

$$V_e[m^3] = \frac{\pi \cdot \left(\frac{d_e[m]}{2}\right)^2 \cdot l_e[m]}{[engine]} \cdot n_e[engine]$$

Eq. (S.4)

$$V_w[m^3] = \frac{l_w[m] \cdot w_w[m] \cdot h_w[m]}{[wing]} \cdot R_F[-] \cdot n_w[wing]$$

Eq. (S.5)

$$V_{ta}[m^3] = l_r[m] \cdot w_r[m] \cdot h_r[m] + \frac{l_s[m] \cdot w_s[m] \cdot h_s[m]}{[stabilizer]} \cdot n_s[stabilizers]$$

**Eq. (S.6)**

$$V_{fuelage}[m^3] = \pi \cdot \left(\frac{d_c[m]}{2}\right)^2 \cdot l_{fuelage}[m] \cdot R_F[-]$$

**Eq. (S.7)**

$$V_{FF}[m^3] = V_e[m^3] + V_w[m^3] + V_{ta}[m^3] + V_{fuelage}[m^3]$$

### **1.C.1.C. Fuel characteristics**

#### **1.C.1.C.1. Fuel type**

##### **1.C.1.C.1.A. Ground combat vehicles and rotary-wing aircraft**

The U.S. military has designed its tactical vehicles to operate on a wide variety of fuel types, to include diesel fuel # 1 (DF-1), diesel fuel # 2 (DF-2), jet propellant 8 (JP-8), diesel fuel-arctic (DF-A), and, in emergency situations, jet propellant 4 (JP-4) and motor gasoline (MOGAS) [60]. However, the U.S. Army has designated JP-8 as the preferred fuel of choice for all diesel compression ignition engines and turbine engines [69]. JP-8 is the military equivalent of Jet A-1 with a military fuel additive package that includes a static dissipater additive, corrosion inhibitor/lubricity improver, fuel system icing inhibitor, and, occasionally, antioxidant and metal deactivators [70]. Standards for JP-8 are outlined in detail specification MIL-DTL-83133E [71]. By adopting a “single fuel standard” on the battlefield, the burden of logistics is greatly reduced and flexibility maximized. This analysis uses JP-8 in the analysis for all tactical vehicle platforms.

##### **1.C.1.C.1.B. Freight locomotives**

Locomotives use DF-2 [72].

##### **1.C.1.C.1.C. Fixed-wing aircraft**

We model military prop planes using JP-8, whereas civilian airliners use Jet-A fuel [60,73].

##### **1.C.1.C.1.D. Watercraft**

We model military waterjet boats using JP-8 as their primary fuel, but they can generally also burn F-24 and ultra-low sulfur diesel (ULSD) [60]. Cargo ships within the U.S. Army’s fleet use marine diesel fuel (MDF) just as most merchant watercraft use heavy fuel oils (HFOs) for vessel propulsion and typically refuel at civilian ports [60,74].

#### **1.C.1.C.2. Density of fossil fuel**

$(\rho_{FF})$

We use published fuel densities at 15°C retrieved from specification sheets and reviews from the military (MIL-DTL-83133E) and industry (Chevron, ExxonMobil, and Shell) as reported in Table S.2. In the workbook, we record values for fuel density in units of kg m<sup>-3</sup> as well as kg L<sup>-1</sup> to facilitate further calculations.

**Table S.2. Density of fuel by type**

Fuel	Density (kg m <sup>-3</sup> )		Source
	Low	High	
JP-8	775	840	[71]
DF-2	850		[75]
Jet-A	780	840	[73]
MDF	981		[76]

A quick note on terminology: military detail specifications (MIL-DTL-#) provide preconceived solutions to requirements and describe exactly how an item is to be produced – to include materials, parts, components, fabrication, and assembly [77]. This is different from performance specifications (MIL-PRF-#) as described in Section 1.C.1.D.7.

### 1.C.1.C.3. Lower heating value (net heat of combustion) of fossil fuel

( $LHV_{FF}$ )

The combustion of hydrogen-rich fuels in ICEs releases water that must be subsequently evaporated within the combustion chamber, which requires some of the heat energy produced by the fuel during combustion. This latent heat of vaporization is lost and does not contribute to the work done by the engine. The water vapor simply passes out of the chamber and into the exhaust stream. Therefore, it is appropriate to use the net heat of combustion, also known as the lower heating value (LHV), of fuel in this analysis. We use reported LHVs as per Table S.3.

**Table S.3. Lower heating value of fuel by type**

Fuel	LHV (MJ kg <sup>-1</sup> )		Source
	Low	High	
JP-8	42.8	43.4	[71,78]
DF-2	42.6		[75]
Jet-A	43.0	43.4	[78]
MDF	42.2	42.6	[75,79,80]

### 1.C.1.C.4. Volume of fossil fuel tank (maximum fuel capacity)

( $V_t$ )

Often, a vehicle platform has multiple fuel tanks. This analysis takes the cumulative volume of all onboard fuel tanks but neglects any internal or external extended range fuel tanks that could be used. When values for usable and/or unusable fuel are available, we use these values in a range across HB to LB since unusable fuel cannot be used for energy but does count against the platform's mass.

### 1.C.1.C.5. Mass of onboard fossil fuel (fuel only) when tank is topped-off

( $m_f$ )

We calculate the topped-off fuel mass as show by Eq. (S.8).

**Eq. (S.8)**

$$m_f[kg] = \rho_{FF} \left[ \frac{kg}{L} \right] \cdot V_t[L]$$

#### **1.C.1.C.6. Volume of onboard fossil fuel (fuel only) when tank is topped-off**

$(V_f)$

In order to prepare for further calculations, we also calculate the volume of fuel in units of  $m^3$  (Eq. (S.9)).

**Eq. (S.9)**

$$V_t[m^3] = \frac{m_f[kg]}{\rho_{FF} \left[ \frac{kg}{m^3} \right]}$$

#### **1.C.1.C.7. Efficiency of storage density for the fossil fuel tank**

$(\eta_{t,FF})$

As a component of the FF system, we also consider the mass and volume of the fuel tank material itself. Manuals rarely cover the construction of fuel tanks. Additionally, tank material and design differs across the different vehicle domains. For example, aircraft use lightweight, crashworthy fuel tanks, locomotive tanks are crashworthy but heavy, and ground combat vehicle fuel tanks have evolved over recent years to incorporate protection against blasts and puncture. Consequently, we found it necessary to use a fuel tank storage density efficiency given by Eq. (S.10) [9,81].

**Eq. (S.10)**

$$\eta_{t,FF}[-] = \frac{m_f[kg]}{m_f[kg] + m_{t,FF}[kg]}$$

##### **1.C.1.C.7.A. Ground combat vehicles**

Ground combat vehicle fuel tanks have evolved over the years. In general, older fuel tanks were cast plastic (polyethylene or Nylon-6) or welded aluminum [82]. Newer fuel tanks use high-density polyethylene (HDPE) [83]. Some use specialized technology to improve safety [84,85]. All of these innovative solutions have the side effect of adding to the overall fuel tank mass and reducing its effective fuel holding volume.

Using the standard, unimproved fuel tank for a wheeled ground combat vehicle, the known value of the mass of a replacement fuel tank, the onboard volume of fuel, and the fuel's density, it is possible to estimate the fuel tank storage density efficiency as approximately 87% using Eq. (S.10). Similarly, using data for an improved fuel tank, the storage density efficiency drops to 72%. Since the exact type of fuel tank is unknown for platforms, we use a HB scenario based upon our improved fuel tank estimate and a LB scenario based upon the unimproved fuel tank. We apply the fuel tank storage density efficiency calculated for the wheeled ground combat vehicle to all other ground combat vehicle transportation platforms in order to estimate the mass of their onboard fuel tanks with their respective capacities.



### 1.C.1.C.7.B. Freight locomotive

Our research into locomotive safety revealed that manufacturers use end plates, side plates/bumpers, bottom plates, long baffles, and short baffles in fuel tank systems to provide crashworthiness in minor derailment and jackknife scenarios [86]. Given the amount of structure used, we estimate a storage density of 70%.

### 1.C.1.C.7.C. Rotary-wing aircraft

To estimate the storage efficiency of helicopter fuel tanks, we investigated tank assemblies that consist of an outer aluminum honeycomb and fiberglass shell container with an internal crashworthy and self-sealing bladder (Eq. (S.8) or Eq. (S.11)).

Eq. (S.11)

$$m_f [kg] = V_t [L] \cdot \left[ \frac{1m^3}{1,000L} \right] \cdot \rho_{FF} \left[ \frac{kg}{m^3} \right]$$

Using these values and Eq. (S.10), we conclude that the storage density for an onboard helicopter fuel tank could be as good as 90%. However, the actual construction of the onboard tanks is unknown, and fuel tanks are typically 75% efficient [9]. We also considered external reserve fuel tank assemblies and calculated a storage density efficiency of about 78% to 88%, which falls within our previous calculations. Consequently, we use a LB value of 88% and a HB value of 75% for this analysis.

### 1.C.1.C.7.D. Fixed-wing aircraft

We use a perfectly efficient (100%) storage density for airplanes because the fuel “tanks” on airplanes are generally essential airplane structure. Airplanes use "wet wings" where the front and rear spars and the upper and lower skins of the wings themselves form the fuel tank walls. Moveable parts of the wings (flaps, slats, spoilers, and speed brakes) are all mounted outside the fuel "box" while joints are made leak-proof [87].

### 1.C.1.C.7.E. Watercraft

We use a value of 75% for fuel tank storage density in our watercraft analysis [9].

### 1.C.1.C.8. Mass of the fossil fuel tank (tank material only)

( $m_{t,FF}$ )

Rearranging Eq. (S.10) allows one to solve for the mass of fuel tank material itself (Eq. (S.12)) using values for the mass of fuel and tank storage density.

Eq. (S.12)

$$m_{t,FF} [kg] = \frac{m_f [kg]}{\eta_{t,FF} [-]} - m_f [kg]$$

### 1.C.1.C.9. Density of fossil fuel tank (tank material only)

( $\rho_{t,FF}$ )

#### 1.C.1.C.9.A. Ground combat vehicles

Plastic fuel tanks have a minimum thickness of 2.54 mm [88]. HDPE density ranges from 944 to 965 kg m<sup>-3</sup> (median value of ~955 kg m<sup>-3</sup>) [89]. A commercial rubber coating example is 14.5 mm-thick at 3.2 lb ft<sup>-2</sup> [90]. Using a thickness of 14.5 mm and Eq. (S.13), this equates to a density of 1,078 kg m<sup>-3</sup>.

Eq. (S.13)

$$\frac{3.2[lb]}{[ft^2]} \times \left[ \frac{0.453592 kg}{lb} \right] \times \left[ \frac{ft^2}{0.092903m^2} \right] \times \frac{1}{0.0145m^2} = 1,077.5 \left[ \frac{kg}{m^3} \right]$$

A range for overall material density of an improved fuel tank can now be roughly estimated (Eq. (S.14), Eq. (S.15)).

Eq. (S.14)

$$\rho_{t,FF} \left[ \frac{kg}{m^3} \right] = \frac{2.54[mm] \cdot 944 \left[ \frac{kg}{m^3} \right] + 14.5[mm] \cdot 1,077.5 \left[ \frac{kg}{m^3} \right]}{2.54[mm] + 14.5[mm]} = 1,058 \left[ \frac{kg}{m^3} \right]$$

Eq. (S.15)

$$\rho_{t,FF} \left[ \frac{kg}{m^3} \right] = \frac{2.54[mm] \cdot 965 \left[ \frac{kg}{m^3} \right] + 14.5[mm] \cdot 1,077.5 \left[ \frac{kg}{m^3} \right]}{2.54[mm] + 14.5[mm]} = 1,061 \left[ \frac{kg}{m^3} \right]$$

Since it is unknown whether a fuel tank in a specific variant is improved or not, we adopt a median value of 955 kg m<sup>-3</sup> for the LB scenario (an unimproved HDPE fuel tank) and a median value of 1,060 kg m<sup>-3</sup> for the HB scenario (an improved fuel tank). We assume that all ground combat vehicles have a similar range of values for fuel tank material density.

#### 1.C.1.C.9.B. Freight locomotive

By law, internal fuel tanks on locomotives must be equivalent to 5/16 in (8 mm) thick steel plates with a yield strength of 25,000 psi (172 MPa) or greater [91,92]. The density of steel is approximately 7,850 kg m<sup>-3</sup> [93].

#### 1.C.1.C.9.C. Rotary-wing aircraft

Aircraft fuel tank densities are generally much lower than those for land vehicles. As we discuss later in the analysis, platform weight equates to required lift, so minimizing weight (mass) is desirable. Helicopters achieve a low density by using an outer fiberglass container with internal crashworthy, self-sealing systems.

If we use an example tank with a total volume of 4.007 m<sup>3</sup> capable of holding 3,028 L (3.028 m<sup>3</sup>) fuel with an empty mass of 275.3 kg, we are able to use the difference between the two volumes to calculate a rough value for the tank material volume (Eq. (S.16)).

**Eq. (S.16)**

$$4.007[m^3] - 3.028[m^3] = 0.979[m^3]$$

Considering the empty mass, we estimate a representative fuel tank density for helicopters using Eq. (S.17).

**Eq. (S.17)**

$$\rho_{t,FF} \left[ \frac{kg}{m^3} \right] = \frac{275.3[kg]}{0.979[m^3]} = 281 \left[ \frac{kg}{m^3} \right]$$

#### **1.C.1.C.9.D. Fixed-wing aircraft**

Fuel tank material density is not necessary for the airplane analysis since airplanes use wet wings (see Section 1.C.1.C.7.D).

#### **1.C.1.C.9.E. Watercraft**

Although MDF tanks can be made from high-carbon steel, black iron, fiberglass, plastic, or stainless steel, they are most generally constructed using aluminum [94]. The American Boat & Yacht Council (ABYC) has set forth guidelines that fuel tanks on watercraft must be constructed of 5000 series aluminum alloy (specifically 5052, 5083, or 5086) with a minimum thickness of 0.090 in (~2.3 mm), though 0.25 in (~6.35 mm) may be more appropriate for frequently wet environments (e.g. under cockpits or in bilges) [94]. Aluminum Alloy 5083 has a density of 2,650 kg m<sup>-3</sup>; we use this value for fuel tank material density on all watercraft [95].

#### **1.C.1.C.10. Volume of the fossil fuel tank (tank material only)**

( $V_{t,FF}$ )

The material volume of onboard fuel tanks for each platform (except fixed-wing aircraft) is calculated by dividing the material mass calculated in Section 1.C.1.C.8 by the material density determined in Section 1.C.1.C.9 (Eq. (S.18)).

**Eq. (S.18)**

$$V_{t,FF}[m^3] = \frac{m_{t,FF}[kg]}{\rho_{t,FF} \left[ \frac{kg}{m^3} \right]}$$

#### **1.C.1.C.11. Combined total mass of fossil fuel and tank**

( $m_{f+t}$ )

The combined total mass of fossil fuel and tank is calculated as the sum of the mass of onboard fossil fuel (fuel only) when the tank is topped off (see Section 1.C.1.C.5) and the mass of the fossil fuel tank (tank material only; empty) (see Section 1.C.1.C.8) (Eq. (S.19)).

**Eq. (S.19)**

$$m_{f+t}[kg] = m_f[kg] + m_{t,FF}[kg]$$

### 1.C.1.C.12. Combined total volume of fossil fuel and tank

( $V_{f+t}$ )

The combined total volume of fossil fuel and tank is calculated as the sum of the volume of onboard fossil fuel (fuel only) when the tank is topped off (see Section 1.C.1.C.6) and the volume of the fossil fuel tank (tank material only) (see Section 1.C.1.C.10) (Eq. (S.20)).

Eq. (S.20)

$$V_{f+t}[m^3] = V_f[m^3] + V_{t,FF}[m^3]$$

### 1.C.1.D. Engine characteristics

#### 1.C.1.D.1. Type and number of fossil fuel engines used

( $n_e$ )

We recorded each vehicle platform's engine type, manufacturer, and number used from applicable manuals and other references [60]. Although cargo ships may also use additional generator sets and bow thruster engines, this analysis only considers main engines. Table S.4 summarizes the engines and manufacturers for the civilian vehicles studied.

**Table S.4. Engine type and number by civilian vehicle platform**

Vehicle platform	Engine	Number	Manufacturer	Source
GE ET44AC	GEVO-12	1	General Electric	[68,96,97]
Boeing 737-700 NG	CFM56-7822	2	CFM International	[98]
Boeing 747-8	GENx-2B	4	General Electric	[99–101]

#### 1.C.1.D.2. Engine dimensions: length, height, width, and/or diameter

( $l_e, h_e, w_e, d_e$ )

We researched and recorded engine dimensions from manuals, industrial manufacturers' specification sheets, textbook examples, or other sources as appropriate [60,68,97,102–122]. Dimensional data was often not published for military vehicle platforms. In such instances, we used dimensional data for similar engines made by the same manufacturer.

#### 1.C.1.D.3. Volume of fossil fuel engine

( $V_e$ )

Depending upon the general shape of the engine and reported dimensional values, we calculate the overall volume of each fossil fuel engine using either Eq. (S.21) or Eq. (S.22).

Eq. (S.21)

$$V_e[m^3] = \pi \cdot \left(\frac{d_e[m]}{2}\right)^2 \cdot l_e[m]$$

Eq. (S.22)

$$V_e[m^3] = l_e[m] \cdot w_e[m] \cdot h_e[m]$$

#### **1.C.1.D.4. Mass of fossil fuel engine**

$(m_e)$

We recorded the “dry weight” (in terms of mass, no fluids) of each engine as per specification sheets, type-certificate data sheets, and other sources as appropriate [60,97,114,117,123–126,101–103,105,106,108,110,111].

#### **1.C.1.D.5. Maximum power of fossil fuel engine**

$(P_{max,e})$

We recorded the maximum power that each individual engine could produce [60,68,96,111,116,127,128]. Unique notes for specific variants follow.

#### **1.C.1.D.5.A. Ground combat vehicles**

The literature reports values for the rated power of vehicles sometimes as brake horsepower (BHP), which is the power delivered directly to (and measured at) the engine’s crankshaft, and other times it does not specify if the values are nominal/rated horsepower (derived from engine size and piston speed), indicated/gross horsepower (theoretically possible from the engine), or brake/net/crankshaft horsepower. To maintain consistency throughout the analysis, we treat all power values as rated horsepower and apply a vehicle engine efficiency (see Section 1.C.1.F.1.A).

#### **1.C.1.D.5.B. Freight locomotive**

The GEVO 12 can produce 3,356 kW (gross) but only 3,274 kW (traction), so we use the effective, tractive power to represent what is actually useable [96].

#### **1.C.1.D.5.C. Rotary-wing aircraft**

We report all helicopter engines in terms of shaft horsepower (SHP). Different SHP values are often quoted for maximum sustainable time periods, such as 2.5 minutes for “contingency,” 10 minutes for “maximum,” 30 minutes for “intermediate,” and unlimited for “maximum continuous” [111]. In such instances, we use the contingency value to be most conservative and challenging for transition within our analysis.

#### **1.C.1.D.5.D. Fixed-wing aircraft**

Both turboprop and turbofan engines generate thrust by accelerating a mass of air, but industry rates turboprop engines in terms of power and turbofan engines in terms of thrust. In a turboprop engine, the majority of thrust comes from the propeller, which spins at a certain speed – revolutions per minute (RPM) – determined by a torque force applied to the shaft. The contribution to thrust from the turboprop’s jet exhaust velocity, or “residual thrust,” is low, generally less than 20% [129]. Since a turboprop engine’s power (and thrust) is a combination of both mechanical prop and residual jet components, manufacturers calculate the power equivalent of the residual thrust and add this to the mechanical power from the prop to arrive at an “equivalent shaft horsepower” [129]. Consequently, we use the rated shaft horsepower for prop planes. We do not use this parameter for jet airliners since turbofan engine ratings are in terms of thrust.

### 1.C.1.D.5.E. Watercraft

We report all watercraft engines in terms of BHP.

### 1.C.1.D.6. Maximum torque of fossil fuel engine

( $\tau_{max,e}$ )

We recorded the maximum torque that each engine could produce for all vehicles other than aircraft [60,102,103,106,130]. It is important to note that power and torque are two separate metrics with distinct units, even though they are often referred to in ways that might appear interchangeable in colloquial discussion or even written work. To understand the differences, it is helpful to review why dynamometer (“dyno”) graphs show torque and power lines crossing at 5,252 RPM for Imperial Units and 9,549 RPM for SI units when graphed at the same scale. We present our own derivation here as we will use this relationship again later in the analysis.

First, consider how power and torque are related in Eq. (S.23) through Eq. (S.27).

Eq. (S.23)

$$power \left[ \frac{ft \cdot lbf}{min} \right] = force[lbf] \cdot velocity \left[ \frac{ft}{min} \right]$$

Eq. (S.24)

$$velocity \left[ \frac{ft}{min} \right] = \frac{distance[ft]}{time[min]}$$

Eq. (S.25)

$$torque[ft \cdot lbf] = force[lbf] \times radius[ft]$$

Eq. (S.26)

$$force[lbf] = \frac{torque[ft \cdot lbf]}{radius[ft]}$$

Eq. (S.27)

$$power \left[ \frac{ft \cdot lbf}{min} \right] = \frac{torque[ft \cdot lbf]}{radius[ft]} \cdot \frac{distance[ft]}{time[min]}$$

Recognizing that engines work by turning a shaft in a circular motion, we can rewrite the distance term as the distance achieved per revolution.

Eq. (S.28)

$$\frac{distance[ft]}{1 \text{ revolution}[rev]} = 2\pi \cdot radius[ft]$$

Eq. (S.29)

$$distance[ft] = 2\pi \cdot radius[ft] \cdot 1 \text{ revolution}[rev]$$

**Eq. (S.30)**

$$1 \text{ revolution}[rev] = \frac{\text{distance}[ft]}{2\pi \cdot \text{radius}[ft]}$$

Combining this concept with Eq. (S.27) above yields Eq. (S.31).

**Eq. (S.31)**

$$\text{power} \left[ \frac{ft \cdot lbf}{min} \right] = \frac{\text{torque}[ft \cdot lbf]}{\text{radius}[ft]} \cdot \frac{2\pi \cdot \text{radius}[ft] \cdot 1 \text{ revolution}[rev]}{\text{time}[min]}$$

Here, we can introduce the metric of revolutions per minute (RPM), Eq. (S.32).

**Eq. (S.32)**

$$RPM = \frac{\text{revolutions}[rev]}{\text{time}[min]}$$

Since a revolution is a distance travelled per circumference distance, it is unitless, as shown by Eq. (S.33).

**Eq. (S.33)**

$$[rev] = \frac{[ft]}{[ft]} = [-]$$

Thus, Eq. (S.31) can be rewritten as Eq. (S.34) using Imperial Units.

**Eq. (S.34)**

$$\text{power} \left[ \frac{ft \cdot lbf}{min} \right] = \text{torque}[ft \cdot lbf] \cdot 2\pi \cdot RPM \left[ \frac{1}{min} \right]$$

When the Scottish entrepreneur James Watt wanted to market his steam engine, he needed to express his engine's capabilities in terms that others would understand. By observation of workhorses in a brewery mill, he concluded that a horse could apply a force of 180 lbf while circling a shaft at a 12 ft radius and walking at a speed that equated to 144 revolutions per hour (2.4 RPM). From this, he defined a metric of power – horsepower (Eq. (S.35)) [131].

**Eq. (S.35)**

$$2\pi \cdot 12[ft] \cdot 180[lbf] \cdot 2.4 \left[ \frac{1}{min} \right] = 32,572 \left[ \frac{ft \cdot lbf}{min} \right] \cong 33,000 \left[ \frac{ft \cdot lbf}{min} \right] = 1[hp]$$

Dividing Eq. (S.34) by Watt's 33,000  $\left[ \frac{ft \cdot lbf}{min} \right]$  gives power in terms of horsepower.

**Eq. (S.36)**

$$1 [hp] = \frac{2\pi}{33,000 \left[ \frac{ft \cdot lbf}{min} \right]} \cdot RPM \left[ \frac{1}{min} \right] \cdot torque [ft \cdot lbf]$$

**Eq. (S.37)**

$$1 [hp] = 0.00019 \cdot RPM \left[ \frac{1}{min} \right] \cdot torque [ft \cdot lbf]$$

**Eq. (S.38)**

$$1 [hp] = \frac{torque [ft \cdot lbf] \cdot RPM \left[ \frac{1}{min} \right]}{5,252.11}$$

From Eq. (S.38), we can see that when torque, in units of ft-lbf, is graphed together with horsepower at the same numerical scale, the lines will cross at 5,252.11 RPM. When the lines do not cross at 5,252 RPM, it is a giveaway that the scales are different.

Applying the same concept to commonly used SI units for power and torque:

**Eq. (S.39)**

$$power [kW] = torque [N \cdot m] \cdot 2\pi \cdot RPM \left[ \frac{1}{min} \right]$$

**Eq. (S.40)**

$$1 [kW] = 1,000 \left[ \frac{J}{s} \right] = 1,000 \left[ \frac{kg \cdot m^2}{s^3} \right]$$

**Eq. (S.41)**

$$1 [N \cdot m] = 1 \left[ \frac{kg \cdot m}{s^2} \cdot m \right] = 1 \left[ \frac{kg \cdot m^2}{s^2} \right]$$

**Eq. (S.42)**

$$1RPM = \frac{revolutions [rev]}{60 [s]}$$

**Eq. (S.43)**

$$1 [kW] = \frac{2\pi}{1,000 \left[ \frac{kg \cdot m^2}{s^3} \right]} \cdot \frac{RPM \left[ \frac{1}{min} \right]}{60 \left[ \frac{s}{min} \right]} \cdot torque \left[ \frac{kg \cdot m^2}{s^2} \right]$$



**Eq. (S.44)**

$$1 [kW] = \frac{\text{torque}[N \cdot m] \cdot \text{RPM} \left[ \frac{1}{\text{min}} \right]}{9,549.3}$$

Thus, when power is in terms of kW and torque in terms of N-m, the lines will cross at 9,549 RPM when graphed at the same scale.

#### **1.C.1.D.7. Oil type**

The volume of engine oil is within the volume of the engine itself. However, we calculate engine mass from “dry weight,” so we must include the mass of this fluid when calculating the fossil fuel system’s overall mass.

The Army publishes lubricant performance specifications (MIL-PRF-#) that state requirements for results (capabilities, operational environments, interfaces, interoperability, compatibility requirements, etc.) without prescribing how those results must be achieved [77]. This is different from detail specifications (MIL-DTL-#) as described in Section 1.C.1.C.2 above.

Industry typically rates oil types using the Society of Automotive Engineers’ (SAE’s) scale, “#W-#” [132]. The first number preceding the “W,” which stands for “winter,” rates the oil’s viscosity (flow) at 0°F (-17.8°C). Lower values represent a more fluid oil that an engine can more easily pump throughout at low temperatures. The second number refers to the oil’s viscosity when hot, at 212°F (100°C). This value reflects an oil’s ability to resist thinning as higher values represent a more viscous (thick) fluid at high temperature [133].

The majority of vehicle platforms analyzed use oil under specification MIL-PRF-2104 [134]. Exceptions include military vehicles with turbine engines that use oil under specification MIL-PRF-23699 and the GE ET44AC Freight Locomotive, which uses a 20W-40 oil [135,136]. We consider the oil negligible in the analysis for large turboprop aircraft [137].

#### **1.C.1.D.8. Volume of oil used in fossil fuel engine**

$(V_{o,e})$

We recorded the volume of lubrication oil used in each engine as detailed by the manual, lubrication order, or other documentation as appropriate [60,96,103,106,119]. Of note are cargo ships that generally have large additional storage tanks, e.g., lubricating oil storage tanks for each main propulsion engine (330 gal), main engine lube oil tanks (630 gal), lube oil settling tanks (670 gal) and waste oil tanks that store dirty oil from the main engines and generators (1,790 gal). Although we know tank capacities, when the vessel is underway, the lube oil settling tank will likely not be completely full and the waste oil tank not completely empty. We neglect the large waste oil tank volume but assume the smaller settling tank is full. To find the oil volume per main propulsion engine for cargo ships, we divide the main engine lube oil tank and settling tank volumes across the two main propulsion engines and then add them to the lube oil storage tank, which is internal to the engine itself. When oil storage tanks are separate from the main engine, our analysis only considers the mass and volume of the oil itself; we do not consider the mass or volume of the external oil tank material.

### 1.C.1.D.9. Density of lubricating oil

( $\rho_o$ )

We researched the density of engine oil lubricants, generally reported at 15°C (~60°F) for the main oil types used; see Table S.5.

**Table S.5. Density of lubricating oil by type**

<b>Military performance specification/SAE grade</b>	<b>Oil type considered</b>	<b>Density (kg L<sup>-1</sup>)</b>	<b>Source</b>
MIL-PRF-2104H/15W-40	EcoPower Diesel Engine Oil	0.879	[138]
MIL-PRF-23699/--	Mobile Jet Oil II	1.004	[139]
	AeroShell Turbine Oil 500	1.005	[140]
--/20W-40	PetroCan 97	0.881	[136]

Since some material safety data sheets (MSDSs) report the specific gravity of engine oil, we converted this value to density by dividing by the reference density of water at 15°C and 1 atm = 0.999  $\left[\frac{kg}{L}\right] = 8.34 \left[\frac{lb}{gal}\right]$  [141,142].

### 1.C.1.D.10. Mass of fossil fuel engine oil

( $m_{o,e}$ )

We calculate the mass of oil using Eq. (S.45).

**Eq. (S.45)**

$$m_o[kg] = V_o[L] \cdot \rho_o \left[\frac{kg}{L}\right]$$

### 1.C.1.D.11. Antifreeze coolant type

The DOD has a Commercial Item Description (CID) for antifreeze coolant under A-A-52624 for use in all tactical/combat liquid-cooled internal combustion engines other than aircraft [121,122]. Antifreeze is not used in aviation (or tank) turbine engines, and water is used in the GE ET44AC Freight Locomotive [68].

### 1.C.1.D.12. Volume of antifreeze (or coolant fluid) used in fossil fuel engine

( $V_{af,e}$ )

We recorded the volume of antifreeze or coolant fluid used in each engine as detailed by manual, lubrication order, or other documentation as appropriate [60,96,106,119,143].

### 1.C.1.D.13. Antifreeze (or coolant fluid) density

( $\rho_{af}$ )

From its MSDS, A-A-52624 specification antifreeze has a specific gravity of 1.13 [121,122,144]. Dividing the specific gravity value by the reference density value for water at 15°C and 1 atm, the density of antifreeze can be taken as 1.129  $\left[\frac{kg}{L}\right] = 9.42 \left[\frac{lb}{gal}\right]$ .

#### 1.C.1.D.14. Mass of antifreeze (or coolant fluid) used in fossil fuel engine

$(m_{af,e})$

We calculate the mass of antifreeze or coolant fluid used using Eq. (S.46).

Eq. (S.46)

$$m_{af,e}[kg] = V_{af,e}[L] \cdot \rho_{af} \left[ \frac{kg}{L} \right]$$

#### 1.C.1.D.15. Total mass of fossil fuel engine(s) to include all engines, lubricating oil, and antifreeze coolant

$(m_{total,e})$

The total engine mass is a function of the engine type, number, oil mass, and antifreeze/coolant fluid mass, as shown in Eq. (S.47).

Eq. (S.47)

$$m_{total,e}[kg] = n_e [engine] \cdot \left( m_e \left[ \frac{kg}{engine} \right] + m_{o,e} \left[ \frac{kg}{engine} \right] + m_{af,e} \left[ \frac{kg}{engine} \right] \right)$$

#### 1.C.1.D.16. Total volume of fossil fuel engine(s) to include all engines

$(V_{total,e})$

We calculate the total engine volume based on the number of engines and the volume of each engine (see Section 1.C.1.D.1 and Section 1.C.1.D.3) as shown by Eq. (S.48).

Eq. (S.48)

$$V_{total,e}[m^3] = n_e [engine] \cdot V_e \left[ \frac{m^3}{engine} \right]$$

### 1.C.1.E. Transmission characteristics

#### 1.C.1.E.1. Type and number of transmissions (gearboxes) used

$(n_T)$

We recorded each vehicle platform's transmission (gearbox) type, manufacturer, and number used from applicable manuals and other references [60,145].

Diesel-electric locomotives already use their diesel engines to generate electricity to power traction motors and transfer rotation to the wheels via gearboxes; unfortunately, data for these motors and gearboxes is not readily available. We could assume that the gearboxes would not change in all-electric variants. However, as we will discuss later, we will size new electric motors and pair them with gearboxes while not subtracting those from the existing platform's mass or volume. Although this favors the FF variant, we want to be able to consider motor and gearbox requirements as variables.

For all aircraft other than prop planes, we use no net change in transmissions/gearboxes. The helicopters use multiple transmissions/gearboxes to take the turboshaft rotation and apply it to the rotors (both main and tail). All-electric variants will likely require similar transmissions.

Therefore, we neglect any net difference in mass or volume when transitioning. Turboprop and turbofan engines include reduction gearing within the engines themselves. As we explain in Section 1.C.2.D, we replace a turboprop engine with both electric motors and an appropriately-sized gearbox and turbofan engines with ducted fans where we can estimate the mass and volume by their “propulsor components.”

Regarding cargo ships, data is not readily available for the actual reduction gearboxes used in-line with main propulsion engines, so we use data for a Masson Marine MM W20200 NR that is appropriately-sized to match each cargo ship’s main engines.

#### **1.C.1.E.2. Transmission dimensions: length, height, width, and/or diameter**

$(l_T, h_T, w_T, d_T)$

We researched and recorded transmission/gearbox dimensions from manuals, industrial manufacturers’ specification sheets, or other sources as appropriate [60,146–153]. When actual dimensions were not available for a vehicle’s transmission, we found dimensions for that transmission’s shipping container and estimated the actual transmission’s size using a 25% reduction in each dimension. Again, since data is unavailable for the cargo ships’ reduction gearboxes, we use values for a Masson Marine MM W20200 NR transmission appropriately-sized to match the main propulsion engines.

#### **1.C.1.E.3. Mass of transmission (gearbox)**

$(m_T)$

We recorded the dry weight (in terms of mass, no fluids) of each transmission (gearbox) as per specification sheets and other sources as appropriate [60,145–147,150–155].

#### **1.C.1.E.4. Automatic transmission fluid type**

We recorded the specification and type of automatic transmission fluid (or transmission oil) acceptable for use in each vehicle platform [60,146,147,155]. Note that, in several instances, engine lubricating oil can be used with the same specifications.

#### **1.C.1.E.5. Volume of automatic transmission fluid (or transmission oil)**

$(V_{ATF})$

We recorded the volume of automatic transmission fluid (oil) used in each transmission (gearbox) as detailed by manual, lubrication order, or other documentation as appropriate [60,146,147,151].

#### **1.C.1.E.6. Density of automatic transmission fluid (or transmission oil)**

$(\rho_{ATF})$

We researched and recorded the densities of specified automatic transmission fluids from applicable industry specification sheets as detailed by Table S.6.

**Table S.6. Density of automatic transmission fluid by type**

Specification/grade	ATF type considered	Density (kg L <sup>-1</sup> )	Source
GM 6297-M	Mobile 1 Synthetic	0.846	[156]
	Total DEXRON III	0.867	[157]
	Pennzoil DEXRON III	0.877	[158]
	Penrite DX-III	0.848	[159]
MIL-L-2104	EcoPower	0.879	[138,160]
	Roshfrans Dexron II	0.881	[161]
MIL-L-2104/SAE 10W-30	--	0.865	[162]
TES 295	Petro-Canada Allison TES 295	0.850	[163]
MIL-PRF-23699	AeroShell Turbine Oil 500	1.005	[140]

**1.C.1.E.7. Mass of automatic transmission fluid (or transmission oil)** $(m_{ATF})$ 

We calculate the mass of the ATF using Eq. (S.49).

**Eq. (S.49)**

$$m_{ATF}[kg] = V_{ATF}[L] \cdot \rho_{ATF} \left[ \frac{kg}{L} \right]$$

**1.C.1.E.8. Total transmission (gearbox) mass to include all transmissions and automatic transmission fluid (or transmission oil)** $(m_{total,T})$ 

We calculate the total transmission mass as the summation of the automatic transmission fluid mass and the dry weight of the transmission as in Eq. (S.50).

**Eq. (S.50)**

$$m_{total,T}[kg] = m_{ATF}[kg] + m_T[kg]$$

**1.C.1.E.9. Total transmission (gearbox) volume to include all transmissions** $(V_{total,T})$ 

We calculate the volume of the transmission as the rectangular cuboid from length, height, and width dimensions described in Section 1.C.1.E.2. This may slightly overestimate the volume as other installed parts may sit within the corners or edges of those dimensions, but we believe the impact is negligible. Additionally, note that we consider the automatic transmission fluid as contained within the volume of the transmission system itself and do not add it here.

**Eq. (S.51)**

$$V_{total,T}[m^3] = n_T [\text{transmissions}] \cdot \frac{(l_T[m] \cdot w_T[m] \cdot h_T[m])}{[\text{transmission}]}$$

### 1.C.1.F. Overall fossil fuel system efficiency

We graphically summarize the overall FF system efficiency by vehicle type in Fig. S.1. Detailed explanations for each vehicle type follow. Note that the empty spaces for each vehicle type are left on purpose for ease of reference between Fig. S.1, Fig. S.11, and Fig. S.12 when comparing the components of overall system efficiency across FF, BE, and HFC variants.

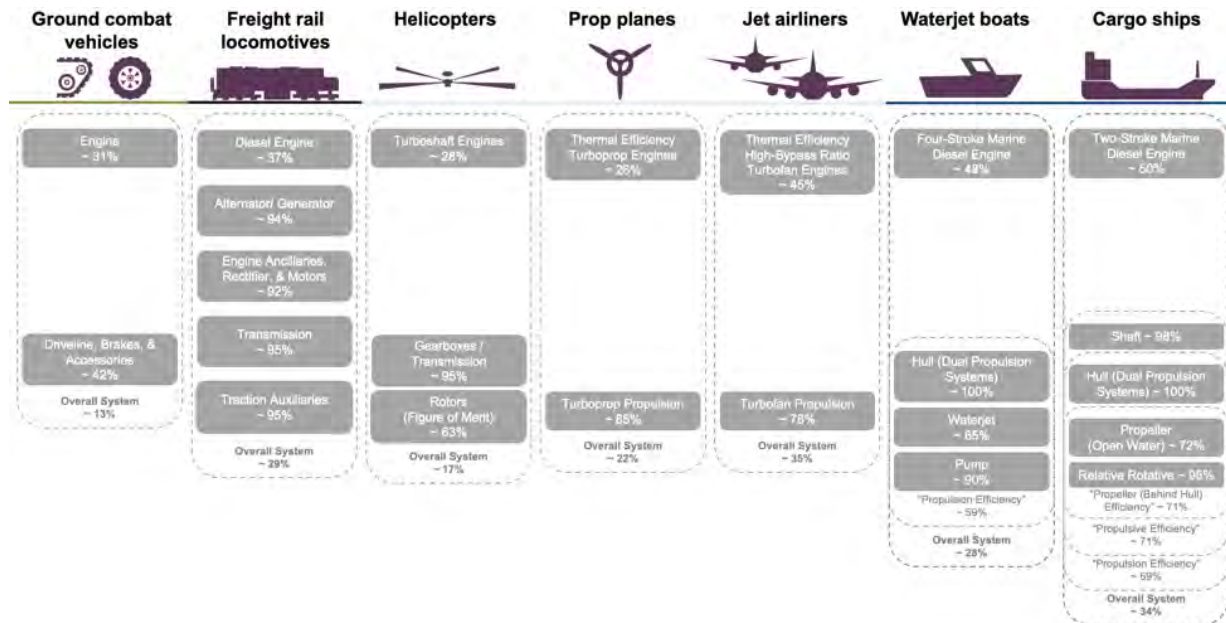


Fig. S.1. Overall fossil fuel system efficiency by vehicle type (same as Fig. 1(a))

#### 1.C.1.F.1. Ground combat vehicles

The energy contained within the chemical bonds of FF used in cars and trucks goes to seven different categories: engine losses, drivetrain losses, standby, accessory use, braking, aerodynamic drag, or rolling resistance. Only two of those categories actually represent the energy used to overcome the “road load” and propel the vehicle forward: aerodynamic drag and rolling resistance (see Section 1.C.2.A.1).

A review of previous research revealed that civilian wheeled diesel vehicles have overall “tank-to-wheels” efficiencies between 19.4% to 21.1% with commonly-cited overall efficiencies of 20% for conventional diesel vehicles and 17% for gasoline vehicles [164–166].

Table S.7 shows typical values for energy loss in civilian vehicles for both city and highway usage along with what this paper assumes for ground combat vehicles based on measurements of a wheeled ground combat vehicle. This analysis does not yet consider the additional efficiency that could be gained from regenerative braking.

**Table S.7. Comparison of energy loss in vehicles**

<b>Component</b>	<b>City use</b>	<b>Highway use</b>	<b>Ground combat vehicle estimates</b>
<b>Engine loss</b>	62%	69%	69%
<b>Drivetrain loss</b>	6%	5%	8%
<b>Standby</b>	17%	4%	0%
<b>Accessories</b>	2%	2%	8%
<b>Braking</b>	6%	2%	2%
<b>Aerodynamic drag</b>	3%	11%	3%
<b>Rolling resistance</b>	4%	7%	10%

\* All columns add to 100%. Data from [167,168].

**1.C.1.F.1.A. Efficiency of tactical vehicle fossil fuel engine**

$(\eta_{TV,e})$

As shown in Table S.7, a ground ICE vehicle is only 31% efficient in converting the chemical energy contained in the fuel to usable energy. This value represents the efficiency of the FF engine; the balance of 69% is loss. In reality, the efficiency constantly changes and can range from 0%, when the vehicle is idling, to the very best diesel engines which are 45% efficient [169]. “Whereas a standard gasoline engine is typically about 25% efficient in converting chemical energy in fuel to mechanical energy, a diesel engine is typically 37% efficient, with some reaching higher values” [170]

As an additional reference point, research into long haul heavy duty trucks in the European Union concluded that the best-in-class diesel engines had a 46% thermal efficiency when kept in their “sweet-spot” of highest efficiency, and average trucks had engines that were 39% efficient [5]. These average trucks experience 61% engine energy loss, which is in the same ballpark as the lightweight wheeled vehicle, especially considering that the trucks are built for efficient transport of commodities on paved freeways at relatively constant speeds as opposed to off-road terrain.

**1.C.1.F.1.B. Combined efficiency of tactical vehicle driveline, brakes, and accessories**

$(\eta_{TV,dl})$

Ground combat vehicles operate off-road and at slower speeds than civilian cars on a highway. Of useful energy produced from the engine, 33% goes to overcoming rolling resistance and 9% goes to overcoming aerodynamic drag for a total of 42% of the 31% useable energy produced [168]. This value represents the combined efficiency of the vehicle driveline, brakes, and accessories (standby is neglected in the analysis and assumed zero under testing conditions). The balance of 58% is lost.

**1.C.1.F.1.C. Overall tactical vehicle fossil fuel system efficiency**

$(\eta_{TV,FF})$

Considered as a percentage of the original chemical energy content of the FF itself, the component percentages of 33% to overcoming rolling resistance and 9% to overcoming aerodynamic drag reduce to just 10% and 3%, respectively, as shown in Table S.7 and by Eq. (S.52) and Eq. (S.53), for a total of 13% efficiency.

**Eq. (S.52)**

$$0.31 \cdot 0.33 = 0.1023 \cong 10\%$$

**Eq. (S.53)**

$$0.31 \cdot 0.09 = 0.0279 \cong 3\%$$

Taken another way, the product of the engine efficiency and the combined efficiency of the driveline, brakes, and accessories is the overall system efficiency, as shown by Eq. (S.54) and Eq. (S.55).

**Eq. (S.54)**

$$\eta_{TV,e}[-] \cdot \eta_{TV,dl}[-] = \eta_{TV,FF}[-]$$

**Eq. (S.55)**

$$0.31 \cdot 0.42 = 0.1302 \cong 13\%$$

One study suggests that just 13% of the chemical energy content of the fuel actually goes towards overcoming aerodynamic drag and rolling resistance to result in forward motion in a military vehicle [168]. Given the lack of specific information for each individual vehicle platform, we use this same value for all ground combat vehicles included in this study. It is important to note, however, that medium- and heavy-duty wheeled vehicles as well as tracked vehicles will likely have even lower efficiencies in overcoming rolling resistance, which is the major contributor to road load at low speeds (see Section 1.C.2.A.1). Therefore, this is likely a conservative assumption.

### **1.C.1.F.2. Freight locomotives**

#### **1.C.1.F.2.A. Efficiency of freight locomotive diesel engine**

$(\eta_{L,e})$

The efficiency of locomotive diesel engines is reported to be in the vicinity of 37.5% to 40% [53,171].

#### **1.C.1.F.2.B. Efficiency of freight locomotive alternator/generator**

$(\eta_{L,alt})$

The efficiency of a locomotive's alternator/generator ranges from about 92% to 96.5% [53,171].

#### **1.C.1.F.2.C. Combined efficiency of freight locomotive engine ancillaries, rectifier, and electric motors**

$(\eta_{L,anc})$

Different analyses report component efficiencies in different ways; some report just an engine ancillaries efficiency of 94% while others report the rectifier (98%) and electric motors (92%) separately (combined 90.16%) [53,171]. We combine these into a singular efficiency of 90.2% to 94% to cover discrepancies between studies.



### 1.C.1.F.2.D. Efficiency of freight locomotive transmission and traction auxiliaries

$(\eta_{L,T}, \eta_{L,trac})$

Here again, different analyses report efficiency components in different ways. For example, one study reported only a “onboard conversion to traction work” efficiency of 90% whereas another study reported values of transmission efficiency (95%) and traction auxiliaries efficiency (95%) separately (combined 90.25%) [53,171]. We combine these into a singular efficiency with a range of 90% to 90.25%.

### 1.C.1.F.2.E. Overall freight locomotive fossil fuel system efficiency

$(\eta_{L,FF})$

The overall fossil fuel system efficiency for a diesel-electric locomotive is the product of the onboard diesel engine efficiency, alternator/generator efficiency, the combined efficiency of engine ancillaries, rectifier, and electric motors, the transmission efficiency, and the efficiency of traction auxiliaries as shown by Eq. (S.56).

Eq. (S.56)

$$\eta_{L,FF}[-] = \eta_{L,e}[-] \cdot \eta_{L,alt}[-] \cdot \eta_{L,anc}[-] \cdot \eta_{L,T}[-] \cdot \eta_{L,trac}[-]$$

Using the combinations of high and low values as described above, we found an overall FF system efficiency of 28% to 32.7% for the freight locomotive, which reasonably matches the overall results found in previous studies of 27.7% and 31% [53,171].

### 1.C.1.F.3. Rotary-wing aircraft

#### 1.C.1.F.3.A. Efficiency of helicopter turboshaft engine

$(\eta_{H,e})$

Research on a single-rotor helicopter revealed turboshaft engine efficiencies of 0.2986 to 0.3262 at hover, 0.2144 to 0.2357 at minimum-powered forward flight, and 0.2968 to 0.3047 for high-speed forward flight [172]. Since a helicopter will conduct each of these maneuvers, it would be inaccurate to use high and low values from these ranges that would then be applied to the LB, MK, or HB cases. Thus, we use a singular value of 28% and apply it to all scenarios.

#### 1.C.1.F.3.B. Efficiency of helicopter transmissions (gearboxes)

$(\eta_{H,T})$

A published estimate for transmission losses in a helicopter is 5% [173]. Thus, we use a value of 0.95 for the helicopter transmission (gearbox) efficiency.

#### 1.C.1.F.3.C. Efficiency of helicopter rotors (“figure of merit”)

$(\eta_{H,r})$

There are many factors that contribute to the overall efficiency of a helicopter’s main rotor. To overcome this challenge, a single, non-dimensional measure of rotor thrust efficiency at hover, called the “figure of merit,” was introduced by Richard H. Prewitt of Kellett Aircraft Corporation in 1940, as shown by Eq. (S.57) [173,174].

Eq. (S.57)

$$\eta_{H,r}[-] = \frac{\text{ideal power required to hover}}{\text{actual power required to hover}} < 1.0$$

Typical values for the figure of merit are 0.55 to 0.60 at design loading whereas well-designed rotors can have a maximum figure of merit of 0.75 to 0.80 and inefficient rotors can be as low as 0.50 [175]. A good figure of merit is typically taken as 0.75 [176]. We use a figure of merit value of 0.75 for all rotary-wing aircraft in this study.

#### 1.C.1.F.3.D. Overall helicopter fossil fuel system efficiency

( $\eta_{H,FF}$ )

The overall fossil fuel system efficiency for a helicopter is the product of the engine efficiency, the transmission/gearbox efficiency, and the rotor efficiency (figure of merit), as shown by Eq. (S.58).

Eq. (S.58)

$$\eta_{H,FF}[-] = \eta_{H,e}[-] \cdot \eta_{H,T}[-] \cdot \eta_{H,r}[-]$$

Using the values described above, we calculate the overall fossil fuel system efficiency of all helicopters in this study as 17%. We do not consider additional losses to the tail rotor or accessory requirements as such losses would likely be similar for all variants, whether FF, BE, or HFC, unless further design changes are made.

#### 1.C.1.F.4. Fixed-wing aircraft

Prop planes use turboprop engines while jet airliners use turbofan engines. Though they have different efficiencies, the overall fossil fuel system efficiency for these aircraft is a matter of the engine converting the chemical energy in the fuel flow to propulsive power [177].

##### 1.C.1.F.4.A. Efficiency of turboprop engine (thermal efficiency)

( $\eta_{TP,e}$ )

The engine efficiency is the thermodynamic efficiency of converting the energy in the fuel flow to shaft power. As discussed in Section 1.C.1.D.5, the average takeoff power for turboprop engines in this study is 895 kW. Plots of commercial turboprop motors suggest a thermodynamic efficiency at cruise of 26% [177]. We only consider efficiency at cruise for this analysis, though we acknowledge that efficiency will constantly change during the various stages of flight as conditions change.

##### 1.C.1.F.4.B. Efficiency of turboprop airplane (propulsion efficiency)

( $\eta_{TP,P}$ )

The propulsion efficiency is the product of the propulsive efficiency and the transmission efficiency or converting shaft power to propulsive power. Propeller efficiency, as it is generally called, can vary widely from 50% to 87% depending upon propeller design, aircraft maneuvers, and environmental conditions [178]. Others have provided simplified rules of thumb values of between 79% to 90% [179]. For this analysis, we use a range of 79% to 90%.

#### 1.C.1.F.4.C. Overall turboprop airplane fossil fuel system efficiency

$(\eta_{TP,FF})$

The overall turboprop airplane fossil fuel system efficiency is the product of the engine thermodynamic efficiency and the propulsion efficiency, as shown by Eq. (S.59).

Eq. (S.59)

$$\eta_{TP,FF}[-] = \eta_{TP,e}[-] \cdot \eta_{TP,p}[-]$$

For this analysis, we use a range of 20.5% to 23.4% for the overall efficiency.

#### 1.C.1.F.4.D. Efficiency of high bypass ratio turbofan engine (thermal efficiency)

$(\eta_{TF,e})$

Numerous studies, reports, and presentations illustrate the efficiency of high bypass ratio (HBR) turbofan engines using graphs that generally appear in one of two main formats like those in [180–182]. The difference in these graphs is where their authors decide to include the transmission (or transfer) efficiency – either with the propulsive efficiency or with the engine thermodynamic (thermal) efficiency. Either way, the overall system efficiency is still the same: the product of all three efficiencies. In this analysis, we combine the engine thermodynamic and transmission efficiencies for a range of 42% to 49% [183].

#### 1.C.1.F.4.E. Efficiency of high bypass ratio turbofan airplane (propulsion efficiency)

$(\eta_{TF,p})$

We estimate the propulsion efficiency of turbofan airplanes as 72.5% to 82.5% [183].

#### 1.C.1.F.4.F. Overall turbofan airplane fossil fuel system efficiency

$(\eta_{TF,FF})$

The overall turbofan airplane fossil fuel system efficiency is the product of the thermal (and transfer) efficiency and the propulsive efficiency, shown by Eq. (S.60).

Eq. (S.60)

$$\eta_{TF,FF}[-] = \eta_{TF,e}[-] \cdot \eta_{TF,p}[-]$$

We use a range of 30.5% to 40.4% for overall efficiency using data from [183]. This strongly correlates to the overall efficiency of HBR turbofan engines reported by [184].

#### 1.C.1.F.5. Watercraft

The components of waterjet boats and propeller-driven cargo ships are unique, and we must calculate their efficiencies in separate ways as described below.

##### 1.C.1.F.5.A. Efficiency of waterjet marine diesel engine

$(\eta_{WJB,e})$

Four-stroke medium and high speed marine diesel engines have thermal efficiencies “slightly lower” than 50% [185]. We use a range of values from 45% to 50%.

### 1.C.1.F.5.B. Efficiency of waterjet boat hull

$(\eta_{WJB,h})$

The hull efficiency of a watercraft is defined as the ratio of the effective towing power, which is the product of the total hull towing resistance and the boat's velocity, to the thrust power, which is the product of the thrust force and the velocity of water arriving at the advance of the propulsion device [186]. It is possible for the effective towing power to exceed the thrust power and hence possible for the hull efficiency to exceed 1.0.

The hull efficiency depends upon the number of propulsion systems (generally one or two) and the boat's block coefficient. The block coefficient is the ratio of the displaced volume to the volume of a rectangular cuboid calculated by the external dimensions of the submerged (below waterline) portions of the vessel. Higher block coefficients correspond to higher hull efficiencies [186].

Given the lack of published values on hull resistance for smaller watercraft, we use a range of 95% to 105% for the hull efficiency, which corresponds to the typical hull efficiency of a larger ship with two propellers and a conventional hull form [186].

### 1.C.1.F.5.C. Efficiency of waterjet jet

$(\eta_{WJB,j})$

Studies on waterjet propulsion in boats reveal a jet efficiency of 42% to 70% over a range of velocity ratios from 0.3 to 0.9, where the velocity ratio is found by dividing the boat velocity by the jet velocity [187]. We model the Army's waterjet boats with operational velocity ratios between 0.5 and 0.9, which correspond to 60% to 70% jet efficiency.

### 1.C.1.F.5.D. Efficiency of waterjet pump

$(\eta_{WJB,p})$

Although the value will constantly vary, 90% is a generally accepted achievable pump efficiency in waterjet propulsion [188]. Studies on mixed flow pumps, which are typically used in waterjet propulsion, suggest operational pump efficiencies between 86.2% and 99.4% [189]. Since this value will constantly change given conditions, we simply use a singular value of 90%.

### 1.C.1.F.5.E. Efficiency of waterjet propulsion

$(\eta_{WJB,p})$

The propulsion efficiency is the product of the hull efficiency, the waterjet jet efficiency, and the waterjet pump efficiency, as shown by Eq. (S.61). We use a range of values from 51.3% to 66.2%.

**Eq. (S.61)**

$$\eta_{WJB,p}[-] = \eta_{WJB,h}[-] \cdot \eta_{WJB,j}[-] \cdot \eta_{WJB,p}[-]$$

### 1.C.1.F.5.F. Overall waterjet boat fossil fuel system efficiency

$(\eta_{WJB,FF})$

The overall waterjet boat fossil fuel system efficiency is the product of the engine efficiency and the propulsion efficiency, shown by Eq. (S.62). We use a range of values in this analysis from 23.1% to 33.1%.

**Eq. (S.62)**

$$\eta_{WJB,FF}[-] = \eta_{WJB,e}[-] \cdot \eta_{WJB,P}[-]$$

#### **1.C.1.F.5.G. Efficiency of propeller ship marine diesel engine**

$(\eta_{PS,e})$

Two-stroke, slow speed marine diesel engines have thermal efficiencies of 50% [185].

#### **1.C.1.F.5.H. Efficiency of propeller ship shaft**

$(\eta_{PS,s})$

The shaft efficiency is a function of the alignment and lubrication of shaft bearings as well as any reduction gears that may be used and is calculated as the ratio between the power delivered to the propeller and the brake power delivered by the main engine [186]. It is normally considered around 99%, but it can vary between 96% to 99.5%, which is the range of values we use in this analysis [186].

#### **1.C.1.F.5.I. Efficiency of propeller ship hull**

$(\eta_{PS,h})$

We describe hull efficiency in Section 1.C.1.F.5.B above. Since the cargo ships in this study have dual propulsion systems, we use a range of 95% to 105% [186].

#### **1.C.1.F.5.J. Open water efficiency of propeller ship**

$(\eta_{PS,ow})$

The term “open water” propeller efficiency refers to the propeller working in a homogeneous wake field with no hull in front of it (which is then corrected by the relative rotative efficiency considered next) [186]. Values can range from 35% to 75% with higher values corresponding to a higher velocity of water in advance of the propeller [186]. We use a range of 68% to 75% for this analysis

#### **1.C.1.F.5.K. Relative rotative efficiency of propeller ship**

$(\eta_{PS,rr})$

Since the actual water that arrives to the propeller is not in “open water” with a constant velocity but rather has a rotational flow, changing velocity, and changing direction, the “relative rotative efficiency” must also be considered [186]. Ships with dual propellers typically have a relative rotative efficiency of approximately 98%, though ships with single propellers can actually have 100% to 107%; the values are high because the rotation of water arriving at the propeller can actually have a beneficial effect [186]. We select the value of 98% to reflect the use of dual propulsion systems on cargo ships.

#### **1.C.1.F.5.L. Behind hull efficiency of propeller ship**

$(\eta_{PS,bh})$

The propeller efficiency working behind the ship, or behind hull efficiency, is the product of the open water propeller efficiency and the relative rotative propeller efficiency, as in Eq. (S.63). We derive a range of values from 66.6% to 73.5% for this analysis.

**Eq. (S.63)**

$$\eta_{PS,bh}[-] = \eta_{PS,ow}[-] \cdot \eta_{PS,rr}[-]$$

#### **1.C.1.F.5.M. Propulsive efficiency of propeller ship**

$(\eta_{PS,p})$

The propulsive efficiency is the product of the hull efficiency and the behind hull efficiency, shown by Eq. (S.64). We derive a range of values from 63.3% to 77.2%.

**Eq. (S.64)**

$$\eta_{PS,p}[-] = \eta_{PS,h}[-] \cdot \eta_{PS,bh}[-]$$

#### **1.C.1.F.5.N. Propulsion efficiency of propeller ship**

$(\eta_{PS,P})$

The propulsion efficiency is the product of the shaft efficiency and the propulsive efficiency, as in Eq. (S.65). We derive a range of values from 60.8% to 76.8%.

**Eq. (S.65)**

$$\eta_{PS,P}[-] = \eta_{PS,S}[-] \cdot \eta_{PS,p}[-]$$

#### **1.C.1.F.5.O. Overall propeller ship fossil fuel system efficiency**

$(\eta_{PS,FF})$

The overall propeller ship fossil fuel system efficiency is the product of the engine efficiency and the propulsion efficiency, shown by Eq. (S.66).

**Eq. (S.66)**

$$\eta_{PS,FF}[-] = \eta_{PS,e}[-] \cdot \eta_{PS,P}[-]$$

We calculate a range of values from 30.4% to 38.4% for cargo ships. For comparison, a study on a Handymax-sized vessel with 37,600 deadweight tonnage (DWT) predicted overall ship efficiency values of 30% to 35% [190]. DWT is a measure of how much the vessel can carry when fully loaded and does not include the weight of the ship itself (i.e., it is a different metric from displacement). Note that “tonnage” is given in terms of a tonne, or metric ton (1,000 kg = 2,204 lb), and not long ton (2,240 lb) or short ton (2,000 lb) [191]. The average DWT of cargo ships in this study is about 1,800,000 kg, only 5% the size of the Handymax [60]. Another “typical” estimate for the net thrusting energy efficiency of a ship is 24% [192]. Overall, our values appear to correlate reasonably well for this analysis. Although we do not consider liquefied natural gas (LNG) solutions, it is interesting to note that a study on a 33,000 DWT vessel using LNG calculated an overall efficiency of 56.6% [74].

## 1.C.1.G. Performance characteristics

### 1.C.1.G.1. Chemical energy content of onboard fossil fuel (less latent heat of vaporization)

( $E_{c,FF}$ )

We calculate the chemical energy content of the onboard fuel less the latent heat of vaporization, Eq. (S.67), as the product of the onboard fuel tank capacity and the LHV of the fuel type used.

Eq. (S.67)

$$E_{c,FF}[Wh] = LHV_{FF} \left[ \frac{MJ}{L} \right] \cdot V_t[L] \cdot \left\{ [W] \cdot \left[ \frac{sec}{J} \right] \cdot \left[ \frac{1,000,000J}{MJ} \right] \cdot \left[ \frac{min}{60sec} \right] \cdot \left[ \frac{hr}{60min} \right] \right\}$$

### 1.C.1.G.2. Onboard useful energy of fossil fuel variant (includes overall system efficiency)

( $OUE_{FF}$ )

Since vehicles cannot convert all of the chemical energy of fuel into useful mechanical energy and vehicular movement, we must also consider the overall system efficiency. We define “onboard useful energy” for fossil fuel variants as the energy that can be applied to vehicular movement, calculated as the product of the chemical energy content of onboard fuel and the overall fossil fuel system efficiency (Eq. (S.68)).

Eq. (S.68)

$$OUE_{FF}[Wh] = E_{c,FF}[Wh] \cdot \eta_{FF}[-]$$

### 1.C.1.G.3. Maximum range of the fossil fuel variant

( $R_{max,FF}$ )

We recorded the maximum range of most vehicle platforms as published in manuals or other documents [60,66,193]. For several vehicle platforms, however, a “range” metric is inappropriate. For example, the Army does not use its waterjet boats to move from a point A to point B, but rather to move about on inland lakes or to move pontoon bridge sections and/or hold them in place against a river’s current. Consequently, the manuals do not give ranges but instead statements like: the boat “carries enough fuel for \_\_\_ hours of operation at \_\_\_% of max power with a crew of \_\_\_” [60]. Also, freight locomotives do not use range as a metric; their performance depends upon the tractive effort required to pull a desired number of rail cars. With rotary-wing aircraft, the “range” is often quoted as the helicopter’s maximum operating radius, assuming that it must return to home station. A helicopter’s “ferry range” is the maximum distance it can fly with zero payload and a full tank of fuel and perhaps ancillary fuel tanks, i.e., a one-way flight mission. With ground combat vehicles, values for maximum range are not based off of a single standardized drive cycle. The US Army does have Test Operating Procedures (TOPs) for test courses on different terrains, to include the Harford Loop (primary roads), the Munson Standard Fuel Consumption Course (secondary roads), Churchville B Course (cross-country), and Perryman 2 & 3 (trails) [194,195]. However, manuals record maximum cruising ranges with a multitude of drive cycle descriptions. For example: GCWR over mixed terrain, 45 miles per hour (mph) on highway, 40 mph on hard-surfaced roads over rolling terrain, 30 to 40 mph on hard surfaces and hilly terrain, 25 mph on dry, level, secondary roads, etc. [60].

#### 1.C.1.G.4. Fuel economy of fossil fuel variant

( $FE_{FF}$ )

We calculate a traditional fossil fuel variant fuel economy in terms of mpg and km L<sup>-1</sup> using Eq. (S.69) and Eq. (S.70).

Eq. (S.69)

$$FE_{FF} \left[ \frac{mi}{gal} \right] = \frac{R_{max,FF} [mi]}{V_t [gal]}$$

Eq. (S.70)

$$FE_{FF} \left[ \frac{km}{L} \right] = \frac{R_{max,FF} [km]}{V_t [L]}$$

Though not calculated explicitly, it is interesting to consider the inverse of this value for several vehicle platforms. For instance, some vehicles can require up to 1.8 gallons of JP-8 just to travel one mile.

Since electric vehicles measure “fuel efficiency” in terms of energy used per distance traveled, we also calculate the fossil fuel variant fuel economy in terms of Wh mi<sup>-1</sup>, and Wh km<sup>-1</sup> for further comparison to BE and HFC variants using Eq. (S.71) and Eq. (S.72).

Eq. (S.71)

$$FE_{FF} \left[ \frac{Wh}{mi} \right] = \frac{E_{c,FF} [Wh]}{R_{max,FF} [mi]}$$

Eq. (S.72)

$$FE_{FF} \left[ \frac{Wh}{km} \right] = \frac{E_{c,FF} [Wh]}{R_{max,FF} [km]}$$

#### 1.C.1.G.5. Velocity (cruise)

( $v$ )

We recorded the maximum forward speed of each variant and converted units such that this metric is recorded in terms of mph, km h<sup>-1</sup>, ft s<sup>-1</sup>, and m s<sup>-1</sup> [60,61,193,196]. We acknowledge that, in the air and sea domains, vehicular speed is generally given in terms of knots (nautical miles per hour) or knots true airspeed (KTAS). For consistency in the analysis, we convert these values to estimates with the same units as described above.

#### 1.C.1.G.6. Maximum torque of fossil fuel variant

( $\tau_{FF}$ )

We can derive the maximum torque that each vehicle platform is capable of producing by finding the product of the maximum engine torque and the number of engines. However, we currently do not use this parameter in our analysis (see Section 1.C.3.A.10), and do not record it for aircraft.



**Eq. (S.73)**

$$\tau_{FF}[N \cdot m] = n_e [engine] \cdot \tau_e \left[ \frac{N \cdot m}{engine} \right]$$

### **1.C.1.G.7. Maximum power of fossil fuel variant**

( $P_{FF}$ )

The total, maximum vehicle power is the product of the number of engines and the maximum power output per engine. This parameter is not calculated for jet airliners since their analyses are based on thrust and TWR (see Sections 1.C.1.D.5.D and 1.C.2.D).

**Eq. (S.74)**

$$P_{FF}[W] = n_e [engine] \cdot P_{max,e} \left[ \frac{kW}{engine} \right] \cdot \left[ \frac{1,000W}{kW} \right]$$

### **1.C.1.G.8. Maximum power-to-weight ratio of fossil fuel variant at curb weight**

( $PWR_{FF,c}$ )

The maximum PWR is a means by which we can compare vehicular performance. In this analysis, we calculate the PWR for both the curb weight and the gross weight for a more complete analysis. Researchers should carefully consider which relationship to use when comparing values from this analysis to common industry/commercial values. For vehicles like cars and trucks, the PWR is typically taken with relation to the curb weight, whereas, for aircraft, the TWR is typically taken with standard day conditions at design takeoff weight and maximum throttle [129,197]. Furthermore, it should be noted that common units for the PWR are either hp lb<sup>-1</sup> (Imperial) or kW kg<sup>-1</sup> (SI). Thus, in SI units, the PWR is technically a “power-to-mass” ratio, whereas the TWR is unitless (a thrust force divided by a weight force).

**Eq. (S.75)**

$$PWR_{c,FF} \left[ \frac{W}{kg} \right] = \frac{P_{FF}[W]}{m_{c,FF}[kg]}$$

### **1.C.1.G.9. Maximum power-to-weight ratio of fossil fuel variant at gross weight**

( $PWR_{FF,g}$ )

As we discuss in Section 1.C.1.G.8, we also calculate the PWR in terms of gross vehicle weight (Eq. (S.76)).

**Eq. (S.76)**

$$PWR_{g,FF} \left[ \frac{W}{kg} \right] = \frac{P_{FF}[W]}{m_{g,FF}[kg]}$$

## 1.C.1.H. Analysis of platform stripped of all fossil fuel components

### 1.C.1.H.1. Combined mass of fossil fuel system components

$(m_{sys,FF})$

We calculate the total FF system mass as the summation of the total fuel mass (including tanks), the total engine mass (including oil and coolant), and the total transmission mass (including ATF) as shown in Eq. (S.77).

Eq. (S.77)

$$m_{sys,FF}[kg] = m_{f+t}[kg] + m_{total,e}[kg] + m_{total,T}[kg]$$

Exceptions to Eq. (S.77) include all aircraft. For rotary-wing aircraft, we model all-electric variants requiring gearboxes of similar volume and mass, so we model leaving the existing transmissions within the “stripped” platform. For fixed-wing aircraft, we model the transmission/gearboxes as integral to the engines themselves (see Section 1.C.1.E.1).

### 1.C.1.H.2. Combined volume of fossil fuel system components

$(V_{sys,FF})$

Similarly, we calculate the total FF system volume as the summation of the total fuel volume (including tanks), the total engine volume, and the total transmission volume as shown in Eq. (S.78).

Eq. (S.78)

$$V_{sys,FF}[m^3] = V_{f+t}[m^3] + V_{total,e}[m^3] + V_{total,T}[m^3]$$

As with the combined FF system mass calculation above, the combined FF system volume does not include transmission volume for the freight locomotive or any aircraft.

### 1.C.1.H.3. Curb mass of vehicle stripped of all fossil fuel system components

$(m_{c,strippedFF})$

We calculate a baseline curb mass for each vehicle platform by subtracting the FF system mass from the FF platform’s curb mass (Eq. (S.79)). This value represents a vehicle platform at curb weight after having been stripped of all its FF system components.

Eq. (S.79)

$$m_{c,strippedFF}[kg] = m_{c,FF}[kg] - m_{sys,FF}[kg]$$

### 1.C.1.H.4. Gross mass of vehicle stripped of all fossil fuel system components

$(m_{g,strippedFF})$

Similarly, we calculate a baseline gross mass for each vehicle platform by subtracting the FF system mass from the FF platform’s gross mass (Eq. (S.80)). This value represents a vehicle

platform with its maximum payload at gross weight after having been stripped of all its FF system components.

**Eq. (S.80)**

$$m_{g,strippedFF}[kg] = m_{g,FF}[kg] - m_{sys,FF}[kg]$$

#### 1.C.1.H.5. Volume of vehicle stripped of all fossil fuel system components

$(V_{strippedFF})$

We calculate the volume of each vehicle platform after having been stripped of its FF system components using Eq. (S.81).

**Eq. (S.81)**

$$V_{strippedFF}[m^3] = V_{FF}[m^3] - V_{sys,FF}[m^3]$$

#### 1.C.1.H.6. Percent reduction in curb vehicle weight, gross vehicle weight, and vehicle volume by removing the fossil fuel system

Finally, we calculate the percent reduction in curb weight, gross weight, and volume for each vehicle platform after having stripped away the FF system components using Eq. (S.82) through Eq. (S.84).

**Eq. (S.82)**

$$\% \text{ reduction in curb weight} = \frac{m_{sys,FF}[kg]}{m_{c,FF}[kg]}$$

**Eq. (S.83)**

$$\% \text{ reduction in gross weight} = \frac{m_{sys,FF}[kg]}{m_{g,FF}[kg]}$$

**Eq. (S.84)**

$$\% \text{ reduction in volume} = \frac{V_{sys,FF}[m^3]}{V_{FF}[m^3]}$$

#### 1.C.2. Calculating vehicular force required

The definition of energy is the ability to do work, and the definition of work is a force times distance (Eq. (S.85) and Eq. (S.86)).

**Eq. (S.85)**

$$\text{energy} = \text{ability to do work}$$

**Eq. (S.86)**

$$\text{work} = \text{force} \times \text{distance}$$

Thus, we can say that we require a certain amount of energy to produce a force across a distance. If we consider a vehicle’s onboard useful energy available (calculated in Section 1.C.1.G.2 above), then the distance that the vehicle can travel (its range) can be related by the force required to move the vehicle as in Eq. (S.87). For reference, the base units for a watt are:

$$W = \frac{J}{s} = \frac{\frac{kg \cdot m^2}{s^2}}{s} \text{ and the base units for a newton are: } N = \frac{kg \cdot m}{s^2}.$$

**Eq. (S.87)**

$$distance [m] = \frac{energy [Wh] \cdot \left[ \frac{3,600s}{hr} \right]}{force [N]}$$

Although this neglects ancillary energy requirements, it does provide a convenient means of comparing the force required for movement of vehicle platform variants, which will be useful in ensuring that we maintain range capabilities from FF to BE and HFC systems. In our analysis, it is the comparison across variants that is most important, not the actual value of a vehicle platform’s range.

For each vehicle type, there exists a set of conditions where the vehicle is moving but no longer accelerating, i.e., the forces acting on the vehicle platform are in equilibrium and the vehicle has a constant velocity. Understanding the forces acting on a vehicle under such conditions facilitates the calculation of vehicular capabilities necessary to overcome those forces, as well as provides a means of comparison between variants to consider capability equivalency. We have summarized the force terms and components in Table S.8.

**Table S.8. Summary of force terms and force components acting on vehicles at equilibrium**

<b>Domain</b>	<b>Type</b>	<b>Conditions</b>	<b>Force to overcome</b>	<b>Major force components</b>	<b>Force generated by vehicle</b>
Land	Ground combat vehicles	At constant speed, grade, and surface; no wind	Tractive resistance “road load”	Air resistance, rolling resistance, gradient resistance	Tractive effort
	Freight locomotive	At constant speed, grade, and rail quality; no wind	Tractive effort	Rolling resistance, grade, curvature	Tractive effort
Air	Rotary-wing	At stationary hover; no wind	Weight	Gravity	Lift
	Fixed-wing	At cruise with constant speed and altitude	Drag, weight	Air resistance, gravity	Thrust, lift
Sea	Watercraft	At constant speed; no current or wind	Total hull towing resistance	Air resistance, friction resistance, residuary resistance	Thrust

## 1.C.2.A. Ground combat vehicles

### 1.C.2.A.1. Road load

(RL)

Terminology regarding forces in automotive engineering have variations in meaning from source to source. For example, the International Standard definition for “road load” is “the force which opposes the movement of a vehicle, including total resistance...” [198]. The EPA defines “road load” as “the force imparted on a vehicle while driving at constant speed over a smooth level surface from sources such as tire rolling resistance, driveline losses, and aerodynamic drag” [199]. “Tractive effort” is the force that acts at the contact area between the tires and the ground surface and propels the vehicle forward [200]. Some sources combine rolling resistance and grade resistance together and call it “road resistance” [200]. In general, the overall “vehicle resistance” or “tractive resistance” for an automobile has three major components: aerodynamic drag (air resistance), rolling resistance, and grade resistance [167,198,200]. Although other formulations exist (to include the influence of rotational inertia, correction factors, and additional dependencies), a commonly used form of the equation for road load is given by Eq. (S.88) where the three major components are air resistance, rolling resistance, and grade resistance, respectively grouped in parentheses. Note that we subtract half the mass of fuel from the overall vehicle mass to roughly account for the fact that the vehicle becomes lighter by consuming fuel during operation.

**Eq. (S.88)**

$$RL_{FF,g}[N] = \left( \frac{1}{2} \cdot \rho_{air} \left[ \frac{kg}{m^3} \right] \cdot A_f[m^2] \cdot C_d[-] \cdot \left( v \left[ \frac{m}{s} \right] \right)^2 \right) \\ + \left( C_{rr}[-] \cdot \left( m_{g,FF}[kg] - \frac{m_f[kg]}{2} \right) \cdot g \left[ \frac{m}{s^2} \right] \right) \\ + \left( \left( m_{g,FF}[kg] - \frac{m_f[kg]}{2} \right) \cdot g \left[ \frac{m}{s^2} \right] \cdot \sin(\theta) \right)$$

The three components of road load acting on a ground combat vehicle are air resistance, rolling resistance, and grade resistance. The air resistance acts as a pressure (force over area) across the front of the vehicle, which we resolve into a single point load acting at the center of the frontal area. The rolling resistance shows up as torque at the front and rear wheels. The grade resistance adds to the tractive force required at the wheels as a function of the incline angle. Each of these component forces are discussed in further detail below.

Regarding the impact of each component force on the overall road load, it should be noted that, over a vehicle’s range of achievable velocity, the rolling resistance force is relatively constant whereas the aerodynamic drag force, or air resistance, is highly dependent upon the vehicle’s speed [201]. At speeds below 40 km h<sup>-1</sup> (~25 mph), road load is predominantly based on rolling resistance and, at speeds above 80 km h<sup>-1</sup> (~50 mph), road load is predominantly based on aerodynamic drag [202]. This is important because ground combat vehicles can be very heavy and generally operate at relatively slow speeds. Thus, for ground combat vehicles, it can reasonably be expected that air resistance contributes less to the overall road load than rolling resistance. Referring to Table S.7, one can see from tests conducted on a wheeled ground combat vehicle that rolling resistance has over three times the effect of aerodynamic drag on

overall efficiency. Previous studies have set a precedence for comparing existing vehicle fleet variants with theoretical variants through a simplified road load equation that uses a constant speed, a flat road, no surface deformation, and no tire slip [5]. We use a similar methodology with specifics described below.

### 1.C.2.A.1.A. Air resistance

The first component of the overall road load is air resistance, as shown by Eq. (S.89). We use the density of air,  $\rho_{air}$ , at sea level (1.225 kg m<sup>-3</sup>) as a standard across all tactical vehicle road load calculations.

**Eq. (S.89)**

$$air\ resistance = \left( \frac{1}{2} \cdot \rho_{air} \left[ \frac{kg}{m^3} \right] \cdot A_f [m^2] \cdot C_d [-] \cdot \left( v \left[ \frac{m}{s} \right] \right)^2 \right)$$

To estimate the front cross-sectional area of each vehicle,  $A_f$ , we simply find the product of the maximum height and width values used in calculating the overall vehicular volume (see Section 1.C.1.B). Throughout the analysis, this value does not change; i.e., any design changes to BE or HFC variants will change the vehicle platform’s length but not its width or height. This is a reasonable assumption because ground combat vehicles must maintain critical dimension restrictions for intermodal transport on military aircraft and waterborne vessels as well as wheelbase widths for crossing combat bridges. For example, military aircraft transporting ground combat vehicles have limits for acceptable mass, height, and width. Whereas the length may limit how many vehicles can fit on an aircraft, modest increases in length will not preclude their loading in the first place.

The coefficient of aerodynamic drag,  $C_d$ , represents the combined effects of form drag, skin friction, and resistance due to air flow through the radiator and interior of the vehicle (due to open windows or hatches) [203]. A notional value used by GVSC in their own research studies and estimations is 0.7 [204]. In this analysis, we estimate coefficients of drag from 0.55 to 0.70 based upon each vehicle’s front angle and profile. For a comparison to civilian vehicles, see Table S.9.

**Table S.9. Coefficient of aerodynamic drag for ground combat vehicles and typical civilian vehicle values**

Vehicle type	C <sub>d</sub>
<i>Wheeled ground combat vehicles (average)</i>	<i>0.69</i>
<i>Tracked ground combat vehicles (average)</i>	<i>0.65</i>
Passenger car	0.30 – 0.60
Convertible	0.40 – 0.65
Racing car	0.25 – 0.30
Bus	0.60 – 0.70
Truck	0.80 – 1.00
Tractor-trailer	1.30
Motorcycle and rider	1.80

[203]

For all calculations, we use the vehicle’s velocity as its maximum or cruise velocity (see Section 1.C.1.G.5). This will also remain constant across all variants of a vehicle platform. Since there are no changes to the air density, front cross-sectional area, coefficient of aerodynamic drag, or velocity between variants, the air resistance will remain constant for FF, BE, and HFC variants of each vehicular platform.

### 1.C.2.A.1.B. Rolling resistance

The second component of the overall road load is rolling resistance, shown by Eq. (S.90).

**Eq. (S.90)**

$$rolling\ resistance = \left( C_{rr}[-] \cdot \left( m_{g,FF}[kg] - \frac{m_f[kg]}{2} \right) \cdot g \left[ \frac{m}{s^2} \right] \right)$$

Rolling resistance is complex with seven major components: energy loss due to deflection of the tire sidewall near the contact area, energy loss due to deflection of tread, scrubbing in the contact area, tire slip in the longitudinal and lateral directions, deflection of the road (terrain) surface, air drag on the inside and outside of the tire, and energy loss on bumps [203]. In general, however, the cause of rolling resistance primarily depends upon the surface driven on. On hard surfaces, hysteresis in the tire materials is the main cause of rolling resistance, which results in an asymmetric distribution of ground reaction forces. The pressure on the leading half of the tire-surface contact area is larger than that in the trailing half, shifting the ground reaction force (normal force) forward of the center of mass of the wheel, which creates a moment (torque) that acts against the rolling of the wheel [200]. The normal force counteracting vehicular weight acts through the center of each wheel as well as the torque resulting from rolling resistance acting against the direction of wheel rotation. On soft surfaces, rolling resistance is primarily caused by deformation of the ground surface itself, and the ground reaction force nearly completely occurs in the leading half of the tire-surface contact area [200]. Ultimately, rolling resistance is a function of the deformation of the vehicle tires and deformation of the road (terrain) surface. Driving in soft soil significantly increases rolling resistance. Table S.10 shows typical values for the coefficient of rolling resistance.

**Table S.10. Coefficient of rolling resistance for ground combat vehicles and typical civilian vehicle values**

Vehicle type	Surface type		
	Hard (dry asphalt/concrete)	Medium (wet earth road)	Soft (sand)
Passenger cars (tourism tires)	0.011 - 0.015	0.080	0.300
Heavy trucks (truck tires)	0.008 - 0.012	0.060	0.250
Tractors (off-road tires)	0.020	0.040	0.200
<i>Wheeled ground combat vehicles (average)</i>	0.02		
<i>Tracked ground combat vehicles (average)</i>	0.04		

[203,205]

Selecting a coefficient of rolling resistance is a complicated matter as ground combat vehicles can be either tracked or wheeled and must be capable of traversing everything from paved roads to soft, loose, off-road terrain. Consequently, there has been a wide range of values used for the coefficient of rolling resistance. For example, recent research on developing a standard drive cycle for military vehicles used 0.15 as a notional vehicle parameter [204]. Solicitation for the new Joint Light Tactical Vehicle specifies an average 44 lbf ton<sup>-1</sup> rolling resistance over the entire Munson Standard Fuel Economy Course, which equates to a coefficient of rolling resistance equal to 0.022 [194]. Researchers have stated that “the rolling resistance of a tracked vehicle would be expected to be greater than for a wheeled vehicle” [206]. For tracked vehicles, performance prediction estimates range from 0.04 to 0.2 [206,207]. A 1984 Australian Army report from their Engineering Development Establishment simply assumed a coefficient of rolling resistance for tracked vehicles as twice that for wheeled vehicles within their models [206]. For this analysis, we model all tracked vehicles with a coefficient of rolling resistance equal to 0.04 and wheeled vehicles equal to 0.02. This acknowledges a variety of terrain to include both improved and unimproved road conditions as well as the difference between tracked and wheeled contact with the ground surface. Nevertheless, these values will not change between the variants analyzed, so they will affect FF variant calculations just the same as they will BE or HFC variant calculations. Finally, we use the mass of the vehicle platform (either gross or curb) along with the gravity constant to calculate the vehicle variant’s weight within the equation.

### 1.C.2.A.1.C. Grade resistance

The third and final component of the overall road load is grade resistance (Eq. (S.91)).

Eq. (S.91)

$$grade\ resistance = \left( \left( m_{g,FF} [kg] - \frac{m_f [kg]}{2} \right) \cdot g \left[ \frac{m}{s^2} \right] \cdot \sin(\theta) \right)$$



Just as in the rolling resistance equation, we use either the gross or curb mass of the vehicle platform along with the gravity constant to calculate the vehicle variant's weight.

The term  $\sin(\theta)$  is the grade and we can write it as a percentage. For example, Fig. S.2 and Eq. (S.92) show a 2% grade where a vehicle will gain 2 m in elevation for every 100 m traveled.

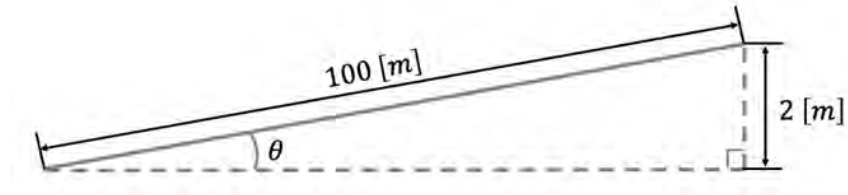


**Fig. S.2. Road grade**

**Eq. (S.92)**

$$\sin^{-1}\left(\frac{2[m]}{100[m]}\right) = 0.02 = 2\%$$

#### **1.C.2.A.1.D. Drive cycle and range possible**

We model a “drive cycle” to compare FF, BE, and HFC variants. The drive cycle begins with the tactical vehicle already having accelerated to its maximum velocity with the full onboard useful energy available from a full tank of diesel, battery charge, or hydrogen tank. The vehicle then proceeds at a constant velocity and coefficient of rolling resistance on a 2% grade with no turns and no braking until the vehicle runs out of fuel or charge, thereby defining the extent of its range. As discussed in Section 1.C.2.A.1, in terms of overall vehicle mass, we model the FF vehicle’s fuel tank as half empty the entire time. Battery mass does not change, and we neglect any changes to vehicle mass due to hydrogen use because such changes are largely insignificant.

#### **1.C.2.A.1.E. Ratio of onboard useful energy to road load**

Dividing the onboard useful energy found using Eq. (S.68) by the road load calculated using Eq. (S.88) yields a ratio by which comparisons between variants can be made (Eq. (S.93)).

**Eq. (S.93)**

$$OUE:RL \left[ \frac{Wh}{N} \right] = \frac{OUE [Wh]}{RL[N]}$$

If we hold this ratio constant between FF, BE, and HFC variants, then we can expect the variants to have the same range under the same driving conditions. (It is interesting to note here that, as shown in Eq. (S.87), multiplying this ratio by the conversion  $3,600 \text{ sec hr}^{-1}$  will yield the vehicle’s expected range (in meters) under the driving conditions defined.)

Eq. (S.93) illustrates why research that only compares onboard energy or onboard useful energy between fossil fuel variants and all-electric variants is inadequate, especially if the mass of the variants differ. If a BE variant has more mass than its FF variant counterpart, then the

rolling resistance and grade resistance will increase, increasing the road load. The increased road load means that we require more onboard useful energy to maintain this ratio and, thereby, maintain range equivalency between the variants. However, increasing the onboard useful energy requires more batteries (BE variants) or hydrogen and storage (HFC variants), which again increases the mass, which increases the road load, which mandates a further increase in onboard useful energy. Therefore, it is possible during the analysis that the condition will arise where this cycle spirals and the ratio for FF and all-electric variants can never be equivalent.

## 1.C.2.B. Freight locomotives

### 1.C.2.B.1. Tractive effort

(TE)

Terminology for forces on trains and locomotives is slightly different from automotive engineering with the term “tractive effort” used to refer to both the pulling effort (or drawbar) provided by a locomotive and the total resistance caused by a line of rail cars. Industry sizes locomotives based on two types of tractive effort: starting and continuous. The starting tractive effort is higher and reflects getting a line of rail cars moving from a standstill. The continuous tractive effort is lower and reflects keeping the line of rail cars moving. Locomotives can either push or pull a train, and they can work in tandem with more than one locomotive serving a single train.

Traction is most important for locomotives and their pulling ability, and maximizing the weight of the locomotive is critical for maximizing traction. Locomotives using alternating current (AC) traction have better adhesion and reliability than those using direct current (DC) traction, so many locomotives today use a variable frequency drive to convert the traction alternator’s output to DC and then reconvert it to a variable frequency AC to power the AC traction motors [208]. AC traction has several advantages over DC traction, to include the ability to minimize wheel slip and compensate for weight transfer. When pulling a load, the distribution of weight will shift from the front axles to the rear axles. This significantly reduces the tractive effort from the front axels in DC systems, but AC systems can compensate for this weight transfer by reducing power to the front axels and applying more power to the rear axles.

The governing equations for a locomotive’s tractive effort are shown in Eq. (S.94) and Eq. (S.95) [208].

**Eq. (S.94)**

$$\text{tractive effort} = \text{weight on drivers} \times \text{adhesion}$$

**Eq. (S.95)**

$$\text{adhesion} = \text{coefficient of friction} \times \text{locomotive adhesion factor}$$

In Eq. (S.94), the weight on drivers is a function of the mass of the locomotive, demonstrating the importance of maximizing this value within allowable railway infrastructure limits. In fact, one experimental HFC switch locomotive used a 9,000 kg ballast to increase its overall mass [209].

In Eq. (S.95), adhesion represents the ability of the locomotive to use friction at the rail-wheel interface to produce tractive effort. The coefficient of friction is generally 0.40 to 0.45 for clear, dry rail in working condition, no matter the locomotive type [208]. However, the

locomotive adhesion variable varies from about 0.45 for DC systems to 0.90 for AC systems [208]. Thus, modern DC systems have adhesion values of 25% to 27% while modern AC systems have adhesion values of 37% to 39% [208]. General Electric (GE) reports a starting tractive effort of 814,024 N (183,000 lbf) and a continuous tractive effort of 711,715 N (160,000 lbf) for its ET44AC locomotive [61]. In the specific case of the GE ET44AC operating at a continuous tractive effort of 711,715 N with a mass of 195,952 kg, the adhesion value is approximately 37%, as shown in Eq. (S.96).

**Eq. (S.96)**

$$\text{adhesion} = \frac{\text{tractive effort}}{\text{weight on drivers}} = \frac{711,715 [N]}{195,952 [kg] \cdot 9.81 \left[ \frac{m}{s^2} \right]} = 0.37$$

The tractive effort required to pull a train,  $TE_{req}$ , is calculated based upon four major components: the tractive effort required to overcome rolling resistance,  $TE_{RR}$ , the tractive effort required to overcome grade,  $TE_G$ , the tractive effort required to overcome curvature,  $TE_C$ , and the tractive effort required to accelerate,  $TE_A$ , as shown by Eq. (S.97). Although aerodynamic drag is also a factor when speeds are above 30 to 40 mph, we do not consider it in our analysis [210].

**Eq. (S.97)**

$$TE_{req} = TE_{RR} + TE_G + TE_C + TE_A$$

The tractive effort required to overcome rolling resistance,  $TE_{RR}$ , is approximately 2 to 5 lbf per ton train weight (2 lbf ton<sup>-1</sup> at low speed and 5 lbf ton<sup>-1</sup> at high speed) [210]. The tractive effort required to overcome grade,  $TE_G$ , is approximately 20 lbf per ton train weight per 1% grade (20 lbf ton<sup>-1</sup> %grade<sup>-1</sup>); a 1% grade for a train is considered steep [210]. The tractive effort required to overcome curvature,  $TE_C$ , is approximately 0.8 lbf per ton per degree curvature (0.8 lbf ton<sup>-1</sup> °curvature<sup>-1</sup>); 4° is the preferred limit where speeds may exceed 15 mph [64,210]. The tractive effort required to accelerate,  $TE_A$ , is approximately 10 lbf per ton train weight to accelerate to 12 mph in two minutes [210]. Eq. (S.98) shows the approximate tractive effort required for a train hauling 100 hopper cars at 100 ton apiece at moderate speed with a maximum 1% grade, maximum 4° curvature, and typical acceleration.

**Eq. (S.98)**

$$\begin{aligned} TE_{req} = & \left( 4 \left[ \frac{\text{lbf}}{\text{ton}} \right] \times 100 \left[ \frac{\text{ton}}{\text{car}} \right] \times 100[\text{car}] \right) \\ & + \left( 20 \left[ \frac{\text{lbf}}{\text{ton} \cdot \% \text{ grade}} \right] \times 100 \left[ \frac{\text{ton}}{\text{car}} \right] \times 100[\text{car}] \times 1\% \right) \\ & + \left( 0.8 \left[ \frac{\text{lbf}}{\text{ton} \cdot ^\circ \text{ curvature}} \right] \times 100 \left[ \frac{\text{ton}}{\text{car}} \right] \times 100[\text{car}] \times 4^\circ \right) \\ & + \left( 10 \left[ \frac{\text{lbf}}{\text{ton}} \right] \times 100 \left[ \frac{\text{ton}}{\text{car}} \right] \times 100[\text{car}] \right) = 372,000[\text{lbf}] = 1,654,738[N] \end{aligned}$$

Since the maximum starting tractive effort of an ET44AC is 814,024 N, it would require just over two (2.03) locomotives to start this train from a standstill and accelerate it to cruising speed under the given conditions. Note that, once the train has accelerated to its cruising speed, the last component of this equation, the tractive effort required for acceleration, is no longer necessary. Removing this 100,000 lbf from the tractive effort means that the train would only need 1.7 locomotives to keep moving and meet the tractive effort required to overcome rolling resistance, grade, and curvature. However, if the train had to slow down or stop for traffic management, then it would need to accelerate again. Thus, it is important to keep the tractive effort required for acceleration under consideration. In a case like this, a rail company could accept some loss in the time required to accelerate the train and simply stick with just two locomotives rather than rounding 2.03 up to 3.0 locomotives.

It is also interesting to consider a locomotive pulling a train at a constant velocity (acceleration has ended), on a straight, flat track. The last three terms of Eq. (S.98) are equal to zero, and just the first term, representing the tractive effort to overcome rolling resistance, remains. If the locomotive were moving at high speed, the rolling resistance term could be as high as 5 lbf ton<sup>-1</sup>. Given a continuous tractive effort of 160,000 lbf, that means a single locomotive could pull a 32,000-ton train (Eq. (S.99)).

**Eq. (S.99)**

$$\frac{160,000 \left[ \frac{\text{lbf}}{\text{locomotive}} \right]}{5 \left[ \frac{\text{lbf}}{\text{ton train}} \right]} = 32,000 \left[ \frac{\text{ton train}}{\text{locomotive}} \right]$$

However, getting that train moving from a standstill at 10 lbf ton<sup>-1</sup> (to achieve 12 mph in 2 minutes) would require 320,000 lbf tractive effort, and a single locomotive only has a starting tractive effort of 183,000 lbf. This illustrates why rail companies have to carefully manage their trains and locomotives with knowledge of gradient and curvature on routes, timing of trains on tracks (such that two trains do not occupy the same location at the same time), the ability of a locomotive to accelerate a train to a desired velocity, fuel resupply locations, etc. All of these concerns translate to the required capabilities of a proposed BE or HFC locomotive.

### **1.C.2.B.2. Ratio of onboard useful energy to tractive effort**

Since, with locomotives, we consider how many vehicle platforms we need to move a payload (rather than how much payload a single platform can move), this analysis will simply consider the ET44AC's continuous tractive effort capability.

Dividing the onboard useful energy found using Eq. (S.68) by the ET44AC's continuous tractive effort of 711,715 N yields a ratio by which we can make comparisons between variants.

**Eq. (S.100)**

$$OUE: TE \left[ \frac{Wh}{N} \right] = \frac{OUE [Wh]}{TE [N]}$$

If we hold this ratio constant between FF, BE, and HFC variants, then we can expect to have the same range given the same conditions. As with ground combat vehicles and shown in

Eq. (S.87), multiplying this ratio by the conversion  $3,600 \text{ sec hr}^{-1}$  will yield the locomotive's expected range (in meters) if it worked at 100% of its drawbar (tractive effort) 100% of the time. Of course, locomotives do not do this in practice, so estimates here are significantly lower than what locomotives typically achieve. Nevertheless, it provides a convenient basis of comparison between variant designs. Note that, in the freight locomotive case, we do not subtract half the mass of fuel from Eq. (S.94) because the tractive effort is also the force required for the locomotive to pull the train behind it. In this case, a BE or HFC locomotive would be advantageous over a FF locomotive because the weight on the drivers would not decrease (or decrease significantly in the HFC case) as the locomotive uses energy.

To perform a check on these assumptions, consider CSX's North American rail-based freight statistics for 2015. In that year, CSX moved 229,562,353,000 ton-miles of freight with a reported fuel usage of 487,540,790 gallons for an efficiency of 471 ton-miles gallon<sup>-1</sup>; as CSX claims, they can "move a ton of freight nearly 500 miles on a gallon of fuel" (see Eq. (S.101)) [211].

**Eq. (S.101)**

$$\frac{229,562,353,000 \text{ [ton} \cdot \text{mile]}}{487,540,790 \text{ [gal]}} = 471 \left[ \frac{\text{ton} \cdot \text{mile}}{\text{gal}} \right]$$

As found in Section 1.C.1.C.4, the GE ET44AC has 4,800 gal of usable fuel. Thus, if CSX were running only GE ET44AC locomotives, then each locomotive could, on average, haul 2,260,800 ton-miles per tank of fuel (Eq. (S.102)).

**Eq. (S.102)**

$$471 \left[ \frac{\text{ton} \cdot \text{mile}}{\text{gal}} \right] \cdot 4,800 \text{ [gal]} = 2,260,800 \text{ [ton} \cdot \text{mile]}$$

Put another way, a single locomotive could move a 10,000-ton train 226 miles (364 km) on a single tank of fuel. Whether or not a single locomotive could get that train moving from a standstill and keep it moving under given rail conditions is another matter, as detailed by Eq. (S.98) above (which also considers a 10,000-ton train with 100 hopper cars weighing 100 ton per car). Using two locomotives, this 10,000-ton train could theoretically travel 452 miles on average CSX rails (with average rail quality, curvature, and grade) while being capable of handling 4° curvature and a 1% grade as examined in Eq. (S.98).

### 1.C.2.C. Rotary-wing aircraft

Helicopters produce a force, rotor thrust, to generate both lift and propulsion for forward flight [173]. With ground combat vehicles and locomotives, we use a ratio between the onboard useful energy and tractive resistance (road load or tractive effort) to estimate the potential range of a vehicle platform. When it comes to aircraft, however, other methods exist for estimating range and endurance (time of flight).

One important metric that aviators closely track is Specific Fuel Consumption (SFC), with units of  $\frac{\text{lb}}{\text{hr} \cdot \text{hr}}$  or  $\frac{\text{kg}}{\text{kWh}}$ , which represents the mass of fuel consumed per unit of power per unit of time. With knowledge of the SFC, the power required, and the amount of onboard fuel, one

can obtain an estimate of the time available for flight. Knowing the airspeed and the time available for flight, one can obtain an estimate of the possible range, as shown by Eq. (S.103).

**Eq. (S.103)**

$$range[m] = velocity \left[ \frac{m}{s} \right] \cdot time[s]$$

### 1.C.2.C.1. First approximation of range

In his textbook, *Principles of Helicopter Aerodynamics*, J. Gordon Leishman offers a “first approximation” for calculating the maximum range of a helicopter, as shown by Eq. (S.104), which we have modified with a reordering of terms and a conversion to SI units in order to facilitate our explanation of the equation’s usefulness below [173].

**Eq. (S.104)**

$$R[m] = \left( \frac{v \left[ \frac{m}{s} \right] \cdot \left[ \frac{3,600s}{hr} \right]}{P[W]} \right) \cdot \left( \frac{m_f[kg]}{SFC \left[ \frac{kg}{Wh} \right]} \right)$$

Note that the first portion in parentheses results in units of the inverse of force, N<sup>-1</sup>. The second portion in parentheses results in units of energy, Wh. This portion of the equation represents the energy that a helicopter gets from its fuel, or *power* × *time*. Taking range as distance, this “first approximation” equation is simply a modified form of *work* = *force* × *distance*.

If we divide just the second portion in parentheses by the average power from the first portion in parentheses, the result is in units of time (or “endurance”) of flight. When we further multiply by the average velocity from the first portion in parentheses, the result is the estimated range. Across the denominator, multiplying power by the SFC yields the “fuel flow,” another closely tracked metric in aviation, in terms of kg hr<sup>-1</sup>.

To better understand how this equation applies to helicopters [173] produces three helpful graphs using an unidentified example helicopter: the first relates engine torque and airspeed, the second relates power required and airspeed, and the third relates fuel flow and power. The torque curve in the first graph indicates that his example helicopter can achieve a maximum range at an airspeed of 93 kts (172 km h<sup>-1</sup>, 47.8 m s<sup>-1</sup>) and 53% torque per engine. Drawing a line from the origin tangent to the torque curve indicates the point at which torque divided by velocity achieved is at a minimum; i.e., the helicopter is able to go the furthest distance in the least amount of time for the minimum amount of effort. Applying the same procedure to the power curve in the second graph indicates that the engine power required at which maximum range is possible is 1,075 hp (802 kW). The third graph indicates that, at that horsepower, the SFC is 0.323 lb hp<sup>-1</sup> hr<sup>-1</sup> (0.000196 kg Wh<sup>-1</sup>) and the fuel flow is ~347 lb hr<sup>-1</sup> (157 kg hr<sup>-1</sup>).

To understand the sensitivity of maximum range to fuel flow and airspeed, one can use published cruise tables for a helicopter of interest. Helicopter manuals often have hundreds of pages of cruise charts, detailing conditions for every 2,000 ft altitude (from sea level to about 20,000 ft) and 10°C (from -50° to 60°C) as appropriate. Each chart shows the maximum range possible for a given indicated airspeed, true airspeed, fuel flow, and torque per engine. Applying cruise chart values for the helicopters in this study to Leishman’s first approximation of range

equation returns results that are 25% to 57% below their reported ferry ranges at 10,000 ft altitude and 9% to 52% below their reported ferry ranges at 20,000 ft altitude. Clearly, the estimation method, the helicopter type, and the consideration of flight conditions play significant roles in accurately calculating the maximum range attainable.

It should be noted that cruise charts generally give the percent torque at 100% RPM under specific flight conditions, which can be as low as 40% torque for some maximum range scenarios. Most helicopters use a constant speed rotor (same RPM); no matter what phase of flight the helicopter is in, i.e., the rotor always spins at the same speed [212]. The pilot is able to achieve variation in rotor thrust by changing the pitch of the rotor's blades through maneuvering the collective control. 100% torque is determined by fatigue limits, and it is not uncommon to exceed 100% torque levels for short periods of time [212].

As discussed earlier in Section 1.C.1.D.6, torque can be related to power as shown in Eq. (S.105).

**Eq. (S.105)**

$$1 [hp] = \frac{\text{torque}[ft \cdot lbf] \cdot RPM \left[ \frac{1}{min} \right]}{5,252.11} \quad \text{or} \quad 1 [kW] = \frac{\text{torque}[N \cdot m] \cdot RPM \left[ \frac{1}{min} \right]}{9,549.3}$$

Using this relationship, we can deduce that change of one percent torque directly relates to a change of one percent power at the same RPM. However, we do not assume that 100% torque corresponds to 100% of the maximum power that a helicopter's engines might be capable of producing. Furthermore, we should note that the overall efficiency for rotary-wing aircraft calculated in Section 1.C.1.F.3 is a singular value, but in reality, the efficiency changes based upon conditions. The power required for a helicopter to obtain maximum range can actually be less than the power required to maintain hover (about 60% to 70%), which itself can be about 40% less than the power available [213].

During straight, level, forward flight, the fuel flow increases with power required, and the power required is a function of several major components (Eq. (S.106)) [173].

**Eq. (S.106)**

$$\begin{aligned} \text{total power required} \\ = \text{induced power} + \text{profile power} + \text{parasitic power} + \text{tail rotor power} \end{aligned}$$

Induced power is the power required to overcome drag developed during the creation of rotor thrust. Increasing the angle of attack causes airflow to move down through the rotor and the total reaction lift vector of the blade to tilt rearward, inducing drag [214]. Profile power is the power required to overcome friction drag on the blades as the rotor blades push through the viscous air [214]. Parasitic power is the power required to overcome the drag resulting from the helicopter fuselage and everything else beyond the main rotor(s); it increases with the cube of airspeed [214]. For single-rotor aircraft, tail rotor power must also be considered to stop the helicopter from rotating, but this component is not applicable for tandem rotor helicopters. Tail rotor power is sometimes estimated as 5% to 10% of the main rotor power [215].

Referring back to the first approximation equation for maximum range (Eq. (S.104)), we previously described how this equation is of the form:  $distance = 1/force \times work$ . Since the

SFC is relates how much fuel is actually used to produce a certain amount of work, it necessarily includes the overall system efficiency and can be related to the onboard useful energy by Eq. (S.107).

**Eq. (S.107)**

$$OUE_{FF}[Wh] = \left( \frac{m_f[kg]}{SFC \left[ \frac{kg}{Wh} \right]} \right)$$

Also, the fuel flow value is related by the SFC and the power produced (Eq. (S.108)).

**Eq. (S.108)**

$$SFC \left[ \frac{kg}{Wh} \right] = \frac{FF \left[ \frac{kg}{hr} \right]}{P[W]}$$

Combining Eq. (S.107) and Eq. (S.108) results in Eq. (S.109).

**Eq. (S.109)**

$$OUE_{FF}[Wh] = \left( \frac{m_f[kg] \cdot P[W]}{FF \left[ \frac{kg}{hr} \right]} \right)$$

At this point, we should consider a challenge in this analysis. If we assume a generalized overall system efficiency for helicopters and then try to compare results from our equations to expected performance from cruise charts, we find that there can be significant differences due to the flight conditions, operating assumptions, and the type of helicopter itself. If we use the notional helicopter described by [173] to help understand the helicopters in this study, then we can calculate the power required for hover using Eq. (S.110) and Eq. (S.111). From [173], the typical power available is 1.7 times the power required for hover, and from Section 1.C.1.G.7, the average maximum power available is 3,388 hp.

**Eq. (S.110)**

$$1.7 = \frac{P}{P_h} = \frac{3,388 [hp]}{P_h}$$

**Eq. (S.111)**

$$P_h = \frac{3,388 [hp]}{1.7} = 1,993 [hp]$$

Furthermore, from [173] we can estimate that the cruising power at which the helicopter can achieve maximum range is approximately 63% of the power required to hover.



Eq. (S.112)

$$0.63 \cdot 1,993[hp] = 1,256 [hp]$$

Thus, in terms of this notional helicopter, the maximum cruising range occurs when operating at 37% of the maximum power, as shown by Eq. (S.113).

Eq. (S.113)

$$\frac{1,256 [hp]}{3,388 [hp]} \cong 0.37$$

To consider the power required for a helicopter to hover in more specific detail, consider the power loading and disk loading values in Table S.11. Power loading, PL, is a measure of hovering efficiency and the ratio of rotor thrust produced to the rotor power required at hover, while disk loading, DL, is a measure of the rotor thrust (i.e., helicopter weight at hover) divided by the main rotor(s) swept area [173]. Increasing a helicopter's weight increases its DL. Using the average known total rotor area and estimates of the disc loading and power loading values shown in Table S.11, we can calculate the power used at hover for our average helicopter platform using Eq. (S.114).

**Table S.11. Example design parameters for helicopters**

Parameter	Units	Average helicopter	Source
Power loading	lbf hp <sup>-1</sup>	7.6	[216]
Disk loading	lbf ft <sup>-2</sup>	9.3	[216]
Total rotor area	ft <sup>2</sup>	3,959	[60,217]
Power required at hover	hp	4,844	Derived
Ratio of typical power available to power required at hover	-	1.40	Derived; compare to 1.7 in [173]
Ratio of cruise power at maximum range to power required at hover	-	0.56	Derived; compare to 0.63 in [173]

Eq. (S.114)

$$\frac{\text{total rotor area [ft}^2\text{]} \cdot \text{disc loading } \left[ \frac{\text{lbf}}{\text{ft}^2} \right]}{\text{power loading } \left[ \frac{\text{lbf}}{\text{hp}} \right]} = \text{power at hover [hp]}$$

As a check on input values, either multiplying the power loading by the power required at hover or multiplying the disc loading by the total rotor area yields a maximum rotor thrust force that is approximately equal to the maximum gross helicopter weight. Our check on input values is within 1% for the helicopters in this study.

We believe it is important to report all of these comparisons and checks with relation to Leishman’s first approximation of range for several reasons. First, they illustrate fundamental relationships between fuel mass, fuel flow/consumption, efficiency, power, and energy as applied to helicopters and provide a good cognitive framework. Second, the variability in results when comparing generalized analysis conditions to specific flight conditions illustrates just how much values can change based upon starting assumptions. Third, although our analysis uses vehicle range as one of four critical characteristics, using Leishman’s first approximation of range may not actually provide an appropriate means of comparison between existing and theoretical BE or HFC helicopters.

### 1.C.2.C.2. Improved approximation for range in fossil fuel helicopters

Leishman noted that Eq. (S.104) is only good for a first approximation because of several factors. First, a helicopter’s mission profile is more than just cruising at a given altitude and airspeed; it requires startup, taxi, hover, takeoff, climb, descent, landing, taxiing again, and shutdown procedures as well. All of these requirements consume fuel, and there should always be fuel reserves for safety. Second, Eq. (S.104) does not consider the change in weight of the helicopter during flight. Leishman states that “the fuel weight is normally a small fraction of the total gross weight of the helicopter (usually, but not always)” [173]. However, in the case of one helicopter in this study, the fuel is approximately 39% of its curb weight. We can use numerical integration to properly estimate the range of FF helicopters that get lighter over time as they consume fuel, but BE helicopters will not decrease in weight during flight and the decrease in weight from consumed hydrogen in HFC helicopters will be negligible. The decrease in fuel weight during flight is advantageous to FF variants.

In his textbook, *Helicopter Theory*, Wayne Johnson notes that, if one assumes the power-to-thrust ratio, speed, and SFC are independent of helicopter weight, then the range and endurance can be evaluated analytically by the Breguet range equation, shown by Eq. (S.115) (with our reordering of terms and conversion to SI units) [175].

**Eq. (S.115)**

$$R[m] = \frac{T[N] \cdot v \left[ \frac{m}{s} \right]}{P[W] \cdot SFC \left[ \frac{kg}{Wh} \right] \cdot g \left[ \frac{m}{s^2} \right] \cdot \left[ \frac{1hr}{3,600s} \right]} \cdot \left( -\ln \left( 1 - \frac{W_i[N] - W_f[N]}{W_i[N]} \right) \right)$$

To explain this equation, we provide the following derivation. Since the helicopter burns fuel during flight and becomes lighter over time, we can define the weight of the helicopter as a function of time:

**Eq. (S.116)**

$$W(t)[N]$$

The rate of change of the helicopter’s weight during cruise is thus:

**Eq. (S.117)**

$$\frac{dW(t)[N]}{dt[s]}$$

And the SFC is the mass of fuel consumed per unit power per unit time:

**Eq. (S.118)**

$$SFC = \left[ \frac{kg}{Wh} \right] = \left[ \frac{kg}{Wh} \right]$$

Multiplying the SFC by gravity converts the mass of fuel consumed into the weight of fuel consumed per unit energy obtained:

**Eq. (S.119)**

$$SFC \left[ \frac{kg}{Wh} \right] \cdot g \left[ \frac{m}{s^2} \right] = (SFC \cdot g) \left[ \frac{N}{Wh} \right]$$

Multiplying Eq. (S.119) by the average power (or rate of energy use) tells us the rate of change of helicopter weight during flight from burning fuel. Since the weight of the helicopter decreases as it consumes fuel, we can apply a negative to Eq. (S.117) or simply move it to the other side of the relationship, as shown in Eq. (S.120). We include a unit conversion for time to maintain proper units.

**Eq. (S.120)**

$$\frac{dW(t)[N]}{dt[s]} = -(SFC \cdot g) \left[ \frac{N}{Wh} \right] \cdot \left[ \frac{1hr}{3,600s} \right] \cdot P[W]$$

A key parameter for helicopters is power loading, PL, which is a measure of hovering efficiency and the ratio of rotor thrust produced to the rotor power required at hover (Eq. (S.121)) [173,175].

**Eq. (S.121)**

$$PL \left[ \frac{N}{W} \right] = \frac{T[N]}{P[W]}$$

A large portion of rotor thrust goes to providing lift and maintaining altitude [173]. At a hover, the propulsive force is zero, and the rotor thrust is equal in magnitude and opposite in direction to the weight of the helicopter. Leishman notes that, “helicopters spend a good proportion of their flight time in hover or low speed forward flight and the use of the hover condition as an initial design point is clear” [173]. Professor Cunha at the Instituto Superior Técnico in Portugal, who teaches helicopter theory, states that, “because a helicopter spends considerable portions of time in hover, designers attempt to optimize the rotor for hover” [174]. Clearly, the hover condition is a key component of design. Note, however, that the value used

for power in Eq. (S.121) is not the maximum power available, but rather the power required to hover. In this instance, a low magnitude for power is desirable, whereas an overall high “power available”-to-weight ratio is simultaneously desirable.

We can write a relationship for the power at hover using Eq. (S.121) as in Eq. (S.122):

**Eq. (S.122)**

$$\frac{P[W]}{T[N]} \cdot T[N] = P[W]$$

And then rewrite Eq. (S.120) as Eq. (S.123):

**Eq. (S.123)**

$$\frac{dW(t)[N]}{dt[s]} = -(SFC \cdot g) \left[ \frac{N}{Wh} \right] \cdot \left[ \frac{1hr}{3,600s} \right] \cdot \frac{P[W]}{T[N]} \cdot T[N]$$

Additionally, if we assume there is no wind and the helicopter is not changing altitude, then rotor thrust is equal to the helicopter weight at hover, so the last two terms are the inverse of PL and helicopter weight:

**Eq. (S.124)**

$$\frac{dW(t)[N]}{dt[s]} = -(SFC \cdot g) \left[ \frac{N}{Wh} \right] \cdot \left[ \frac{1hr}{3,600s} \right] \cdot \frac{P[W]}{T[N]} \cdot W[N]$$

At this point, we can introduce the change in distance “x” (helicopter range) into the equation by multiplying either side by  $\frac{dx}{dx} = 1$ , which does nothing to change the overall result:

**Eq. (S.125)**

$$\frac{dx[m]}{dx[m]} \cdot \frac{dW(t)[N]}{dt[s]} = -(SFC \cdot g) \left[ \frac{N}{Wh} \right] \cdot \left[ \frac{1hr}{3,600s} \right] \cdot \frac{P[W]}{T[N]} \cdot W[N]$$

Rearranging terms:

**Eq. (S.126)**

$$\frac{dx[m]}{dt[s]} \cdot \frac{dW(t)[N]}{dx[m]} = -(SFC \cdot g) \left[ \frac{N}{Wh} \right] \cdot \left[ \frac{1hr}{3,600s} \right] \cdot \frac{P[W]}{T[N]} \cdot W[N]$$

Note that  $\frac{dx[m]}{dt[s]}$  is the change in distance per change in time, which we can simply replace with the term velocity (v). The  $dx[m]$  that remains then is distance, which we will call the “cruising range (CR)” to remind ourselves that this range value is valid only under these specific assumptions. Thus, we can further rewrite Eq. (S.126) as Eq. (S.127) and Eq. (S.128):

**Eq. (S.127)**

$$v \left[ \frac{m}{s} \right] \cdot \frac{dW(t)[N]}{dx[m]} = -(SFC \cdot g) \left[ \frac{N}{Wh} \right] \cdot \left[ \frac{1hr}{3,600s} \right] \cdot \frac{P[W]}{T[N]} \cdot W[N]$$

**Eq. (S.128)**

$$dx[m] = \frac{dW(t)[N]}{W[N]} \cdot \frac{T[N]}{P[W]} \cdot \frac{v \left[ \frac{m}{s} \right]}{-(SFC \cdot g) \left[ \frac{N}{Wh} \right] \cdot \left[ \frac{1hr}{3,600s} \right]}$$

Integrating from the initial (*i*) to final (*f*) points of cruise:

**Eq. (S.129)**

$$\int_i^f dx[m] = \int_i^f \frac{dW(t)[N]}{W[N]} \cdot \frac{T[N]}{P[W]} \cdot \frac{v \left[ \frac{m}{s} \right]}{-(SFC \cdot g) \left[ \frac{N}{Wh} \right] \cdot \left[ \frac{1hr}{3,600s} \right]}$$

**Eq. (S.130)**

$$\int_i^f dx[m] = \left( \frac{T[N]}{P[W]} \cdot \frac{v \left[ \frac{m}{s} \right]}{-(SFC \cdot g) \left[ \frac{N}{Wh} \right] \cdot \left[ \frac{1hr}{3,600s} \right]} \right) \cdot \int_i^f \frac{dW(t)[N]}{W[N]}$$

**Eq. (S.131)**

$$(x_f - x_i)[m] = \left( \frac{T[N]}{P[W]} \cdot \frac{v \left[ \frac{m}{s} \right]}{-(SFC \cdot g) \left[ \frac{N}{Wh} \right] \cdot \left[ \frac{1hr}{3,600s} \right]} \right) \cdot \int_i^f \frac{dW(t)[N]}{W[N]}$$

Since the derivative of a natural logarithm is its reciprocal, we can evaluate the integral of the reciprocal as shown by Eq. (S.132):

**Eq. (S.132)**

$$\int \frac{1}{x} dx = \ln|x| + c$$

Thus, we evaluate Eq. (S.131) from initial to final points of cruise using Eq. (S.133).

**Eq. (S.133)**

$$(x_f - x_i)[m] = \left( \frac{T[N]}{P[W]} \cdot \frac{v \left[ \frac{m}{s} \right]}{-(SFC \cdot g) \left[ \frac{N}{Wh} \right] \cdot \left[ \frac{1hr}{3,600s} \right]} \right) \cdot (\ln(W_f[N]) - \ln(W_i[N]))$$

Moving the negative from the SFC and applying the quotient rule for natural logarithms yields Eq. (S.134) and Eq. (S.135).

**Eq. (S.134)**

$$(x_f - x_i)[m] = \left( \frac{T[N]}{P[W]} \cdot \frac{v \left[ \frac{m}{s} \right]}{(SFC \cdot g) \left[ \frac{N}{Wh} \right] \cdot \left[ \frac{1hr}{3,600s} \right]} \right) \cdot (-\ln(W_f[N]) + \ln(W_i[N]))$$

**Eq. (S.135)**

$$CR[m] = \left( \frac{v \left[ \frac{m}{s} \right]}{(SFC \cdot g) \left[ \frac{N}{Wh} \right] \cdot \left[ \frac{1hr}{3,600s} \right]} \right) \cdot \left( \frac{T[N]}{P[W]} \right) \cdot \ln \left( \frac{W_i[N]}{W_f[N]} \right)$$

Eq. (S.135) is our derived equivalent to Johnson's Eq. (S.115) with a reordering of terms for clarity. As already shown during the derivation of this equation (see Eq. (S.124)), we can replace thrust with the initial helicopter weight (equal values while at hover with no wind and no change in altitude), which is a necessary working assumption with precedence in helicopter modeling [215,218]. Dividing weight by gravity leaves mass, and the product of the SFC and power yields fuel flow. Combined, these adjustments convert Eq. (S.135) to Eq. (S.136), which is a convenient form for estimating the cruising range using values obtained from charts in manuals.

**Eq. (S.136)**

$$CR[m] = \left( \frac{v \left[ \frac{m}{s} \right] \cdot m_i[kg]}{FF \left[ \frac{kg}{s} \right]} \right) \cdot \ln \left( \frac{m_i[kg]}{m_f[kg]} \right)$$

When we apply Eq. (S.136) to the flight condition scenarios we previously discussed while evaluating Leishman's "first approximation" equation, the results are now within 5% to 15% of the reported maximum ferry ranges for helicopters. Thus, accounting for the change in weight during flight has a significant impact on estimating maximum range. It is also important to remember that approximately 10% to 15% of the engine's power will be delivered to the tail rotor to counteract torque in single rotor helicopters [219]. For tandem rotor helicopters, 100% of the power (less accessory power requirements) goes to the main rotors since the tandem rotors offset torque on the helicopter's body and a tail rotor is not required.

### 1.C.2.C.3. Ratio of onboard useful energy to lift force

Although our analysis above demonstrates how to calculate helicopter range by two methods, we have also demonstrated just how variable such calculated estimates can be when comparing results from these methods to known helicopter performance values. Our main concern in this analysis is not to calculate a helicopter's range, but rather to compare a BE or HFC variant's capability to achieve the range of the existing FF helicopter. Consequently, we

believe that a better approach for this analysis is to simply compare variants based upon their onboard useful energy and the lift force required for hovering.

We adopt this course of action for the following reasons: first, the main benefit of using a helicopter over an airplane is its ability to hover, and the amount of useful energy carried onboard dictates how long a variant can maintain a hover. As described by the Federal Aviation Administration in its Helicopter Flying Handbook: “helicopter performance revolves around whether or not the helicopter can be hovered. More power is required during the hover than in any other flight regime” [220]. Cunha puts it this way: “since the ability of the helicopter is to hover, this operation is more important than all other factors” [215].

Second, the propulsive force is related to the lift force by an angle defined by the rotor blades’ angle of attack less the flight path angle [173]. In design, this angle is assumed small for forward flight, and the lift force is equal to the rotor thrust at hover with no wind, no acceleration, no drag, and zero velocity. In this scenario, the helicopter is at equilibrium with forces in balance, and the lift force (rotor thrust) is equal to the helicopter weight. This greatly reduces complexity in the analysis when the intent is simply to provide a fair comparison between variants.

Third, as demonstrated above, the maximum range of a helicopter is highly sensitive to flight conditions. Significant challenges exist in estimating range due to different overall system efficiencies. By simply comparing a ratio of onboard useful energy to the lift force required, this analysis will ensure that heavier variants require more onboard energy whereas lighter variants can carry less onboard energy – regardless of specific conditions.

Fourth, when comparing variants, we consider equivalency between variants using the total PWR. The cruise power used when helicopters achieve maximum range is significantly less than the total power available. To that end, when comparing variants, we could have estimated the cruise power as a specific percentage of the total power from cruise charts in manuals, which, after already having applied an equivalent total PWR, would have the same effect as creating a comparable cruise PWR. However, it is not a requirement that the cruise PWR be equivalent between variants, so this would be unfair to assume that it must be.

Fifth, comparing maximum range between variants does not account for the energy required to taxi, hover, conduct systems checks, climb, descend, or land; it assigns all energy to go toward achieving maximum range. Achieving maximum range is not the primary purpose of rotary-wing aircraft. In fact, “ferry range” values are much less cited than “radius” values. The values are also very different because of different flight conditions and configurations.

Sixth, since helicopters operate near the ground (near sea level) most of the time, they cannot take advantage of higher-altitude conditions (lower pressure, density, and temperature) throughout the majority of their flight time, except while on long distance or ferry missions. Thus, it does not seem applicable to consider equivalency between FF, BE, and HFC variants based on near-perfect flight conditions necessary for maximum ferry range.

For all these reasons, we decided to consider equivalency between helicopter variants as an equal ratio of onboard useful energy to lift force (rotor thrust) required at hover, given by Eq. (S.137), where the lift force is equal to either the helicopter’s curb or gross vehicle weight (Eq. (S.138) and Eq. (S.139)).

**Eq. (S.137)**

$$OUE: L_{FF} \left[ \frac{Wh}{N} \right] = \frac{OUE [Wh]}{L_{FF} [N]}$$

**Eq. (S.138)**

$$L_{FF,c}[N] = m_{FF,c}[kg] \cdot g \left[ \frac{m}{s^2} \right]$$

**Eq. (S.139)**

$$L_{FF,g}[N] = m_{FF,g}[kg] \cdot g \left[ \frac{m}{s^2} \right]$$

We acknowledge that increasing a helicopter variant's volume will increase its parasite drag, the effect of which we do not capture in our ratio of onboard useful energy to lift force required at hover. In general, "parasite drag increases with the gross weight, roughly as [the equivalent flat plate area  $\sim$  gross weight<sup>2/3</sup>], so parasite power increases with helicopter size" [175]. Later in our analysis, this may specifically give a benefit to HFC helicopters where the lift force (vehicle weight) is less than FF variants due to a lighter energy source, but the helicopter's volume is larger due to bulky hydrogen storage requirements, therefore increasing drag and power requirements.

#### **1.C.2.D. Fixed-wing aircraft**

Unlike helicopters that have the primary purpose of being able to hover and conduct low speed forward flight near the ground, planes have the purpose of maximizing range and endurance. Our analysis considers both turboprop and turbofan airplanes.

##### **1.C.2.D.1. Turbofan thrust at takeoff**

( $T_{TO}$ )

Jet airliners use turbofan engines, and manufacturers report turbofan capabilities in terms of thrust. Therefore, we must calculate maximum engine power from manufacturers' reported values for takeoff thrust.

When analyzing airplanes, there are several distinct phases of flight: taxiing, takeoff, climb, cruise, descent, landing, and taxiing again. We will consider two critical phases: takeoff, which requires maximum thrust and, consequently, the airplane's TWR is most important, and cruise, where the onboard useful energy directly relates to maximum cruising range. To illustrate the difference in thrust requirements between takeoff and cruise, NASA's X-57 Maxwell Electric Research Plane uses 14 electric motors for takeoff but just two motors mounted at the wingtips during cruise [221].

Thrust is a reaction force. Turbojet and turbofan engines work by accelerating a mass of air in one direction, causing a force (thrust) of equal magnitude in the opposite direction. This analysis is particularly concerned with "static thrust," which is the thrust developed when the engine is at rest (zero velocity), e.g., a stationary airplane positioned at the end of the runway and poised for takeoff.

The major components of a turbofan engine include a jet core and a ducted fan. The central core of the turbofan engine is essentially a turbojet engine where compressors raise the pressure of inlet air, the high-pressure air enters the combustor where fuel is injected, the fuel-air mixture is ignited, and the resulting hot gases pass through the turbines that drive the compressors [222]. In a turbofan engine, a ducted fan surrounds this jet core. A portion of the inlet air is "bypassed" around the jet core and through the fan. This is referred to as a "two spool" engine, one for the fan and one for the jet core [223]. The mass of air that flows through



the jet core is called the “core airflow” ( $\dot{m}_c$ ), while the mass of air that flows through the fan is called the “bypass flow” or “fan flow” ( $\dot{m}_f$ ) [223]. The bypass ratio (BPR) is the mass flow rate of air that enters through the fan divided by the mass flow rate of air that passes through the jet core (Eq. (S.140)). The bypass flow provides additional thrust for takeoff while the jet core produces the primary thrust used for cruise [224].

**Eq. (S.140)**

$$BPR[-] = \frac{\dot{m}_f \left[ \frac{kg}{s} \right]}{\dot{m}_c \left[ \frac{kg}{s} \right]}$$

We adopt our turbofan station terminology from NASA: the entrance to the turbofan is station “0” where the velocity of air is called the “free stream” velocity; the exit of the jet core is station “e,” and the exit from the ducted fan is station “f” [223]. At the inlet, the total air mass flow rate for station 0 is the summation of the air mass flow rates entering the jet core and the ducted fan (Eq. (S.141)).

**Eq. (S.141)**

$$\dot{m}_0 \left[ \frac{kg}{s} \right] = \dot{m}_c \left[ \frac{kg}{s} \right] + \dot{m}_f \left[ \frac{kg}{s} \right]$$

Manufacturer’s data sheets for turbofan engines typically do not report  $\dot{m}_c$  or  $\dot{m}_f$ ; they simply report the “air mass flow at takeoff” ( $\dot{m}_0$ ) and the BPR [100]. Thus, it is convenient to express the air mass flow rates through the ducted fan and jet core as per Eq. (S.142) and Eq. (S.143), solely in terms of  $\dot{m}_0$  and BPR.

**Eq. (S.142)**

$$\dot{m}_c \left[ \frac{kg}{s} \right] = \frac{\dot{m}_0 \left[ \frac{kg}{s} \right]}{BPR[-] + 1}$$

**Eq. (S.143)**

$$\dot{m}_f \left[ \frac{kg}{s} \right] = \frac{\dot{m}_0 \left[ \frac{kg}{s} \right] \cdot BPR[-]}{BPR[-] + 1}$$

We can derive an equation for thrust using Newton’s Second Law (Eq. (S.144)).

**Eq. (S.144)**

$$F[N] = m[kg] \cdot a \left[ \frac{m}{s^2} \right]$$

Since momentum is the product of an object’s mass and velocity, and acceleration is the change of velocity with respect to time, force is equal to the change in an object’s momentum.

Considering the change from an object with a certain mass and velocity at station 1, time 1 to an object with a certain mass and velocity at station 2, time 2, we can rewrite Eq. (S.144) as Eq. (S.145) or Eq. (S.146).

**Eq. (S.145)**

$$F[N] = \frac{(m_2[kg] \cdot v_2 \left[\frac{m}{s}\right]) - (m_1[kg] \cdot v_1 \left[\frac{m}{s}\right])}{t_2[s] - t_1[s]}$$

**Eq. (S.146)**

$$F[N] = \frac{d}{dt} \left( m[kg] \cdot v \left[\frac{m}{s}\right] \right)$$

Since mass flow rate ( $\dot{m}$ ) is in terms of mass per unit time, we can further rewrite Eq. (S.145) and Eq. (S.146) as Eq. (S.147).

**Eq. (S.147)**

$$F[N] = \left( \dot{m}_2 \left[\frac{kg}{s}\right] \cdot v_2 \left[\frac{m}{s}\right] \right) - \left( \dot{m}_1 \left[\frac{kg}{s}\right] \cdot v_1 \left[\frac{m}{s}\right] \right)$$

However, Eq. (S.147) assumes a constant pressure across stations 1 and 2. Pressure ( $p$ ) is a force divided by an area ( $A$ ); thus, if the cross-sectional area is constant but there is a net change in pressure from station 1 to station 2, the force resulting from the pressure change must also be considered in the calculation of total force, as in Eq. (S.148).

**Eq. (S.148)**

$$F[N] = \left( \dot{m}_2 \left[\frac{kg}{s}\right] \cdot v_2 \left[\frac{m}{s}\right] \right) - \left( \dot{m}_1 \left[\frac{kg}{s}\right] \cdot v_1 \left[\frac{m}{s}\right] \right) + ((p_2[Pa] - p_1[Pa]) \cdot A_2[m^2])$$

Eq. (S.148) would be appropriate for rockets, but in cases of turbofan engines, the magnitude of the force due to pressure change is small relative to the rest of the equation [225]. Since the propulsive jet from the turbofan discharges and expands to atmospheric pressure, we can proceed using Eq. (S.147) [226].

Returning to the two spool concept of simultaneous flows through the turbofan engine, we can rewrite Eq. (S.147) such that the overall engine thrust force ( $T$ ) is the summation of the thrust force from the ducted fan and the thrust force from the jet core (Eq. (S.149)).

**Eq. (S.149)**

$$\begin{aligned} T_{TF}[N] &= T_F[N] + T_{JC}[N] \\ &= \left( \left( \dot{m}_f \left[\frac{kg}{s}\right] \cdot v_f \left[\frac{m}{s}\right] \right) - \left( \dot{m}_f \left[\frac{kg}{s}\right] \cdot v_0 \left[\frac{m}{s}\right] \right) \right) \\ &\quad + \left( \left( \dot{m}_e \left[\frac{kg}{s}\right] \cdot v_e \left[\frac{m}{s}\right] \right) - \left( \dot{m}_c \left[\frac{kg}{s}\right] \cdot v_0 \left[\frac{m}{s}\right] \right) \right) \end{aligned}$$

In a turbojet engine,  $\dot{m}_c \left[ \frac{kg}{s} \right] = \dot{m}_0 \left[ \frac{kg}{s} \right]$ , and Eq. (S.149) reduces to Eq. (S.150).

**Eq. (S.150)**

$$T_{TJ}[N] = \left( \dot{m}_e \left[ \frac{kg}{s} \right] \cdot v_e \left[ \frac{m}{s} \right] \right) - \left( \dot{m}_0 \left[ \frac{kg}{s} \right] \cdot v_0 \left[ \frac{m}{s} \right] \right)$$

The first component of this equation,  $\left( \dot{m}_e \left[ \frac{kg}{s} \right] \cdot v_e \left[ \frac{m}{s} \right] \right)$ , is known as “gross thrust.” The second component,  $\left( \dot{m}_0 \left[ \frac{kg}{s} \right] \cdot v_0 \left[ \frac{m}{s} \right] \right)$ , is known as “ram drag.” The result,  $T_{TJ}[N]$ , is known as the “net thrust.” At static thrust, the engine (and airplane) is stationary and the air that flows through the engine starts from still air. Thus, at static thrust,  $v_0 = 0$ , and the ram drag is also zero [226].

Combining Eq. (S.140), Eq. (S.141), and Eq. (S.149), we can rewrite the equation for turbofan engine thrust as Eq. (S.151).

**Eq. (S.151)**

$$T_e[N] = \left( \dot{m}_e \left[ \frac{kg}{s} \right] \cdot v_e \left[ \frac{m}{s} \right] \right) - \left( \dot{m}_0 \left[ \frac{kg}{s} \right] \cdot v_0 \left[ \frac{m}{s} \right] \right) + BPR \cdot \left( \dot{m}_c \left[ \frac{kg}{s} \right] \cdot v_f \left[ \frac{m}{s} \right] \right)$$

To better understand these values, let us consider a performance analysis of a turbofan engine [227]. Although their analysis was performed on a different model of GENX high-bypass ratio turbofan engine than that used on the Boeing 747-8, they conveniently recorded results for a similar engine under three different phases of flight, as summarized in Table S.12.

**Table S.12. Summary of selected analysis results for the GENx-1B70 turbofan engine**

Parameter	Takeoff thrust (maximum five minutes)	Continuous maximum thrust	Cruise thrust
Thrust, $T$ (kN)	320.48 (static)	293.25 (static)	60.64
Bypass ratio, BPR	9.1 : 1	--	--
Total air mass flow rate, $\dot{m}_0$ (kg s <sup>-1</sup> )	1,155.43	1,155.43	597.88
Bypass air flow rate, $\dot{m}_f$ (kg s <sup>-1</sup> )	1,041.03	--	--
Core air flow rate, $\dot{m}_c$ (kg s <sup>-1</sup> )	114.399	--	--
Fan exit velocity “cold jet velocity,” $v_f$ (m s <sup>-1</sup> )	262.67	237.88	308.39
Jet core exit velocity “hot jet velocity,” $v_e$ (m s <sup>-1</sup> )	401.92	389.14	395.58
Thrust specific fuel consumption, TSFC (kg s <sup>-1</sup> kN <sup>-1</sup> )	0.01	0.01	0.02

Data from [227].

We can perform a check by calculating the same values for  $\dot{m}_f$  and  $\dot{m}_c$  for takeoff from  $\dot{m}_0$  and the BPR according to Eq. (S.142) and Eq. (S.143). Using the published values for  $v_f$  and  $v_e$ , we can also calculate the mass flow rate of air exhaust from the turbofan jet core,  $\dot{m}_e$  using a rearranged Eq. (S.151), as shown by Eq. (S.152).

**Eq. (S.152)**

$$\frac{320,480[N] + \left(1,155.43 \left[\frac{kg}{s}\right] \cdot 0 \left[\frac{m}{s}\right]\right) - 9.1 \cdot \left(114.399 \left[\frac{kg}{s}\right] \cdot 262.67 \left[\frac{m}{s}\right]\right)}{401.92 \left[\frac{m}{s}\right]} = 117.019 \left[\frac{kg}{s}\right]$$

Furthermore, applying these values for the GEnx-1B70 engine to the static thrust at takeoff scenario using Eq. (S.149) illustrates an interesting point (Eq. (S.153)). From applying these values to the equation, we can see that the thrust produced by the fan component of the turbofan engine at takeoff is nearly six-times that produced by the jet core, as conceptually described by Moran et al [224]. In fact, ~85% of the takeoff thrust is from the fan. This upholds the conclusion made by researchers at NASA's Glenn Research Center who chose to use a factor of 0.8 when estimating fan thrust from total turbofan thrust after analyzing proprietary data derived from a range of turbofan engines capable of producing between 66,700 N and 444,800 N thrust [57].

**Eq. (S.153)**

$$\begin{aligned} T_{TF}[N] &= T_F[N] + T_{JC}[N] \\ &= \left( \left( \dot{m}_f \left[\frac{kg}{s}\right] \cdot v_f \left[\frac{m}{s}\right] \right) - \left( \dot{m}_f \left[\frac{kg}{s}\right] \cdot v_0 \left[\frac{m}{s}\right] \right) \right) \\ &\quad + \left( \left( \dot{m}_e \left[\frac{kg}{s}\right] \cdot v_e \left[\frac{m}{s}\right] \right) - \left( \dot{m}_c \left[\frac{kg}{s}\right] \cdot v_0 \left[\frac{m}{s}\right] \right) \right) \end{aligned}$$

with values:

$$\begin{aligned} 320,480[N] &= 273,447.0[N] + 47,032.3[N] \\ &= \left( \left( 1,041.03 \left[\frac{kg}{s}\right] \cdot 262.67 \left[\frac{m}{s}\right] \right) - \left( 1,041.03 \left[\frac{kg}{s}\right] \cdot 0 \left[\frac{m}{s}\right] \right) \right) \\ &\quad + \left( \left( 117.019 \left[\frac{kg}{s}\right] \cdot 401.92 \left[\frac{m}{s}\right] \right) - \left( 114.399 \left[\frac{kg}{s}\right] \cdot 0 \left[\frac{m}{s}\right] \right) \right) \end{aligned}$$

To investigate turbofan engines further, let us now consider the GEnx-2B67 engines used on the Boeing 747-8, as discussed in Section 1.C.1.D.1. GE's published specifications of the GEnx-2B67 engines are summarized in Table S.13 [100,113,125].

**Table S.13. Summary of manufacturer’s reported GENx-2B67 turbofan engine specifications**

Parameter	Value
Takeoff (static) thrust, $T_{TO,FF,i}$ (N)	295,807
Bypass ratio at takeoff, BPR	8.0 : 1
Air mass flow at takeoff, $\dot{m}_0$ ( $\text{kg s}^{-1}$ )	1,042

Unfortunately, we cannot readily obtain values for the exhaust velocity of the fan and jet core ( $v_f, v_e$ ) as well as for the mass flow rate of air from the jet core exhaust ( $\dot{m}_e$ ) for the GENx-2B67 engine. Therefore, in order to proceed with the analysis, we assume that the GENx-2B67 engine is capable of producing the same exhaust velocities as the GENx-1B70 engine. Calculating the separate air mass flow rates into the engine using Eq. (S.142) and Eq. (S.143), and using  $v_0 = 0$  to acknowledge airflow starting from still air in the static thrust case for takeoff, we estimate  $\dot{m}_e$  for the GENx-2B67 using Eq. (S.149) and show all values used in both Eq. (S.154) and Table S.14.

**Eq. (S.154)**

$$\begin{aligned}
 T_{TF}[N] &= T_F[N] + T_{JC}[N] \\
 &= \left( \left( \dot{m}_f \left[ \frac{\text{kg}}{\text{s}} \right] \cdot v_f \left[ \frac{\text{m}}{\text{s}} \right] \right) - \left( \dot{m}_f \left[ \frac{\text{kg}}{\text{s}} \right] \cdot v_0 \left[ \frac{\text{m}}{\text{s}} \right] \right) \right) \\
 &\quad + \left( \left( \dot{m}_e \left[ \frac{\text{kg}}{\text{s}} \right] \cdot v_e \left[ \frac{\text{m}}{\text{s}} \right] \right) - \left( \dot{m}_c \left[ \frac{\text{kg}}{\text{s}} \right] \cdot v_0 \left[ \frac{\text{m}}{\text{s}} \right] \right) \right)
 \end{aligned}$$

with values:

$$\begin{aligned}
 295,807[N] &= 243,291[N] + 52,516[N] \\
 &= \left( \left( 926.222 \left[ \frac{\text{kg}}{\text{s}} \right] \cdot 262.67 \left[ \frac{\text{m}}{\text{s}} \right] \right) - \left( 926.222 \left[ \frac{\text{kg}}{\text{s}} \right] \cdot 0 \left[ \frac{\text{m}}{\text{s}} \right] \right) \right) \\
 &\quad + \left( \left( 130.663 \left[ \frac{\text{kg}}{\text{s}} \right] \cdot 401.92 \left[ \frac{\text{m}}{\text{s}} \right] \right) - \left( 115.778 \left[ \frac{\text{kg}}{\text{s}} \right] \cdot 0 \left[ \frac{\text{m}}{\text{s}} \right] \right) \right)
 \end{aligned}$$

**Table S.14. Reported, adopted, and calculated values for the GENx-2B67 turbofan engine**

Parameter	Value	Source
Takeoff (static) thrust, $T_{TO,FF,i}$	295,807 (N)	Reported by manufacturer
Bypass ratio at takeoff, BPR	8.0 : 1	Reported by manufacturer
Air mass flow at takeoff, $\dot{m}_0$	1,042 (kg s <sup>-1</sup> )	Reported by manufacturer
Bypass air flow rate, $\dot{m}_f$	926.222 (kg s <sup>-1</sup> )	Calculated Eq. (S.143)
Core air flow rate, $\dot{m}_c$	115.778 (kg s <sup>-1</sup> )	Calculated Eq. (S.142)
Fan exit velocity “cold jet velocity,” $v_f$	262.67 (m s <sup>-1</sup> )	Adopted, based on GENx-1B70
Jet core exit velocity “hot jet velocity,” $v_e$	401.92 (m s <sup>-1</sup> )	Adopted, based on GENx-1B70
Initial airflow velocity, $v_0$	0 (m s <sup>-1</sup> )	Static; still air at start with no wind and airplane stationary
Core air exhaust flow rate, $\dot{m}_e$	130.663 (kg s <sup>-1</sup> )	Calculated Eq. (S.154)
Takeoff thrust from fan, $T_F$	243,291 (N)	Calculated Eq. (S.154)
Takeoff thrust from jet core, $T_{JC}$	52,516 (N)	Calculated Eq. (S.154)

Note that using these results in Eq. (S.155) yields a scaling factor of ~82.2% of the total takeoff thrust coming from the ducted fan, which relates very well to research done by [57,224,227].

**Eq. (S.155)**

$$F_{T,DF_{TF}} [\%] = \frac{T_F [N]}{T_{TO,FF,i} [N]}$$

### 1.C.2.D.2. Thrust-to-weight ratio

An increase in aircraft weight decreases both aircraft performance and fuel economy, and the TWR is one of the most important parameters affecting aircraft performance [129,227]. Airplanes with a higher TWR can accelerate more quickly, climb more rapidly, sustain higher turn rates, and reach higher maximum speeds [129]. It is important to note, however, that an airplane’s TWR is not constant throughout all phases of flight for several reasons. First, as the airplane consumes fuel, the weight of the airplane decreases. Second, the required engine thrust varies with altitude and velocity. Consequently, it is critical to consider the TWR at takeoff conditions when designing the number and size of engines required for a specific airframe [129]. One should also note that the TWR is used for jet aircraft whereas “power loading” is used for propeller (“prop”) aircraft, of which the inverse is the PWR [129]. In flight, the two ratios can be related for a turboprop aircraft using the propulsion efficiency and airplane velocity as shown in Eq. (S.156). However, this relationship does not apply to takeoff where, at start, static thrust

exists but the airplane's velocity is zero and the air ahead of the propeller must be accelerated from stationary [129].

**Eq. (S.156)**

$$\frac{T[N]}{W[N]} = \frac{\eta_{TP,P}[-]}{v \left[ \frac{m}{s} \right]} \cdot \frac{P[W]}{W[N]}$$

The TWR is generally quoted as the ratio of the maximum static takeoff thrust at sea-level to the MTOW and, for jets, is typically in the range of 0.25 to 0.40 [129,228]. For example, a Boeing 747-400 has a TWR of 0.27 [229]. In order to be consistent across the entire analysis of all vehicle platforms, we calculate a TWR for both the “gross weight” and “curb weight” scenarios according to Eq. (S.157) and Eq. (S.158).

**Eq. (S.157)**

$$TWR_{TO,FF,g} \left[ \frac{N}{N} \right] = \frac{T_{TO,FF,i} \left[ \frac{N}{engine} \right] \cdot n_e [engines]}{m_{g,FF} [kg] \cdot g \left[ \frac{m}{s^2} \right]}$$

**Eq. (S.158)**

$$TWR_{TO,FF,c} \left[ \frac{N}{N} \right] = \frac{T_{TO,FF,i} \left[ \frac{N}{engine} \right] \cdot n_e [engines]}{m_{c,FF} [kg] \cdot g \left[ \frac{m}{s^2} \right]}$$

### 1.C.2.D.3. Relating takeoff thrust and power

As discussed in Section 1.C.2.D.2, when considering new variants of a specific aircraft design, it is imperative that the TWR is either met or exceeded (Eq. (S.159), Eq. (S.160)) in order to maintain takeoff capability as well as other performance characteristics.

**Eq. (S.159)**

$$TWR_{TO,FF,g} \left[ \frac{N}{N} \right] \leq \begin{cases} TWR_{TO,BE,g} \left[ \frac{N}{N} \right] \\ TWR_{TO,HFC,g} \left[ \frac{N}{N} \right] \end{cases}$$

**Eq. (S.160)**

$$TWR_{TO,FF,c} \left[ \frac{N}{N} \right] \leq \begin{cases} TWR_{TO,BE,c} \left[ \frac{N}{N} \right] \\ TWR_{TO,HFC,c} \left[ \frac{N}{N} \right] \end{cases}$$

This requirement is complicated by our desire to switch from FF turbofan engines to an all-electric system, sometimes referred to in the literature as “Universally-Electric Systems

Architecture” or “universally-electric architecture” [230,231]. Two methods by which this can be theoretically be achieved is by using propellers or ducted fans.

Props are best suited (i.e., most efficient) where they can accelerate a high mass of air to a low velocity (e.g., at lower altitude where the air density is higher and at lower speeds) as opposed to jets that accelerate a relatively low mass of air to a high velocity (e.g., at higher altitude where the air density is lower and drag is lower) [226,232]. At speeds above Mach 0.5 (~166 m s<sup>-1</sup>), propeller efficiency decreases [233]. NASA’s Pathfinder solar-electric aircraft used propellers at over 21,300 m (70,000 ft) altitude and its Helios Prototype achieved 29,524 m (96,863 ft) [234,235]. However, these experimental aircraft are exceptionally lightweight, the Helios having a gross weight of just 726 kg [235]. Such lightweight high-altitude aircraft are not suited for long distance transport operations.

Ducted fans are propellers mounted within a cylindrical shroud, or “duct,” that prevents losses in thrust from the tips of the propeller; they have more and shorter blades than propellers and can operate at higher rotational speeds [236]. Some recent proposals for all-electric transport aircraft call for using ducted fans run by High-Temperature Super-conducting (HTS) electric motors [230,237,238]. Airbus has recently test flown a two-seater electric airplane using ducted fans [239].

We consider replacing turboprops with all-electric driven props and turbofan engines with ducted fans driven by electric motors. An analysis on a notional BE or HFC airliner will therefore require estimates of the characteristics of suitable all-electric driven ducted fans. Research from NASA has already covered this topic.

As a part of NASA’s Glenn Research Center Program in High Power Density motors for Aeropropulsion, Brown et al. conducted weight comparisons of motors, engines, fuel cells, and gearboxes [57]. Using proprietary data for large turbofan engines, they determined that the “engine weight less propulsor [klb]” (*y*) is related to the “effective replacement shaft power [khp]” (*x*) shown by Eq. (S.161).

**Eq. (S.161)**

$$y[klb] = 0.1439 \cdot (x[khp])^{0.9108}$$

The “engine weight less propulsor” includes the jet core and associated FF components, so subtracting this value from the total mass of a turbofan engine will yield the mass of the ducted fan (or “propulsor components”) that remain. In other words, the “propulsor” mass is the mass of the turbofan engine with all of its FF components stripped away. To find this value, we must first calculate the “effective replacement shaft power,” which we also need to properly size the electric motors used to spin the ducted fan.

Brown et al. determined that, for jet engines between 15,000 and 100,000 lbf (66,700 to 444,800 N) thrust, the power supplied to the fan at takeoff rotation (Mach 0.25) is 0.97 times the total engine sea-level static thrust (Eq. (S.162)).

**Eq. (S.162)**

$$P_{F,TO,FF}[hp] = 0.97 \left[ \frac{hp}{lbf} \right] \cdot T_{TO,FF,tot}[lbf]$$

Using unit conversions of 1 hp = 745.7 W and 1 lbf = 4.44822 N, we can rewrite Eq. (S.162) as Eq. (S.163).



**Eq. (S.163)**

$$P_{F,TO,FF} [W] = 162.6108 \left[ \frac{W}{N} \right] \cdot T_{TO,FF,tot} [N]$$

However, this relationship is between fan power and the total thrust of a FF turbofan with both a ducted fan and jet core. Brown et al. note that the jet thrust, which does not exist for an electric motor-driven fan, accounts for ~20% of the total thrust at takeoff (~17.8% as we determined in Section 1.C.2.D.1 above for the GENx-2B67 engine). “If an electric motor were to drive the fan used in a particular turbofan engine (at the same speed and with the same torque), the resulting thrust would be lower than the total thrust of the turbofan including its jet” [57]. Therefore, to use the power-thrust relationship shown in Eq. (S.162) and Eq. (S.163), we must account that only 80% of the thrust of a turbofan comes from the fans at takeoff (Eq. (S.164)). (Note that we could use 82.2% here, as estimated for the GENx-2B67 engines, but we elect to use Brown et al.’s general estimate of 80% in order to apply the same analysis across multiple aircraft without requiring specific data on other turbofan engines.)

**Eq. (S.164)**

$$0.8 \cdot T_{TO,FF,tot} [N] = T_{TO,FF,Only} [N]$$

Combining Eq. (S.163) and Eq. (S.164) yields Eq. (S.165), which directly relates the power supplied to a ducted fan at takeoff to the ducted fan’s thrust alone (i.e., no longer the total turbofan engine thrust).

**Eq. (S.165)**

$$P_{F,TO,FF} [W] = 162.6108 \left[ \frac{W}{N} \right] \cdot \frac{T_{TO,FF,Only} [N]}{0.8}$$

Since  $\frac{1}{0.8} = 1.25$ , Eq. (S.165) can just as easily be written as Eq. (S.166) or Eq. (S.167).

**Eq. (S.166)**

$$P_{F,TO,FF} [W] = 1.25 \cdot \left( 162.6108 \left[ \frac{W}{N} \right] \cdot T_{TO,FF,Only} [N] \right) = 203.264 \left[ \frac{W}{N} \right] \cdot T_{TO,FF,Only} [N]$$

**Eq. (S.167)**

$$T_{TO,FF,Only} [N] = \frac{P_{F,TO,FF} [W]}{203.264 \left[ \frac{W}{N} \right]}$$

If all-electric ducted fans in either a BE or an HFC variant provide the same thrust required for takeoff as the original FF turbofans, then  $T_{TO,electric}$  (either  $T_{TO,BE}$  or  $T_{TO,HFC}$ ) must have the same value as  $T_{TO,FF,tot}$ . Thus, Eq. (S.166) can be rewritten as Eq. (S.168) to show the all-electric ducted fan power required for a given takeoff thrust. This is what Brown et al. calls the “effective replacement shaft power.”

**Eq. (S.168)**

$$P_{F,TO,electric}[W] = 203.264 \left[ \frac{W}{N} \right] \cdot T_{TO,electric}[N]$$

To relate the all-electric effective replacement shaft power required for takeoff thrust to the power supplied to the fan component of a FF turbofan engine that produces the same takeoff thrust, we combine Eq. (S.163) with Eq. (S.168) and  $T_{TO,electric}[N] = T_{TO,FF,tot}[N]$  as shown by Eq. (S.169) through Eq. (S.172).

**Eq. (S.169)**

$$P_{F,TO,FF}[W] = 162.6108 \left[ \frac{W}{N} \right] \cdot T_{TO,FF,tot}[N]$$

**Eq. (S.170)**

$$T_{TO,electric}[N] = T_{TO,FF,tot}[N] = \frac{P_{F,TO,electric}[W]}{203.264 \left[ \frac{W}{N} \right]}$$

**Eq. (S.171)**

$$P_{F,TO,FF}[W] = 162.6108 \left[ \frac{W}{N} \right] \cdot \frac{P_{F,TO,electric}[W]}{203.264 \left[ \frac{W}{N} \right]}$$

**Eq. (S.172)**

$$P_{F,TO,electric}[W] = 1.25 \cdot (P_{F,TO,FF}[W])$$

This derivation explains the finding made by Brown et al. – that the “replacement effective power output” of a turbofan engine is 1.25 times the fan power, and that “this power reasonably represents the power that a motor would have to produce to give the same thrust as a turbine engine” [57].

As an example, let us consider the Boeing 747-8 with its four GENx-2B67 engines capable of producing a total static thrust of 1,183,227 N. If we imagine that we have either a BE or an HFC aircraft of the same mass and volume and we want all-electric ducted fans capable of producing the same amount of thrust for takeoff, we can substitute 1,183,227 N into Eq. (S.165) for  $T_F$ , which reveals that a power supply of 240,506,893 W is required for equivalent takeoff capability. To check, using the total static thrust of 1,183,227 N in Eq. (S.163) yields a fan power of 192,405,514 W, 1.25 times which equals 240,506,893 W, and this upholds Eq. (S.169).

As Brown et al. notes: “the published weights of turbine engines usually include the ‘propulsor,’ that is, the propulsive fan and related components such as the fan frame, brackets, supports, exit guide vanes and containment” [57]. Thus, “the first step in making an appropriate comparison of motors and turbofan engines... is to subtract the propulsor weight from the total weight of a turbofan engine” [57]. This will give us the weight of the engine less the jet core, but we will later have to add in electric motors needed to drive the fan shaft.

Having calculated the “replacement effective power output” as 240,506,861 W, 1/4<sup>th</sup> of which is 60,126,715 W or (80.631 khp), we can return to Eq. (S.161) and calculate the “engine weight less propulsor [klb]” per GENx-2B67 engine (Eq. (S.173)).

**Eq. (S.173)**

$$y[klb] = 0.1439 \cdot (80.631[khp])^{0.9108} = 7.8434[klb] = 3,557.71[kg]$$

Since the original mass of the GENx-2B67 turbofan engine is 5,623 kg (see Section 1.C.1.D.4) and there are four engines on the airplane, the total mass of turbofan engines can be calculated using Eq. (S.174), and the total mass of propulsor components across the four engines can be calculated using Eq. (S.175).

**Eq. (S.174)**

$$m_e \left[ \frac{kg}{engine} \right] \cdot n_e [engines] = 5,623 \left[ \frac{kg}{engine} \right] \cdot 4 [engines] = 22,492[kg]$$

**Eq. (S.175)**

$$3,557.71 \left[ \frac{kg}{engine} \right] \cdot 4 [engines] = 14,231[kg]$$

The “engine weight less propulsor” includes the jet core and associated FF components, so subtracting the result of Eq. (S.173) from the total mass of GENx-2B67 turbofan engines found in Eq. (S.174) yields the mass of the ducted fans (or “propulsor components”) of the GENx-2B67 engines after having stripped away all FF components (Eq. (S.176)).

**Eq. (S.176)**

$$22,492[kg] - 14,231[kg] = 8,261[kg]$$

It is interesting to note here that the structure and ducted fan portion is just ~37% of the overall turbofan engine’s mass while the jet core and associated FF components is ~63%.

Our analysis will require the ability to change the thrust and weight of an all-electric airplane such that the TWR is either met or exceeded when compared to the original FF variant. For example, if a BE airplane design weighs more than the original FF variant, we must increase the design takeoff thrust until we can achieve the appropriate TWR. Increasing the takeoff thrust requires increasing the engine size, and its mass, which in turn increases the mass (and weight) of the aircraft. Eq. (S.161) only relates the effective replacement power output to the engine weight less propulsor, but what we need for this analysis is a way to calculate the mass of the propulsor based upon a desired thrust. Fortunately, Brown et al. also published a linear regression equation that relates “takeoff thrust at sea-level [klb]” (x) to “total engine weight [klb]” (y) for the range of turbofan engines that they studied (Eq. (S.177)). (Note that units for thrust are technically klbf and units of “weight” are klbm.)

**Eq. (S.177)**

$$y[klb] = 0.2446 \cdot (x[klb])^{0.9108}$$

To proceed with our analysis, we created Table S.15 using a *notional* set of engines to further investigate the relationships described by [57] within the range of engines they considered and the mathematical relationships they developed. We convert all units to SI and develop a ratio of thrust achieved by ducted fans only to the mass of propulsor components.

**Table S.15. Analysis of the relationships presented by Brown et al. and development of a relationship between ducted fan thrust and propulsor mass**

Takeoff thrust, $T_{TO,FF,tot}$ or $T_{TO,electric}$ (N)	FF turbofan total engine mass (kg)	Thrust achieved by fan only in turbofan engine, $T_{TO,FF,Fonly}$ (N)	Power supplied to fan in FF turbofan engine $P_{F,TO,FF}$ (W)	All-electric replacement effective power output to achieve takeoff thrust, $P_{F,TO}$ (W)	Engine mass less propulsor (kg)	Propulsor mass (kg)	Ratio of propulsor mass to total FF turbofan engine mass ( $kg\ kg^{-1}$ )	Ratio of thrust achieved by all-electric fan only to propulsor mass ( $N\ kg^{-1}$ )
66,723	1,307	53,379	10,849,935	13,562,419	916	391	0.30	136.66
88,964	1,699	71,172	14,466,580	18,083,225	1,191	508	0.30	140.21
111,206	2,081	88,964	18,083,225	22,604,031	1,459	622	0.30	143.03
133,447	2,457	106,757	21,699,870	27,124,838	1,723	734	0.30	145.37
155,688	2,828	124,550	25,316,515	31,645,644	1,983	845	0.30	147.39
177,929	3,194	142,343	28,933,160	36,166,450	2,239	954	0.30	149.15
200,170	3,555	160,136	32,549,805	40,687,256	2,493	1,062	0.30	150.73
222,411	3,913	177,929	36,166,450	45,208,063	2,744	1,169	0.30	152.15
244,652	4,268	195,722	39,783,095	49,728,869	2,993	1,275	0.30	153.45
266,893	4,620	213,515	43,399,740	54,249,675	3,240	1,381	0.30	154.65
289,134	4,970	231,307	47,016,385	58,770,481	3,485	1,485	0.30	155.75
311,375	5,317	249,100	50,633,030	63,291,288	3,728	1,589	0.30	156.79
333,617	5,661	266,893	54,249,675	67,812,094	3,970	1,692	0.30	157.75
355,858	6,004	284,686	57,866,320	72,332,900	4,210	1,794	0.30	158.67
378,099	6,345	302,479	61,482,965	76,853,706	4,449	1,896	0.30	159.53
400,340	6,684	320,272	65,099,610	81,374,513	4,687	1,997	0.30	160.34
422,581	7,022	338,065	68,716,255	85,895,319	4,923	2,098	0.30	161.12
444,822	7,357	355,858	72,332,900	90,416,125	5,159	2,199	0.30	161.86
295,807	5,074	236,645	48,101,379	60,126,723	3,558	1,516	0.30	156.07
1,183,227	20,296	946,581	192,405,514	240,506,893	14,231	6,065	0.30	156.07

The red text is data specific to GENx-2B67 engines (the first row being one engine and the second row four engines). Note that the engine mass less propulsor is the same as found using Eq. (S.175), but the actual mass of the GENx-2B67 engine is ~11% greater than that suggested by Brown et al. (5,623 kg as opposed to 5,074 kg). The GENx-2B67 engine was actually introduced after Brown et al.’s work was published. Also note that the ratio of propulsor mass to FF turbine mass matches Brown et al.’s statement that “the average fraction of total engine weight represented by the propulsor components is 30 percent” [57]. Furthermore, note that the ratio of thrust achieved by the ducted fan only to propulsor mass changes, i.e., the relationship is non-linear. We can also see this by plotting the results as shown in Fig. S.3.

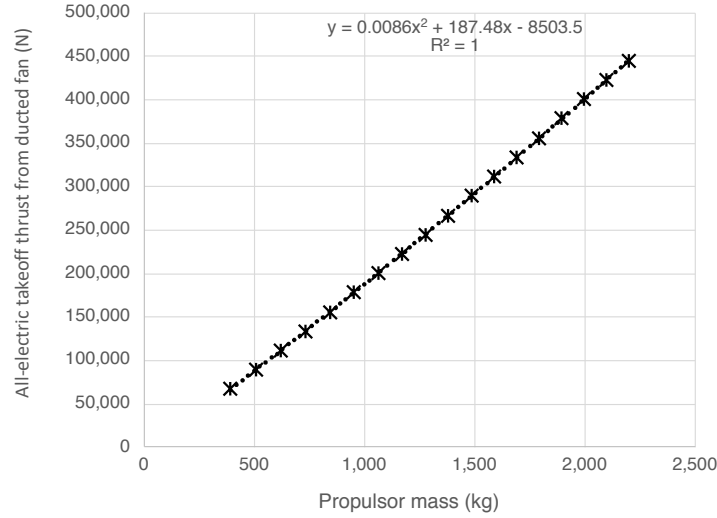


**Fig. S.3. Thrust achieved by fan only vs propulsor mass, second-order polynomial regression**

However, the values in Fig. S.3 are already an estimation, and, as shown in Fig. S.4, a simple linear regression of the data achieves an acceptable coefficient of multiple determination for multiple regression (R-squared value) of 0.9996. Thus, to keep our analysis linear, we proceed using the relationship developed in Fig. S.4 and shown by Eq. (S.178) and Eq. (S.179).

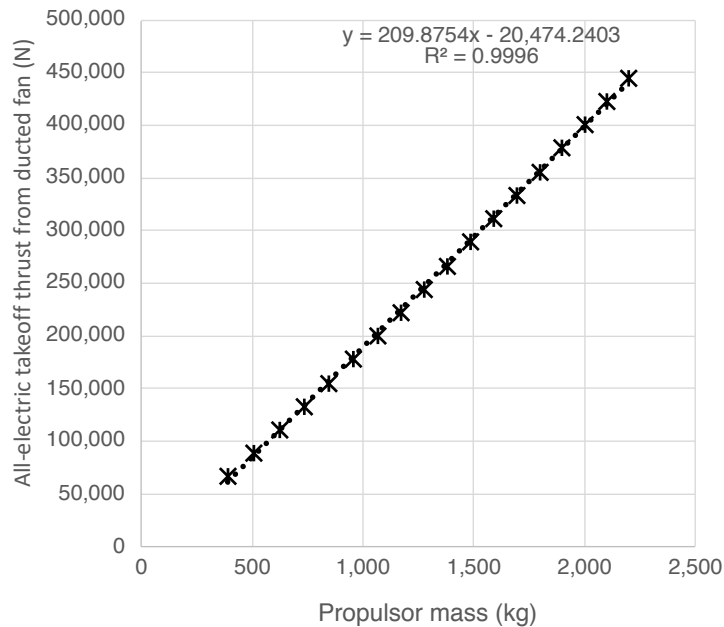


**Fig. S.4. Thrust achieved by fan only vs propulsor mass, linear regression**

**Eq. (S.178)**

$$T_{TO,electric} [N] = 209.8754 \left[ \frac{N}{kg} \right] \cdot m_{PC} [kg] + (-20,474.2403 [N])$$

**Eq. (S.179)**

$$m_{PC} [kg] = \frac{T_{TO,electric}[N] - (-20,474[N])}{209.8754 \left[ \frac{N}{kg} \right]}$$

With this relationship now developed, we can return to Eq. (S.159) and Eq. (S.160) in Section 1.C.2.D.3. In order to get Eq. (S.159) and Eq. (S.160) into terms of two unknown variables,  $m_m[kg]$  and either  $m_B[kg]$  (for BE variants) or  $m_{H_2storage}[kg]$  (for HFC variants), we must take one further series of steps. Eq. (S.180) combines Eq. (S.167) and Eq. (S.178) to relate the ducted fan (propulsor) mass to both fan power and fan thrust.

**Eq. (S.180)**

$$T_{TO,electric}[N] = \frac{P_{F,TO,electric}[W]}{203.264 \left[ \frac{W}{N} \right]} = 209.8754 \left[ \frac{N}{kg} \right] \cdot m_{PC} [kg] + (-20,474.2403[N])$$

We henceforth assign  $203.264 \left[ \frac{W}{N} \right] = \frac{P_{F,TO,electric}[W]}{T_{TO,electric}[N]}$  as  $R_{DFTOP\_TOT} \left[ \frac{W}{N} \right]$ , the “ratio of electric ducted fan takeoff power to takeoff thrust.” We rewrite Eq. (S.180) as Eq. (S.181) to relate the power necessary to generate the takeoff thrust required to the mass of propulsor components in the equation of a line format,  $y = m \cdot x + b$ .

**Eq. (S.181)**

$$m_{PC} [kg] = 0.0000234 \left[ \frac{kg}{W} \right] \cdot P_{F,TO,electric}[W] + 97.55[kg]$$

We now assign  $0.0000234 \left[ \frac{kg}{W} \right]$  as  $c_m$ , the “slope constant” and  $97.55[kg]$  as  $c_b$ , the “y-intercept constant” in our “propulsor component mass – fan power at takeoff” line. Since we want to relate the mass of electric motors necessary to produce sufficient shaft power for the ducted fans to produce the required takeoff thrust, we can write Eq. (S.182).

**Eq. (S.182)**

$$P_{F,TO,electric}[W] = m_m[kg] \cdot PWR_{m,c} \left[ \frac{W}{kg} \right]$$

Combining Eq. (S.181) and Eq. (S.182) yields a relationship between the propulsor mass and the mass of motors required (Eq. (S.183)).

**Eq. (S.183)**

$$m_{PC} [kg] = \left( c_m \left[ \frac{kg}{W} \right] \cdot m_m[kg] \cdot PWR_{m,c} \left[ \frac{W}{kg} \right] \right) + c_b[kg]$$

Combining Eq. (S.180) and Eq. (S.182) yields a relationship between takeoff thrust and the mass of motors required (Eq. (S.184)).

**Eq. (S.184)**

$$T_{TO,electric}[N] = \frac{m_m[kg] \cdot PWR_{m,c} \left[ \frac{W}{kg} \right]}{R_{DFTOP\_TOT} \left[ \frac{W}{N} \right]}$$

#### **1.C.2.D.4. Cruising range of the fossil fuel variant**

$(CR_{FF})$

Recall that we already recorded the maximum range for the aircraft platforms in Section 1.C.1.G.3. However, it will become important later in the analysis to have an understanding of the mathematical relationships that led to these values. Similar to the improved approximation for estimating range in rotary-wing aircraft, we can use the Breguet range equation, named for French aviation pioneer Louis Charles Breguet, to consider the range of FF fixed-wing aircraft that consume fuel during flight [240,241]. We present here our own derivation of the Breguet range equation for jet aircraft (where engine data is in terms of thrust) because it is important to understand the underlying assumptions that make this formulation acceptable and also because we will need to consider the derivation of a range equations for turboprop airplanes (where engine data is in terms of power) and all-electric airplanes (where power is delivered by electric motors).

We begin by assuming steady, level flight with no wind and constants for velocity, lift coefficient, drag coefficient, and specific fuel consumption, i.e., the plane is at “cruise.” Range depends upon the amount (weight) of fuel onboard, the rate at which the airplane burns that fuel, and the thrust the engines produce from burning the fuel. Since the airplane releases waste products from fuel combustion to the atmosphere, the weight of the aircraft decreases during flight. Thus, the weight of the aircraft is a function of time (Eq. (S.185)):

**Eq. (S.185)**

$$W(t)[N]$$

We can express the rate of change of the aircraft’s weight during cruise as Eq. (S.186):

**Eq. (S.186)**

$$\frac{dW(t)[N]}{dt[s]}$$

The Thrust Specific Fuel Consumption (TSFC) is the mass of fuel consumed per unit time (mass flow rate) per unit thrust (T) produced (Eq. (S.187)). For reference, the cruising TSFC is  $\sim 3.09 \times 10^{-5} \text{ kg s}^{-1} \text{ N}^{-1}$  for a Boeing 737-700 NG and  $\sim 3.06 \times 10^{-5} \text{ kg s}^{-1} \text{ N}^{-1}$  for the Boeing 747-8 [242,243].

**Eq. (S.187)**

$$TSFC = \left[ \frac{kg}{s} \right] \left[ \frac{1}{N} \right]$$

When multiplied by gravity (i.e., converting the mass of fuel consumed to the weight of fuel consumed), the units become:

**Eq. (S.188)**

$$TSFC \left[ \frac{kg}{N} \right] \cdot g \left[ \frac{m}{s^2} \right] = (TSFC \cdot g) \left[ \frac{1}{s} \right]$$

Since the weight of the airplane decreases as it burns fuel, we can relate Eq. (S.186) and Eq. (S.188) applying a negative to the equation (to either side) and introducing the amount of thrust produced by the engines (Eq. (S.189)).

**Eq. (S.189)**

$$\frac{dW(t)[N]}{dt[s]} = -TSFC \left[ \frac{kg}{N} \right] \cdot g \left[ \frac{m}{s^2} \right] \cdot T[N]$$

At cruise, the plane is flying at a constant velocity and altitude; it is neither accelerating nor climbing. Thus, forces acting on the plane are in equilibrium with no net force acting upon it. As illustrated in Fig. S.5, lift ( $L$ ) is equal in magnitude and opposite in direction of weight ( $W$ ), whereas thrust ( $T$ ) is equal and opposite of drag ( $D$ ).

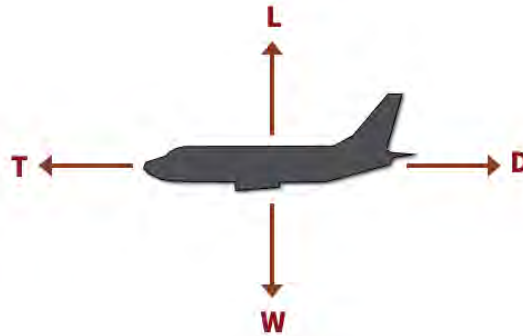


**Fig. S.5. Forces acting on an airplane flying at constant velocity and altitude**

Since thrust is equal to drag in magnitude, we can rewrite Eq. (S.189) as Eq. (S.190).

**Eq. (S.190)**

$$\frac{dW(t)[N]}{dt[s]} = -TSFC \left[ \frac{kg}{N} \right] \cdot g \left[ \frac{m}{s^2} \right] \cdot D[N]$$

A common metric for airplane performance is the lift-to-drag ratio ( $L/D$ ). At cruise, the following relationship is true:



**Eq. (S.191)**

$$\frac{L}{D} = \frac{W}{T}$$

Note that, at cruise, we are interested in the inverse of the TWR, whereas the TWR itself is our major concern at takeoff. However, the thrust requirement at takeoff is much higher than that required at cruise, as previously shown in Table S.12, so the two metrics are not directly related.

We can introduce the inverse of the L/D ratio into our derivation as shown by Eq. (S.192).

**Eq. (S.192)**

$$\frac{dW(t)[N]}{dt[s]} = -TSFC \left[ \frac{kg}{s} \right] \cdot g \left[ \frac{m}{s^2} \right] \cdot \frac{D[N]}{L[N]} \cdot L[N]$$

Since lift is equal to weight at cruise, we can replace a lift term with weight as in Eq. (S.193).

**Eq. (S.193)**

$$\frac{dW(t)[N]}{dt[s]} = -TSFC \left[ \frac{kg}{s} \right] \cdot g \left[ \frac{m}{s^2} \right] \cdot \frac{D[N]}{L[N]} \cdot W[N]$$

Now, we need to introduce range, or the change in distance “x” into the equation. Multiplying either side by  $\frac{dx}{dx} = 1$  does nothing to the result:

**Eq. (S.194)**

$$\frac{dx[m]}{dx[m]} \cdot \frac{dW(t)[N]}{dt[s]} = -TSFC \left[ \frac{kg}{s} \right] \cdot g \left[ \frac{m}{s^2} \right] \cdot \frac{D[N]}{L[N]} \cdot W[N]$$

Rearranging terms:

**Eq. (S.195)**

$$\frac{dx[m]}{dt[s]} \cdot \frac{dW(t)[N]}{dx[m]} = -TSFC \left[ \frac{kg}{s} \right] \cdot g \left[ \frac{m}{s^2} \right] \cdot \frac{D[N]}{L[N]} \cdot W[N]$$

Note that  $\frac{dx[m]}{dt[s]}$  is the change in distance per change in time, which is velocity (v). The  $dx[m]$  that remains is our distance, or “cruising range (CR),” so we can further rewrite the equation as Eq. (S.196) and Eq. (S.197).

**Eq. (S.196)**

$$v \left[ \frac{m}{s} \right] \cdot \frac{dW(t)[N]}{dx[m]} = -TSFC \left[ \frac{kg}{N} \right] \cdot g \left[ \frac{m}{s^2} \right] \cdot \frac{D[N]}{L[N]} \cdot W[N]$$

**Eq. (S.197)**

$$dx[m] = CR[m] = \frac{dW(t)[N]}{W[N]} \cdot \frac{L[N]}{D[N]} \cdot \frac{v \left[ \frac{m}{s} \right]}{-TSFC \left[ \frac{kg}{N} \right] \cdot g \left[ \frac{m}{s^2} \right]}$$

Integrating from the initial (*i*) to final (*f*) points of cruise:

**Eq. (S.198)**

$$\int_i^f dx[m] = \int_i^f \frac{dW(t)[N]}{W[N]} \cdot \frac{L[N]}{D[N]} \cdot \frac{v \left[ \frac{m}{s} \right]}{-TSFC \left[ \frac{kg}{N} \right] \cdot g \left[ \frac{m}{s^2} \right]}$$

**Eq. (S.199)**

$$\int_i^f dx[m] = \left( \frac{L[N]}{D[N]} \cdot \frac{v \left[ \frac{m}{s} \right]}{-TSFC \left[ \frac{kg}{N} \right] \cdot g \left[ \frac{m}{s^2} \right]} \right) \cdot \int_i^f \frac{dW(t)[N]}{W[N]}$$

**Eq. (S.200)**

$$(x_f - x_i)[m] = \left( \frac{L[N]}{D[N]} \cdot \frac{v \left[ \frac{m}{s} \right]}{-TSFC \left[ \frac{kg}{N} \right] \cdot g \left[ \frac{m}{s^2} \right]} \right) \cdot (\ln W_f[N] - \ln W_i[N])$$

Moving the negative, applying the quotient rule for natural logarithms, and changing Newtons to its base units of  $\left[ \frac{kg \cdot m}{s^2} \right]$  gives us Eq. (S.201) and Eq. (S.202).

**Eq. (S.201)**

$$(x_f - x_i)[m] = \left( \frac{L[N]}{D[N]} \cdot \frac{v \left[ \frac{m}{s} \right]}{TSFC \left[ \frac{kg}{N} \right] \cdot g \left[ \frac{m}{s^2} \right]} \right) \cdot (-\ln W_f[N] + \ln W_i[N])$$

**Eq. (S.202)**

$$CR[m] = \left( \frac{v \left[ \frac{m}{s} \right]}{TSFC \left[ \frac{kg}{N} \right] \cdot g \left[ \frac{m}{s^2} \right]} \right) \cdot \left( \frac{L[N]}{D[N]} \right) \cdot \ln \left( \frac{W_i[N]}{W_f[N]} \right)$$

Eq. (S.202) gives us a convenient way to estimate the jet aircraft's range if we only consider travel at cruise conditions.

As mentioned earlier, ratings for propeller aircraft engines are in terms of power, and the derivation of a range equation is therefore slightly different [244]. Since the derivation is different and we will need the Breguet range equation to estimate the L/D ratio for prop planes, we present our own derivation below.

Instead of using the TSFC (Eq. (S.203)), we must use the Power Specific Fuel Consumption (PSFC), as in Eq. (S.204).

**Eq. (S.203)**

$$TSFC \left[ \frac{kg}{N} \right] \cdot g \left[ \frac{m}{s^2} \right] = (TSFC \cdot g) \left[ \frac{1}{s} \right]$$

**Eq. (S.204)**

$$PSFC \left[ \frac{kg}{W} \right] \cdot g \left[ \frac{m}{s^2} \right]$$

Since the base units for a watt are  $\left[ \frac{kg \cdot m^2}{s^3} \right]$ , we can simplify the units from Eq. (S.204) to those in Eq. (S.205).

**Eq. (S.205)**

$$PSFC \left[ \frac{\frac{kg}{s}}{\frac{kg \cdot m^2}{s^3}} \right] \cdot g \left[ \frac{m}{s^2} \right] = (PSFC \cdot g) \left[ \frac{1}{m} \right]$$

Also, for propeller aircraft, the relationship between power and thrust is based on the turboprop propulsion efficiency and velocity:

**Eq. (S.206)**

$$\eta_{TP,P}[-] \cdot P[W] = T[N] \cdot v \left[ \frac{m}{s} \right]$$

We show a quick check on base units in Eq. (S.207).

**Eq. (S.207)**

$$\eta_{TP,P}[-] \cdot P \left[ \frac{kg \cdot m^2}{s^3} \right] = T \left[ \frac{kg \cdot m}{s^2} \right] \cdot v \left[ \frac{m}{s} \right]$$

Again, we assume that, in cruise at constant velocity and altitude, thrust is equal in magnitude to drag. Therefore, we can replace thrust with drag in Eq. (S.206) to find an expression for power (Eq. (S.208)).

**Eq. (S.208)**

$$P[W] = \frac{D[N] \cdot v \left[ \frac{m}{s} \right]}{\eta_{TP,P}[-]}$$

At this point, we can follow the same derivation process we previously did for jet aircraft. Since the airplane burns fuel and releases the by-products of combustion to the atmosphere, the weight of the aircraft decreases during flight, and the weight of the aircraft is a function of time (Eq. (S.209) and Eq. (S.210)).

**Eq. (S.209)**

$$W(t)[N]$$

**Eq. (S.210)**

$$\frac{dW(t)[N]}{dt[s]}$$

In propeller airplanes, the change of weight over time (a decrease, so with a negative applied) is a function of the PSFC and the power (constant) applied during cruise (Eq. (S.211)).

**Eq. (S.211)**

$$\frac{dW(t)[N]}{dt[s]} = -PSFC \left[ \frac{\frac{kg}{s}}{\frac{kg \cdot m^2}{s^3}} \right] \cdot g \left[ \frac{m}{s^2} \right] \cdot P[W]$$

Again, we can check this step of our derivation by checking if base units balance (Eq. (S.212)).

**Eq. (S.212)**

$$\frac{dW(t) \left[ \frac{kg \cdot m}{s^2} \right]}{dt[s]} = -(PSFC \cdot g) \left[ \frac{1}{m} \right] \cdot P \left[ \frac{kg \cdot m^2}{s^3} \right]$$

Now, we can conveniently replace the power term and introduce drag into our derivation using Eq. (S.208) to get Eq. (S.213).

**Eq. (S.213)**

$$\frac{dW(t)[N]}{dt[s]} = -(PSFC \cdot g) \left[ \frac{1}{m} \right] \cdot \frac{D[N] \cdot v \left[ \frac{m}{s} \right]}{\eta_{TP,P}[-]}$$

Additionally, we can introduce the inverse of the L/D ratio at cruise into our derivation by simultaneously adding a lift term, which cancels with the lift term in the L/D ratio to leave drag (Eq. (S.214)).

**Eq. (S.214)**

$$\frac{dW(t)[N]}{dt[s]} = -(PSFC \cdot g) \left[ \frac{1}{m} \right] \cdot \frac{v \left[ \frac{m}{s} \right]}{\eta_{TP,P}[-]} \cdot \frac{D[N]}{L[N]} \cdot L[N]$$

Since lift is equal in magnitude to weight at cruise, we can replace a lift term with weight (Eq. (S.215)).

**Eq. (S.215)**

$$\frac{dW(t)[N]}{dt[s]} = -(PSFC \cdot g) \left[ \frac{1}{m} \right] \cdot \frac{v \left[ \frac{m}{s} \right]}{\eta_{TP,P}[-]} \cdot \frac{D[N]}{L[N]} \cdot W[N]$$

As with the helicopters and jet airplanes, we can now introduce range into our derivation as shown by Eq. (S.216).

**Eq. (S.216)**

$$\frac{dx[m]}{dx[m]} \cdot \frac{dW(t)[N]}{dt[s]} = -(PSFC \cdot g) \left[ \frac{1}{m} \right] \cdot \frac{v \left[ \frac{m}{s} \right]}{\eta_{TP,P}[-]} \cdot \frac{D[N]}{L[N]} \cdot W[N]$$

Rearranging terms, we get Eq. (S.217).

**Eq. (S.217)**

$$\frac{dx[m]}{dt[s]} \cdot \frac{dW(t)[N]}{dx[m]} = -(PSFC \cdot g) \left[ \frac{1}{m} \right] \cdot \frac{v \left[ \frac{m}{s} \right]}{\eta_{TP,P}[-]} \cdot \frac{D[N]}{L[N]} \cdot W[N]$$

Note that  $\frac{dx[m]}{dt[s]}$  is the change in distance per change in time, which is our constant velocity ( $v$ ). The  $dx[m]$  that remains is our distance, or “cruising range (CR),” so we can rewrite Eq. (S.217) as Eq. (S.218).

**Eq. (S.218)**

$$v \left[ \frac{m}{s} \right] \cdot \frac{dW(t)[N]}{dx[m]} = -(PSFC \cdot g) \left[ \frac{1}{m} \right] \cdot \frac{v \left[ \frac{m}{s} \right]}{\eta_{TP,P}[-]} \cdot \frac{D[N]}{L[N]} \cdot W[N]$$

Canceling the velocity term from both sides and rearranging to solve for the cruising range gives us Eq. (S.219).

**Eq. (S.219)**

$$dx[m] = CR[m] = \frac{\eta_{TP,P}[-]}{-(PSFC \cdot g) \left[ \frac{1}{m} \right]} \cdot \frac{L[N]}{D[N]} \cdot \frac{dW(t)[N]}{W[N]}$$

Integrating from the initial ( $i$ ) to final ( $f$ ) points of cruise:

**Eq. (S.220)**

$$\int_i^f dx[m] = \int_i^f \frac{\eta_{TP,P}[-]}{-(PSFC \cdot g) \left[ \frac{1}{m} \right]} \cdot \frac{L[N]}{D[N]} \cdot \frac{dW(t)[N]}{W[N]}$$

**Eq. (S.221)**

$$\int_i^f dx[m] = \left( \frac{\eta_{TP,P}[-]}{-(PSFC \cdot g) \left[ \frac{1}{m} \right]} \cdot \frac{L[N]}{D[N]} \right) \cdot \int_i^f \frac{dW(t)[N]}{W[N]}$$

**Eq. (S.222)**

$$(x_f - x_i)[m] = \left( \frac{\eta_{TP,P}[-]}{-(PSFC \cdot g) \left[ \frac{1}{m} \right]} \cdot \frac{L[N]}{D[N]} \right) \cdot (\ln W_f[N] - \ln W_i[N])$$

And finally, moving the negative, applying the quotient rule for natural logarithms, and rearranging terms:

**Eq. (S.223)**

$$(x_f - x_i)[m] = \left( \frac{\eta_{TP,P}[-]}{(PSFC \cdot g) \left[ \frac{1}{m} \right]} \cdot \frac{L[N]}{D[N]} \right) \cdot (-\ln W_f[N] + \ln W_i[N])$$

**Eq. (S.224)**

$$CR[m] = \left( \frac{\eta_{TP,P}[-]}{(PSFC \cdot g) \left[ \frac{1}{m} \right]} \right) \cdot \left( \frac{L[N]}{D[N]} \right) \cdot \ln \left( \frac{W_i[N]}{W_f[N]} \right)$$

Eq. (S.224) gives us a convenient way to estimate a turboprop aircraft's range if we only consider travel at cruise conditions.

#### **1.C.2.D.5. Lift-to-drag ratio**

*(L/D)*

Eq. (S.224) is also useful when we do not know an airplane's typical L/D ratio during cruise. From Section 1.C.1.F.4.B, we know that the average of our assumed range of turboprop efficiency is ~84.5%. We can look up each prop plane's maximum range and weight with full fuel tanks. Manuals report estimates of fuel consumption for engine starting, taxiing, and takeoff; fuel consumption for climbing to a cruising altitude; and fuel consumption for descent. Subtracting the weight of fuel consumed during the takeoff, climbing, and descent phases of flight leaves the fuel remaining for the cruise phase (plus whatever excess is desired for taxiing and reserve).

At this point, only two unknowns remain in Eq. (S.224), the L/D ratio that we are trying to estimate and the PSFC. To find the PSFC, we can use data from tables and charts published in manuals under International Standard Atmosphere (ISA) "standard day" conditions to find the percent torque on, and fuel flow rate to, the engine(s). Applying the percent torque to the maximum torque and relating this to power from the relationship in Eq. (S.38), we can find the power required at cruise for a given RPM and flight conditions. From Eq. (S.204), we know that the PSFC is fuel flow divided by power, so we can solve for the PSFC using Eq. (S.225) [244]. Finally, we can return to Eq. (S.224) and solve for the average L/D ratio.

Eq. (S.225)

$$PSFC \left[ \frac{s^2}{m^2} \right] = \frac{fuel\ flow \left[ \frac{kg}{s} \right]}{power [W]}$$

In the case of the medium- and long-haul jet airliners, several estimates for the cruising L/D ratio can be found in the literature [245–247]. Table S.16 summarizes typical L/D ratios for different aircraft types as well as for the airplane types we studied.

**Table S.16. Typical L/D ratios for different aircraft types and the airplanes studied in this analysis**

<b>Airplane type, <i>platform</i></b>	<b>Typical L/D ratios</b>	<b>Source</b>
Gliders	20 to 35	[248]
Jets	12 to 20	[248]
<i>Long-haul jet airliner</i>	~17.7	[247]
<i>Medium-haul jet airliner</i>	~17	[245]
General aviation	10 to 15	[248]
Ultralight	8 to 15	[248]
Subsonic military	8 to 11	[248]
<i>Average of prop planes</i>	~8.9	Derived, Section 1.C.2.D.5
Supersonic fighter	5 to 8	[248]
Helicopters	2 to 4	[248]

### 1.C.2.E. Watercraft

#### 1.C.2.E.1. Watercraft dimensions: height, beam, length overall, length at water line, and length between perpendiculars

( $h, L_B, L_{OA}, L_{WL}, L_{PP}$ )

We recorded each watercraft’s dimensions from its manual [60]. The height of a watercraft refers to the distance from the water’s surface to the highest point, generally a mast. This value does not include draft, the distance from the water’s surface to the lowest point of the hull. Neither manuals nor other available documents record height data for cargo ships, so we estimate it using schematics of the ships and ratios of known measurements, averaged, to the unknown height.

The beam is the watercraft’s width at its widest point, sometimes called the “breadth on waterline.” The overall length of a watercraft is its length at its longest point, generally above the water line. For boats that use rub rails for pushing objects in the water, we include them in these dimensions. The length at the waterline is the length from the foremost point on the bow to the aftmost point on the stern where the water surface touches the watercraft’s hull. This value is not readily available for any watercraft, presumably because it changes with a watercraft’s load. To estimate this value for use in future equations, we use Eq. (S.226), which estimates the length at the waterline as equal to 95% of the watercraft’s overall length [186].



**Eq. (S.226)**

$$L_{WL}[m] = 0.95 \cdot L_{OA}[m]$$

The length between perpendiculars is the length between vertical lines drawn at the foremost to aftmost perpendiculars (generally the same point on the bow as the reference for the length at the waterline to the rudder axis on the stern). It is usually slightly less than the waterline length and can be estimated by Eq. (S.227) [186].

**Eq. (S.227)**

$$L_{PP}[m] = 0.97 \cdot L_{WL}[m]$$

For cargo ships, the average overall length and length between perpendiculars are 83.2 m and 78 m, respectively; thus, in the average cargo ship case, the length between perpendiculars is 93.75% of the overall length. Since we have known values for cargo ships, we use them in our analysis. For waterjet boats, however, we estimate the length between perpendiculars using Eq. (S.227).

#### **1.C.2.E.2. Draft, loaded and light**

$(D_{loaded}, D_{light})$

A ship's draft (also spelled draught or abbreviated as D) is defined as the vertical distance from the waterline to the deepest point of the hull within the water [186]. We recorded drafts for each watercraft from the appropriate manuals [60].

For cargo ships, the manuals provide a distinction between light (or "empty") and loaded (or "heavy") values for the draft. This is not the case for waterjet boats where the manuals only cite an operational draft, which we consider as the "loaded" draft. Consequently, we estimate a value for the light draft using Eq. (S.228) (previously unintroduced terms are explained next in Sections 1.C.2.E.3 and 1.C.2.E.4).

**Eq. (S.228)**

$$D_{light}[m] = \frac{\nabla_{light} [m^3]}{C_{B,loaded} [-] \cdot L_{WL}[m] \cdot L_B[m]}$$

#### **1.C.2.E.3. Displacement weight and volume, loaded and light**

$(\Delta_{loaded}, \Delta_{light}, \nabla_{loaded}, \nabla_{light})$

We can measure a ship's displacement in terms of either weight (mass) or volume. When referenced in terms of weight (mass), we use the symbol  $\Delta$ . This value corresponds to the buoyancy force (or the mass used in calculating the buoyancy force). When referenced in terms of volume, we use the symbol  $\nabla$ .

We recorded values for the displacement weight from the manuals as appropriate, which report in terms of either long (imperial) ton or (metric) tonne. To calculate the displacement volume, we use Eq. (S.229) and Eq. (S.230) as well as either the density of fresh water at 15°C (1,000 kg m<sup>-3</sup>) for waterjet boats or the density of sea water at 15°C (1,025 kg m<sup>-3</sup>) for cargo ships, according to primary location of use. Since the manuals for boats do not provide a "light"

displacement weight, we subtract each boat's payload mass from the loaded displacement mass to find an approximate value, as shown by Eq. (S.231).

**Eq. (S.229)**

$$\nabla_{loaded} [m^3] = \frac{\Delta_{loaded} [kg]}{\rho_{water} \left[ \frac{kg}{m^3} \right]}$$

**Eq. (S.230)**

$$\nabla_{light} [m^3] = \frac{\Delta_{light} [kg]}{\rho_{water} \left[ \frac{kg}{m^3} \right]}$$

**Eq. (S.231)**

$$\nabla_{light} [kg] = \Delta_{loaded} [kg] - m_{p,FF} [kg]$$

Sometimes, there are discrepancies in manuals' values. Theoretically, the difference between the loaded displacement weight ("gross") and the light displacement weight ("curb") should be the payload. However, for one cargo ship, this difference would be 3,028,000 kg, which is 67% higher than the reported maximum cargo load of 1,814,368 kg [60]. For one waterjet boat, the manual's value for loaded displacement mass of ~7,300 kg is heavier than the gross vehicle mass reported on the boat's data plate of 6,979 kg (presumably the later value is useful for trailer transport and the former value allows for crew and equipment while in the water) [60]. For this analysis, we use reported values of displacement for the total hull towing resistance calculations rather than gross and curb weights or derived payloads.

#### 1.C.2.E.4. Block coefficient

( $C_B$ )

The block coefficient is a value used to describe the shape of a ship's hull and is defined as the ratio between the displacement volume and the volume of a rectangular cuboid formed by the dimensions of the draft, the length (generally at the waterline but sometimes at perpendiculars), and the beam; values typically range from 0.50 to 0.90 and can be found using the method shown by Eq. (S.232) and Eq. (S.233) [186]. Note that, due to the lack of detailed hull shape data, we model no change to the value of the length at the waterline as the displacement changes. Many other estimates exist for the block coefficient for use when the actual displacement is not known [249].

**Eq. (S.232)**

$$C_{B,loaded}[-] = \frac{\nabla_{loaded} [m^3]}{D_{loaded} [m] \cdot L_{WL} [m] \cdot L_B [m]}$$

**Eq. (S.233)**

$$C_{B,light}[-] = \frac{\nabla_{light} [m^3]}{D_{light} [m] \cdot L_{WL} [m] \cdot L_B [m]}$$

### 1.C.2.E.5. Total hull towing resistance

( $R_T$ )

The force that boats and ships must overcome to move is called “towing resistance.” Naval architects typically determine its value by building ship models and measuring the resistance force as they are “towed” across a tank [250]. There are three principle components, called “source resistances,” to the total hull towing resistance as a ship moves through calm water and calm air, which are influenced by the ship’s speed, displacement, and hull form: viscous (or friction) resistance, air resistance, and wave and eddy (or residual) resistance (Eq. (S.234)) [186,192].

**Eq. (S.234)**

$$R_T[N] = R_F[N] + R_A[N] + R_R[N]$$

Using Bernoulli’s Law, it is known that a fluid with a given velocity and density will exert a dynamic pressure given by Eq. (S.235).

**Eq. (S.235)**

$$\frac{1}{2} \cdot \rho \left[ \frac{kg}{m^3} \right] \cdot \left( v \left[ \frac{m}{s} \right] \right)^2 = \left[ \frac{kg \cdot m^2}{m^3 \cdot s^2} \right] = \left[ \frac{kg \cdot m}{s^2} \right] = \left[ \frac{N}{m^2} \right]$$

If we tow a body through water and the body completely stops the water, then the water will exert a reaction pressure on the body’s surface according to the dynamic pressure. For the friction and residual source resistances, we can use this dynamic pressure to calculate a reference force that is dependent upon the wetted surface area of the hull. We can then use this reference force multiplied by a resistance coefficient to find the source resistance.

#### 1.C.2.E.5.A. Reference force, loaded and light

( $K_{loaded}, K_{light}$ )

The reference force is given by Eq. (S.236) or Eq. (S.237), where the water density is either that of fresh water or seawater as appropriate for watercraft type. (We introduce the wetted surface area in the next section.)

**Eq. (S.236)**

$$K_{loaded}[N] = \frac{1}{2} \cdot \rho_{water} \left[ \frac{kg}{m^3} \right] \cdot \left( v \left[ \frac{m}{s} \right] \right)^2 \cdot A_{s,loaded}[m^2]$$

**Eq. (S.237)**

$$K_{light}[N] = \frac{1}{2} \cdot \rho_{water} \left[ \frac{kg}{m^3} \right] \cdot \left( v \left[ \frac{m}{s} \right] \right)^2 \cdot A_{s,light}[m^2]$$

Knowing the reference force is useful because we can then calculate the total hull towing resistance using a dimensionless coefficient (Eq. (S.238)).

Eq. (S.238)

$$R_T[N] = C_T[-] \cdot K[N]$$

### 1.C.2.E.5.B. Wetted surface area (below water line), loaded and light

$(A_{s,loaded}, A_{s,light})$

There are numerous equations for estimating the wetted surface area of watercraft. In our analysis, we first compared the Denny-Mumford Method (Eq. (S.239) and Eq. (S.240)), the Schneekluth-Bertram Method (Eq. (S.241) and Eq. (S.242)), the Baier-Bragg Method (Eq. (S.243) and Eq. (S.244)), and the Froude Method (Eq. (S.247) and Eq. (S.248)) [249,251,252]. To use these methods, recall that we assume that the length between perpendiculars and the length at the water line do not change between loaded and light cases – a necessary assumption given the lack of available detailed hull shape data. We provide each of the equations below, along with a summary of results as applied to each watercraft type in Table S.17.

#### *Denny-Mumford Method:*

Eq. (S.239)

$$A_{s,loaded}[m^2] = 1.7 \cdot L_{PP}[m] \cdot D_{loaded}[m] + \frac{\nabla_{loaded}[m^3]}{D_{loaded}[m]}$$

Eq. (S.240)

$$A_{s,light}[m^2] = 1.7 \cdot L_{PP}[m] \cdot D_{light}[m] + \frac{\nabla_{light}[m^3]}{D_{light}[m]}$$

#### *Schneekluth-Bertram Method:*

Eq. (S.241)

$$A_{s,loaded}[m^2] = \left( 3.4 \cdot (\nabla_{loaded}[m^3])^{\frac{1}{3}} + 0.5 \cdot L_{WL}[m] \right) \cdot (\nabla_{loaded}[m^3])^{\frac{1}{3}}$$

Eq. (S.242)

$$A_{s,light}[m^2] = \left( 3.4 \cdot (\nabla_{light}[m^3])^{\frac{1}{3}} + 0.5 \cdot L_{WL}[m] \right) \cdot (\nabla_{light}[m^3])^{\frac{1}{3}}$$

#### *Baier-Bragg Method:*

Eq. (S.243)

$$A_{s,loaded}[m^2] = C_{B-B}[-] \cdot (L_{WL}[m])^{\frac{2}{10}}$$

Eq. (S.244)

$$A_{s,light}[m^2] = C_{B-B}[-] \cdot (L_{WL}[m])^{\frac{2}{10}}$$

The Brier-Bragg Coefficient ( $C_{B-B}$ ) can be estimated using the displacement weight (in long ton, 1 lt = 2,240 lb) as given by Eq. (S.245) and Eq. (S.246) [251].

**Eq. (S.245)**

$$C_{B-B,light}[-] = -0.00000906385 \cdot \left( \frac{\Delta_{light} [lt]}{\left(\frac{L_{WL}}{100}\right)^3} \right)^2 + 0.00954632 \cdot \left( \frac{\Delta_{light} [lt]}{\left(\frac{L_{WL}}{100}\right)^3} \right) + 0.776457$$

**Eq. (S.246)**

$$C_{B-B,loaded}[-] = -0.00000906385 \cdot \left( \frac{\Delta_{loaded} [lt]}{\left(\frac{L_{WL}}{100}\right)^3} \right)^2 + 0.00954632 \cdot \left( \frac{\Delta_{loaded} [lt]}{\left(\frac{L_{WL}}{100}\right)^3} \right) + 0.776457$$

**Froude Method:**

**Eq. (S.247)**

$$A_{s,loaded} [m^2] = \left( (\nabla_{loaded} [ft^3])^{\frac{2}{3}} \cdot \left( 3.4 + \frac{L_{WL} [ft]}{2 \cdot (\nabla_{loaded} [ft^3])^{\frac{1}{3}}} \right) \right) \cdot \left[ \frac{1m^2}{10.7639ft^2} \right]$$

**Eq. (S.248)**

$$A_{s,light} [m^2] = \left( (\nabla_{light} [ft^3])^{\frac{2}{3}} \cdot \left( 3.4 + \frac{L_{WL} [ft]}{2 \cdot (\nabla_{light} [ft^3])^{\frac{1}{3}}} \right) \right) \cdot \left[ \frac{1m^2}{10.7639ft^2} \right]$$

**Table S.17. Comparison of various wetted surface area estimates**

Method	Waterjet boats		Cargo ships	
	Light [m <sup>2</sup> ]	Loaded [m <sup>2</sup> ]	Light [m <sup>2</sup> ]	Loaded [m <sup>2</sup> ]
Denny-Mumford	18.0	18.5	893.2	1,601.8
Schneekluth-Bertram	18.8	19.4	789.6	1,505.7
Baier-Bragg	11.5	11.2	378.5	1,102.8
Froude	10.1	10.4	525.1	889.7

There is significant discrepancy between the various methods, which illustrates why so many different methods exist for different types of ships. For example, the Schneekluth-Bertram Method was primarily developed for cargo ships and ferries [252]. Throughout our analysis, we will find it useful to be able to calculate the wetted surface area independent of the draft, which eliminates the Denny-Mumford method. Unfortunately, as we can see from the equations for the other methods, that means our calculations and optimizations will become non-linear for

watercraft. We have elected to use the Schneekluth-Bertram Method for all watercraft and all variants, whether FF, BE, or HFC, in our analysis for consistency and simplicity.

### 1.C.2.E.5.C. Frictional resistance

( $R_F$ )

The frictional resistance of a ship's hull depends upon the wetted surface area and speed, and it can account for 40% to 90% of a ship's total hull resistance [186]. We calculate the frictional resistance using Eq. (S.249), where  $C_F$  is the frictional resistance coefficient and  $K$ , the reference force, can be for either loaded or light scenarios as calculated above.

Eq. (S.249)

$$R_F[N] = C_F[-] \cdot K[N]$$

There are several methods for estimating the frictional resistance coefficient, as shown by the Schoenherr Formula (Eq. (S.250)) and the Holtrop & Mennen Formula (Eq. (S.251)) [249,253,254]. We calculate the frictional resistance coefficient using both methods for an initial comparison, but we only used the Holtrop & Mennen Formula for further calculations. Results are within 0.5%.

Eq. (S.250)

$$C_F[-] = \frac{0.4631}{(\log Re[-])^{2.6}}$$

Eq. (S.251)

$$C_F[-] = \frac{0.075}{(\log Re[-] - 2)^2}$$

The Reynolds Number ( $Re$ ) is given by Eq. (S.252) and is dependent upon the kinematic viscosity of water ( $\nu$ ), taken as  $1.1300 \times 10^{-6} \left[ \frac{m^2}{s} \right]$  for fresh water and  $1.1883 \times 10^{-6} \left[ \frac{m^2}{s} \right]$  for salt water, both at 59°F (15°C) [192,255–257].

Eq. (S.252)

$$Re[-] = \frac{L_{WL}[m] \cdot v \left[ \frac{m}{s} \right]}{\nu \left[ \frac{m^2}{s} \right]}$$

Note that, for external flow over flat plates (like a watercraft's hull), typical Reynolds number magnitudes are  $< 5 \times 10^5$  for laminar flow,  $> 1 \times 10^6$  for turbulent flow, and values in-between represent the transition between laminar to turbulent flow [192]. Typical water flow around a ship's hull transitions from laminar to turbulent with the Reynolds number increasing as the length increases from the front of the hull (at 0[m]) to the end of the submerged portion (at  $L_{WL}[m]$ ).

#### 1.C.2.E.5.D. Air resistance

( $R_A$ )

The air resistance is a factor of the ship's profile above the waterline in a plane perpendicular to the direction of travel and the ship's speed. We do not consider the effect of wind in this analysis. Air resistance is typically about 2% to 8% of a ship's total hull towing resistance [186,192]. Although we can calculate the air resistance using an air resistance coefficient in a similar manner to the frictional and residual resistances, it can also be estimated as 90% of the dynamic pressure of air with a velocity equal to the ship's velocity [186].

Eq. (S.253)

$$R_A[N] = 0.90 \cdot \frac{1}{2} \cdot \rho_{air} \left[ \frac{kg}{m^3} \right] \cdot \left( v \left[ \frac{m}{s} \right] \right)^2 \cdot A_{air}[m^2]$$

To estimate the front cross-sectional area of the watercraft above the waterline, we used drawings from the manuals and data for height and beam dimensions [60]. Since height is measured from the water surface to the top of the mast, we use a reduction factor of 40% for the average waterjet boat and 80% for the average cargo ship (i.e., 60% of the rectangular area given by  $height \times beam$  is empty space for waterjet boats and 20% is empty space for cargo ships).

#### 1.C.2.E.5.E. Residual resistance

( $R_R$ )

When William Froude conducted his pioneering ship experiments in the 1860s, he assumed that the total resistance was a factor of the skin friction and "wave-making and pressure form," or friction + "the rest," which he termed "residuary" resistance [255]. As discussed above, air resistance is only a small component to overall ship drag. It turns out that, for a typical naval vessel, the frictional resistance is the largest component of the total hull towing resistance (drag) at low speeds, while the residual resistance becomes dominant at high speeds [254]. At low speeds, the residual resistance is about 8% to 25% of the total hull towing resistance, but at high speeds it can grow to 40% to 60% [186].

Whereas the frictional resistance is a factor of the Reynolds number, the residual resistance is a factor of the Froude number given by Eq. (S.254) [192,254,255].

Eq. (S.254)

$$Fr[-] = \frac{v \left[ \frac{m}{s} \right]}{\sqrt{g \left[ \frac{m}{s^2} \right] \cdot L_{WL}[m]}}$$

Scale models in towing tanks are generally used to calculate the total hull towing resistance with the total hull towing resistance coefficient being the summation of the frictional and residual coefficients [254,255].

Eq. (S.255)

$$C_T[N] = C_F[-] + C_R[-]$$

Some methods include a “correlation allowance” between the model and the actual ship. Since we generally must find the residual resistance coefficient,  $C_R$  using experimental methods or computer models, we simply estimate  $C_R$  using [254]. This suggests that, for an average cargo ship and Froude number of 0.17, the frictional resistance coefficient is about 0.0016, which correlates to our calculated value of 0.00178 from Eq. (S.250) and Eq. (S.251) above. In this case, the residual resistance coefficient is about 0.001.

The Froude number for the average waterjet boat is beyond that presented by [254], and references like the Lap-Keller Chart used to estimate  $C_R$  are not readily available [253]. Given the higher speed of waterjet boats (about twice that of cargo ships) and the fact that residual resistance can be ~50% of the total hull towing resistance at higher speeds, we use a residual resistance coefficient of 0.0023 for the average waterjet boat, roughly equal to the frictional resistance coefficient.

We can calculate the residual resistance using Eq. (S.256) for both the loaded (gross) and light (curb) scenarios.

**Eq. (S.256)**

$$R_R[N] = C_R[-] \cdot K[N]$$

Now that we can independently calculate the friction resistance, the air resistance, and the residual resistance, we add all three to find the total hull towing resistance for a watercraft (Eq. (S.234)).

### **1.C.3. Characteristics of electric motors and gearboxes for battery electric and hydrogen fuel cell systems**

Whether used in BE or HFC variants, we must appropriately size electric motors and gearboxes to ensure we achieve desired performance characteristics.

#### **1.C.3.A. Electric Motors**

Electric motors are plentiful. In 2011, the International Energy Agency (IEA) estimated that electric motor-driven systems accounted for 43% to 46% of all global electricity consumption (giving rise to 6,040 Mt of CO<sub>2</sub> emissions annually due to their sources of electricity) [258]. For all-electric BE and HFC variants, electric motors can be used to replace ICEs as the power plant [200].

EVs use many different types of motors, both DC and AC. Pros and cons exist for each type. For example, DC motors do not require inverters, but AC motors are better suited for regenerative braking [259]. Several decades ago, researchers wrote that “recent technological developments have pushed AC motors to a new era, leading to definite advantages over DC motors: higher efficiency, higher power density, lower cost, more reliable, and almost maintenance free” [260].

AC induction motors work by supplying an alternating current to windings in the stator (the fixed portion that either inside or surrounding the rotating rotor), which creates a rotating magnetic field that changes with the current’s oscillation [261]. The rotor (the central shaft that spins within or outside the stationary stator) lags and rotates at a slower speed. The stator’s magnetic field changes relative to the rotor, and this induces an opposing current [262]. This induced opposing current in the rotor’s windings in turn creates a magnetic field that reacts



against the stator's magnetic field. Faraday's Law combined with Lenz's Law defines that the direction of the magnetic field opposes change in current through the rotor's windings, causing the rotor to rotate in the direction of the rotating stator magnetic field. The rotor then accelerates until the magnitude of the induced rotor current and torque balances the applied mechanical load on the rotor. The difference between the synchronous speed (where the motor's speed is exactly proportional to the supply current's frequency) and the operating speed at the same frequency is called "slip" and is either expressed in RPM or as a percent ratio of the synchronous speed [262]. For reference, the Tesla Model S uses AC induction, liquid-cooled, variable frequency drive motors paired with a single-speed fixed gear transmission [263]. Whereas AC induction motors rely upon their induced opposing current and magnetic field and are therefore asynchronous, there are synchronous motors where the rotor turns at the same rate as the stator field [264]. In synchronous motors, the rotor has permanent magnets or DC-powered electromagnets that turn in step with the stator field.

Typical commercial electric motors are radial flux, meaning the orientation of the magnetic flux is radial to the rotor shaft. However, new axial flux synchronous motors (where the magnetic flux is parallel to, or along the axis of, the rotor shaft) can apply to transportation applications as well [265]. Axial flux motors can be more efficient and lightweight than traditional radial flux motors because the copper can be limited to an orientation perpendicular to magnet rotation (i.e., none is left overhanging on the ends of the coils) and the copper can be placed against the exterior motor case to enhance cooling and heat transfer [266]. For example, Magnax, a company in Belgium, claims that their AXF225 yokeless axial flux motor can produce 170 kW peak power with a mass of just 14 kg, yielding a peak PWR of 12.1 kW kg<sup>-1</sup>; they also claim motors with peak power densities of up to 15 kW kg<sup>-1</sup> (7.5 kW kg<sup>-1</sup> continuous) with nominal efficiencies of 94% to 95% and peak efficiency of 98% [267,268]. In comparison, BMW's hybrid synchronous machine radial flux motor used in their i3 model has a peak power of 125 kW with a mass of 42 kg, yielding a peak PWR of 3.0 kW kg<sup>-1</sup> [11]. This suggests that axial flux motors may someday prove to be better suited for applications where vehicle mass is an issue.

Another company, Emrax, produces electric motors for EVs with peak PWRs of ~7.5 to 11.3 kW kg<sup>-1</sup> and continuous PWRs of ~3.8 to 4.9 kW kg<sup>-1</sup> with efficiencies of 92% to 98% [269,270]. Tesla Motors, Inc. uses two, 70 lb motors (~63.5 kg total) to produce 362 hp (~270 kW) in its Model S, yielding a PWR of ~4.3 kW kg<sup>-1</sup> [271]. BorgWarner (formerly Remy, Inc.), produces motors for electric vehicles with PWRs of ~4.3 kW kg<sup>-1</sup> and peak efficiencies >95% (typical 74.0% to 95.8%) [272–278]. Another company in the UK, YASA, produces electric motors for transportation applications with a continuous PWR of 2.1 kW kg<sup>-1</sup> [279].

We conducted a survey of 15 different commercially-available, off-the-shelf (COTS) electric motors from five different manufacturers (BorgWarner, Emrax, Remy, Magnax, YASA) and compared their continuous power, mass, and volume as shown in Fig. S.6 through Fig. S.8. Blue dots represent radial flux electric motors and red dots represent axial flux motors [267,269,270,273,275–279].

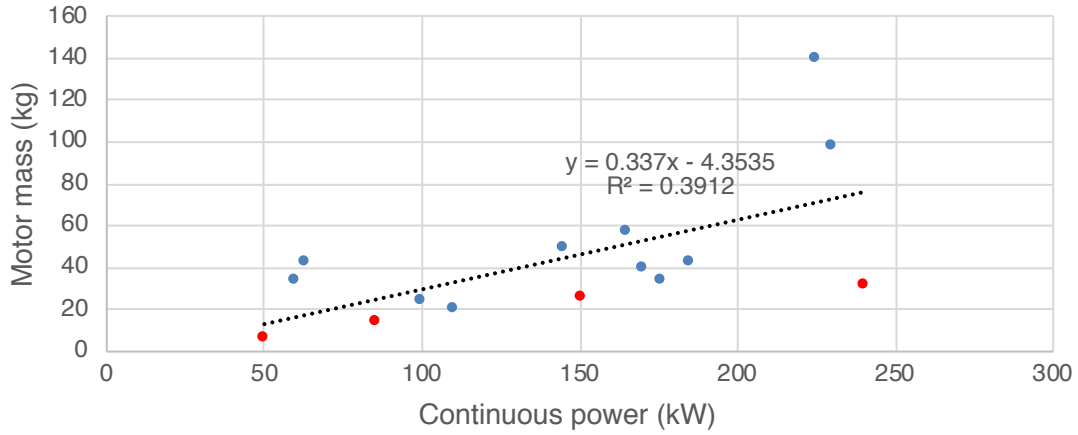


**Fig. S.6. Relationship between electric motor mass and continuous power output capability.**

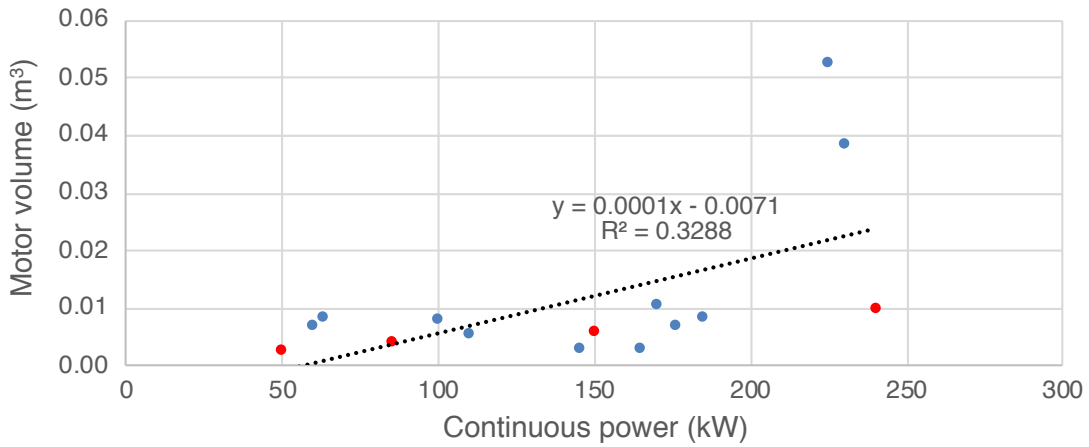


**Fig. S.7. Relationship between electric motor volume and continuous power output capability.**

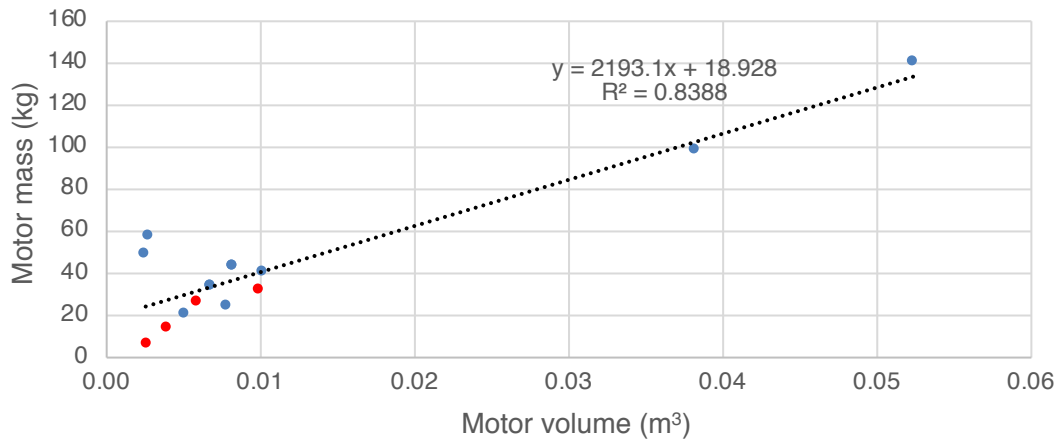


**Fig. S.8. Relationship between electric motor mass and volume.**

For this analysis, we first want to consider a LB scenario that uses COTS technology and a HB scenario that uses published technological targets for the near future (we will later use the MK values for each vehicle platform to apply defined commercial and future feasible technologies, but for now we want to investigate just near-term technologies). We selected the radial flux, air cooled Emrax 348 electric motor as a basis for the LB scenario and the axial flux Magnax AXF225 for the HB scenario. We recorded data for each motor from industry specification sheets [16,267,270].

In application, we can use multiple electric motors at different wheels on a single vehicle or have multiple motors work together along a single shaft. (As a side note, using multiple electric motors may provide a benefit over a single ICE by providing redundancy.) Since our focus is on the overall changes to mass and volume for the variants of each vehicle platform, of which the electric motor is just a small fraction, we define “parity” between an existing FF vehicle’s peak torque and peak power as meeting or exceeding the cumulative torque and cumulative continuous power output possible from “stacking” electric motors [267]. (We will later use electric motor peak, not continuous, power.) In the sections that follow, the HB scenario may sometimes have values for individual motor parameters that seem worse than those in the LB scenario. However, readers must remember that we are stacking motors to achieve the desired torque and power, and what ultimately matters is the calculated motor specific power and power density, which is always better in the HB scenario using axial flux motors.

With regards to fixed-wing aircraft, future-seeking concepts consider the use of High-Temperature Super-conducting (HTS) electric motors whose superconducting materials, when operated below a critical temperature, are able to carry current with negligible resistive losses [230,237,238,280]. Such motors are still in the research and development phase, so we limit our analysis to the motors presented above. With regards to the diesel-electric freight locomotive, it already has a transmission paired to electric motors and traction auxiliaries (i.e., the diesel engine produces electricity to power electric motors). Although we could model the freight locomotive as retaining its electric motors, we consider adding new motors and gearboxes without subtracting the existing ones and acknowledge that we short the available mass and volume budgets in this transition (see Section 1.C.1.E.1).

#### **1.C.3.A.1. Torque output from individual electric motor**

$(\tau_{m,i})$

The Emrax 348 can produce a torque of 500 N-m whereas the Magnax AXF225 can produce a peak torque of 250 N-m [267,270]. It should be noted that Emrax quotes this parameter as “continuous” torque. We do not consider limits for how long a motor can sustain a given torque output level.

#### **1.C.3.A.2. Continuous power output of individual electric motor**

$(P_{m,c,i})$

The Emrax 348 can sustain a continuous power output of 140 kW [270]. Magnax does not overtly report the continuous power output of their motors – only the peak. However, included in an article posted to their company website is the statement: “continuous power figures for the Magnax motor come out at 50 percent of what it can make at its peak” [281]. Thus, we consider the continuous power output of the Magnax AXF225 as 85 kW, half of its peak [267].

### 1.C.3.A.3. Peak power output of individual electric motor

$(P_{m,p,i})$

The Emrax 348 has a peak power output of 290 kW, which can only be maintained for a few minutes at cold start or a few seconds at hot start [270]. The Magnax AXF225 has a peak power output of 170 kW [267]. Data for how long the motor can sustain this peak power output is unavailable.

### 1.C.3.A.4. Electric motor dimensions: length and diameter

$(l_{m,i}, d_{m,i})$

The Emrax 348 has a length (reported as “width”) of 107 mm and a diameter of 348 mm [270]. The exact length of the Magnax AXF225 is not reported, but what is reported is that the AXF185, 225, 275, and 355 have lengths between 75 and 100 mm [268]. To be conservative, we use a value of 100 mm. The width is given in the nomenclature of the motor itself – the AXF225 has a diameter of 225 mm [268].

### 1.C.3.A.5. Volume of individual electric motor

$(V_{m,i})$

We estimate the physical size of each individual motor by calculating the volume of a cylinder using data for the length and diameter (Eq. (S.257)).

Eq. (S.257)

$$V_{m,i}[m^3] = \pi \cdot \left(\frac{1}{2} d_{m,i}[m]\right)^2 \cdot l_{m,i}[m]$$

### 1.C.3.A.6. Mass of individual electric motor

$(m_{m,i})$

We recorded the mass of each individual motor from published data; the Emrax 348 has a mass of 39 kg, and the Magnax AXF225 has a mass of 14 kg [267,270]. It is worthy of noting here that the DOE does not cite technical targets for electric motor mass; presumably because the PWR of electric motors is not of primary concern for light-duty passenger vehicle applications.

### 1.C.3.A.7. Power density of electric motor(s)

$(PD_m)$

We calculate the power density of electric motors by dividing the individual motor’s peak power output by its volume (Eq. (S.258)).

Eq. (S.258)

$$PD_m \left[ \frac{W}{L} \right] = \frac{P_{m,p,i} \left[ \frac{W}{motor} \right]}{V_{m,i} \left[ \frac{m^3}{motor} \right] \cdot \left[ \frac{1,000L}{m^3} \right]}$$

The DOE published a technical target for the year 2025 of 50,000 W L<sup>-1</sup> based on a 100,000 W peak power electric motor operating at 650 V (nominal, DC) with a motor volume of

2.0 L [282]. The Magnax AXF225 almost meets this technical target today with a power density of nearly 43,000 W L<sup>-1</sup>.

### 1.C.3.A.8. Power-to-weight ratio (continuous) of electric motor(s)

( $PWR_{m,c}$ )

A convenient way to compare electric motor performance is by PWR. Using manufacturer's data, we calculate the continuous PWR for the Emrax 348 and Magnax AXF225 as 3.59 kW kg<sup>-1</sup> and 6.07 kW kg<sup>-1</sup>, respectively, using Eq. (S.259).

Eq. (S.259)

$$PWR_{m,c} \left[ \frac{W}{kg} \right] = \frac{P_{m,c,i} \left[ \frac{W}{motor} \right]}{m_{m,i} \left[ \frac{kg}{motor} \right]}$$

### 1.C.3.A.9. Power-to-weight ratio (peak) of electric motor(s)

( $PWR_{m,p}$ )

Similarly, we can calculate the peak PWR for the Emrax 348 and Magnax AXF225 as 7.44 kW kg<sup>-1</sup> and 12.1 kW kg<sup>-1</sup>, respectively, using Eq. (S.260).

Eq. (S.260)

$$PWR_{m,p} \left[ \frac{W}{kg} \right] = \frac{P_{m,p,i} \left[ \frac{W}{motor} \right]}{m_{m,i} \left[ \frac{kg}{motor} \right]}$$

The type of electric motor selected for an application matters. To provide a means of reference, we derived an equation to estimate the mass of an electric motor based upon maximum (peak) output power using data from a full range of Class F, continuous duty, 60 Hz, 460 V motors (see Fig. S.9). Class F is a National Electrical Manufacturers Association (NEMA) motor winding insulation rating indicating a maximum temperature of 155°C [283]. Fig. S.9 suggests a peak PWR of ~0.1435 kW kg<sup>-1</sup> for electric motors [284]. This is very low compared to the Emrax and Magnax motors under consideration, but these TECO motors are for industrial applications, like drive pumps, fans, compressors, and other tasks where mass is not an issue. When using electric motors developed for specialty applications like transportation, the peak PWR can be much better. It is interesting to note that claimed specifications for the Magnax axial flux motor already exceed recently published forecasts for future electric motor PWRs of >10 kW kg<sup>-1</sup> [10].

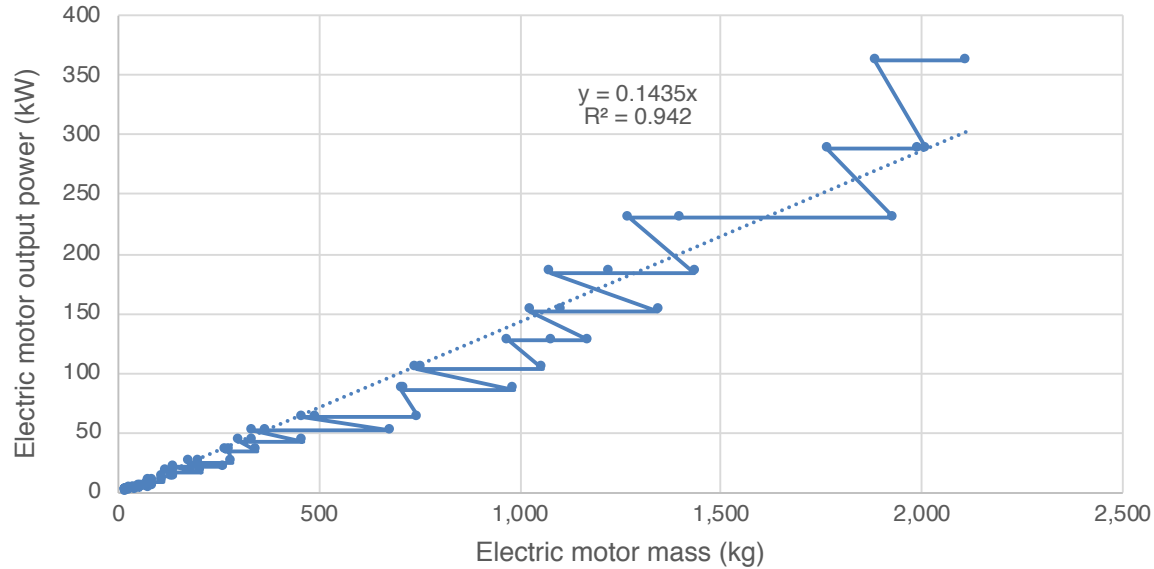


**Fig. S.9. Example electric motor power-to-weight ratio relationship for common, squirrel-cage induction motors.**

### 1.C.3.A.10. Number of electric motors

( $n_m$ )

There are several ways by which we could estimate the number of electric motors needed to meet or exceed each FF vehicle platform’s capabilities. All of the methods presented here model electric motors manufactured specific to the application’s needs and the overall electric motor volume, mass, torque, and power are cumulative, as if the individual motors are “stacked” to obtain the required output.

One method is to consider the FF variant’s maximum power output and meet that value with an equivalent amount of electric motor peak power (Eq. (S.261)). Since we rarely operate vehicles at their “red line” and, if we do, it is only for a very brief period of time, this may be a reasonable assumption. For example, as already discussed in Section 1.C.1.D.5.C, one example helicopter can only operate at its contingency engine horsepower for 2.5 minutes, its maximum horsepower for 10 minutes at, and its intermediate horsepower for 30 minutes.

**Eq. (S.261)**

$$n_m[motor] = \frac{P_{FF}[W]}{P_{m,p,i} \left[ \frac{W}{motor} \right]}$$

A second method is to consider the FF variant’s maximum power output and meet that value with an equivalent amount of electric motor continuous power that can be sustained indefinitely (Eq. (S.262)). This is a significantly conservative analysis.

**Eq. (S.262)**

$$n_m[motor] = \frac{P_{FF}[W]}{P_{m,c,i} \left[ \frac{W}{motor} \right]}$$

A third method is to consider both the FF variant's peak torque and peak power, calculate the number of electric motors needed to meet both metrics individually, and then take the larger number of motors as the governing factor, as illustrated by Eq. (S.263).

**Eq. (S.263)**

$$n_m[motor] = \max \left\{ \begin{array}{l} \frac{T_{FF}[N \cdot m]}{T_{m,i} \left[ \frac{N \cdot m}{motor} \right]} \\ \frac{P_{FF}[W]}{P_{m,c,i} \left[ \frac{W}{motor} \right]} \end{array} \right.$$

Although the third method, which considers both torque and power, may appear to be best, it fails to provide a convenient means of comparison that allows for design changes in all-electric variants according to a desired PWR. Consequently, we adopt the first and second methods for our analysis. Recall that, unlike an ICE that must obtain a certain speed and power output before maximum torque can be achieved, an electric motor starts from zero RPM with maximum torque, placing torque availability where it is generally most needed for a vehicle.

### 1.C.3.A.11. Continuous power output of combined electric motors

$(P_{m,c})$

If we consider stacking or combining electric motors to achieve the desired power output for a vehicle platform, we can calculate the total power output using Eq. (S.264) for continuous power, though the same method can be used for peak power.

**Eq. (S.264)**

$$n_m[motor] \cdot P_{m,c,i} \left[ \frac{W}{motor} \right] = P_{m,c}[W]$$

### 1.C.3.A.12. Mass of electric motor(s)

$(m_m)$

Upon calculating the number of electric motors required to meet or exceed existing FF/ICE capabilities, we calculate the resulting mass of electric motors needed using Eq. (S.265).

**Eq. (S.265)**

$$m_m[kg] = n_m[motor] \cdot m_{m,i} \left[ \frac{kg}{motor} \right]$$

### 1.C.3.A.13. Volume of electric motor(s)

( $V_m$ )

Similarly, we calculate the resulting volume of electric motors needed using Eq. (S.266).

Eq. (S.266)

$$V_m[m^3] = n_m[motor] \cdot V_{m,i} \left[ \frac{m^3}{motor} \right]$$

### 1.C.3.B. Gearbox (transmission)

#### 1.C.3.B.1. Ground combat vehicles

Electric vehicles can use a “direct-drive” gear (1:1 ratio between motor RPM and wheel RPM) which is 99.5% efficient [285]. Electric motors produce useable torque across a wide RPM range starting from zero, so there is no need for a clutch or multi-speed transmission. However, many manufacturers design for an appropriate single-speed (constant gear ratio) that allows for a specific top speed yet still is useful at lower RPM [286]. For example, in 2008, Tesla’s Chief Technical Officer (CTO), JB Straubel, wrote that Tesla’s “Powertrain 1.5” would use a single-speed gearbox with a constant ratio of 8.2752:1 and a mass of 45 kg [287]. This provides simplicity, reduces inefficiencies, and reduces both mass and volume required for the drivetrain.

To illustrate this mathematically, consider the dynamometer (“dyno”) graph for a wheeled vehicle using a 6.5L V8 engine from [288]. (As an aside, the “PS” shown next to “HP” on the graph stands for the German *Pferdestärke*, or “horse-strength,” which is ~98.6% of BHP [289]. The vehicle uses size 335/80R20 tires [290]. From the naming convention, the width of the tires is 335 mm, the aspect ratio is 80 (meaning the tire sidewall height is 80% of the tire’s width, which equals 268 mm), the construction, R = Radial, and the wheel diameter is 20 in [291]. From these dimensions, we can calculate the tire diameter using Eq. (S.267) and the tire circumference using Eq. (S.268).

Eq. (S.267)

$$tire\ diameter = \left( \left( 20[in] \cdot \left[ \frac{25.4mm}{1in} \right] \right) + \left( 2 \cdot (0.80 \cdot 335[mm]) \right) \right) \cdot \left[ \frac{1m}{1,000mm} \right] = 1.044[m]$$

Eq. (S.268)

$$tire\ circumference = 2 \cdot \pi \cdot \left( \frac{1.044[m]}{2} \right) = 3.28[m]$$

Therefore, for every revolution of the tire, the vehicle travels 3.28 m. Let us assume that this vehicle has a top speed of 55 mph (~24.6 m s<sup>-1</sup>). Referring to [288], the vehicle’s power reaches a maximum of ~200 hp at an RPM as low as ~2,500 RPM. We can use Eq. (S.269) to match a vehicle’s top speed with its engine crankshaft RPM [286].



**Eq. (S.269)**

$$\text{top speed} = \frac{\text{engine RPM}}{\text{gear ratio}} \cdot \text{tire circumference}$$

Using Eq. (S.270), we can see that an appropriate gear ratio to take the crankshaft's 2,500 RPM and convert it to the tire's RPM that equates to 55 mph is ~4.8:1. From the dyno graph, at this engine RPM, the vehicle can produce ~550 N-m of torque [288].

**Eq. (S.270)**

$$28.2 \left[ \frac{m}{s} \right] = \frac{2,500 \left[ \frac{rev}{min} \right]}{\text{gear ratio} \cdot \left[ \frac{60s}{min} \right]} \cdot 3.28 \left[ \frac{m}{rev} \right]$$

However, a ground combat vehicle generally does not travel at 55 mph on the battlefield. A more likely speed would be about 15 mph (~6.7 m s<sup>-1</sup>) for supporting dismounted patrols. If the FF variant only had a single gear with a ratio of 4.8:1, we could again use Eq. (S.269) to solve for the engine RPM needed to match this slower vehicle speed (Eq. (S.271)).

**Eq. (S.271)**

$$6.7 \left[ \frac{m}{s} \right] = \frac{\text{engine RPM} \left[ \frac{rev}{min} \right]}{4.8 \cdot \left[ \frac{60s}{min} \right]} \cdot 3.28 \left[ \frac{m}{rev} \right]$$

From Eq. (S.271), we see that the engine RPM would need to be ~588 RPM for this gear ratio and vehicle speed combination to work. This is far too low for the ICE, and dyno graphs reflect that an ICE is incapable of producing usable torque at that speed.

This illustrates why multiple gears and transmissions are employed in conjunction with ICEs to improve performance. ICEs produce little torque at low RPM and maximum torque only within narrow RPM range [292]. This stands in stark contrast to electric vehicles like the Tesla Roadster and Model S whose motors can spin up to ~14,000 RPM and ~18,000 RPM, respectively while producing usable, maximum torque from zero RPM [293]. Although the vehicle systems are different, it is interesting to note that the maximum speed of the average ground combat vehicle is already within the constant torque range for electric motors as applied to the Tesla Model S system.

Recently, some manufacturers have begun developing multi-speed transmissions for electric vehicles to increase the average motor efficiency, improve the drive range, or even reduce the electric motor size required [285,294,295]. Proterra, the maker of electric buses for mass transportation, uses a two-speed auto-shift transmission in order to maximize efficiency while either traveling at freeway speed or climbing steep hills [296,297]. The benefit of using a two-speed transmission is increased torque in the first gear and increased vehicle speed in the second gear [28]. As validated by the DOE at Oak Ridge National Laboratory, tests on ten-ton Smith-Newton medium-duty EV delivery trucks using either an Eaton single-speed gearbox or an Eaton three-speed gearbox show improvements of 7.7% improvement in overall efficiency,

18.4% in top speed, 3.9% in acceleration from 0 to 50 mph, and 6.4% in gradeability by using a three-speed transmission [29].

Whether an EV uses a single-speed or multi-speed gearbox, our analysis should consider more than just the mass and volume of the electric motor itself. Although a smaller, lighter single-speed gearbox may be sufficient, we will consider a two-speed gearbox used in all tactical vehicle variants.

### **1.C.3.B.2. Freight locomotive**

The diesel-electric locomotive already has a transmission paired to electric motors and the traction auxiliaries. However, as discussed in Sections 1.C.1.E.1 and 1.C.3.A, in the absence of data for their mass and volume, we take a conservative approach and model adding a two-speed gearbox with electric motors without subtracting away the existing ones.

### **1.C.3.B.3. Rotary-wing aircraft**

Since we model removing the ICEs but not the transmission systems in the helicopters, we do not consider replacement gearboxes in our analysis.

### **1.C.3.B.4. Fixed-wing aircraft**

Propeller propulsion uses gearboxes to adapt the performance characteristics of the core engine to the characteristics of the prop, and turbofan propulsion uses gearboxes to decouple the fan from the turbine; both instances considerably increase maximum efficiency in the FF variant [56]. For example, the Pipistrel Alpha Electro all-electric prop airplane uses an integrated electric motor/gearbox [298]. Our analysis will consider a two-speed gearbox for all-electric prop planes and no gearboxes for jet airliners using ducted fans.

### **1.C.3.B.5. Watercraft**

Since the electric motor in waterjet boats will operate a pump for waterjet propulsion, we do not need a gearbox for that platform type. However, cargo ships will require gearboxes to properly match motor RPM to individual propeller RPM, just as smaller electric propeller boat motors use gearboxes [299].

### **1.C.3.B.6. Scaling factor, dry weight (mass) of gearbox used per dry weight (mass) of electric motor**

$(F_{m_{GB-m_m}})$

Due to the limited availability of data on gearboxes designed specifically for heavy-duty vehicle applications, we will use a two-speed gearbox manufactured to match the motor size required for each vehicle platform. The Eaton Corporation manufactures a two-speed EV transmission with a dry mass of 81 kg, a volume of 0.085 m<sup>3</sup>, and an oil capacity of 4.6 L [30,295]. However, this two-speed gearbox is for vehicles up to 18 tons. In the previously mentioned analysis regarding ten-ton Smith-Newton medium-duty EV delivery trucks using Eaton single-speed and three-speed gearboxes, the DOE provided data on the combined motor + gearbox mass and volume (see Table S.18) [29]. Note that the baseline vehicle and motor is the same, but there is a difference in the calculated motor volume between the two gearbox combinations. This is likely due to the method of measurement used by the DOE; they report

size as maximum dimensions in length, height, and width, and the motor/gearbox combination is not a complete rectangular cuboid.

**Table S.18. Eaton gearboxes sized to Smith-Newton medium duty electric vehicle delivery trucks**

Parameter	Single-speed gearbox	Three-speed gearbox
Motor mass	83.5 kg	83.5 kg
Gearbox mass	27.2 kg	90.7 kg
Motor volume	0.0572 m <sup>3</sup>	0.0719 m <sup>3</sup>
Gearbox volume	0.0236 m <sup>3</sup>	0.1242 m <sup>3</sup>

Using these values, we calculate ratios of gearbox mass to motor mass and gearbox volume to motor volume. Graphing these values and creating trendlines, we are able to make rough estimates for sizing factors of a two-speed gearbox in terms of the required electric motor mass and volume (Fig. S.10).

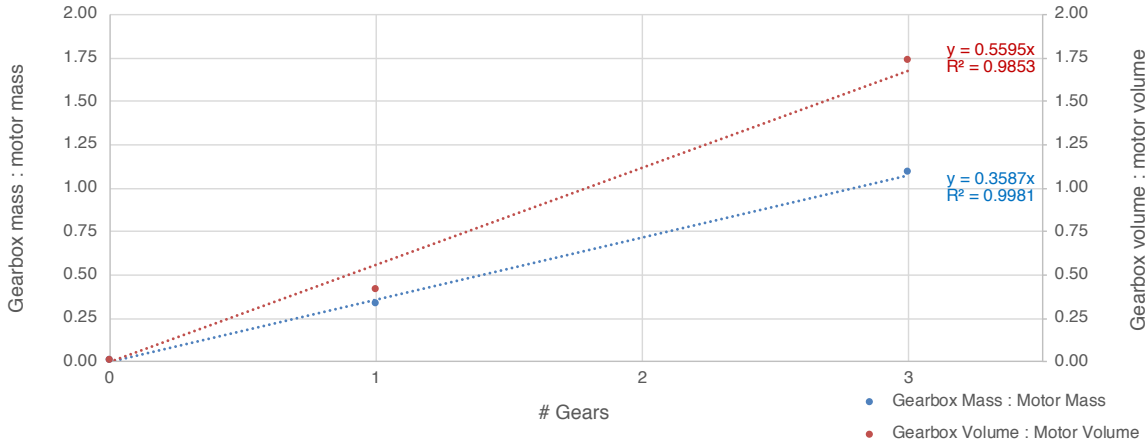


**Fig. S.10. Linear trendlines for mass and volume ratios, gearbox : electric motor**

Fig. S.10 suggests that an estimate for the mass of a two-speed gearbox is  $2 \cdot 0.3587 = 0.7174$  times the mass of its paired electric motor. We define this factor as  $F_{m_{GB}-m_m}$ , which allows for easy estimation of a dry mass for a gearbox defined by the size of electric motors used in an all-electric variant.

**1.C.3.B.7. Mass of gearbox**

$(m_{GB})$

Having defined a scaling factor for the dry mass of a two-speed gearbox, we can now estimate the required gearbox mass based upon the mass of electric motors using Eq. (S.272).

**Eq. (S.272)**

$$m_{GB}[kg] = F_{m_{GB}-m_m} \cdot m_m[kg]$$

### 1.C.3.B.8. Scaling factor, volume of gearbox used per volume of electric motor

$(F_{V_{GB-V_m}})$

Similarly, Fig. S.10 suggests an estimate for the volume of a two-speed gearbox is  $2 \cdot 0.5595 = 1.119$  times the volume of its paired electric motor.

### 1.C.3.B.9. Volume of gearbox

$(V_{GB})$

Having defined a scaling factor for the volume of a two-speed gearbox, we can also estimate the required gearbox volume based upon the volume of electric motors using Eq. (S.273).

Eq. (S.273)

$$V_{GB} [m^3] = F_{V_{GB-V_m}} \cdot V_m [m^3]$$

### 1.C.3.B.10. Scaling factor, volume of gearbox oil used per volume of gearbox

$(F_{V_{o,GB-V_{GB}}})$

We cannot forget that the gearbox requires lubricating oil, and just as we included the mass of oil in our formulation of a mass budget from stripping away the FF system, we need to account for the oil necessary in an all-electric system. To find the mass of oil necessary, we must first find the volume of oil necessary.

The Eaton two-speed electric vehicle transmission, which has a total volume of  $0.085 \text{ m}^3$ , uses  $4.6 \text{ L}$  ( $\sim 0.0046 \text{ m}^3$ ) of SAE50 Eaton PS 164 lubricating oil [30]. This equates to a scaling factor of  $0.05412$  for the overall gearbox volume used. We therefore consider  $5.412\%$  of any two-speed gearbox volume as oil for a rough estimate.

### 1.C.3.B.11. Volume of oil used in gearbox

$(V_{o,GB})$

Using the scaling factor for the volume of gearbox oil required per volume of gearbox, we can calculate the volume of oil used in an appropriately-sized, two-speed gearbox using Eq. (S.274).

Eq. (S.274)

$$V_{o,GB} [L] = F_{V_{o,GB-V_{GB}}} \cdot V_{GB} [m^3] \cdot \left[ \frac{1,000L}{m^3} \right]$$

### 1.C.3.B.12. Gearbox oil type

Eaton's Service Manual for its two-speed TRSM7202 transmission specifies the use of SAE50 Eaton PS 164 gear oil for transmission lubricant [30]. We will model this same oil for all gearboxes in our analysis because we are simply seeking an estimate for the mass of oil that a gearbox will use. In practice, the type of oil may be different based on vehicle platform type.

### 1.C.3.B.13. Density of gearbox lubricating oil

( $\rho_o$ )

From a specifications sheet for SAE50 transmission lubricant, the density of oil is 0.860 kg L<sup>-1</sup> at 15.6°C (~60°F) [300].

### 1.C.3.B.14. Mass of gearbox oil

( $m_{o,GB}$ )

We can now calculate the mass of oil using Eq. (S.275).

Eq. (S.275)

$$m_{o,GB}[kg] = V_{o,GB}[L] \cdot \rho_o \left[ \frac{kg}{L} \right]$$

### 1.C.3.B.15. Total electric gearbox mass to include all gearboxes and lubricating oil

( $m_{total,GB}$ )

Although the volume of oil is contained within the volume of the gearbox, the mass of oil will add to the dry mass of the gearbox, as shown in Eq. (S.276).

Eq. (S.276)

$$m_{total,GB}[kg] = m_{GB}[kg] + m_{o,GB}[kg]$$

### 1.C.3.B.16. Combined electric motor and gearbox factors

As a check on the above assumptions, let us consider a wheeled vehicle with a mass of 3,697 kg (curb) and 5,488 kg (gross). This vehicle would require 1.26 electric motors with a mass of 26.5 kg motor<sup>-1</sup> and volume of 0.007 m<sup>3</sup> motor<sup>-1</sup> to meet or exceed the power in the FF variant.

Using Eq. (S.272), we can calculate the mass of a matching two-speed gearbox using Eq. (S.277).

Eq. (S.277)

$$0.7174 \cdot 1.26[motors] \cdot 26.5 \left[ \frac{kg}{motor} \right] = 23.95[kg]$$

Using Eq. (S.273), we can calculate the volume of a matching two-speed gearbox using Eq. (S.278).

Eq. (S.278)

$$1.119 \cdot 1.26[motors] \cdot 0.0067 \left[ \frac{m^3}{motor} \right] = 0.0094[m^3]$$

Using Eq. (S.274), we can calculate the volume of gearbox oil using Eq. (S.279).

**Eq. (S.279)**

$$0.05412 \cdot 0.0094[m^3] \cdot \left[ \frac{1,000L}{m^3} \right] = 0.509[L]$$

Using Eq. (S.275), we can calculate the mass of gearbox oil using Eq. (S.280).

**Eq. (S.280)**

$$0.860 \left[ \frac{kg}{L} \right] \cdot 0.509[L] = 0.438[kg]$$

Using Eq. (S.276), we find the total mass of the gearbox and oil as shown by Eq. (S.281).

**Eq. (S.281)**

$$23.95[kg] + 0.438[kg] = 24.4[kg]$$

Thus, a rough estimate for a two-speed gearbox for this vehicle would be about 24 kg dry mass and 0.01 m<sup>3</sup> volume. We conducted a survey of COTS gearboxes for EVs and summarized the available specifications in Table S.19. Compared to the table's values, our estimated gearbox mass and volume values seem low. However, we calculated these results using values for some of the best electric motors on the market today, whereas the table's values reflect gearboxes paired with electric motors that have already been on the market for some time now. Our estimates for gearbox mass and volume may therefore be reasonable for near-term/future applications.

**Table S.19. Mass and volume of COTS EV gearboxes**

Brand	Model	Platform characteristics	Mass (kg)	Volume (m <sup>3</sup> )	Source
xTrac	P1166 (Single-speed)	2,000 kg GVW electric motor: < 10,000 RPM < 500 N-m	17	--	[301]
MAGNA/ GETRAG	1eDT200 (Single-speed)	“Mid-size” EVs electric motor: < 200 N-m	20	0.033	[302]
xTrac	P1227 (Single-speed)	Electric motor: < 10,000 RPM < 500 N-m	23	--	[303]
MAGNA/ GETRAG	2eDT200 (Two-speed)	Electric motor: < 200 N-m	26	0.034	[304]
Eaton	Single-speed	Vehicle < 9,072 kg	27.2	0.024	[29]
MAGNA/ GETRAG	1eDT350 (Single-speed)	Light commercial vehicles < 3,175 kg	28	--	[305]
Punch Powertrain	EVS28 TwinSpeed	Electric motor: < 12,000 RPM < 400 N-m	45	--	[28,306]
Tesla	Single-speed	Electric motor: < 14,000 RPM < 400 N-m	45	--	[287]
Tesla	Two-speed	--	53	--	[287]
Eaton	Two-speed	Vehicle < 16,330 kg	81	0.085	[30]
Eaton	Three-speed	Vehicle < 9,072 kg	90.7	0.124	[29]
MAGNA/ GETRAG	1eDT330 (Single-speed)	Electric motor: < 2x320 N-m	150 (w/motors)	0.119	[307,308]

**1.C.3.B.17. Combined mass of electric motor, gearbox, and oil**

$(m_{m+GB+o})$

We can calculate the combined mass of the electric motor, gearbox, and gearbox oil, based upon the individual electric motor mass and volume and the three scaling factors previously introduced, as shown by Eq. (S.282). Since we have already performed some of the intermediate steps, we can also find the same result using Eq. (S.283).

**Eq. (S.282)**

$$\begin{aligned}
 m_{m+GB+o} \left[ \frac{kg}{motor} \right] &= \left( m_{m,i} \left[ \frac{kg}{motor} \right] \right) + \left( F_{m_{GB}-m_m} [-] \cdot m_{m,i} \left[ \frac{kg}{motor} \right] \right) \\
 &+ \left( \left( F_{V_o,GB-V_{GB}} [-] \cdot \left( F_{V_{GB}-V_m} [-] \cdot V_{m,i} \left[ \frac{m^3}{motor} \right] \right) \cdot \left[ \frac{1,000L}{m^3} \right] \right) \cdot \rho_o \left[ \frac{kg}{L} \right] \right)
 \end{aligned}$$

**Eq. (S.283)**

$$m_{m+GB+o} \left[ \frac{kg}{motor} \right] = \frac{m_m[kg] + m_{total,GB}[kg]}{n_m[motor]}$$

### 1.C.3.B.18. Combined volume of electric motor and gearbox

$(V_{m+GB})$

In a similar fashion, we can calculate the combined volume of the electric motor and gearbox using either Eq. (S.284) or Eq. (S.285).

Eq. (S.284)

$$V_{m+GB} \left[ \frac{m^3}{motor} \right] = \left( V_{m,i} \left[ \frac{m^3}{motor} \right] \right) + \left( F_{V_{GB-V_m}} [-] \cdot V_{m,i} \left[ \frac{m^3}{motor} \right] \right)$$

Eq. (S.285)

$$V_{m+GB} \left[ \frac{m^3}{motor} \right] = \frac{V_m [m^3] + V_{GB} [m^3]}{n_m [motor]}$$

### 1.C.3.B.19. Scaling factor, total mass of electric motor, gearbox, and oil used per dry weight (mass) of electric motor

$(F_{m_{m+GB+o-m_m}})$

In our analysis, we will find it necessary to use the mass of electric motors as a variable in order to meet or exceed the FF vehicle's PWR. However, when calculating a proposed all-electric variant's mass, we must know not just the electric motor mass but the total mass of the electric motor, gearbox, and gearbox oil package. Therefore, we have defined a scaling factor that yields the total mass as a function of the electric motor mass.

To accomplish this, we first must find the ratio of the gearbox (and its oil) mass to the electric motor mass, which we place within the parentheses of Eq. (S.286). Adding this value to 1 yields a scaling factor that will yield the total electric motor, gearbox, and gearbox oil mass per unit of electric motor mass desired.

Eq. (S.286)

$$F_{m_{m+GB+o-m_m}} = 1 + \left( \frac{m_{m+GB+o} \left[ \frac{kg}{motor} \right] - m_{m,i} \left[ \frac{kg}{motor} \right]}{m_{m,i} \left[ \frac{kg}{motor} \right]} \right) = \frac{m_{m+GB+o} \left[ \frac{kg}{motor} \right]}{m_{m,i} \left[ \frac{kg}{motor} \right]}$$

### 1.C.3.B.20. Ratio of total volume of electric motor and gearbox used per dry weight (mass) of electric motors

$(R_{V_{m+GB-m_m}})$

Similarly, when calculating the volume of a proposed all-electric variant based upon the mass of electric motors used, we need a ratio of the total electric motor and gearbox volume in relation to electric motor mass. We can do this using Eq. (S.287).



Eq. (S.287)

$$R_{V_{m+GB}.m_m} \left[ \frac{m^3}{kg} \right] = \frac{V_{m+GB} \left[ \frac{m^3}{motor} \right]}{m_{m,i} \left[ \frac{kg}{motor} \right]}$$

#### 1.C.4. Characteristics of battery electric platforms

##### 1.C.4.A. Battery density standards

The lithium ion battery (LIB) has become the single dominant technological design that private industry has scaled up for BE transportation, threatening technological lock-in for the long-term [309]. Manufacturers of BE vehicles prefer LIBs because of their energy storage capacity, ability to maintain a high current, ability to maintain a charge, ability to supply power in the cold, and ability to provide numerous cycles with minimal degradation [310]. This may change in the future as research continues into different battery types. For example, Lithium-Oxygen batteries can theoretically deliver a specific energy of 5.2 kWh kg<sup>-1</sup> and energy density of 10.5 kWh L<sup>-1</sup> at the cell-level [311]. There are many such estimates for different battery types throughout the literature. In our analysis, we will eventually calculate tipping point values for these variables. We specifically do not put a cap on future feasible battery specific energy or energy density values because we do not restrict the type or chemistry of batteries that can be used for transportation applications.

Often, research will quote very favorable-sounding values for battery specific energy (gravimetric energy density) and energy density (volumetric energy density), but we must be careful to consider whether those values are theoretical or commercial and whether they are at the “cell” or “pack” level. For example, consider the LIB with a 339 mAh g<sup>-1</sup> LiC<sub>6</sub> anode and 278 mAh g<sup>-1</sup> LiNi<sub>1/3</sub>Co<sub>1/3</sub>Mn<sub>1/3</sub>O<sub>2</sub> cathode – it has a theoretical specific energy of 421 Wh kg<sup>-1</sup>, but the commercial version by Tesla and Panasonic has a specific energy of 272 Wh kg<sup>-1</sup>, a decrease of 35% [312]. This is at the cell-level. At the pack (or “system”) level, additional mass and volume are required to support control management, cooling, electronics, and housing components [5]. Consequently, at the pack-level, the specific energy drops to approximately 170 Wh kg<sup>-1</sup> [313]. This is a 60% decrease in the same metric for the same battery. Clearly, applied research must use the appropriate value to avoid unrealistic and unfair results. Although some may claim that basing an analysis on the lower, pack-level values is inexact (for instance, a manufacturer might find synergy by incorporating battery housing into the structure of the vehicle itself), this analysis will use the more conservative pack-level values. We will discuss the pack-level specific energy, energy density, and physical density of battery systems in more detail below.

##### 1.C.4.A.1. System (pack)-level gravimetric battery energy density (specific energy) and volumetric battery energy density

( $SE_B, ED_B$ )

###### 1.C.4.A.1.A. Ground combat vehicles

With regard to today’s technology, EPA Certification Summary Information Reports state that current lithium-ion batteries in Tesla vehicles have a gravimetric energy density

(specific energy) of 150 Wh kg<sup>-1</sup> (Model X and Model 3) and 170 Wh kg<sup>-1</sup> (Model S) at the pack level [313–316]. Proterra and LG Chem, manufacturers of battery electric busses, use a lithium-ion battery with a specific energy of 157 Wh kg<sup>-1</sup> and a volumetric energy density of 260 Wh L<sup>-1</sup> [12,317,318]. One source reports the Tesla Model X has a pack-level specific energy of 183.8 Wh kg<sup>-1</sup>, but the Certification Summary Information Report says it is just 150 Wh kg<sup>-1</sup> [316,319]. Some individuals have documented detailed teardowns of commercial vehicle systems and report their independently measured values. For example, the Tesla Model 3 uses 4,416 individual lithium-ion (Li-ion) 2170 cells in its 80.5 kWh battery pack [315,320]. Estimates place cell-level useable values at 246 Wh kg<sup>-1</sup> and 711 Wh L<sup>-1</sup> [320,321]. The cells are arranged 46 cells to a brick and either 23 or 25 bricks to a module depending upon the module's placement within the battery pack [320]. Given measurements of the modules, this equates to approximately 217 Wh kg<sup>-1</sup> and 430 Wh L<sup>-1</sup> at the module-level. The modules are arranged into a pack including the frame and penthouse, which contains the charge cable connector, power conversion unit, fuses, and controls [320]. The total pack weighs about 480 kg and is about 235 L in volume, resulting in pack-level values of approximately 168 Wh kg<sup>-1</sup> and 343 Wh L<sup>-1</sup>. This equates to a 32% and 52% decrease, respectively, in the gravimetric and volumetric energy density moving from the cell- to pack-level.

The DOE unfortunately no longer publishes technical targets for battery energy density by 2025. However, a 2012 report from Germany's Fraunhofer Institute for Systems and Innovation Research reports that the DOE once stated a technical target of 250 Wh kg<sup>-1</sup> by 2020, and that China reported a target of 300 Wh kg<sup>-1</sup> [322]. Currently, the United States Advanced Battery Consortium states a commercialization target of 235 Wh kg<sup>-1</sup> useable specific energy and 500 Wh L<sup>-1</sup> useable energy density at the system level (350 Wh kg<sup>-1</sup>, 750 Wh L<sup>-1</sup> at the cell level) by calendar year 2020 [18]. Lion Smart, a German engineering firm, claims to have achieved an automotive battery pack for the BMW i3 with an energy density of >230 Wh kg<sup>-1</sup> and energy density of 460 Wh L<sup>-1</sup> at the pack level [323]. Recent claims for cell-level solid state battery specific energy and energy density values include Solid Power's 320 to 700 Wh kg<sup>-1</sup>, 700 to 1,000 Wh L<sup>-1</sup>; Solid Energy's 450 Wh kg<sup>-1</sup>, 1,200 Wh L<sup>-1</sup>; C4V's 380 Wh kg<sup>-1</sup>, 700 Wh L<sup>-1</sup>; and Sion Power's 500 Wh kg<sup>-1</sup>, 1,000 Wh L<sup>-1</sup> [20,32,33,324].

Given these COTS and published technical targets, we will conduct the first portion of our analysis using specific energy, energy density values of 170 Wh kg<sup>-1</sup>, 260 Wh L<sup>-1</sup> for the low benefit scenario and 235 Wh kg<sup>-1</sup>, 500 Wh L<sup>-1</sup> for the high benefit scenario.

#### **1.C.4.A.1.B. Freight locomotive**

GE is currently working on a demonstration model for a BE freight locomotive that uses approximately 20,000 LIB cells “similar to what you might find under the hood of an electric car,” and future versions are expected to have ~50,000 cells [325]. Just as we propose the method of starting with an existing vehicle platform and stripping away the FF components to create a mass and volume budget for new components, GE will “strip out the engine and cooling systems from a diesel locomotive to make way for the battery under the hood... from the outside, the battery-powered locomotive won't look much different from its diesel counterparts” [325]. GE's BE freight locomotive design will be able to generate up to 2,400 kWh of energy and save 10% to 15% fuel [325]. Current efforts seem to use the same technology as commercial BE light-duty vehicles, just with a much larger battery pack. Therefore, our analysis will use the same values as for ground combat vehicles.

### 1.C.4.A.1.C. Rotary-wing aircraft

Since helicopters spend a significant portion of their time in low-level flight, this analysis will not consider any potential benefits that could possibly improve the specific energy from that of land-based systems (e.g., less cooling hardware required for batteries operating at high altitudes). Since there are no known commercial BE helicopters at this point, we adopt the same values used for ground combat vehicles and freight locomotives for helicopters.

### 1.C.4.A.1.D. Fixed-wing aircraft

BE aircraft developers seem to avoid publishing working values for battery specific energy and energy density, though there is some data from recent test aircraft. The Swiss Solar Impulse 2, which completed the first ever piloted, fixed-wing, solar-powered circumnavigation of the globe in 2016, used four 38.5 kWh Kokam Ultra High Energy Nickel Manganese Cobalt (NMC) Oxide battery packs with 150 Ah cells totaling 154 kWh of energy storage at a reported 260 Wh kg<sup>-1</sup> [326]. However, Kokam’s website only advertises a best specific energy of 186 Wh kg<sup>-1</sup> [327]. Recent research that summarizes flyable, manned electric aircraft lists specific energy values as high as 207 Wh kg<sup>-1</sup> for the Airbus E-Fan, 204 Wh kg<sup>-1</sup> for the IFB Stuttgart eGenius, 180 Wh kg<sup>-1</sup> for the Pipistrel Taurus Electro, and 171 Wh kg<sup>-1</sup> for the Pipistrel Alpha Electro [55]. Another publication estimates the Pipistrel Taurus Electro at ~150 Wh kg<sup>-1</sup> [328]. However, as described above, these values raise concern because it is not clear if they are for the cell or pack level, and the calculations below do not support reports of such high values. For example, commercially available BE aircraft manufactured by Pipistrel include the Taurus Electro and the Alpha Electro. The Taurus Electro has a 7.1 kWh (total) battery pack using four battery boxes weighing 13.9 kg each; Pipistrel recommends only considering 80% capacity as a “sensible” discharge level, so the Taurus Electro can be considered to have a specific energy as calculated by Eq. (S.288) [329].

Eq. (S.288)

$$\frac{7,100 [Wh]}{4 [battery\ boxes] \cdot 13.9 \left[ \frac{kg}{battery\ box} \right]} \cdot 0.8 \cong 102 \left[ \frac{Wh}{kg} \right]$$

The Pipistrel Alpha Electro is a single-engine trainer airplane that uses six swappable 20 kg batteries for a 17 kWh system, which suggests a specific energy of ~142 Wh kg<sup>-1</sup> [298,330,331]. However, this value does not consider the housing, rack, or connections for the batteries. The NASA X-57 Maxwell BE airplane uses 69.1 kWh of LIB weighing 390 kg for a specific energy of 177 Wh kg<sup>-1</sup>, but NASA’s press release carefully notes that only 47 kWh is usable, resulting in an effective 120 Wh kg<sup>-1</sup> [332].

Given the variability of values for aircraft, we select a low benefit value for specific energy of 120 Wh kg<sup>-1</sup> to reflect NASA’s X-57 and a likely value for Pipistrel’s Alpha Electro after considering housing requirements. For the high benefit value, we select 300 Wh kg<sup>-1</sup> to reflect what some BE aircraft designers have personally conveyed to us as their “working target” for achievable technology within the next several years. Given the lack of reliable data for volume and energy density, we adopt the same values as those used previously in other platforms: 260 Wh L<sup>-1</sup> for the low benefit scenario and 500 Wh L<sup>-1</sup> for the high benefit scenario.

### 1.C.4.A.1.E. Watercraft

Watercraft manufacturers are also using LIBs. Cigarette and Mercedes-AMG have partnered to build a battery-electric racing boat that uses 12 electric motors to produce 2,220 hp and 2,213 ft-lb torque [333]. Torqeedo, a German electric boat manufacturer, cooperates with BMW to use automotive batteries for marine applications [334]. Torqeedo uses modified versions of the BMW i3 and i8 batteries as highlighted below in Table S.20.

**Table S.20. Summary of characteristics for example batteries used in marine applications**

Parameter	Units	BMW i3	BMW i8	Source
Capacity	Wh	30,500	9,100	[310,335]
Mass	kg	256	98	
Volume	L	278	147	
Specific energy	Wh kg <sup>-1</sup>	119	93	
Energy density	Wh L <sup>-1</sup>	110	62	

Note that these batteries have lower specific energy values than do their typical automotive counterparts because “very rugged design is ideal for boat applications that place high demands on shock resistance” [310]. Rather than using lightweight foil-sealed cells, boats use welded steel cylinders to encapsulate the battery cells. Furthermore, electrolytic gas can be generated if water were to mix with the components of LIBs, so battery packs for watercraft applications must be completely waterproof [310].

We elect to use low benefit values of 119 Wh kg<sup>-1</sup> and 110 Wh L<sup>-1</sup> for the specific energy and energy density of watercraft batteries, which correspond with Torqeedo’s use of the BMW i3 battery pack. For high benefit values, we use 235 Wh kg<sup>-1</sup> and 500 Wh L<sup>-1</sup>, reflecting the technical targets set by the United States Advanced Battery Consortium, LLC [18].

### 1.C.4.A.2. Physical density of battery pack system

( $\rho_{B,sys}$ )

Having described the battery pack’s gravimetric energy density (specific energy) and volumetric energy density (energy density), we can also consider its actual physical density using Eq. (S.289).

**Eq. (S.289)**

$$\frac{ED_B \left[ \frac{Wh}{L} \right] \cdot \left[ \frac{1,000 L}{m^3} \right]}{SE_B \left[ \frac{Wh}{kg} \right]} = \rho_{B,sys} \left[ \frac{kg}{m^3} \right]$$

### 1.C.4.B. Overall battery electric system efficiency

We summarize our findings for the overall BE system efficiency by vehicle type in Fig. S.11. Those items in gray are the same as previously shown in Fig. S.1 for FF systems, i.e., these system components remain the same in the BE variant. Items in blue represent system components we added for a BE system, which we describe in detail below.

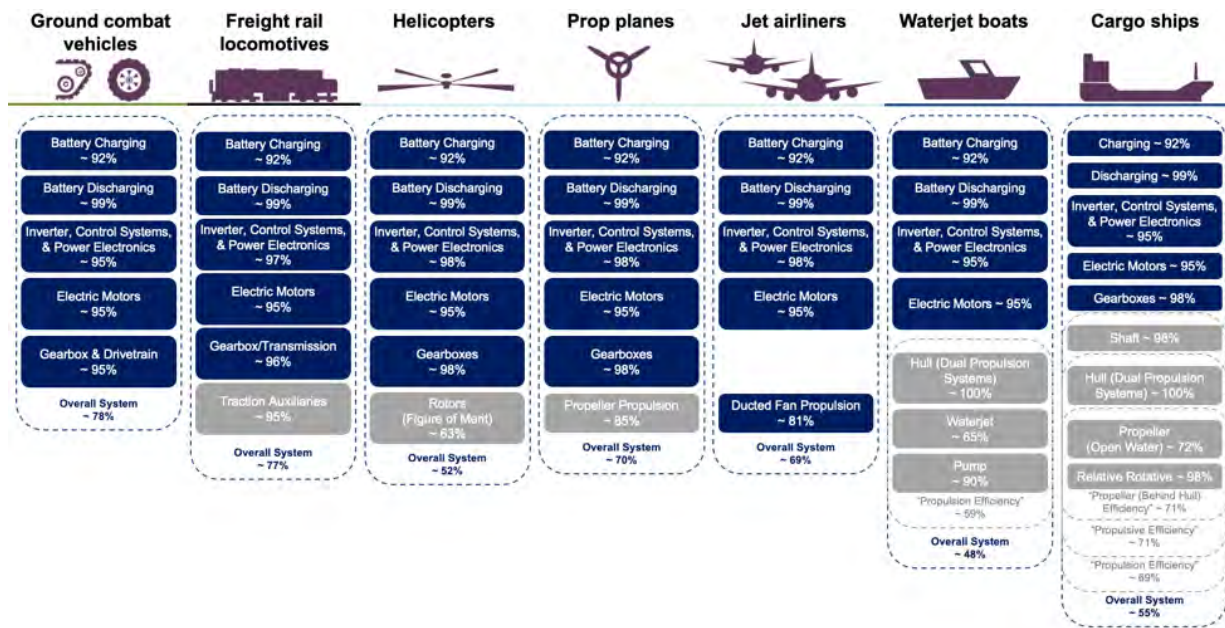


Fig. S.11. Overall battery electric system efficiency by vehicle type (same as Fig. 1(b))

### 1.C.4.B.1. Ground combat vehicles

Just as diesel has conversion losses from chemical to mechanical energy, so do BE vehicles, albeit much less. Since the Army must transport JP-8 fuel to any given location on the battlefield, it is appropriate to consider an energy analysis boundary in-between the typical well-to-wheels (WTW) and tank-to-wheels (TTW). Losses in energy from a JP-8 pump (or refueling truck) to a vehicle are negligible. However, there are losses experienced in charging batteries for battery electric vehicles. Thus, we will consider a “charge-to-wheels (CTW)” value for comparison.

We replace the ICE efficiency with the charging efficiency of batteries, the battery discharge efficiency, a combination of the efficiencies for inverters that convert DC to AC, control systems, and power electronics, and an electric motor efficiency. Despite replacing one efficiency for four different efficiencies, the overall result is much higher for the BE variant. We replace the FF vehicle’s driveline, brakes, and accessories combined efficiency with a combined gearbox and drivetrain efficiency. We neglect any potential benefits from brake recovery.

#### 1.C.4.B.1.A. Efficiency of battery charging

( $\eta_c$ )

In their 2018 textbook, *Electric Powertrain: Energy Systems, Power Electronics and Drives for Hybrid, Electric and Fuel Cell Vehicles*, the authors cite 85% as a “reasonable estimate of efficiency from the plug to the battery” [164]. Others estimate values as high as 95% [336]. A 2017 study revealed that EV charging losses ranged from 12.38% at 40 Amps (A) AC to 17.22% at 10 A AC [337]. We calculate the overall charging loss by including not just the battery (which only has losses of 0.64% to 1.69%) but the power electronics unit, the electric vehicle supply equipment (charging station), breakers (that protect the charging station), and transformers (that step voltage down from 480 V at the building or street to 240 V at the breaker panel) [337]. In fact, the transformers are a significant portion of the losses (10.2% at 10 A and

3.33% at 40 A), but unlike the other components, the transformers apply to everything within the building – not just vehicle charging [337]. In order to establish a boundary for calculating charging efficiency separate from building energy use efficiency, we subtract transformer losses from the overall battery charging losses, which results in a total loss of 7.02% at 10 A and 9.05% at 40%. This suggests a battery charging efficiency of ~92% when considering the batteries, breaker panel, charging station, and power electronics unit. Rather than present a range of values, we use a singular value of 92% that agrees well with other estimates.

#### **1.C.4.B.1.B. Efficiency of battery discharging**

( $\eta_B$ )

The coulombic efficiency (or “faradaic efficiency”) describes the efficiency of electron transfer within batteries during a single charge-discharge cycle, i.e., the ratio of total energy extracted from the battery to the energy put into the battery [338]. LIBs have a very high coulombic efficiency, exceeding 99%, which has been shown to even improve with cycling [338]. Generally, the coulombic efficiency can be assumed as 1 for discharge, but it is actually influenced by operating conditions such as the battery state of charge, temperature, and current [339]. We only found one claim of battery “leakage” of 85% to 90%, but without reference or further cited source [336]. We use a discharge battery discharge efficiency of 99% for this analysis.

#### **1.C.4.B.1.C. Combined efficiency of DC-to-AC inverter, control systems, and power electronics**

( $\eta_I$ )

Often, the values for inverter efficiency, control systems, and power electronics get wrapped up into a larger reported “battery-to-wheel” efficiency [164]. In an attempt to better understand the efficiency of each aspect of the BE system, we separate these values and use a value of 95% for inverter efficiency as suggested several sources [5,336]. This correlates well with the inverter efficiency map for a Nissan Leaf as published by the DOE’s Oak Ridge National Laboratory, which suggests that the inverter operates in the 90% to 99% efficiency range over the vast majority of its paired electric motor’s RPM range.

#### **1.C.4.B.1.D. Efficiency of electric motor**

( $\eta_m$ )

Electric motors tend to operate with efficiencies of 80% to 90% across their entire RPM range [336]. The lowest efficiencies occur at the extremes of torque (N-m)–speed (RPM) efficiency maps (i.e., high-torque, low-speed or low-torque, high-speed applications) [276]. Although we consider both HB and LB scenarios, an electric motor in a transportation platform will operate across a range of efficiencies as drive cycle characteristics require from moment to moment. To apply a lower efficiency to the LB scenario and a higher efficiency to the HB scenario would be an unfair comparison as it would imply that the motor only operates at a single efficiency (good or bad) in each case. Therefore, we use a singular electric motor efficiency of 95% for both the LB and HB scenarios, which correlates to other research on the conversion of heavy-duty trucks from FF to BE variants [5]. Given the range of overestimation and underestimation this assumption provides, our analysis will cover the majority of operable conditions for an electric motor.

When considering the efficiency maps of electric motors, one must be careful to consider what the values actually include; it is commonplace for motor efficiency contours to be published combined with their paired inverter efficiencies [11]. With regard to the two electric motors specifically considered in this portion of the analysis, the Emrax 348 has a published efficiency range of 92% to 98% and the Magnax AXF225 has a published nominal efficiency of 94% to 95% with a peak efficiency of 98% [268,270].

#### 1.C.4.B.1.E. Efficiency of gearbox/transmission

$(\eta_{GB})$

A direct-drive system (1:1 ratio) from an electric motor to the drivetrain is ~99.5% efficient [285]. Although incorporating a two-speed gearbox does introduce another component to the system that decreases overall system efficiency, it simultaneously improves the vehicle's efficiency by increasing torque in the first gear and speed in the second gear. Studies on 10-ton medium-duty trucks reveal a gearbox efficiency of 93.4% for a single-speed transmission and 98% for a three-speed transmission [29]. We use an efficiency of 95% for a two-speed electric gearbox.

#### 1.C.4.B.1.F. Overall tactical vehicle battery electric system efficiency

$(\eta_{TV,BE})$

We can calculate the overall tactical vehicle BE system efficiency ( $\eta_{TV,BE}$ ) as the product of the battery charging efficiency ( $\eta_C$ ), battery discharging efficiency ( $\eta_B$ ), the combined DC-to-AC inverter, control systems, and power electronics efficiency ( $\eta_I$ ), the motor efficiency ( $\eta_m$ ), and the gearbox efficiency ( $\eta_{GB}$ ) as shown by Eq. (S.290).

**Eq. (S.290)**

$$\eta_{TV,BE}[-] = \eta_C[-] \cdot \eta_B[-] \cdot \eta_I[-] \cdot \eta_m[-] \cdot \eta_{GB}[-]$$

Using the values above, this results in an overall system efficiency for a BE tactical vehicle of ~78%. This value reasonably correlates with other estimates. Markowitz claims an overall system efficiency between 68% to 73% but uses lower efficiency values for the motor and drivetrain (combined 90%) and battery discharge (90%) [336]. Hayes and Goodarzi claim an overall system efficiency of 68%, but they simply use an 85% charging efficiency and 80% battery-to-wheels efficiency [164]. A study on long-haul BE trucks in the European Union claims an overall system efficiency of 85% (less charging), citing a higher value of transmission efficiency of 99% [5]. Combining this with a 92% charging efficiency as described in Section 1.C.4.B.1.A, the overall system efficiency would be 78.2%. We use a singular value of 78.1% across all scenarios (LB, MK, and HB).

#### 1.C.4.B.2. Freight locomotives

The only difference in values used for system components from those described in ground combat vehicles above are those for the combined efficiency of the inverter, control systems, and power electronics and the transmission efficiency. Voltage conversion in a catenary-electric locomotive is 97% [171]. Control system/power electronics are 97.5% efficient and transmission is 96% efficient in electric locomotives [53]. We use values of 97% and 96%, respectively, for these two component efficiencies.

#### 1.C.4.B.2.A. Overall freight locomotive battery electric system efficiency

$(\eta_{L,BE})$

Considering an overall “charge-to-track” efficiency, we calculate the overall freight locomotive BE system efficiency ( $\eta_{L,BE}$ ) as the product of the battery charging efficiency ( $\eta_C$ ), the battery discharge efficiency ( $\eta_B$ ), the combined efficiency of the inverter, control systems, and power electronics ( $\eta_I$ ), the motor efficiency ( $\eta_m$ ), the gearbox efficiency ( $\eta_{GB}$ ), and the traction auxiliaries efficiency ( $\eta_{TA}$ ) as shown in Eq. (S.291).

Eq. (S.291)

$$\eta_{L,BE}[-] = \eta_C[-] \cdot \eta_B[-] \cdot \eta_I[-] \cdot \eta_m[-] \cdot \eta_{GB}[-] \cdot \eta_{TA}[-]$$

This results in an estimated overall BE system efficiency of 76.5%, which agrees well with the literature (76% for electric locomotives using overhead electric lines). A catenary line feed cable is 95% efficient, and a transformer is also 95% efficient (resulting in a combined efficiency of 90.25%). Removing these efficiencies and replacing them with battery charging efficiency of 92% and battery discharging efficiency of 99% (a combined efficiency of 91.08%) is of minimal difference.

#### 1.C.4.B.3. Rotary-wing aircraft

We use the same efficiency values for battery charging and discharging in helicopters as those for ground combat vehicles and freight locomotives. However, we also use values from the German Aerospace Center for the combined efficiency of the inverter, control systems, and power electronics (98% “controller” efficiency) and for the gearbox efficiency (98%) [56]. Although we do not model removing the existing transmissions from the FF helicopters, we do assume that their efficiency when paired with electric motors improves. It is worth noting that the German Aerospace Center also assumes a 95% efficiency for electric motors, just as we used in other vehicle platforms [56].

#### 1.C.4.B.3.A. Overall helicopter battery electric system efficiency

$(\eta_{H,BE})$

Considering an overall “charge-to-rotor” efficiency, we calculate the overall helicopter BE system efficiency ( $\eta_{H,BE}$ ) as the product of the battery charging efficiency ( $\eta_C$ ), the battery discharge efficiency ( $\eta_B$ ), the combined efficiency of the inverter, control systems, and power electronics ( $\eta_I$ ), the motor efficiency ( $\eta_m$ ), the gearbox efficiency ( $\eta_{GB}$ ), and rotor figure of merit ( $\eta_{H,r}$ ) using Eq. (S.292).

Eq. (S.292)

$$\eta_{H,BE}[-] = \eta_C[-] \cdot \eta_B[-] \cdot \eta_I[-] \cdot \eta_m[-] \cdot \eta_{GB}[-] \cdot \eta_{H,r}[-]$$

This results in an estimated overall BE system efficiency of 51.9%.



#### 1.C.4.B.4. Fixed-wing aircraft

We model the component efficiencies for airplanes the same as for helicopters, except for the propeller or ducted fan efficiency that replaces the rotor's figure of merit.

##### 1.C.4.B.4.A. Overall prop airplane battery electric system efficiency

( $\eta_{PA,BE}$ )

Considering an overall “charge-to-prop” efficiency, we calculate the overall prop airplane BE system efficiency ( $\eta_{PA,BE}$ ) as the product of the battery charging efficiency ( $\eta_C$ ), the battery discharge efficiency ( $\eta_B$ ), the combined efficiency of the inverter, control systems, and power electronics ( $\eta_I$ ), the motor efficiency ( $\eta_m$ ), the gearbox efficiency ( $\eta_{GB}$ ), and the propeller propulsion efficiency ( $\eta_{TP,P}$ ) as show in Eq. (S.293).

Eq. (S.293)

$$\eta_{PA,BE}[-] = \eta_C[-] \cdot \eta_B[-] \cdot \eta_I[-] \cdot \eta_m[-] \cdot \eta_{GB}[-] \cdot \eta_{TP,P}[-]$$

We previously determined the propeller propulsion efficiency to range from 79% to 90% (see Section 1.C.1.F.4.B). The resulting overall BE system efficiency ranges from 65.6% to 74.8%. This agrees with the German Aerospace Center's estimate of 73%, which used an 80% efficient propeller but did not consider battery charging or discharging efficiencies. Note that, in this case, the range of 79% to 90% propeller efficiency flips from the LB/HB scenarios in the FF system to the BE system; whereas a 90% propeller in the FF system applies to the LB scenario, it corresponds to the HB scenario for the BE system.

##### 1.C.4.B.4.B. Efficiency of ducted fan

( $\eta_{DF}$ )

Ducted fans can increase thrust, allow for more and shorter blades, and achieve higher rotational speeds because the duct will prevent losses in thrust from the tips of the propeller [236,239,340]. Additionally, research shows that propulsive efficiencies on the order of turbofan engine aircraft can be achieved using distributed fan propulsion along the wing [341,342]. As discussed in Section 1.C.1.F.4.E, the propulsion efficiency of HBR turbofan engines is ~72.5% to 82.5%. Tests on ducted fan propulsion units have found efficiencies ranging from 74.2% to 88.5% [340]. We assume this same range of values for the ducted fan efficiency.

##### 1.C.4.B.4.C. Overall ducted fan airplane battery electric system efficiency

( $\eta_{DFA,BE}$ )

Considering an overall “charge-to-fan” efficiency, the overall ducted fan airplane BE system efficiency ( $\eta_{DFA,BE}$ ) is the product of the battery charging efficiency ( $\eta_C$ ), the battery discharge efficiency ( $\eta_B$ ), the combined efficiency of the inverter, control systems, and power electronics ( $\eta_I$ ), the motor efficiency ( $\eta_m$ ), and the ducted fan propulsion efficiency ( $\eta_{DF}$ ), as shown in Eq. (S.294). We do not model a gearbox in the ducted fan electric airplane. The overall BE system efficiency for a ducted fan airplane ranges from 62.9% to 75.0%.

Eq. (S.294)

$$\eta_{DFA,BE}[-] = \eta_C[-] \cdot \eta_B[-] \cdot \eta_I[-] \cdot \eta_m[-] \cdot \eta_{DF}[-]$$

### 1.C.4.B.5. Watercraft

#### 1.C.4.B.5.A. Overall waterjet boat battery electric system efficiency

$(\eta_{WJB,BE})$

We calculate the overall BE system efficiency for a waterjet boat ( $\eta_{WJB,BE}$ ) as the product of the battery charging efficiency ( $\eta_C$ ), the battery discharge efficiency ( $\eta_B$ ), the combined efficiency of the inverter, control systems, and power electronics ( $\eta_I$ ), the motor efficiency ( $\eta_m$ ), and the propulsion efficiency ( $\eta_{WJB,P}$ ) as shown by Eq. (S.295). We do not model a gearbox in the waterjet boat.

Eq. (S.295)

$$\eta_{WJB,BE}[-] = \eta_C[-] \cdot \eta_B[-] \cdot \eta_I[-] \cdot \eta_m[-] \cdot \eta_{WJB,P}[-]$$

Note that we previously calculated the waterjet boat propulsion efficiency, which includes the hull, waterjet, and pump efficiencies, in Section 1.C.1.F.5.E. The propulsion efficiency ranges from 51.3% to 66.2%, but we must flip the values from the LB and HB scenarios from the FF system to the BE system, i.e., whereas 66.2% correlated to the LB scenario in the FF system, it corresponds to the HB scenario in the BE system. We adopt all other efficiency values from those used in ground combat vehicles. The resulting overall BE system efficiency ranges from 42.2% to 54.4%.

#### 1.C.4.B.5.B. Overall propeller ship battery electric system efficiency

$(\eta_{PS,BE})$

Just as with the waterjet boat, the battery charging efficiency, discharge efficiency, combined efficiency of the inverter, control systems, and power electronics, and the motor efficiency are all modeled the same as in ground combat vehicles. In the case of propeller ships, we use a gearbox with an efficiency of 98% as suggested by a study on crude oil tanker vessels [185]. These efficiencies are combined with the propulsion efficiency ( $\eta_{PS,P}$ ) previously calculated in Section 1.C.1.F.5.N, which ranges from 60.8% to 76.8%. Here again, we must flip the values from the LB and HB scenarios from the FF system to the BE system. The resulting overall BE system efficiency ranges from 49.0% to 61.9%, as we calculate using Eq. (S.296). This seems reasonable given that Torqeedo claims 44% to 56% system efficiency for their BE outboard prop systems [343].

Eq. (S.296)

$$\eta_{PS,BE}[-] = \eta_C[-] \cdot \eta_B[-] \cdot \eta_I[-] \cdot \eta_m[-] \cdot \eta_{GB}[-] \cdot \eta_{PS,P}[-]$$

### 1.C.5. Characteristics of hydrogen fuel cell platforms

Hydrogen (especially non-combustion hydrogen fuel cell) systems have the potential for carrying vast quantities of energy with very little mass while producing very little pollution. However, some researchers underestimate this potential because they focus on the mass and volume requirements for onboard hydrogen storage. As one paper puts it: the “physical constraints of gravimetric and volumetric energy density likely preclude battery- or hydrogen-powered aircraft for long-distance cargo or passenger service... to contain the same total energy

as a diesel fuel storage system, a liquid hydrogen storage system would weigh roughly six times more and be about eight times larger” [4].

This claim raises two questions. First, how did the authors arrive at this estimate? Second, although the authors do mention elsewhere that improved efficiency over ICE vehicles may make energy storage requirements less in HFC vehicles to achieve the same range, what about the vehicle system as a whole? By stripping away all unnecessary FF components and expanding the budget for onboard energy storage, a HFC vehicle may actually have greater range than an ICE vehicle. Answering both questions is an important part of our analysis.

We attempt to verify the claim regarding comparative energy storage requirements by considering a theoretical example of storing both 1kg of hydrogen (H<sub>2</sub>) and the equivalent chemical energy content of diesel. The DOE uses a value of 33.3 kWh kg<sup>-1</sup> for the LHV of H<sub>2</sub> [37]. Number 2 Diesel has an LHV of 11,833 Wh kg<sup>-1</sup> (36.24 MJ L<sup>-1</sup>) [75]. Therefore, as shown in Eq. (S.297), 2.81 kg of diesel and 1 kg of H<sub>2</sub> are equivalent strictly in terms of chemical energy content.

**Eq. (S.297)**

$$\frac{33,300 \left[ \frac{Wh}{kg H_2} \right]}{11,833 \left[ \frac{Wh}{kg diesel} \right]} = \frac{2.81 \left[ \frac{kg diesel}{kg H_2} \right]}{1.00 \left[ \frac{kg H_2}{kg H_2} \right]}$$

Auto manufacturers seem to have reached a consensus on 700-bar compressed gas hydrogen (CGH<sub>2</sub>) as the most suitable nominal working pressure for the near term [344]. Already at the commercial retail level are the Hyundai Tucson, Toyota Mirai, Honda Clarity, and Mercedes-Benz GLC F-Cell vehicles, all using 700-bar storage technology [13]. The density of H<sub>2</sub> at 700 bar is approximately 41.0 kg m<sup>-3</sup> [13,164]. Liquid hydrogen (LH<sub>2</sub>) has a density of 70.9 kg m<sup>-3</sup> [9]. Diesel has a density of about 850 kg m<sup>-3</sup> [75]. Eq. (S.298) through Eq. (S.300) calculate the volume required for each fuel source to contain 33,300 Wh of energy. We tabulate data in Table S.21.

**Eq. (S.298)**

$$\frac{2.81 [kg diesel]}{850 \left[ \frac{kg}{m^3} \right]_{diesel}} = 3.31 \times 10^{-3} [m^3]_{diesel}$$

**Eq. (S.299)**

$$\frac{1.00 [kg H_2]}{41.0 \left[ \frac{kg}{m^3} \right]_{H_2, 700 bar}} = 2.44 \times 10^{-2} [m^3]_{H_2, 700 bar}$$

**Eq. (S.300)**

$$\frac{1.00 [kg H_2]}{70.9 \left[ \frac{kg}{m^3} \right]_{LH_2}} = 1.41 \times 10^{-2} [m^3]_{LH_2}$$

The DOE, through its United States Driving Research and Innovation for Vehicle efficiency and Energy sustainability (US DRIVE) partnership, which includes three car manufacturers, five energy companies, two utilities, and one research institute, updates technical targets every five years to help guide realistic research and development into hydrogen storage and fuel cells for light-duty vehicles. As of their last publication in 2017, their 2020 technical target for onboard hydrogen storage system gravimetric capacity was 1.5 kWh kg<sup>-1</sup> storage system, or (when divided by the specific energy of H<sub>2</sub> at 33,300 Wh kg<sup>-1</sup>) 0.045 kg H<sub>2</sub> kg<sup>-1</sup> storage system (a storage efficiency of 4.5%). Similarly, their 2020 target for system volumetric capacity was 1.0 kWh L<sup>-1</sup> storage system, or 0.030 kg H<sub>2</sub> L<sup>-1</sup> storage system (30 kg H<sub>2</sub> m<sup>-3</sup> storage system) [37]. Of note, there are already three commercially available fuel cell electric vehicles: the Honda Clarity Fuel Cell, the Hyundai Tucson Fuel Cell/ix35 Fuel Cell, and the Toyota Mirai [345].

Returning to our example using 1 kg H<sub>2</sub>, we can calculate the mass and volume of hydrogen storage systems used in light-duty transportation using Eq. (S.301) and Eq. (S.302).

**Eq. (S.301)**

$$\frac{1 [kg H_2]}{0.045 \left[ \frac{kg H_2}{kg \text{ storage system}} \right]} = 22.2 [kg \text{ storage system}]$$

**Eq. (S.302)**

$$\frac{1 [kg H_2]}{30 \left[ \frac{kg H_2}{m^3} \right]} = 3.33 \times 10^{-2} [m^3 \text{ storage system}]$$

US DRIVE makes two important notes on their target values. First, these targets are “for a complete system, including tank, material, valves, regulators, piping, mounting brackets, insulation, added cooling capacity, and all other balance-of-plant components.” Second, “capacities are defined as the usable quantity of hydrogen deliverable to the fuel cell system divided by the total mass/volume of the complete storage system, including all stored hydrogen, media, reactants, and system components” [37].

LH<sub>2</sub> storage must stay at -253°C to prevent boil-off at standard atmospheric pressure. LH<sub>2</sub> tanks must therefore be super insulated. BMW and Linde state that their LH<sub>2</sub> tank used in the BMW Hydrogen 7 (which combusts the hydrogen rather than using a fuel cell to generate electricity) uses vacuum insulation across double walls with several layers of fiberglass and aluminum to equal the R-value of 17 meters thickness of Styrofoam [346]. Research by Winnefeld et al. suggests that a best-case, “exemplary cylindrical” cryogenic tank with spherically-rounded ends would have a storage density of 0.64 (equal to the mass of the fuel divided by the sum of the mass of the fuel and tank, as shown in Eq. (S.303) [9]. We can calculate the total mass of LH<sub>2</sub> fuel and tank in our theoretical example using Eq. (S.304).

**Eq. (S.303)**

$$0.64 = \frac{1 [kg H_2]}{1 [kg H_2] + x [kg \text{ tank}]} \quad x = 0.5625 [kg \text{ tank}]$$

**Eq. (S.304)**

$$1 [kg H_2] + 0.5625 [kg tank] = 1.5625 [kg]$$

However, the Winnefeld et al. estimate does not include some critical components, “such as maintaining cryogenic temperatures inside the tank, safety periphery, and heat exchangers” [9]. An actual LH2 storage tank for vehicle transportation manufactured by Linde (the CoolH2 Tank System) has many components beyond the tank such as cooling tubes, cooling plates, dryer heat exchanger, cooling water heat exchanger, reversing valve, shut-off valve, safety valve, electrical heater, shields, and filling port [347]. Although Winnefeld et al. use a mean density of  $67.3 \text{ kg m}^{-3}$  for hydrogen to consider the gas fraction available for venting (reduced from  $70.9 \text{ kg m}^{-3}$ ), the Argonne National Laboratory instead uses a tank ullage (unfilled space within the tank) factor of 7.5% and also notes that only 57% of the stored hydrogen is actually recoverable (including a 40% boil-off based on industry feedback) [347].

There is a noticeable lack of current data on the mass and volume of LH2 tanks. Journal articles often skip the LH2 storage density in tables of values, filling the voids with descriptions such as “size dependent” or “varies” [348,349]. The only reported values we have discovered for LH2 are  $2.0 \text{ kWh kg}^{-1}$  storage ( $0.060 \text{ kg LH}_2 \text{ kg}^{-1}$  storage) and  $1.6 \text{ kWh L}^{-1}$  storage ( $0.05 \text{ kg LH}_2 \text{ L}^{-1}$  storage) [350,351]. These values are listed in a table titled “Current Status of On-Board Hydrogen Systems,” but were published over a decade ago. Also, they exist in tables alongside those for 10,000-psi tanks ( $\sim 700\text{-bar}$ ) of  $1.9 \text{ kWh kg}^{-1}$  storage and  $1.3 \text{ kWh L}^{-1}$  storage, which, as shown above, were republished by US DRIVE in 2017 as  $1.5 \text{ kWh kg}^{-1}$  and  $1.0 \text{ kWh L}^{-1}$ , respectively [37]. It is odd that “current status values” decreased for 700-bar systems, which suggests different boundary definitions for what was considered a part of the storage system. Using the latest values, we can use Eq. (S.305) and Eq. (S.306) to calculate an estimated mass and volume for LH2 storage systems.

**Eq. (S.305)**

$$\frac{1 [kg LH_2]}{2,000 \left[ \frac{Wh}{kg \text{ storage system}} \right]_{LH_2}} = 16.7 [kg \text{ storage system}]$$

$$\frac{1 [kg LH_2]}{33,300 \left[ \frac{Wh}{kg LH_2} \right]}$$

**Eq. (S.306)**

$$\frac{1 [kg LH_2]}{1,600 \left[ \frac{Wh}{L \text{ storage system}} \right]_{LH_2} \cdot 1,000 \left[ \frac{L \text{ storage system}}{m^3 \text{ storage system}} \right]} = 2.08 \times 10^{-2} [m^3 \text{ storage system}]$$

$$\frac{1 [kg LH_2]}{33,300 \left[ \frac{Wh}{kg LH_2} \right]}$$

Some diesel fuel tanks are made of high strength steel, like those for locomotives, which has a material density of about  $7,850 \text{ kg m}^{-3}$  [91–93]. Sometimes, fuel tanks for vehicles include special end plates, side plates, bottom plates, long baffles, and short baffles to improve crashworthiness and safety [86]. Using known values for the mass of replacement fuel tanks, we estimate a storage energy density of 70% for locomotive fuel tanks and 80% for tactical vehicle fuel tanks. This agrees with the suggested storage density of kerosene tanks at 75% [9]. Using

the estimated diesel fuel tank storage densities, Eq. (S.307) calculates the tank mass using high strength steel and Eq. (S.308) using HDPE.

**Eq. (S.307)**

$$0.70 = \frac{1 [kg H_2]}{1 [kg H_2] + x [kg tank]} \quad x = 0.43 [kg tank]$$

**Eq. (S.308)**

$$0.80 = \frac{1 [kg H_2]}{1 [kg H_2] + x [kg tank]} \quad x = 0.25 [kg tank]$$

Using the diesel fuel tank material densities, we can calculate the volume of the fuel tank material itself (Eq. (S.309) and Eq. (S.310)).

**Eq. (S.309)**

$$\frac{0.43 [kg]}{7,850 \left[ \frac{kg}{m^3} \right]} = 5.50 \times 10^{-5} [m^3]$$

**Eq. (S.310)**

$$\frac{0.25 [kg]}{1,107 \left[ \frac{kg}{m^3} \right]} = 2.26 \times 10^{-4} [m^3]$$

Table S.21 tabulates the above calculated values and illustrates the mass and volume ratios between hydrogen and diesel fuel tanks. The cells highlighted in gray indicate values that we derive directly from data within the table.

**Table S.21. Comparison between diesel, compressed hydrogen, and liquid hydrogen storage mass & volume**

	Mass (kg)				Volume (m <sup>3</sup> )			
	Diesel		Hydrogen		Diesel		Hydrogen	
	HSS	HDPE	H <sub>2,700 bar</sub>	LH <sub>2</sub>	HSS	HDPE	H <sub>2,700 bar</sub>	LH <sub>2</sub>
<b>Fuel:</b>	2.81	2.81	1.00	1.00	3.31x10 <sup>-3</sup>		2.44x10 <sup>-2</sup>	1.41x10 <sup>-2</sup>
<b>Tank:</b>	0.43	0.25	21.2	15.7	5.5x10 <sup>-5</sup>	2.26x10 <sup>-4</sup>	8.90x10 <sup>-3</sup>	6.70x10 <sup>-3</sup>
<b>Total:</b>	3.24	3.06	22.2	16.7	3.37x10 <sup>-3</sup>	3.54x10 <sup>-3</sup>	3.33x10 <sup>-2</sup>	2.08x10 <sup>-2</sup>
<b>Average:</b>	3.15				3.45x10 <sup>-3</sup>			
<b>Ratio:</b>	1 : 1		7.0 : 1	5.3 : 1	1 : 1		9.7 : 1	6.0 : 1

Returning to claim that an LH2 system would “weigh roughly six times more and be about eight times larger,” we find that these are reasonable estimates, yet still high by about 12% and 25%, respectively.

Other hydrogen storage options exist, too. As US DRIVE notes: “while [LH2] systems exhibit higher hydrogen densities, their overall system densities are reduced due to the need for insulation as well as the boil-off and venting that occurs from extended dormancy... as a result, this technology is not currently being pursued for light duty vehicles” [37]. An interesting option

that US DRIVE reports in their “Projected Performance of Hydrogen Storage Systems” tables is cryogenic compressed hydrogen (CCH<sub>2</sub>) at 500-bar [37]. “While compressed hydrogen storage is typically at ambient temperatures, cold and cryogenic compressed hydrogen storage is also being investigated for light-duty vehicles due to their higher gas densities. These systems offer potential advantages for heavy-duty vehicles and fleet applications that utilize consistent drive cycles and require long driving ranges” [37]. The DOE defines “cold” hydrogen as capable of being delivered to fueling stations as a compressed gas, whereas “cryogenic” must be delivered as LH<sub>2</sub> [37]. Both LH<sub>2</sub> and CCH<sub>2</sub> are stored in super-insulated tanks at approximately -253°C, but LH<sub>2</sub> is stored in low-pressure (1 to 10 bar) tanks while CCH<sub>2</sub> is kept in high-pressure (5 to 700 bar) tanks [352]. This is an important distinction because both storage systems will experience “boil-off” as heat from the ambient environment transfers through the tank material to the low-temperature hydrogen, increasing tank pressure and requiring venting to protect the integrity of the tank. A CCH<sub>2</sub> tank will allow for internal pressure to build up much higher than a LH<sub>2</sub> tank, which reduces losses and extends fuel storage residence time.

US DRIVE reports a projected performance of CCH<sub>2</sub> at a 2.3 kWh kg<sup>-1</sup> and 1.4 kWh L<sup>-1</sup> at the system-level, which we can use in Eq. (S.311) and Eq. (S.312) to expand our analysis [37].

**Eq. (S.311)**

$$\frac{1 \text{ [kg CcH}_2\text{]}}{2,300 \left[ \frac{\text{Wh}}{\text{kg storage system}} \right]_{\text{CcH}_2}} = 14.5 \text{ [kg storage system]}$$

$$\frac{1 \text{ [kg CcH}_2\text{]}}{33,300 \left[ \frac{\text{Wh}}{\text{kg CcH}_2} \right]}$$

**Eq. (S.312)**

$$\frac{1 \text{ [kg CcH}_2\text{]}}{1,400 \left[ \frac{\text{Wh}}{\text{L storage system}} \right]_{\text{CcH}_2} \cdot 1,000 \left[ \frac{\text{L storage system}}{\text{m}^3 \text{ storage system}} \right]}{33,300 \left[ \frac{\text{Wh}}{\text{kg CcH}_2} \right]} = 2.38 \times 10^{-2} \text{ [m}^3 \text{ storage system]}$$

Recent work on CCH<sub>2</sub> tanks for heavy-duty applications (like buses) use four tanks of 141 L storage each (564 L or 0.564 m<sup>3</sup> total) at 500-bar to hold 40 kg usable H<sub>2</sub>, with a hydrogen density of 70.9 kg m<sup>-3</sup> [352,353]. Taking these values and updating Table S.21 from above allows for comparison of CCH<sub>2</sub> within Table S.22.

**Table S.22. Comparison between diesel, compressed hydrogen, liquid hydrogen, and cryo-compressed hydrogen storage mass and volume**

	Mass [kg]					Volume [m <sup>3</sup> ]				
	Diesel		Hydrogen			Diesel		Hydrogen		
	HSS	HDPE	H <sub>2,700 bar</sub>	LH <sub>2</sub>	CcH <sub>2</sub>	HSS	HDPE	H <sub>2,700 bar</sub>	LH <sub>2</sub>	CcH <sub>2</sub>
<b>Fuel:</b>	2.81	2.81	1.00	1.00	1.00	3.31x10 <sup>-3</sup>		2.44x10 <sup>-2</sup>	1.41x10 <sup>-2</sup>	1.41x10 <sup>-2</sup>
<b>Tank:</b>	0.43	0.25	21.2	15.7	14.5	5.5x10 <sup>-5</sup>	2.26x10 <sup>-4</sup>	8.90x10 <sup>-3</sup>	6.70x10 <sup>-3</sup>	9.70x10 <sup>-3</sup>
<b>Total:</b>	3.24	3.06	22.2	16.7	15.5	3.37x10 <sup>-3</sup>	3.54x10 <sup>-3</sup>	3.33x10 <sup>-2</sup>	2.08x10 <sup>-2</sup>	2.38x10 <sup>-2</sup>
<b>Average:</b>	3.15					3.45x10 <sup>-3</sup>				
<b>Ratio:</b>	1 : 1		7.0 : 1	5.3 : 1	4.9 : 1	1 : 1		9.7 : 1	6.0 : 1	6.9 : 1

It is also interesting to note that, with the 2017 edition technical targets for hydrogen storage, US DRIVE reports: “targets relating to ICE were removed. At one time, hydrogen powered ICEs were seen as a logical evolution step to fuel cell vehicles powered by hydrogen. Focus has shifted entirely to [Fuel Cell Electric Vehicles] FCEVs and thus there is no longer a need to include specific targets as related to ICEs” [37]. There is no need to combust the hydrogen if we use an HFC system.

Having done the above exercise and gained a better understanding of the circumstances surrounding hydrogen’s use in transportation, we decided to use two systems for this first part of our analysis: CcH<sub>2</sub> for the HB scenario and H<sub>2,700 bar</sub> for the LB scenario. The MK scenario will be an average of these two systems.

### 1.C.5.A. Characteristics of hydrogen

We summarize the most important characteristics of hydrogen systems in Table S.23. To help avoid confusion, we include the various units common to the literature. We describe these characteristics in detail in the sections that follow.

**Table S.23. Summary of hydrogen system characteristics**

<b>System:</b>	<b>H<sub>2,700 bar</sub> (CGH<sub>2</sub>)</b>	<b>CcH<sub>2</sub></b>
<b>Pressure</b>	700 bar = 70 MPa = 10,153 psi = 691 atm	1.01 bar = 0.101 MPa = 14.7 psi = 1 atm or 500 bar = 50 MPa = 7,252 psi = 493 atm
<b>Density</b>	41 kg m <sup>-3</sup> = 0.041 kg L <sup>-1</sup> = 41 g L <sup>-1</sup>	71 kg m <sup>-3</sup> = 0.071 kg L <sup>-1</sup> = 71 g L <sup>-1</sup>
<b>LHV</b>	120 MJ kg <sup>-1</sup>	120 MJ kg <sup>-1</sup>
<b>Specific energy</b>	33.3 kWh kg <sup>-1</sup>	33.3 kWh kg <sup>-1</sup>
<b>Energy density</b>	1.4 kWh L <sup>-1</sup> = 1,400,000 Wh m <sup>-3</sup>	1.4 kWh L <sup>-1</sup> = 1,400,000 Wh m <sup>-3</sup>

#### 1.C.5.A.1. Density of hydrogen

( $\rho_{H_2}$ )

At 700-bar (also 70 MPa, 10,153 psi, or 691 atm), the density of hydrogen ( $\rho_{H_2,700}$ ) is approximately 41 kg m<sup>-3</sup>. Some sources report 0.042 kg L<sup>-1</sup> while other report 40 g L<sup>-1</sup> [13,164]. Storage calculations use 70.7 kg m<sup>-3</sup> hydrogen density for cryogenic-capable pressure vessels, i.e., LH<sub>2</sub> at 20 K (-253.15°C) and 1 atm [353,354]. Note that other research publications



consider CcH2 at a storage pressure of 500-bar but still use a storage density of 0.071 kg L<sup>-1</sup> [352].

### 1.C.5.A.2. Lower heating value (net calorific value) of hydrogen

( $LHV_{H_2}$ )

Although we do not consider burning hydrogen for fuel, we can still use this value to demonstrate hydrogen's specific energy. The LHV of hydrogen is approximately 120 MJ kg<sup>-1</sup> [9,355].

### 1.C.5.A.3. Gravimetric energy density (specific energy) of hydrogen

( $SE_{H_2}$ )

We can do a unit conversion to determine the specific energy of hydrogen alone ( $SE_{H_2}$ ) from its LHV, converting energy units from MJ to Wh (Eq. (S.313)). Values of 33,330 Wh kg<sup>-1</sup> or 33.3 kWh kg<sup>-1</sup> are commonly used [13,356]. Note that this value is for hydrogen only; we will later need to reduce this value to report a storage system-level specific energy.

Eq. (S.313)

$$120 \left[ \frac{MJ}{kg} \right] \cdot \left[ \frac{277.78 Wh}{MJ} \right] = 33,333 \left[ \frac{Wh}{kg} \right]$$

### 1.C.5.A.4. Volumetric energy density of hydrogen

( $ED_{H_2}$ )

We can calculate the energy density of hydrogen alone by multiplying the specific energy of hydrogen by the density of hydrogen (with an appropriate unit conversion). We will later need to reduce this value as well to report a storage system-level energy density.

Eq. (S.314)

$$\rho_{H_2} \left[ \frac{kg}{m^3} \right] \cdot SE_{H_2} \left[ \frac{Wh}{kg} \right] \cdot \left[ \frac{m^3}{1,000L} \right] = ED_{H_2} \left[ \frac{Wh}{L} \right]$$

### 1.C.5.B. Fuel cell stack standards

The DOE's Fuel Cell Technical Team, through US DRIVE, publishes and updates technical targets for fuel cell stack system-level specific power, power density, and overall system efficiency. For this portion of our analysis, we will use DOE's published values, from November 2017, using 2020 technical targets for the LB scenario and 2025 technical targets for the HB scenario [14].

The DOE has focused their efforts on polymer electrolyte membrane fuel cells (PEMFCs) (also known as proton exchange membrane fuel cells) [14,39]. Fuel cells generate a flow of current by converting the chemical energy of a fuel (in this case, hydrogen) into electrical energy through an electrochemical reaction, known as "cold combustion" [357]. In a PEMFC, oxygen serves as the oxidant in the reaction with the byproducts of just water and heat. PEMFCs operate at relatively low temperatures (~90°C, 194°F) [358]. Bi-polar "plates" serve as a flow field to surround the electrolyte membrane and make up a single fuel "cell." Individual fuel "cells"

make up the fuel cell “stack.” A fuel cell “stack” is generally encased using a thermoplastic case [357].

In order to better understand the current state of PEMFC technology, we conducted a survey of PEMFCs on the market today and recorded their published values in Table S.24. Note that some manufacturers do not record net (continuous) power output levels or the entire PEMFC case dimensions.

**Table S.24. Survey of commercial PEMFCs**

Company	Ballard	Ballard	ElringKlinger	HES	Hydrogenics	Intelligent Energy	Re-Fire
Location	Canada	Canada	Germany	Singapore	Canada	United Kingdom	China
Product/application	FCveloCity/ Medium duty	FCveloCity-HD200/ Heavy duty	NM5/ Commercial vehicles	Ultra-light Aerostak/ aircraft	HD 180/ Heavy duty	AC64/ UAV	CAVEN-4/ Medium duty
Rated power at 1 atm (W)	30,000 (net)	100,000 (net)	13,100	1,000 (continuous), 1,300 (peak) at 0.5 to 0.7-bar	180 (continuous)	2,070 (gross) at 0.4 to 0.7-bar	46,000
Mass (kg)	125	285	13.7	1.77	720	2.9	160
Volume (L)	162	527	10.9 (stack cells only)	4.56	1,200	2.85	208
Specific power (W kg <sup>-1</sup> )	240	351	956	565 734 (peak)	250	714	287
Power density (W L <sup>-1</sup> )	185	190	1207	219 285 (peak)	150	726	221
Source	[359]	[360]	[361]	[362]	[363]	[364–366]	[367]

### 1.C.5.B.1. Specific power and power density of proton-exchange membrane fuel cell stack

( $SP_{FCS}, PD_{FCS}$ )

The 2018 Toyota Mirai’s fuel cell stack has a specific power of 2,000 W kg<sup>-1</sup> and an output power density of 3,100 W L<sup>-1</sup> [40,368]. These values are significantly higher than the DOE’s published “ultimate” technical targets of 650 W kg<sup>-1</sup> and 850 W L<sup>-1</sup> [14]. It is important to note that the DOE targets are “system-level” and include not just the fuel cell stack itself but its balance-of-plant (BOP) components and thermal management system; they exclude hydrogen storage, batteries, electric drive, and power electronics, which will be considered elsewhere in our analysis. Table S.25 summarizes this comparison. The “Integrated transportation fuel cell power system” columns exclude hydrogen storage, power electronics, and electric drive, whereas the “Fuel cell stack” columns exclude hydrogen storage, power electronics, and electric drive, *as well as* fuel cell ancillaries to include thermal, water, and air management systems.

**Table S.25. Department of Energy’s published technical targets for fuel cells**

	“Fuel cell stack”			“Integrated transportation fuel cell power system”		
	2015 Status	2020 Target	Ultimate target	2015 Status	2020 Target	Ultimate target
<b>Specific power (W kg<sup>-1</sup>)</b>	2,000	2,000	2,000	659	650	650 (900)*
<b>Power density (W L<sup>-1</sup>)</b>	3,000	2,250	2,500	640	650	850

Data from [369].

\* The DOE website reports an ultimate target of 650 W kg<sup>-1</sup>, but a 2017 DOE Fuel Cell Technical Team Roadmap published a “2025” target of 900 W kg<sup>-1</sup> [14].

Despite these targets, research suggests that the specific power of PEMFCs can significantly increase in the short term due to improvements in both the “active” and “passive” components of the fuel cell [10]. For example, active components are likely to improve with the development of new electrocatalysts in the membrane electrode assembly, which “showed a tremendous performance increase in the past while still having large room for improvement” [10]. Furthermore, passive components, such as bipolar plates, account for approximately 80% of a fuel cell stack’s mass and hold several promising areas for improvement [10]. The bipolar plates (which conduct heat and current, distribute reactant gases, and provide mechanical stability) are currently made of a graphite-polymer composite, which has good corrosion resistance but arguably poor conductivity and stability. Metals could better serve these needs, but they are corrosive. Research into non-corrosive metallic coatings can significantly reduce the thickness and mass of metallic bipolar plates. Combined with further reduction of peripherals (end plates, screws, etc.), researchers expect a 5x increase in stack specific power to levels >10,000 W kg<sup>-1</sup> and justify using 8,000 W kg<sup>-1</sup> for analysis of long-distance passenger air flight [10]. Significant room for improvement still exists for PEMFCs because they were largely developed for automotive applications and technical targets have already been reached; ultra-lightweight applications have yet to be strongly pursued. Additionally, a fuel cell stack’s operating environment will play a role in its required size. Current liquid-cooled fuel cell stacks require ~17% of their mass and ~29% of their volume for cooling equipment, to include the working liquid, container, pumps, radiator, and cooling fan [38]. At higher elevations, it may be possible to reduce cooling requirements due to lower ambient temperatures (see Table S.26).

**Table S.26. US Standard Atmosphere altitude and temperature**

Altitude	Temperature	
	(°C)	(°F)
0 m (0 ft)	15.0	59.0
4,000 m (~13,000 ft)	-10.8	12.6
11,300 m (~37,000 ft)	-56.5	-69.7

[370]

In our analysis, we use the DOE’s Integrated transportation fuel cell power system 2020 targets for the LB scenario and ultimate targets (or higher 2025 targets) for the HB scenario

across all vehicle platforms. One could argue that this assumption is too conservative and should only apply to vehicles that predominantly operate at sea level while fixed-wing aircraft should consider the lower ambient temperatures at altitude that can either reduce or eliminate the need for thermal management. As we will discuss in Section 1.C.5.C.3, though, PEMFCs operating at altitude may require additional equipment not needed at sea-level.

### 1.C.5.C. Hydrogen storage standards

Anubhav Datta of the US Army Aviation and Missile Research, Development, and Engineering Center (AMRDEC) Aeroflightdynamics Directorate and Wayne Johnson of NASA’s Ames Research Center summarize the issues surrounding hydrogen storage in their 2012 paper published by the American Institute of Aeronautics and Astronautics. They find that type-1 and -2 tanks are for storage pressures below 350 bar and are too heavy for aviation, but type-3 tanks (with metal liners) and type-4 tanks (with plastic liners) may be acceptable [54].

Our research will focus on Type-4 tanks. As an example, Table S.27 details a commercially available Type-4 hydrogen storage tank manufactured by Quantum (we will explain the specific energy and energy density ratios in Section 1.C.5.C.1).

**Table S.27. Commercially available Type-4 hydrogen storage tank parameters**

Storage system	Manufacturer/ model	H <sub>2</sub>	Tank		Specific energy ratio	Energy density ratio	Source
		(kg)	(kg)	(L)	(kg H <sub>2</sub> kg storage <sup>-1</sup> )	(kg H <sub>2</sub> L storage <sup>-1</sup> )	
Type 4, 700-bar	Quantum Technologies/ 110463	5.00	92.0	129	0.0543	0.0388	[54]

We should note that there are multiple means of storing hydrogen. While BMW uses a cylindrical, super-insulated cryogenic pressure vessel hydrogen tank, other companies like Volute (now exclusively licensed by Linamar) are developing conformable hydrogen tanks that are more akin to the ~6 m long human small intestine where many loops can be fit into various available locations within the vehicle’s frame [371,372].

#### 1.C.5.C.1. Gravimetric energy density (specific energy), volumetric energy density (energy density), ratio of usable hydrogen specific energy (net useful energy) to maximum hydrogen storage system mass, and ratio of usable hydrogen energy density (net useful energy) to maximum hydrogen storage system volume

$$(SE_{H_2storage}, ED_{H_2storage}, R_{SE}, R_{ED})$$

The DOE reports technical targets for system level hydrogen storage from their Hydrogen Storage Technical Team through US DRIVE [13]. We will use published values from July 2017 shown in Table S.28. Cells in gray indicate values not reported by the DOE but rather derived using Eq. (S.315) and Eq. (S.316). These ratios are a useful way to compare the useable specific energy of hydrogen itself to the useable, system-level specific energy and energy density of a hydrogen storage system. Our results from these equations match the values published by US DRIVE.

Eq. (S.315)

$$R_{SE} \left[ \frac{kg H_2}{kg storage} \right] = \frac{SE_{H_2 storage} \left[ \frac{Wh}{kg storage} \right]}{SE_{H_2} \left[ \frac{Wh}{kg H_2} \right]}$$

Eq. (S.316)

$$R_{ED} \left[ \frac{kg H_2}{L storage} \right] = \frac{ED_{H_2, sys} \left[ \frac{Wh}{L storage} \right]}{SE_{H_2} \left[ \frac{Wh}{kg H_2} \right]}$$

**Table S.28. DOE technical targets for onboard hydrogen storage systems**

Parameter	Units	Onboard hydrogen storage			Predicted performance		
		2020 Target	2025 Target	Ultimate target	300-bar CGH <sub>2</sub>	700-bar CGH <sub>2</sub>	500-bar CcH <sub>2</sub>
Specific energy	Wh kg <sup>-1</sup>	1,500	1,800	2,200	1,800	1,400	2,300
	$\frac{kg H_2}{kg storage}$	0.045	0.054	0.065	0.054	0.042	0.069
Energy density	Wh L <sup>-1</sup>	1,000	1,300	1,700	600	800	1,400
	$\frac{kg H_2}{L storage}$	0.030	0.040	0.050	0.018	0.024	0.042

Data from [13].

As an example of what is commercially available, the 2017 Toyota Mirai has a hydrogen storage system specific energy ratio of 0.044 (kg H<sub>2</sub> kg storage<sup>-1</sup>) and an energy density ratio of 0.025 (kg H<sub>2</sub> kg storage<sup>-1</sup>). Multiplying each of these values by the specific energy of hydrogen (33.3 kWh kg<sup>-1</sup>) yields values of 1,465 Wh kg<sup>-1</sup> and 833 Wh L<sup>-1</sup> for the hydrogen storage system specific energy and energy density, respectively [13].

Since the DOE reports their values as “net usable hydrogen,” we will model that 100% of the hydrogen stored can be used and that the volume values in the tables above account for the ullage required to allow for thermal expansion of the liquid hydrogen. We further model the values as accounting for the fraction of hydrogen that is actually recoverable (e.g. Argonne National Laboratory calculations on LH<sub>2</sub> storage consider 57% hydrogen stored as recoverable due to boil-off, but boil-off can be significantly reduced by using 500-bar CcH<sub>2</sub> tanks) [347]. As per the Hydrogen Storage Technical Team Roadmap from 2017, the DOE values include the mass of the fuel tank, material, valves, regulators, piping, mounting brackets, insulation, added cooling capacity, and all other BOP components; the values exclude the unusable energy as a result of maintaining minimum fuel cell system pressure, flow, and temperature requirements [13].

Regarding potential economies of scale, referring to Table S.28 (which considers storage of 5.6 kg useable H<sub>2</sub>), approximately 93% of the mass and 96% of the volume of a 500-bar CcH<sub>2</sub> storage system belongs to non-fuel components (tank, material, valves, regulators, piping, mounting brackets, insulation, cooling, and BOP). One study suggests that storing a larger amount of fuel in a larger tank would gain storage efficiency; 350-bar, 700-bar, and LH<sub>2</sub> systems show similar performance up to 5 kg H<sub>2</sub> stored, but a LH<sub>2</sub> system will occupy significantly less mass (and volume) than the other systems beyond that point [38]. These researchers concluded

that 700-bar CGH2 systems are best for storing 5 kg hydrogen or less, but LH2 systems will be more efficient for storage beyond 5 kg [38].

Other researchers reason that high-altitude aircraft can use hydrogen storage systems with fewer non-fuel storage requirements. Although heat transfer will lead to increased pressure and boil-off in a liquid hydrogen tank, if hydrogen extraction compensates the incoming heat flow at all times, the insulation or active cooling may not be necessary [10]. “In aircraft operation, sufficient extraction of hydrogen happens during all phases of the flight; the holding times on the ground before and after the flight with little or no hydrogen extraction are critical and determine the tank design” [10].

Excluding the low-temperature benefit at higher altitudes, this concept may also be applicable for other forms of transportation where constant fuel extraction occurs between refueling ports or stations. If a ship sailing across the ocean, for example, uses hydrogen at a rate equal to or faster than boil-off and venting requirements, it may be possible to optimize (minimize) insulation and reduce BOP hydrogen storage system components.

### 1.C.5.C.2. Physical density of hydrogen storage system

( $\rho_{H_2,sys}$ )

Having described the hydrogen storage system’s gravimetric energy density (specific energy) and volumetric energy density (energy density), one can also consider its actual physical density.

Eq. (S.317)

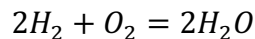
$$\frac{ED_{H_2storage} \left[ \frac{Wh}{L} \right] \cdot \left[ \frac{1,000 L}{m^3} \right]}{SE_{H_2storage} \left[ \frac{Wh}{kg} \right]} = \rho_{H_2,sys} \left[ \frac{kg}{m^3} \right]$$

### 1.C.5.C.3. Fuel cell oxidant supply requirements

The PEMFC electrochemical process requires both hydrogen and oxygen (O<sub>2</sub>). PEMFCs can either extract oxygen from the ambient air (in which case they are called “air breathing”) or from storage tanks, similar to H<sub>2</sub>. Oxygen accounts for ~20.95% of air volume at any altitude, but as air density becomes thinner at higher altitudes, less oxygen molecules are available. Research shows that, at an altitude of 4,000 m (~13,000 ft), PEMFCs need compressors to meet inlet air mass flow requirements, and this accounts for a significant portion of operating power load [38]. The power required to compress inlet air in order to provide sufficient oxygen for PEMFC operation can be calculated as a function of altitude. Some researchers believe that “air breathing” PEMFC designs can be used below 4,000 m but, above that altitude, pure O<sub>2</sub> should be stored onboard using liquid oxygen (LO<sub>2</sub>) as the most efficient (in terms of mass and volume) storage solution [38].

Eq. (S.318) shows the chemical reaction in PEMFC operation.

Eq. (S.318)



A hydrogen atom has the mass of 1.008 u (unified atomic mass, or dalton). An oxygen atom has a mass of 15.999 u. Using a mass balance in Eq. (S.318), the mass ratio of oxygen : hydrogen required is:

**Eq. (S.319)**

$$\frac{2 \cdot 15.999}{2 \cdot 2 \cdot 1.008} = \frac{7.94 [kg O_2]}{1 [kg H_2]}$$

We roughly estimated trendlines for the LO2 storage mass and volume plotted in [38], respectively, as Eq. (S.320) and Eq. (S.321).

**Eq. (S.320)**

$$Total Storage Mass [kg storage] = 1.1 \left[ \frac{kg storage}{kg O_2} \right] \cdot Mass O_2 Stored [kg O_2] + 10 [kg storage]$$

**Eq. (S.321)**

$$Total Storage Volume [L storage] = 0.9 \left[ \frac{L storage}{kg O_2} \right] \cdot Mass O_2 Stored [kg O_2]$$

Therefore, for every 1 kg of H<sub>2</sub> stored, a high-altitude airplane must also store ~7.9 kg of O<sub>2</sub>, which translates into a total of ~19 kg and ~7.1 L (0.0071 m<sup>3</sup>) of O<sub>2</sub> storage per 1 kg of H<sub>2</sub> stored. This is a significant increase in “fuel” storage requirements to support high-altitude flight.

Our analysis neither dictates a cruising altitude for all-electric airplanes nor does it take advantage of lower values of gravity at higher altitudes. We will therefore not consider oxygen storage requirements in our analysis, but we acknowledge that, if high-altitude applications are desired, additional requirements may be necessary.

#### **1.C.5.D. Overall hydrogen fuel cell system efficiency**

We graphically summarize the overall HFC system efficiency by vehicle type in Fig. S.12. The system components shown in gray are the same as previously shown in Fig. S.1 for FF systems, and those in blue are the same as previously shown in Fig. S.11 for BE systems, i.e., these system components remain the same in the HFC variant. System components shown in purple are those added specifically for the HFC variant, which we describe in detail below. Blanks correspond to system components that were necessary for either the FF and/or BE variants but not the HFC variant. We specifically position each system component (and blanks) to allow for comparison between FF, BE, and HFC variants between figures.

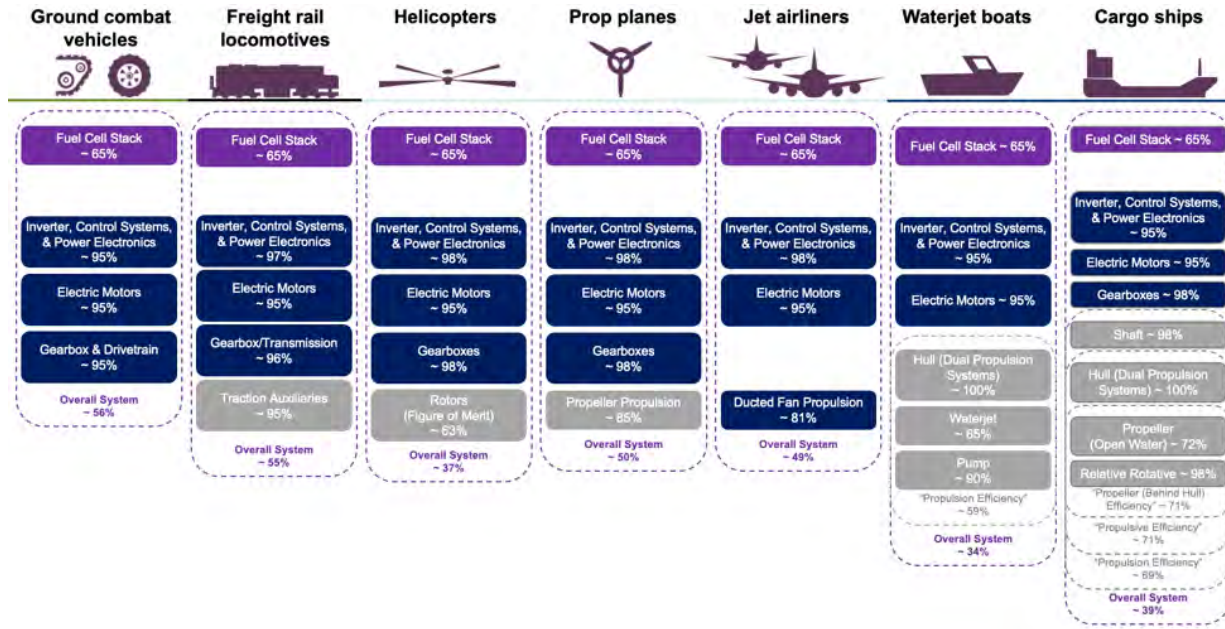


Fig. S.12. Overall HFC system efficiency by vehicle type (same as Fig. 1(c))

### 1.C.5.D.1. Efficiency of fuel cell stack

( $\eta_{FCS}$ )

The DOE reports an achieved peak energy efficiency ( $\eta_{FCS}$ ) of 60% and a technical target of 65% for both 2020 and 2025, calculated as shown in Eq. (S.322) [14].

Eq. (S.322)

$$\eta_{FCS} = \frac{DC \text{ output energy}}{LHV_{H_2}}$$

We use a constant 65% efficiency for the LB, MK, and HB scenarios. As this efficiency covers the system process from the hydrogen fuel to the output DC energy produced, we will further reduce the overall system efficiency with the inverter, electric motor, and drivetrain efficiencies.

### 1.C.5.D.2. Ground combat vehicles

#### 1.C.5.D.2.A. Overall tactical vehicle hydrogen fuel cell system efficiency

( $\eta_{TV,HFC}$ )

We can estimate the overall tactical vehicle HFC system efficiency ( $\eta_{TV,HFC}$ ) as the product of the fuel cell stack efficiency ( $\eta_{FCS}$ ), the combined DC-to-AC inverter, control systems, and power electronics efficiency ( $\eta_i$ ), the motor efficiency ( $\eta_m$ ), and the gearbox/transmission efficiency ( $\eta_{GB}$ ) as show by Eq. (S.323).

Eq. (S.323)

$$\eta_{TV,HFC}[-] = \eta_{FCS}[-] \cdot \eta_i[-] \cdot \eta_m[-] \cdot \eta_{GB}[-]$$



Using the values we previously discussed, this results in an overall system efficiency of ~56%. This matches well to research published in 2004 that used 50% efficiency for fuel cell stacks and found an overall light-duty vehicle efficiency of 44.5% (if we decrease our 65% efficient fuel cell stack to 50%, our overall system efficiency becomes 43%, suggesting the rest of our system component efficiencies are similar) [373]. Over the past 15 years, PEMFCs have become more efficient.

### 1.C.5.D.3. Freight locomotives

#### 1.C.5.D.3.A. Overall freight locomotive hydrogen fuel cell system efficiency

$(\eta_{L,HFC})$

The overall freight locomotive HFC system efficiency ( $\eta_{L,HFC}$ ) is the product of the fuel cell stack efficiency ( $\eta_{FCS}$ ), the combined efficiency of the inverter, control systems, and power electronics ( $\eta_I$ ), the motor efficiency ( $\eta_m$ ), the gearbox/transmission efficiency ( $\eta_{GB}$ ), and the traction auxiliaries efficiency ( $\eta_{TA}$ ) as shown in Eq. (S.324).

Eq. (S.324)

$$\eta_{L,HFC}[-] = \eta_{FCS}[-] \cdot \eta_I[-] \cdot \eta_m[-] \cdot \eta_{GB}[-] \cdot \eta_{TA}[-]$$

This results in an estimated overall locomotive HFC system efficiency of ~55%.

### 1.C.5.D.4. Rotary-wing aircraft

#### 1.C.5.D.4.A. Overall helicopter hydrogen fuel cell system efficiency

$(\eta_{H,HFC})$

The overall helicopter HFC system efficiency ( $\eta_{H,HFC}$ ) is the product of the fuel cell stack efficiency ( $\eta_{FCS}$ ), the combined efficiency of the inverter, control systems, and power electronics ( $\eta_I$ ), the motor efficiency ( $\eta_m$ ), the gearbox/transmission efficiency ( $\eta_{GB}$ ), and the rotor figure of merit ( $\eta_{H,r}$ ) as shown in Eq. (S.325).

Eq. (S.325)

$$\eta_{H,HFC}[-] = \eta_{FCS}[-] \cdot \eta_I[-] \cdot \eta_m[-] \cdot \eta_{GB}[-] \cdot \eta_{H,r}[-]$$

This results in an estimated overall HFC system efficiency of ~37%.

### 1.C.5.D.5. Fixed-wing aircraft

#### 1.C.5.D.5.A. Overall prop airplane hydrogen fuel cell system efficiency

$(\eta_{PA,HFC})$

The overall prop airplane HFC system efficiency ( $\eta_{PA,HFC}$ ) is the product of the fuel cell stack efficiency ( $\eta_{FCS}$ ), the combined efficiency of the inverter, control systems, and power electronics ( $\eta_I$ ), the motor efficiency ( $\eta_m$ ), the gearbox/transmission efficiency ( $\eta_{GB}$ ), and the propeller propulsion efficiency ( $\eta_{TP,P}$ ) as shown in Eq. (S.326).

**Eq. (S.326)**

$$\eta_{PA,HFC}[-] = \eta_{FCS}[-] \cdot \eta_I[-] \cdot \eta_m[-] \cdot \eta_{GB}[-] \cdot \eta_{TP,P}[-]$$

Since the propeller propulsion efficiency was already determined to range from 79% to 90% (see Section 1.C.1.F.4.B), the overall HFC system efficiency will range from 46.9% to 53.4%. This agrees relatively well with the German Aerospace Center's estimate of 44%, which used a 60% efficient fuel cell stack [56]. Note that, as with the BE case, the range of 79% to 90% propeller efficiency flips from the LB to HB scenario and vice versa between the FF system and the HFC system; i.e., whereas a 90% propeller in the FF system corresponded to a LB scenario, it corresponds to the HB scenario in the HFC system.

**1.C.5.D.5.B. Overall ducted fan airplane hydrogen fuel cell system efficiency****( $\eta_{DFA,HFC}$ )**

The overall ducted fan airplane HFC system efficiency ( $\eta_{DFA,HFC}$ ) is the product of the fuel cell stack efficiency ( $\eta_{FCS}$ ), the combined efficiency of the inverter, control systems, and power electronics ( $\eta_I$ ), the motor efficiency ( $\eta_m$ ), and the ducted fan propulsion efficiency ( $\eta_{DF}$ ) as shown in Eq. (S.327). Again, we do not model a gearbox with the ducted fan.

**Eq. (S.327)**

$$\eta_{DFA,HFC}[-] = \eta_{FCS}[-] \cdot \eta_I[-] \cdot \eta_m[-] \cdot \eta_{DF}[-]$$

The overall HFC system efficiency for a ducted fan airplane ranges from 44.0% to 52.5%.

**1.C.5.D.6. Watercraft****1.C.5.D.6.A. Overall waterjet boat hydrogen fuel cell system efficiency****( $\eta_{WJB,HFC}$ )**

The overall HFC system efficiency for a waterjet boat ( $\eta_{WJB,HFC}$ ) is the product of the fuel cell stack efficiency ( $\eta_{FCS}$ ), the combined efficiency of the inverter, control systems, and power electronics ( $\eta_I$ ), the motor efficiency ( $\eta_m$ ), and the propulsion efficiency ( $\eta_{WJB,P}$ ) as shown in Eq. (S.328). A waterjet boat does not require a gearbox.

**Eq. (S.328)**

$$\eta_{WJB,HFC}[-] = \eta_{FCS}[-] \cdot \eta_I[-] \cdot \eta_m[-] \cdot \eta_{WJB,P}[-]$$

Note that we previously calculated the waterjet boat propulsion efficiency in Section 1.C.1.F.5.E, and it includes the hull, waterjet, and pump efficiencies. It ranges from 51.3% to 66.2%, and we must flip the values from the LB to HB scenarios and vice versa from the FF system to the HFC system, i.e., whereas 66.2% correlated to the LB scenario in the FF system, it corresponds to the HB scenario in the HFC system. We model all other efficiency values the same as those used in ground combat vehicles. The resulting overall HFC system efficiency ranges from 30.1% to 38.8%.

### 1.C.5.D.6.B. Overall propeller ship hydrogen fuel cell system efficiency

$(\eta_{PS,HFC})$

Just as with the waterjet boat, the fuel cell stack efficiency, combined efficiency of the inverter, control systems, and power electronics, and the motor efficiency are all modeled the same as in ground combat vehicles. (As a point of reference, Siemens manufactures a PEMFC for submarines with modules that achieve 59% to 69% efficiency [374]). In the case of propeller ships, we must also consider a gearbox with an efficiency of 98% as suggested by a study on crude oil tanker vessels [185]. These efficiencies are combined with the propulsion efficiency ( $\eta_{PS,P}$ ) previously calculated in Section 1.C.1.F.5.N, which ranges from 60.8% to 76.8%. Here again, we must flip the values from the LB to HB scenario and vice versa from the FF system to the HFC system, i.e., whereas 76.8% correlated to the LB scenario in the FF system, it corresponds to the HB scenario in the HFC system. The resulting overall propeller ship HFC system efficiency ( $\eta_{PS,HFC}$ ) ranges from 34.9% to 44.1%, as calculated using Eq. (S.329) which agrees with published estimated for overall efficiency of HFC surface ships of 39% to 42% [375–378].

Eq. (S.329)

$$\eta_{PS,HFC}[-] = \eta_{FCS}[-] \cdot \eta_I[-] \cdot \eta_m[-] \cdot \eta_{GB}[-] \cdot \eta_{PS,P}[-]$$

## 1.D. Part 1: Comparison of equivalent platform “raw” energy by variant

In Part 1 of our analysis, we demonstrate why comparisons that only consider equivalency between onboard storage systems are inadequate. This is a problem because leaders often have little to no engineering expertise and must make decisions on future initiatives and investments based upon incongruent recommendations. Consequently, we believe it is important to demonstrate upfront why such comparisons are inadequate before proceeding to our improved comparison.

### 1.D.1. Fossil fuel variants

#### 1.D.1.A. Mass and volume of onboard fuel in the existing fossil fuel vehicle

$(m_f, V_f)$

This comparison is based upon meeting the raw chemical energy content of a vehicle’s onboard fossil fuel. To begin, we first return to Sections 1.C.1.C.5 and 1.C.1.C.6 and record the mass and volume of fossil fuel carried onboard each vehicle platform.

### 1.D.2. Battery electric variants

#### 1.D.2.A. Mass of battery pack

$(m_B)$

Next, we return to Section 1.C.1.G.1 for the chemical energy content contained within the mass and volume of onboard fossil fuel as well as Section 1.C.4.A.1 for the specific energy of the battery pack. Dividing the chemical energy content by the specific energy of the battery pack yields the mass of battery pack required to hold the same amount of “raw” energy as the mass of fossil fuel in the existing ICE vehicle (Eq. (S.330)).

**Eq. (S.330)**

$$m_B[kg] = \frac{E_{c,FF}[Wh]}{SE_B \left[ \frac{Wh}{kg} \right]}$$

### **1.D.2.B. Volume of battery pack**

$(V_B)$

Similarly, we take the chemical energy content of the onboard fossil fuel from Section 1.C.1.G.1 and divide it by the energy density of a battery pack from Section 1.C.4.A.1 to find the volume of battery pack required to hold the same amount of “raw” energy as the volume of fossil fuel in the existing ICE vehicle (Eq. (S.331)).

**Eq. (S.331)**

$$V_B[m^3] = \frac{E_{c,FF}[Wh]}{ED_B \left[ \frac{Wh}{m^3} \right]}$$

### **1.D.2.C. Mass ratio of battery pack to onboard fossil fuel**

$(m_B : m_f)$

Dividing the mass of battery pack required (Section 1.D.2.A) by the mass of onboard fossil fuel (Section 1.D.1.A) yields the mass ratio of a BE variant’s battery pack to the existing FF vehicle’s fuel. A value greater than one means the battery pack is heavier than fuel with an equivalent raw energy content. A value of one means they are equally as heavy, and a value less than one means the battery pack weighs less than the fuel.

**Eq. (S.332)**

$$m_B[kg] : m_f[kg] = \frac{m_B[kg]}{m_f[kg]}$$

### **1.D.2.D. Volumetric ratio of battery pack to onboard fossil fuel**

$(V_B : V_f)$

Similarly, dividing the volume of battery pack required (Section 1.D.2.B) by the volume of onboard fossil fuel (Section 1.D.1.A) yields the volume ratio of a BE variant’s battery pack to the existing FF vehicle’s fuel with equivalent raw energy content (Eq. (S.333)). A value greater than one means the battery pack is larger than fuel with an equivalent raw energy content. A value of one means they are equal in size, and a value less than one means the battery pack takes up less space than the fuel.

**Eq. (S.333)**

$$V_B[m^3] : V_f[m^3] = \frac{V_B[m^3]}{V_f[m^3]}$$

### 1.D.3. Hydrogen fuel cell variants

#### 1.D.3.A. Mass of stored hydrogen and hydrogen storage system

$(m_{H_2}, m_{H_2storage})$

We can calculate the mass of hydrogen required by taking the chemical energy content of onboard fossil fuel (Section 1.C.1.G.1) and dividing it by the specific energy of hydrogen itself (Section 1.C.5.A.3) as in Eq. (S.334) or by the specific energy of the hydrogen storage system (Section 1.C.5.C.1) as in Eq. (S.335). The former describes the mass of hydrogen that an HFC variant must carry to have the same raw energy content as the FF vehicle, whereas the latter describes the mass of the complete hydrogen storage system required. Even without numbers, one can see that this comparison is unfair in that we do not consider the mass of the fossil fuel tank itself, though its contribution to overall mass is likely relatively small.

Eq. (S.334)

$$m_{H_2} [kg] = \frac{E_{c,FF} [Wh]}{SE_{H_2} \left[ \frac{Wh}{kg} \right]}$$

Eq. (S.335)

$$m_{H_2storage} [kg] = \frac{E_{c,FF} [Wh]}{SE_{H_2storage} \left[ \frac{Wh}{kg} \right]}$$

#### 1.D.3.B. Volume of stored hydrogen and hydrogen storage system

$(V_{H_2}, V_{H_2storage})$

Similarly, the volume of hydrogen required is found by taking the chemical energy content of onboard fossil fuel (Section 1.C.1.G.1) and dividing it by the energy density of hydrogen itself (Section 1.C.5.A.4) as in Eq. (S.336) or by the energy density of the hydrogen storage system (Section 1.C.5.C.1) as in Eq. (S.337). The former describes the volume of hydrogen that an HFC variant carry to have the same raw energy content as the FF vehicle, whereas the latter describes volume of the complete hydrogen storage system required.

Eq. (S.336)

$$V_{H_2} [m^3] = \frac{E_{c,FF} [Wh]}{ED_{H_2} \left[ \frac{Wh}{m^3} \right]}$$

Eq. (S.337)

$$V_{H_2storage} [m^3] = \frac{E_{c,FF} [Wh]}{ED_{H_2storage} \left[ \frac{Wh}{m^3} \right]}$$

### 1.D.3.C. Mass ratio of stored hydrogen to fossil fuel

$(m_{H_2} : m_f)$

Dividing the mass of hydrogen required (Section 1.D.3.A) by the mass of onboard fossil fuel (Section 1.D.1.A) yields the mass ratio of an HFC variant's hydrogen to the existing FF vehicle's fuel (Eq. (S.338)).

**Eq. (S.338)**

$$m_{H_2}[kg] : m_f[kg] = \frac{m_{H_2}[kg]}{m_f[kg]}$$

### 1.D.3.D. Volumetric ratio of stored hydrogen to fossil fuel

$(V_{H_2} : V_f)$

Similarly, dividing the volume of hydrogen required (Section 1.D.3.B) by the volume of onboard fossil fuel (Section 1.D.1.A) yields the volumetric ratio of an HFC variant's hydrogen to the existing FF vehicle's fuel (Eq. (S.339)).

**Eq. (S.339)**

$$V_{H_2}[m^3] : V_f[m^3] = \frac{V_{H_2}[m^3]}{V_f[m^3]}$$

### 1.D.3.E. Mass ratio of hydrogen and storage system to fossil fuel

$(m_{H_2storage} : m_f)$

Dividing the mass of the complete hydrogen storage system (with BOP components) required (Section 1.D.3.A) by the mass of onboard fossil fuel (Section 1.D.1.A) yields the mass ratio of an HFC variant's hydrogen storage system to the existing FF vehicle's fuel (Eq. (S.340)).

**Eq. (S.340)**

$$m_{H_2storage}[kg] : m_f[kg] = \frac{m_{H_2storage}[kg]}{m_f[kg]}$$

### 1.D.3.F. Volumetric ratio of hydrogen and storage system to fossil fuel

$(V_{H_2storage} : V_f)$

Similarly, dividing the volume of the complete hydrogen storage system (with BOP components) required (Section 1.D.3.B) by the volume of onboard fossil fuel (Section 1.D.1.A) yields the volumetric ratio of an HFC variant's hydrogen storage system to the existing FF vehicle's fuel (Eq. (S.341)).

**Eq. (S.341)**

$$V_{H_2storage}[m^3] : V_f[m^3] = \frac{V_{H_2storage}[m^3]}{V_f[m^3]}$$

## 1.E. Part 2: Comparison of equivalent platform “useful” energy by variant

In Part 2 of our analysis, we expand the comparison made in Part 1 by including each variant’s (FF, BE, and HFC) overall system efficiency. Only a certain amount of a vehicle’s onboard energy is actually “useful,” i.e., converting stored chemical energy into useful mechanical energy for vehicular movement is not a 100% efficient process. As we illustrated in Sections 1.C.1.F, 1.C.4.B, and 1.C.5.D, the overall efficiency can be strikingly different based upon the variant’s energy conversion process. Not taking this factor into account results in an unfair and inadequate comparison. By incorporating useful energy, we can obtain a much more accurate comparison than that shown in Part 1.

The equations in Part 2 are the same as those shown above in Part 1 with the exception that some now include the overall system efficiency for either the FF, BE, or HFC system as appropriate. Note that the efficiencies include a “\_\_” prior to the variant designator. This blank is for designating the vehicle type for which we have already calculated the overall system efficiency value: tactical vehicle (TV), locomotive (L), helicopter (H), turboprop airplane (TP), propeller airplane (PA), turbofan airplane (TF), ducted fan airplane (DFA), waterjet boat (WJB), or propeller-driven ship (PS).

### 1.E.1. Fossil fuel variants

#### 1.E.1.A. Mass and volume of onboard fuel in the existing fossil fuel vehicle

$(m_f, V_f)$

No change from Section 1.D.1.A.

### 1.E.2. Battery electric variants

#### 1.E.2.A. Mass of battery pack

$(m_B)$

We take the chemical energy content contained within the mass and volume of onboard fossil fuel (Section 1.C.1.G.1) and multiply it by the overall system efficiency for the appropriate FF vehicle type (Section 1.C.1.F) to find the onboard useful energy for the FF vehicle. We then divide this value by the product of the specific energy of a battery pack (Section 1.C.4.A.1) and the overall system efficiency for the appropriate BE vehicle type (Section 1.C.4.B). The result is the mass of battery pack required to hold the same amount of useful energy as the mass of fossil fuel in the existing ICE vehicle (Eq. (S.342)).

Eq. (S.342)

$$m_B [kg] = \frac{E_{c,FF} [Wh] \cdot \eta_{\_FF}}{SE_B \left[ \frac{Wh}{kg} \right] \cdot \eta_{\_BE}}$$

#### 1.E.2.B. Volume of battery pack

$(V_B)$

We take the same onboard useful energy for the FF vehicle found in the numerator of Eq. (S.342) and divide this value by the product of the energy density of a battery pack (Section 1.C.4.A.1) and the overall system efficiency for the appropriate BE vehicle type (Section

1.C.4.B). The result is the volume of battery pack required to hold the same amount of useful energy as the volume of fossil fuel in the existing ICE vehicle (Eq. (S.343)).

**Eq. (S.343)**

$$V_B[m^3] = \frac{E_{C,FF}[Wh] \cdot \eta_{FF}}{ED_B \left[ \frac{Wh}{m^3} \right] \cdot \eta_{BE}}$$

### 1.E.2.C. Mass ratio of battery pack to onboard fossil fuel

$(m_B : m_f)$

We can now calculate the mass ratio of battery pack to onboard fossil fuel the same as we did in Section 1.D.2.C using Eq. (S.332).

### 1.E.2.D. Volumetric ratio of battery pack to onboard fossil fuel

$(V_B : V_f)$

Similarly, we can calculate the volumetric ratio of battery pack to onboard fossil fuel the same as we did in Section 1.D.2.D using Eq. (S.333).

## 1.E.3. Hydrogen fuel cell variants

### 1.E.3.A. Mass of stored hydrogen and hydrogen storage system

$(m_{H_2}, m_{H_2storage})$

We calculate the mass of hydrogen required by taking the same onboard useful energy for the FF vehicle found in the numerator of Eq. (S.342) and dividing it by the product of the specific energy of hydrogen itself (Section 1.C.5.A.3) and the overall system efficiency of the HFC variant as in Eq. (S.344) or by the product of the specific energy of the hydrogen storage system (Section 1.C.5.C.1) and the overall system efficiency of the HFC variant as in Eq. (S.345). The former describes the mass of hydrogen that an HFC variant must carry to have the same useful energy content as the FF vehicle, whereas the latter describes the mass of the complete hydrogen storage system required.

**Eq. (S.344)**

$$m_{H_2}[kg] = \frac{E_{C,FF}[Wh] \cdot \eta_{FF}}{SE_{H_2} \left[ \frac{Wh}{kg} \right] \cdot \eta_{HFC}}$$

**Eq. (S.345)**

$$m_{H_2storage}[kg] = \frac{E_{C,FF}[Wh] \cdot \eta_{FF}}{SE_{H_2storage} \left[ \frac{Wh}{kg} \right] \cdot \eta_{HFC}}$$



### 1.E.3.B. Volume of stored hydrogen and hydrogen storage system

$(V_{H_2}, V_{H_2storage})$

Similarly, we can calculate the volume of hydrogen required by taking the same onboard useful energy for the FF vehicle found in the numerator of Eq. (S.342) and dividing it by the product of the energy density of hydrogen itself (Section 1.C.5.A.4) and the overall system efficiency of the HFC variant as in Eq. (S.346) or by the product of the energy density of the hydrogen storage system (Section 1.C.5.C.1) and the overall system efficiency of the HFC variant as in Eq. (S.347). The former describes the volume of hydrogen that an HFC variant must carry to have the same useful energy content as the FF vehicle, whereas the latter describes the volume of the complete hydrogen storage system required.

Eq. (S.346)

$$V_{H_2} [m^3] = \frac{E_{c,FF} [Wh] \cdot \eta_{FF}}{ED_{H_2} \left[ \frac{Wh}{m^3} \right] \cdot \eta_{HFC}}$$

Eq. (S.347)

$$V_{H_2storage} [m^3] = \frac{E_{c,FF} [Wh] \cdot \eta_{FF}}{ED_{H_2storage} \left[ \frac{Wh}{m^3} \right] \cdot \eta_{HFC}}$$

### 1.E.3.C. Mass ratio of stored hydrogen to fossil fuel

$(m_{H_2} : m_f)$

No change from Section 1.D.3.C and Eq. (S.338).

### 1.E.3.D. Volumetric ratio of stored hydrogen to fossil fuel

$(V_{H_2} : V_f)$

No change from Section 1.D.3.D and Eq. (S.339).

### 1.E.3.E. Mass ratio of hydrogen and storage system to fossil fuel

$(m_{H_2storage} : m_f)$

No change from Section 1.D.3.E and Eq. (S.340).

### 1.E.3.F. Volumetric ratio of hydrogen and storage system to fossil fuel

$(V_{H_2storage} : V_f)$

No change from Section 1.D.3.F and Eq. (S.341).

### 1.F. Part 3: Calculating solutions for BE and HFC variants with equivalent or improved capabilities compared to existing FF vehicles

In Part 3 of our analysis, we use both graphical and computational optimization methods to find solutions for BE and HFC variants with equivalent or improved capabilities compared to existing FF vehicles. Our equations are based on four characteristics of vehicles that define their performance as well as defined technology levels for seven major variables across two scenarios. The four characteristics that we consider are overall vehicle mass, volume, PWR (or TWR) and range. The seven major variables are electric motor PWR, battery pack-level specific energy and energy density, hydrogen storage system specific energy and energy density, and fuel cell stack system specific power and power density. We consider two scenarios that define the values for the seven major variables: current technology (what is commercially-available today) and future technology (what researchers cite as feasible within the literature or, in a few instances, claims of current technology achievements with reductions applied when applicable), as shown in Table S.29. The electric motor specific power (or PWR) ranges from the radial flux motor used in the BMW i3 to the new axial flux motor produced by Magnax. Although we previously calculated a peak electric motor PWR of  $\sim 12.1 \text{ kW kg}^{-1}$  for the Magnax AXF225, Magnax further claims it has achieved peak values of  $15 \text{ kW kg}^{-1}$ , which we will adopt as our future (feasible) value [379]. Note that, for airplanes, maximum power is required for takeoff and climb portions of the flight profile; consequently, we model the electric motors as capable of sustaining the necessary output to get to cruising altitude and velocity. The battery (pack-level) specific energy and energy density values range from what is currently used by Proterra in electric buses to Sion Power's claimed achievements with an estimated 33% reduction from the cell-level to pack-level applied (the same reduction as used by the DOE and the USABC in creating their technical targets). Hydrogen storage system specific energy and energy density values range from what the 2017 Toyota Mirai currently uses (with BOP components added) to what researchers state is possible for LH2 and what the DOE publishes as an ultimate target. Fuel cell stack (with BOP components) specific power and power density values range from what US DRIVE states is the current status to what researchers and the DOE publish as achievable.

**Table S.29. Current commercial and future feasible technology values for BE and HFC variant design.**

Variable	Units	Current (commercial)	Source	Future (feasible)	Source
Electric motor specific power (PWR)	W kg <sup>-1</sup>	2,976	[11]	15,000	[16]
Battery (pack-level) specific energy	Wh kg <sup>-1</sup>	157	[12]	335	[17,18,20]
Battery (pack-level) energy density	Wh L <sup>-1</sup>	260	[12]	670	[17,18,20]
Hydrogen storage system (w/ BOP) specific energy	Wh kg <sup>-1</sup>	1,465	[13]	21,000	[9] *no BOP
Hydrogen storage system (w/ BOP) energy density	Wh L <sup>-1</sup>	833	[13]	1,700	[13]
Fuel cell stack (w/ BOP) specific power	W kg <sup>-1</sup>	659	[14]	8,000	[10]
Fuel cell stack (w/ BOP) power density	W L <sup>-1</sup>	640	[15]	850	[19]

## 1.F.1. Graphical optimization of solutions

One of the most unique contributions of our research is the method we developed to find solutions for meeting or exceeding the four vehicle characteristics using just two variables: the mass of electric motors and mass of battery pack required for BE variants and the mass of electric motors and mass of hydrogen storage system required for HFC variants. Below, we show the derivation of equations for the lines (and curves for watercraft range) that define equivalency between BE or HFC variants and the existing FF vehicles for each vehicle type and each vehicle characteristic. Note that we can write the relationships that follow either in terms of the gross vehicle weight condition or the curb vehicle weight condition. We conduct our analysis using the gross vehicle weight condition, i.e., including vehicle payload.

### 1.F.1.A. Battery electric variants

#### 1.F.1.A.1. Ground combat vehicles

##### 1.F.1.A.1.A. Equivalent power-to-weight ratio

For BE ground combat vehicles (tactical vehicles), we begin with the first relationship that the BE variant must have an overall PWR greater than or equal to that of the existing FF vehicle (Eq. (S.348)).

**Eq. (S.348)**

$$PWR_{FF,g} \left[ \frac{W}{kg} \right] \leq PWR_{BE,g} \left[ \frac{W}{kg} \right]$$

We previously calculated the PWR of the FF vehicle (see Sections 1.C.1.G.8 and 1.C.1.G.9). We can calculate the overall power of a BE variant using the mass of electric motors and the specific power (or PWR) of the electric motors (Eq. (S.349)).

**Eq. (S.349)**

$$P_{BE,g} [W] = m_m [kg] \cdot PWR_m \left[ \frac{W}{kg} \right]$$

Since the PWR is actually in terms of mass (not weight), we can rewrite Eq. (S.348) as Eq. (S.350).

**Eq. (S.350)**

$$PWR_{FF,g} \left[ \frac{W}{kg} \right] = \frac{P_{FF} [W]}{m_g [kg]} \leq \frac{P_{BE,g} [W]}{m_{BE,g} [kg]}$$

Since ground combat vehicles can benefit from gearboxes paired with the electric motors, we use a scaling factor (see Section 1.C.3.B.19) to estimate the total mass of motors, gearboxes, and oil. We can then calculate the mass of a BE variant by starting with the mass of the FF variant stripped of all its FF components and adding to it the mass of motors, gearboxes, oil, and battery pack required (Eq. (S.351)).

**Eq. (S.351)**

$$m_{BE,g}[kg] = m_{g,strippedFF}[kg] + (F_{m_m+GB+o\_m_m}[-] \cdot m_m[kg]) + m_B[kg]$$

Combining Eq. (S.350) and Eq. (S.351) yields Eq. (S.352).

**Eq. (S.352)**

$$PWR_{FF,g} \left[ \frac{W}{kg} \right] \leq \frac{m_m[kg] \cdot PWR_m \left[ \frac{W}{kg} \right]}{m_{g,strippedFF}[kg] + (F_{m_m+GB+o\_m_m}[-] \cdot m_m[kg]) + m_B[kg]}$$

We can rearrange Eq. (S.352) into Eq. (S.353), which takes the familiar form of the equation of a line:  $y = m \cdot x + b$  where the variable  $y$  is the mass of battery pack required and the variable  $x$  is the mass of electric motors required.

**Eq. (S.353)**

$$m_B[kg] \leq \left( \frac{PWR_m \left[ \frac{W}{kg} \right]}{PWR_{FF,g} \left[ \frac{W}{kg} \right]} - F_{m_m+GB+o\_m_m}[-] \right) \cdot m_m[kg] + (-m_{g,strippedFF}[kg])$$

For ease of use in a spreadsheet and graphing programs, we define the PWR equation as the first vehicle characteristic relationship and, therefore (with subscripts) the slope is given by Eq. (S.354) and the y-intercept by Eq. (S.355).

**Eq. (S.354)**

$$m_1[-] = \left( \frac{PWR_m \left[ \frac{W}{kg} \right]}{PWR_{FF,g} \left[ \frac{W}{kg} \right]} - F_{m_m+GB+o\_m_m}[-] \right)$$

**Eq. (S.355)**

$$b_1[kg] = (-m_{g,strippedFF}[kg])$$

### 1.F.1.A.1.B. Equivalent ratio of onboard useful energy to road load force

Our second vehicle characteristic relationship is that, for the BE variant to have equivalent or improved range, the BE variant must have a ratio of onboard useful energy to road load force greater than or equal to that of the existing FF vehicle (Eq. (S.356)). We previously calculated the left side of the equation using Eq. (S.93) in Section 1.C.2.A.1.E.

**Eq. (S.356)**

$$\frac{OUE_{FF}[Wh]}{RL_{FF,g}[N]} \leq \frac{OUE_{BE,g}[Wh]}{RL_{BE,g}[N]}$$

We calculate the onboard useful energy of the BE variant as a function of the battery pack mass, the specific energy of the battery pack, and the overall system efficiency (Eq. (S.357)).

**Eq. (S.357)**

$$OUE_{BE,g}[Wh] = m_B[kg] \cdot SE_B \left[ \frac{Wh}{kg} \right] \cdot \eta_{TV,BE}[-]$$

The road load force of the BE variant is found the same way as for the FF variant in Section 1.C.2.A.1, except we now use the mass of the BE variant in the gross vehicle weight scenario instead of the gross mass of the FF vehicle (Eq. (S.358)). The mass of the BE variant is the same as in Eq. (S.351).

**Eq. (S.358)**

$$RL_{BE,g}[N] = \left( C_{rr}[-] \cdot m_{BE,g}[kg] \cdot g \left[ \frac{m}{s^2} \right] \right) + \left( \frac{1}{2} \cdot \rho_{air} \left[ \frac{kg}{m^3} \right] \cdot C_d[-] \cdot A_f[m^2] \cdot \left( v \left[ \frac{m}{s} \right] \right)^2 \right) + \left( m_{BE,g}[kg] \cdot g \left[ \frac{m}{s^2} \right] \cdot \sin\theta[-] \right)$$

We can now rewrite Eq. (S.356) as Eq. (S.359) and substitute Eq. (S.357) and Eq. (S.358) to get Eq. (S.360).

**Eq. (S.359)**

$$OUE_{BE,g}[Wh] \geq \left( \frac{OUE_{FF}[Wh]}{RL_{FF,g}[N]} \right) \cdot RL_{BE,g}[N]$$

**Eq. (S.360)**

$$\begin{aligned} & m_B[kg] \cdot SE_B \left[ \frac{Wh}{kg} \right] \cdot \eta_{TV,BE}[-] \\ & \geq \left( \frac{OUE_{FF}[Wh]}{RL_{FF,g}[N]} \right) \\ & \cdot \left( \left( C_{rr}[-] \cdot m_{BE,g}[kg] \cdot g \left[ \frac{m}{s^2} \right] \right) + \left( \frac{1}{2} \cdot \rho_{air} \left[ \frac{kg}{m^3} \right] \cdot C_d[-] \cdot A_f[m^2] \cdot \left( v \left[ \frac{m}{s} \right] \right)^2 \right) \right. \\ & \left. + \left( m_{BE,g}[kg] \cdot g \left[ \frac{m}{s^2} \right] \cdot \sin\theta[-] \right) \right) \end{aligned}$$

Rearranging terms to get our equation of a line format, we get Eq. (S.361) where the slope is given by Eq. (S.362) and the y-intercept by Eq. (S.363).

Eq. (S.361)

$$m_B[kg] \geq \left( \frac{C_{rr}[-] \cdot F_{m_{m+GB+o\_m_m}}[-] + \sin\theta[-] \cdot F_{m_{m+GB+o\_m_m}}[-]}{\frac{SE_B \left[ \frac{Wh}{kg} \right] \cdot \eta_{TV,BE}[-]}{\left( \frac{OUE_{FF}[Wh]}{RL_{FF,g}[N]} \right) \cdot g \left[ \frac{m}{s^2} \right]} - C_{rr}[-] - \sin\theta[-]} \right) \cdot m_m[kg] + \left( \frac{C_{rr}[-] \cdot m_{g,strippedFF}[kg] + \frac{\left( \frac{1}{2} \cdot \rho_{air} \left[ \frac{kg}{m^3} \right] \cdot C_d[-] \cdot A_f[m^2] \cdot \left( v \left[ \frac{m}{s} \right) \right)^2}{g \left[ \frac{m}{s^2} \right]} + \sin\theta[-] \cdot m_{g,strippedFF}[kg]}{\frac{SE_B \left[ \frac{Wh}{kg} \right] \cdot \eta_{TV,BE}[-]}{\left( \frac{OUE_{FF}[Wh]}{RL_{FF,g}[N]} \right) \cdot g \left[ \frac{m}{s^2} \right]} - C_{rr}[-] - \sin\theta[-]} \right)$$

Eq. (S.362)

$$m_2[-] = \left( \frac{C_{rr}[-] \cdot F_{m_{m+GB+o\_m_m}}[-] + \sin\theta[-] \cdot F_{m_{m+GB+o\_m_m}}[-]}{\frac{SE_B \left[ \frac{Wh}{kg} \right] \cdot \eta_{TV,BE}[-]}{\left( \frac{OUE_{FF}[Wh]}{RL_{FF,g}[N]} \right) \cdot g \left[ \frac{m}{s^2} \right]} - C_{rr}[-] - \sin\theta[-]} \right)$$

Eq. (S.363)

$$b_2[kg] = \left( \frac{C_{rr}[-] \cdot m_{g,strippedFF}[kg] + \frac{\left( \frac{1}{2} \cdot \rho_{air} \left[ \frac{kg}{m^3} \right] \cdot C_d[-] \cdot A_f[m^2] \cdot \left( v \left[ \frac{m}{s} \right) \right)^2}{g \left[ \frac{m}{s^2} \right]} + \sin\theta[-] \cdot m_{g,strippedFF}[kg]}{\frac{SE_B \left[ \frac{Wh}{kg} \right] \cdot \eta_{TV,BE}[-]}{\left( \frac{OUE_{FF}[Wh]}{RL_{FF,g}[N]} \right) \cdot g \left[ \frac{m}{s^2} \right]} - C_{rr}[-] - \sin\theta[-]} \right)$$

### 1.F.1.A.1.C. Equivalent overall vehicle volume

Our third vehicle characteristic relationship is the overall volume of the BE variant must be less than or equal to that of the existing FF vehicle (Eq. (S.364)). We previously calculated the right side of the equation using Eq. (S.2) in Section 1.C.1.B.

Eq. (S.364)

$$V_{BE,g}[m^3] \leq V_{FF,g}[m^3]$$

Here again, since ground combat vehicles can benefit from gearboxes paired with the electric motors, we must use a ratio (see Section 1.C.3.B.20) to estimate the total volume of

motors and gearboxes (we consider the volume of oil contained within the volume of the gearboxes). We can then calculate the volume of a BE variant by starting with the volume of the FF variant stripped of all its FF components and adding to it the volume of motors, gearboxes, and battery pack required (Eq. (S.365)).

**Eq. (S.365)**

$$V_{BE}[m^3] = V_{FF,stripped}[m^3] + \left( m_m[kg] \cdot R_{V_{m+GB} \cdot m_m} \left[ \frac{m^3}{kg} \right] \right) + \left( \frac{m_B[kg] \cdot SE_B \left[ \frac{Wh}{kg} \right]}{ED_B \left[ \frac{Wh}{L} \right] \cdot 1,000 \left[ \frac{L}{m^3} \right]} \right)$$

Rearranging terms to get our equation of a line format, we get Eq. (S.366) where the slope is given by Eq. (S.367) and the y-intercept by Eq. (S.368).

**Eq. (S.366)**

$$m_B[kg] \leq \left( - \frac{ED_B \left[ \frac{Wh}{L} \right] \cdot 1,000 \left[ \frac{L}{m^3} \right] \cdot R_{V_{m+GB} \cdot m_m} \left[ \frac{m^3}{kg} \right]}{SE_B \left[ \frac{Wh}{kg} \right]} \right) \cdot m_m[kg] + \left( \left( \frac{1,000 \left[ \frac{L}{m^3} \right] \cdot ED_B \left[ \frac{Wh}{L} \right]}{SE_B \left[ \frac{Wh}{kg} \right]} \right) \cdot (V_{FF,g}[m^3] - V_{FF,stripped}[m^3]) \right)$$

**Eq. (S.367)**

$$m_3[-] = \left( - \frac{ED_B \left[ \frac{Wh}{L} \right] \cdot 1,000 \left[ \frac{L}{m^3} \right] \cdot R_{V_{m+GB} \cdot m_m} \left[ \frac{m^3}{kg} \right]}{SE_B \left[ \frac{Wh}{kg} \right]} \right)$$

**Eq. (S.368)**

$$b_3[kg] = \left( \left( \frac{1,000 \left[ \frac{L}{m^3} \right] \cdot ED_B \left[ \frac{Wh}{L} \right]}{SE_B \left[ \frac{Wh}{kg} \right]} \right) \cdot (V_{FF,g}[m^3] - V_{FF,stripped}[m^3]) \right)$$

#### 1.F.1.A.1.D. Equivalent overall vehicle mass

The fourth and final vehicle characteristic relationship is the overall mass of the BE variant must be less than or equal to that of the existing FF vehicle (Eq. (S.369)). We previously recorded the values for right side of the equation in Section 1.C.1.A.

**Eq. (S.369)**

$$m_{BE,g}[kg] \leq m_{FF,g}[kg]$$

Substituting Eq. (S.351) for the left side of Eq. (S.369) we get Eq. (S.370).

**Eq. (S.370)**

$$m_{g,strippedFF}[kg] + (F_{m_{m+GB+o\_}m_m}[-] \cdot m_m[kg]) + m_B[kg] \leq m_{FF,g}[kg]$$

Rearranging terms to get our equation of a line format, we get Eq. (S.371) where the slope is given by Eq. (S.372) and the y-intercept by Eq. (S.373).

**Eq. (S.371)**

$$m_B[kg] \geq (-F_{m_{m+GB+o\_}m_m}[-]) \cdot m_m[kg] + (m_{FF,g}[kg] - m_{g,strippedFF}[kg])$$

**Eq. (S.372)**

$$m_4[-] = (-F_{m_{m+GB+o\_}m_m}[-])$$

**Eq. (S.373)**

$$b_4[kg] = (m_{FF,g}[kg] - m_{g,strippedFF}[kg])$$

### 1.F.1.A.2. Freight locomotive

#### 1.F.1.A.2.A. Equivalent power-to-weight ratio

For the first vehicle characteristic relationship, we use the same derivation and equations for BE freight locomotives as we did for ground combat vehicles in Section 1.F.1.A.1.A (Eq. (S.348) through Eq. (S.355)). Again, as previously discussed in Sections 1.C.1.E.1, 1.C.3.A, and 1.C.3.B.2, we take a conservative approach and, in the absence of data, do not first subtract away the mass and volume of existing electric motors and gearboxes in the diesel electric locomotive in order to consider these requirements as variables for an all-electric system.

#### 1.F.1.A.2.B. Equivalent ratio of onboard useful energy to tractive effort force

Our second vehicle characteristic relationship is that, for the BE to have equivalent or improved range, the BE variant must have a ratio of onboard useful energy to tractive effort force greater than or equal to that of the existing FF vehicle (Eq. (S.374)). We previously calculated the left side of the equation using Eq. (S.100) in Section 1.C.2.B.2.

**Eq. (S.374)**

$$\frac{OUE_{FF}[Wh]}{TE_{FF,g}[N]} \leq \frac{OUE_{BE,g}[Wh]}{TE_{BE,g}[N]}$$

We calculate the onboard useful energy of the BE variant as a function of the battery pack mass, the specific energy of the battery pack, and the overall system efficiency (Eq. (S.375)).

**Eq. (S.375)**

$$OUE_{BE,g}[Wh] = m_B[kg] \cdot SE_B \left[ \frac{Wh}{kg} \right] \cdot \eta_{L,BE}[-]$$



The tractive effort force of the BE variant is found the same way as for the FF variant in Section 1.C.2.B.1, except we now use the mass of the BE variant in the gross vehicle weight scenario instead of the gross mass of the FF vehicle (Eq. (S.376)). The mass of the BE variant is the same as by Eq. (S.351).

**Eq. (S.376)**

$$TE_{BE,g}[N] = m_{BE}[kg] \cdot g \left[ \frac{m}{s^2} \right] \cdot C_f[-] \cdot F_a[-]$$

We can now rewrite Eq. (S.374) as Eq. (S.377) and substitute Eq. (S.375) and Eq. (S.376) to get Eq. (S.378).

**Eq. (S.377)**

$$OUE_{BE,g}[Wh] \geq \left( \frac{OUE_{FF}[Wh]}{TE_{FF,g}[N]} \right) \cdot TE_{BE,g}[N]$$

**Eq. (S.378)**

$$m_B[kg] \cdot SE_B \left[ \frac{Wh}{kg} \right] \cdot \eta_{L,BE}[-] \geq \left( \frac{OUE_{FF}[Wh]}{TE_{FF,g}[N]} \right) \cdot \left( m_{BE}[kg] \cdot g \left[ \frac{m}{s^2} \right] \cdot C_f[-] \cdot F_a[-] \right)$$

Rearranging terms to get our equation of a line format, we get Eq. (S.379) where the slope is given by Eq. (S.380) and the y-intercept by Eq. (S.381).

**Eq. (S.379)**

$$m_B[kg] \geq \left( \frac{F_{m_m+GB+o_m_m}[-]}{SE_B \left[ \frac{Wh}{kg} \right] \cdot \eta_{L,BE}[-]} \right) \cdot m_m[kg] + \left( \frac{m_{g,strippedFF}[kg]}{SE_B \left[ \frac{Wh}{kg} \right] \cdot \eta_{L,BE}[-]} \right) \cdot \left( \frac{OUE_{FF}[Wh]}{TE_{FF,g}[N]} \right) \cdot g \left[ \frac{m}{s^2} \right] \cdot C_f[-] \cdot F_a[-]$$

Eq. (S.380)

$$m_2[-] = \left( \frac{F_{m_m+GB+o_m}[-]}{SE_B \left[ \frac{Wh}{kg} \right] \cdot \eta_{L,BE}[-]} \right) \cdot \left( \frac{\left( \frac{OUE_{FF}[Wh]}{TE_{FF,g}[N]} \right) \cdot g \left[ \frac{m}{s^2} \right] \cdot C_f[-] \cdot F_a[-]}{-1} \right)$$

Eq. (S.381)

$$b_2[kg] = \left( \frac{m_{g,strippedFF}[kg]}{SE_B \left[ \frac{Wh}{kg} \right] \cdot \eta_{L,BE}[-]} \right) \cdot \left( \frac{\left( \frac{OUE_{FF}[Wh]}{TE_{FF,g}[N]} \right) \cdot g \left[ \frac{m}{s^2} \right] \cdot C_f[-] \cdot F_a[-]}{-1} \right)$$

### 1.F.1.A.2.C. Equivalent overall vehicle volume

For the freight locomotive's third vehicle characteristic relationship, there is no change from Eq. (S.364) through Eq. (S.368) in our derivation from Section 1.F.1.A.1.C.

### 1.F.1.A.2.D. Equivalent overall vehicle mass

For the freight locomotive's fourth vehicle characteristic relationship, there is no change from Eq. (S.369) through Eq. (S.373) in our derivation from Section 1.F.1.A.1.D. However, with locomotives, there is no real benefit to decreasing mass. Locomotive design maximizes weight to maximize the adhesion generated between wheels and rail. The GE ET44AC is already at the maximum weight allowed by infrastructure constraints. We will conduct our freight locomotive analysis in the same manner as the other vehicle types but will remember to consider solutions that maximize allowable vehicle mass.

### 1.F.1.A.3. Rotary-wing aircraft

#### 1.F.1.A.3.A. Equivalent power-to-weight ratio

For the helicopters' first vehicle characteristic relationship, there is no change from Eq. (S.348) through Eq. (S.355) in our derivation from Section 1.F.1.A.1.A.

#### 1.F.1.A.3.B. Equivalent ratio of onboard useful energy to lift force

Our second vehicle characteristic relationship is that, for the BE variant to have equivalent or improved range, the BE variant must have a ratio of onboard useful energy to lift force greater than or equal to that of the existing FF vehicle (Eq. (S.382)). We previously calculated the left side of the equation using Eq. (S.137) in Section 1.C.2.C.3.

**Eq. (S.382)**

$$\frac{OUE_{FF}[Wh]}{L_{FF,g}[N]} \leq \frac{OUE_{BE,g}[Wh]}{L_{BE,g}[N]}$$

We calculate the onboard useful energy of the BE variant as a function of the battery pack mass, the specific energy of the battery pack, and the overall system efficiency (Eq. (S.383)).

**Eq. (S.383)**

$$OUE_{BE,g}[Wh] = m_B[kg] \cdot SE_B \left[ \frac{Wh}{kg} \right] \cdot \eta_{H,BE}[-]$$

The lift force of the BE variant is found the same way as for the FF variant in Section 1.C.2.C.3, except we now use the mass of the BE variant in the gross vehicle weight scenario instead of the gross mass of the FF vehicle (Eq. (S.384)). The mass of the BE variant is the same as by Eq. (S.351).

**Eq. (S.384)**

$$L_{BE,g}[N] = m_{BE,g}[kg] \cdot g \left[ \frac{m}{s^2} \right]$$

We can now rewrite Eq. (S.382) as Eq. (S.385) and substitute Eq. (S.383) and Eq. (S.384) to get Eq. (S.386).

**Eq. (S.385)**

$$OUE_{BE,g}[Wh] \geq \left( \frac{OUE_{FF}[Wh]}{L_{FF,g}[N]} \right) \cdot L_{BE,g}[N]$$

**Eq. (S.386)**

$$m_B[kg] \cdot SE_B \left[ \frac{Wh}{kg} \right] \cdot \eta_{H,BE}[-] \geq \left( \frac{OUE_{FF}[Wh]}{L_{FF,g}[N]} \right) \cdot m_{BE,g}[kg] \cdot g \left[ \frac{m}{s^2} \right]$$

Rearranging terms to get our equation of a line format, we get Eq. (S.387) where the slope is given by Eq. (S.388) and the y-intercept by Eq. (S.389).

**Eq. (S.387)**

$$m_B[kg] \geq \left( \frac{F_{m_m+GB+o} \cdot m_m[-]}{SE_B \left[ \frac{Wh}{kg} \right] \cdot \eta_{H,BE}[-] \cdot \left( \frac{OUE_{FF}[Wh]}{L_{FF,g}[N]} \right) \cdot g \left[ \frac{m}{s^2} \right]} - 1 \right) \cdot m_m[kg] + \left( \frac{m_{g,strippedFF}[kg]}{SE_B \left[ \frac{Wh}{kg} \right] \cdot \eta_{H,BE}[-] \cdot \left( \frac{OUE_{FF}[Wh]}{L_{FF,g}[N]} \right) \cdot g \left[ \frac{m}{s^2} \right]} - 1 \right)$$

Eq. (S.388)

$$m_2[-] = \left( \frac{F_{m_m+GB+o_m}[-]}{SE_B \left[ \frac{Wh}{kg} \right] \cdot \eta_{H,BE}[-]} \right) \left( \frac{OUE_{FF}[Wh]}{L_{FF,g}[N]} \right) \cdot g \left[ \frac{m}{s^2} \right] - 1$$

Eq. (S.389)

$$b_2[kg] = \left( \frac{m_{g,strippedFF}[kg]}{SE_B \left[ \frac{Wh}{kg} \right] \cdot \eta_{H,BE}[-]} \right) \left( \frac{OUE_{FF}[Wh]}{L_{FF,g}[N]} \right) \cdot g \left[ \frac{m}{s^2} \right] - 1$$

#### 1.F.1.A.3.C. Equivalent overall vehicle volume

For the helicopters' third vehicle characteristic relationship, there is no change from Eq. (S.364) through Eq. (S.368) in our derivation from Section 1.F.1.A.1.C.

#### 1.F.1.A.3.D. Equivalent overall vehicle mass

For the helicopters' fourth vehicle characteristic relationship, there is no change from Eq. (S.369) through Eq. (S.373) in our derivation from Section 1.F.1.A.1.D.

#### 1.F.1.A.4. Fixed-wing aircraft

##### 1.F.1.A.4.A. Turboprop airplanes (all-electric propeller airplanes)

##### 1.F.1.A.4.A.1. Equivalent power-to-weight ratio

For the turboprop airplane's first vehicle characteristic relationship, there is only one slight change in terminology from our derivation in Section 1.F.1.A.1.A. Instead of using the maximum rated power of the FF vehicle, we use the maximum rated takeoff power of the turboprop engines to find the overall airplane PWR ( $PWR_{TO,FF,g}$ ). Following the same process as before, we begin with the first relationship that the BE variant must have an overall takeoff PWR greater than or equal to that of the existing FF vehicle (Eq. (S.390)).

Eq. (S.390)

$$PWR_{TO,FF,g} \left[ \frac{W}{kg} \right] \leq PWR_{TO,BE,g} \left[ \frac{W}{kg} \right]$$

We previously calculated the PWR of the FF vehicle at takeoff (see Sections 1.C.1.G.8 and 1.C.1.G.9). We calculate the overall power of a BE variant using the mass of electric motors and the specific power (or PWR) of the electric motors as in Eq. (S.349). Since the PWR is actually in terms of mass (not weight), we can rewrite Eq. (S.390) as Eq. (S.391).

**Eq. (S.391)**

$$PWR_{TO,FF,g} \left[ \frac{W}{kg} \right] = \frac{P_{TO,FF}[W]}{m_g[kg]} \leq \frac{P_{TO,BE,g}[W]}{m_{BE,g}[kg]}$$

As we previously discussed in Section 1.C.1.E.1, turboprop engines make use of reduction gearing, so we assume that all-electric prop planes also use some sort of gearing and use the same scaling factor to approximate an overall mass of combined electric motors and gearboxes (i.e., no change from Eq. (S.351)). An example of this application is Pipistrel's Alpha Trainer Electro BE airplane that uses propeller reduction gears integrated with its electric motor [298]. Combining Eq. (S.391) and Eq. (S.351) yields Eq. (S.392).

**Eq. (S.392)**

$$PWR_{TO,FF,g} \left[ \frac{W}{kg} \right] \leq \frac{m_m[kg] \cdot PWR_m \left[ \frac{W}{kg} \right]}{m_{g,strippedFF}[kg] + \left( F_{m_m+GB+o\_m_m}[-] \cdot m_m[kg] \right) + m_B[kg]}$$

We can rearrange Eq. (S.392) into Eq. (S.393) to get the equation of a line format where Eq. (S.394) is the slope and Eq. (S.395) is the y-intercept.

**Eq. (S.393)**

$$m_B[kg] \leq \left( \frac{PWR_m \left[ \frac{W}{kg} \right]}{PWR_{TO,FF,g} \left[ \frac{W}{kg} \right]} - F_{m_m+GB+o\_m_m}[-] \right) \cdot m_m[kg] + (-m_{g,strippedFF}[kg])$$

**Eq. (S.394)**

$$m_1[-] = \left( \frac{PWR_m \left[ \frac{W}{kg} \right]}{PWR_{TO,FF,g} \left[ \frac{W}{kg} \right]} - F_{m_m+GB+o\_m_m}[-] \right)$$

**Eq. (S.395)**

$$b_1[kg] = (-m_{g,strippedFF}[kg])$$

#### 1.F.1.A.4.A.2. Equivalent cruising range

Our second vehicle characteristic relationship for the turboprop airplane is the cruising range of the BE variant must be greater than or equal to the cruising range of the FF vehicle (Eq. (S.396)).

**Eq. (S.396)**

$$CR_{FF}[m] \leq CR_{BE,g}[m]$$

We previously recorded the maximum cruising range of a turboprop airplane in Section 1.C.1.G.3 and showed how to derive the Breguet range equation estimate of this value. However, at this point, we must derive an estimate of cruising range for an all-electric airplane. The derivation below is useful for all BE and HFC variants of turboprop and turbofan airplanes used within our analysis.

#### **1.F.1.A.4.A.2.A. Deriving a cruising range equation for all-electric aircraft**

$(CR_{BE}, CR_{HFC})$

For a FF airplane, we can use the Breguet range equations to account for the fuel it burns and the airplane becoming lighter over time. With BE aircraft, however, the weight does not change over time, and as an HFC aircraft uses hydrogen, the overall change in weight is negligible. The weight of hydrogen is just a small fraction of the overall airplane's mass, so the extra range achieved due to the HFC aircraft becoming lighter during the later parts of cruise is minimal. Similar to our Breguet range equation derivations, we can derive a cruising range estimate for all-electric airplanes.

We begin by making several basic assumptions. First, all energy goes toward movement, i.e., we do not consider ancillary power loads for instruments, lights, controls, passenger accessories, etc. Second, we only consider cruising flight, i.e., we neglect energy requirements for taxiing, take-off, climb, descent, landing, and safety reserves. Third, we consider cruising flight is at a constant velocity (zero acceleration) and constant altitude (no change in air density).

Returning to basic principles:

**Eq. (S.397)**

$$\text{energy} = \text{capacity to do work}$$

**Eq. (S.398)**

$$\text{work} = \text{force} \times \text{distance}$$

The force required by an aircraft for forward movement is thrust,  $T[N]$ . Therefore, energy is equal to the thrust produced times the distance covered:

**Eq. (S.399)**

$$\text{energy} = \text{thrust} \times \text{distance}$$

We can calculate the onboard useful energy for an all-electric airplane using Eq. (S.400) for a BE variant or Eq. (S.401) for an HFC variant where the “\_\_\_” can be designated as either “PA” for a propeller airplane or “DFA” for a ducted fan airplane. Note that, for units to balance in future equations, the specific energy of the battery pack must be in units of  $\left[\frac{Ws}{kg}\right]$ .

**Eq. (S.400)**

$$OUE_{BE}[Ws] = m_B[kg] \cdot SE_B \left[ \frac{Ws}{kg} \right] \cdot \eta_{\_BE}$$

**Eq. (S.401)**

$$OUE_{HFC}[Ws] = m_{H_2storage}[kg] \cdot SE_{H_2storage} \left[ \frac{Ws}{kg} \right] \cdot \eta_{\_HFC}$$

From our assumptions, Eq. (S.402) through Eq. (S.404) apply at cruise.

**Eq. (S.402)**

$$L = W$$

**Eq. (S.403)**

$$T = D$$

**Eq. (S.404)**

$$\frac{L}{D} = \frac{W}{T}$$

We can rearrange Eq. (S.404) to get Eq. (S.405).

**Eq. (S.405)**

$$T = W \frac{D}{L}$$

Combining Eq. (S.399), Eq. (S.400), and Eq. (S.405) (and calling “distance” the “cruising range”) gives us Eq. (S.406) for a BE variant and Eq. (S.407) for an HFC variant.

**Eq. (S.406)**

$$m_B[kg] \cdot SE_B \left[ \frac{Ws}{kg} \right] \cdot \eta_{\_BE}[-] = W[N] \frac{D[N]}{L[N]} \cdot CR[m]$$

**Eq. (S.407)**

$$m_{H_2storage}[kg] \cdot SE_{H_2storage} \left[ \frac{Ws}{kg} \right] \cdot \eta_{\_HFC}[-] = W[N] \frac{D[N]}{L[N]} \cdot CR[m]$$

We can now solve for the cruising range to get Eq. (S.408) for BE variants and Eq. (S.409) for HFC variants.

**Eq. (S.408)**

$$CR[m] = \frac{m_B[kg] \cdot SE_B \left[ \frac{Ws}{kg} \right] \cdot \eta_{\_,BE}[-]}{m_{BE}[kg] \cdot g \left[ \frac{m}{s^2} \right]} \cdot \frac{L[N]}{D[N]}$$

**Eq. (S.409)**

$$CR[m] = \frac{m_{H_2storage}[kg] \cdot SE_{H_2storage} \left[ \frac{Ws}{kg} \right] \cdot \eta_{\_,HFC}[-]}{m_{HFC}[kg] \cdot g \left[ \frac{m}{s^2} \right]} \cdot \frac{L[N]}{D[N]}$$

We can further make these two equations more succinct by substituting Eq. (S.400) and Eq. (S.401) into the numerator of each.

**Eq. (S.410)**

$$CR[m] = \frac{OUE_{BE}[Ws]}{m_{BE}[kg] \cdot g \left[ \frac{m}{s^2} \right]} \cdot \frac{L[N]}{D[N]}$$

**Eq. (S.411)**

$$CR[m] = \frac{OUE_{HFC}[Ws]}{m_{HFC}[kg] \cdot g \left[ \frac{m}{s^2} \right]} \cdot \frac{L[N]}{D[N]}$$

Our Eq. (S.410) is, essentially, the same equation derived and used by multiple other researchers [56,380–382]. A useful way to rearrange the terms of this equation is shown by Eq. (S.412) for BE variants and Eq. (S.413) for HFC variants.

**Eq. (S.412)**

$$CR[km] = \left( \frac{m_B[kg]}{m_{g,BE}[kg]} \right) \cdot \left( \frac{1}{g \left[ \frac{m}{s^2} \right]} \right) \cdot \left( \frac{L[N]}{D[N]} \right) \cdot \left( SE_B \left[ \frac{Wh}{kg} \right] \right) \cdot (\eta_{\_,BE}[-]) \cdot \left[ \frac{3,600 \left[ \frac{s}{hr} \right]}{1,000 \left[ \frac{m}{km} \right]} \right]$$

**Eq. (S.413)**

$$CR[km] = \left( \frac{m_{H_2storage}[kg]}{m_{g,HFC}[kg]} \right) \cdot \left( \frac{1}{g \left[ \frac{m}{s^2} \right]} \right) \cdot \left( \frac{L[N]}{D[N]} \right) \cdot \left( SE_{H_2storage} \left[ \frac{Wh}{kg} \right] \right) \cdot (\eta_{\_,BE}[-]) \cdot \left[ \frac{3,600 \left[ \frac{s}{hr} \right]}{1,000 \left[ \frac{m}{km} \right]} \right]$$

Note that we have changed the units on cruising range to kilometers, the units on specific energy to watt-hours per kilogram, and included unit conversions. This form of these two equations is helpful because each term has a useful meaning. The first term is a ratio of energy



storage mass to the overall airplane mass. Put in other words, this is the percent of the airplane's mass that goes toward onboard energy storage. Higher values for this term are desirable because they will increase the airplane's range, but lower values are desirable for practicality. We want airplanes with a high payload capacity, but the more we use an airplane's payload to carry energy storage, the less payload remains for transporting cargo or passengers. To put this term into perspective, the mass ratio of jet fuel to MTOW is  $\sim 0.22$  for our average prop plane,  $\sim 0.30$  for the Boeing 737-700 NG, and  $\sim 0.43$  for the Boeing 747-8. The second term is the inverse of gravity. Although gravity decreases with altitude, we neglect any changes to the gravity term in this analysis and use the gravitational constant at sea level in all calculations; the difference in results is small, and it eliminates discrepancies that may result from operating different variants of an airplane platform at different altitudes. The third term is the L/D ratio. Because the L/D ratio depends upon airplane design parameters outside the scope of this analysis, we model the L/D ratio as constant upon transitioning from a FF airplane to an all-electric variant. The third term is the specific energy, or gravimetric energy density, of the energy storage in terms of typically-used units of Wh kg<sup>-1</sup>. We can see that a percent increase in the specific energy will increase range by the same percentage. The fourth term is the overall system efficiency of the variant. For comparison, we have summarized the values for the approximate average overall system efficiency by platform and variant in Table S.30.

**Table S.30. Approximate average overall system efficiency by airplane platform and variant**

<b>Platform / Variant:</b>	<b>FF</b>	<b>BE</b>	<b>HFC</b>
Average prop plane	22%	70%	50%
Medium-haul jet airliner	32%	69%	49%
Long-haul jet airliner	35%	69%	49%

Eq. (S.412) and Eq. (S.413) are also helpful because they allow us to graph design estimates for maximum cruising range based upon energy storage technology achievements as shown in Fig. S.13 and Fig. S.14.

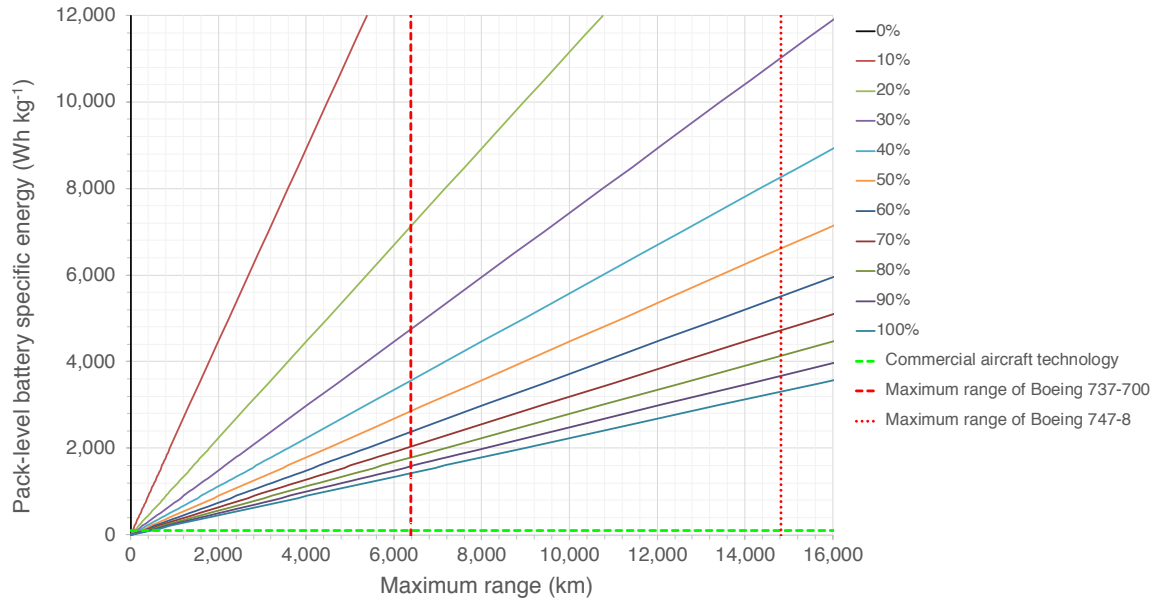


**Fig. S.13. Estimates of maximum range for a BE airplane by percent total airplane mass attributed to the battery pack and the pack-level battery specific energy.**

Calculations use a specified L/D ratio of 17.7 and BE airplane overall system efficiency of 69.0%. Solid lines represent the ratio (by percentage) of battery pack mass to MGTOW. The horizontal dashed green line denotes pack-level battery specific energy in commercial BE aircraft [329]. Vertical dashed and dotted red lines denote the maximum range of select commercial aircraft.

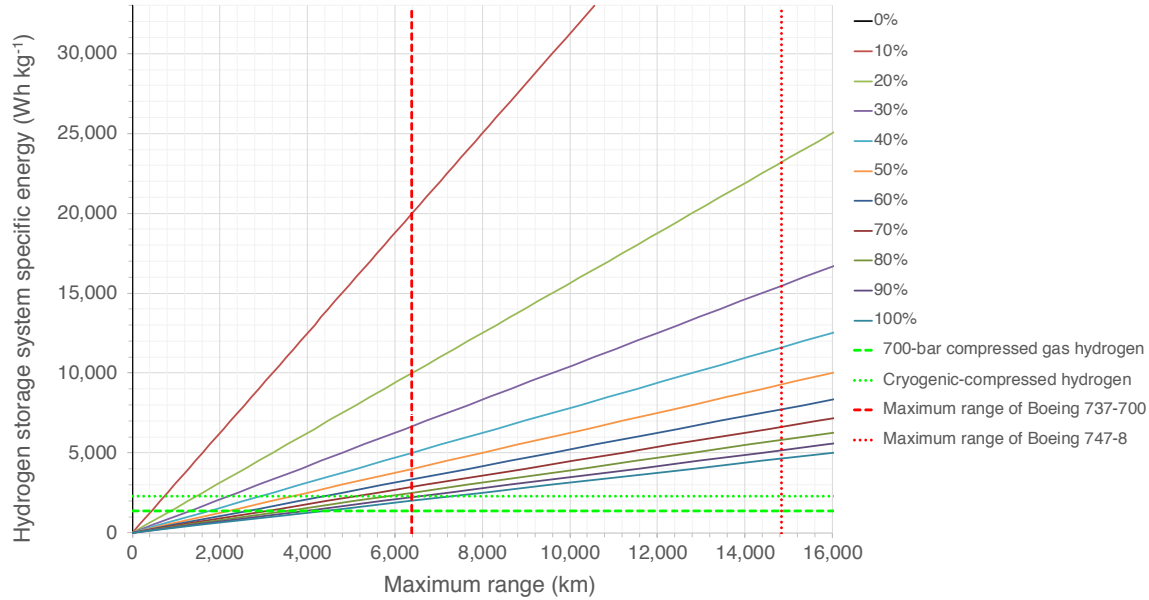


**Fig. S.14. Estimates of maximum range for an HFC airplane by percent total airplane mass attributed to the hydrogen storage system and the hydrogen storage system specific energy.**

Calculations use a specified L/D ratio of 17.7 and HFC airplane overall system efficiency of 49.2%. Solid lines represent the ratio (by percentage) of hydrogen storage system mass to MGTOW. The horizontal dashed and dotted green lines denote the specific energy of commercial 700-bar compressed gas and projected cryogenic-compressed hydrogen systems, respectively [13]. Vertical dashed and dotted red lines denote the maximum range of select commercial aircraft.

Because our methodology changes with fixed-wing aircraft, we believe it is worth taking a moment to check if our concept of comparing ratios of onboard useful energy to the force that must be overcome for movement is valid for estimating range equivalency between variants. If we start with the definition of work (Eq. (S.414)) and relate the work that can be accomplished by an airplane to its onboard useful energy, the force that must be overcome during cruise to aerodynamic drag, and the distance to cruising range, we get Eq. (S.415) and Eq. (S.416).

**Eq. (S.414)**

$$\text{work} = \text{force} \times \text{distance}$$

**Eq. (S.415)**

$$\text{onboard useful energy} = \text{drag} \times \text{cruising range}$$

**Eq. (S.416)**

$$\frac{OUE}{CR} = D$$

Using a BE airplane as an example, we can expand Eq. (S.416) to get Eq. (S.417) using our previously derived Eq. (S.400) and Eq. (S.410).

**Eq. (S.417)**

$$\frac{OUE_{BE,g}[Ws]}{CR_{BE,g}[m]} = \frac{m_B[kg] \cdot SE_B \left[ \frac{Ws}{kg} \right] \cdot \eta_{-,BE}[-]}{\frac{OUE_{BE,g}[Ws] \cdot \left( \frac{L[N]}{D[N]} \right)}{m_{BE,g}[kg] \cdot g \left[ \frac{m}{s^2} \right]}}$$

Further expanding the onboard useful energy and lift in the denominator yields Eq. (S.418), which, when further reduced, shows that our equations and applications are consistent.

**Eq. (S.418)**

$$\frac{OUE_{BE,g}[Ws]}{CR_{BE,g}[m]} = \frac{m_B[kg] \cdot SE_B \left[ \frac{Ws}{kg} \right] \cdot \eta_{-,BE}[-]}{\frac{\left( m_B[kg] \cdot SE_B \left[ \frac{Ws}{kg} \right] \cdot \eta_{-,BE}[-] \right) \cdot \left( \frac{m_{BE,g}[kg] \cdot g \left[ \frac{m}{s^2} \right]}{D[N]} \right)}{m_{BE,g}[kg] \cdot g \left[ \frac{m}{s^2} \right]}} = D[N]$$

Therefore, we could have been consistent in our methodology and continued to use a ratio of onboard useful energy to force that must be overcome for movement. In the case of fixed-wing aircraft, the force that must be overcome, drag, is given by Eq. (S.419).

**Eq. (S.419)**

$$D[N] = C_d[-] \cdot \left( \frac{\rho_{air} \left[ \frac{kg}{m^3} \right] \cdot \left( v \left[ \frac{m}{s} \right] \right)^2}{2} \right) \cdot A_{ref}[m^2]$$

At this point, however, we would have some challenges in making fair comparisons between variants. For example, the drag reference area ( $A_{ref}$ ) can be the total surface area, the frontal area, or the wing area, so long as all calculations are consistent and the corresponding drag coefficient ( $C_d$ ) is used. For ground combat vehicles, we model the front profile area as staying the same and that new variants are simply different in length. Freight locomotives are so heavy that air resistance is negligible when calculating the tractive effort required. For rotary-wing aircraft, we neglect drag altogether and simply consider the lift force at hover. With watercraft, we model the front profile area exposed to air as staying the same and that changes in air resistance are negligible compared to water resistance from changes to the hull. For fixed-wing aircraft then, we could assume that the reference area does not change between variants, but if we want to maintain the same cruising velocity, then the onboard useful energy must be equal between variants to achieve equal cruising range. Since we already have equations for estimating range, we elect to use those equations directly in our analysis. This requires assuming that the lift-to-drag ratio, which depends upon many design variables, stays constant between variants, but it avoids specifically dictating that the reference surface area does not change.

Returning to our second vehicle characteristic relationship, we can now substitute Eq. (S.410) into Eq. (S.396) to get Eq. (S.420).

**Eq. (S.420)**

$$CR_{FF}[m] \leq CR_{BE,g}[m] = \frac{OUE_{BE,g}[Ws]}{m_{BE,g}[kg] \cdot g \left[ \frac{m}{s^2} \right]} \cdot \left( \frac{L[N]}{D[N]} \right)$$

Further substituting Eq. (S.400) and Eq. (S.351) into Eq. (S.420) yields Eq. (S.421).

**Eq. (S.421)**

$$CR_{FF}[m] \leq \frac{m_B[kg] \cdot SE_B \left[ \frac{Ws}{kg} \right] \cdot \eta_{PA,BE}[-]}{\left( m_{g,strippedFF}[kg] + (F_{m_{m+GB+o\_}m_m}[-] \cdot m_m[kg]) + m_B[kg] \right) \cdot g \left[ \frac{m}{s^2} \right]} \cdot \left( \frac{L[N]}{D[N]} \right)$$

Rearranging Eq. (S.421) into the equation of a line format, we get Eq. (S.422) where the slope is given by Eq. (S.423) and the y-intercept by Eq. (S.424).

**Eq. (S.422)**

$$m_B[kg] \geq \left( \frac{\frac{F_{m_{m+GB+o\_}m_m}[-]}{SE_B \left[ \frac{Ws}{kg} \right] \cdot \eta_{PA,BE}[-] \cdot \left( \frac{L[N]}{D[N]} \right)} - 1}{CR_{FF}[m] \cdot g \left[ \frac{m}{s^2} \right]} \right) \cdot m_m[kg] + \left( \frac{\frac{m_{g,strippedFF}[kg]}{SE_B \left[ \frac{Ws}{kg} \right] \cdot \eta_{PA,BE}[-] \cdot \left( \frac{L[N]}{D[N]} \right)} - 1}{CR_{FF}[m] \cdot g \left[ \frac{m}{s^2} \right]} \right)$$

**Eq. (S.423)**

$$m_2[-] = \left( \frac{\frac{F_{m_{m+GB+o\_}m_m}[-]}{SE_B \left[ \frac{Ws}{kg} \right] \cdot \eta_{PA,BE}[-] \cdot \left( \frac{L[N]}{D[N]} \right)} - 1}{CR_{FF}[m] \cdot g \left[ \frac{m}{s^2} \right]} \right)$$

Eq. (S.424)

$$b_2[kg] = \left( \frac{m_{g,strippedFF}[kg]}{\frac{SE_B \left[ \frac{WS}{kg} \right] \cdot \eta_{PA,BE}[-] \cdot \left( \frac{L[N]}{D[N]} \right)}{CR_{FF}[m] \cdot g \left[ \frac{m}{s^2} \right]} - 1 \right)$$

#### 1.F.1.A.4.A.3. Equivalent overall vehicle volume

For the turboprop airplane's third vehicle characteristic relationship, there is no change from Eq. (S.364) through Eq. (S.368) in our derivation from Section 1.F.1.A.1.C.

#### 1.F.1.A.4.A.4. Equivalent overall vehicle mass

For the turbofan airplane's fourth vehicle characteristic relationship, there is no change from Eq. (S.369) through Eq. (S.373) in our derivation from Section 1.F.1.A.1.D.

#### 1.F.1.A.4.B. Turbofan airplanes (all-electric ducted fan airplanes)

##### 1.F.1.A.4.B.1. Equivalent thrust-to-weight ratio

Instead of terms of power, turbofan airplanes are rated in terms of thrust, so the first vehicle characteristic relationship is that the takeoff TWR of the BE variant must be greater than or equal to that of the FF vehicle (Eq. (S.425)).

Eq. (S.425)

$$TWR_{TO,FFg} \left[ \frac{N}{N} \right] \leq TWR_{TO,BE,g} \left[ \frac{N}{N} \right]$$

We previously found the TWR at takeoff for the FF vehicle in Section 1.C.2.D.2. For all-electric variants, we related takeoff thrust and power in Section 1.C.2.D.3. We calculate the mass of the BE variant by taking the same equation used for other vehicles (Eq. (S.351)) and adding the mass of propulsor components (Eq. (S.183)). Note that, since we model direct drive fans with no gearboxes, the scaling factor for the total mass of electric motors, gearboxes, and oil used per dry mass of electric motors used is simply 1.0 (see Section 1.C.3.B.19). Combining Eq. (S.183) and Eq. (S.184) from Section 1.C.2.D.3 with Eq. (S.425) yields Eq. (S.426), which we can rearrange into the equation of a line format (Eq. (S.427)) where the slope is given by Eq. (S.428) and the y-intercept by Eq. (S.429).

Eq. (S.426)

$$TWR_{TO,FFg} \left[ \frac{N}{N} \right] \leq \frac{\frac{m_m[kg] \cdot PWR_m \left[ \frac{W}{kg} \right]}{R_{DFTOP,TOT} \left[ \frac{W}{N} \right]}}{\left( m_{g,strippedFF}[kg] + (F_{m_m+GB+o,m_m}[-] \cdot m_m[kg]) + \left( c_m \left[ \frac{kg}{W} \right] \cdot m_m[kg] \cdot PWR_m \left[ \frac{W}{kg} \right] + c_b[kg] \right) + m_B[kg] \right) \cdot g \left[ \frac{m}{s^2} \right]}$$

**Eq. (S.427)**

$$m_B[kg] \leq \left( \frac{PWR_m \left[ \frac{W}{kg} \right]}{R_{DFTOP\_TOT} \left[ \frac{W}{N} \right] \cdot TWR_{TO,FFg} \left[ \frac{N}{N} \right] \cdot g \left[ \frac{m}{s^2} \right]} - F_{m_m+GB+o\_m_m}[-] \right. \\ \left. - \left( c_m \left[ \frac{kg}{W} \right] \cdot PWR_m \left[ \frac{W}{kg} \right] \right) \right) \cdot m_m[kg] + \left( -(c_b[kg] + m_{g,strippedFF}[kg]) \right)$$

**Eq. (S.428)**

$$m_1[-] = \left( \frac{PWR_m \left[ \frac{W}{kg} \right]}{R_{DFTOP\_TOT} \left[ \frac{W}{N} \right] \cdot TWR_{TO,FFg} \left[ \frac{N}{N} \right] \cdot g \left[ \frac{m}{s^2} \right]} - F_{m_m+GB+o\_m_m}[-] \right. \\ \left. - \left( c_m \left[ \frac{kg}{W} \right] \cdot PWR_m \left[ \frac{W}{kg} \right] \right) \right)$$

**Eq. (S.429)**

$$b_1[kg] = \left( -(c_b[kg] + m_{g,strippedFF}[kg]) \right)$$

#### 1.F.1.A.4.B.2. Equivalent cruising range

For the second vehicle characteristic relationship, we begin with the same relationship for cruising range that we used for turboprop airplanes in Eq. (S.420). Using our estimated efficiency for BE ducted fan airplanes (see Section 1.C.4.B.4.C) and our method for calculating the mass of BE ducted fan airplanes (see Section 1.F.1.A.4.B.1), we can expand Eq. (S.420) to get Eq. (S.430).

**Eq. (S.430)**

$$CR_{FF}[m] \leq \frac{m_B[kg] \cdot SE_B \left[ \frac{WS}{kg} \right] \cdot \eta_{DFA,BE}[-]}{\left( m_{g,strippedFF}[kg] + (F_{m_m+GB+o\_m_m}[-] \cdot m_m[kg]) + \left( \left( c_m \left[ \frac{kg}{W} \right] \cdot m_m[kg] \cdot PWR_m \left[ \frac{W}{kg} \right] \right) + c_b[kg] \right) + m_B[kg] \right) \cdot g \left[ \frac{m}{s^2} \right]} \cdot \left( \frac{L[N]}{D[N]} \right)$$

Rearranging Eq. (S.430) into the equation of a line format gives us Eq. (S.431), where the slope is given by Eq. (S.432) and the y-intercept by Eq. (S.433).

Eq. (S.431)

$$m_B[kg] \geq \left( \frac{c_m \left[ \frac{kg}{W} \right] \cdot PWR_m \left[ \frac{W}{kg} \right] + F_{m_{m+GB+o\_m_m}}[-]}{SE_B \left[ \frac{WS}{kg} \right] \cdot \eta_{DFA, BE}[-] \cdot \left( \frac{L[N]}{D[N]} \right) - 1} \right) \cdot m_m[kg]$$

$$+ \left( \frac{c_b[kg] + m_{g,strippedFF}[kg]}{SE_B \left[ \frac{WS}{kg} \right] \cdot \eta_{DFA, BE}[-] \cdot \left( \frac{L[N]}{D[N]} \right) - 1} \right) \cdot \left( \frac{CR_{FF}[m] \cdot g \left[ \frac{m}{s^2} \right]}{CR_{FF}[m] \cdot g \left[ \frac{m}{s^2} \right]} - 1 \right)$$

Eq. (S.432)

$$m_2[-] = \left( \frac{c_m \left[ \frac{kg}{W} \right] \cdot PWR_m \left[ \frac{W}{kg} \right] + F_{m_{m+GB+o\_m_m}}[-]}{SE_B \left[ \frac{WS}{kg} \right] \cdot \eta_{DFA, BE}[-] \cdot \left( \frac{L[N]}{D[N]} \right) - 1} \right) \cdot \left( \frac{CR_{FF}[m] \cdot g \left[ \frac{m}{s^2} \right]}{CR_{FF}[m] \cdot g \left[ \frac{m}{s^2} \right]} - 1 \right)$$

Eq. (S.433)

$$b_2[kg] = \left( \frac{c_b[kg] + m_{g,strippedFF}[kg]}{SE_B \left[ \frac{WS}{kg} \right] \cdot \eta_{DFA, BE}[-] \cdot \left( \frac{L[N]}{D[N]} \right) - 1} \right) \cdot \left( \frac{CR_{FF}[m] \cdot g \left[ \frac{m}{s^2} \right]}{CR_{FF}[m] \cdot g \left[ \frac{m}{s^2} \right]} - 1 \right)$$

### 1.F.1.A.4.B.3. Equivalent overall vehicle volume

The third vehicle characteristic relationship, that the overall volume of the BE variant must be less than or equal to that of the existing FF vehicle, is the same as Eq. (S.364) in Section 1.F.1.A.1.C. However, since we model a BE variant as using the ducted fan portion of turbofan engines for propulsion, we must add back in the volume of the FF engines (which we removed to find the stripped volume of the FF variant) to estimate their size. Therefore, we calculate the volume of a BE ducted fan airplane by taking Eq. (S.365) and adding the original engine volume (Eq. (S.434)).



**Eq. (S.434)**

$$V_{BE}[m^3] = V_{FF,stripped}[m^3] + \left( m_m[kg] \cdot R_{V_{m+GB} \cdot m_m} \left[ \frac{m^3}{kg} \right] \right) + \left( \frac{m_B[kg] \cdot SE_B \left[ \frac{Wh}{kg} \right]}{ED_B \left[ \frac{Wh}{L} \right] \cdot 1,000 \left[ \frac{L}{m^3} \right]} \right) + V_{total,e}[m^3]$$

Rearranging Eq. (S.434) into the equation of a line format gives us Eq. (S.435), where the slope is given by Eq. (S.436) and the y-intercept by Eq. (S.437).

**Eq. (S.435)**

$$m_B[kg] \leq \left( - \frac{ED_B \left[ \frac{Wh}{L} \right] \cdot 1,000 \left[ \frac{L}{m^3} \right] \cdot R_{V_{m+GB} \cdot m_m} \left[ \frac{m^3}{kg} \right]}{SE_B \left[ \frac{Wh}{kg} \right]} \right) \cdot m_m[kg] + \left( \left( \frac{1,000 \left[ \frac{L}{m^3} \right] \cdot ED_B \left[ \frac{Wh}{L} \right]}{SE_B \left[ \frac{Wh}{kg} \right]} \right) \cdot (V_{FF,g}[m^3] - V_{FF,stripped}[m^3] - V_{total,e}[m^3]) \right)$$

**Eq. (S.436)**

$$m_3[-] = \left( - \frac{ED_B \left[ \frac{Wh}{L} \right] \cdot 1,000 \left[ \frac{L}{m^3} \right] \cdot R_{V_{m+GB} \cdot m_m} \left[ \frac{m^3}{kg} \right]}{SE_B \left[ \frac{Wh}{kg} \right]} \right)$$

**Eq. (S.437)**

$$b_3[kg] = \left( \left( \frac{1,000 \left[ \frac{L}{m^3} \right] \cdot ED_B \left[ \frac{Wh}{L} \right]}{SE_B \left[ \frac{Wh}{kg} \right]} \right) \cdot (V_{FF,g}[m^3] - V_{FF,stripped}[m^3] - V_{total,e}[m^3]) \right)$$

#### **1.F.1.A.4.B.4. Equivalent overall vehicle mass**

The fourth vehicle characteristic relationship, that the overall mass of the BE variant must be less than or equal to that of the existing FF vehicle, is the same as Eq. (S.369) in Section 1.F.1.A.1.D. However, as described above in Section 1.F.1.A.4.B.1, the mass of the BE variant must also include the mass of propulsor components (Eq. (S.183)), as shown by Eq. (S.438).

**Eq. (S.438)**

$$m_{BE,g}[kg] = m_{g,strippedFF}[kg] + (F_{m_m+GB+o\_m_m}[-] \cdot m_m[kg]) + m_{PC}[kg] + m_B[kg]$$

Substituting Eq. (S.438) and Eq. (S.183) into Eq. (S.369) yields Eq. (S.439).

**Eq. (S.439)**

$$m_{g,strippedFF}[kg] + (F_{m_m+GB+o\_m_m}[-] \cdot m_m[kg]) + \left( \left( c_m \left[ \frac{kg}{W} \right] \cdot m_m[kg] \cdot PWR_m \left[ \frac{W}{kg} \right] \right) + c_b[kg] \right) + m_B[kg] \leq m_{FF,g}[kg]$$

Rearranging Eq. (S.439) into the equation of a line format gives us Eq. (S.440), where the slope is given by Eq. (S.441) and the y-intercept by Eq. (S.442).

**Eq. (S.440)**

$$m_B[kg] \geq \left( -F_{m_m+GB+o\_m_m}[-] - \left( c_m \left[ \frac{kg}{W} \right] \cdot PWR_m \left[ \frac{W}{kg} \right] \right) \right) \cdot m_m[kg] + (m_{FF,g}[kg] - m_{g,strippedFF}[kg] - c_b[kg])$$

**Eq. (S.441)**

$$m_4[-] = \left( -F_{m_m+GB+o\_m_m}[-] - \left( c_m \left[ \frac{kg}{W} \right] \cdot PWR_m \left[ \frac{W}{kg} \right] \right) \right)$$

**Eq. (S.442)**

$$b_4[kg] = (m_{FF,g}[kg] - m_{g,strippedFF}[kg] - c_b[kg])$$

## 1.F.1.A.5. Watercraft

### 1.F.1.A.5.A. Waterjet boats

#### 1.F.1.A.5.A.1. Equivalent power-to-weight ratio

There is no change from Eq. (S.348) through Eq. (S.355) in our derivation from Section 1.F.1.A.1.A when deriving the first vehicle characteristic relationship for waterjet boats.

#### 1.F.1.A.5.A.2. Equivalent ratio of onboard useful energy to total hull towing resistance

Our second vehicle characteristic relationship is that, for the BE to have equivalent or improved range, the BE variant must have a ratio of onboard useful energy to total hull towing resistance force greater than or equal to that of the existing FF vehicle (Eq. (S.443)).

**Eq. (S.443)**

$$\frac{OUE_{FF}[Wh]}{R_{T,FF,g}[N]} \leq \frac{OUE_{BE,g}[Wh]}{R_{T,BE,g}[N]}$$

We previously calculated the onboard useful energy and the total hull towing resistance of the FF vehicle in Sections 1.C.1.G.2 and 1.C.2.E.5, respectively; this provides the values for the left side of Eq. (S.443).

For the right side of Eq. (S.443), we calculate the onboard useful energy of the BE variant using Eq. (S.444).

**Eq. (S.444)**

$$OUE_{BE,g}[Wh] = m_B[kg] \cdot SE_B \left[ \frac{Wh}{kg} \right] \cdot \eta_{WJB,BE}[-]$$

We previously discussed calculating the total hull towing resistance in Section 1.C.2.E.5. Expanding Eq. (S.234) with the equations for friction resistance, residual resistance, and air resistance yields Eq. (S.445), where we calculate the wetted surface area using the Schneekluth-Bertram Method (Eq. (S.241)) and the displacement volume by Eq. (S.229), which we rewrite as Eq. (S.446).

**Eq. (S.445)**

$$R_{T,BE}[N] = (C_f[-] + C_R[-]) \left( \frac{1}{2} \cdot \rho_w \left[ \frac{kg}{m^3} \right] \cdot \left( v \left[ \frac{m}{s} \right] \right)^2 \cdot A_s[m^2] \right) + \left( 0.90 \cdot \frac{1}{2} \cdot \rho_{air} \left[ \frac{kg}{m^3} \right] \cdot \left( v \left[ \frac{m}{s} \right] \right)^2 \cdot A_{air}[m^2] \right)$$

**Eq. (S.446)**

$$\nabla[m^3] = \frac{m_{BE,g}[kg]}{\rho_w \left[ \frac{kg}{m^3} \right]}$$

Substituting Eq. (S.241) and Eq. (S.446) into Eq. (S.445) and further substituting the result along with Eq. (S.444) into Eq. (S.443) yields Eq. (S.447).

**Eq. (S.447)**

$$\left( \frac{OUE_{FF}[Wh]}{R_{T,FF,g}[N]} \right) \leq \frac{m_B[kg] \cdot SE_B \left[ \frac{Wh}{kg} \right] \cdot \eta_{WJB,BE}[-]}{\left( (C_f[-] + C_R[-]) \left( \frac{1}{2} \cdot \rho_w \left[ \frac{kg}{m^3} \right] \cdot \left( v \left[ \frac{m}{s} \right] \right)^2 \cdot \left( \left( 3.4 \cdot (\zeta)^{\frac{1}{3}} + 0.5 \cdot L_{WL}[m] \right) \cdot (\zeta)^{\frac{1}{3}} \right) \right) + \left( 0.90 \cdot \frac{1}{2} \cdot \rho_{air} \left[ \frac{kg}{m^3} \right] \cdot \left( v \left[ \frac{m}{s} \right] \right)^2 \cdot A_{air}[m^2] \right) \right)}$$

where:

$$\zeta = \frac{m_{g,strippedFF}[kg] + (F_{m_{m+GB+o\_m_m}}[-] \cdot m_m[kg]) + m_B[kg]}{\rho_w \left[ \frac{kg}{m^3} \right]}$$

This is a non-linear equation, so we are unable to rearrange terms into the equation of a line format as we have done for all other vehicles and characteristics. In order to make this

complex equation easier to work with in spreadsheets and graphing tools, we created six constants (Eq. (S.448) through Eq. (S.453)) which combine to form Eq. (S.454):

**Eq. (S.448)**

$$c_1 \left[ \frac{Wh}{N} \right] = \frac{OUE_{FF} [Wh]}{R_{T,FF,g} [N]}$$

**Eq. (S.449)**

$$c_2 \left[ \frac{Wh}{kg} \right] = SE_B \left[ \frac{Wh}{kg} \right] \cdot \eta_{WJB,BE}$$

**Eq. (S.450)**

$$c_3 [-] = C_f [-] + C_R [-]$$

**Eq. (S.451)**

$$c_4 \left[ \frac{kg}{m \cdot s^2} \right] = \frac{1}{2} \cdot \rho_w \left[ \frac{kg}{m^3} \right] \cdot \left( v \left[ \frac{m}{s} \right] \right)^2$$

**Eq. (S.452)**

$$c_5 [m] = 0.5 \cdot L_{WL} [m]$$

**Eq. (S.453)**

$$c_6 [N] = 0.90 \cdot \frac{1}{2} \cdot \rho_{air} \left[ \frac{kg}{m^3} \right] \cdot \left( v \left[ \frac{m}{s} \right] \right)^2 \cdot A_{air} [m^2]$$

**Eq. (S.454)**

$$c_1 \left[ \frac{Wh}{N} \right] \leq \frac{m_B [kg] \cdot c_2 \left[ \frac{Wh}{kg} \right]}{\left( (c_3 [-]) \left( c_4 \left[ \frac{kg}{m \cdot s^2} \right] \cdot \left( \left( 3.4 \cdot (\zeta)^{\frac{1}{3}} + c_5 [m] \right) \cdot (\zeta)^{\frac{1}{3}} \right) \right) + c_6 [N] \right)}$$

where:

$$\zeta = \frac{m_{g,strippedFF} [kg] + (F_{m_m+GB+o_m} [-] \cdot m_m [kg]) + m_B [kg]}{\rho_w \left[ \frac{kg}{m^3} \right]}$$

### 1.F.1.A.5.A.3. Equivalent overall vehicle volume

There is no change from Eq. (S.364) through Eq. (S.368) in our derivation from Section 1.F.1.A.1.C when deriving the third vehicle characteristic relationship for waterjet boats.

#### **1.F.1.A.5.A.4. Equivalent overall vehicle mass**

There is no change from Eq. (S.369) through Eq. (S.373) in our derivation from Section 1.F.1.A.1.D when deriving the fourth vehicle characteristic relationship for waterjet boats.

#### **1.F.1.A.5.B. Propeller ships**

##### **1.F.1.A.5.B.1. Equivalent power-to-weight ratio**

There is no change from Eq. (S.355) in our derivation from Section 1.F.1.A.1.A when deriving the first vehicle characteristic relationship for propeller ships.

##### **1.F.1.A.5.B.2. Equivalent ratio of onboard useful energy to total hull towing resistance**

There is only one difference in our derivation from Section 1.F.1.A.5.A.2 when deriving the second vehicle characteristic relationship for propeller ships. Instead of using the efficiency of BE waterjet boats in Eq. (S.444) and Eq. (S.449), we use the efficiency of BE propeller ships (see Section 1.C.4.B.5.B).

We should also note that, since waterjet boats are predominately used in freshwater and cargo (propeller) ships in seawater, we use different values for water density as appropriate.

##### **1.F.1.A.5.B.3. Equivalent overall vehicle volume**

There is no change from Eq. (S.364) through Eq. (S.368) in our derivation from Section 1.F.1.A.1.C when deriving the third vehicle characteristic relationship for propeller ships.

##### **1.F.1.A.5.B.4. Equivalent overall vehicle mass**

There is no change from Eq. (S.369) through Eq. (S.373) in our derivation from Section 1.F.1.A.1.D when deriving the fourth vehicle characteristic relationship for propeller ships.

#### **1.F.1.B. Hydrogen fuel cell variants**

##### **1.F.1.B.1. Ground combat vehicles**

###### **1.F.1.B.1.A. Equivalent power-to-weight ratio**

For HFC ground combat vehicles (tactical vehicles), we begin with the first relationship that the HFC variant must have an overall PWR greater than or equal to that of the existing FF vehicle (Eq. (S.455)).

**Eq. (S.455)**

$$PWR_{FF,g} \left[ \frac{W}{kg} \right] \leq PWR_{HFC,g} \left[ \frac{W}{kg} \right]$$

Again, we previously calculated the PWR of the FF vehicle (see Sections 1.C.1.G.8 and 1.C.1.G.9). We can calculate the overall power of an HFC variant using the mass of electric motors and the specific power (or PWR) of the electric motors (Eq. (S.456)).

**Eq. (S.456)**

$$P_{HFC,g}[W] = m_m[kg] \cdot PWR_m \left[ \frac{W}{kg} \right]$$

Since the PWR is actually in terms of mass (not weight), we can rewrite Eq. (S.455) as Eq. (S.457).

**Eq. (S.457)**

$$PWR_{FF,g} \left[ \frac{W}{kg} \right] = \frac{P_{FF}[W]}{m_g[kg]} \leq \frac{P_{HFC,g}[W]}{m_{HFC,g}[kg]}$$

Since ground combat vehicles can benefit from gearboxes paired with the electric motors, we use a scaling factor (see Section 1.C.3.B.19) to estimate the total mass of motors, gearboxes, and oil. We can then calculate the mass of an HFC variant by starting with the mass of the FF variant stripped of all its FF components and adding to it the mass of motors, gearboxes, oil, fuel cell stack, and hydrogen storage system (Eq. (S.458)).

**Eq. (S.458)**

$$m_{HFC,g}[kg] = m_{g,strippedFF}[kg] + (F_{m_m+GB+o,m_m}[-] \cdot m_m[kg]) + m_{FCS}[kg] + m_{H_2storage}[kg]$$

We calculate the mass of fuel cell stack required by matching its maximum power output with the maximum power output from the electric motors (Eq. (S.459)).

**Eq. (S.459)**

$$m_{FCS}[kg] = \left( \frac{m_m[kg] \cdot PWR_m \left[ \frac{W}{kg} \right]}{SP_{FCS} \left[ \frac{W}{kg} \right]} \right)$$

Combining Eq. (S.457) through Eq. (S.459) yields Eq. (S.460), which relates the PWR between the existing FF vehicle and an HFC variant with just the electric motor mass and hydrogen storage system mass as variables.

**Eq. (S.460)**

$$PWR_{FF,g} \left[ \frac{W}{kg} \right] \leq \frac{m_m[kg] \cdot PWR_m \left[ \frac{W}{kg} \right]}{m_{g,strippedFF}[kg] + (F_{m_m+GB+o,m_m}[-] \cdot m_m[kg]) + \left( \frac{m_m[kg] \cdot PWR_m \left[ \frac{W}{kg} \right]}{SP_{FCS} \left[ \frac{W}{kg} \right]} \right) + m_{H_2storage}[kg]}$$

We can rearrange Eq. (S.460) into Eq. (S.461), to get our equation of a line format:  $y = m \cdot x + b$  where the variable  $y$  is the mass of hydrogen storage system (to include hydrogen)

required and the variable  $x$  is the mass of electric motors required. Eq. (S.462) is the slope and Eq. (S.463) is the y-intercept.

**Eq. (S.461)**

$$m_{H_2storage} [kg] \leq \left( \frac{PWR_m \left[ \frac{W}{kg} \right]}{PWR_{FF,g} \left[ \frac{W}{kg} \right]} - F_{m+GB+o} \cdot m_m [-] - \frac{PWR_m \left[ \frac{W}{kg} \right]}{SP_{FCS} \left[ \frac{W}{kg} \right]} \right) \cdot m_m [kg] + (-m_{g,strippedFF} [kg])$$

**Eq. (S.462)**

$$m_1 [-] = \left( \frac{PWR_m \left[ \frac{W}{kg} \right]}{PWR_{FF,g} \left[ \frac{W}{kg} \right]} - F_{m+GB+o} \cdot m_m [-] - \frac{PWR_m \left[ \frac{W}{kg} \right]}{SP_{FCS} \left[ \frac{W}{kg} \right]} \right)$$

**Eq. (S.463)**

$$b_1 [kg] = (-m_{g,strippedFF} [kg])$$

#### 1.F.1.B.1.B. Equivalent ratio of onboard useful energy to road load force

Our second vehicle characteristic relationship is that, for the HFC variant to have equivalent or improved range, the HFC variant must have a ratio of onboard useful energy to road load force greater than or equal to that of the existing FF vehicle (Eq. (S.464)). We previously calculated the left side of the equation using Eq. (S.93) in Section 1.C.2.A.1.E.

**Eq. (S.464)**

$$\frac{OUE_{FF} [Wh]}{RL_{FF,g} [N]} \leq \frac{OUE_{HFC,g} [Wh]}{RL_{HFC,g} [N]}$$

We calculate the onboard useful energy of the HFC variant as a function of the hydrogen storage system mass, the specific energy of the hydrogen storage system, and the overall system efficiency (Eq. (S.465)).

**Eq. (S.465)**

$$OUE_{HFC,g} [Wh] = m_{H_2storage} [kg] \cdot SE_{H_2storage} \left[ \frac{Wh}{kg} \right] \cdot \eta_{TV,HFC} [-]$$

The road load force of the HFC variant is found the same way as for the FF variant in Section 1.C.2.A.1, except we now use the mass of the HFC variant in the gross vehicle weight scenario instead of the gross mass of the FF vehicle (Eq. (S.466)). The mass of the HFC variant is the same as in Eq. (S.458).

**Eq. (S.466)**

$$RL_{HFC,g}[N] = \left( C_{rr}[-] \cdot m_{HFC,g}[kg] \cdot g \left[ \frac{m}{s^2} \right] \right) + \left( \frac{1}{2} \cdot \rho_{air} \left[ \frac{kg}{m^3} \right] \cdot C_d[-] \cdot A_f[m^2] \cdot \left( v \left[ \frac{m}{s} \right] \right)^2 \right) + \left( m_{HFC,g}[kg] \cdot g \left[ \frac{m}{s^2} \right] \cdot \sin\theta[-] \right)$$

We can now rewrite Eq. (S.464) as Eq. (S.467) and substitute Eq. (S.465) and Eq. (S.466) to get Eq. (S.468).

**Eq. (S.467)**

$$OUE_{HFC,g}[Wh] \geq \left( \frac{OUE_{FF}[Wh]}{RL_{FF,g}[N]} \right) \cdot RL_{HFC,g}[N]$$

**Eq. (S.468)**

$$m_{H_2storage}[kg] \cdot SE_{H_2storage} \left[ \frac{Wh}{kg} \right] \cdot \eta_{TV,HFC}[-] \geq \left( \frac{OUE_{FF}[Wh]}{RL_{FF,g}[N]} \right) \cdot \left( \left( C_{rr}[-] \cdot m_{HFC,g}[kg] \cdot g \left[ \frac{m}{s^2} \right] \right) + \left( \frac{1}{2} \cdot \rho_{air} \left[ \frac{kg}{m^3} \right] \cdot C_d[-] \cdot A_f[m^2] \cdot \left( v \left[ \frac{m}{s} \right] \right)^2 \right) + \left( m_{HFC,g}[kg] \cdot g \left[ \frac{m}{s^2} \right] \cdot \sin\theta[-] \right) \right)$$

Substituting Eq. (S.458) for the mass of the HFC variant into Eq. (S.468) and rearranging terms to get our equation of a line format, we get Eq. (S.469) where the slope is given by Eq. (S.470) and the y-intercept by Eq. (S.471).

**Eq. (S.469)**

$$m_{H_2storage}[kg] \geq \left( \frac{C_{rr}[-] \cdot F_{m_{+GB+o},m_m}[-] + \frac{C_{rr}[-] \cdot PWR_{m,c} \left[ \frac{W}{kg} \right]}{SP_{FCS} \left[ \frac{W}{kg} \right]} + \sin\theta[-] \cdot F_{m_{+GB+o},m_m}[-] + \frac{\sin\theta[-] \cdot PWR_{m,c} \left[ \frac{W}{kg} \right]}{SP_{FCS} \left[ \frac{W}{kg} \right]}}{\frac{SE_{H_2storage} \left[ \frac{Wh}{kg} \right] \cdot \eta_{TV,HFC}[-]}{\left( \frac{OUE_{FF}[Wh]}{RL_{FF}[N]} \right) \cdot g \left[ \frac{m}{s^2} \right]} - C_{rr}[-] - \sin\theta[-]} \right) \cdot m_m[kg] + \left( \frac{C_{rr}[-] \cdot m_{g,strippedFF}[kg] + \frac{\left( \frac{1}{2} \cdot \rho_{air} \left[ \frac{kg}{m^3} \right] \cdot C_d[-] \cdot A_f[m^2] \cdot \left( v \left[ \frac{m}{s} \right] \right)^2 \right)}{g \left[ \frac{m}{s^2} \right]} + \sin\theta[-] \cdot m_{g,strippedFF}[kg]}{\frac{SE_{H_2storage} \left[ \frac{Wh}{kg} \right] \cdot \eta_{TV,HFC}[-]}{\left( \frac{OUE_{FF}[Wh]}{RL_{FF}[N]} \right) \cdot g \left[ \frac{m}{s^2} \right]} - C_{rr}[-] - \sin\theta[-]} \right)$$



**Eq. (S.470)**

$$m_2[-] = \left( \frac{C_{rr}[-] \cdot F_{m_m+GB+o_m}[-] + \frac{C_{rr}[-] \cdot PWR_{m,c} \left[ \frac{W}{kg} \right]}{SP_{FCS} \left[ \frac{W}{kg} \right]} + \sin\theta[-] \cdot F_{m_m+GB+o_m}[-] + \frac{\sin\theta[-] \cdot PWR_{m,c} \left[ \frac{W}{kg} \right]}{SP_{FCS} \left[ \frac{W}{kg} \right]}}{\frac{SE_{H_2storage} \left[ \frac{Wh}{kg} \right] \cdot \eta_{TV,HFC}[-]}{\left( \frac{OUE_{FF} [Wh]}{RL_{FF} [N]} \right) \cdot g \left[ \frac{m}{s^2} \right]} - C_{rr}[-] - \sin\theta[-]} \right)$$

**Eq. (S.471)**

$$b_2[kg] = \left( \frac{C_{rr}[-] \cdot m_{g,strippedFF} [kg] + \frac{\left( \frac{1}{2} \cdot \rho_{air} \left[ \frac{kg}{m^3} \right] \cdot C_d[-] \cdot A_f [m^2] \cdot \left( v \left[ \frac{m}{s} \right) \right)^2 \right)}{g \left[ \frac{m}{s^2} \right]} + \sin\theta[-] \cdot m_{g,strippedFF} [kg]}{\frac{SE_{H_2storage} \left[ \frac{Wh}{kg} \right] \cdot \eta_{TV,HFC}[-]}{\left( \frac{OUE_{FF} [Wh]}{RL_{FF} [N]} \right) \cdot g \left[ \frac{m}{s^2} \right]} - C_{rr}[-] - \sin\theta[-]} \right)$$

### 1.F.1.B.1.C. Equivalent overall vehicle volume

Our third vehicle characteristic relationship is the overall volume of the HFC variant must be less than or equal to that of the existing FF vehicle (Eq. (S.472)). We previously calculated the right side of the equation using Eq. (S.2) in Section 1.C.1.B.

**Eq. (S.472)**

$$V_{HFC,g} [m^3] \leq V_{FF,g} [m^3]$$

Here again, since ground combat vehicles can benefit from gearboxes paired with the electric motors, we must use a ratio (see Section 1.C.3.B.20) to estimate the total volume of motors and gearboxes (we consider the volume of oil contained within the volume of the gearboxes). We can calculate the volume of an HFC variant by starting with the volume of the FF variant stripped of all its FF components and adding to it the volume of motors, gearboxes, fuel cell stack, and hydrogen storage system required (Eq. (S.473)).

**Eq. (S.473)**

$$V_{HFC} [m^3] = V_{FF,stripped} [m^3] + \left( m_m [kg] \cdot R_{V_{m+GB} \cdot m_m} \left[ \frac{m^3}{kg} \right] \right) + \left( \frac{m_m [kg] \cdot PWR_m \left[ \frac{W}{kg} \right]}{PD_{FCS} \left[ \frac{W}{L} \right] \cdot 1,000 \left[ \frac{L}{m^3} \right]} \right) + \left( \frac{m_{H_2storage} [kg] \cdot SE_{H_2storage} \left[ \frac{Wh}{kg} \right]}{ED_{H_2storage} \left[ \frac{Wh}{L} \right] \cdot 1,000 \left[ \frac{L}{m^3} \right]} \right)$$

Rearranging terms to get our equation of a line format, we get Eq. (S.474) where the slope is given by Eq. (S.475) and the y-intercept by Eq. (S.476).

Eq. (S.474)

$$\begin{aligned}
 m_{H_2storage}[kg] & \leq \left( - \left( \frac{ED_{H_2storage} \left[ \frac{Wh}{L} \right] \cdot 1,000 \left[ \frac{L}{m^3} \right] \cdot R_{V_{m+GB}m_m} \left[ \frac{m^3}{kg} \right]}{SE_{H_2storage} \left[ \frac{Wh}{kg} \right]} \right) \right. \\
 & \quad + \left. \left( \frac{ED_{H_2storage} \left[ \frac{Wh}{L} \right] \cdot PWR_m \left[ \frac{W}{kg} \right]}{PD_{FCS} \left[ \frac{W}{L} \right] \cdot SE_{H_2storage} \left[ \frac{Wh}{kg} \right]} \right) \right) \cdot m_m[kg] \\
 & \quad + \left( \left( \frac{1,000 \left[ \frac{L}{m^3} \right] \cdot ED_{H_2storage} \left[ \frac{Wh}{L} \right]}{SE_{H_2storage} \left[ \frac{Wh}{kg} \right]} \right) \cdot (V_{FF,g}[m^3] - V_{FF,stripped}[m^3]) \right)
 \end{aligned}$$

Eq. (S.475)

$$\begin{aligned}
 m_3[-] & = \left( - \left( \frac{ED_{H_2storage} \left[ \frac{Wh}{L} \right] \cdot 1,000 \left[ \frac{L}{m^3} \right] \cdot R_{V_{m+GB}m_m} \left[ \frac{m^3}{kg} \right]}{SE_{H_2storage} \left[ \frac{Wh}{kg} \right]} \right) \right. \\
 & \quad + \left. \left( \frac{ED_{H_2storage} \left[ \frac{Wh}{L} \right] \cdot PWR_m \left[ \frac{W}{kg} \right]}{PD_{FCS} \left[ \frac{W}{L} \right] \cdot SE_{H_2storage} \left[ \frac{Wh}{kg} \right]} \right) \right)
 \end{aligned}$$

Eq. (S.476)

$$b_3[kg] = \left( \left( \frac{1,000 \left[ \frac{L}{m^3} \right] \cdot ED_{H_2storage} \left[ \frac{Wh}{L} \right]}{SE_{H_2storage} \left[ \frac{Wh}{kg} \right]} \right) \cdot (V_{FF,g}[m^3] - V_{FF,stripped}[m^3]) \right)$$

#### 1.F.1.B.1.D. Equivalent overall vehicle mass

The fourth and final vehicle characteristic relationship is the overall mass of the HFC variant must be less than or equal to that of the existing FF vehicle (Eq. (S.477)). We previously recorded the values for right side of the equation in Section 1.C.1.A.

Eq. (S.477)

$$m_{HFC,g}[kg] \leq m_{FF,g}[kg]$$

Substituting Eq. (S.458) for the left side of Eq. (S.477) we get Eq. (S.478).

**Eq. (S.478)**

$$m_{g,strippedFF}[kg] + (F_{m_m+GB+o\_m_m}[-] \cdot m_m[kg]) + \left( \frac{m_m[kg] \cdot PWR_m \left[ \frac{W}{kg} \right]}{SP_{FCS} \left[ \frac{W}{kg} \right]} \right) + m_{H_2storage}[kg] \leq m_{FF,g}[kg]$$

Rearranging terms to get our equation of a line format, we get Eq. (S.479) where the slope is given by Eq. (S.480) and the y-intercept by Eq. (S.481).

**Eq. (S.479)**

$$m_{H_2storage}[kg] \geq \left( -F_{m_m+GB+o\_m_m}[-] - \frac{PWR_m \left[ \frac{W}{kg} \right]}{SP_{FCS} \left[ \frac{W}{kg} \right]} \right) \cdot m_m[kg] + (m_{FF,g}[kg] - m_{g,strippedFF}[kg])$$

**Eq. (S.480)**

$$m_4[-] = \left( -F_{m_m+GB+o\_m_m}[-] - \frac{PWR_m \left[ \frac{W}{kg} \right]}{SP_{FCS} \left[ \frac{W}{kg} \right]} \right)$$

**Eq. (S.481)**

$$b_4[kg] = (m_{FF,g}[kg] - m_{g,strippedFF}[kg])$$

## 1.F.1.B.2. Freight locomotive

### 1.F.1.B.2.A. Equivalent power-to-weight ratio

For the first vehicle characteristic relationship, we use the same derivation and equations for HFC freight locomotives as we did for ground combat vehicles in Section 1.F.1.B.1.A (Eq. (S.455) through Eq. (S.463)). Again, as previously discussed in Sections 1.C.1.E.1, 1.C.3.A, and 1.C.3.B.2, we take a conservative approach and, in the absence of data, do not first subtract away the mass and volume of existing electric motors and gearboxes in the diesel electric locomotive in order to consider these requirements as variables for an all-electric system.

### 1.F.1.B.2.B. Equivalent ratio of onboard useful energy to tractive effort force

Our second vehicle characteristic relationship is that, for the HFC to have equivalent or improved range, the HFC variant must have a ratio of onboard useful energy to tractive effort force greater than or equal to that of the existing FF vehicle (Eq. (S.482)). We previously calculated the left side of the equation using Eq. (S.100) in Section 1.C.2.B.2.

**Eq. (S.482)**

$$\frac{OUE_{FF}[Wh]}{TE_{FF,g}[N]} \leq \frac{OUE_{HFC,g}[Wh]}{TE_{HFC,g}[N]}$$

We calculate the onboard useful energy of the HFC variant as a function of the hydrogen storage system mass, the specific energy of the hydrogen storage system, and the overall system efficiency (Eq. (S.483)).

**Eq. (S.483)**

$$OUE_{HFC,g}[Wh] = m_{H_2storage}[kg] \cdot SE_{H_2storage} \left[ \frac{Wh}{kg} \right] \cdot \eta_{L,HFC}[-]$$

The tractive effort force of the HFC variant is found the same way as for the FF variant in Section 1.C.2.B.1, except we now use the mass of the HFC variant in the gross vehicle weight scenario instead of the gross mass of the FF vehicle (Eq. (S.484)). The mass of the HFC variant is the same as by Eq. (S.458).

**Eq. (S.484)**

$$TE_{HFC,g}[N] = m_{HFC,g}[kg] \cdot g \left[ \frac{m}{s^2} \right] \cdot C_f[-] \cdot F_a[-]$$

We can now rewrite Eq. (S.482) as Eq. (S.485) and substitute Eq. (S.483) and Eq. (S.484) to get Eq. (S.486).

**Eq. (S.485)**

$$OUE_{HFC,g}[Wh] \geq \left( \frac{OUE_{FF}[Wh]}{TE_{FF,g}[N]} \right) \cdot TE_{HFC,g}[N]$$

**Eq. (S.486)**

$$\begin{aligned} m_{H_2storage}[kg] \cdot SE_{H_2storage} \left[ \frac{Wh}{kg} \right] \cdot \eta_{L,HFC}[-] \\ \geq \left( \frac{OUE_{FF}[Wh]}{TE_{FF,g}[N]} \right) \cdot \left( m_{HFC,g}[kg] \cdot g \left[ \frac{m}{s^2} \right] \cdot C_f[-] \cdot F_a[-] \right) \end{aligned}$$

Rearranging terms to get our equation of a line format, we get Eq. (S.487) where the slope is given by Eq. (S.488) and the y-intercept by Eq. (S.489).

Eq. (S.487)

$$m_{H_2storage}[kg] \geq \left( \frac{F_{m+GB+o\_m}[-] + \frac{PWR_m \left[ \frac{W}{kg} \right]}{SP_{FCS} \left[ \frac{W}{kg} \right]}}{\frac{SE_{H_2storage} \left[ \frac{Wh}{kg} \right] \cdot \eta_{L,HFC}[-]}{\left( \frac{OUE_{FF}[Wh]}{TE_{FF}[N]} \right) \cdot g \left[ \frac{m}{s^2} \right] \cdot C_f[-] \cdot F_a[-]} - 1} \right) \cdot m_m[kg] + \left( \frac{m_{g,strippedFF}[kg]}{\frac{SE_{H_2storage} \left[ \frac{Wh}{kg} \right] \cdot \eta_{L,HFC}[-]}{\left( \frac{OUE_{FF}[Wh]}{TE_{FF}[N]} \right) \cdot g \left[ \frac{m}{s^2} \right] \cdot C_f[-] \cdot F_a[-]} - 1} \right)$$

Eq. (S.488)

$$m_2[-] = \left( \frac{F_{m+GB+o\_m}[-] + \frac{PWR_m \left[ \frac{W}{kg} \right]}{SP_{FCS} \left[ \frac{W}{kg} \right]}}{\frac{SE_{H_2storage} \left[ \frac{Wh}{kg} \right] \cdot \eta_{L,HFC}[-]}{\left( \frac{OUE_{FF}[Wh]}{TE_{FF}[N]} \right) \cdot g \left[ \frac{m}{s^2} \right] \cdot C_f[-] \cdot F_a[-]} - 1} \right)$$

Eq. (S.489)

$$b_2[kg] = \left( \frac{m_{g,strippedFF}[kg]}{\frac{SE_{H_2storage} \left[ \frac{Wh}{kg} \right] \cdot \eta_{L,HFC}[-]}{\left( \frac{OUE_{FF}[Wh]}{TE_{FF}[N]} \right) \cdot g \left[ \frac{m}{s^2} \right] \cdot C_f[-] \cdot F_a[-]} - 1} \right)$$

### 1.F.1.B.2.C. Equivalent overall vehicle volume

For the freight locomotive's third vehicle characteristic relationship, there is no change from Eq. (S.472) through Eq. (S.476) in our derivation from Section 1.F.1.B.1.C.

### 1.F.1.B.2.D. Equivalent overall vehicle mass

For the freight locomotive's fourth vehicle characteristic relationship, there is no change from Eq. (S.477) through Eq. (S.481) in our derivation from Section 1.F.1.B.1.D.

### 1.F.1.B.3. Rotary-wing aircraft

#### 1.F.1.B.3.A. Equivalent power-to-weight ratio

For the helicopters' first vehicle characteristic relationship, there is no change from Eq. (S.455) through Eq. (S.463) in our derivation from Section 1.F.1.B.1.A.

#### 1.F.1.B.3.B. Equivalent ratio of onboard useful energy to lift force

Our second vehicle characteristic relationship is that, for the HFC variant to have equivalent or improved range, the HFC variant must have a ratio of onboard useful energy to lift force greater than or equal to that of the existing FF vehicle (Eq. (S.490)). We previously calculated the left side of the equation using Eq. (S.137) in Section 1.C.2.C.3.

Eq. (S.490)

$$\frac{OUE_{FF}[Wh]}{L_{FF,g}[N]} \leq \frac{OUE_{HFC,g}[Wh]}{L_{HFC,g}[N]}$$

We calculate the onboard useful energy of the HFC variant as a function of the hydrogen storage system mass, the specific energy of the hydrogen storage system, and the overall system efficiency (Eq. (S.491)).

Eq. (S.491)

$$OUE_{HFC,g}[Wh] = m_{H_2storage}[kg] \cdot SE_{H_2storage} \left[ \frac{Wh}{kg} \right] \cdot \eta_{L,HFC}[-]$$

The lift force of the HFC variant is found the same way as for the FF variant in Section 1.C.2.C.3, except we now use the mass of the HFC variant in the gross vehicle weight scenario instead of the gross mass of the FF vehicle (Eq. (S.492)). The mass of the HFC variant is the same as by Eq. (S.458).

Eq. (S.492)

$$L_{HFC,g}[N] = m_{HFC,g}[kg] \cdot g \left[ \frac{m}{s^2} \right]$$

We can now rewrite Eq. (S.490) as Eq. (S.493) and substitute Eq. (S.491) and Eq. (S.492) to get Eq. (S.494).

Eq. (S.493)

$$OUE_{HFC,g}[Wh] \geq \left( \frac{OUE_{FF}[Wh]}{L_{FF,g}[N]} \right) \cdot L_{HFC,g}[N]$$

Eq. (S.494)

$$m_{H_2storage}[kg] \cdot SE_{H_2storage} \left[ \frac{Wh}{kg} \right] \cdot \eta_{L,HFC}[-] \geq \left( \frac{OUE_{FF}[Wh]}{L_{FF,g}[N]} \right) \cdot m_{HFC,g}[kg] \cdot g \left[ \frac{m}{s^2} \right]$$

Rearranging terms to get our equation of a line format, we get Eq. (S.495) where the slope is given by Eq. (S.496) and the y-intercept by Eq. (S.497).

**Eq. (S.495)**

$$m_{H_2storage}[kg] \geq \left( \frac{F_{m_m+GB+o\_m_m}[-] + \frac{PWR_m \left[ \frac{W}{kg} \right]}{SP_{FCS} \left[ \frac{W}{kg} \right]}}{\frac{SE_{H_2storage} \left[ \frac{Wh}{kg} \right] \cdot \eta_{H,HFC}[-]}{\left( \frac{OUE_{FF}[Wh]}{L_{FF,g}[N]} \right) \cdot g \left[ \frac{m}{s^2} \right]} - 1} \right) \cdot m_m[kg] + \left( \frac{m_{g,strippedFF}[kg]}{\frac{SE_{H_2storage} \left[ \frac{Wh}{kg} \right] \cdot \eta_{H,HFC}[-]}{\left( \frac{OUE_{FF}[Wh]}{L_{FF,g}[N]} \right) \cdot g \left[ \frac{m}{s^2} \right]} - 1} \right)$$

**Eq. (S.496)**

$$m_2[-] = \left( \frac{F_{m_m+GB+o\_m_m}[-] + \frac{PWR_m \left[ \frac{W}{kg} \right]}{SP_{FCS} \left[ \frac{W}{kg} \right]}}{\frac{SE_{H_2storage} \left[ \frac{Wh}{kg} \right] \cdot \eta_{H,HFC}[-]}{\left( \frac{OUE_{FF}[Wh]}{L_{FF,g}[N]} \right) \cdot g \left[ \frac{m}{s^2} \right]} - 1} \right)$$

**Eq. (S.497)**

$$b_2[kg] = \left( \frac{m_{g,strippedFF}[kg]}{\frac{SE_{H_2storage} \left[ \frac{Wh}{kg} \right] \cdot \eta_{H,HFC}[-]}{\left( \frac{OUE_{FF}[Wh]}{L_{FF,g}[N]} \right) \cdot g \left[ \frac{m}{s^2} \right]} - 1} \right)$$

### 1.F.1.B.3.C. Equivalent overall vehicle volume

For the helicopters' third vehicle characteristic relationship, there is no change from Eq. (S.472) through Eq. (S.476) in our derivation from Section 1.F.1.B.1.C.

#### 1.F.1.B.3.D. Equivalent overall vehicle mass

For the helicopters' fourth vehicle characteristic relationship, there is no change from Eq. (S.477) through Eq. (S.481) in our derivation from Section 1.F.1.B.1.D.

#### 1.F.1.B.4. Fixed-wing aircraft

##### 1.F.1.B.4.A. Turboprop airplanes (all-electric propeller airplanes)

##### 1.F.1.B.4.A.1. Equivalent power-to-weight ratio

As with our BE analysis, for the turboprop airplane's first vehicle characteristic relationship, there is only one slight change in terminology from our derivation in Section 1.F.1.A.1.A. Instead of using the maximum rated power of the FF vehicle, we use the maximum rated takeoff power of the turboprop engines to find the overall airplane PWR ( $PWR_{TO,FF,g}$ ). Following the same process as before, we begin with the first relationship that the HFC variant must have an overall takeoff PWR greater than or equal to that of the existing FF vehicle (Eq. (S.498)).

**Eq. (S.498)**

$$PWR_{TO,FF,g} \left[ \frac{W}{kg} \right] \leq PWR_{TO,HFC,g} \left[ \frac{W}{kg} \right]$$

We previously calculated the PWR of the FF vehicle at takeoff (see Sections 1.C.1.G.8 and 1.C.1.G.9). We calculate the overall power of an HFC variant using the mass of electric motors and the specific power (or PWR) of the electric motors as in Eq. (S.456). Since the PWR is actually in terms of mass (not weight), we can rewrite Eq. (S.498) as Eq. (S.499).

**Eq. (S.499)**

$$PWR_{TO,FF,g} \left[ \frac{W}{kg} \right] = \frac{P_{TO,FF}[W]}{m_g[kg]} \leq \frac{P_{TO,HFC,g}[W]}{m_{HFC,g}[kg]}$$

As we previously discussed in Section 1.C.1.E.1, turboprop engines make use of reduction gearing, so we believe that all-electric variants will also benefit from gearboxes and use the same scaling factor to approximate an overall mass of combined electric motors and gearboxes (i.e., no change from Eq. (S.458)). Combining Eq. (S.499) with Eq. (S.458) and Eq. (S.459) yields Eq. (S.500).

**Eq. (S.500)**

$$PWR_{TO,FF,g} \left[ \frac{W}{kg} \right] \leq \frac{m_m[kg] \cdot PWR_m \left[ \frac{W}{kg} \right]}{m_{g,strippedFF}[kg] + (F_{m_m+GB+o\_m_m}[-] \cdot m_m[kg]) + \left( \frac{m_m[kg] \cdot PWR_m \left[ \frac{W}{kg} \right]}{SP_{FCS} \left[ \frac{W}{kg} \right]} \right) + m_{H_2storage}[kg]}$$



We can rearrange Eq. (S.500) into Eq. (S.501) to get the equation of a line format where Eq. (S.502) is the slope and Eq. (S.503) is the y-intercept.

**Eq. (S.501)**

$$m_{H_2storage} [kg] \leq \left( \frac{PWR_m \left[ \frac{W}{kg} \right]}{PWR_{TO,FF,g} \left[ \frac{W}{kg} \right]} - F_{m_m+GB+o\_m_m} [-] - \frac{PWR_m \left[ \frac{W}{kg} \right]}{SP_{FCS} \left[ \frac{W}{kg} \right]} \right) \cdot m_m [kg] + (-m_{g,strippedFF} [kg])$$

**Eq. (S.502)**

$$m_1 [-] = \left( \frac{PWR_m \left[ \frac{W}{kg} \right]}{PWR_{TO,FF,g} \left[ \frac{W}{kg} \right]} - F_{m_m+GB+o\_m_m} [-] - \frac{PWR_m \left[ \frac{W}{kg} \right]}{SP_{FCS} \left[ \frac{W}{kg} \right]} \right)$$

**Eq. (S.503)**

$$b_1 [kg] = (-m_{g,strippedFF} [kg])$$

#### 1.F.1.B.4.A.2. Equivalent cruising range

Our second vehicle characteristic relationship for the turboprop airplane is the cruising range of the HFC variant must be greater than or equal to the cruising range of the FF vehicle (Eq. (S.504)).

**Eq. (S.504)**

$$CR_{FF} [m] \leq CR_{HFC,g} [m]$$

We previously recorded the maximum cruising range of a turboprop airplane in Section 1.C.1.G.3 and showed how to derive the Breguet range equation estimate of this value. We also derived an estimate of cruising range for an all-electric airplane. We can substitute Eq. (S.411) into Eq. (S.504) to get Eq. (S.505).

**Eq. (S.505)**

$$CR_{FF} [m] \leq CR_{HFC,g} [m] = \frac{OUE_{HFC,g} [Ws]}{m_{BE,g} [kg] \cdot g \left[ \frac{m}{s^2} \right]} \cdot \left( \frac{L [N]}{D [N]} \right)$$

Further substituting Eq. (S.401), Eq. (S.458), and Eq. (S.459) into Eq. (S.505) yields Eq. (S.506).

**Eq. (S.506)**

$$CR_{FF}[m] \leq \frac{m_{H_2storage}[kg] \cdot SE_{H_2storage} \left[ \frac{WS}{kg} \right] \cdot \eta_{PA,HFC}[-]}{\left( m_{g,strippedFF}[kg] + (F_{m+GB+o\_}m_m[-] \cdot m_m[kg]) + \left( \frac{m_m[kg] \cdot PWR_m \left[ \frac{W}{kg} \right]}{SP_{FCS} \left[ \frac{W}{kg} \right]} \right) + m_{H_2storage}[kg] \right) \cdot g \left[ \frac{m}{s^2} \right]} \cdot \left( \frac{L[N]}{D[N]} \right)$$

Rearranging Eq. (S.506) into the equation of a line format, we get Eq. (S.507) where the slope is given by Eq. (S.508) and the y-intercept by Eq. (S.509).

**Eq. (S.507)**

$$m_{H_2storage}[kg] \geq \left( \frac{F_{m+GB+o\_}m_m[-] + \frac{PWR_m \left[ \frac{W}{kg} \right]}{SP_{FCS} \left[ \frac{W}{kg} \right]}}{SE_{H_2storage} \left[ \frac{WS}{kg} \right] \cdot \eta_{PA,HFC}[-] \cdot \left( \frac{L[N]}{D[N]} \right) - 1} \right) \cdot m_m[kg] + \left( \frac{m_{g,strippedFF}[kg]}{SE_{H_2storage} \left[ \frac{WS}{kg} \right] \cdot \eta_{PA,HFC}[-] \cdot \left( \frac{L[N]}{D[N]} \right) - 1} \right) \cdot g \left[ \frac{m}{s^2} \right]$$

**Eq. (S.508)**

$$m_2[-] = \left( \frac{F_{m+GB+o\_}m_m[-] + \frac{PWR_m \left[ \frac{W}{kg} \right]}{SP_{FCS} \left[ \frac{W}{kg} \right]}}{SE_{H_2storage} \left[ \frac{WS}{kg} \right] \cdot \eta_{PA,HFC}[-] \cdot \left( \frac{L[N]}{D[N]} \right) - 1} \right)$$

Eq. (S.509)

$$b_2[kg] = \left( \frac{m_{g,strippedFF}[kg]}{SE_{H_2storage} \left[ \frac{WS}{kg} \right] \cdot \eta_{PA,HFC}[-] \cdot \left( \frac{L[N]}{D[N]} \right)} - 1 \right) \frac{1}{(CR_{FF}[m]) \cdot g \left[ \frac{m}{s^2} \right]}$$

### 1.F.1.B.4.A.3. Equivalent overall vehicle volume

For the turboprop airplane's third vehicle characteristic relationship, there is no change from Eq. (S.472) through Eq. (S.476) in our derivation from Section 1.F.1.B.1.C.

### 1.F.1.B.4.A.4. Equivalent overall vehicle mass

For the turbofan airplane's fourth vehicle characteristic relationship, there is no change from Eq. (S.477) through Eq. (S.481) in our derivation from Section 1.F.1.B.1.D.

## 1.F.1.B.4.B. Turbofan airplanes (all-electric ducted fan airplanes)

### 1.F.1.B.4.B.1. Equivalent thrust-to-weight ratio

Instead of terms of power, turbofan airplanes are rated in terms of thrust, so the first vehicle characteristic relationship is that the takeoff TWR of the HFC variant must be greater than or equal to that of the FF vehicle (Eq. (S.425)).

Eq. (S.510)

$$TWR_{TO,FFg} \left[ \frac{N}{N} \right] \leq TWR_{TO,HFC,g} \left[ \frac{N}{N} \right]$$

We previously found the TWR at takeoff for the FF vehicle in Section 1.C.2.D.2. For all-electric variants, we related takeoff thrust and power in Section 1.C.2.D.3. We calculate the mass of the HFC variant by taking the same equation used for other vehicles (Eq. (S.458)) and adding the mass of propulsor components (Eq. (S.183)). Note that, since we model direct drive fans with no gearboxes, the scaling factor for the total mass of electric motors, gearboxes, and oil used per dry mass of electric motors used is simply 1.0 (see Section 1.C.3.B.19). Combining Eq. (S.183) and Eq. (S.184) from Section 1.C.2.D.3 with Eq. (S.510) yields Eq. (S.511), which we can rearrange into the equation of a line format (Eq. (S.512)) where the slope is given by Eq. (S.513) and the y-intercept by Eq. (S.514).

Eq. (S.511)

$$TWR_{TO,FFg} \left[ \frac{N}{N} \right] \leq \frac{m_m[kg] \cdot PWR_m \left[ \frac{W}{kg} \right]}{R_{DFTOProt} \left[ \frac{W}{N} \right]} \left( m_{g,strippedFF}[kg] + (F_{m_m+GB+o\_m_m}[-] \cdot m_m[kg]) + \left( c_m \left[ \frac{kg}{W} \right] \cdot m_m[kg] \cdot PWR_m \left[ \frac{W}{kg} \right] \right) + c_b[kg] \right) + \left( \frac{m_m[kg] \cdot PWR_m \left[ \frac{W}{kg} \right]}{SP_{FCS} \left[ \frac{W}{kg} \right]} \right) + m_{H_2storage}[kg] \cdot g \left[ \frac{m}{s^2} \right]$$

Eq. (S.512)

$$m_{H_2storage}[kg] \leq \left( \frac{PWR_m \left[ \frac{W}{kg} \right]}{R_{DFTOP\_TOT} \left[ \frac{W}{N} \right] \cdot TWR_{TO,FFg} \left[ \frac{N}{N} \right] \cdot g \left[ \frac{m}{s^2} \right]} - \frac{PWR_m \left[ \frac{W}{kg} \right]}{SP_{FCS} \left[ \frac{W}{kg} \right]} - F_{m_{m+GB+o\_}m_m}[-] \right. \\ \left. - \left( c_m \left[ \frac{kg}{W} \right] \cdot PWR_m \left[ \frac{W}{kg} \right] \right) \right) \cdot m_m[kg] + \left( -(c_b[kg] + m_{g,strippedFF}[kg]) \right)$$

Eq. (S.513)

$$m_1[-] = \left( \frac{PWR_m \left[ \frac{W}{kg} \right]}{R_{DFTOP\_TOT} \left[ \frac{W}{N} \right] \cdot TWR_{TO,FFg} \left[ \frac{N}{N} \right] \cdot g \left[ \frac{m}{s^2} \right]} - \frac{PWR_m \left[ \frac{W}{kg} \right]}{SP_{FCS} \left[ \frac{W}{kg} \right]} - F_{m_{m+GB+o\_}m_m}[-] \right. \\ \left. - \left( c_m \left[ \frac{kg}{W} \right] \cdot PWR_m \left[ \frac{W}{kg} \right] \right) \right)$$

Eq. (S.514)

$$b_1[kg] = \left( -(c_b[kg] + m_{g,strippedFF}[kg]) \right)$$

### 1.F.1.B.4.B.2. Equivalent cruising range

For the second vehicle characteristic relationship, we begin with the same relationship for cruising range that we used for turboprop airplanes in Eq. (S.505). Using our estimated efficiency for HFC ducted fan airplanes (see Section 1.C.5.D.5.B) and our method for calculating the mass of HFC ducted fan airplanes (see Section 1.F.1.B.4.B.1), we can expand Eq. (S.505) to get Eq. (S.515).

Eq. (S.515)

$$CR_{FF}[m] \leq \frac{m_{H_2storage}[kg] \cdot SE_{H_2storage} \left[ \frac{Ws}{kg} \right] \cdot \eta_{DFA,HFC}[-]}{\left( m_{g,strippedFF}[kg] + (F_{m_{m+GB+o\_}m_m}[-] \cdot m_m[kg]) + (\zeta) + \left( \frac{m_m[kg] \cdot PWR_m \left[ \frac{W}{kg} \right]}{SP_{FCS} \left[ \frac{W}{kg} \right]} \right) + m_{H_2storage}[kg] \right) \cdot g \left[ \frac{m}{s^2} \right]} \cdot \left( \frac{L[N]}{D[N]} \right)$$

where:

$$\zeta = \left( c_m \left[ \frac{kg}{W} \right] \cdot m_m[kg] \cdot PWR_m \left[ \frac{W}{kg} \right] \right) + c_b[kg]$$

Rearranging Eq. (S.515) into the equation of a line format gives us Eq. (S.516), where the slope is given by Eq. (S.517) and the y-intercept by Eq. (S.518).

**Eq. (S.516)**

$$m_{H_2storage} [kg] \geq \left( \frac{\frac{PWR_m \left[ \frac{W}{kg} \right]}{SP_{FCS} \left[ \frac{W}{kg} \right]} + \left( c_m \left[ \frac{kg}{W} \right] \cdot PWR_m \left[ \frac{W}{kg} \right] \right) + F_{m_m+GB+o_m} [-]}{\frac{SE_{H_2storage} \left[ \frac{WS}{kg} \right] \cdot \eta_{DFA,HFC} [-] \cdot \left( \frac{L[N]}{D[N]} \right) - 1}{CR_{FF} [m] \cdot g \left[ \frac{m}{s^2} \right]}} \right) \cdot m_m [kg] + \left( \frac{c_b [kg] + m_{g,strippedFF} [kg]}{\frac{SE_{H_2storage} \left[ \frac{WS}{kg} \right] \cdot \eta_{DFA,HFC} [-] \cdot \left( \frac{L[N]}{D[N]} \right) - 1}{CR_{FF} [m] \cdot g \left[ \frac{m}{s^2} \right]}} \right)$$

**Eq. (S.517)**

$$m_2 [-] = \left( \frac{\frac{PWR_m \left[ \frac{W}{kg} \right]}{SP_{FCS} \left[ \frac{W}{kg} \right]} + \left( c_m \left[ \frac{kg}{W} \right] \cdot PWR_m \left[ \frac{W}{kg} \right] \right) + F_{m_m+GB+o_m} [-]}{\frac{SE_{H_2storage} \left[ \frac{WS}{kg} \right] \cdot \eta_{DFA,HFC} [-] \cdot \left( \frac{L[N]}{D[N]} \right) - 1}{CR_{FF} [m] \cdot g \left[ \frac{m}{s^2} \right]}} \right)$$

**Eq. (S.518)**

$$b_2 [kg] = \left( \frac{c_b [kg] + m_{g,strippedFF} [kg]}{\frac{SE_{H_2storage} \left[ \frac{WS}{kg} \right] \cdot \eta_{DFA,HFC} [-] \cdot \left( \frac{L[N]}{D[N]} \right) - 1}{CR_{FF} [m] \cdot g \left[ \frac{m}{s^2} \right]}} \right)$$

### 1.F.1.B.4.B.3. Equivalent overall vehicle volume

The third vehicle characteristic relationship, that the overall volume of the HFC variant must be less than or equal to that of the existing FF vehicle, is the same as Eq. (S.472) in Section 1.F.1.B.1.C. However, since we model an HFC variant as using the ducted fan portion of turbofan engines for propulsion, we must add back in the volume of the FF engines (which we removed to find the stripped volume of the FF variant) to estimate their size. Therefore, we

calculate the volume of an HFC ducted fan airplane by taking Eq. (S.473) and adding the original engine volume (Eq. (S.519)).

**Eq. (S.519)**

$$V_{HFC}[m^3] = V_{FF,stripped}[m^3] + \left( m_m[kg] \cdot R_{V_{m+GB\_m_m}} \left[ \frac{m^3}{kg} \right] \right) + \left( \frac{m_m[kg] \cdot PWR_m \left[ \frac{W}{kg} \right]}{PD_{FCS} \left[ \frac{W}{L} \right] \cdot 1,000 \left[ \frac{L}{m^3} \right]} \right) + \left( \frac{m_{H_2storage}[kg] \cdot SE_{H_2storage} \left[ \frac{Wh}{kg} \right]}{ED_{H_2storage} \left[ \frac{Wh}{L} \right] \cdot 1,000 \left[ \frac{L}{m^3} \right]} \right) + V_{total,e}[m^3]$$

Rearranging Eq. (S.519) into the equation of a line format gives us Eq. (S.520), where the slope is given by Eq. (S.521) and the y-intercept by Eq. (S.522).

**Eq. (S.520)**

$$m_{H_2storage}[kg] \leq \left( - \left( \frac{ED_{H_2storage} \left[ \frac{Wh}{L} \right] \cdot 1,000 \left[ \frac{L}{m^3} \right] \cdot R_{V_{m+GB\_m_m}} \left[ \frac{m^3}{kg} \right]}{SE_{H_2storage} \left[ \frac{Wh}{kg} \right]} \right) + \left( \frac{ED_{H_2storage} \left[ \frac{Wh}{L} \right] \cdot PWR_m \left[ \frac{W}{kg} \right]}{PD_{FCS} \left[ \frac{W}{L} \right] \cdot SE_{H_2storage} \left[ \frac{Wh}{kg} \right]} \right) \right) \cdot m_m[kg] + \left( \left( \frac{1,000 \left[ \frac{L}{m^3} \right] \cdot ED_{H_2storage} \left[ \frac{Wh}{L} \right]}{SE_{H_2storage} \left[ \frac{Wh}{kg} \right]} \right) \cdot (V_{FF,g}[m^3] - V_{FF,stripped}[m^3] - V_{total,e}[m^3]) \right)$$

Eq. (S.521)

$$m_3[-] = \left( - \left( \frac{ED_{H_2storage} \left[ \frac{Wh}{L} \right] \cdot 1,000 \left[ \frac{L}{m^3} \right] \cdot R_{V_{m+GB_{mm}}} \left[ \frac{m^3}{kg} \right]}{SE_{H_2storage} \left[ \frac{Wh}{kg} \right]} \right) + \left( \frac{ED_{H_2storage} \left[ \frac{Wh}{L} \right] \cdot PWR_m \left[ \frac{W}{kg} \right]}{PD_{FCS} \left[ \frac{W}{L} \right] \cdot SE_{H_2storage} \left[ \frac{Wh}{kg} \right]} \right) \right)$$

Eq. (S.522)

$$b_3[kg] = \left( \left( \frac{1,000 \left[ \frac{L}{m^3} \right] \cdot ED_{H_2storage} \left[ \frac{Wh}{L} \right]}{SE_{H_2storage} \left[ \frac{Wh}{kg} \right]} \right) \cdot (V_{FF,g}[m^3] - V_{FF,stripped}[m^3] - V_{total,e}[m^3]) \right)$$

#### 1.F.1.B.4.B.4. Equivalent overall vehicle mass

The fourth vehicle characteristic relationship, that the overall mass of the HFC variant must be less than or equal to that of the existing FF vehicle, is the same as Eq. (S.477) in Section 1.F.1.B.1.D. However, as described above in Section 1.F.1.B.4.B.1, the mass of the HFC variant must also include the mass of propulsor components (Eq. (S.183)), as shown by Eq. (S.523).

Eq. (S.523)

$$m_{HFC,g}[kg] = m_{g,strippedFF}[kg] + (F_{m_{m+GB+o\_}m_m}[-] \cdot m_m[kg]) + \left( \frac{m_m[kg] \cdot PWR_m \left[ \frac{W}{kg} \right]}{SP_{FCS} \left[ \frac{W}{kg} \right]} \right) + m_{PC}[kg] + m_{H_2storage}[kg]$$

Substituting Eq. (S.523) and Eq. (S.183) into Eq. (S.369) yields Eq. (S.439).

Eq. (S.524)

$$m_{g,strippedFF}[kg] + (F_{m_{m+GB+o\_}m_m}[-] \cdot m_m[kg]) + \left( \frac{m_m[kg] \cdot PWR_m \left[ \frac{W}{kg} \right]}{SP_{FCS} \left[ \frac{W}{kg} \right]} \right) + m_{PC}[kg] + m_{H_2storage}[kg] \leq m_{FF,g}[kg]$$

Rearranging Eq. (S.524) into the equation of a line format gives us Eq. (S.525), where the slope is given by Eq. (S.526) and the y-intercept by Eq. (S.527).

**Eq. (S.525)**

$$m_{H_2storage}[kg] \geq \left( -F_{m_m+GB+o_m_m}[-] - \frac{PWR_m \left[ \frac{W}{kg} \right]}{SP_{FCS} \left[ \frac{W}{kg} \right]} - \left( c_m \left[ \frac{kg}{W} \right] \cdot PWR_m \left[ \frac{W}{kg} \right] \right) \right) \cdot m_m[kg] + (m_{FF,g}[kg] - m_{g,strippedFF}[kg] - c_b[kg])$$

**Eq. (S.526)**

$$m_4[-] = \left( -F_{m_m+GB+o_m_m}[-] - \frac{PWR_m \left[ \frac{W}{kg} \right]}{SP_{FCS} \left[ \frac{W}{kg} \right]} - \left( c_m \left[ \frac{kg}{W} \right] \cdot PWR_m \left[ \frac{W}{kg} \right] \right) \right)$$

**Eq. (S.527)**

$$b_4[kg] = (m_{FF,g}[kg] - m_{g,strippedFF}[kg] - c_b[kg])$$

### 1.F.1.B.5. Watercraft

#### 1.F.1.B.5.A. Waterjet boats

##### 1.F.1.B.5.A.1. Equivalent power-to-weight ratio

There is no change from Eq. (S.455) through Eq. (S.463) in our derivation from Section 1.F.1.B.1.A when deriving the first vehicle characteristic relationship for waterjet boats.

##### 1.F.1.B.5.A.2. Equivalent ratio of onboard useful energy to total hull towing resistance

Our second vehicle characteristic relationship is that, for the HFC variant to have equivalent or improved range, it must have a ratio of onboard useful energy to total hull towing resistance force greater than or equal to that of the existing FF vehicle (Eq. (S.528)).

**Eq. (S.528)**

$$\frac{OUE_{FF}[Wh]}{R_{T,FF,g}[N]} \leq \frac{OUE_{HFC,g}[Wh]}{R_{T,HFC,g}[N]}$$

We previously calculated the onboard useful energy and the total hull towing resistance of the FF vehicle in Sections 1.C.1.G.2 and 1.C.2.E.5, respectively; this provides the values for the left side of Eq. (S.528).

For the right side of Eq. (S.528), we calculate the onboard useful energy of the HFC variant using Eq. (S.529).



**Eq. (S.529)**

$$OUE_{HFC,g}[Wh] = m_{H_2storage}[kg] \cdot SE_{H_2storage} \left[ \frac{Wh}{kg} \right] \cdot \eta_{WJB,HFC}[-]$$

We previously discussed calculating the total hull towing resistance in Section 1.C.2.E.5. Expanding Eq. (S.234) with the equations for friction resistance, residual resistance, and air resistance yields Eq. (S.530), where we calculate the wetted surface area using the Schneekluth-Bertram Method (Eq. (S.241)) and the displacement volume by Eq. (S.229), which we rewrite as Eq. (S.531).

**Eq. (S.530)**

$$R_{T,HFC}[N] = (C_f[-] + C_R[-]) \left( \frac{1}{2} \cdot \rho_w \left[ \frac{kg}{m^3} \right] \cdot \left( v \left[ \frac{m}{s} \right] \right)^2 \cdot A_s[m^2] \right) + \left( 0.90 \cdot \frac{1}{2} \cdot \rho_{air} \left[ \frac{kg}{m^3} \right] \cdot \left( v \left[ \frac{m}{s} \right] \right)^2 \cdot A_{air}[m^2] \right)$$

**Eq. (S.531)**

$$\nabla[m^3] = \frac{m_{HFC,g}[kg]}{\rho_w \left[ \frac{kg}{m^3} \right]}$$

Substituting Eq. (S.241) and Eq. (S.531) into Eq. (S.530) and further substituting the result along with Eq. (S.529) into Eq. (S.528) yields Eq. (S.532).

**Eq. (S.532)**

$$\left( \frac{OUE_{FF}[Wh]}{R_{T,FF}[N]} \right) \leq \frac{m_{H_2storage}[kg] \cdot SE_{H_2storage} \left[ \frac{Wh}{kg} \right] \cdot \eta_{HFC}[-]}{\left( (C_f[-] + C_R[-]) \left( \frac{1}{2} \cdot \rho_w \left[ \frac{kg}{m^3} \right] \cdot \left( v \left[ \frac{m}{s} \right] \right)^2 \cdot \left( \left( 3.4 \cdot (\zeta)^{\frac{1}{3}} + 0.5 \cdot L_{WL}[m] \cdot (\zeta)^{\frac{1}{3}} \right) \right) \right) + \left( 0.90 \cdot \frac{1}{2} \cdot \rho_{air} \left[ \frac{kg}{m^3} \right] \cdot \left( v \left[ \frac{m}{s} \right] \right)^2 \cdot A_{air}[m^2] \right) \right)}$$

where:

$$\zeta = \frac{m_{g,strippedFF}[kg] + (F_{m_m+GB+o}[-] \cdot m_m[kg]) + \left( \frac{m_m[kg] \cdot PWR_m \left[ \frac{W}{kg} \right]}{SP_{FCS} \left[ \frac{W}{kg} \right]} \right) + m_{H_2storage}[kg]}{\rho_w \left[ \frac{kg}{m^3} \right]}$$

This is a non-linear equation, so we are unable to rearrange terms into the equation of a line format as we have done for all other vehicles and characteristics. In order to make this complex equation easier to work with in spreadsheets and graphing tools, we created seven constants (Eq. (S.533) through Eq. (S.539)) which combine to form Eq. (S.540):

Eq. (S.533)

$$c_1 \left[ \frac{Wh}{N} \right] = \frac{OUE_{FF} [Wh]}{R_{T,FF,g} [N]}$$

Eq. (S.534)

$$c_2 \left[ \frac{Wh}{kg} \right] = SE_{H_2storage} \left[ \frac{Wh}{kg} \right] \cdot \eta_{WJB,HFC}$$

Eq. (S.535)

$$c_3 [-] = C_f [-] + C_R [-]$$

Eq. (S.536)

$$c_4 \left[ \frac{kg}{m \cdot s^2} \right] = \frac{1}{2} \cdot \rho_w \left[ \frac{kg}{m^3} \right] \cdot \left( v \left[ \frac{m}{s} \right] \right)^2$$

Eq. (S.537)

$$c_5 [m] = 0.5 \cdot L_{WL} [m]$$

Eq. (S.538)

$$c_6 [N] = 0.90 \cdot \frac{1}{2} \cdot \rho_{air} \left[ \frac{kg}{m^3} \right] \cdot \left( v \left[ \frac{m}{s} \right] \right)^2 \cdot A_{air} [m^2]$$

Eq. (S.539)

$$c_7 [-] = \frac{PWR_m \left[ \frac{W}{kg} \right]}{SP_{FCS} \left[ \frac{W}{kg} \right]}$$

Eq. (S.540)

$$c_1 \left[ \frac{Wh}{N} \right] \leq \frac{m_{H_2storage} [kg] \cdot c_2 \left[ \frac{Wh}{kg} \right]}{\left( (c_3 [-]) \left( c_4 \left[ \frac{kg}{m \cdot s^2} \right] \cdot \left( \left( 3.4 \cdot (\zeta)^{\frac{1}{3}} + c_5 [m] \right) \cdot (\zeta)^{\frac{1}{3}} \right) \right) + c_6 [N] \right)}$$

where:

$$\zeta = \frac{m_{g,strippedFF} [kg] + (F_{m_m+GB+o_m} [-] \cdot m_m [kg]) + (c_7 [-] \cdot m_m [kg]) + m_{H_2storage} [kg]}{\rho_w \left[ \frac{kg}{m^3} \right]}$$

### 1.F.1.B.5.A.3. Equivalent overall vehicle volume

There is no change from Eq. (S.472) through Eq. (S.476) in our derivation from Section 1.F.1.B.1.C when deriving the third vehicle characteristic relationship for waterjet boats.

#### **1.F.1.B.5.A.4. Equivalent overall vehicle mass**

There is no change from Eq. (S.477) through Eq. (S.481) in our derivation from Section 1.F.1.B.1.D when deriving the fourth vehicle characteristic relationship for waterjet boats.

#### **1.F.1.B.5.B. Propeller ships**

##### **1.F.1.B.5.B.1. Equivalent power-to-weight ratio**

There is no change from Eq. (S.348) through Eq. (S.355) in our derivation from Section 1.F.1.A.1.A when deriving the first vehicle characteristic relationship for propeller ships.

##### **1.F.1.B.5.B.2. Equivalent ratio of onboard useful energy to total hull towing resistance**

There are only two differences in our derivation from Section 1.F.1.B.5.A.2 when deriving the second vehicle characteristic relationship for propeller ships. Instead of using the efficiency of HFC waterjet boats in Eq. (S.529) and Eq. (S.534), we use the efficiency of HFC propeller ships (see Section 1.C.5.D.6.B). Additionally, waterjet boats are predominately used in freshwater and cargo (propeller) ships in seawater, so we use different values for water density as appropriate.

##### **1.F.1.B.5.B.3. Equivalent overall vehicle volume**

There is no change from Eq. (S.472) through Eq. (S.476) in our derivation from Section 1.F.1.B.1.C when deriving the third vehicle characteristic relationship for propeller ships.

##### **1.F.1.B.5.B.4. Equivalent overall vehicle mass**

There is no change from Eq. (S.477) through Eq. (S.481) in our derivation from Section 1.F.1.B.1.D when deriving the fourth vehicle characteristic relationship for propeller ships.

#### **1.F.1.C. Solving the system of equations by substitution and by graphing the feasible region: electric motor mass vs battery pack mass or hydrogen storage system mass**

Thus far, we have developed lines (or curves in the case of watercraft range characteristics) to describe the vehicle characteristic relationships using “design variables” of electric motor mass and either battery pack mass for BE variants or hydrogen storage system mass for HFC variants. Unless lines for vehicle characteristics are parallel or along the same line, plotting the four lines for any variant will result in six unique intersections. The intersections are important because they represent solutions where at least two of the proposed vehicle’s characteristics are 100% of the existing vehicle’s characteristics. Fig. S.15 illustrates this concept for an HFC variant. For each vehicle characteristic relationship (PWR in blue, range in green, volume in red, and mass in orange), the line shown represents the combination of electric motor mass and hydrogen storage system mass that results in equivalency between the HFC variant and the existing FF vehicle. Shaded regions show combinations that result in improved capabilities for the HFC variant. Shaded regions may overlap. The area shown in yellow in Fig. S.15 denotes combinations of electric motor mass and hydrogen storage system mass where all four vehicle characteristics are either met or improved, i.e., all four shaded regions overlap. Using values for each intersection, we can calculate the resulting HFC variant mass, volume, PWR (or TWR), and range, and then compare the results to the existing FF variant to see how each vehicle characteristic has either improved or regressed with the HFC

variant (Eq. (S.541) through Eq. (S.544), note that “range” may refer to either cruising range or a ratio of onboard useful energy to force required as appropriate per vehicle type). The inset table in Fig. S.15 gives an example of such comparisons.

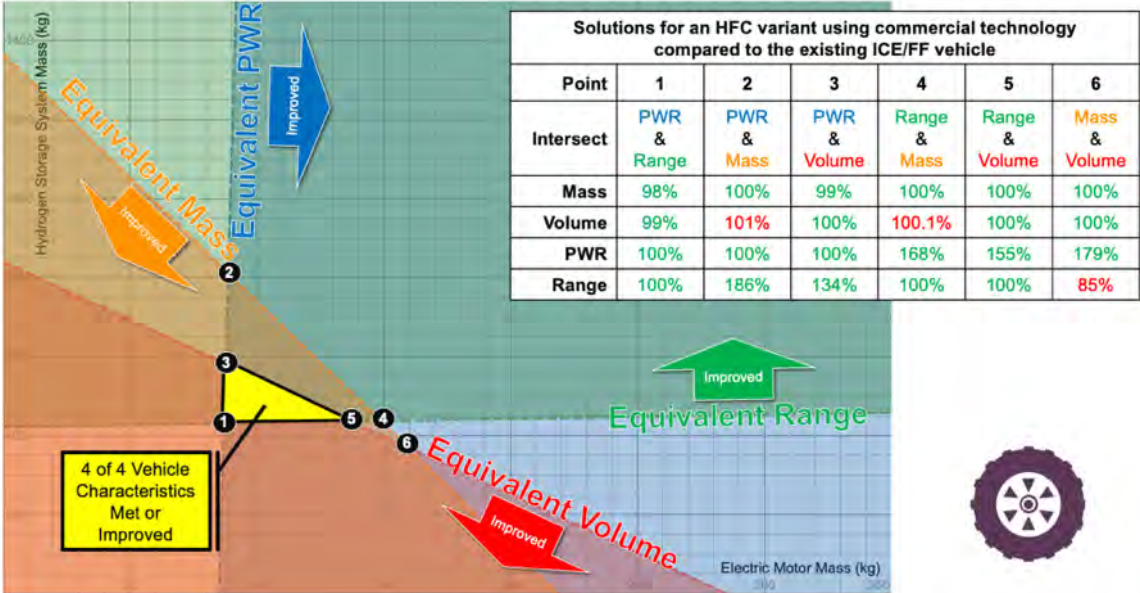


**Fig. S.15. Example of the four vehicle characteristics considered graphed for an HFC variant with intersections and feasible region marked.**

Any intersections that lie outside of quadrant I (positive values for x- and y-axes) are clearly unacceptable solutions. Green text indicates improved results (decreased mass and/or volume and increased PWR and/or range), while red text indicates areas of regression from the existing FF vehicle characteristics.

Eq. (S.541)

$$100\% \cdot \begin{cases} \frac{m_{g,BE}}{m_{g,FF}} \\ \frac{m_{g,HFC}}{m_{g,FF}} \end{cases}$$

Eq. (S.542)

$$100\% \cdot \begin{cases} \frac{V_{g,BE}}{V_{FF}} \\ \frac{V_{g,HFC}}{V_{FF}} \end{cases}$$

Eq. (S.543)

$$100\% \cdot \begin{cases} \frac{PWR_{g,BE}}{PWR_{g,FF}} \\ \frac{PWR_{g,HFC}}{PWR_{g,FF}} \end{cases} \text{ or } 100\% \cdot \begin{cases} \frac{TWR_{TO,g,BE}}{TWR_{TO,g,FF}} \\ \frac{TWR_{TO,g,HFC}}{TWR_{TO,g,FF}} \end{cases}$$

Eq. (S.544)

$$100\% \cdot \begin{cases} \frac{\text{range}_{g,BE}}{\text{range}_{FF}} \\ \frac{\text{range}_{g,HFC}}{\text{range}_{FF}} \end{cases}$$

In optimization language, if we consider the desired vehicle characteristics as “constraints” that must be satisfied, then their graphed lines form “behavior constraints” [383]. The “feasible region,” if one exists where all four vehicle characteristics can be satisfied, is bounded by these behavior constraints. Since the vehicle must have a positive value for both battery pack mass (or hydrogen storage system mass) and electric motor mass, the x- and y-axes (abscissa = 0 and/or ordinate = 0) would form “side constraints,” due to the “positivity constraint” requirements. However, extremely low values (say 0.000001 kg for instance) would also not be acceptable for either energy storage or electric motor mass, so results must be carefully interpreted. Solution combinations for our “design variables” that fall within the feasible region but not on a constraint line are called “acceptable free point” solutions [383]. Design solutions along one or more constraint line(s) are called “acceptable bound point” solutions and any associated constraint line is considered an “active constraint” [383].

We have arranged our optimization analyses such that the battery pack mass (or hydrogen storage system mass) and electric motor mass are the “decision variables,” and the optimization problems are “deterministic” – parameter inputs dictate that there is one global solution that can be reached every time depending upon the optimization function chosen. Most vehicles in this study are linear problems, but the watercraft are non-linear because of their equations for range. Although we will report our results in terms of integers for readability, our analysis is not of an “integer programming problem” but of a “real-valued programming problem” and the design variables are permitted to take any real value [383]. Thus, there are an infinite number of design solutions that can be selected, especially when one considers that a design team can chose to ignore a behavior constraint line and accept certain deviations (e.g., a 10% increase in vehicle volume is deemed acceptable). In many cases, it may not be possible for all four vehicle characteristics to be simultaneously met with given technology levels, so a design team may need to settle for three of the four being met and accept a deviation in the other.

Optimization is a method to select one of these infinite number of design solutions by minimizing or maximizing an “objective function.” We can define the objective function to investigate that which matters most to a design team. Do we want to maximize range or PWR? Or do we want to minimize overall vehicle volume or mass? Or do we want to do all four simultaneously? If we have multiple objective functions, then our analysis becomes a “multi-objective programming problem.” We have chosen to draw our optimization graphs in two-dimensions using terms of mass on both axes because it provides a consistent, convenient, and

useful way to examine design possibilities across all vehicle types. Those familiar with graphical optimization techniques will look at our graphs and lean toward selecting the acceptable bound point at the intersection of the two active constraints closest to the origin as the “optimal” solution (see Point 1 in Fig. S.15). However, this would only be optimal if our goal was to optimize for mass and minimize the mass of an acceptable BE or HFC variant. For example, a design team may determine that an all-electric variant of a tracked ground combat vehicle should be as light as possible to ensure it can traverse combat bridges and that its existing range is acceptable. However, minimizing mass may not be a design team’s goal for a certain vehicle. For example, a design team may want to maximize a new vehicle’s range while limiting it to the same mass and PWR as the existing vehicle yet allowing it to be larger in volume (see Point 2 in Fig. S.15).

To find the intersection of behavior constraint lines, we can use Eq. (S.545), which shows how to find the x-value (battery pack mass) for the intersection of the PWR and range lines, our first and second compared vehicle characteristics. Once we calculate the x-value (battery pack mass), we can then find the y-value (electric motor mass required) by substituting the x-value and solving in either line equation, PWR or range. Using this same process, we can calculate values for all linear intersections in our model.

**Eq. (S.545)**

$$m_B[kg] = \frac{b_1[kg] \cdot m_2[-] + b_2[kg] \cdot m_1[-]}{m_1[-] - m_2[-]}$$

For watercraft, three of the intersections can be solved linearly because both vehicle characteristics are defined by lines. However, since range is a non-linear equation, the three intersections that involve range can be found using add-in optimization software in Microsoft Excel. To do so, we must first input a guess value in the cell for the battery pack mass, which then populates a value for the electric motor mass using Eq. (S.546).

**Eq. (S.546)**

$$m_m[kg] = \left( \frac{m_B[kg] - b_1[kg]}{m_1[-]} \right)$$

Next, we can rewrite Eq. (S.454) as Eq. (S.547), moving the left side of the equation to the right and making the left side equal to zero.

Eq. (S.547)

$$0 = \frac{m_B[kg] \cdot c_2 \left[ \frac{Wh}{kg} \right]}{\left( (c_3[-]) \left( c_4 \left[ \frac{kg}{m \cdot s^2} \right] \cdot \left( \left( 3.4 \cdot (\zeta)^{\frac{1}{3}} + c_5[m] \right) \cdot (\zeta)^{\frac{1}{3}} \right) \right) + c_6[N] \right)} - c_1 \left[ \frac{Wh}{N} \right]$$

where:

$$\zeta = \frac{m_{g,strippedFF}[kg] + (F_{m_m+GB+o_m}[-] \cdot m_m[kg]) + m_B[kg]}{\rho_w \left[ \frac{kg}{m^3} \right]}$$

Using the cell value for electric motor mass and our initial guess for a value of the battery pack mass, we can calculate the right side of Eq. (S.547). The result may be less than, greater than, or equal to zero, depending upon our guess value. Using Microsoft Excel’s add-in Solver software, we can define a cell by the right side of Eq. (S.547) as our “objective,” which we want to “set” to a “value of” zero “by changing the variable cell” that holds our initial guess for a battery pack mass value. We use the “solving method” of “GRG Nonlinear” to find a result. The algorithm tests new values for the battery pack mass, which changes the value for electric motor mass using Eq. (S.546), both of which change the right side of Eq. (S.547). Once the algorithm has found a solution that satisfies Eq. (S.547) (i.e., the right side equals zero), it stops.

At this point, it is worth noting that the algorithm may converge upon a local solution rather than a global solution depending upon our initial guess. The GRG (or “Generalized Reduced Gradient”) Nonlinear solver works by determining the slope (or gradient) of the objective function as it tries values for the variable cell(s). It determines that it has reached an optimum solution when the partial derivatives equal zero. If the initial guess is near a local solution, the solver may converge and stop, reporting the local solution rather than the global solution [384].

The Microsoft Excel Solver has multiple solver options. The “Evolutionary” method works according to the “Theory of Natural Selection” and starts with a random “population” of input sets of values for the variable cell(s). The solver can run the model for each set and find the one that has a solution closest to the target value (in this case, zero). Then it runs again with the best offspring, continuing until there is little change from one population to the next. Unfortunately, although this method is more likely to find a global optimum solution than the GRG Nonlinear solver, it is computationally expensive and takes significant time to run [384].

As a compromise, the Microsoft Excel Solver has a “Multistart” option for its GRG Nonlinear solver. This creates a randomly distributed population of initial values, and the model evaluates each one. Because the model starts multiple times from different initial conditions, there is a greater chance of finding the global solution rather than a local solution, but it too can be computationally expensive and increase the time required for the solver to run [384].

### 1.F.2. Computational optimization of solutions

There are many ways to find potential solutions for all-electric variants and to visualize results. One useful way, convenient for graphing results when using a spreadsheet, is to establish a range of values for one parameter and then calculate a range of output that can be compared to

the existing FF vehicle's characteristics. This allows design teams to visualize and understand how technology advancements might affect all-electric variant characteristics and compare them against known FF vehicle characteristics. We have selected several methods (three for BE variants and six for HFC variants) which we describe below in order to create graphs that, we believe, will be helpful to design teams and decision-makers alike in assessing the potential for transitioning to all-electric variants.

### **1.F.2.A. Battery pack-level specific energy technology improvements and the effect on variant mass**

In this analysis, we use the intersection between PWR (or TWR) and range lines (or curves) to visualize the effects that technology improvements to battery pack-level specific energy will have on BE variant mass. We model the gross vehicle weight condition and use medial/known values for each vehicle. We input a newly specified value for the electric motor specific power (electric motor PWR) and create a range of values for the specific energy (gravimetric energy density) of a battery pack from 1 to 12,000 Wh kg<sup>-1</sup>. (Note that the theoretical energy density of lithium-air (Li-O<sub>2</sub>) batteries at the material level is 11,400 Wh kg<sup>-1</sup>, so this scale is well-beyond any foreseeable battery pack-level values [35]. We show this scale in order to visualize all vehicle types.) From here, we can calculate the mass of battery pack required (Section 1.F.2.A.1), the mass of motors required (Section 1.F.2.A.2), the overall mass of the BE variant (Section 1.F.2.A.3), and the mass ratio (using medial/known values) between the BE variant and the existing FF vehicle (Section 1.F.2.A.4). We can then graph the mass ratio (y-axis) against the battery pack-level specific energy (x-axis) to see how technology improvement to batteries will affect resulting BE variant mass.

#### **1.F.2.A.1. Mass of battery pack required**

##### **1.F.2.A.1.A. Ground combat vehicles, freight locomotive, rotary-wing aircraft, and fixed-wing aircraft**

If we take Eq. (S.549) from Section 1.F.2.A.2.A (or Eq. (S.550) from Section 1.F.2.A.2.B for propeller airplanes or Eq. (S.551) from Section 1.F.2.A.2.C for ducted fan airplanes) below and substitute it into our range equation (using the equation of a line format) for select vehicle types from Section 1.F.1.A above, we can rearrange terms to solve for the mass of battery pack required. The resulting equation can take the same format as Eq. (S.545) (shown again as Eq. (S.548) for clarity). There are three major differences now from our previous use of these equations. First, the battery pack-level specific energy variable will come from the range of values created (1 to 12,000 Wh kg<sup>-1</sup>). Second, the electric motor PWR is newly specified to allow for investigating proposed technology achievements. Third, all other parameters will come from medial/known vehicle values, as described above.



Eq. (S.548)

$$m_B[kg] = \frac{b_1[kg] \cdot m_2[-] + b_2[kg] \cdot m_1[-]}{m_1[-] - m_2[-]}$$

where:

**Table S.31. Previously defined equations used to solve for battery pack mass required**

Vehicle characteristic:	PWR (or TWR)		Range	
Vehicle type	$m_1[-]$	$b_1[kg]$	$m_2[-]$	$b_2[kg]$
Ground combat vehicles	Eq. (S.354)	Eq. (S.355)	Eq. (S.362)	Eq. (S.363)
Freight locomotive	Eq. (S.354)	Eq. (S.355)	Eq. (S.380)	Eq. (S.381)
Rotary-wing aircraft	Eq. (S.354)	Eq. (S.355)	Eq. (S.388)	Eq. (S.389)
Propeller airplane	Eq. (S.394)	Eq. (S.395)	Eq. (S.423)	Eq. (S.424)
Ducted fan airplanes	Eq. (S.428)	Eq. (S.429)	Eq. (S.432)	Eq. (S.433)

### 1.F.2.A.1.B. Watercraft

For watercraft, we can still take Eq. (S.549) from Section 1.F.2.A.2.A below and substitute it into our range equation for watercraft from Section 1.F.1.A above. However, since the range equation for watercraft is nonlinear, we use the Microsoft Excel add-in Solver to find its intersection with the PWR line (see process described in Section 1.F.1.C). Here again, there are three major differences now from previous use of these equations. First, the battery pack-level specific energy variable will come from the range of values created (1 to 12,000 Wh kg<sup>-1</sup>). Second, the electric motor PWR is newly specified. Third, all other parameters will come from medial/known vehicle values, as described above.

**Table S.32. Previously defined equations used to solve for battery pack mass required – watercraft only**

Vehicle characteristic:	PWR		Range
Vehicle type	$m_1[-]$	$b_1[kg]$	$c_1$ through $c_6$
Waterjet boat	Eq. (S.354)	Eq. (S.355)	Nonlinear; must use Eq. (S.448) through Eq. (S.454) and Solver process from Section 1.F.1.C
Cargo (propeller) ship	Eq. (S.354)	Eq. (S.355)	Nonlinear; must use Eq. (S.448) through Eq. (S.454) with notes in Section 1.F.1.A.5.B.2 and Solver process from Section 1.F.1.C

### 1.F.2.A.2. Mass of motors required

#### 1.F.2.A.2.A. Ground combat vehicles, freight locomotive, rotary-wing aircraft, and watercraft

To solve for the mass of motors required for most vehicle types, we simply rearrange Eq. (S.353) to get Eq. (S.549).

Eq. (S.549)

$$m_m[kg] = \frac{m_{g,strippedFF}[kg] + m_B[kg]}{\left( \frac{PWR_m \left[ \frac{Wh}{kg} \right]}{PWR_{FF,g} \left[ \frac{Wh}{kg} \right]} \right) - F_{m_m+GB+o\_m_m}[-]}$$

### 1.F.2.A.2.B. Propeller airplanes

To solve for the mass of motors required for propeller airplanes, we rearrange Eq. (S.393) to get Eq. (S.550).

Eq. (S.550)

$$m_m[kg] = \frac{m_{g,strippedFF}[kg] + m_B[kg]}{\left( \frac{PWR_m \left[ \frac{Wh}{kg} \right]}{PWR_{TO,FF,g} \left[ \frac{Wh}{kg} \right]} \right) - F_{m_m+GB+o\_m_m}[-]}$$

### 1.F.2.A.2.C. Ducted fan airplanes

To solve for the mass of motors required for ducted fan airplanes, we rearrange Eq. (S.427) to get Eq. (S.551).

Eq. (S.551)

$$m_m[kg] = \frac{c_b[kg] + m_{g,strippedFF}[kg] + m_B[kg]}{\left( \frac{PWR_m \left[ \frac{Wh}{kg} \right]}{R_{DFTOP\_TOT} \left[ \frac{W}{N} \right] \cdot TWR_{TO,FFg} \left[ \frac{N}{N} \right] \cdot g \left[ \frac{m}{s^2} \right]} \right) - F_{m_m+GB+o\_m_m}[-] - \left( c_m \left[ \frac{kg}{W} \right] \cdot PWR_m \left[ \frac{W}{kg} \right] \right)}$$

### 1.F.2.A.3. Mass of battery electric variant

#### 1.F.2.A.3.A. Ground combat vehicles, freight locomotive, rotary-wing aircraft, propeller airplanes, and watercraft

No change from Eq. (S.351).

#### 1.F.2.A.3.B. Ducted fan airplanes

No change from Eq. (S.438).

#### 1.F.2.A.4. Mass ratio

##### 1.F.2.A.4.A. All vehicle types

For all vehicle types, we calculate the mass ratio between BE variants and existing FF vehicles by dividing the mass of the BE variant found in Section 1.F.2.A.3 by the mass of the existing FF vehicle recorded in Section 1.C.1.A.2.

Eq. (S.552)

$$m_{g,BE} : m_{g,FF} = \frac{m_{g,BE}}{m_{g,FF}}$$

##### 1.F.2.A.5. Battery pack-level specific energy for overall mass equivalency between the BE variant and the FF vehicle

Finally, to find the battery pack-level specific energy at which each BE variant will have a 1:1 ratio in Eq. (S.552) (i.e., equivalent mass between the BE variant and the FF vehicle), we can again turn to Microsoft Excel's add-in Solver. We create an objective cell using Eq. (S.553) and establish a variable cell with an initial guess. We then run the Solver to find the variable value at which the objective is set to zero.

Eq. (S.553)

$$0 = 1 - \frac{m_{g,BE}}{m_{g,FF}}$$

##### 1.F.2.B. Battery pack-level energy density technology improvements and the effect on variant volume

In this analysis, we use the intersection between PWR (or TWR) and range lines (or curves) to visualize the effects that technology improvements to battery pack-level energy density will have on BE variant volume. We continue to model the gross vehicle weight condition, use medial/known values for each vehicle, and use the newly specified value for the electric motor specific power (electric motor PWR). Different from Section 1.F.2.A above where we created a range of values for battery pack-level specific energy, here we input and use a singular value, which allows us to investigate specific technology achievements. We create a range of values for the energy density (volumetric energy density) of a battery pack from 1 to 12,000 Wh L<sup>-1</sup>. (Note that the theoretical energy density of iron-air batteries at the material level is 9,700 Wh L<sup>-1</sup> [36], which, again, is well-beyond currently foreseeable pack-level values.) From here, we can calculate the mass of battery pack required (Section 1.F.2.B.1), the mass of motors required (Section 1.F.2.B.2), the overall volume of the BE variant (Section 1.F.2.B.3), and the volume ratio (using medial/known values) between the BE variant and the existing FF vehicle (Section 1.F.2.B.4). We can then graph the volume ratio (y-axis) against the battery pack-level energy density (x-axis) to see how technology improvement to batteries will affect resulting BE variant volume.

### **1.F.2.B.1. Mass of battery pack required**

#### **1.F.2.B.1.A. All vehicles**

We use the same equations and processes described in Section 1.F.2.A.1, with the exception that now, instead of using a range of values for the battery pack-level specific energy, we select and input a new, single value for investigation. This results in a single value for the mass of battery pack required throughout our range of pack-level battery energy density values because pack-level battery energy density is neither a variable in Eq. (S.548) nor the equations used by the Microsoft Excel add-in Solver for watercraft.

#### **1.F.2.B.2. Mass of motors required**

Here again, since pack-level battery energy density is not a variable within the equations used to calculate the mass of motors required, we will have a single value for mass of motors required across our range of values for pack-level battery energy density.

##### **1.F.2.B.2.A. Ground combat vehicles, freight locomotive, rotary-wing aircraft, propeller airplanes, and watercraft**

No change from Eq. (S.549).

##### **1.F.2.B.2.B. Propeller airplanes**

No change from Eq. (S.550).

##### **1.F.2.B.2.C. Ducted fan airplanes**

No change from Eq. (S.551).

### **1.F.2.B.3. Volume of battery electric variant**

#### **1.F.2.B.3.A. Ground combat vehicles, freight locomotive, rotary-wing aircraft, propeller airplanes, and watercraft**

No change from Eq. (S.365).

#### **1.F.2.B.3.B. Ducted fan airplanes**

No change from Eq. (S.434).

### **1.F.2.B.4. Volume ratio**

#### **1.F.2.B.4.A. All vehicle types**

For all vehicle types, we calculate the volume ratio between BE variants and existing FF vehicles by dividing the volume of the BE variant found in Section 1.F.2.B.3 by the volume of the existing FF vehicle recorded in Section 1.C.1.B.2.

Eq. (S.554)

$$V_{g,BE}:V_{g,FF} = \frac{V_{g,BE}}{V_{g,FF}}$$

#### **1.F.2.B.5. Battery pack-level energy density for overall volume equivalency between the BE variant and the FF vehicle**

Finally, to find the battery pack-level energy density at which each BE variant will have a 1:1 ratio in Eq. (S.554) (i.e., equivalent volume between the BE variant and the FF vehicle), we can again turn to Microsoft Excel's add-in Solver. We create an objective cell using Eq. (S.555) and establish a variable cell with an initial guess. We then run the Solver to find the variable value at which the objective is set to zero.

**Eq. (S.555)**

$$0 = 1 - \frac{V_{g,BE}}{V_{g,FF}}$$

If the optimization solver cannot find a solution and/or the result for Eq. (S.555) does not equal zero, the user should check if the mass of battery pack required and/or mass of motors required are negative values throughout. If they are, then no feasible solution exists when using the user-specified battery pack-level specific energy value.

#### **1.F.2.C. Battery pack-level energy density technology improvements and the effect on variant volume using solutions for battery pack-level specific energy that result in equivalent mass between BE variants and existing FF vehicles**

In this portion of our analysis, we repeat our procedure from Section 1.F.2.B, but instead of using a newly selected value for pack-level battery specific energy, we use our value found via optimization from Section 1.F.2.A. Since we began this process using lines (or curves) defined by PWR (or TWR) and range equivalency between the BE variant and the existing FF vehicle, and we now use values that are known to result in an equivalent mass between the BE variant and the existing FF vehicle, when we ultimately find the value for pack-level battery energy density that results in a 1:1 ratio for overall volume, we satisfy the requirement for all four vehicle characteristics (PWR (or TWR), range, volume, and mass) to be simultaneously equivalent between our BE variant design and the existing FF vehicle.

#### **1.F.2.D. Hydrogen storage system specific energy technology improvements and the effect on variant mass**

In this analysis, we use the intersection between PWR (or TWR) and range lines (or curves) to visualize the effects that technology improvements to hydrogen storage system specific energy will have on HFC variant mass. We model the gross vehicle weight condition and use medial/known values for each vehicle. We input a newly specified value for the electric motor specific power (electric motor PWR) and create a range of values for the specific energy (gravimetric energy density) of a hydrogen storage system from 1 to 33,000 Wh kg<sup>-1</sup>. (Note that the net calorific value of hydrogen itself is 120 MJ kg<sup>-1</sup> (~33.3 kWh kg<sup>-1</sup>), so with storage components included, the value for a complete hydrogen storage system must be less than that of hydrogen itself, see Section 1.C.5.A.2.) We also input a newly specified value for fuel cell stack specific power, which allows us to run the model with various inputs to investigate the affect that fuel cell stack technology has on overall variant mass. (Unlike the BE analysis above in Section 1.F.2.A that only considers mass requirements for energy storage and electric motors, the HFC analysis must also consider mass requirements for the fuel cell stack, which adds another

variable.) From here, we can calculate the mass of a hydrogen storage system required (Section 1.F.2.D.1), the mass of motors required (Section 1.F.2.D.2), the overall mass of the HFC variant (Section 1.F.2.D.3), and the mass ratio (using medial/known values) between the HFC variant and the existing FF vehicle (Section 1.F.2.D.4). We can then graph the mass ratio (y-axis) against the hydrogen storage system specific energy (x-axis) to see how technology improvement to hydrogen storage systems will affect resulting HFC variant mass.

### 1.F.2.D.1. Mass of hydrogen storage system required

#### 1.F.2.D.1.A. Ground combat vehicles, freight locomotive, rotary-wing aircraft, and fixed-wing aircraft

If we take Eq. (S.557) from Section 1.F.2.D.2.A (or Eq. (S.558) from Section 1.F.2.D.2.B for propeller airplanes or Eq. (S.559) from Section 1.F.2.D.2.C for ducted fan airplanes) below and substitute it into our range equation (using the equation of a line format) for select vehicle types from Section 1.F.1.B above, we can rearrange terms to solve for the mass of hydrogen storage system required. The resulting equation can take the same format as Eq. (S.545) (shown again as Eq. (S.556) for clarity and modified for HFC variants). There are three major differences now from our previous use of these equations. First, the hydrogen storage system specific energy variable will come from the range of values created (1 to 33,000 Wh kg<sup>-1</sup>). Second, the electric motor PWR and fuel cell stack specific power are both newly specified to allow for investigating proposed technology achievements. Third, all other parameters now come from medial/known vehicle values.

Eq. (S.556)

$$m_{H_2storage}[kg] = \frac{b_1[kg] \cdot m_2[-] + b_2[kg] \cdot m_1[-]}{m_1[-] - m_2[-]}$$

where  $m_1$ ,  $m_2$ ,  $b_1$ , and  $b_2$  are defined according to Table S.33:

**Table S.33. Previously defined equations used to solve for hydrogen storage system mass required**

Vehicle characteristic:	PWR (or TWR)		Range	
	$m_1[-]$	$b_1[kg]$	$m_2[-]$	$b_2[kg]$
Ground combat vehicles	Eq. (S.462)	Eq. (S.463)	Eq. (S.470)	Eq. (S.471)
Freight locomotive	Eq. (S.462)	Eq. (S.463)	Eq. (S.488)	Eq. (S.489)
Rotary-wing aircraft	Eq. (S.462)	Eq. (S.463)	Eq. (S.496)	Eq. (S.497)
Propeller airplane	Eq. (S.502)	Eq. (S.503)	Eq. (S.508)	Eq. (S.509)
Ducted fan airplanes	Eq. (S.513)	Eq. (S.514)	Eq. (S.517)	Eq. (S.518)

#### 1.F.2.D.1.B. Watercraft

For watercraft, we can still take Eq. (S.557) from Section 1.F.2.D.2.A below and substitute it into our range equation for watercraft from Section 1.F.1.B above. However, since the range equation for watercraft is nonlinear, we use the Microsoft Excel add-in Solver to find its intersection with the PWR line (see process described in Section 1.F.1.C). Here again, there

are three major differences now from previous use of these equations. First, the hydrogen storage system specific energy variable will come from the range of values created (1 to 33,000 Wh kg<sup>-1</sup>). Second, the electric motor PWR and fuel cell stack specific power are both newly specified. Third, all other parameters will come from medial/known vehicle values.

**Table S.34. Previously defined equations used to solve for hydrogen storage system mass required – watercraft only**

Vehicle characteristic:	PWR		Range
Vehicle type	$m_1[-]$	$b_1[kg]$	$c_1$ through $c_7$
Waterjet boat	Eq. (S.462)	Eq. (S.463)	Nonlinear; must use Eq. (S.533) through Eq. (S.540) and Solver process from Section 1.F.1.C
Cargo (propeller) ship	Eq. (S.462)	Eq. (S.463)	Nonlinear; must use Eq. (S.533) through Eq. (S.540) with notes in Section 1.F.1.B.5.B.2 and Solver process from Section 1.F.1.C

### 1.F.2.D.2. Mass of motors required

#### 1.F.2.D.2.A. Ground combat vehicles, freight locomotive, rotary-wing aircraft, and watercraft

To solve for the mass of motors required for most vehicle types, we simply rearrange Eq. (S.461) to get Eq. (S.557).

Eq. (S.557)

$$m_m[kg] = \frac{m_{g,strippedFF}[kg] + m_{H_2storage}[kg]}{\left( \frac{PWR_m \left[ \frac{W}{kg} \right]}{PWR_{FF,g} \left[ \frac{W}{kg} \right]} - F_{m_m+GB+o\_m_m}[-] - \frac{PWR_m \left[ \frac{W}{kg} \right]}{SP_{FCS} \left[ \frac{W}{kg} \right]} \right)}$$

#### 1.F.2.D.2.B. Propeller airplanes

To solve for the mass of motors required for propeller airplanes, we rearrange Eq. (S.501) to get Eq. (S.558).

Eq. (S.558)

$$m_m[kg] = \frac{m_{g,strippedFF}[kg] + m_{H_2storage}[kg]}{\left( \frac{PWR_m \left[ \frac{W}{kg} \right]}{PWR_{TO,FF,g} \left[ \frac{W}{kg} \right]} - F_{m_m+GB+o\_m_m}[-] - \frac{PWR_m \left[ \frac{W}{kg} \right]}{SP_{FCS} \left[ \frac{W}{kg} \right]} \right)}$$

### 1.F.2.D.2.C. Ducted fan airplanes

To solve for the mass of motors required for ducted fan airplanes, we rearrange Eq. (S.512) to get Eq. (S.559).

Eq. (S.559)

$$m_m[kg] = \frac{c_b[kg] + m_{g,strippedFF}[kg] + m_{H_2storage}[kg]}{\left( \frac{PWR_m \left[ \frac{W}{kg} \right]}{R_{DFTOP\_TOT} \left[ \frac{W}{N} \right] \cdot TWR_{TO,FFg} \left[ \frac{N}{N} \right] \cdot g \left[ \frac{m}{s^2} \right]} - \frac{PWR_m \left[ \frac{W}{kg} \right]}{SP_{FCS} \left[ \frac{W}{kg} \right]} - F_{m_m+GB+o\_m_m}[-] - \left( c_m \left[ \frac{kg}{W} \right] \cdot PWR_m \left[ \frac{W}{kg} \right] \right) \right)}$$

### 1.F.2.D.3. Mass of hydrogen fuel cell variant

#### 1.F.2.D.3.A. Ground combat vehicles, freight locomotive, rotary-wing aircraft, propeller airplanes, and watercraft

No change from Eq. (S.458).

#### 1.F.2.D.3.B. Ducted fan airplanes

No change from Eq. (S.523).

### 1.F.2.D.4. Mass ratio

#### 1.F.2.D.4.A. All vehicle types

For all vehicle types, we calculate the mass ratio between HFC variants and existing FF vehicles by dividing the mass of the HFC variant found in Section 1.F.2.D.3 by the mass of the existing FF vehicle recorded in Section 1.C.1.A.2.

Eq. (S.560)

$$m_{g,HFC} : m_{g,FF} = \frac{m_{g,HFC}}{m_{g,FF}}$$

#### 1.F.2.D.5. Hydrogen storage system specific energy for overall mass equivalency between the HFC variant and the FF vehicle

Finally, to find the hydrogen storage system specific energy at which each HFC variant will have a 1:1 ratio in Eq. (S.560) (i.e., equivalent mass between the HFC variant and the FF vehicle), we can again turn to Microsoft Excel's add-in Solver. We create an objective cell using Eq. (S.561) and establish a variable cell with an initial guess. We then run the Solver to find the variable value at which the objective is set to zero.

Eq. (S.561)

$$0 = 1 - \frac{m_{g,HFC}}{m_{g,FF}}$$



### **1.F.2.E. Hydrogen storage system energy density technology improvements and the effect on variant volume**

In this analysis, we use the intersection between PWR (or TWR) and range lines (or curves) to visualize the effects that technology improvements to hydrogen storage system energy density will have on HFC variant volume. We continue to model the gross vehicle weight condition, use medial/known values for each vehicle, and use the newly specified values for the electric motor specific power (electric motor PWR) and fuel cell stack specific power. Different from Section 1.F.2.D above where we created a range of values for hydrogen storage system specific energy, here we input and use a singular value, which allows us to investigate specific technology achievements. We also must input a value for the fuel cell stack power density, as this, too, will affect the overall HFC variant volume. We create a range of values for the energy density (volumetric energy density) of a hydrogen storage system from 1 to 3,000 Wh L<sup>-1</sup>. (Recall from Section 1.C.5.A.1 that LH2 is more dense than 700-bar CGH2 (0.071 vs 0.041 kg L<sup>-1</sup>). If we use the density for LH2 and hydrogen's specific energy of 33.3 kWh kg<sup>-1</sup>, we can calculate the theoretical maximum volumetric energy density of LH2 alone as ~2,367 Wh L<sup>-1</sup>. Including the hydrogen storage tank with its BOP requires the hydrogen storage system to have an energy density less than this value.) From here, we can calculate the mass of hydrogen storage system required (Section 1.F.2.E.1), the mass of motors required (Section 1.F.2.E.2), the overall volume of the HFC variant (Section 1.F.2.E.3), and the volume ratio (using medial/known values) between the HFC variant and the existing FF vehicle (Section 1.F.2.E.4). We can then graph the volume ratio (y-axis) against the hydrogen storage system energy density (x-axis) to see how technology improvement to hydrogen storage will affect resulting HFC variant volume.

#### **1.F.2.E.1. Mass of hydrogen storage system required**

##### **1.F.2.E.1.A. All vehicles**

We use the same equations and processes described in Section 1.F.2.D.1, with the exception that now, instead of using a range of values for the hydrogen storage system specific energy, we select and input a new, single value for investigation. This results in a single value for the mass of hydrogen storage system required throughout our range of hydrogen storage system energy density values because hydrogen storage system energy density is neither a variable in Eq. (S.556) nor the equations used by the Microsoft Excel add-in Solver for watercraft.

##### **1.F.2.E.2. Mass of motors required**

Here again, since the hydrogen storage system energy density is not a variable within the equations used to calculate the mass of motors required, we will have a single value for mass of motors required across our range of values for hydrogen storage system energy density.

##### **1.F.2.E.2.A. Ground combat vehicles, freight locomotive, rotary-wing aircraft, propeller airplanes, and watercraft**

No change from Eq. (S.557).

### **1.F.2.E.2.B. Propeller airplanes**

No change from Eq. (S.558).

### **1.F.2.E.2.C. Ducted fan airplanes**

No change from Eq. (S.559).

### **1.F.2.E.3. Volume of hydrogen fuel cell variant**

#### **1.F.2.E.3.A. Ground combat vehicles, freight locomotive, rotary-wing aircraft, propeller airplanes, and watercraft**

No change from Eq. (S.473).

#### **1.F.2.E.3.B. Ducted fan airplanes**

No change from Eq. (S.519).

### **1.F.2.E.4. Volume ratio**

#### **1.F.2.E.4.A. All vehicle types**

For all vehicle types, we calculate the volume ratio between HFC variants and existing FF vehicles by dividing the volume of the HFC variant found in Section 1.F.2.E.3 by the volume of the existing FF vehicle recorded in Section 1.C.1.B.2.

**Eq. (S.562)**

$$V_{g,HFC}:V_{g,FF} = \frac{V_{g,HFC}}{V_{g,FF}}$$

#### **1.F.2.E.5. Hydrogen storage system energy density for overall volume equivalency between the HFC variant and the FF vehicle**

To find the hydrogen storage system energy density at which each HFC variant will have a 1:1 ratio in Eq. (S.562) (i.e., an equivalent volume between the HFC variant and the FF vehicle), we can use Microsoft Excel's add-in Solver. We create an objective cell using Eq. (S.563) and establish a variable cell with an initial guess. We then run the Solver to find the variable value at which the objective is set to zero.

**Eq. (S.563)**

$$0 = 1 - \frac{V_{g,HFC}}{V_{g,FF}}$$

Of course, achieving equivalent volume between the HFC variant and existing FF vehicle using the input parameters chosen does not mean that the mass will be equivalent as well. We can use the value found via optimization above, along with the same mass of hydrogen storage system and mass of electric motors used in this portion of the analysis, to find the overall HFC variant mass using the equations listed in Section 1.F.2.D.3. We can then return to Eq. (S.560) to calculate the mass ratio and compare the HFC variant to the existing FF vehicle.

### **1.F.2.F. Fuel cell stack system specific power technology improvements and the effect on variant mass**

In this analysis, we use the intersection between PWR (or TWR) and range lines (or curves for watercraft) to visualize the effects that technology improvements to fuel cell stack specific power will have on HFC variant mass. We model the gross vehicle weight condition and use medial/known values for each vehicle. We input a specified value for the electric motor specific power (electric motor PWR) and create a range of values for the specific power of a fuel cell stack system from 1 to 12,000 Wh kg<sup>-1</sup>. (Note that the literatures cites >10,000 Wh kg<sup>-1</sup> as achievable [10].) We also input a newly specified value for hydrogen fuel cell system specific energy, which allows us to run the model with various inputs to investigate the affect that hydrogen storage technology has on overall variant mass. (Our analysis here is very similar to that in Section 1.F.2.D except that, instead of the fuel cell stack specific power being held constant and testing a range of values for hydrogen storage system specific energy, we now do the reverse.) From here, we can calculate the mass of a hydrogen storage system required (Section 1.F.2.F.1), the mass of motors required (Section 1.F.2.F.2), the overall mass of the HFC variant (Section 1.F.2.F.3), and the mass ratio (using medial/known values) between the HFC variant and the existing FF vehicle (Section 1.F.2.F.4). We can then graph the mass ratio (y-axis) against the fuel cell stack system (x-axis) to see how technology improvement to fuel cell stacks will affect resulting HFC variant mass.

#### **1.F.2.F.1. Mass of hydrogen storage system required**

We use the same equations as those in Section 1.F.2.D.1, with the exception that we now change the input values for fuel cell stack system specific power and hydrogen storage system specific energy, as described above.

#### **1.F.2.F.2. Mass of motors required**

No change from Eq. (S.557) through Eq. (S.559) in Section 1.F.2.D.2.

#### **1.F.2.F.3. Mass of hydrogen fuel cell variant**

##### **1.F.2.F.3.A. Ground combat vehicles, freight locomotive, rotary-wing aircraft, propeller airplanes, and watercraft**

No change from Eq. (S.458).

##### **1.F.2.F.3.B. Ducted fan airplanes**

No change from Eq. (S.523).

#### **1.F.2.F.4. Mass ratio**

##### **1.F.2.F.4.A. All vehicle types**

No change from Eq. (S.560).

#### **1.F.2.F.5. Fuel cell stack system specific power for overall mass equivalency between the HFC variant and the FF vehicle**

No change from Section 1.F.2.D.5 and Eq. (S.561).

#### **1.F.2.G. Fuel cell stack system power density technology improvements and the effect on variant volume**

In this analysis, we use the intersection between PWR (or TWR) and range lines (or curves for watercraft) to visualize the effects that technology improvements to fuel cell stack system power density will have on HFC variant volume. We continue to model the gross vehicle weight condition, use medial/known values for each vehicle, and use the newly specified values for the electric motor specific power (electric motor PWR) and hydrogen storage system specific energy. We now also specify values for the hydrogen storage system energy density and fuel cell stack specific power. We create a range of values for the fuel cell stack system power density from 1 to 12,000 Wh L<sup>-1</sup>. (There is little in the literature regarding forecasts for future fuel cell stack system power density (volumetric) values; the DOE has published a target of 850 W L<sup>-1</sup> [19].) From here, we can calculate the mass of hydrogen storage system required (Section 1.F.2.G.1), the mass of motors required (Section 1.F.2.G.2), the overall volume of the HFC variant (Section 1.F.2.G.3), and the volume ratio (using medial/known values) between the HFC variant and the existing FF vehicle (Section 1.F.2.G.4). We can then graph the volume ratio (y-axis) against the fuel cell stack system power density (x-axis) to see how technology improvement to fuel cell stack systems will affect resulting HFC variant volume.

##### **1.F.2.G.1. Mass of hydrogen storage system required**

###### **1.F.2.G.1.A. All vehicles**

We use the same equations and processes described in Section 1.F.2.E.1, with the exception that now, instead of using a range of values for the hydrogen storage system energy density, we select and input a new, single value for investigation. This results in a single value for the mass of hydrogen storage system required throughout our range of fuel cell stack power density values because hydrogen storage system energy density is neither a variable in Eq. (S.556) nor the equations used by the Microsoft Excel add-in Solver for watercraft.

###### **1.F.2.G.2. Mass of motors required**

Here again, since the hydrogen storage system energy density is not a variable within the equations used to calculate the mass of motors required, we will have a single value for mass of motors required across our range of values for fuel cell stack power density.

###### **1.F.2.G.2.A. Ground combat vehicles, freight locomotive, rotary-wing aircraft, propeller airplanes, and watercraft**

No change from Eq. (S.557).

###### **1.F.2.G.2.B. Propeller airplanes**

No change from Eq. (S.558).

### **1.F.2.G.2.C. Ducted fan airplanes**

No change from Eq. (S.559).

### **1.F.2.G.3. Volume of hydrogen fuel cell variant**

#### **1.F.2.G.3.A. Ground combat vehicles, freight locomotive, rotary-wing aircraft, propeller airplanes, and watercraft**

No change from Eq. (S.473).

#### **1.F.2.G.3.B. Ducted fan airplanes**

No change from Eq. (S.519).

### **1.F.2.G.4. Volume ratio**

#### **1.F.2.G.4.A. All vehicle types**

No change from Eq. (S.562).

### **1.F.2.G.5. Fuel cell stack system power density for overall volume equivalency between the HFC variant and the FF vehicle**

No change from Section 1.F.2.E.5 and Eq. (S.563).

### **1.F.2.H. Balancing the competing interests of hydrogen storage system and fuel cell stack system mass to achieve equivalent mass between HFC variants and existing FF vehicles**

Throughout the majority of our individual analyses, we select and use a certain electric motor PWR technology. Consequently, for BE variants, the only vehicle system technology that impacts overall variant mass is the battery pack. In HFC variants, however, assuming a certain electric motor PWR technology still leaves the hydrogen storage system and fuel cell stack competing for the available mass budget. Therefore, for HFC variants, it is interesting to determine the hydrogen storage system specific energy technology required given a fuel cell stack specific power technology (and vice versa) in order to achieve a desired overall HFC variant mass. To accomplish this, we calculate two ranges of values: one for an HFC variant with equivalent mass to the existing FF vehicle and one for an HFC variant with a specified mass scaling factor. Using the scaling factor in our model allows us to investigate different design scenarios, e.g., what technology combinations are required if a 5% increase in overall vehicle mass is acceptable?

To calculate a design HFC variant mass using a scaling factor, we use the existing FF gross vehicle mass (Eq. (S.564)).

#### **Eq. (S.564)**

$$m_{g,HFC}[kg] = F_{m,s}[\%] \cdot m_{g,FF}[kg]$$

To ensure the proper amount of motors are used in the design in order to achieve overall vehicle PWR equivalency between the HFC variant and the existing FF vehicle, we can use Eq. (S.565) for all vehicle types except turbofan airplanes.

**Eq. (S.565)**

$$m_m[kg] = \frac{m_{g,HFC}[kg] \cdot PWR_{FF,g} \left[ \frac{W}{kg} \right]}{PWR_m \left[ \frac{W}{kg} \right]}$$

Combining Eq. (S.564) and Eq. (S.565) results in Eq. (S.566), which is helpful when considering the turbofan airplanes. Since turbofan airplanes are rated in terms of thrust, we can use our calculated takeoff power required to achieve that thrust,  $P_{F,TO,electric}[W]$ , from Section 1.C.2.D.3 (Eq. (S.567)).

**Eq. (S.566)**

$$m_m[kg] = \frac{F_{m,s}[\%] \cdot P_{FF,g}[W]}{PWR_m \left[ \frac{W}{kg} \right]}$$

**Eq. (S.567)**

$$m_m[kg] = \frac{F_{m,s}[\%] \cdot P_{F,TO,electric}[W]}{PWR_m \left[ \frac{W}{kg} \right]}$$

At this point, we have met two of the four vehicle characteristics: mass and PWR (or TWR). We now use the same range of values for fuel cell stack specific power (first used in Section 1.F.2.F) and calculate a range of values for the required hydrogen storage system specific energy. We do this by taking the equation for vehicle characteristic relationship for range for each vehicle type and rearranging it to solve for the hydrogen storage system specific energy in terms of fuel cell stack specific power (see Eq. (S.568) through Eq. (S.573) in Sections 1.F.2.H.1 through 1.F.2.H.6 below). Solutions in this analysis, therefore, meet three of the four vehicle characteristics: mass, PWR (or TWR), and range.

### 1.F.2.H.1. Ground combat vehicles

Eq. (S.568)

$$\begin{aligned}
 SE_{H_2storage} \left[ \frac{Wh}{kg} \right] &= \left( \frac{\left( \frac{OUE_{FF} [Wh]}{RL_{FF} [N]} \right) \cdot g \left[ \frac{m}{s^2} \right]}{\eta_{TV,HFC} [-]} \right) \\
 &\cdot \left( \frac{\left( C_{rr} [-] \cdot F_{m_m+GB+o,m_m} [-] + \frac{C_{rr} [-] \cdot PWR_{m,c} \left[ \frac{W}{kg} \right]}{SP_{FCS} \left[ \frac{W}{kg} \right]} + \sin\theta [-] \cdot F_{m_m+GB+o,m_m} [-] + \frac{\sin\theta [-] \cdot PWR_{m,c} \left[ \frac{W}{kg} \right]}{SP_{FCS} \left[ \frac{W}{kg} \right]} \right) \cdot m_m [kg]}{\left( m_{g,HFC} [kg] - m_{g,strippedFF} [kg] - (F_{m_m+GB+o,m_m} [-] \cdot m_m [kg]) - \left( \frac{m_m [kg] \cdot PWR_{m,c} \left[ \frac{W}{kg} \right]}{SP_{FCS} \left[ \frac{W}{kg} \right]} \right)} \right)} \right) \\
 &+ \left( \frac{\left( C_{rr} [-] \cdot m_{g,strippedFF} [kg] + \frac{\left( \frac{1}{2} \cdot \rho_{air} \left[ \frac{kg}{m^3} \right] \cdot C_d [-] \cdot A_f [m^2] \cdot \left( v \left[ \frac{m}{s} \right) \right)^2}{g \left[ \frac{m}{s^2} \right]} + \sin\theta [-] \cdot m_{g,strippedFF} [kg] \right)}{\left( m_{g,HFC} [kg] - m_{g,strippedFF} [kg] - (F_{m_m+GB+o,m_m} [-] \cdot m_m [kg]) - \left( \frac{m_m [kg] \cdot PWR_{m,c} \left[ \frac{W}{kg} \right]}{SP_{FCS} \left[ \frac{W}{kg} \right]} \right)} \right)} \right) + C_{rr} [-] + \sin\theta [-] \right)
 \end{aligned}$$

### 1.F.2.H.2. Freight locomotives

Eq. (S.569)

$$SE_{H_2storage} \left[ \frac{Wh}{kg} \right] = \left( \frac{\left( \frac{OUE_{FF} [Wh]}{TE_{FF} [N]} \right) \cdot g \left[ \frac{m}{s^2} \right] \cdot C_f [-] \cdot F_a [-] \cdot m_{g,HFC} [kg]}{\eta_{L,HFC} [-] \cdot \left( m_{g,HFC} [kg] - m_{g,strippedFF} [kg] - (F_{m_m+GB+o,m_m} [-] \cdot m_m [kg]) - \left( \frac{m_m [kg] \cdot PWR_{m,c} \left[ \frac{W}{kg} \right]}{SP_{FCS} \left[ \frac{W}{kg} \right]} \right)} \right)} \right)$$

### 1.F.2.H.3. Rotary-wing aircraft

Eq. (S.570)

$$SE_{H_2storage} \left[ \frac{Wh}{kg} \right] = \left( \frac{\left( \frac{OUE_{FF} [Wh]}{L_{FF} [N]} \right) \cdot g \left[ \frac{m}{s^2} \right] \cdot m_{HFC,g} [kg]}{\eta_{H,HFC} [-] \cdot \left( m_{HFC,g} [kg] - m_{g,strippedFF} [kg] - (F_{m_m+GB+o,m_m} [-] \cdot m_m [kg]) - \left( \frac{m_m [kg] \cdot PWR_{m,c} \left[ \frac{W}{kg} \right]}{SP_{FCS} \left[ \frac{W}{kg} \right]} \right)} \right)} \right)$$

#### 1.F.2.H.4. Propeller airplanes

Eq. (S.571)

$$SE_{H_2storage} \left[ \frac{Wh}{kg} \right] = \left[ \frac{1h}{3,600s} \right] \cdot \left( \frac{CR_{FF}[m] \cdot g \left[ \frac{m}{s^2} \right] \cdot m_{HFC,g}[kg]}{\eta_{PA,HFC}[-] \cdot \left( \frac{L[N]}{D[N]} \right) \cdot \left( m_{HFC,g}[kg] - m_{g,strippedFF}[kg] - (F_{m_m+GB+o,m_m}[-] \cdot m_m[kg]) - \left( \frac{m_m[kg] \cdot PWR_{m,c} \left[ \frac{W}{kg} \right]}{SP_{FCS} \left[ \frac{W}{kg} \right]} \right)} \right)} \right)$$

#### 1.F.2.H.5. Ducted fan airplanes

Eq. (S.572)

$$SE_{H_2storage} \left[ \frac{Wh}{kg} \right] = \left[ \frac{1h}{3,600s} \right] \cdot \left( \frac{CR_{FF}[m] \cdot g \left[ \frac{m}{s^2} \right] \cdot m_{HFC,g}[kg]}{\eta_{DFA,HFC}[-] \cdot \left( \frac{L[N]}{D[N]} \right) \cdot \left( m_{HFC,g}[kg] - m_{g,strippedFF}[kg] - (F_{m_m+GB+o,m_m}[-] \cdot m_m[kg]) - (\zeta + c_b[kg]) - \left( \frac{m_m[kg] \cdot PWR_{m,c} \left[ \frac{W}{kg} \right]}{SP_{FCS} \left[ \frac{W}{kg} \right]} \right)} \right)} \right)$$

where:

$$\zeta = c_m \left[ \frac{kg}{W} \right] \cdot m_m[kg] \cdot PWR_{m,c} \left[ \frac{W}{kg} \right]$$

#### 1.F.2.H.6. Watercraft

Eq. (S.573)

$$SE_{H_2storage} \left[ \frac{Wh}{kg} \right] = \left( \frac{OUE_{FF}[Wh]}{R_{T,FF,g}[N]} \right) \cdot \left( \frac{\left( (C_f[-] + C_R[-]) \cdot \frac{1}{2} \cdot \rho_w \left[ \frac{kg}{m^3} \right] \cdot (v \left[ \frac{m}{s} \right])^2 \cdot \left( \left( 3.4 \cdot \left( \frac{m_{HFC,g}[kg]}{\rho_w \left[ \frac{kg}{m^3} \right]} \right)^{\frac{1}{3}} + 0.5 \cdot L_{WL}[m] \right) \cdot \left( \frac{m_{HFC,g}[kg]}{\rho_w \left[ \frac{kg}{m^3} \right]} \right)^{\frac{1}{3}} \right) + (0.90 \cdot \frac{1}{2} \cdot \rho_{air} \left[ \frac{kg}{m^3} \right] \cdot (v \left[ \frac{m}{s} \right])^2 \cdot A_{air}[m^2])}{\left( m_{HFC,g}[kg] - m_{g,strippedFF}[kg] - (F_{m_m+GB+o,m_m}[-] \cdot m_m[kg]) - \left( \frac{m_m[kg] \cdot PWR_{m,c} \left[ \frac{W}{kg} \right]}{SP_{FCS} \left[ \frac{W}{kg} \right]} \right)} \right) \cdot \eta_{HFC}[-]} \right)$$

#### 1.F.2.I. Balancing the competing interests of hydrogen storage system and fuel cell stack system volume to achieve equivalent volume between HFC variants and existing FF vehicles

To complete our look at HFC variant designs, we consider the fourth vehicle characteristic that we have yet to address: overall variant volume. Here, we want to investigate how fuel cell stack power density technology and hydrogen storage system energy density technology affects their competition for volume budget in the HFC variant. We begin by



establishing a volume scaling factor so our model can consider desired design changes, e.g., a 5% increase in overall variant volume is acceptable. We then calculate the HFC variant volume using Eq. (S.574).

**Eq. (S.574)**

$$V_{g,HFC}[kg] = F_{V,s}[\%] \cdot V_{g,FF}[kg]$$

At this point, our equations dictate that we specify values for fuel cell stack specific power and hydrogen storage system specific energy, which will be required to calculate the hydrogen storage system energy density required given a range of values for fuel cell stack power density (the same range we used in Section 1.F.2.G). We can ensure the HFC variant design is satisfactory in terms of mass by using combinations of these values calculated in Section 1.F.2.H.

Taking our derived vehicle characteristic relationships for volume and rearranging to solve for the hydrogen storage system energy density in terms of fuel cell stack power density (using our selected values of hydrogen storage system specific energy and fuel cell stack specific power that we just calculated as satisfactory in Section 1.F.2.H), we can solve for technology combinations that meet our desired volume requirements. Solutions now, therefore, meet all four of our vehicle characteristics: mass, PWR (or TWR), range, and volume.

### 1.F.2.I.1. Ground combat vehicles, freight locomotive, rotary-wing aircraft, propeller airplanes, and watercraft

**Eq. (S.575)**

$$ED_{H_2storage} \left[ \frac{Wh}{L} \right] = \left( \frac{\left( \left( m_{HFC,g}[kg] - m_{g,strippedFF}[kg] - (F_{m_m+GB+o,m_m}[-] \cdot m_m[kg]) - \left( \frac{m_m[kg] \cdot PWR_{m,c} \left[ \frac{W}{kg} \right]}{SP_{FCS} \left[ \frac{W}{kg} \right]} \right) \right) \cdot SE_{H_2storage} \left[ \frac{Wh}{kg} \right] \right)}{\left( V_{HFC,g}[m^3] - V_{g,strippedFF}[m^3] - \left( R_{V_{m+GB+o,m_m}} \left[ \frac{m^3}{kg} \right] \cdot m_m[kg] \right) - \left( \frac{m_m[kg] \cdot PWR_{m,c} \left[ \frac{W}{kg} \right]}{PD_{FCS} \left[ \frac{W}{L} \right] \cdot \left[ \frac{1,000L}{m^3} \right]} \right)} \right) \cdot \left[ \frac{m^3}{1,000L} \right]$$

### 1.F.2.I.2. Ducted fan airplanes

Eq. (S.576)

$$ED_{H_2\text{storage}} \left[ \frac{Wh}{L} \right] = \frac{\left( \left( m_{HFC,g}[kg] - m_{g,strippedFF}[kg] - (F_{m+GB+o,m_m}[-] \cdot m_m[kg]) - (\zeta + c_b[kg]) - \left( \frac{m_m[kg] \cdot PWR_{m,c} \left[ \frac{W}{kg} \right]}{SP_{FCS} \left[ \frac{W}{kg} \right]} \right) \right) \cdot SE_{H_2\text{storage}} \left[ \frac{Wh}{kg} \right] \right)}{\left( V_{HFC,g}[m^3] - V_{g,strippedFF}[m^3] - (R_{V_{m+GB+o,m_m}} \left[ \frac{m^3}{kg} \right] \cdot m_m[kg]) - \left( \frac{m_m[kg] \cdot PWR_{m,c} \left[ \frac{W}{kg} \right]}{PD_{FCS} \left[ \frac{W}{L} \right] \cdot \left[ \frac{1,000L}{m^3} \right]} \right) - V_{total,e}[m^3] \right)} \cdot \left[ \frac{m^3}{1,000L} \right]$$

where:

$$\zeta = c_m \left[ \frac{kg}{W} \right] \cdot m_m[kg] \cdot PWR_{m,c} \left[ \frac{W}{kg} \right]$$

### 1.F.3. Technological tipping point solutions

In this portion of our analysis, we use both graphical and computational optimization methods to calculate the technological tipping points for battery packs, hydrogen storage systems, and fuel cell stacks given electric motor PWR. Although using Microsoft Excel's add-in Solver is relatively straightforward, it can be repetitive and time consuming, especially when one must run multiple optimizations. In order to automate this repetitive process, we incorporated macros into our model.

We ordered our macros alphabetically to match the order in which they are used within the model. In order to use macros within a Microsoft Excel spreadsheet, users must "Enable Macros" when opening a file. Additionally, users must have the "Solver Add-in" installed. To do so, click on "Tools" and "Add-ins." Check the "Solver Add-in" and "Analysis ToolPak" and click "OK." The "Solver" can then be accessed under the "Data" tab. Further, if users want to use the Solver Visual Basic for Applications (VBA) in the Visual Basic Editor (available under the "Developer" tab), they must first establish a reference to the Solver Add-in. In the Visual Basic Editor, click on "Tools" and "References" and then select "Solver" under "Available References."

Our macros use the GRG Nonlinear solver, discussed in Section 1.F.1.C. It is worth reiterating that, although the GRG Nonlinear solver is one of the fastest of Excel's add-in solvers, it is unfortunately highly-dependent upon the initial "guess" conditions for decision variables – the solver may prematurely stop at local optimal solutions or conclude that no feasible solution exists rather than find the global optimal solution. The Multistart option (also discussed in Section 1.F.1.C), with the "Require Bounds on Variables" box unchecked, can improve the probability of the solver converging to the global optimal solution, but it is more computationally expensive. Some of our macros use Multistart, while others do not. Users must evaluate whether results are correct using other checks.

Table S.35 details the approximate time required to run each macro on a laptop with a 3.5 GHz, i7 processor and 16 GB memory. Since some run times are very long, if a user wants to run a macro, he or she may want to consider "commenting-out" portions code using the Visual Basic Editor that refer to vehicles that are not of interest. Alternatively, a user can simply run single instances of the solver. We spent significant time stressing the model and running solvers to check solutions.

**Table S.35. Computational time requirements for each macro in Data S1**

<b>Macro name</b>	<b>Computational time, approximate (minutes)</b>
A Watercraft Commercial and Future Feasibility	2
B BE Technological Tipping Point Solver	6
C HFC Technological Tipping Point Solver	24
D Watercraft Technological Tipping Points Checks	2
E BE Optimization Solver One	4
F BE Optimization Solver Two	8
G HFC Optimization Solver One	17
H HFC Optimization Solver Two	180
I HFC Optimization Solver Three	80

### 1.F.3.A. Battery electric variants

#### 1.F.3.A.1. Graphical analysis

As discussed in Section 1.F.2.H, because the BE variant analysis only depends upon the battery pack technology levels once we select a value for the electric motor PWR, we can algebraically calculate the battery pack-level specific energy and energy density values that will enable a BE variant to be equivalent to the existing FF vehicle in all four vehicle characteristics simultaneously. We chose three values for the electric motor PWR to investigate: 2,976 W kg<sup>-1</sup> (~3 kW kg<sup>-1</sup>), 10 kW kg<sup>-1</sup>, and 15 kW kg<sup>-1</sup>. The lowest value is commercially available in the BMW i3, the highest value is claimed to be achieved by Magnax with their new axial flux motors, and the intermediate value is used in the literature as an acceptable value for “future” electric motors [10,27,29]. If we run our model (Sections 1.F.2.A and 1.F.2.C) three times (for each of the electric motor PWR values that we want to investigate), we can record the results for the required battery pack-level technology that give us a 1:1 ratio for both vehicle mass and volume using the PWR (or TWR) and range equations. To check our results, we repeat the analysis done in Section 1.F.1.A where we solve for the six intersections between the four vehicle characteristics lines (or curves) using these new battery pack technology values for each vehicle. We can then graph the lines (or curves) for the four vehicle relationships, which should all intersect at the same point (Fig. S.16). As shown by the table inset in Fig. S.16, a BE variant using the specified battery pack technology, mass of electric motors, and mass of battery pack will be equivalent to the FF vehicle (i.e., 100%) for all four vehicle characteristics.

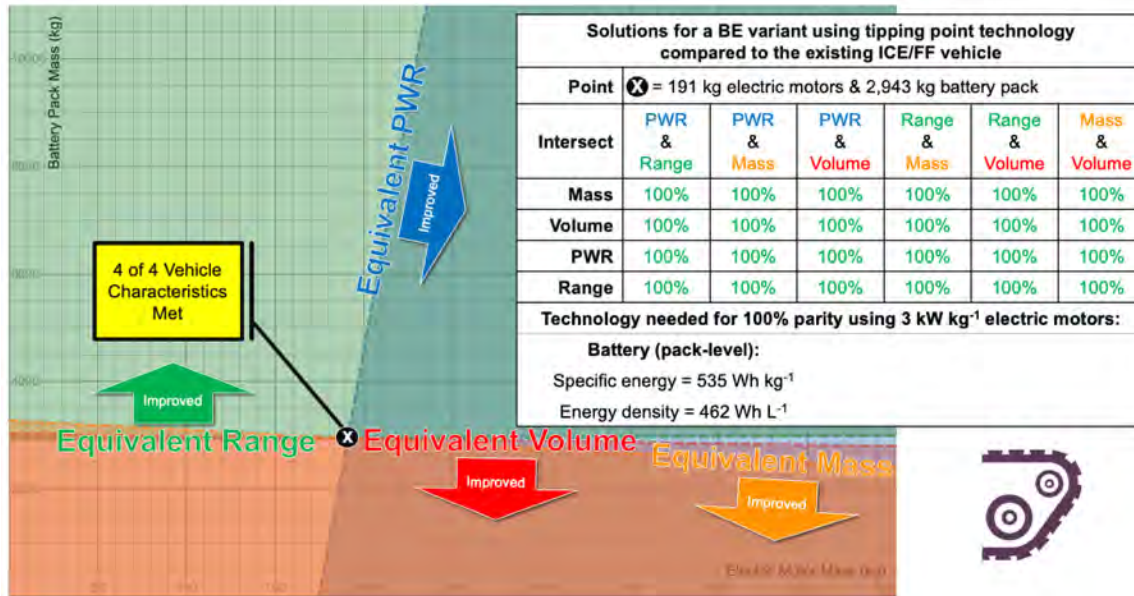


**Fig. S.16. Example of the four vehicle characteristics considered graphed for a BE variant using tipping point battery pack-level technology.**

### 1.F.3.A.2. Computational optimization analysis

Having developed the important relationships in our model, we can now set-up computational optimization solvers to investigate different desired design outcomes. In our BE variant analysis, we develop two optimization solvers: BE Optimization Solver #1 and #2.

#### 1.F.3.A.2.A. BE Optimization Solver #1

Our first solver works to minimize the battery technology improvements (for specific energy and energy density) required given a specified electric motor PWR. We define constraints for the BE variant mass and volume to be less than or equal to the existing FF vehicle and the BE variant PWR (or TWR) and range to be greater than or equal to the existing FF vehicle. The user can define future feasible battery technology values as constraints or, by using artificially-large values like 20,000 Wh kg<sup>-1</sup> and 20,000 Wh L<sup>-1</sup> for battery pack specific energy and energy density, identify the technological tipping points required for vehicle characteristics to be equivalent between the BE variant and the existing FF vehicle.

BE Optimization Solver #1 is useful because users can easily modify design requirements and add weighting factors for battery pack technology levels while investigating questions such as: what are the tipping point technologies required to meet design requirements or, given expected technology levels, what are the electric motor and battery pack requirements for a given BE variant? If no solution is found using BE Optimization Solver #1, then BE Optimization Solver #2 can be used to further investigate potential solutions.

##### 1.F.3.A.2.A.1. Objective function

Our model currently does not use any weighting factors, meaning that a one-unit improvement in battery pack specific energy is equal in value to a one-unit improvement in battery pack energy density. If one technology is deemed more important, a user could easily

add an appropriate weighting factor to Eq. (S.577). Note that, in our objective function equation, we dictate that the decision variable value cannot be less than the commercial value; i.e., the optimization solver cannot create a benefit in minimizing the total objective value result by using degraded technologies. Also note that units matter so far as terms are consistent. The solver will work to minimize the numerical value despite units matching.

**Eq. (S.577)**

$$\text{Total objective value} = \left( SE_{B,DV} \left[ \frac{Wh}{kg} \right] - SE_{B,COTS} \left[ \frac{Wh}{kg} \right] \right) + \left( ED_{B,DV} \left[ \frac{Wh}{L} \right] - ED_{B,COTS} \left[ \frac{Wh}{L} \right] \right)$$

where:

$$0 \leq \begin{cases} SE_{B,DV}[kg] - SE_{B,COTS}[kg] \\ ED_{B,DV}[kg] - ED_{B,COTS}[kg] \end{cases}$$

### 1.F.3.A.2.A.2. Decision variables

We list the decision variables for BE Optimization Solver #1 in Table S.36. Note that the electric motor PWR is a user-defined variable that must be set prior to running the optimization algorithm. Although not a true “decision variable” used by the solver, it is a variable that the user must decide upon prior to running the model.

**Table S.36. Decision variables for BE Optimization Solver #1**

Variable	Units
Battery pack-level specific energy ( $SE_{B,DV}$ )	Wh kg <sup>-1</sup>
Battery pack-level energy density ( $ED_{B,DV}$ )	Wh L <sup>-1</sup>
Mass of electric motors used ( $m_{m,DV}$ )	kg
Mass of battery pack used ( $m_{B,DV}$ )	kg

### 1.F.3.A.2.A.3. Constraints

#### 1.F.3.A.2.A.3.A. Positivity constraints

We assume that the technology level decision variables must be greater than or equal to commercial technology; i.e., neither degraded commercial values nor negative values are acceptable (Eq. (S.578) through Eq. (S.579)).

**Eq. (S.578)**

$$SE_{B,DV}[kg] \geq SE_{B,COTS}[kg]$$

**Eq. (S.579)**

$$ED_{B,DV}[kg] \geq ED_{B,COTS}[kg]$$

We ensure that the optimization solver does not use negative values for the mass of electric motors or the mass of battery pack used in the BE variant design (Eq. (S.580) through Eq. (S.581)).

**Eq. (S.580)**

$$m_{m,DV}[kg] \geq 0$$

**Eq. (S.581)**

$$m_{B,DV}[kg] \geq 0$$

#### **1.F.3.A.2.A.3.B. Future feasible limits constraints**

We also include an option to ensure the optimization solver cannot select technology levels beyond what is feasible (Eq. (S.582) through Eq. (S.583)). Users can either input technology values that support near-term possibilities for design or input large numbers beyond what is expected in order to determine tipping point technologies required.

**Eq. (S.582)**

$$SE_{B,DV}[kg] \leq SE_{B,F}[kg]$$

**Eq. (S.583)**

$$ED_{B,DV}[kg] \leq ED_{B,F}[kg]$$

#### **1.F.3.A.2.A.3.C. Vehicle performance characteristics constraints**

Finally, we include options for meeting vehicle performance characteristics for mass, volume, PWR (or TWR), and range. In our analysis, we consider all four characteristics simultaneously. However, a user could easily select just one, two, or three of these characteristics for inclusion in the optimization solver. Additionally, a user could even change the constraint value for each (e.g., instead of using the original FF vehicle’s gross mass as a constraint, allow for a 5% increase). The relationships are the same as those previously discussed in Section 1.F.1.A – mass: Eq. (S.369), volume: Eq. (S.364), PWR (or TWR: Eq. (S.348), Eq. (S.390) or Eq. (S.425), and range (Eq. (S.356), Eq. (S.374), Eq. (S.382), Eq. (S.396), or Eq. (S.443).

#### **1.F.3.A.2.A.4. Solver parameters**

For clarity, each of our optimization solvers has two sections within our model. In the first section, we organize and present the decision variables, objective function, and constraints with explanations. In the second section, we change that organization and repeat cross-referenced cells to make selecting groups of cells easy when establishing the Solver Parameters. The optimization solver attempts to minimize the objective function result by changing the decision variable cells subject to the defined constraints, which we have arranged into greater-than-or-equal-to and less-than-or-equal-to clusters. To help ensure that the optimization solver finds a global, rather than local, solution, we use the “Multistart” option, discussed in Section 1.F.1.C.

#### **1.F.3.A.2.B. BE Optimization Solver #2**

Our second solver works to minimize the difference in all four vehicle characteristics – mass, volume, PWR (or TWR) and range – between the BE variant and the existing FF vehicle. As with BE Optimization Solver #1, we define constraints to make the BE variant mass and

volume less than or equal to the existing FF vehicle and BE variant PWR (or TWR) and range greater than or equal to the existing FF vehicle. The user has the option of either defining technology levels, which is useful for investigating solutions that are specific to each technology or using future feasible values for the battery pack to produce solutions that are the best that can be achieved within current forecasts. Again, using artificially-large values here will result in identifying the technological tipping points required for vehicle characteristics to be equivalent. Users can select commercial and/or future feasible technology levels and compare results from this computational optimization solver to our results using graphical methods in Section 1.F.1.A.

This solver is useful because users can investigate optimal solutions using a completely different objective function. Whereas BE Optimization Solver #1 might not work for some scenarios, BE Optimization Solver #2 is likely to produce a result (e.g., in cases where technology advancements can never support meeting all four vehicle characteristics simultaneously and a design sacrifice must be made).

#### **1.F.3.A.2.B.1. Objective function**

Here again, our model currently does not use any weighting factors, meaning that meeting each of the four vehicle characteristics is equally important. If one characteristic is deemed more important, a user could easily add an appropriate weighting factor to Eq. (S.584). Eq. (S.584) finds the summation of the relationship ratios described in Section 1.F.1.A – mass: Eq. (S.369), volume: Eq. (S.364), PWR (or TWR): Eq. (S.348), Eq. (S.390) or Eq. (S.425), and range (Eq. (S.356), Eq. (S.374), Eq. (S.382), Eq. (S.396), or Eq. (S.443). The appropriate ratio must be selected for each of the four vehicle characteristics by vehicle type. The objective function takes the summation of each, which the optimization solver will then try to minimize, thereby minimizing the difference in each of the four vehicle characteristics between the BE variant and the existing FF vehicle.

Eq. (S.584)

$$\text{Total objective value} = \left( \frac{m_{g,BE}[kg]}{m_{g,FF}[kg]} \right) + \left( \frac{V_{g,BE}[m^3]}{V_{FF}[m^3]} \right) + \left\{ \begin{array}{l} \left( \frac{PWR_{g,BE} \left[ \frac{W}{kg} \right]}{PWR_{g,FF} \left[ \frac{W}{kg} \right]} \right) \\ \left( \frac{TWR_{g,BE} \left[ \frac{N}{N} \right]}{TWR_{g,FF} \left[ \frac{N}{N} \right]} \right) \end{array} \right\} + \left\{ \begin{array}{l} \frac{OUE_{BE,g}[Wh]}{RL_{BE,g}[N]} \\ \frac{OUE_{FF}[Wh]}{RL_{FF,g}[N]} \\ \frac{OUE_{BE,g}[Wh]}{TE_{BE,g}[N]} \\ \frac{OUE_{FF}[Wh]}{TE_{FF,g}[N]} \\ \frac{OUE_{BE,g}[Wh]}{L_{BE,g}[N]} \\ \frac{OUE_{FF}[Wh]}{L_{FF,g}[N]} \\ \frac{CR_{BE,g}[m]}{CR_{FF}[m]} \\ \frac{OUE_{BE,g}[Wh]}{R_{T,BE,g}[N]} \\ \frac{OUE_{FF}[Wh]}{R_{T,FF,g}[N]} \end{array} \right\}$$

### 1.F.3.A.2.B.2. Decision variables

The decision variables for BE Optimization Solver #2 are listed in Table S.37. This time, the electric motor PWR and the battery pack technology levels for specific energy and energy density are all user-defined decisions made prior to running the optimization solver, which itself uses just the mass of electric motors and mass of battery pack as true decision variables.

**Table S.37. Decision variables for BE Optimization Solver #2**

Variable	Units
Mass of electric motors used ( $m_{m,DV}$ )	kg
Mass of battery pack used ( $m_{B,DV}$ )	kg

### 1.F.3.A.2.B.3. Constraints

#### 1.F.3.A.2.B.3.A. Positivity constraints

Since the battery pack specific energy and energy density are pre-decided, we do not need to define positivity constraints for these variables. We again use Eq. (S.580) and Eq. (S.581) to ensure the optimization solver does not assign negative values to either the mass of electric motors or the mass of battery pack.



### **1.F.3.A.2.B.3.B. Vehicle performance characteristics constraints**

No change from Section 1.F.3.A.2.A.3.C.

### **1.F.3.A.2.B.4. Solver parameters**

No change from Section 1.F.3.A.2.A.4.

## **1.F.3.B. Hydrogen fuel cell variants**

### **1.F.3.B.1. Graphical analysis**

With HFC variants, the hydrogen storage system and the fuel cell stack both compete for available mass and volume budgets. This results in more unknowns than equations, our problem is indeterminate, and we cannot solve directly like we did for BE variants. Consequently, our analysis in Section 1.F.2 no longer provides a fully-optimized solution. (Recall that, as we progressed through Sections 1.F.2.D through 1.F.2.I, we had to periodically assign values for some technologies while finding the results for others.) However, what we can do is run our computational optimization solvers for potential HFC designs (Section 1.F.3.B.2 below), find results, and then test those results using the same graphical analysis procedures as we did for BE variants in Section 1.F.3.A.1.

We use the same three values for the electric motor PWR:  $2,976 \text{ W kg}^{-1}$ ,  $10 \text{ kW kg}^{-1}$ , and  $15 \text{ kW kg}^{-1}$  in our optimization solvers and find results for the hydrogen storage system specific energy and energy density and the fuel cell stack specific power and power density. Then, we repeat our analysis done in Section 1.F.1.B where we solve for the six intersections between the four vehicle characteristics lines (or curves). We can then graph the lines (or curves) for the four vehicle relationships, which should all intersect at the same point, defining the mass of electric motors and the mass of hydrogen storage system required for the HFC variant to be equivalent to the existing FF vehicle. The values defining this point should be the same as those output from the optimization solver(s) in Section 1.F.3.B.2, confirming the procedure.

Returning to the concept that we cannot use the optimized values from our individual parameter curves developed in Section 1.F.2.D through 1.F.2.I, we can, however, select values (for the fuel cell stack technologies for instance), look up the resulting values (for the hydrogen storage system technologies) and test that the resulting required combinations are as expected, i.e., that the HFC variant has 100% of each of the four characteristics of the existing FF vehicle. This should only be used to check our process, though, because, unlike the optimizations below where constraints are applied, this method may produce negative values that satisfy the mathematical equations but not common sense.

### **1.F.3.B.2. Computational optimization analysis**

In our HFC variant analysis, we develop three optimization solvers: HFC Optimization Solver #1, #2, and #3.

#### **1.F.3.B.2.A. HFC Optimization Solver #1**

This solver works to minimize the improvement required in each technology level given a specified electric motor PWR. The user can define the future feasible values, defining upper constraints. Constraints are also in place for the HFC variant mass and volume to be less than or equal to the existing FF vehicle and the HFC variant PWR (or TWR) and range to be greater than

or equal to the existing FF vehicle. If no solution is found by the optimization solver, then HFC Optimization Solver #2 and/or #3 can be used to further investigate potential solutions.

### 1.F.3.B.2.A.1. Objective function

Our model currently does not use any weighting factors, meaning that a one-unit improvement in any one of the four technology levels (hydrogen storage system specific energy or energy density or fuel cell stack specific power or power density) is equal in value to a one-unit improvement in another. If one technology is deemed more important, a user could easily add an appropriate weighting factor to Eq. (S.585).

Eq. (S.585)

Total objective value

$$\begin{aligned}
 &= \left( \frac{SE_{H_2storage,DV} \left[ \frac{Wh}{kg} \right] - SE_{H_2storage,COTS} \left[ \frac{Wh}{kg} \right]}{SE_{H_2storage,COTS} \left[ \frac{Wh}{kg} \right]} \right) \\
 &+ \left( \frac{ED_{H_2storage,DV} \left[ \frac{Wh}{L} \right] - ED_{H_2storage,COTS} \left[ \frac{Wh}{L} \right]}{ED_{H_2storage,COTS} \left[ \frac{Wh}{L} \right]} \right) \\
 &+ \left( \frac{SP_{FCS,DV} \left[ \frac{W}{kg} \right] - SP_{FCS,COTS} \left[ \frac{W}{kg} \right]}{SP_{FCS,COTS} \left[ \frac{W}{kg} \right]} \right) + \left( \frac{PD_{FCS,DV} \left[ \frac{W}{L} \right] - PD_{FCS,COTS} \left[ \frac{W}{L} \right]}{PD_{FCS,COTS} \left[ \frac{W}{L} \right]} \right)
 \end{aligned}$$

### 1.F.3.B.2.A.2. Decision variables

We list the decision variables for HFC Optimization Solver #1 in Table S.38. Note that the electric motor PWR is a user-defined variable that must be set prior to running the optimization algorithm. Although not a true “decision variable” used by the solver, it is a variable that the user must decide upon prior to running the model.

**Table S.38. Decision variables for HFC Optimization Solver #1**

Variable	Units
Hydrogen storage system specific energy ( $SE_{H_2storage,DV}$ )	Wh kg <sup>-1</sup>
Hydrogen storage system energy density ( $ED_{H_2storage,DV}$ )	Wh L <sup>-1</sup>
Fuel cell stack specific power ( $SP_{FCS,DV}$ )	W kg <sup>-1</sup>
Fuel cell stack power density ( $PD_{FCS,DV}$ )	W L <sup>-1</sup>
Mass of electric motors used ( $m_{m,DV}$ )	kg
Mass of hydrogen storage system used ( $m_{H_2storage,DV}$ )	kg

### 1.F.3.B.2.A.3. Constraints

#### 1.F.3.B.2.A.3.A. Positivity constraints

We set up our model so that the technology level decision variables must either be greater than or equal to commercial technology or greater than or equal to zero; i.e., it neither accepts

degraded commercial values nor negative values (Eq. (S.586) through Eq. (S.589)). This allows a user to run the solver and identify technological tipping points either required for the future or that have already been surpassed.

**Eq. (S.586)**

$$SE_{H_2storage,DV} \left[ \frac{Wh}{kg} \right] \geq \begin{cases} SE_{H_2storage,COTS} \left[ \frac{Wh}{kg} \right] \\ 0 \end{cases}$$

**Eq. (S.587)**

$$ED_{H_2storage,DV} \left[ \frac{Wh}{L} \right] \geq \begin{cases} ED_{H_2storage,COTS} \left[ \frac{Wh}{L} \right] \\ 0 \end{cases}$$

**Eq. (S.588)**

$$SP_{FCS,DV} \left[ \frac{W}{kg} \right] \geq \begin{cases} SP_{FCS,COTS} \left[ \frac{W}{kg} \right] \\ 0 \end{cases}$$

**Eq. (S.589)**

$$PD_{FCS,DV} \left[ \frac{W}{L} \right] \geq \begin{cases} PD_{FCS,COTS} \left[ \frac{W}{L} \right] \\ 0 \end{cases}$$

We ensure that the optimization solver does not use negative values for the mass of electric motors or the mass of hydrogen storage system used in the HFC variant design (same as Eq. (S.580) above and Eq. (S.590) below).

**Eq. (S.590)**

$$m_{H_2storage,DV} [kg] \geq 0$$

### 1.F.3.B.2.A.3.B. Future feasible limits constraints

We also include an option to ensure the optimization solver cannot select technology levels beyond what is feasible (Eq. (S.591) through Eq. (S.594)). Users can either input technology values that support near-term possibilities for design or input large numbers beyond what is expected in order to determine tipping point technologies required. Theoretical and practical limits can also be applied.

**Eq. (S.591)**

$$SE_{H_2storage,DV} \left[ \frac{Wh}{kg} \right] \leq SE_{H_2storage,F} \left[ \frac{Wh}{kg} \right]$$

Eq. (S.592)

$$ED_{H_2storage,DV} \left[ \frac{Wh}{L} \right] \leq ED_{H_2storage,F} \left[ \frac{Wh}{L} \right]$$

Eq. (S.593)

$$SP_{FCS,DV} \left[ \frac{W}{kg} \right] \leq SP_{FCS,F} \left[ \frac{W}{kg} \right]$$

Eq. (S.594)

$$PD_{FCS,DV} \left[ \frac{W}{L} \right] \leq PD_{FCS,F} \left[ \frac{W}{L} \right]$$

### 1.F.3.B.2.A.3.C. Vehicle performance characteristics constraints

No change from Section 1.F.3.A.2.A.3.C except that the relationships are now for HFC variants, rather than BE variants, as defined in Section 1.F.1.B – mass: Eq. (S.477), volume: Eq. (S.472), PWR (or TWR): Eq. (S.455), Eq. (S.498) or Eq. (S.510), and range: Eq. (S.464), Eq. (S.482), Eq. (S.490), Eq. (S.504), or Eq. (S.528).

### 1.F.3.B.2.A.4. Solver parameters

No change from Section 1.F.3.A.2.A.4.

### 1.F.3.B.2.B. HFC Optimization Solver #2

The second HFC optimization solver works to minimize the difference in all four characteristics (mass, volume, PWR or TWR, and range) between the existing FF vehicle and the HFC variant. Although the constraints are in still in place (HFC variant mass and volume must be less than or equal to the existing FF vehicle and HFC variant PWR (or TWR) and range must be greater than or equal to the existing FF vehicle), the optimization solver will often find a solution that sacrifices volume if not all four characteristics can be simultaneously met. The user has the option of either defining technology levels or including them as decision variables (i.e., using six or just two decision variables).

This solver is useful for investigating solutions that are specific to technology levels. For example, a user can take the four technology-driven decision variables and define them (making them parameters) as future feasible values and leave just the mass of motors and mass of hydrogen storage system as decision variables. In this case, the optimization solver will find a solution that is the best that can be achieved within specified technology forecasts.

### 1.F.3.B.2.B.1. Objective function

This solver also does not currently use any weighting factors, meaning that meeting each of the four vehicle characteristics is equally important. If one characteristic is deemed more important, a user could easily add an appropriate weighting factor to Eq. (S.595). Eq. (S.595) finds the summation of the relationship ratios described in Section 1.F.1.B – mass: Eq. (S.477), volume: Eq. (S.472), PWR (or TWR): Eq. (S.455), Eq. (S.498) or Eq. (S.510), and range: Eq. (S.464), Eq. (S.482), Eq. (S.490), Eq. (S.504), or Eq. (S.528). The appropriate ratio must be selected for each of the four vehicle characteristics by vehicle type. The objective function takes

the summation of each, which the optimization solver will then try to minimize, thereby minimizing the difference in each of the four vehicle characteristics between the HFC variant and the existing FF vehicle.

**Eq. (S.595)**

$$\text{Total objective value} = \left( \frac{m_{g,HFC}[kg]}{m_{g,FF}[kg]} \right) + \left( \frac{V_{g,HFC}[m^3]}{V_{FF}[m^3]} \right) + \left\{ \begin{array}{l} \left( \frac{PWR_{g,HFC} \left[ \frac{W}{kg} \right]}{PWR_{g,FF} \left[ \frac{W}{kg} \right]} \right) \\ \left( \frac{TWR_{g,HFC} \left[ \frac{N}{N} \right]}{TWR_{g,FF} \left[ \frac{N}{N} \right]} \right) \end{array} \right\} + \left\{ \begin{array}{l} \frac{OUE_{HFC,g}[Wh]}{RL_{HFC,g}[N]} \\ \frac{OUE_{FF}[Wh]}{RL_{FF,g}[N]} \\ \frac{OUE_{HFC,g}[Wh]}{TE_{HFC,g}[N]} \\ \frac{OUE_{FF}[Wh]}{TE_{FF,g}[N]} \\ \frac{OUE_{HFC,g}[Wh]}{L_{HFC,g}[N]} \\ \frac{OUE_{FF}[Wh]}{L_{FF,g}[N]} \\ \frac{CR_{HFC,g}[m]}{CR_{FF}[m]} \\ \frac{OUE_{HFC,g}[Wh]}{R_{T,HFC,g}[N]} \\ \frac{OUE_{FF}[Wh]}{R_{T,FF,g}[N]} \end{array} \right\}$$

### 1.F.3.B.2.B.2. Decision variables

The decision variables for HFC Optimization Solver #2 are the same as those listed in Table S.38. Note that another option is to make the four technology levels (hydrogen storage specific energy and energy density and fuel cell stack specific power and power density) parameters with assigned values, leaving just the mass of electric motors and mass of hydrogen storage system used as decision variables.

### 1.F.3.B.2.B.3. Constraints

#### 1.F.3.B.2.B.3.A. Positivity constraints

We again use Eq. (S.580) and Eq. (S.590) to ensure the optimization solver does not assign negative values to either the mass of electric motors or the mass of hydrogen storage system used.

### 1.F.3.B.2.B.3.B. Vehicle performance characteristics constraints

No change from Section 1.F.3.B.2.A.3.C.

### 1.F.3.B.2.B.3.C. Solver parameters

No change from Section 1.F.3.B.2.A.4.

### 1.F.3.B.2.C. HFC Optimization Solver #3

Our third HFC optimization solver works to minimize the HFC variant's overall volume. It works the same as HFC Optimization Solver #2 with three exceptions: first, the objective function is reduced to only include the volume vehicle characteristic; second, the four technology levels are assigned as parameter values, leaving just the mass of electric motors and mass of hydrogen storage system used as decision variables; and third, the volume constraint is removed.

This solver is useful either as a check on previous work or for finding a solution for those vehicle platforms where not all four characteristics – mass, volume, PWR (or TWR), and range – can be simultaneously met or improved and volume must be sacrificed.

#### 1.F.3.B.2.C.1. Objective function

The objective function (Eq. (S.596)) only considers volume, seeking to minimize the amount that this vehicle characteristic must be exceeded while the other three vehicle characteristics – mass, PWR (or TWR), and range – are met as constraints.

Eq. (S.596)

$$\text{Total objective value} = \left( \frac{V_{g,HFC}[m^3] - V_{FF}[m^3]}{V_{FF}[m^3]} \right)$$

#### 1.F.3.B.2.C.2. Decision variables

Only the mass of electric motors and mass of hydrogen storage system used are decision variables in this solver (Table S.39); all other variables have been made parameters with assigned values.

**Table S.39. Decision variables for BE Optimization Solver #3**

Variable	Units
Mass of electric motors used ( $m_{m,DV}$ )	kg
Mass of hydrogen storage system used ( $m_{H2storage,DV}$ )	kg

#### 1.F.3.B.2.C.3. Constraints

##### 1.F.3.B.2.C.3.A. Positivity constraints

No change from Section 1.F.3.B.2.B.3.A.

##### 1.F.3.B.2.C.3.B. Vehicle performance characteristics constraints

Same as Section 1.F.3.B.2.B.3.B except that the volume constraint is removed; i.e., only mass, PWR (or TWR), and range constraints are applied.

#### **1.F.3.B.2.C.4. Solver parameters**

No change from Section 1.F.3.B.2.A.4.

## **2. SUPPLEMENTARY DISCUSSION AND FIGURES**

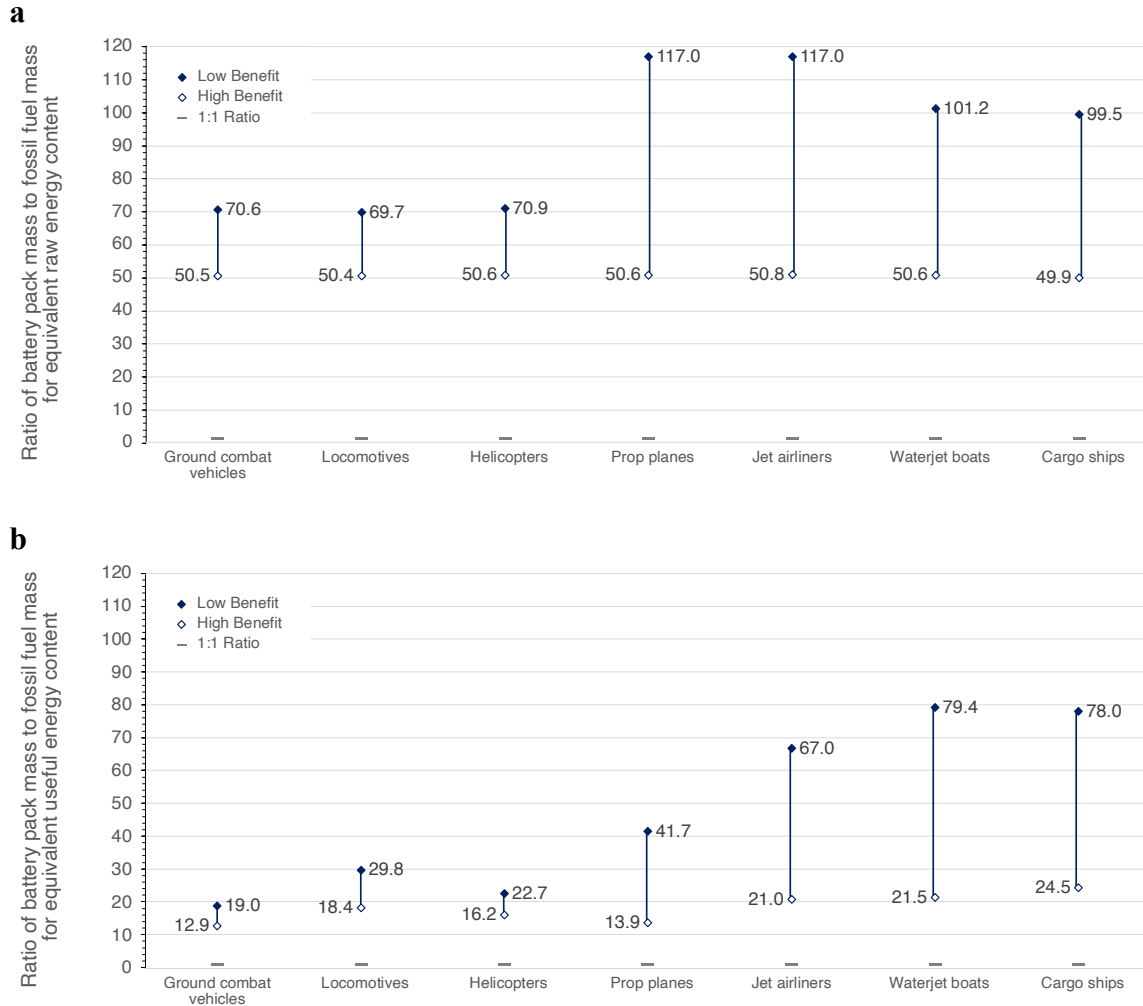
This section provides additional discussion. We demonstrate the inadequacy of other assessments that use too narrow a scope and show how using a whole-system design approach facilitates a better understanding of what is possible in transitioning existing vehicles to all-electric systems. We discuss additional factors to consider when transitioning vehicles, to include fleet modernization, safety, supporting infrastructure, and other aspects that deserve further attention.

### **2.A. Comparison of equivalent platform “raw” energy and “useful” energy by variant (Sections 1.D and 1.E)**

As previously discussed, we encountered comparisons in the literature or in conversation that simply compare mass and volume requirements for raw energy when comparing BE or HFC systems to ICE/FF systems. As Fig. S.17 through Fig. S.22 illustrate, this is an inadequate comparison that may be inaccurately used to convince others that transitioning to all-electric vehicle systems is infeasible.

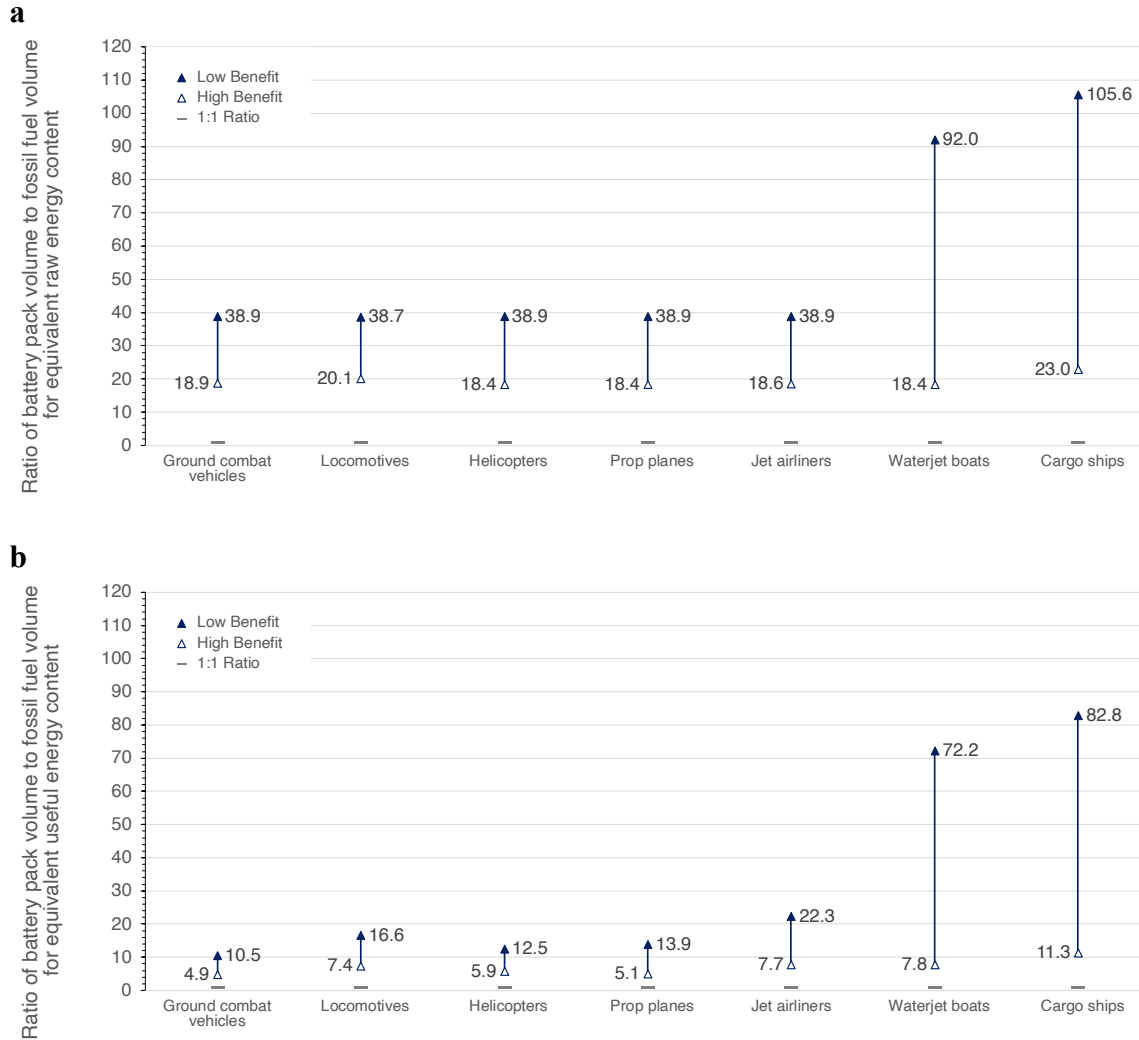
For each figure, we show the “raw” energy content comparison (a) and the “useful” energy content comparison (b). The only difference between the two is that we go one step further in (b) and consider how efficient the overall system is. Although just this single step is enough to illustrate why the comparisons in (a) are insufficient, the comparison in (b) can still be improved upon by holistically considering the vehicle system the extra mass and volume budget available from eliminating ICE/FF components that are no longer needed. When interpreting the results in Fig. S.17 through Fig. S.22, note that variations occur due to different fuel types and the overall system efficiency between variants for the same vehicle type.





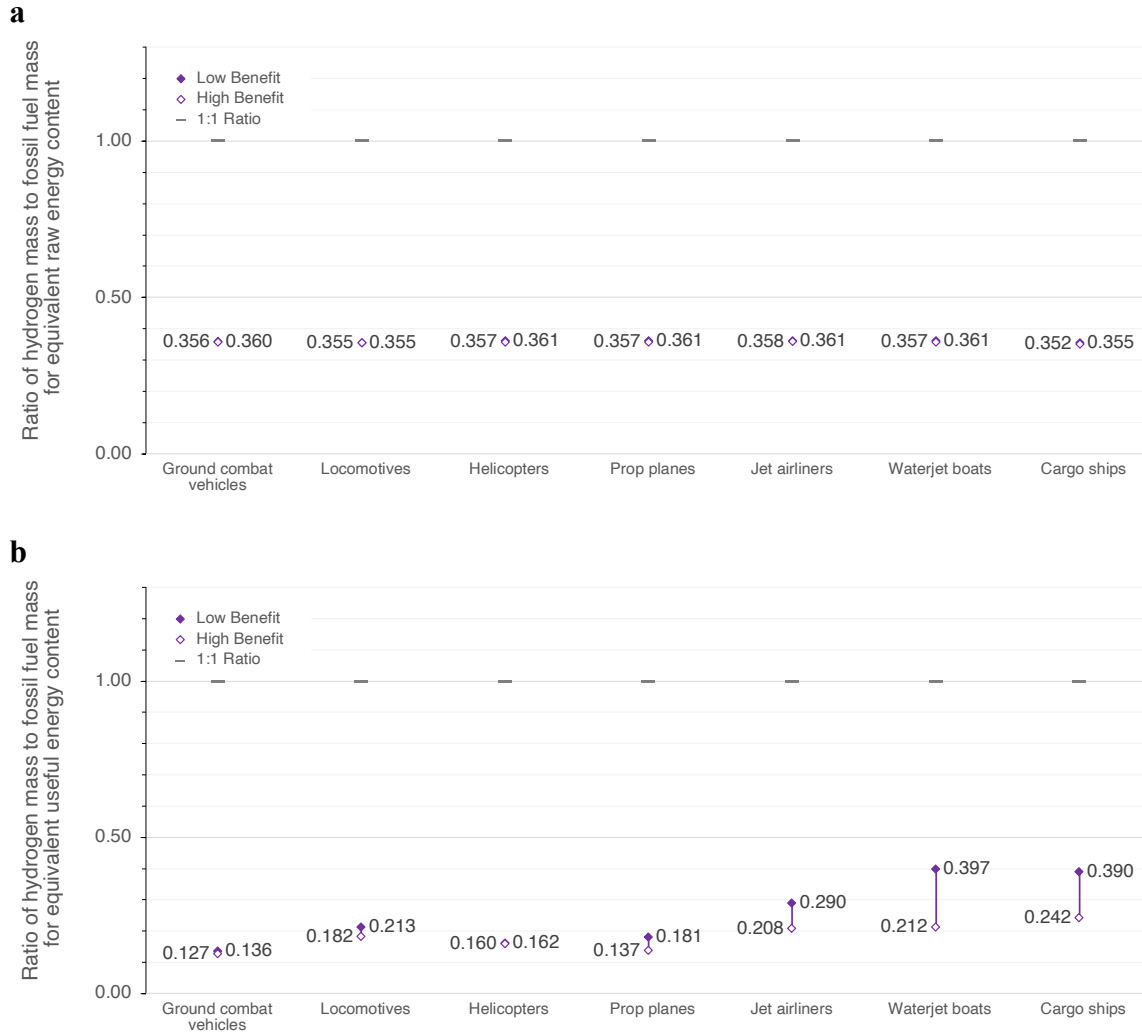
**Fig. S.17. An illustration of battery pack mass required to carry the same raw energy content (a) and useful energy content (b) of one-unit mass of fossil fuel, by vehicle type.**

Calculations determine the chemical energy content of the fossil fuel (JP-8, diesel #2, Jet-A, or marine diesel fuel oil) carried onboard each platform to find the mass ratio of equivalent energy storage. Low benefit values use input parameter combinations that result in the highest mass ratio (e.g., low estimates for battery specific energy and high estimates for the lower heating value of the fossil fuel) and vice versa for high benefit values. Variations are due to the fossil fuel type as well as the commercial/projected values for battery pack-level specific energy for each vehicle type. Calculations in (a) use battery pack-level specific energy values while calculations in (b) also consider the overall system efficiencies for ICE and BE vehicles. Although the comparison in (a) is often used, it is clearly inadequate, and, although improved, (b) still fails to account for efficiencies gained by eliminating FF system components.



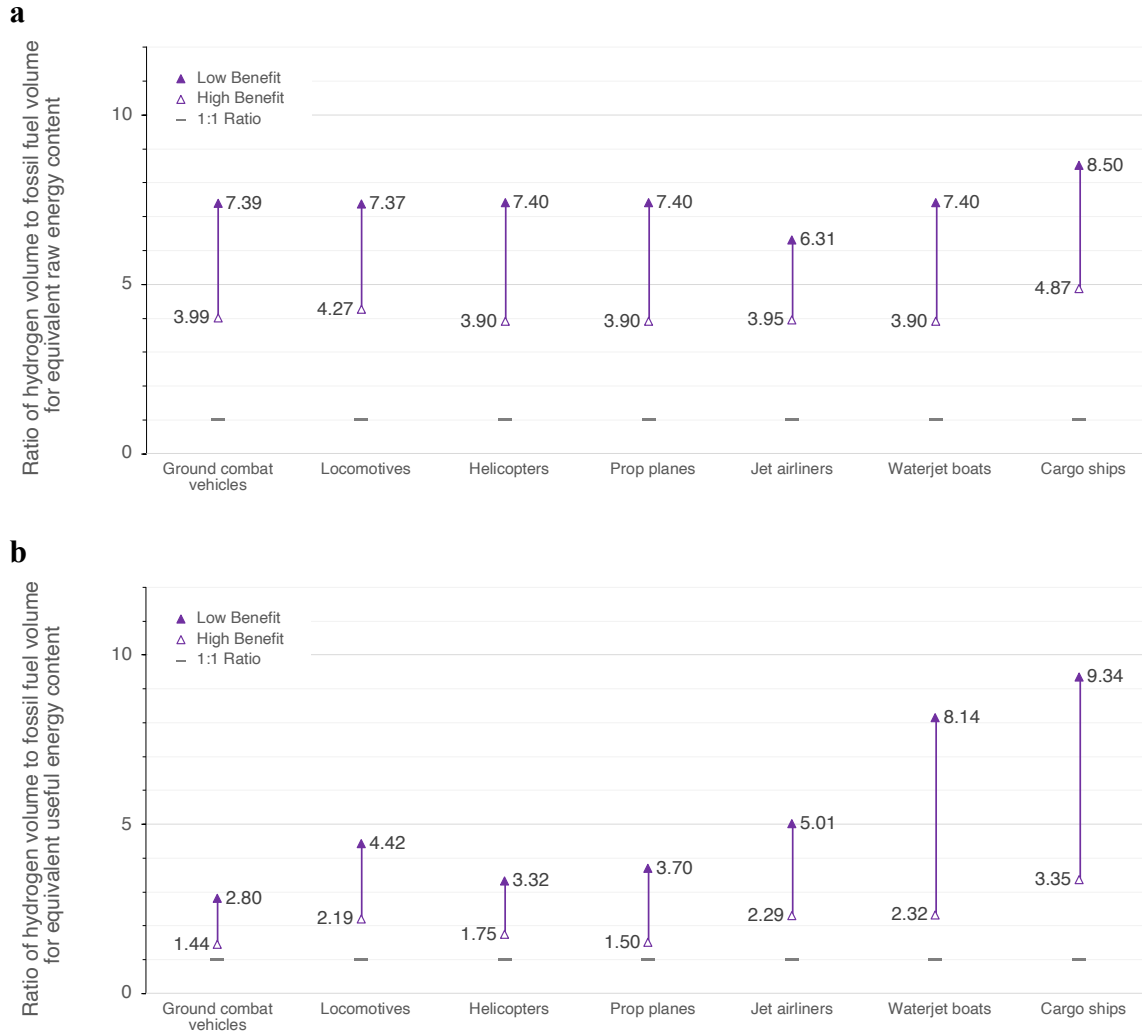
**Fig. S.18. An illustration of battery pack volume required to carry the same raw energy content (a) and useful energy content (b) of one-unit volume of fossil fuel, by vehicle type.**

Calculations determine the chemical energy content of the fossil fuel (JP-8, diesel #2, Jet-A, or marine diesel fuel oil) carried onboard each platform to find the volume ratio of equivalent energy storage. Low benefit values use input parameter combinations that result in the highest volume ratio (e.g., low estimates for battery energy density and high estimates for the lower heating value of the fossil fuel) and vice versa for high benefit values. Variations are due to the fossil fuel type as well as the commercial/projected values for battery pack-level energy density for each vehicle type. Calculations in (a) use battery pack-level energy density values while calculations in (b) also consider the overall system efficiencies for ICE and BE vehicles. Although the comparison in (a) is often used, it is clearly inadequate, and, although improved, (b) still fails to account for efficiencies gained by eliminating FF system components.



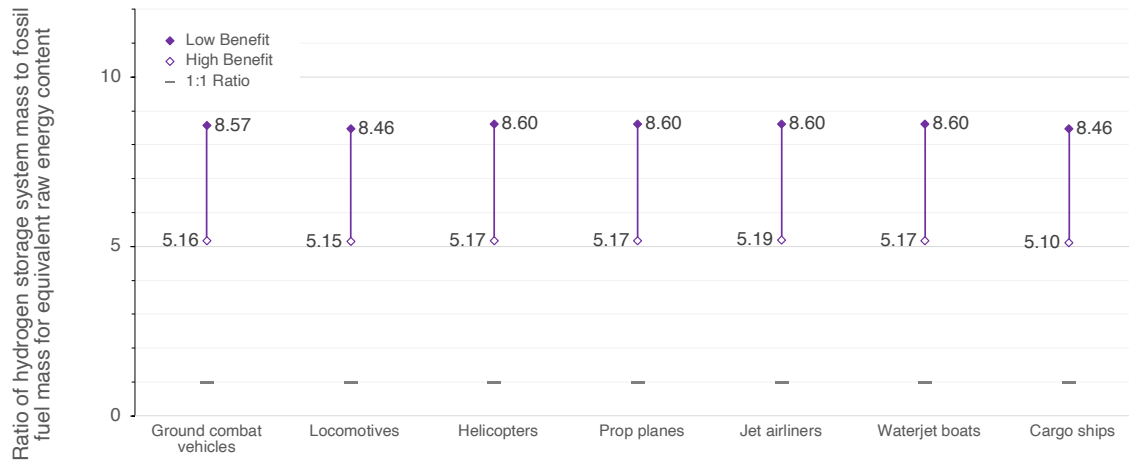
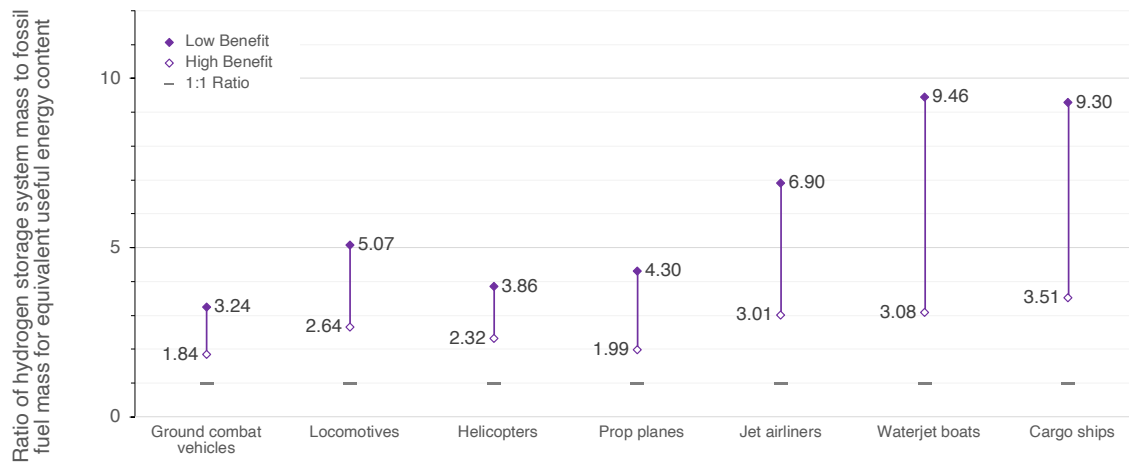
**Fig. S.19. An illustration of hydrogen (gas only) mass required to have the same raw energy content (a) and useful energy content (b) of one-unit mass of fossil fuel, by vehicle type.**

Calculations determine the chemical energy content of the fossil fuel (JP-8, diesel #2, Jet-A, or marine diesel fuel oil) carried onboard each platform to find the mass ratio of equivalent energy storage. Low benefit values use input parameter combinations that result in the highest volume ratio (e.g., high estimates for the lower heating value of the fossil fuel) and vice versa for high benefit values. Variations in (a) are due to the fossil fuel type and in (b) also include the range of overall system efficiencies for each vehicle type. Calculations in (a) use hydrogen (gas only) specific energy while calculations in (b) also consider the overall system efficiencies for ICE and BE vehicles.



**Fig. S.20. An illustration of hydrogen (gas only) volume required to have the same raw energy content (a) and useful energy content (b) of one-unit volume of fossil fuel, by vehicle type.**

Calculations determine the chemical energy content of the fossil fuel (JP-8, diesel #2, Jet-A, or marine diesel fuel oil) carried onboard each platform to find the volume ratio of equivalent energy storage. Low benefit values use input parameter combinations that result in the highest volume ratio (e.g., 700-bar compressed gas hydrogen energy density and high estimates for the lower heating value of the fossil fuel) and vice versa (e.g., liquid hydrogen energy density and low estimates for the lower heating value of the fossil fuel) for high benefit values. Variations in (a) are due to the fossil fuel type and hydrogen storage system type and in (b) also include the range of overall system efficiencies for each vehicle type. Calculations in (a) use hydrogen (gas only) energy density while calculations in (b) also consider the overall system efficiencies for ICE and BE vehicles.

**a****b**

**Fig. S.21. An illustration of hydrogen storage system mass required to have the same raw energy content (a) and useful energy content (b) of one-unit mass of fossil fuel, by vehicle type**

Calculations determine the chemical energy content of the fossil fuel (JP-8, diesel #2, Jet-A, or marine diesel fuel oil) carried onboard each platform to find the mass ratio of equivalent energy storage. Low benefit values use input parameter combinations that result in the highest mass ratio (e.g., 700-bar compressed gas hydrogen specific energy and high estimates for the lower heating value of the fossil fuel) and vice versa (e.g., liquid hydrogen specific energy and low estimates for the lower heating value of the fossil fuel) for high benefit values. Variations in (a) are due to the fossil fuel type and hydrogen storage system type and in (b) also include the range of overall system efficiencies for each vehicle type. Calculations in (a) use hydrogen storage system (700-bar or cryogenic-compressed hydrogen) specific energy values while calculations in (b) also consider the overall system efficiencies for ICE and BE vehicles.

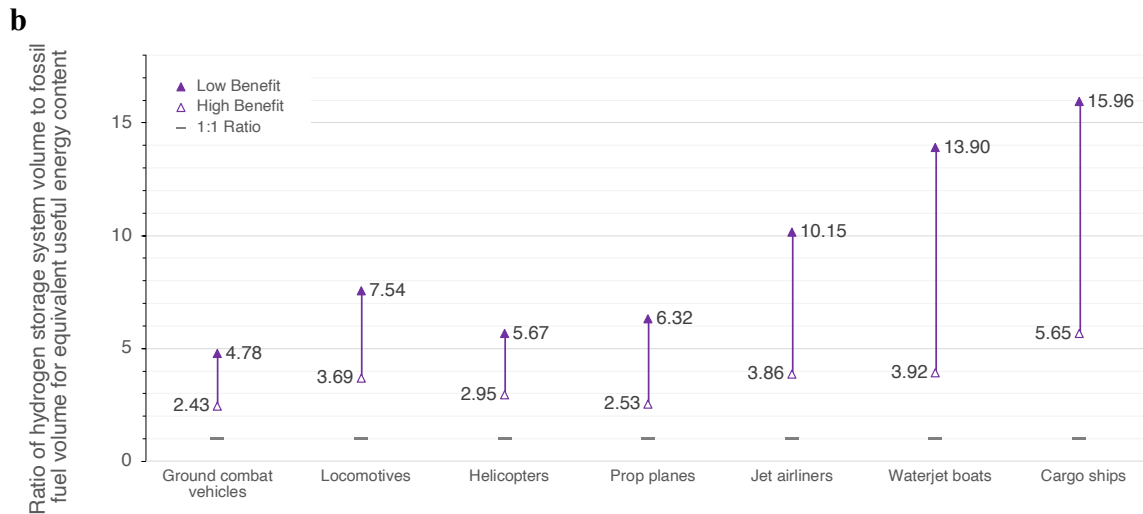
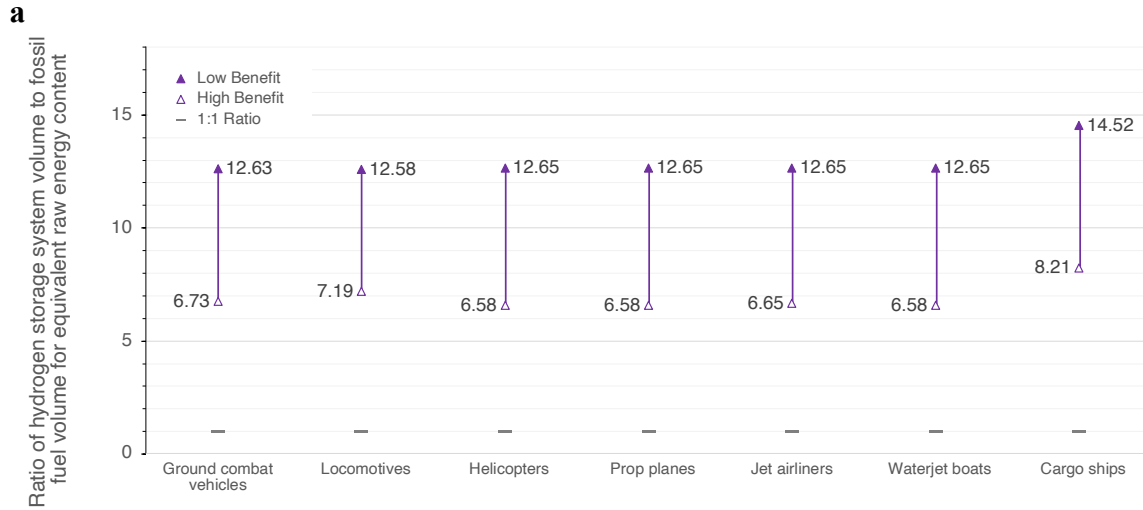


**Fig. S.22. An illustration of hydrogen storage system volume required to have the same raw energy content (a) and useful energy content (b) of one-unit volume of fossil fuel, by vehicle type**

Calculations determine the chemical energy content of the fossil fuel (JP-8, diesel #2, Jet-A, or marine diesel fuel oil) carried onboard each platform to find the volume ratio of equivalent energy storage. Low benefit values use input parameter combinations that result in the highest volume ratio (e.g., 700-bar compressed gas hydrogen energy density and high estimates for the lower heating value of the fossil fuel) and vice versa (e.g., liquid hydrogen energy density and low estimates for the lower heating value of the fossil fuel) for high benefit values. Variations in (a) are due to the fossil fuel type and hydrogen storage system type and in (b) also include the range of overall system efficiencies for each vehicle type. Calculations in (a) use hydrogen storage system (700-bar or cryogenic-compressed hydrogen) energy density values while calculations in (b) also consider the overall system efficiencies for ICE and BE vehicles.

## 2.B. Calculating solutions for BE and HFC variants with equivalent or improved capabilities compared to existing FF vehicles (Section 1.F)

Earlier, we derived equations and conducted both a graphical and computational optimization to compare potential BE and HFC variants of existing FF/ICE vehicles. Fig. S.23 through Fig. S.94 illustrate these results. We show eight graphs for each vehicle platform arranged in sets of two figures per page. The first two figures are for BE variants using commercial and future feasible technologies. The second set of two figures are for HFC variants using commercial and future feasible technologies. The third set of two figures are for BE variant tipping point technologies using  $3 \text{ kW kg}^{-1}$  and  $15 \text{ kW kg}^{-1}$  electric motors. Finally, the fourth set of two figures are for BE variant tipping point technologies using  $3 \text{ kW kg}^{-1}$  and  $15 \text{ kW kg}^{-1}$  electric motors. Below are a few notes on interpreting these graphs:

1. Scales on the x- and y-axes are different for each graph in order to best show the results. For all BE variant graphs, the y-axis is in terms of battery pack mass (kg). For all HFC variant graphs, the y-axis is in terms of hydrogen storage system mass (kg). For all graphs, the x-axis is in terms of electric motor mass (kg).
2. We use a standard color scheme for quick comparison between characteristics of the BE or HFC variant and the existing FF/ICE vehicle. PWR (or TWR) is in blue, range is in green, mass is in orange, and volume is in red.
3. Dashed lines represent combinations of electric motor mass and either battery pack mass or hydrogen storage system mass that result in equivalency between the BE or HFC variant and the existing FF/ICE vehicle for that characteristic.
4. Shaded regions indicate combinations of electric motor mass and either battery pack mass or hydrogen storage system mass that result in an improved capability in the BE or HFC variant over the existing FF/ICE vehicle.
5. Numbered circles highlight the intersection points of vehicle characteristic equivalency lines, and the point numbers always refer to the same intersection of vehicle characteristics: 1 is for PWR (or TWR) and range, 2 for PWR (or TWR) and mass, 3 for PWR (or TWR) and volume, 4 for range and mass, 5 for range and volume, and 6 for mass and volume.
6. When all vehicle characteristic equivalency lines intersect at the same point, we label that point with an “X.”
7. Any point on the graph can be considered a design “solution.” The table inset within each graph gives the numerical comparison between the BE or HFC variant and the existing FF/ICE vehicle at each numbered intersection if the values for that point were used as a design solution. Numbers in green represent equivalent or improved capabilities (i.e., 100% and higher for PWR (or TWR) and range and 100% and lower for mass and volume). Numbers in red represent decreased capabilities in the BE or HFC variant.
8. Yellow shapes call out solutions where either all four vehicle characteristics are simultaneously met/improved or, in instances where that is not possible, where three of four vehicle characteristics are met/improved.
9. Vehicle icons are at the bottom right for quick identification.
10. For the tipping point technology graphs, we also include the technology needed to be achieved within the table.

### Ground combat vehicle (tracked)

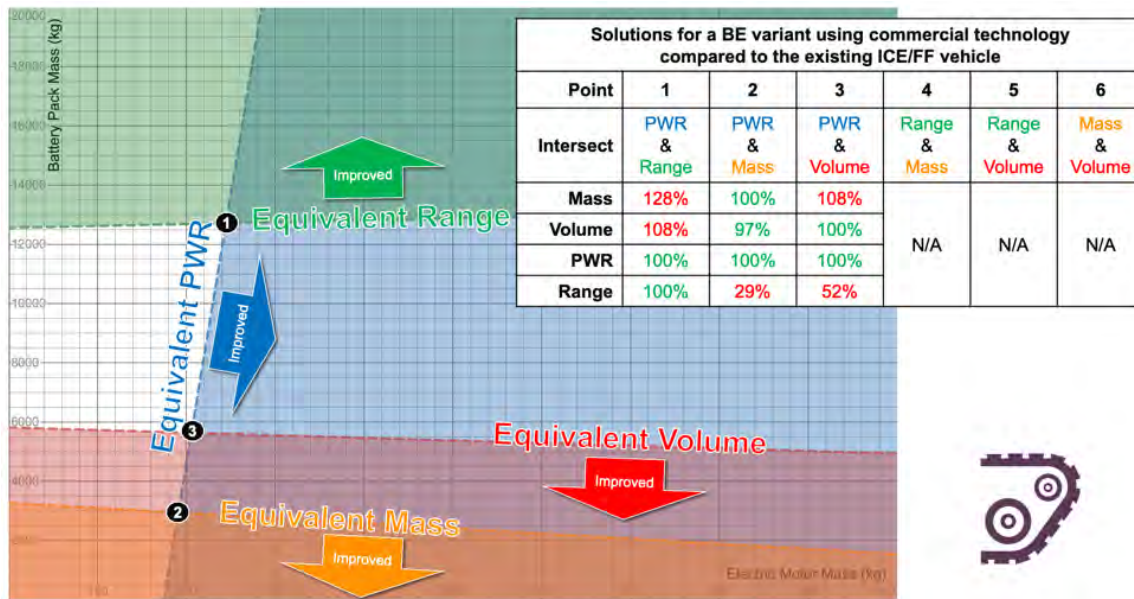


Fig. S.23. Ground combat vehicle (tracked) battery electric variant, commercial technology solutions

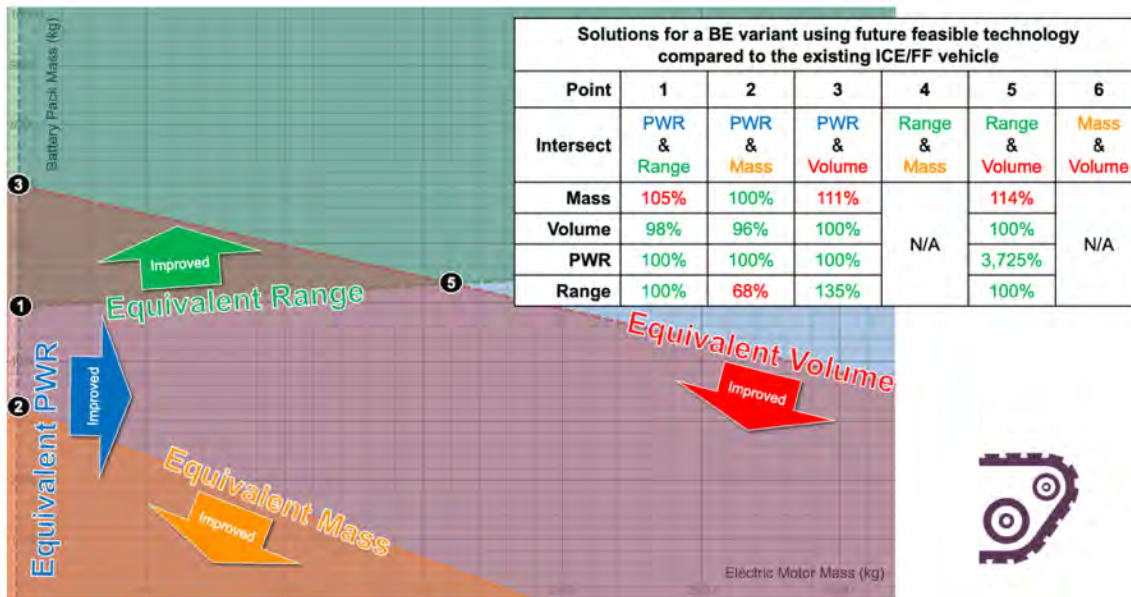


Fig. S.24. Ground combat vehicle (tracked) battery electric variant, future feasible technology solutions



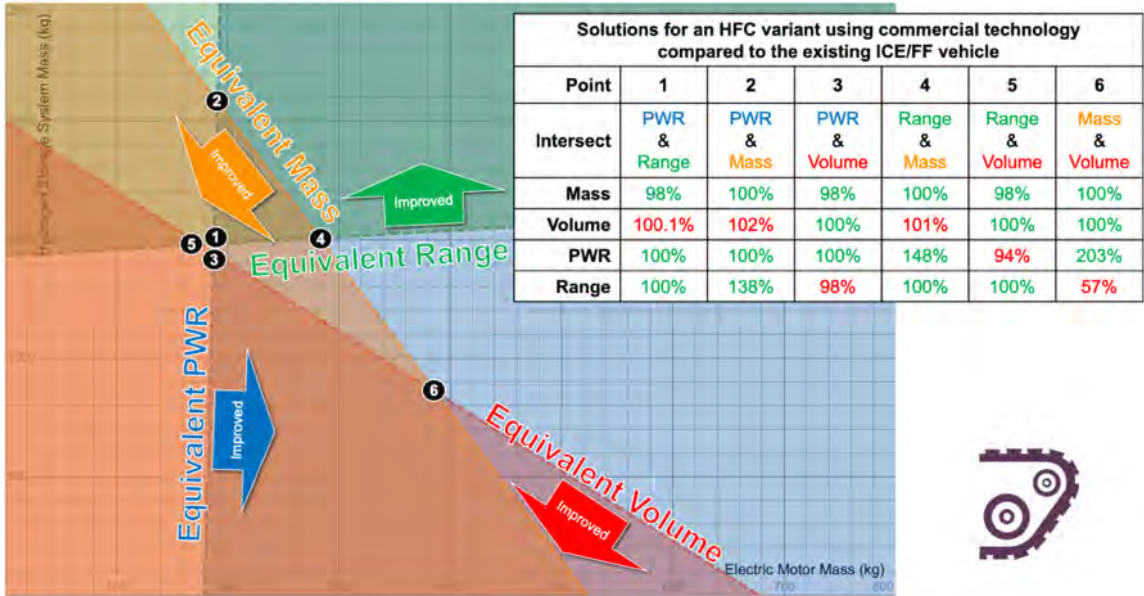


Fig. S.25. Ground combat vehicle (tracked) hydrogen fuel cell variant, commercial technology solutions

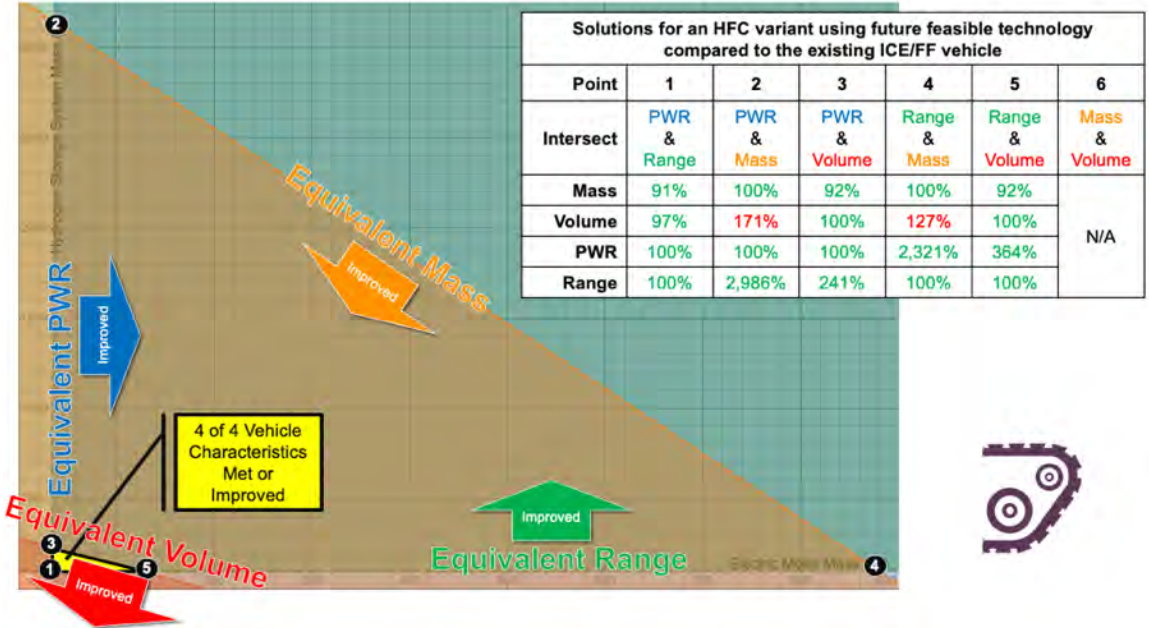


Fig. S.26. Ground combat vehicle (tracked) hydrogen fuel cell variant, future feasible technology solutions

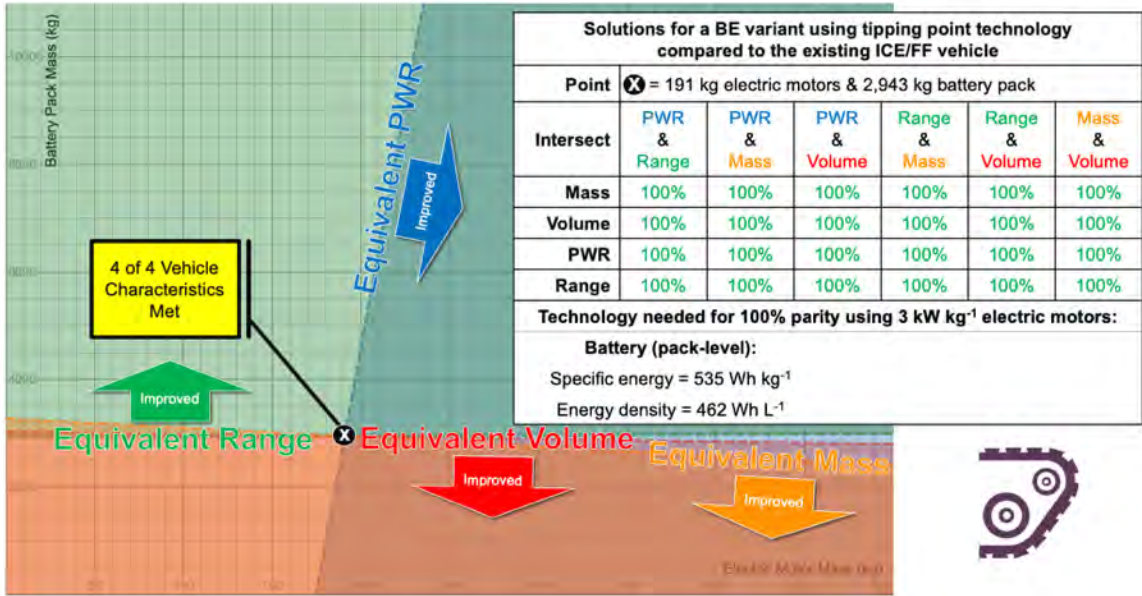


Fig. S.27. Tipping point technology for ground combat vehicle (tracked) battery electric variant using 3 kW kg<sup>-1</sup> electric motors, same as Fig. 4(b)

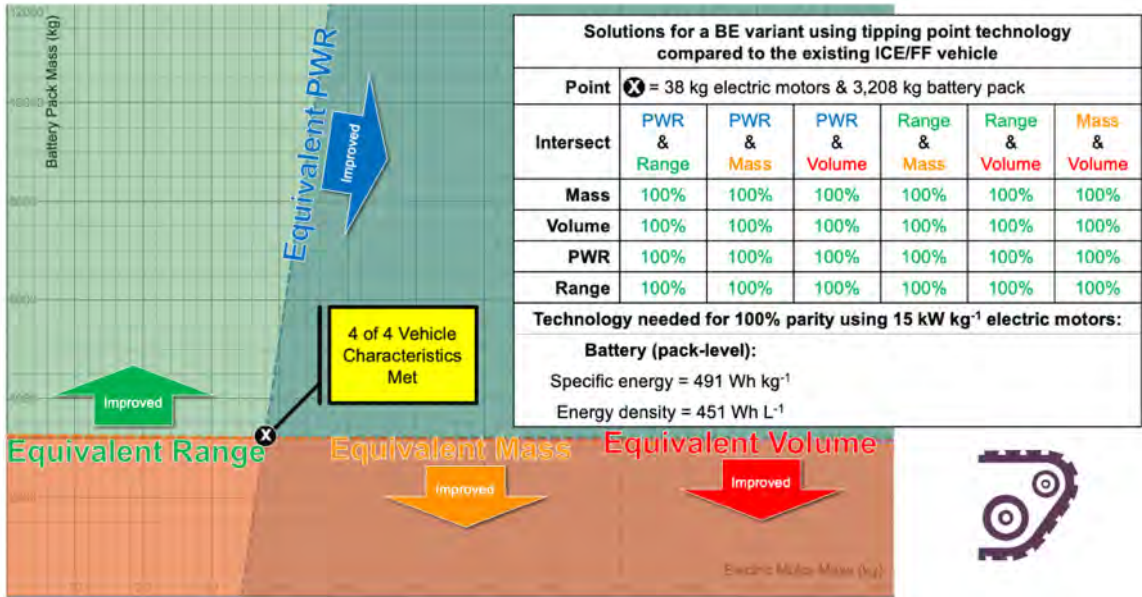


Fig. S.28. Tipping point technology for ground combat vehicle (tracked) battery electric variant using 15 kW kg<sup>-1</sup> electric motors

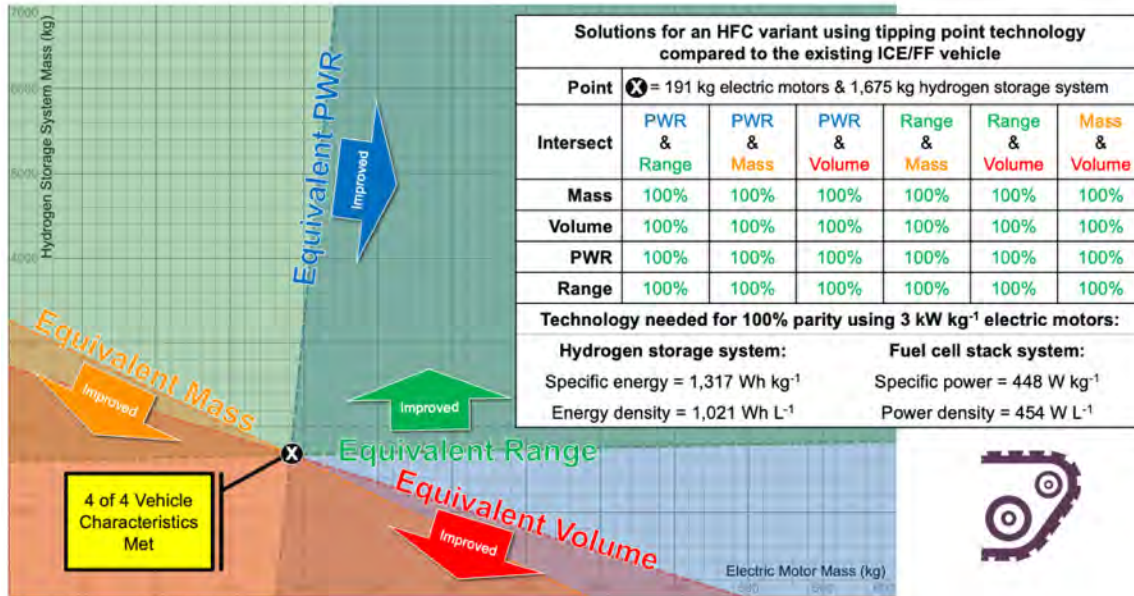


Fig. S.29. Tipping point technology for ground combat vehicle (tracked) hydrogen fuel cell variant using 3 kW kg<sup>-1</sup> electric motors

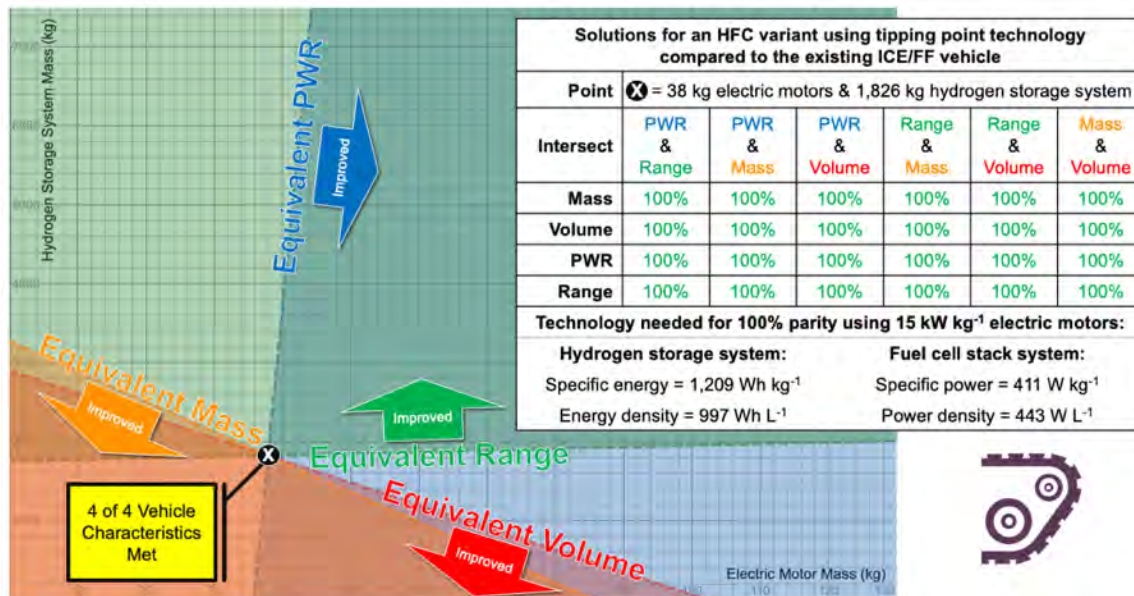


Fig. S.30. Tipping point technology for ground combat vehicle (tracked) hydrogen fuel cell variant using 15 kW kg<sup>-1</sup> electric motors

Ground combat vehicle (wheeled)

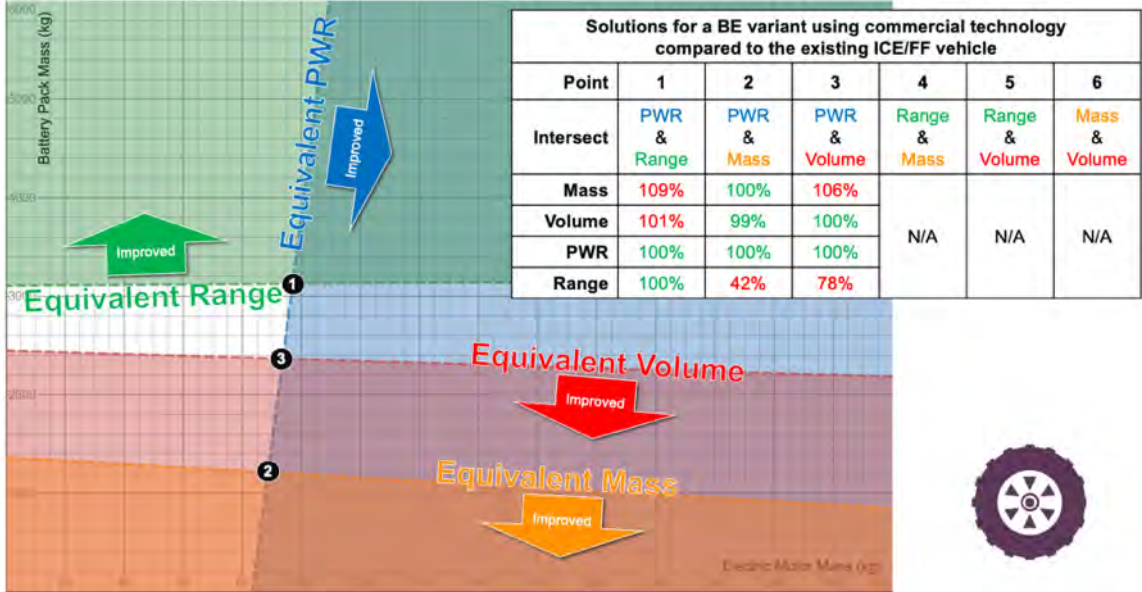


Fig. S.31. Ground combat vehicle (wheeled) battery electric variant, commercial technology solutions

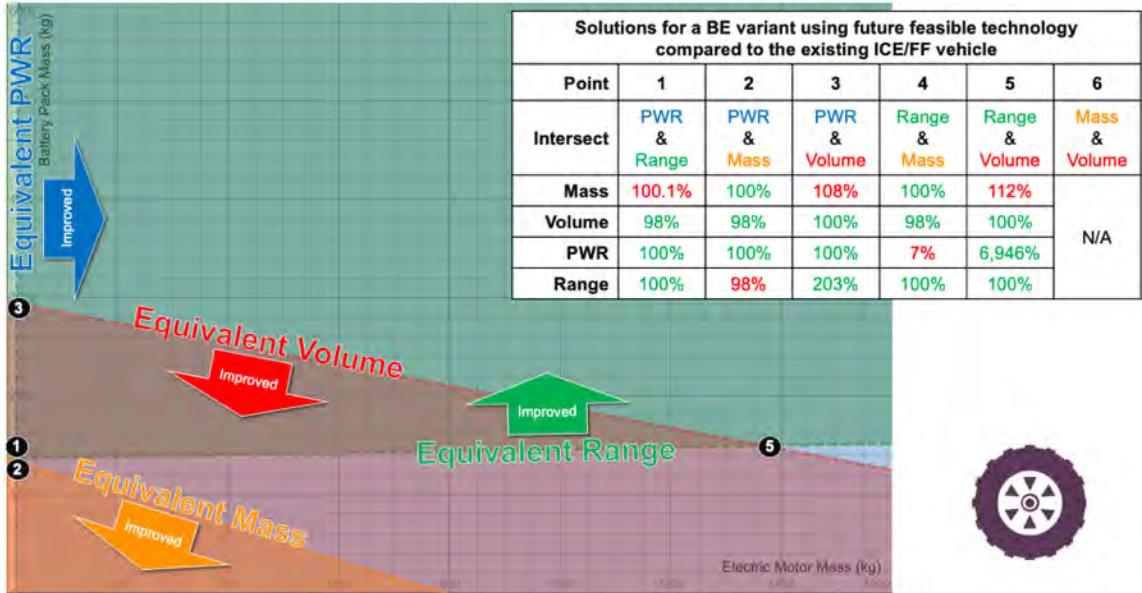


Fig. S.32. Ground combat vehicle (wheeled) battery electric variant, future feasible technology solutions

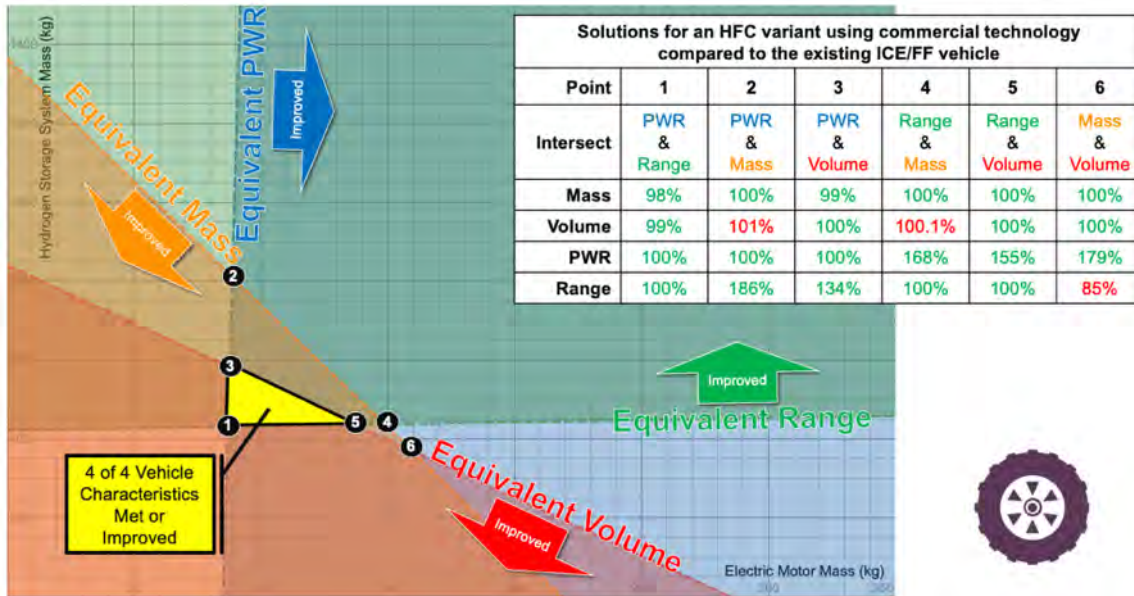


Fig. S.33. Ground combat vehicle (wheeled) hydrogen fuel cell variant, commercial technology solutions, same as Fig. 4(a)

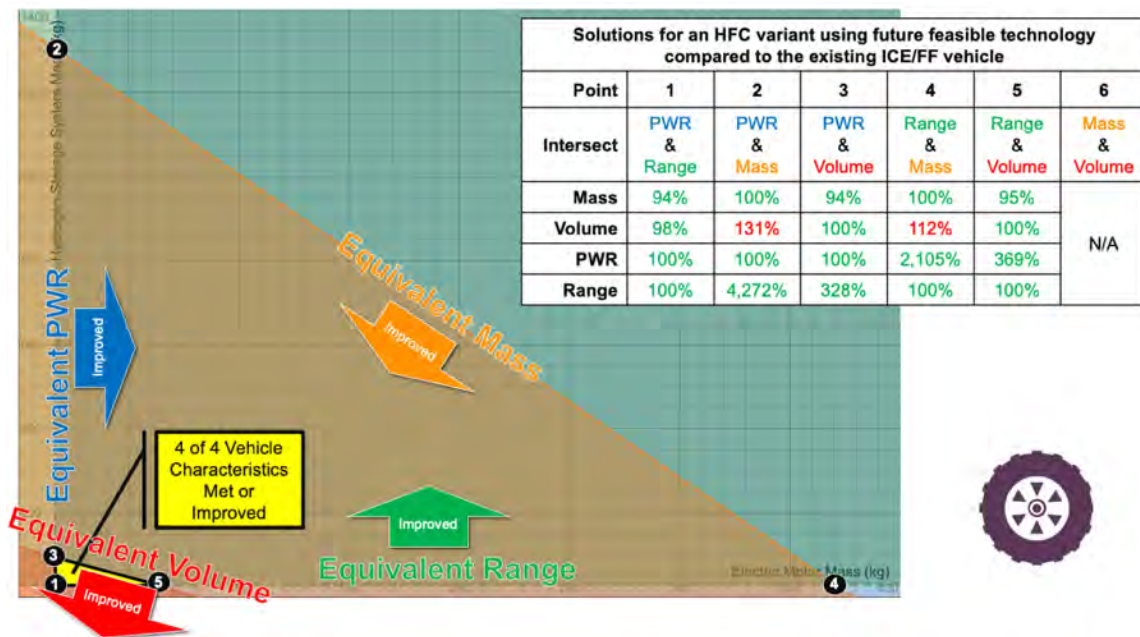


Fig. S.34. Ground combat vehicle (wheeled) hydrogen fuel cell variant, future feasible technology solutions

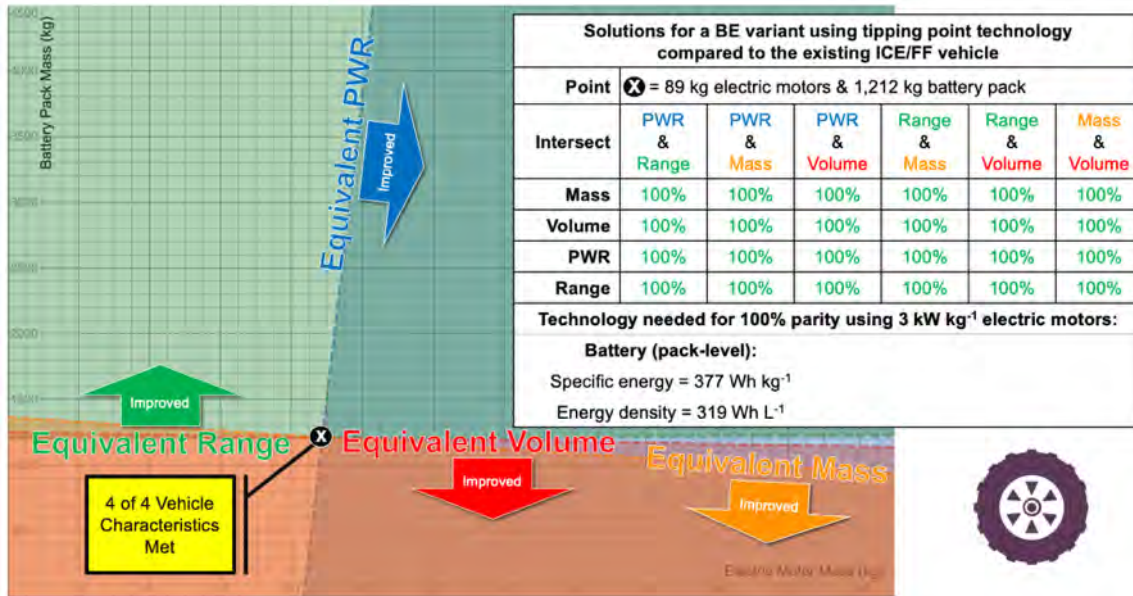


Fig. S.35. Tipping point technology for ground combat vehicle (wheeled) battery electric variant using 3 kW kg<sup>-1</sup> electric motors

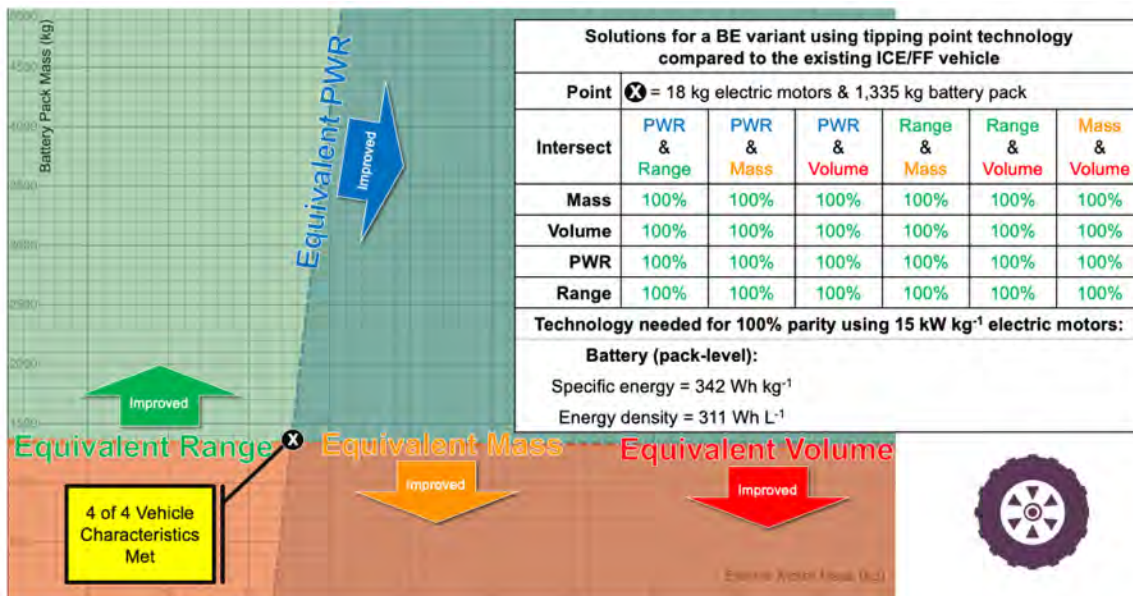


Fig. S.36. Tipping point technology for ground combat vehicle (wheeled) battery electric variant using 15 kW kg<sup>-1</sup> electric motors

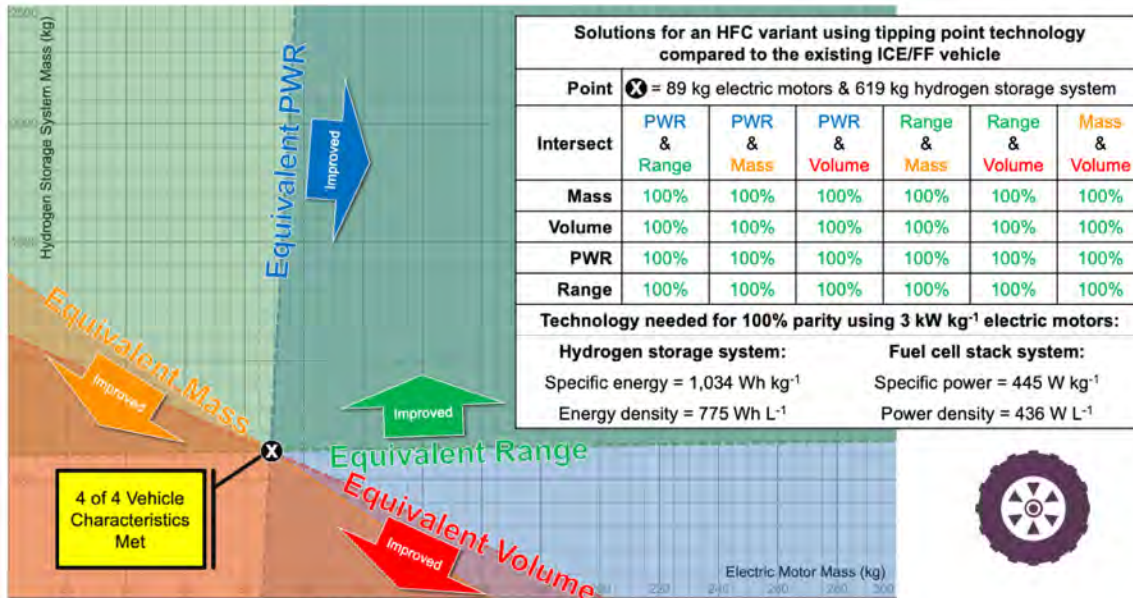


Fig. S.37. Tipping point technology for ground combat vehicle (wheeled) hydrogen fuel cell variant using 3 kW kg<sup>-1</sup> electric motors

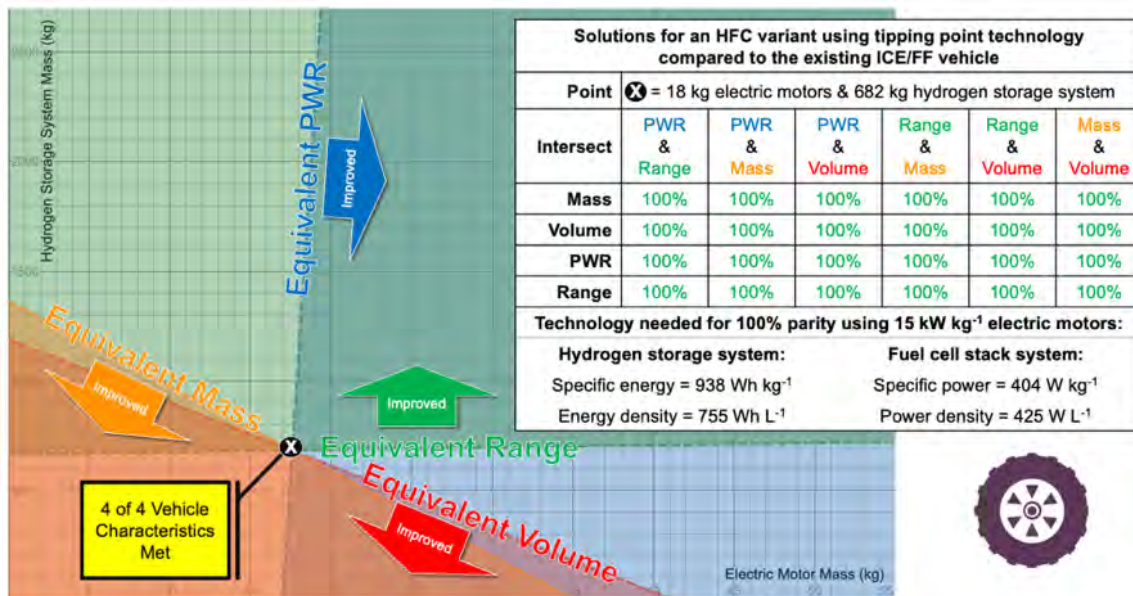


Fig. S.38. Tipping point technology for ground combat vehicle (wheeled) hydrogen fuel cell variant using 15 kW kg<sup>-1</sup> electric motors

## Freight rail locomotive

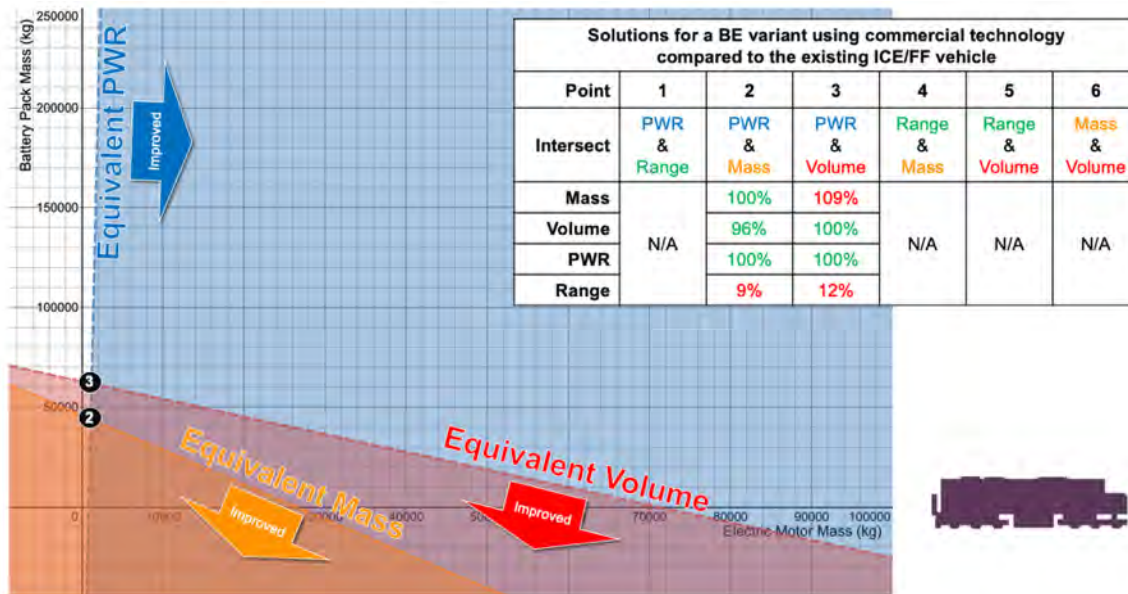


Fig. S.39. Locomotive battery electric variant, commercial technology solutions

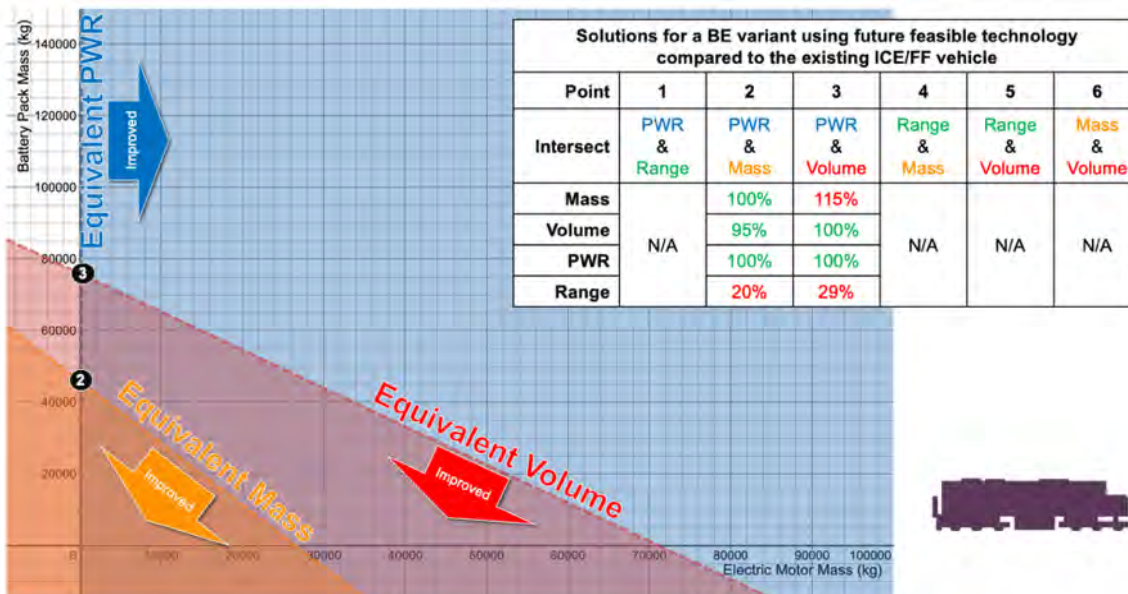


Fig. S.40. Locomotive battery electric variant, future feasible technology solutions



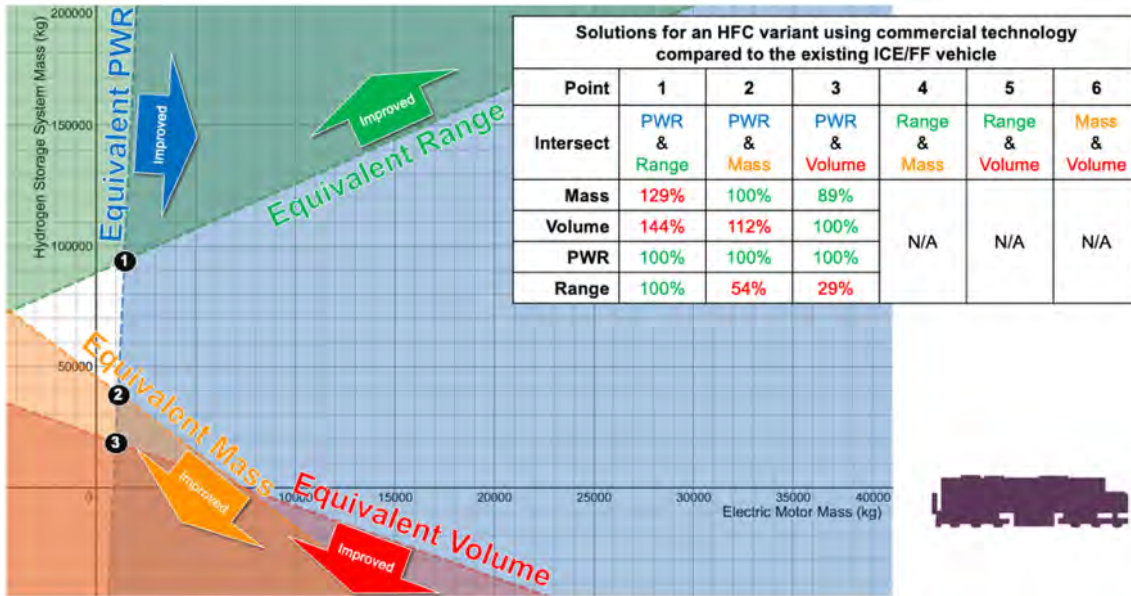


Fig. S.41. Locomotive hydrogen fuel cell variant, commercial technology solutions

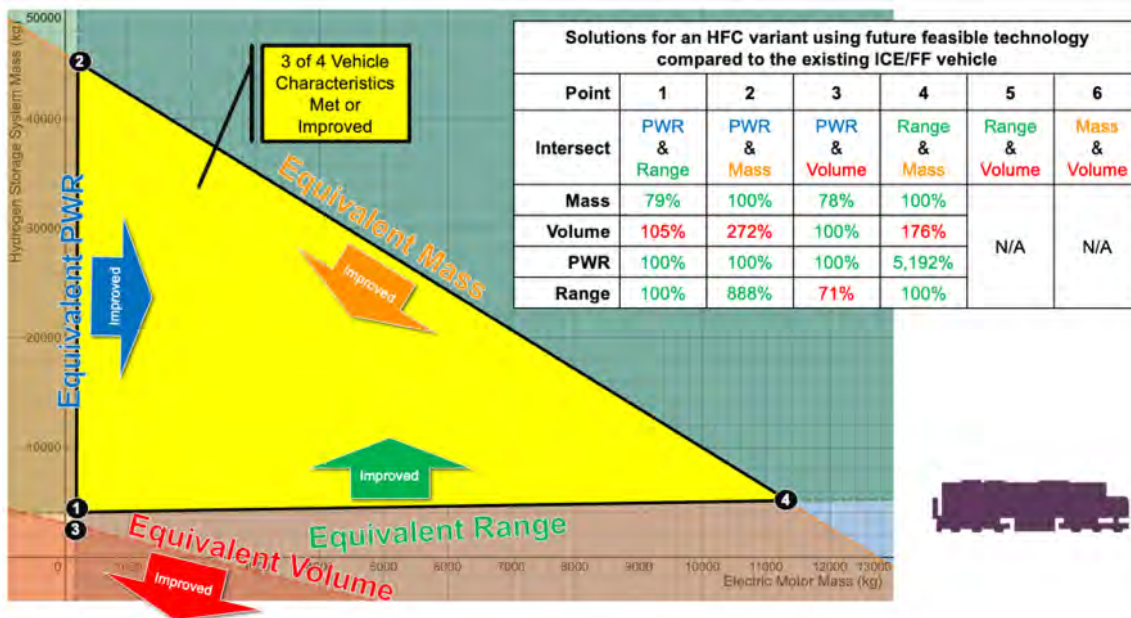


Fig. S.42. Locomotive hydrogen fuel cell variant, future feasible technology solutions

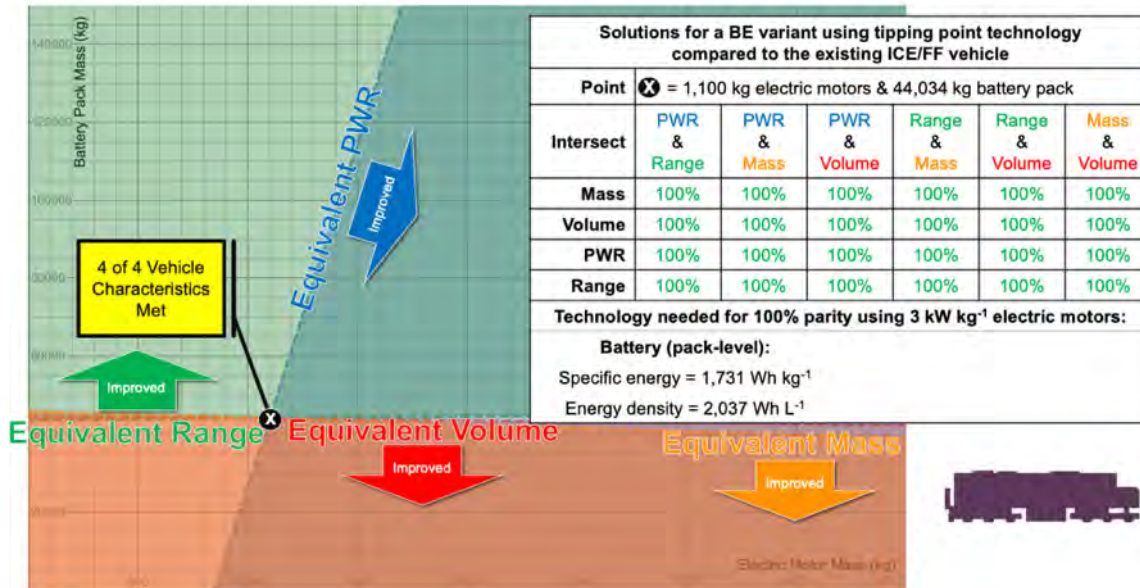


Fig. S.43. Tipping point technology for a locomotive battery electric variant using 3 kW kg<sup>-1</sup> electric motors

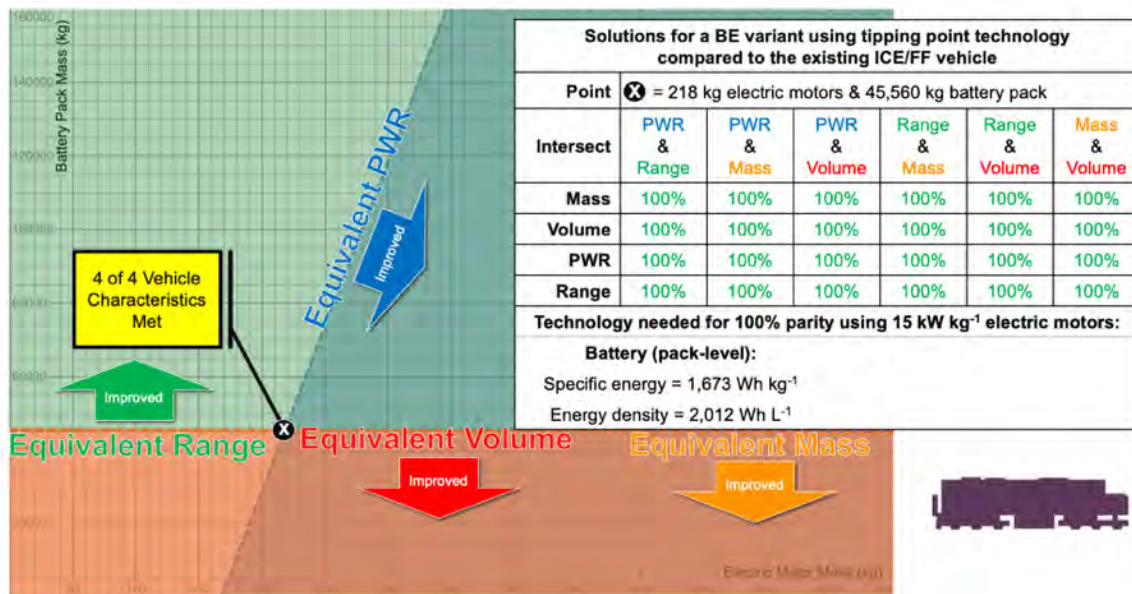


Fig. S.44. Tipping point technology for a locomotive battery electric variant using 15 kW kg<sup>-1</sup> electric motors

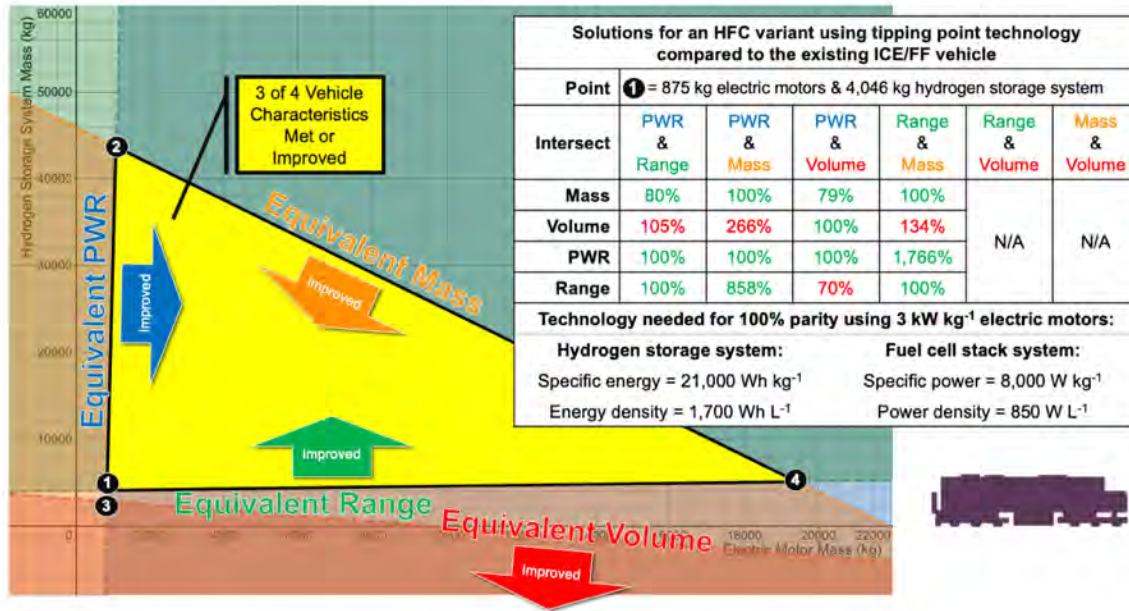


Fig. S.45. Tipping point technology for a locomotive hydrogen fuel cell variant using 3 kW kg<sup>-1</sup> electric motors

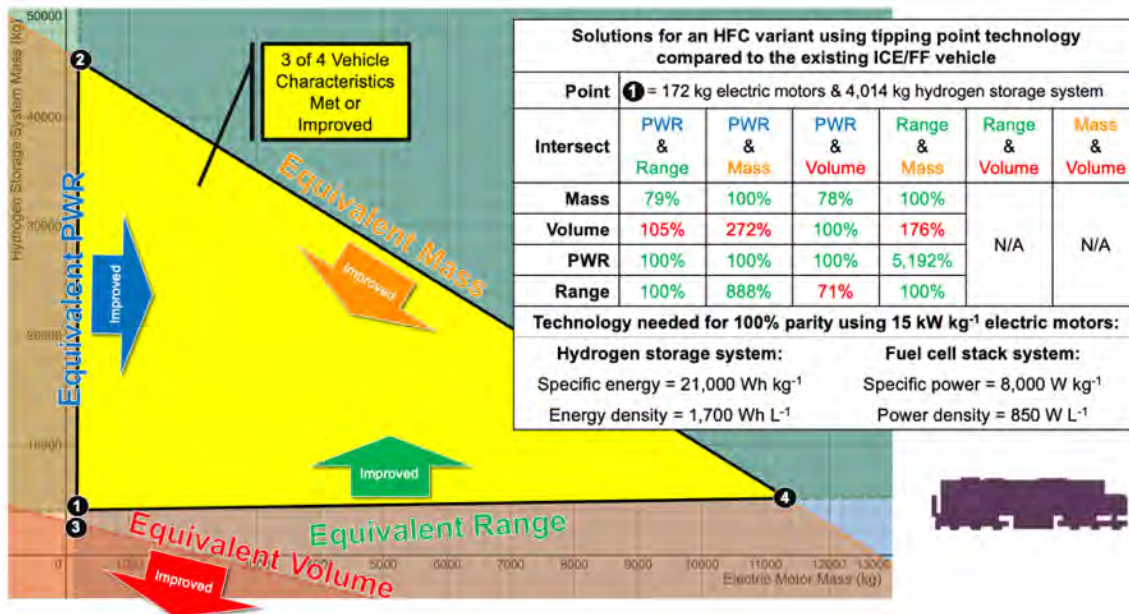


Fig. S.46. Tipping point technology for a locomotive hydrogen fuel cell variant using 15 kW kg<sup>-1</sup> electric motors

Rotary-wing aircraft (helicopters)

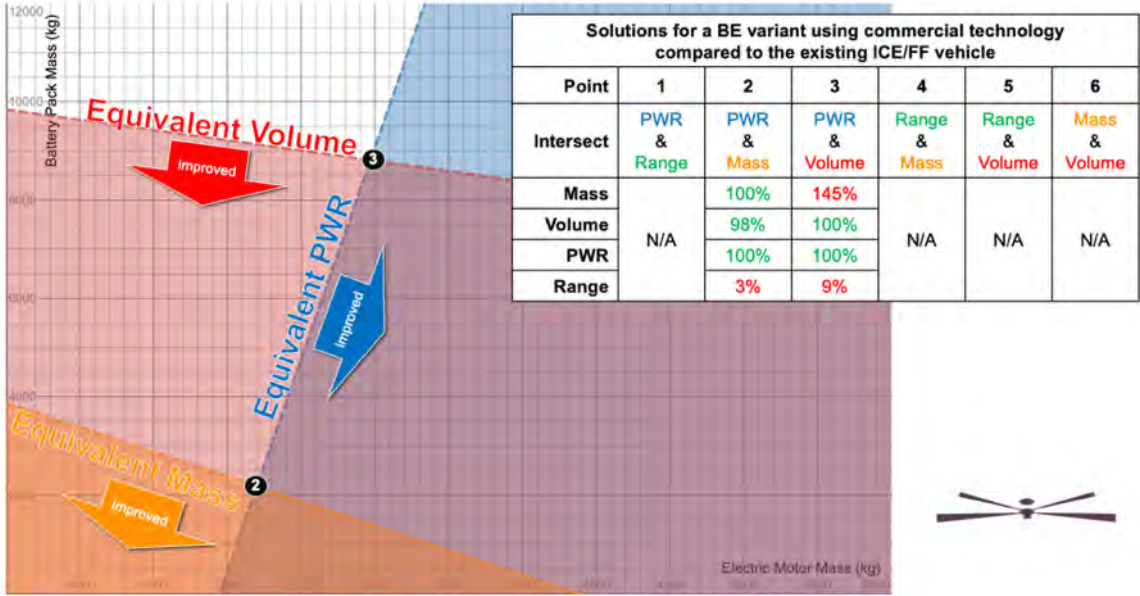


Fig. S.47. Battery electric variant helicopter, commercial technology solutions

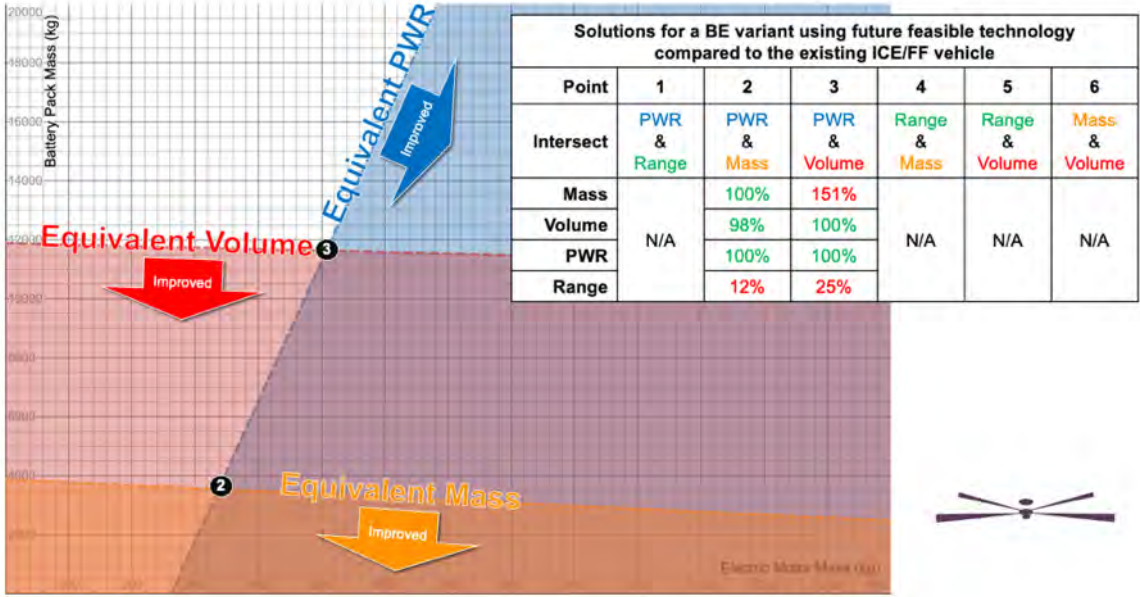


Fig. S.48. Battery electric variant helicopter, future feasible technology solutions

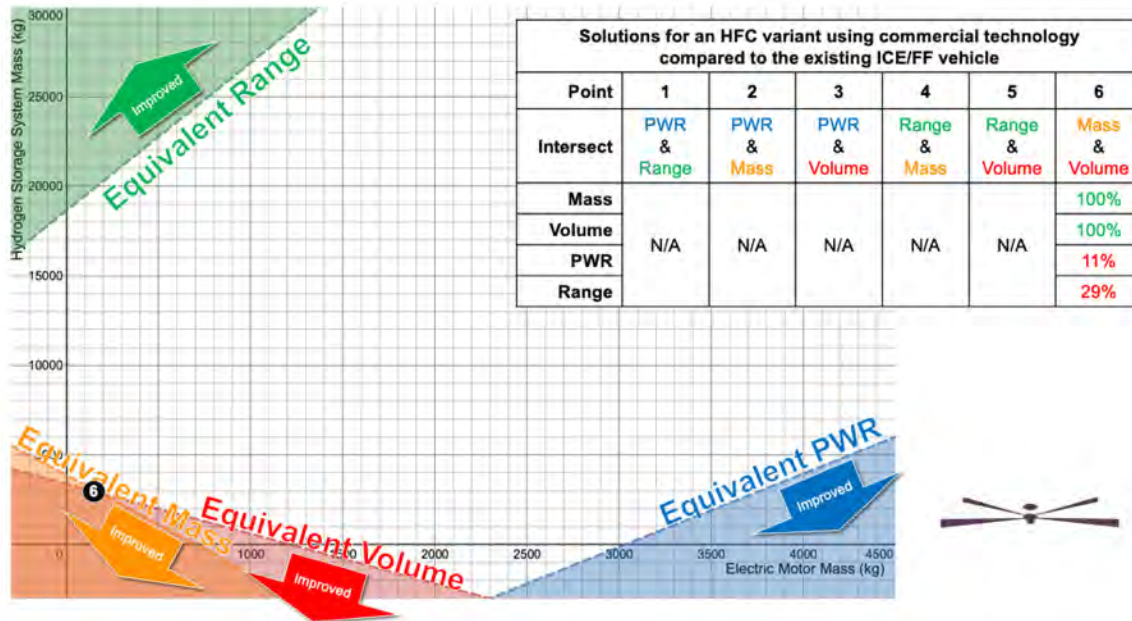


Fig. S.49. Hydrogen fuel cell variant helicopter, commercial technology solutions

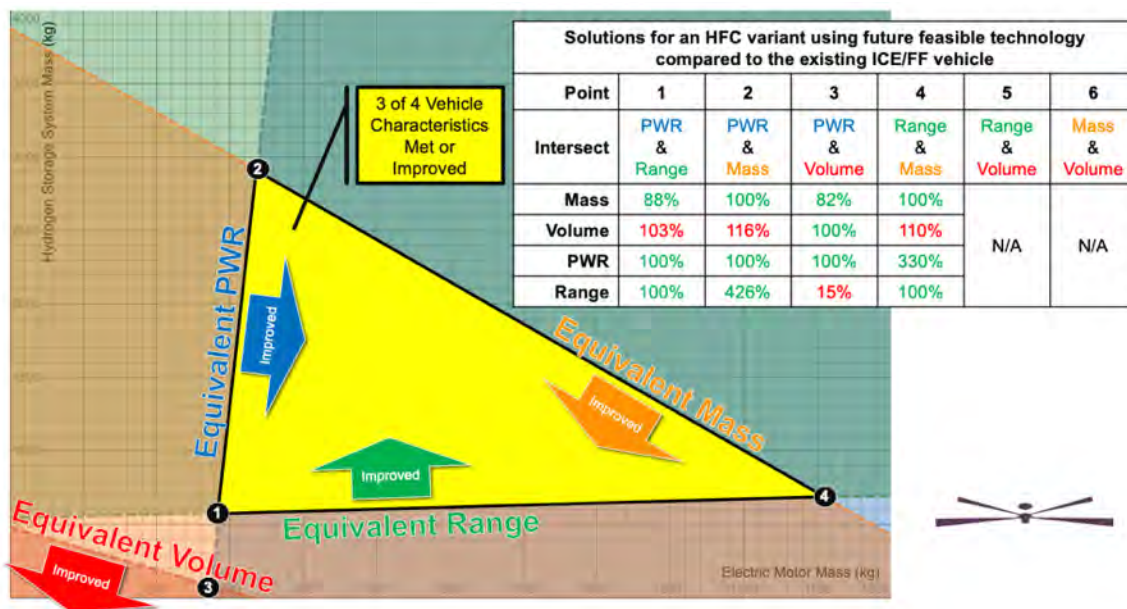


Fig. S.50. Hydrogen fuel cell variant helicopter, future feasible technology solutions

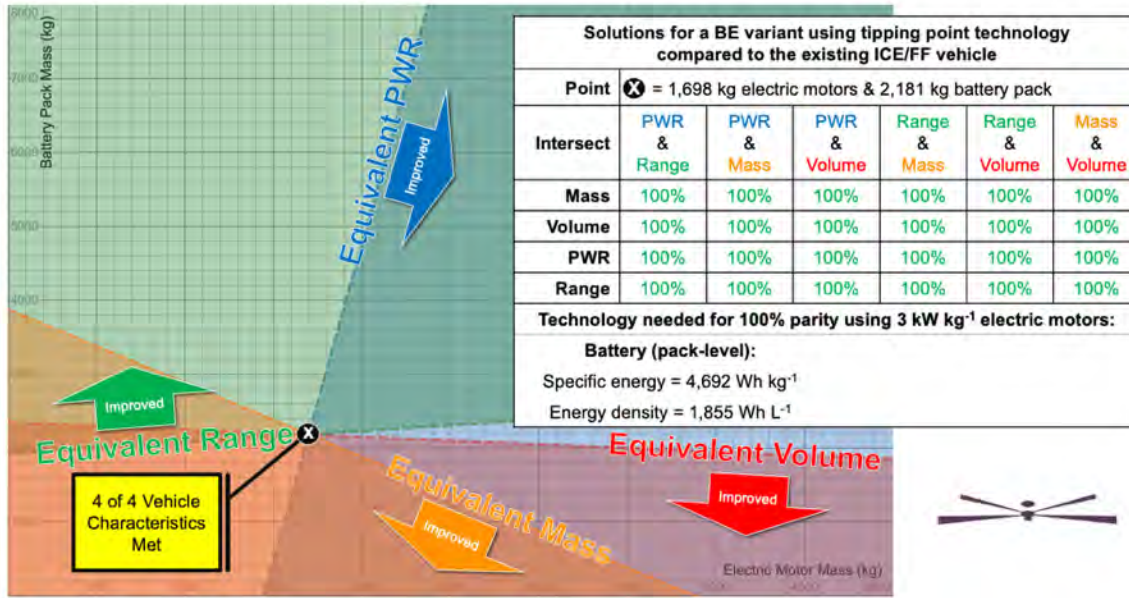


Fig. S.51. Tipping point technology for battery electric variant helicopter using 3 kW kg<sup>-1</sup> electric motors

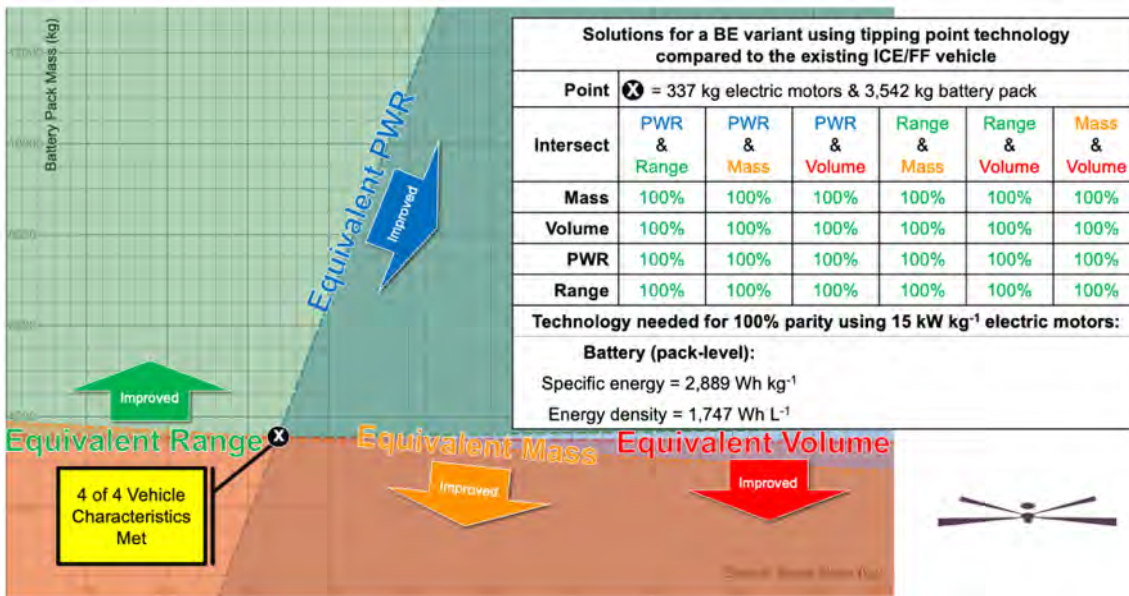


Fig. S.52. Tipping point technology for battery electric variant helicopter using 15 kW kg<sup>-1</sup> electric motors

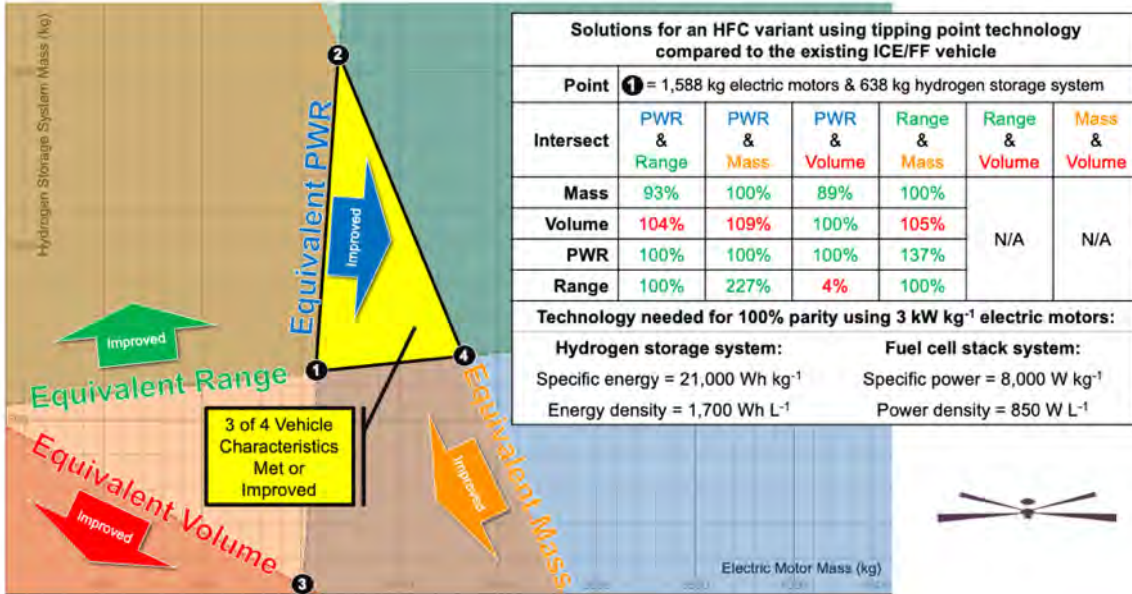


Fig. S.53. Tipping point technology for hydrogen fuel cell variant helicopter using 3 kW kg<sup>-1</sup> electric motors

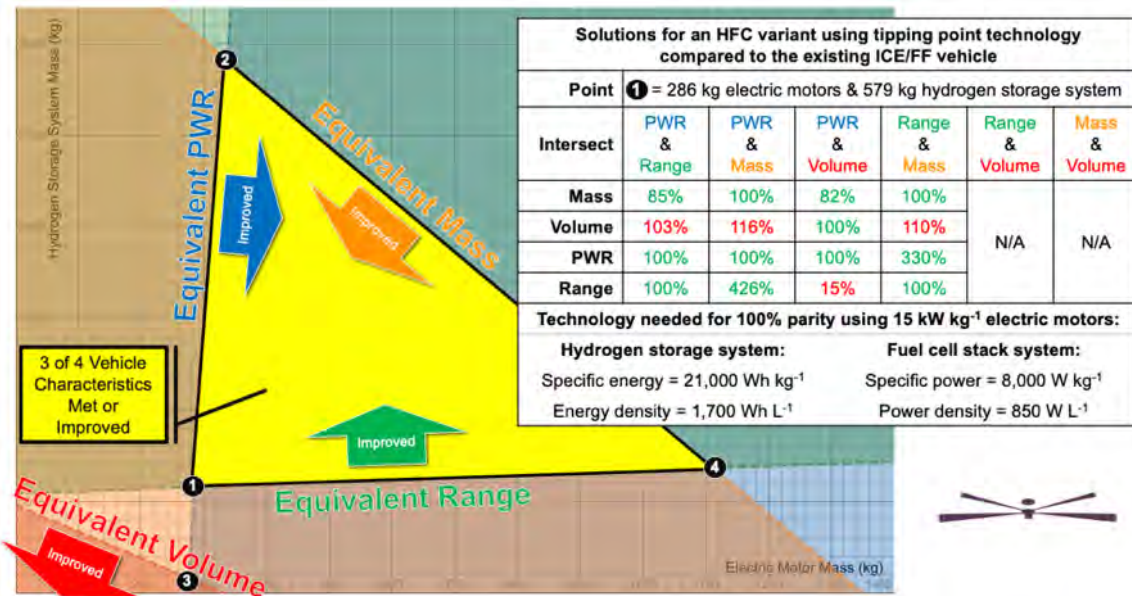


Fig. S.54. Tipping point technology for hydrogen fuel cell variant helicopter using 15 kW kg<sup>-1</sup> electric motors

### Fixed-wing aircraft (prop plane)

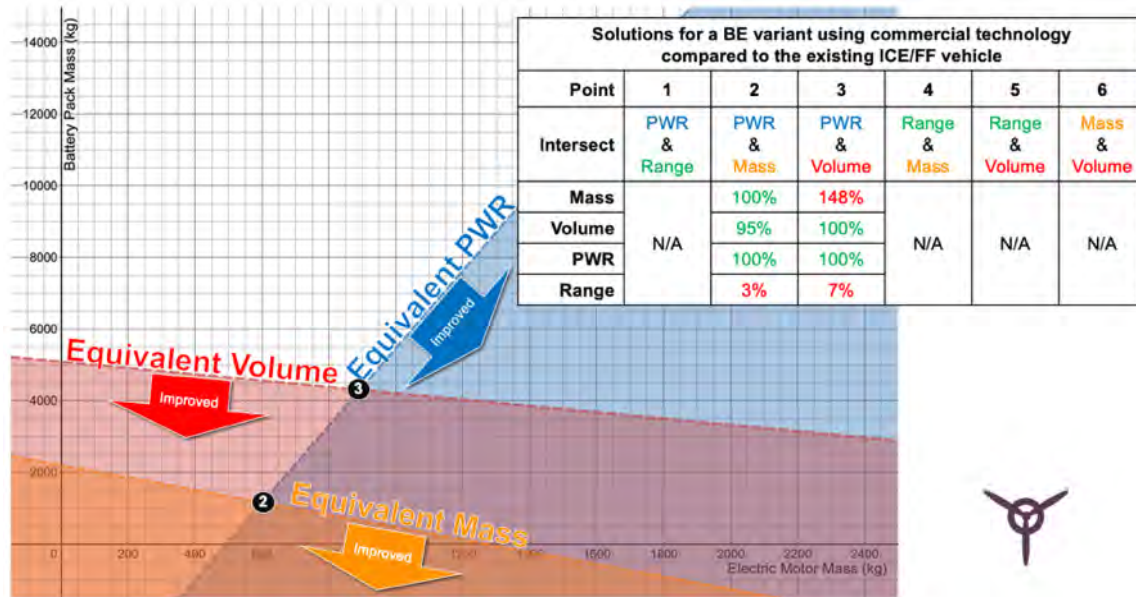


Fig. S.55. Battery electric variant prop plane, commercial technology solutions

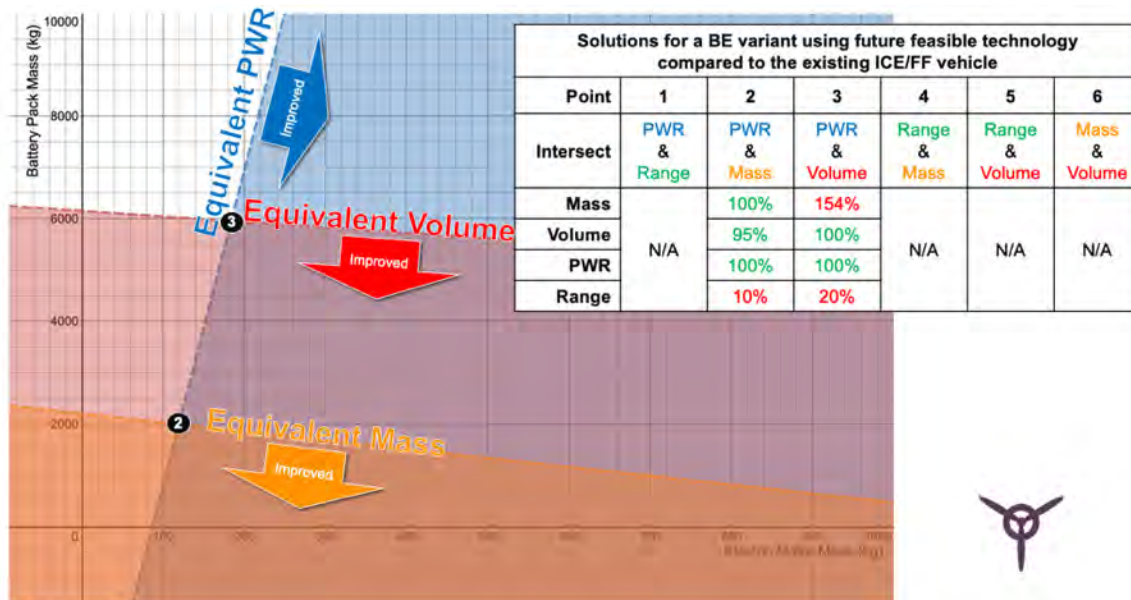


Fig. S.56. Battery electric variant prop plane, future feasible technology solutions



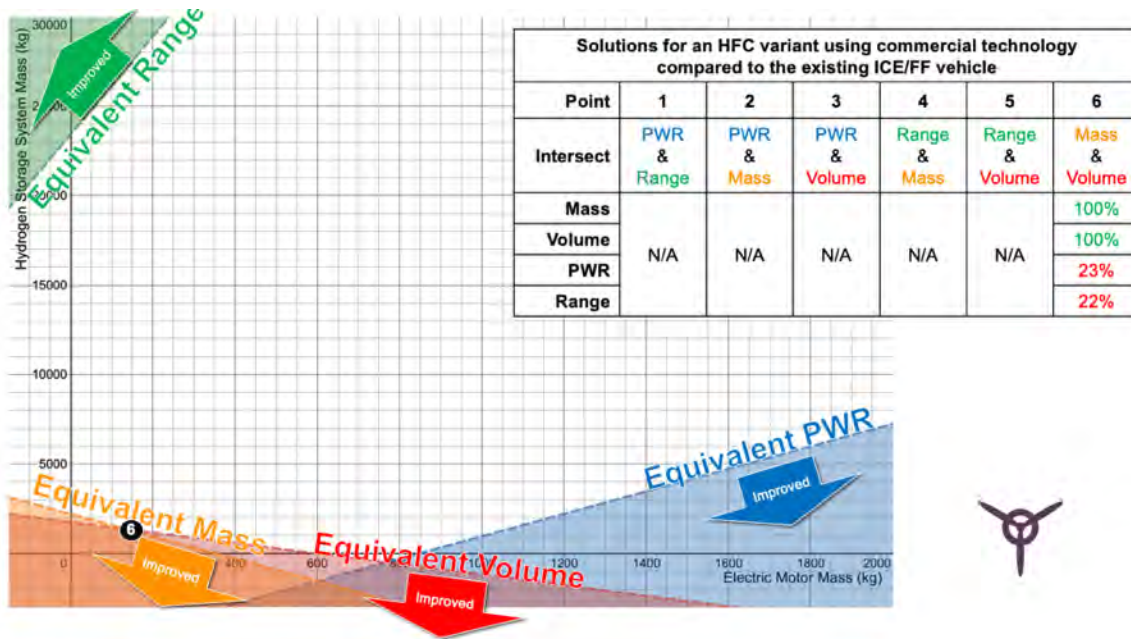


Fig. S.57. Hydrogen fuel cell variant prop plane, commercial technology solutions

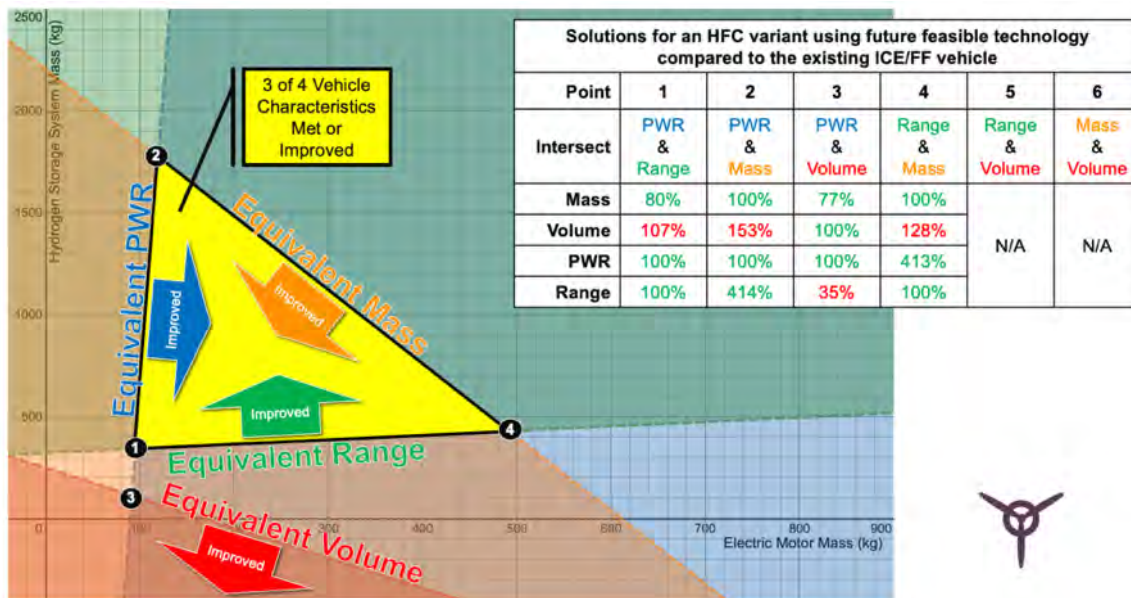


Fig. S.58. Hydrogen fuel cell variant prop plane, future feasible technology solutions

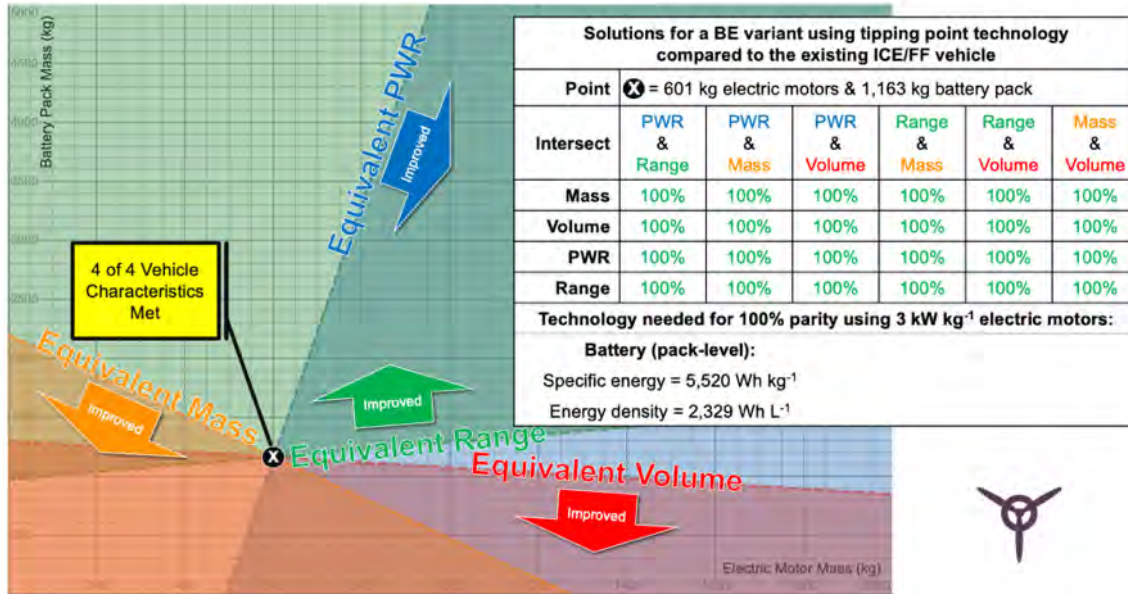


Fig. S.59. Tipping point technology for battery electric variant prop plane using 3 kW kg<sup>-1</sup> electric motors

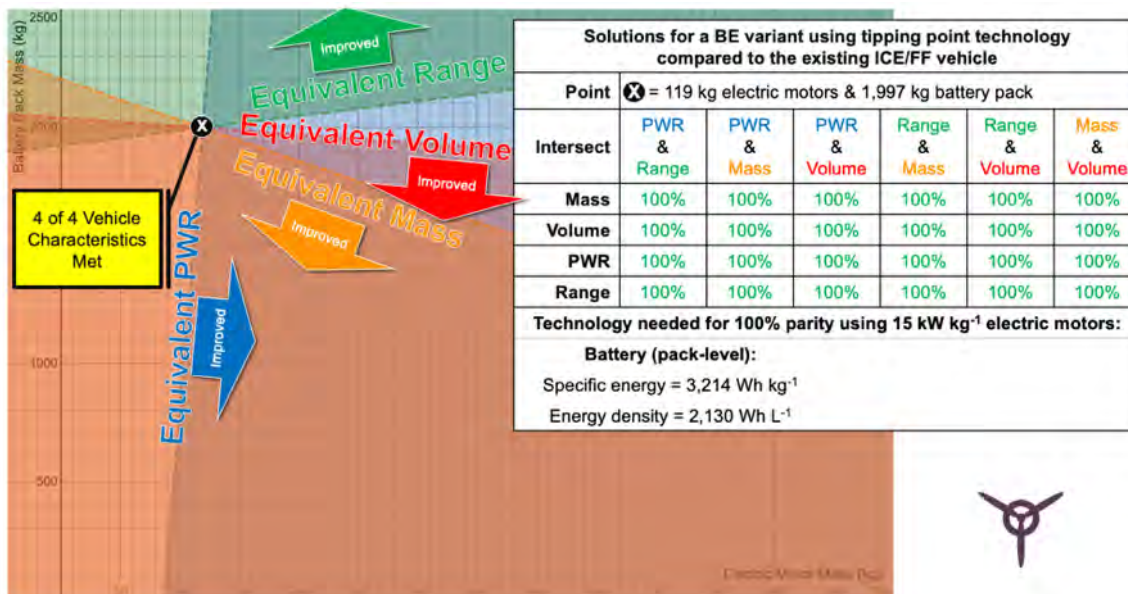


Fig. S.60. Tipping point technology for battery electric variant prop plane using 15 kW kg<sup>-1</sup> electric motors

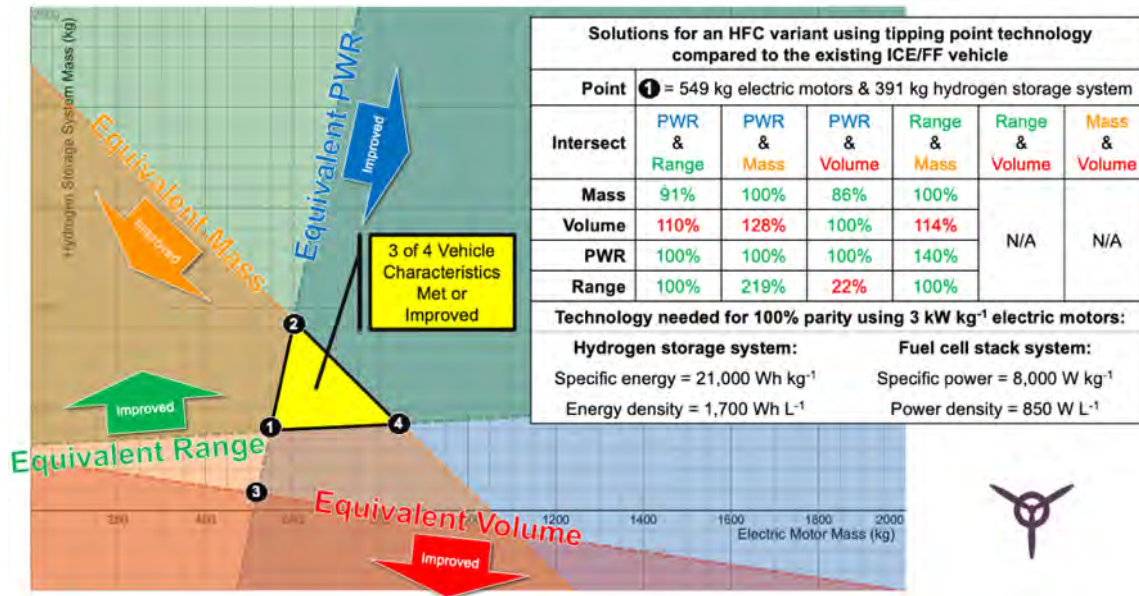


Fig. S.61. Tipping point technology for hydrogen fuel cell variant prop plane using 3 kW kg<sup>-1</sup> electric motors

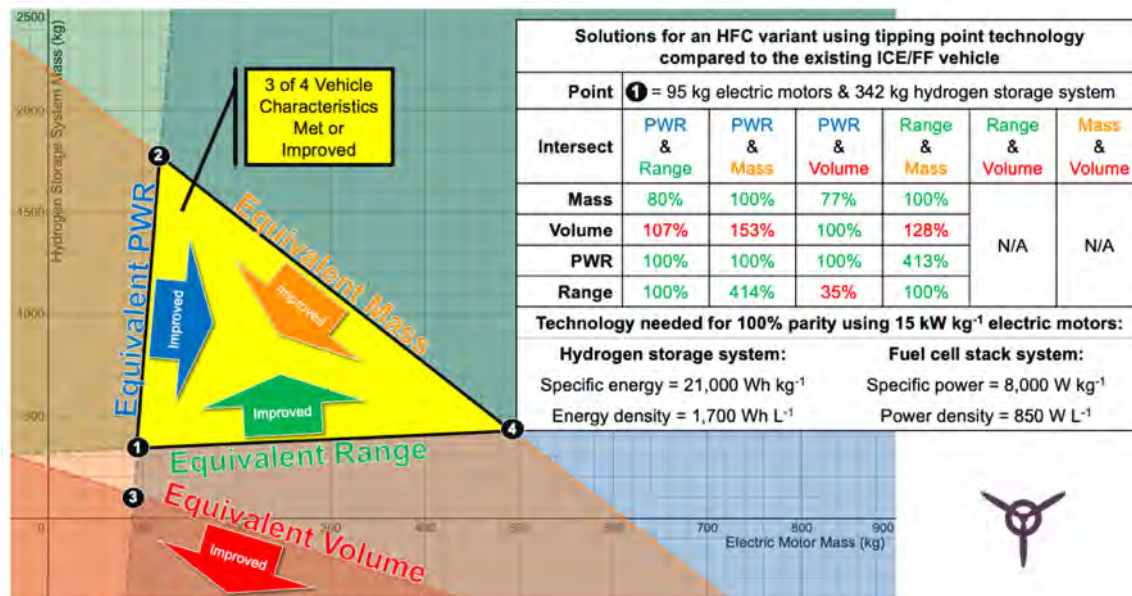


Fig. S.62. Tipping point technology for hydrogen fuel cell variant prop plane using 15 kW kg<sup>-1</sup> electric motors

Fixed-wing aircraft (medium-haul jet airliner)

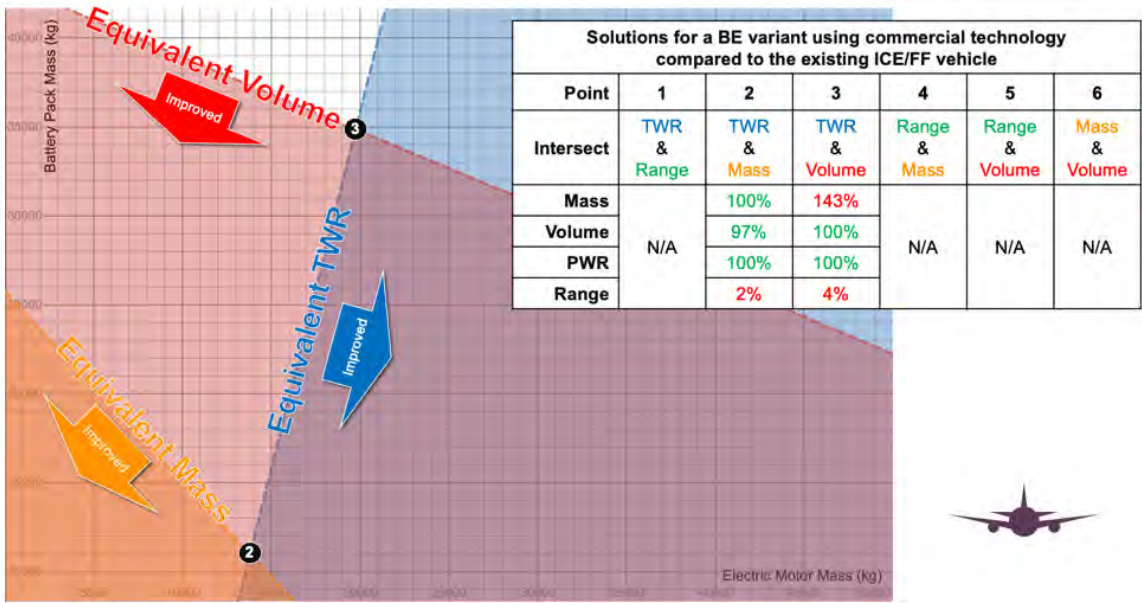


Fig. S.63. Medium-haul jet airliner battery electric variant, commercial technology solutions

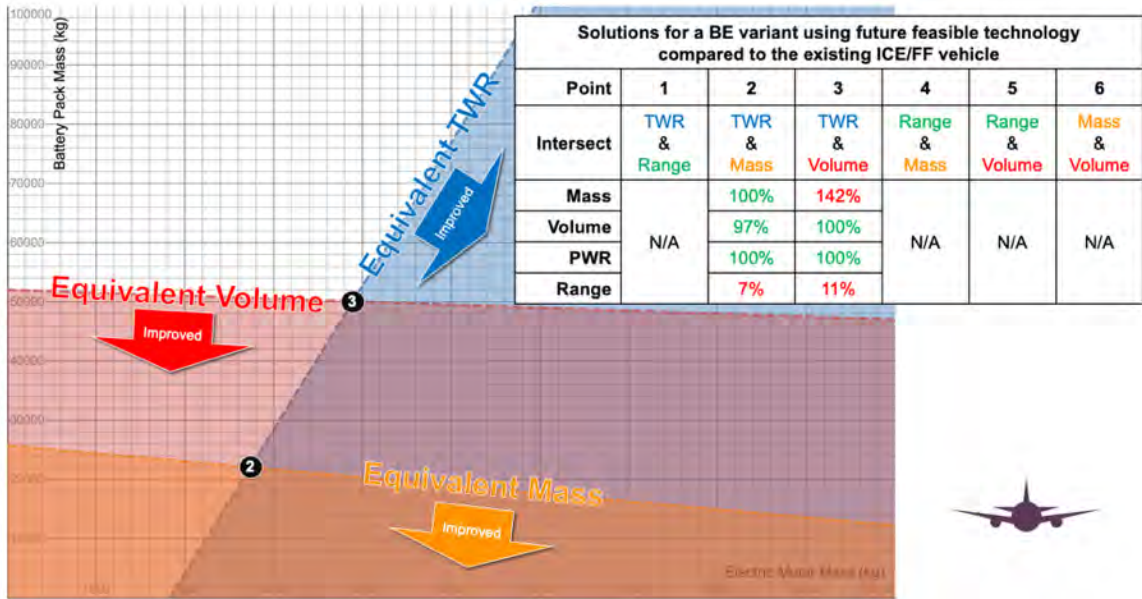


Fig. S.64. Medium-haul jet airliner battery electric variant, future feasible technology solutions

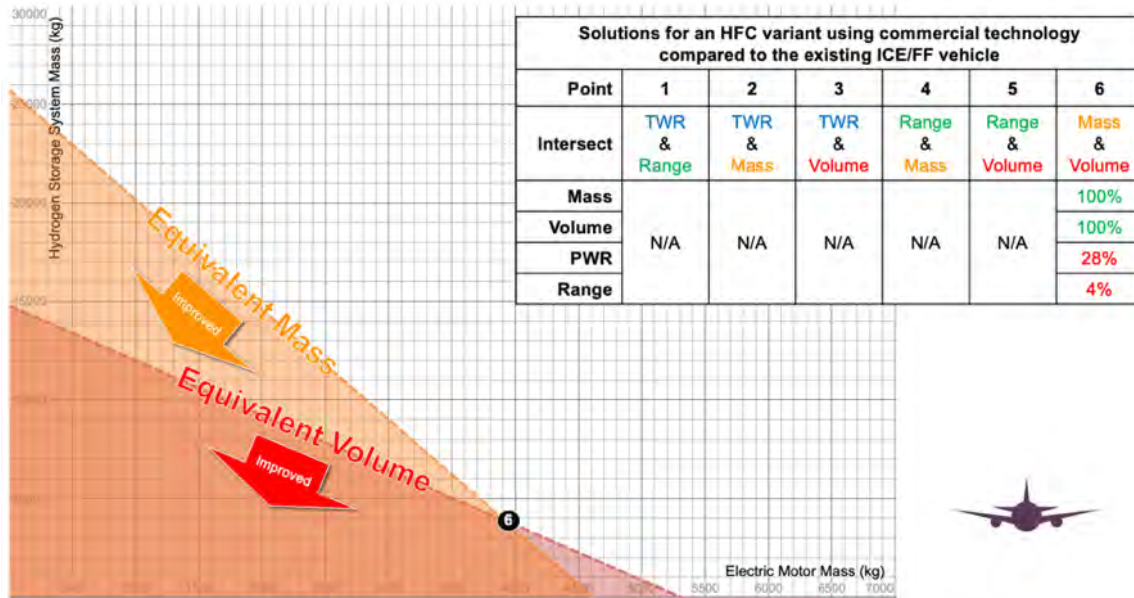


Fig. S.65. Medium-haul jet airliner hydrogen fuel cell variant, commercial technology solutions

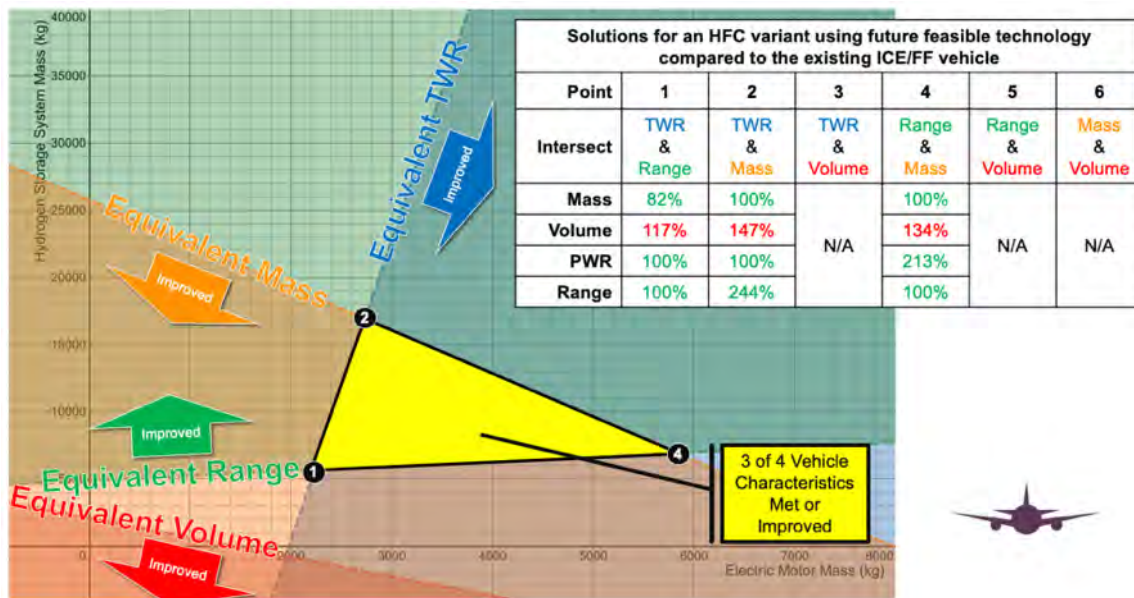


Fig. S.66. Medium-haul jet airliner hydrogen fuel cell variant, future feasible technology solutions

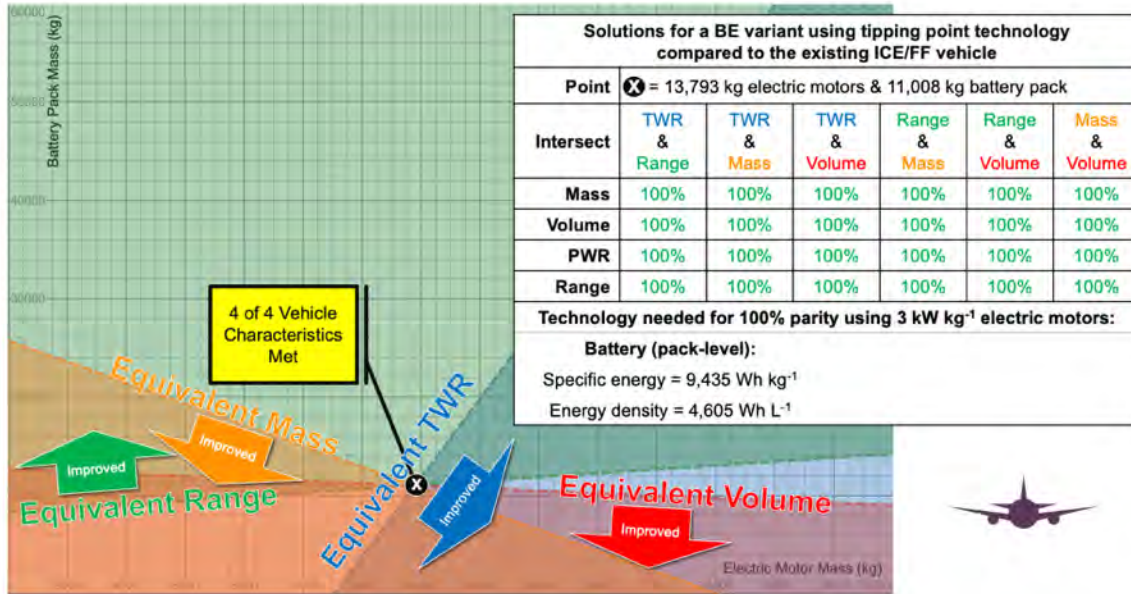


Fig. S.67. Tipping point technology for a medium-haul jet airliner battery electric variant using 3 kW kg<sup>-1</sup> electric motors

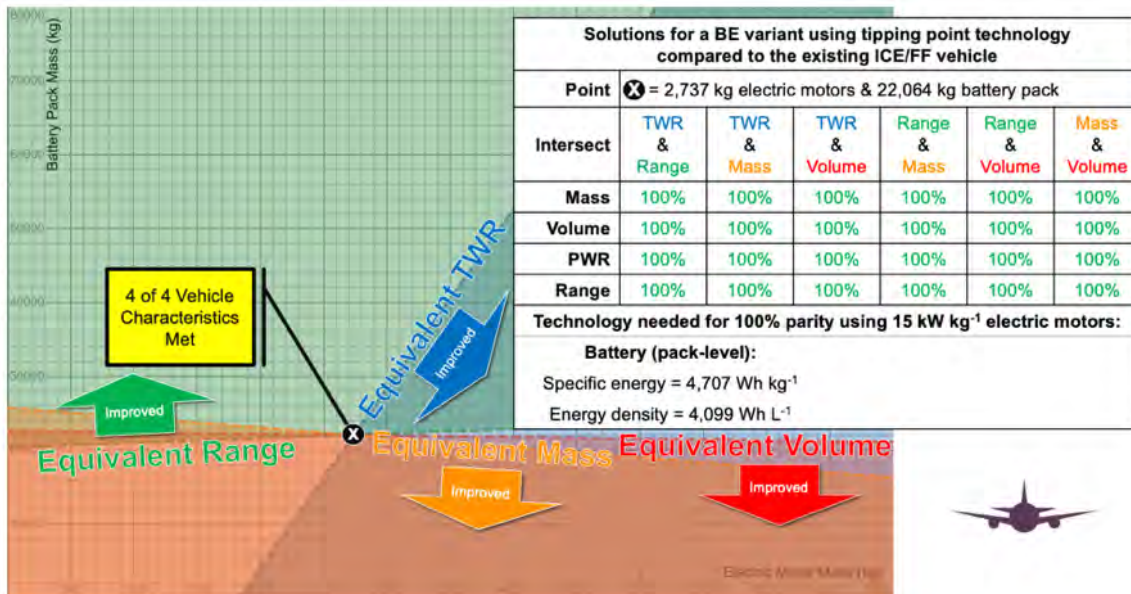


Fig. S.68. Tipping point technology for a medium-haul jet airliner battery electric variant using 15 kW kg<sup>-1</sup> electric motors

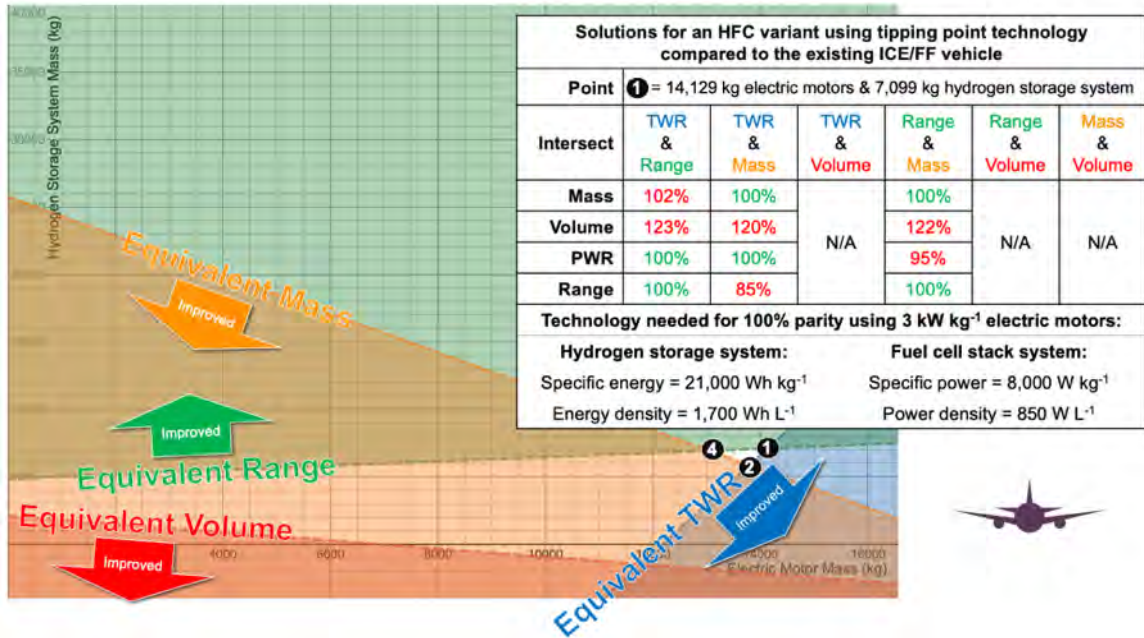


Fig. S.69. Tipping point technology for a medium-haul jet airliner hydrogen fuel cell variant using 3 kW kg<sup>-1</sup> electric motors

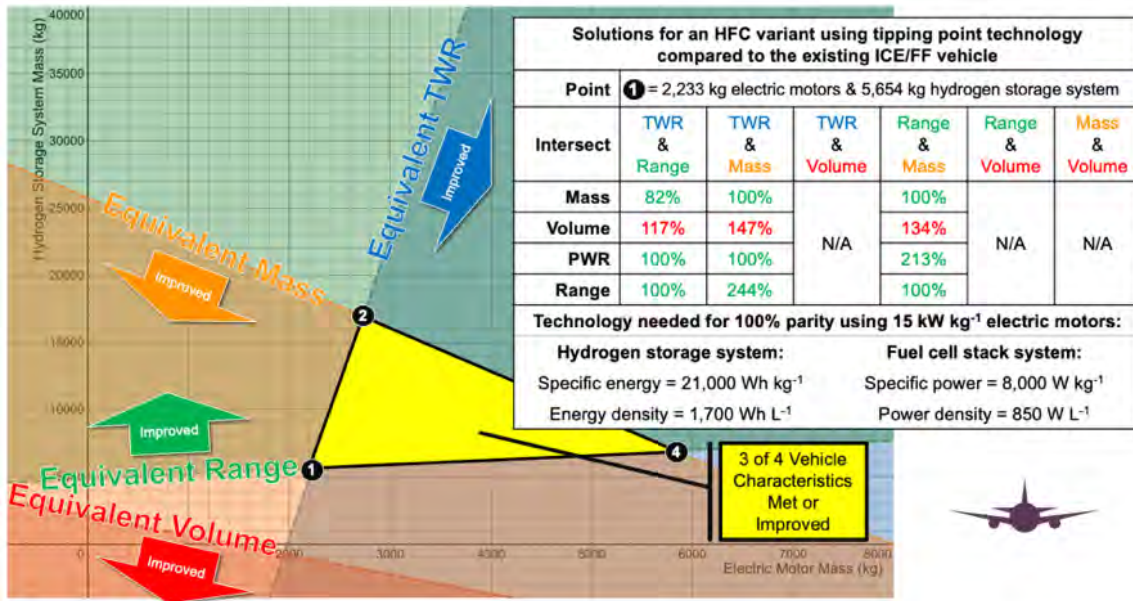


Fig. S.70. Tipping point technology for a medium-haul jet airliner hydrogen fuel cell variant using 15 kW kg<sup>-1</sup> electric motors

Fixed-wing aircraft (long-haul jet airliner)

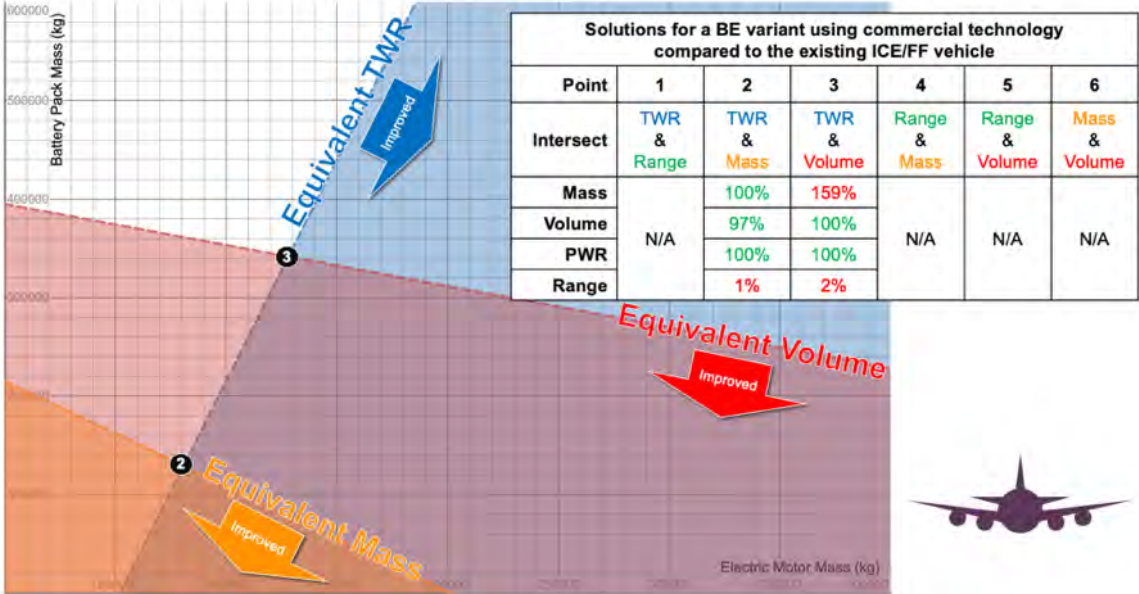


Fig. S.71. Long-haul jet airliner battery electric variant, commercial technology solutions

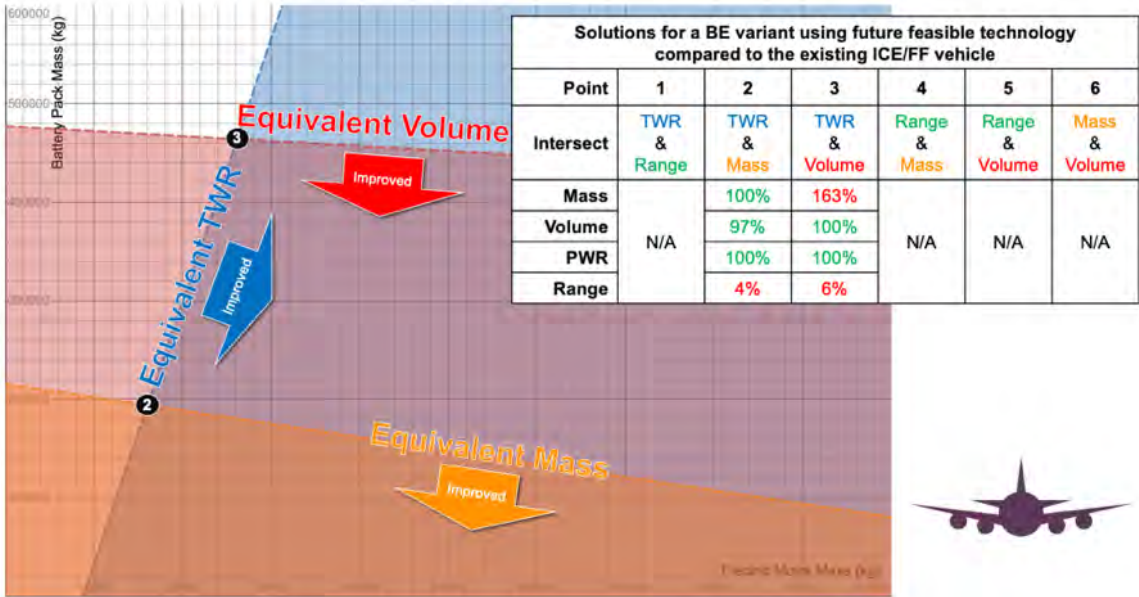


Fig. S.72. Long-haul jet airliner battery electric variant, future feasible technology solutions



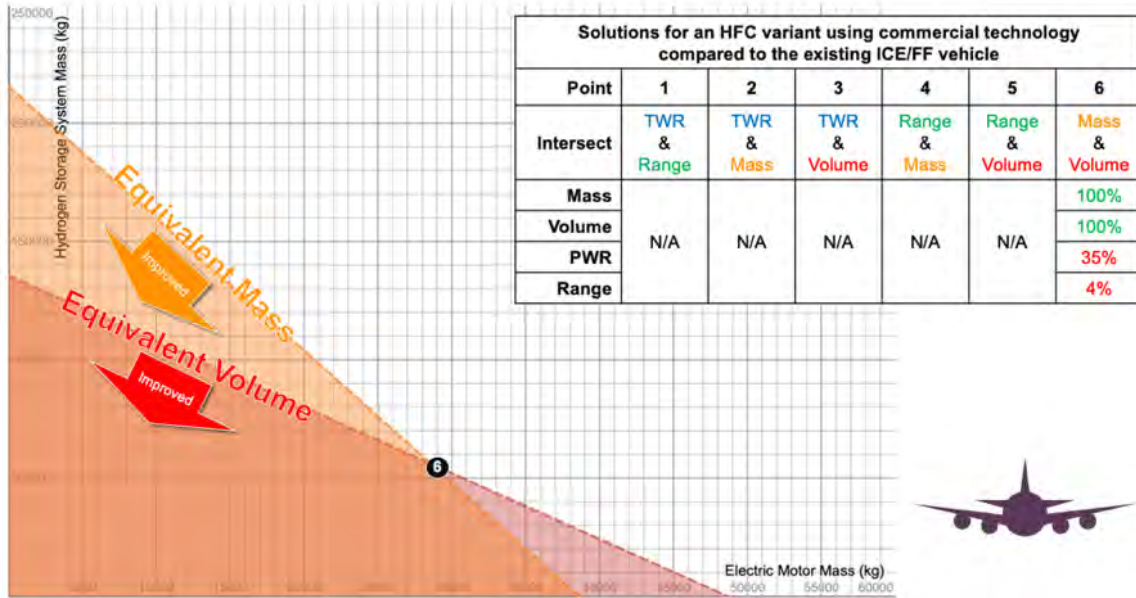


Fig. S.73. Long-haul jet airliner hydrogen fuel cell variant, commercial technology solutions

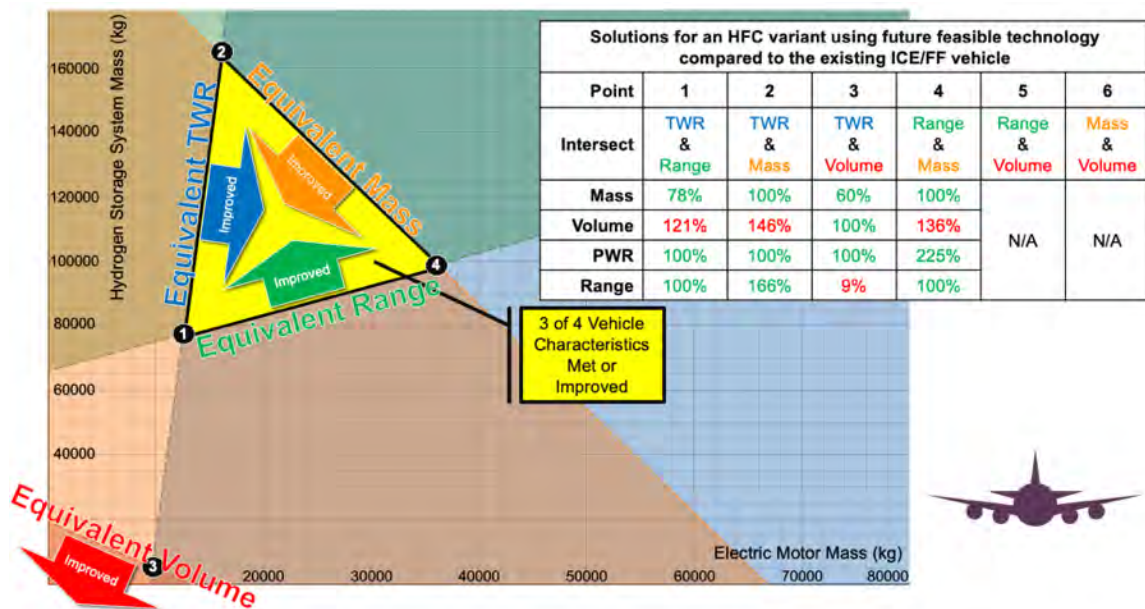


Fig. S.74. Long-haul jet airliner hydrogen fuel cell variant, future feasible technology solutions, same as Fig. 3(a)

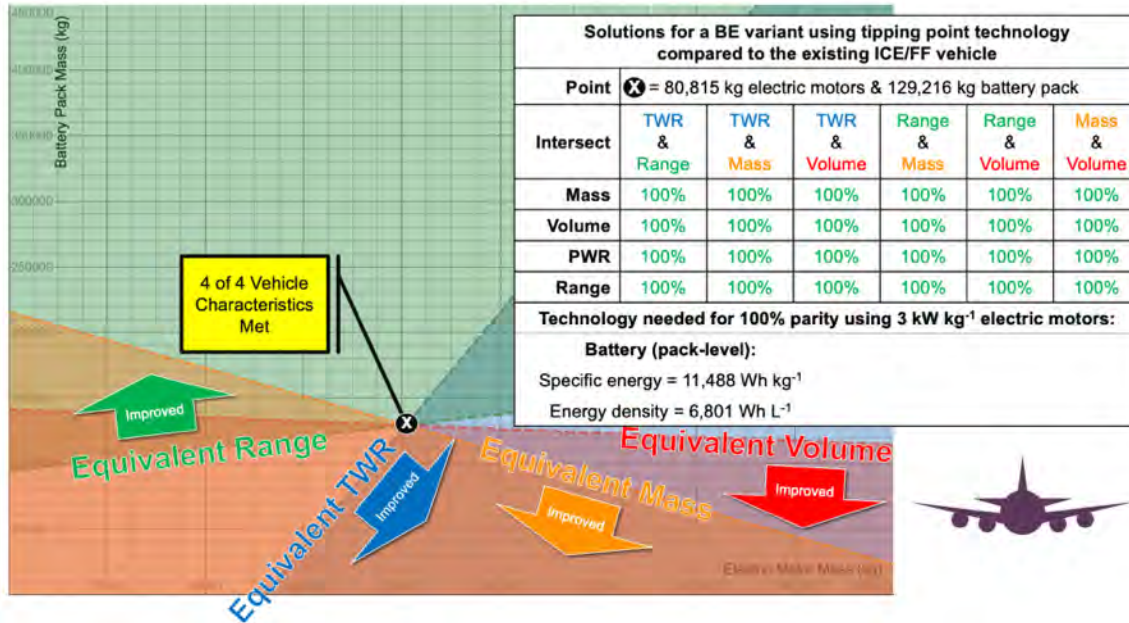


Fig. S.75. Tipping point technology for a long-haul jet airliner battery electric variant using 3 kW kg<sup>-1</sup> electric motors

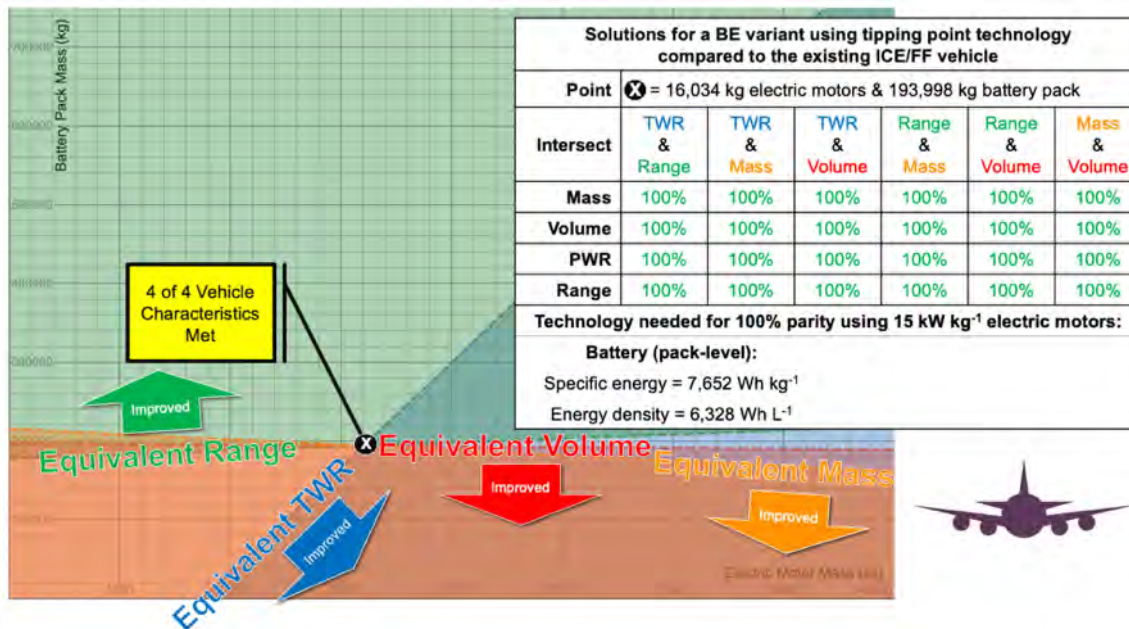


Fig. S.76. Tipping point technology for a long-haul jet airliner battery electric variant using 15 kW kg<sup>-1</sup> electric motors

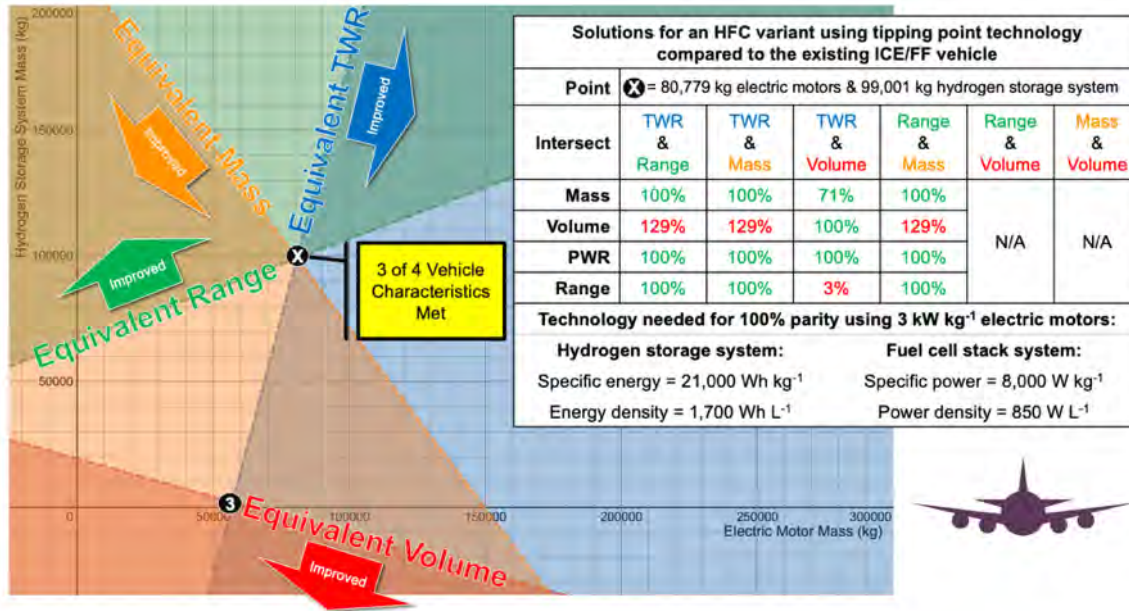


Fig. S.77. Tipping point technology for a long-haul jet airliner hydrogen fuel cell variant using 3 kW kg<sup>-1</sup> electric motors

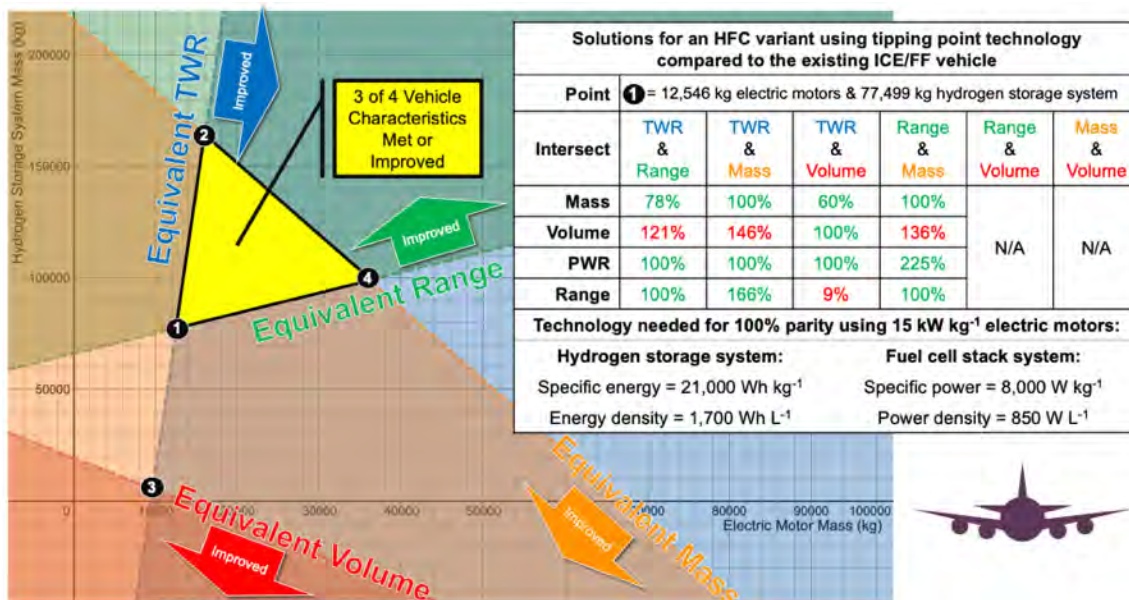


Fig. S.78. Tipping point technology for a long-haul jet airliner hydrogen fuel cell variant using 15 kW kg<sup>-1</sup> electric motors

## Waterjet boats

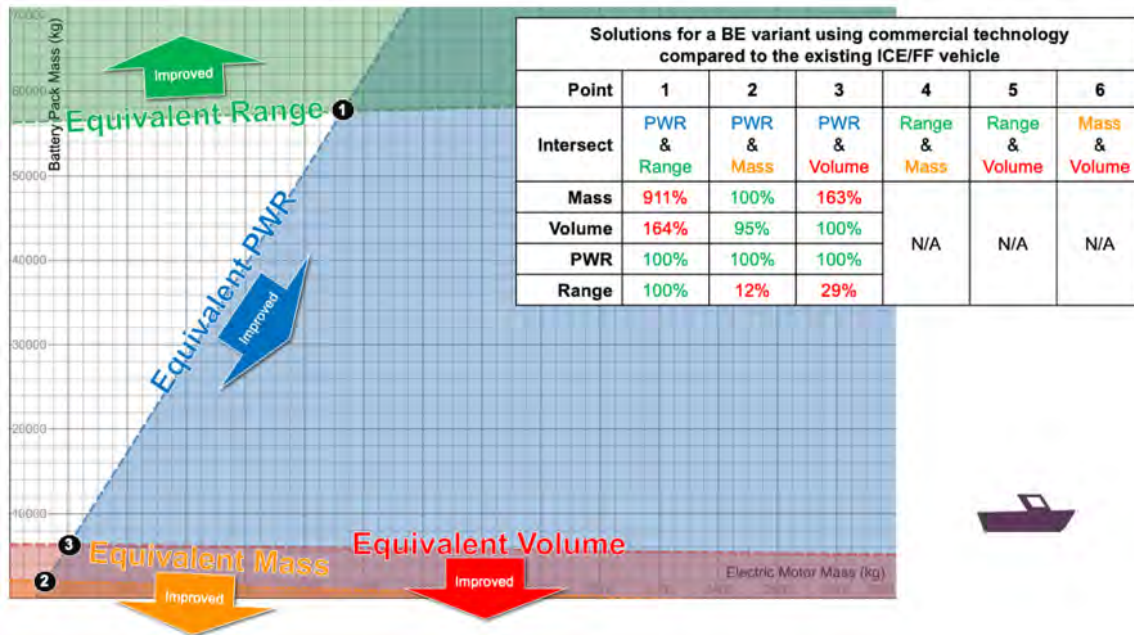


Fig. S.79. Battery electric variant waterjet boat, commercial technology solutions

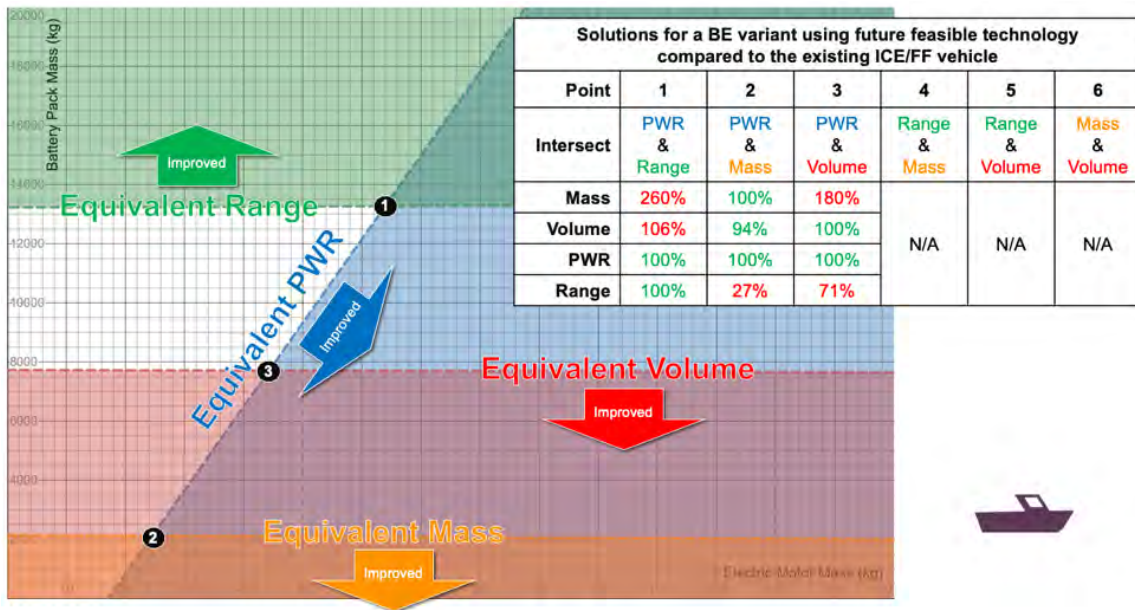


Fig. S.80. Battery electric variant waterjet boat, future feasible technology solutions

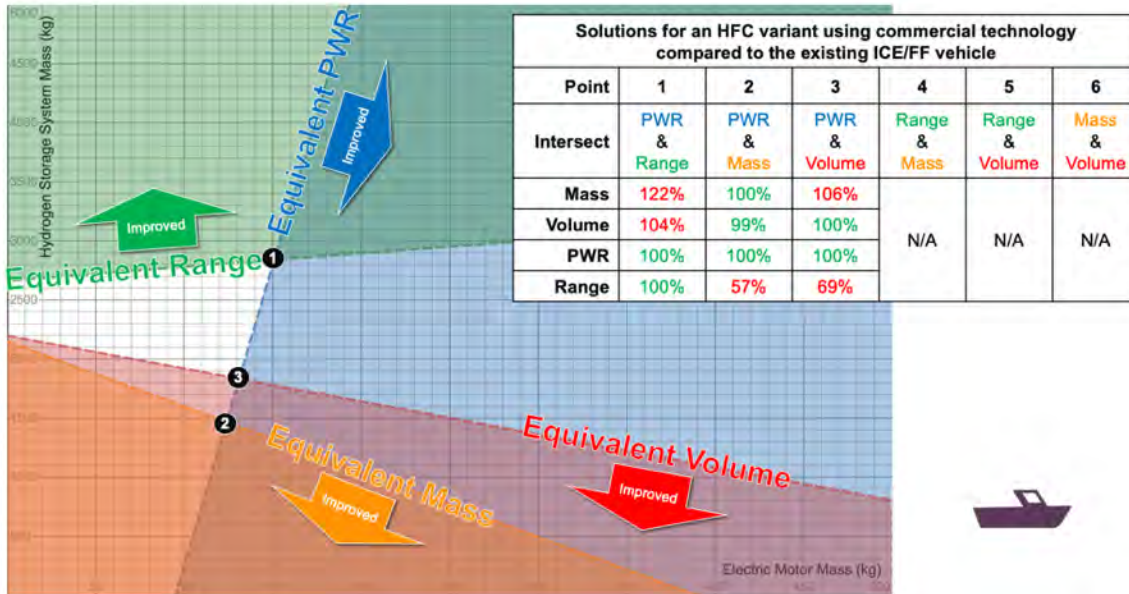


Fig. S.81. Hydrogen fuel cell variant waterjet boat, commercial technology solutions

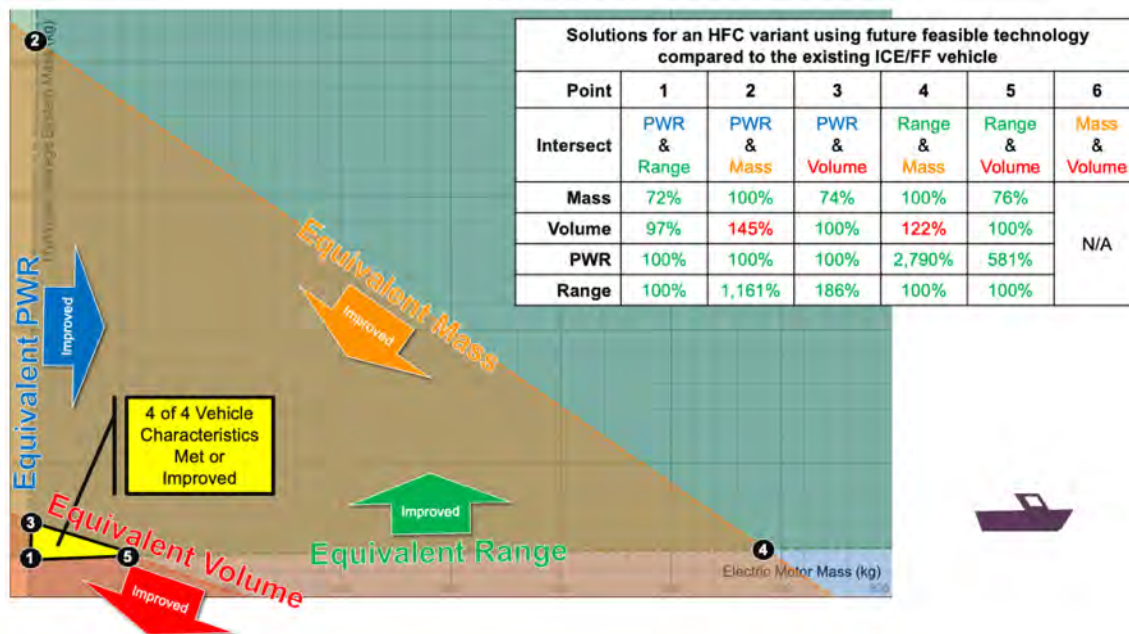


Fig. S.82. Hydrogen fuel cell variant waterjet boat, future feasible technology solutions

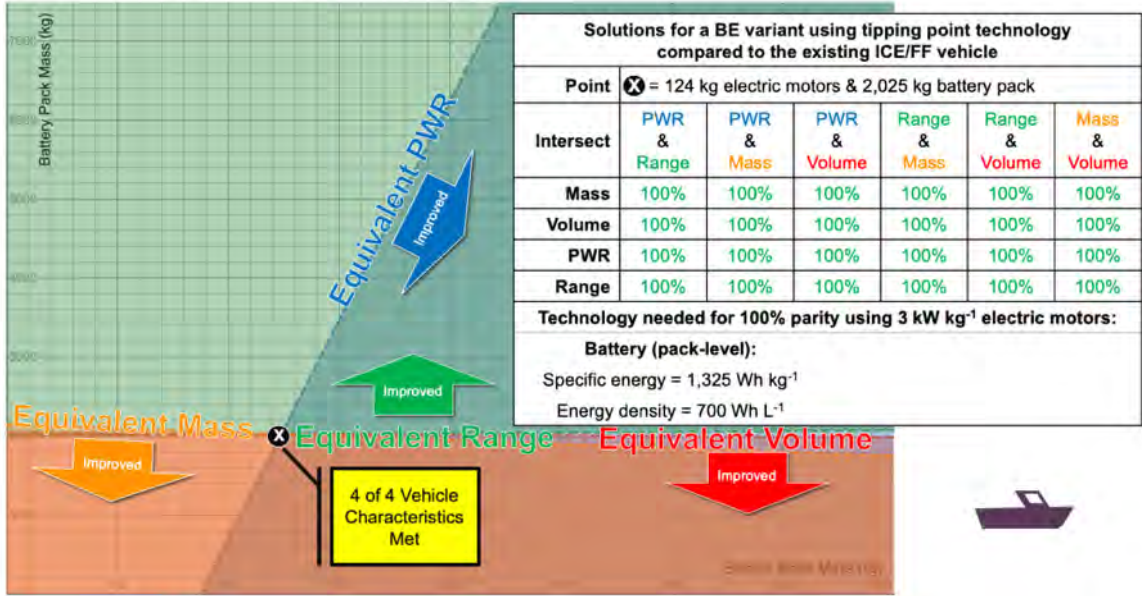


Fig. S.83. Tipping point technology for battery electric variant waterjet boat using 3 kW kg<sup>-1</sup> electric motors

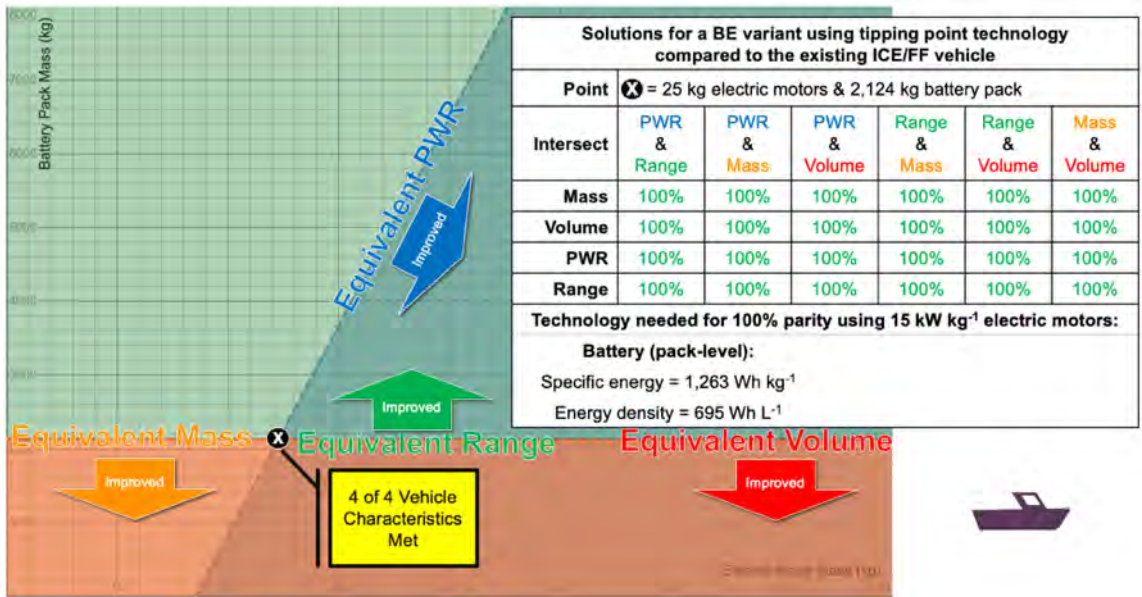


Fig. S.84. Tipping point technology for battery electric variant waterjet boat using 15 kW kg<sup>-1</sup> electric motors

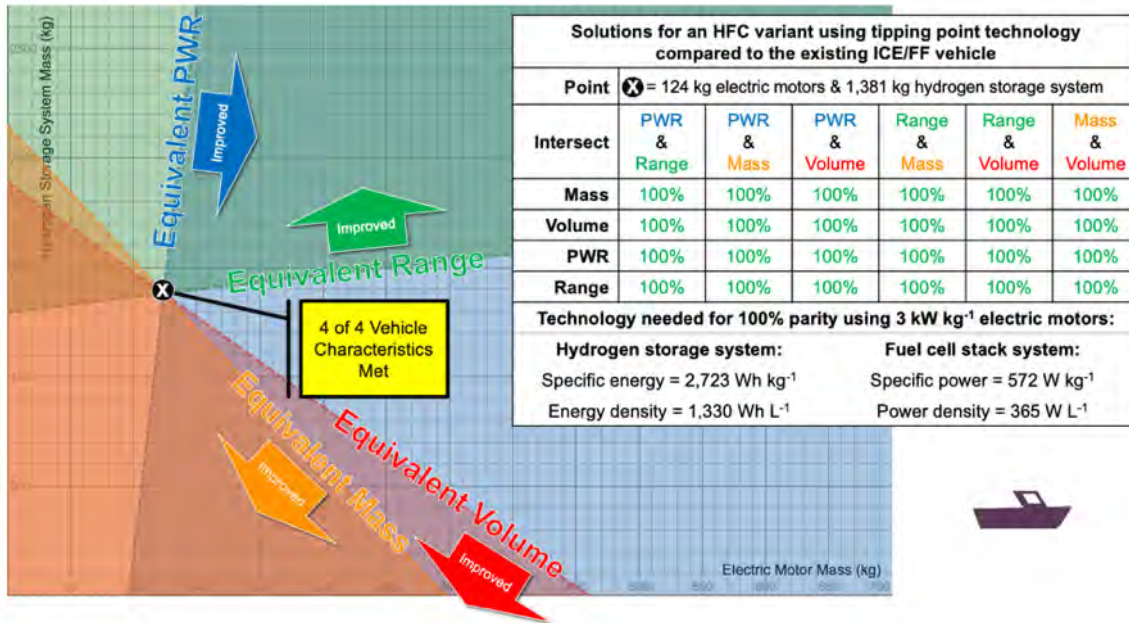


Fig. S.85. Tipping point technology for hydrogen fuel cell variant waterjet boat using 3 kW kg<sup>-1</sup> electric motors

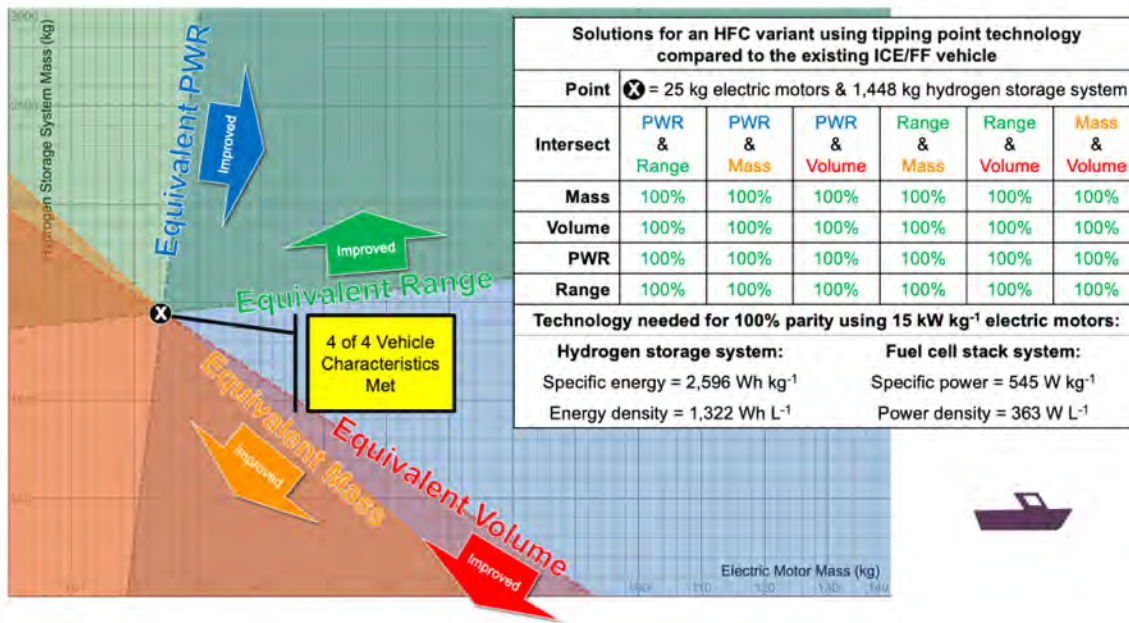


Fig. S.86. Tipping point technology for hydrogen fuel cell variant waterjet boat using 15 kW kg<sup>-1</sup> electric motors

## Cargo ships

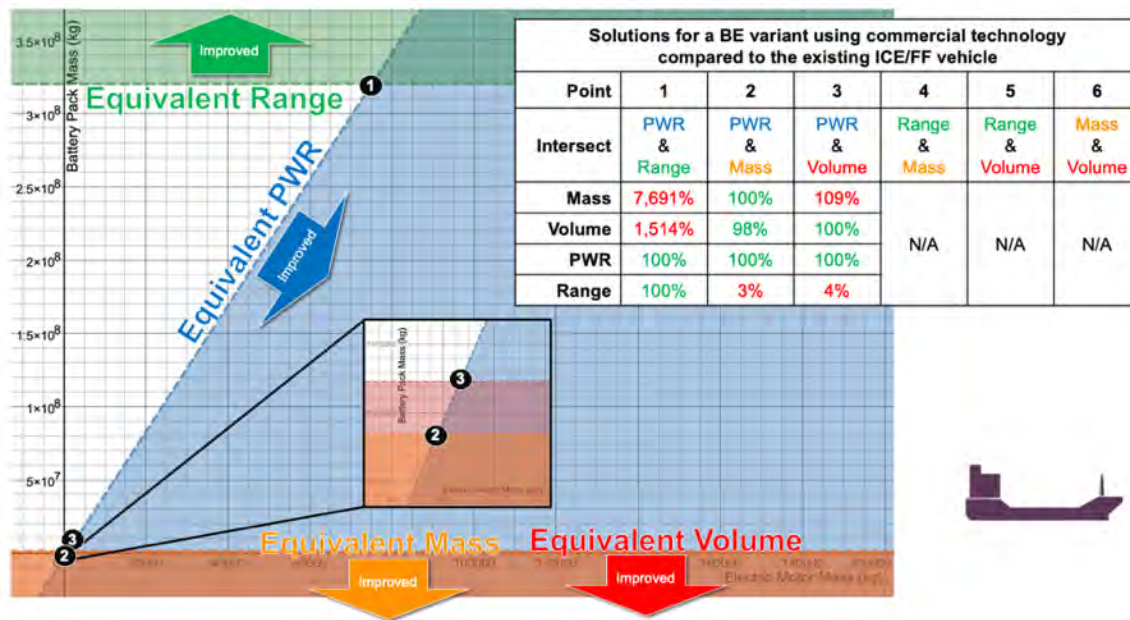


Fig. S.87. Battery electric variant cargo ship, commercial technology solutions

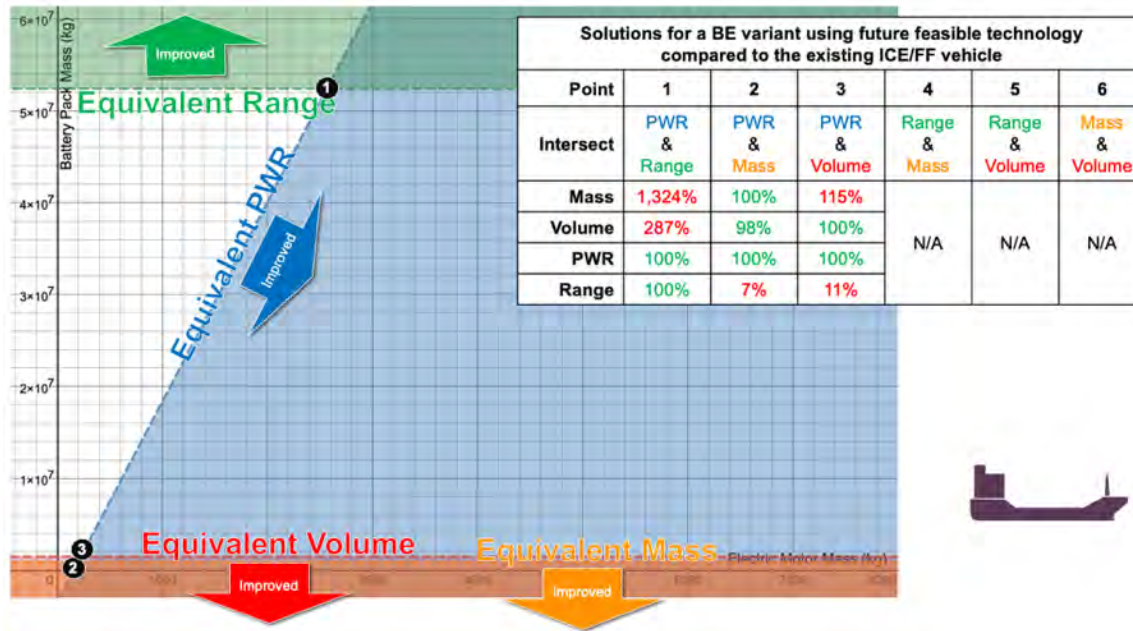


Fig. S.88. Battery electric variant cargo ship, future feasible technology solutions



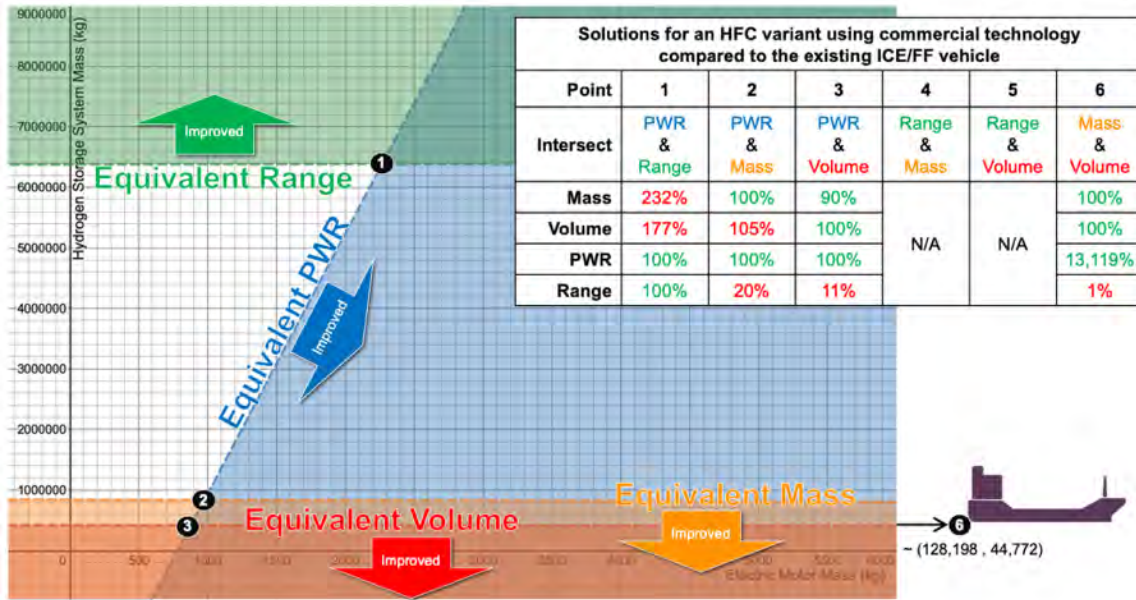


Fig. S.89. Hydrogen fuel cell variant cargo ship, commercial technology solutions

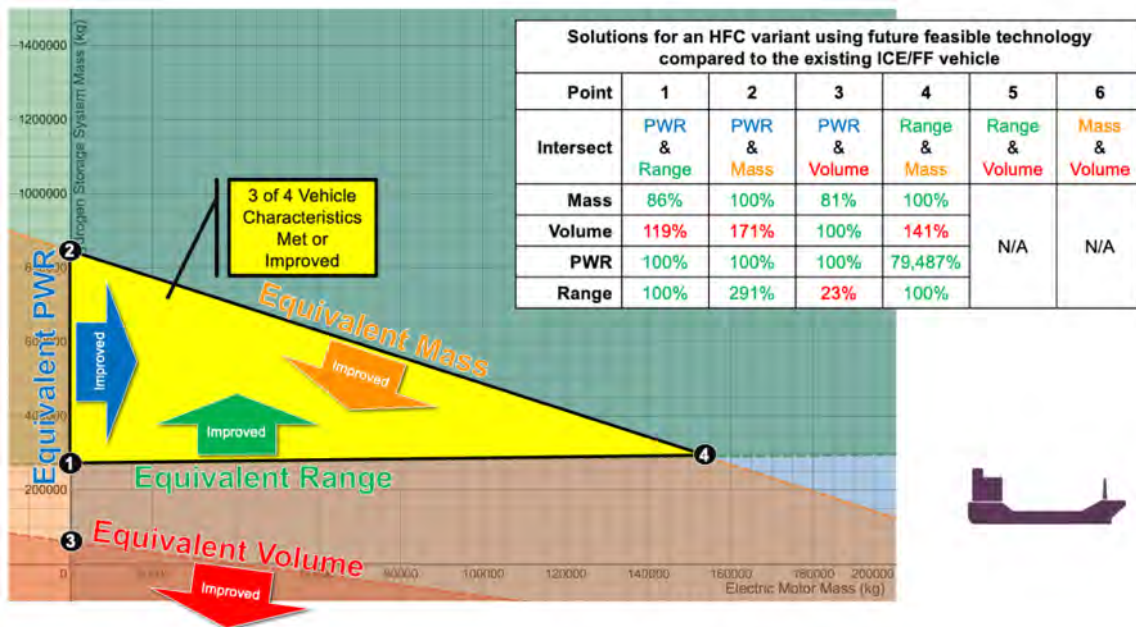


Fig. S.90. Hydrogen fuel cell variant cargo ship, future feasible technology solutions

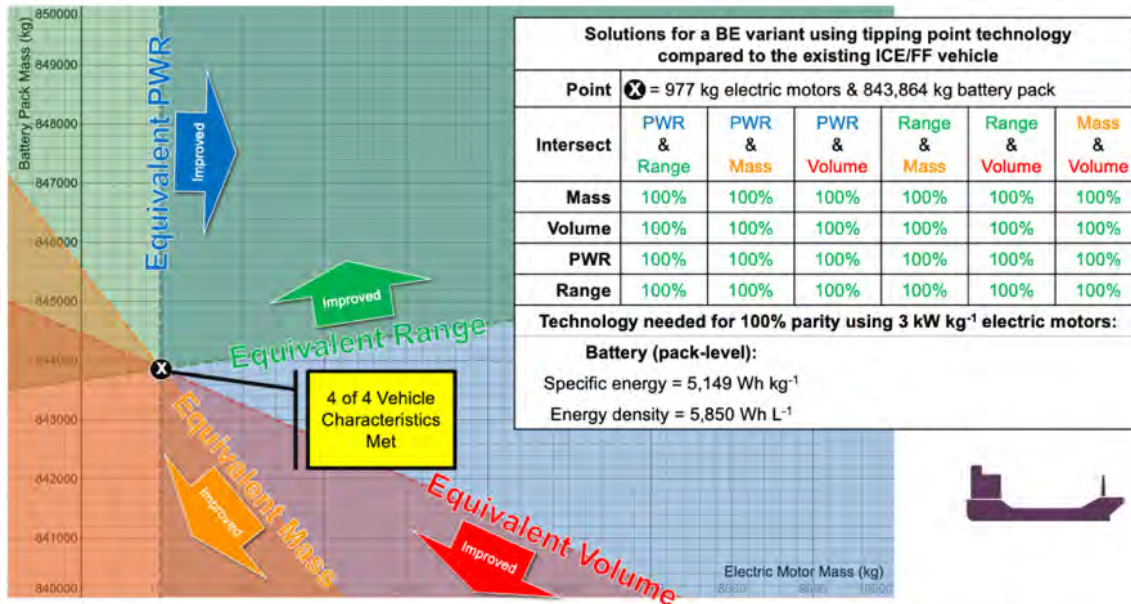


Fig. S.91. Tipping point technology for battery electric variant cargo ship using 3 kW kg<sup>-1</sup> electric motors

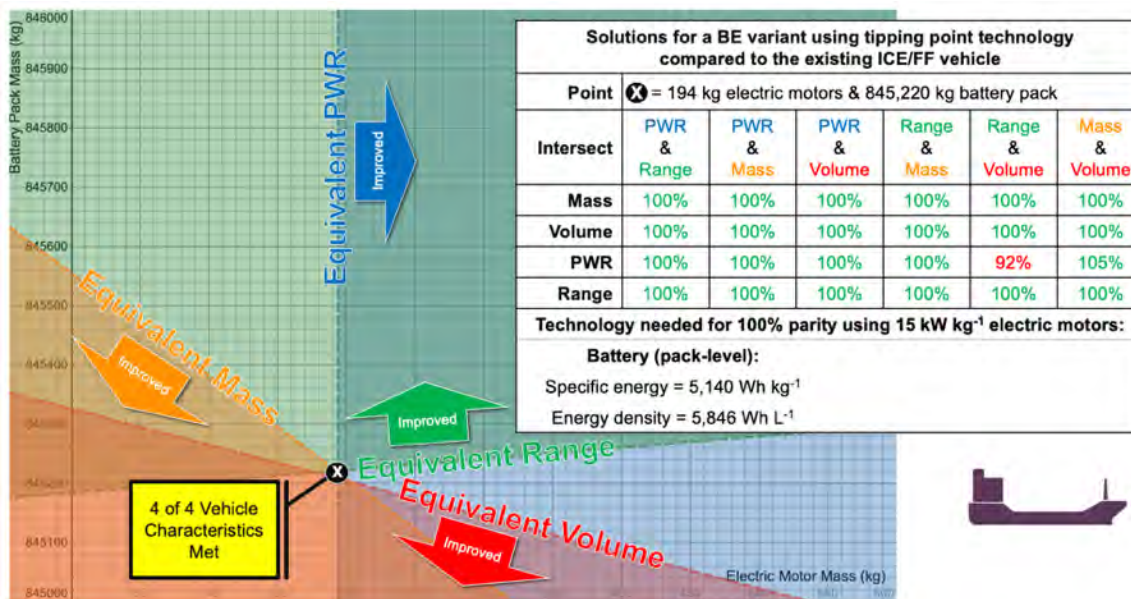


Fig. S.92. Tipping point technology for battery electric variant cargo ship using 15 kW kg<sup>-1</sup> electric motors

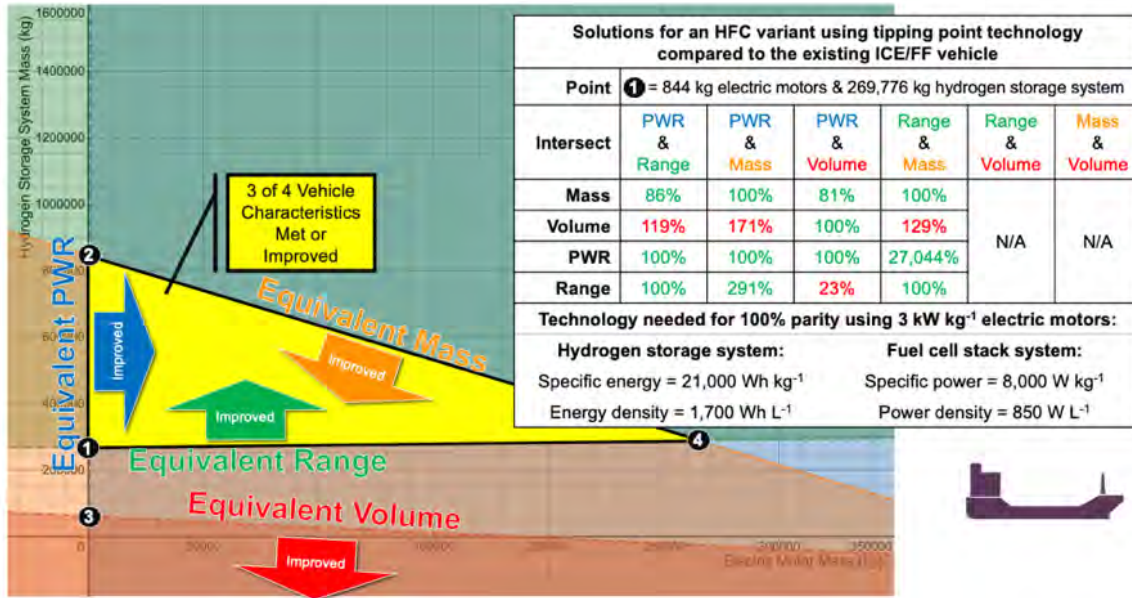


Fig. S.93. Tipping point technology for hydrogen fuel cell variant cargo ship using 3 kW kg<sup>-1</sup> electric motors

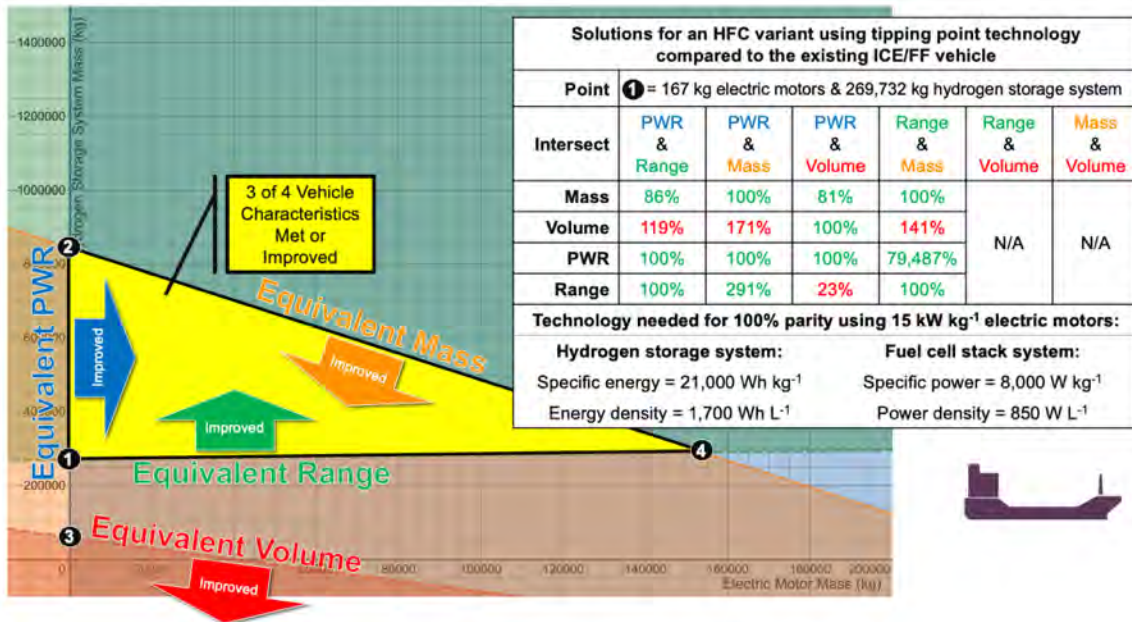
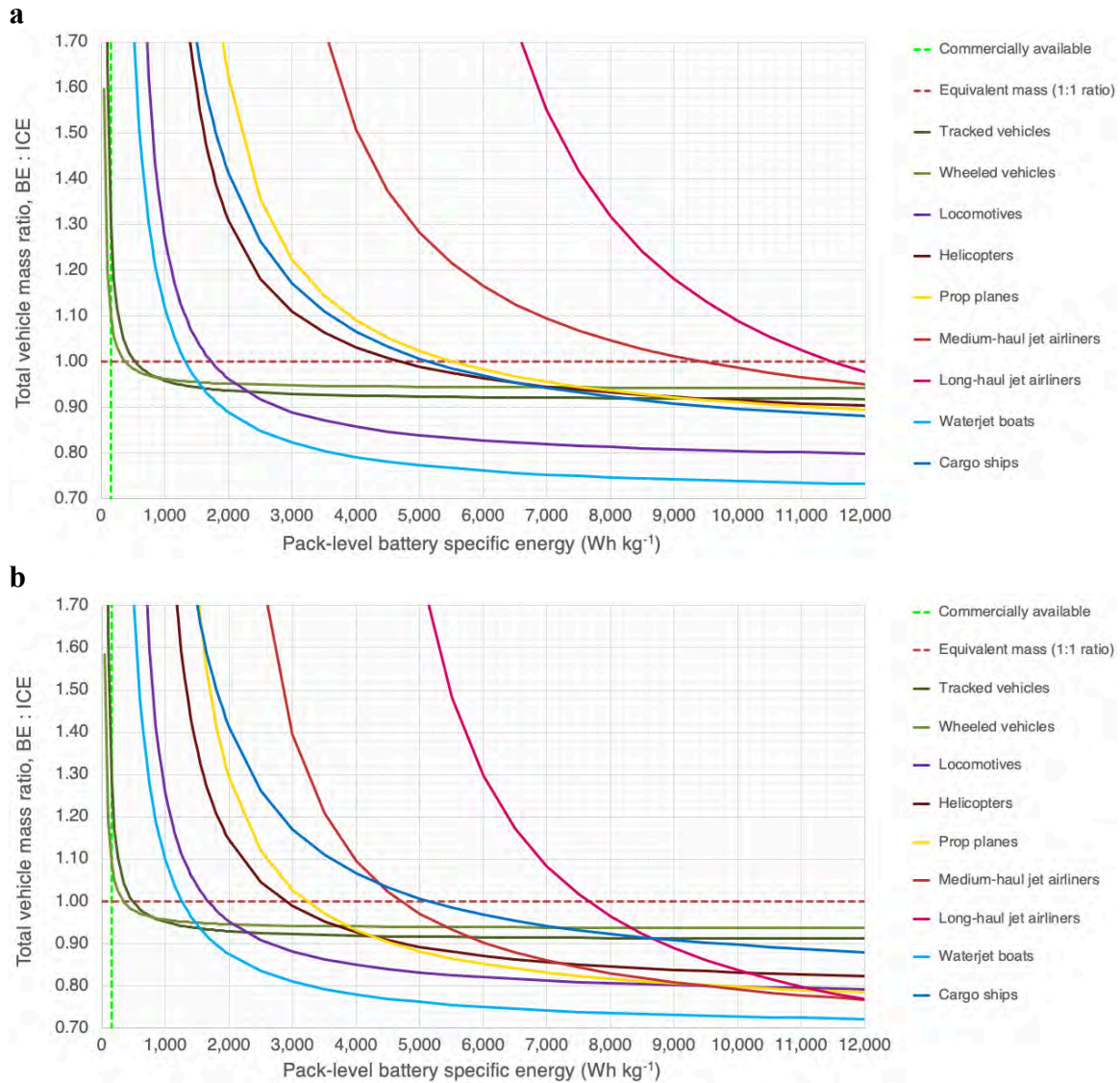


Fig. S.94. Tipping point technology for hydrogen fuel cell variant cargo ship using 15 kW kg<sup>-1</sup> electric motors

The graphs in Fig. S.23 through Fig. S.94 are useful in aiding our understanding as to what is required for BE and HFC variants. However, one limitation to these graphs is each one details the possibilities for a specified combination of values for the key variables involved: electric motor PWR, pack-level battery specific energy and energy density, hydrogen storage system specific energy and energy density, and hydrogen fuel cell stack specific power and power density, as appropriate for the variant. What may be even more useful for designers of all-electric variants and decision-makers considering research and development goals are graphs that show how specific technology levels will affect a certain vehicle characteristic. Fig. S.95 through Fig. S.103 do just that, illustrating our results from Sections 1.F.2.A through 1.F.2.I. In each of these graphs, the BE or HFC variant exactly meets the PWR (or TWR) and range of the existing FF/ICE vehicle.

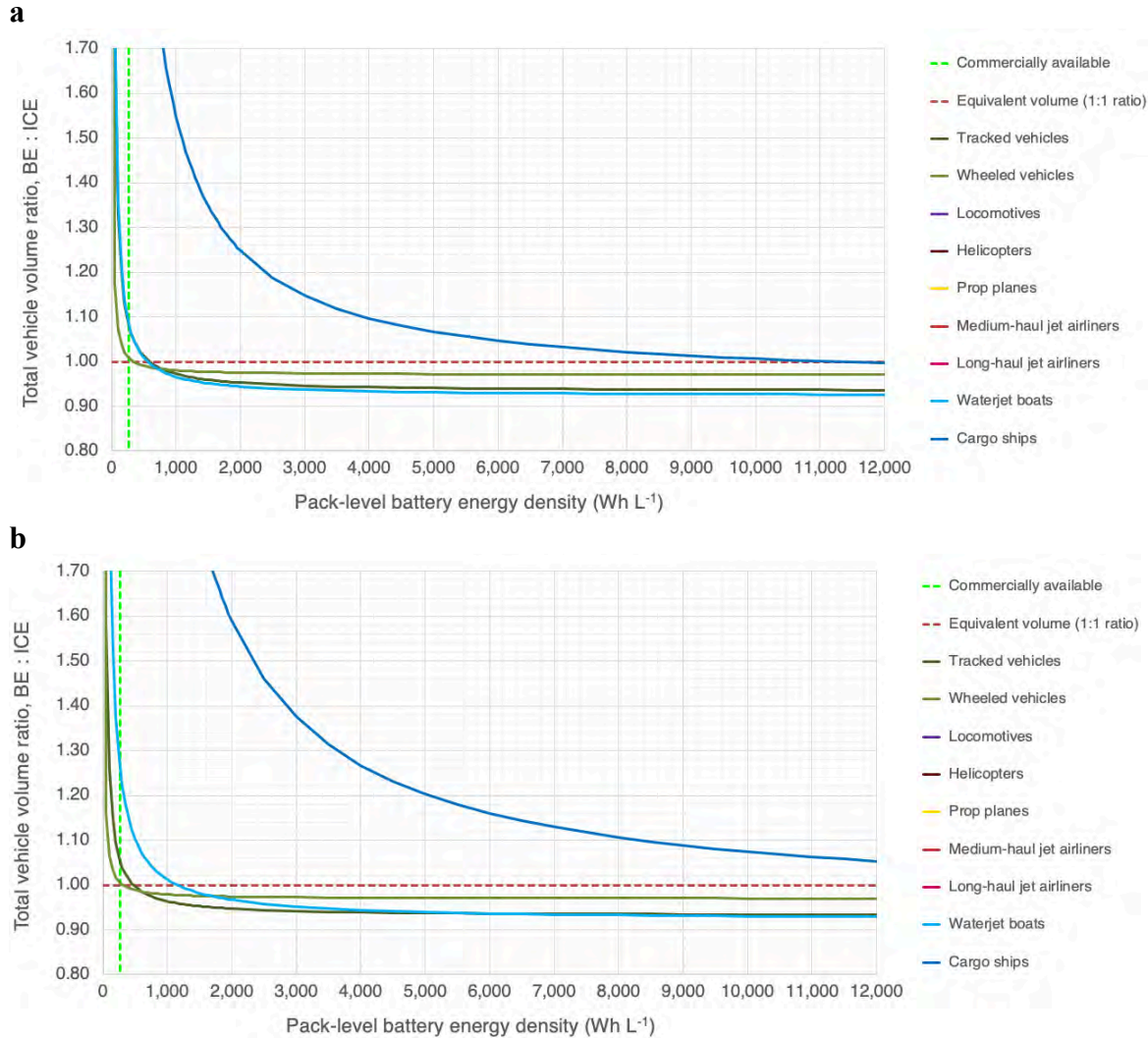
Fig. S.95 through Fig. S.101 illustrate how a range of possible values for one of the key variables affects the overall variant mass or volume. For example, Fig. S.95 shows how pack-level battery specific energy technology affects the overall BE variant with the same PWR (or TWR) and range of the existing FF/ICE vehicle. These graphs are incredibly useful because we can quickly see where commercial technology levels are, assess what future technologies can do for BE or HFC variants, and define acceptable targets. For example, a designer working on a BE variant of a wheeled ground combat vehicle using  $15 \text{ kW kg}^{-1}$  electric motors may know that a 5% increase in overall vehicle mass is acceptable. If that is the case, then pack-level battery specific energy technology only needs to reach  $200 \text{ Wh kg}^{-1}$  for such a design to be possible. Using commercial battery pack specific energy technology of  $157 \text{ Wh kg}^{-1}$  would require a BE wheeled ground combat vehicle to be ~9% heavier.

Fig. S.102 and Fig. S.103 illustrate how the hydrogen storage system and the fuel cell stack compete for mass and volume budget, respectively, in the HFC variant. Technology improvements in the hydrogen storage system allow for lower technology levels in the fuel cell stack to be acceptable, and vice versa. It is evident from Fig. S.102 that ground vehicles can already transition using commercial HFC technology (especially with  $15 \text{ kW kg}^{-1}$  electric motors), and that, because the hydrogen storage system and the fuel cell stacks are only two parts of the overall vehicle system, further technological improvements do little to further reduce overall mass. Although acceptable overall HFC variant mass is achievable given technology values cited as feasible within the literature, Fig. S.103 illustrates the challenge that overall HFC variant volume still poses. Many vehicle platforms (all aircraft, the freight locomotive, and cargo ships) can never achieve the same volume as the existing FF/ICE vehicles due to hydrogen storage density limitations. In such instances, designers must consider if additional volume budget is available (beyond what we estimated in this analysis) and whether additional vehicle volume is acceptable. Many design opportunities exist, such as changing the shape of aircraft, using a rail car with additional stored hydrogen for locomotives, and using otherwise unused on- or below-deck space for hydrogen storage on cargo ships.



**Fig. S.95. Impact of pack-level battery specific energy on total vehicle mass using an electric motor PWR of 3 kW kg<sup>-1</sup> (a) and 15 kW kg<sup>-1</sup> (b).**

Calculations are based on the requirement for BE variants to have the same PWR (or TWR) and range as existing ICE vehicles. Commercial pack-level battery specific energy is shown by the vertical green dashed line. A 1:1 mass ratio between BE and ICE vehicles is shown by the horizontal red dashed line. Where each vehicle platform's line crosses the red dashed line indicates the technological tipping point at which the BE variant will have the same mass as the existing ICE vehicle. A vertical line drawn at any battery specific energy value will indicate the percent increase or decrease in total vehicle mass achieved upon conversion at that technology level. Since onboard useful energy storage is only one component of a vehicle platform, the effect upon total vehicle mass decreases as specific energy increases. (b) is the same as Fig. 5(a).



**Fig. S.96. Impact of pack-level battery energy density on total vehicle volume using an electric motor PWR and pack-level battery specific energy of  $3 \text{ kW kg}^{-1}$  and  $157 \text{ Wh kg}^{-1}$  (a) and  $15 \text{ kW kg}^{-1}$  and  $335 \text{ Wh kg}^{-1}$  (b), respectively.**

Calculations are based on the requirement for BE variants to have the same PWR (or TWR) and range as existing ICE vehicles. Commercial pack-level battery energy density is shown by the vertical green dashed line. A 1:1 volume ratio between BE and ICE vehicles is shown by the horizontal red dashed line. Where each vehicle platform's line crosses the red dashed line indicates the technological tipping point at which the BE variant will have the same volume as the existing ICE vehicle. A vertical line drawn at any battery energy density value will indicate the percent increase or decrease in total vehicle volume achieved upon conversion at that technology level. Since onboard useful energy storage is only one component of a vehicle platform, the effect upon total vehicle volume decreases as specific energy increases. Results are not shown for the locomotive or any aircraft as those platforms do not have feasible results using the singular value for pack-level battery specific energy specified.

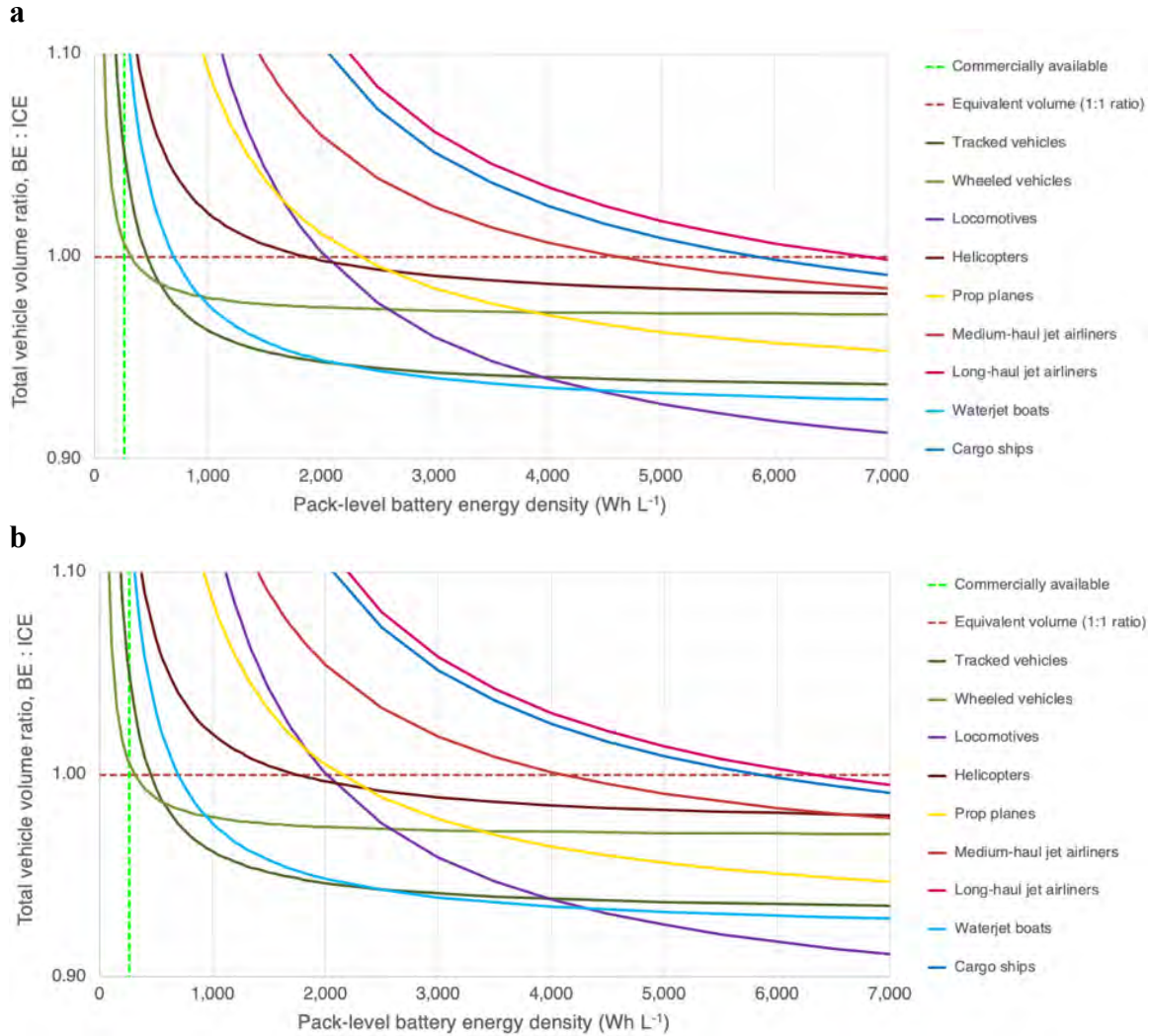


**Fig. S.97. Impact of pack-level battery energy density on total vehicle volume using an electric motor PWR of  $3 \text{ kW kg}^{-1}$  (a) and  $15 \text{ kW kg}^{-1}$  (b) with values for pack-level battery specific energy that result in a 1:1 mass ratio (equivalent mass) between BE and ICE variants for each individual vehicle platform.**

Calculations are based on the requirement for BE variants to have the same PWR (or TWR) and range as existing ICE vehicles. In this scenario, different values for pack-level specific energy are used for each vehicle type to ensure a 1:1 mass ratio between BE and ICE variants. Commercial pack-level battery energy density is shown by the vertical green dashed line. A 1:1 volume ratio between BE and ICE vehicles is shown by the horizontal red dashed line. Where each vehicle platform's line crosses the red dashed line indicates the technological tipping point at which the BE variant will have the same volume as the existing ICE vehicle. A vertical line drawn at any battery energy density value will indicate the percent increase or decrease in total vehicle volume achieved upon conversion at that technology level. Since onboard useful energy storage is only one component of a vehicle platform, the effect upon total vehicle volume decreases as specific energy increases. (b) is the same as Fig. 5(b).

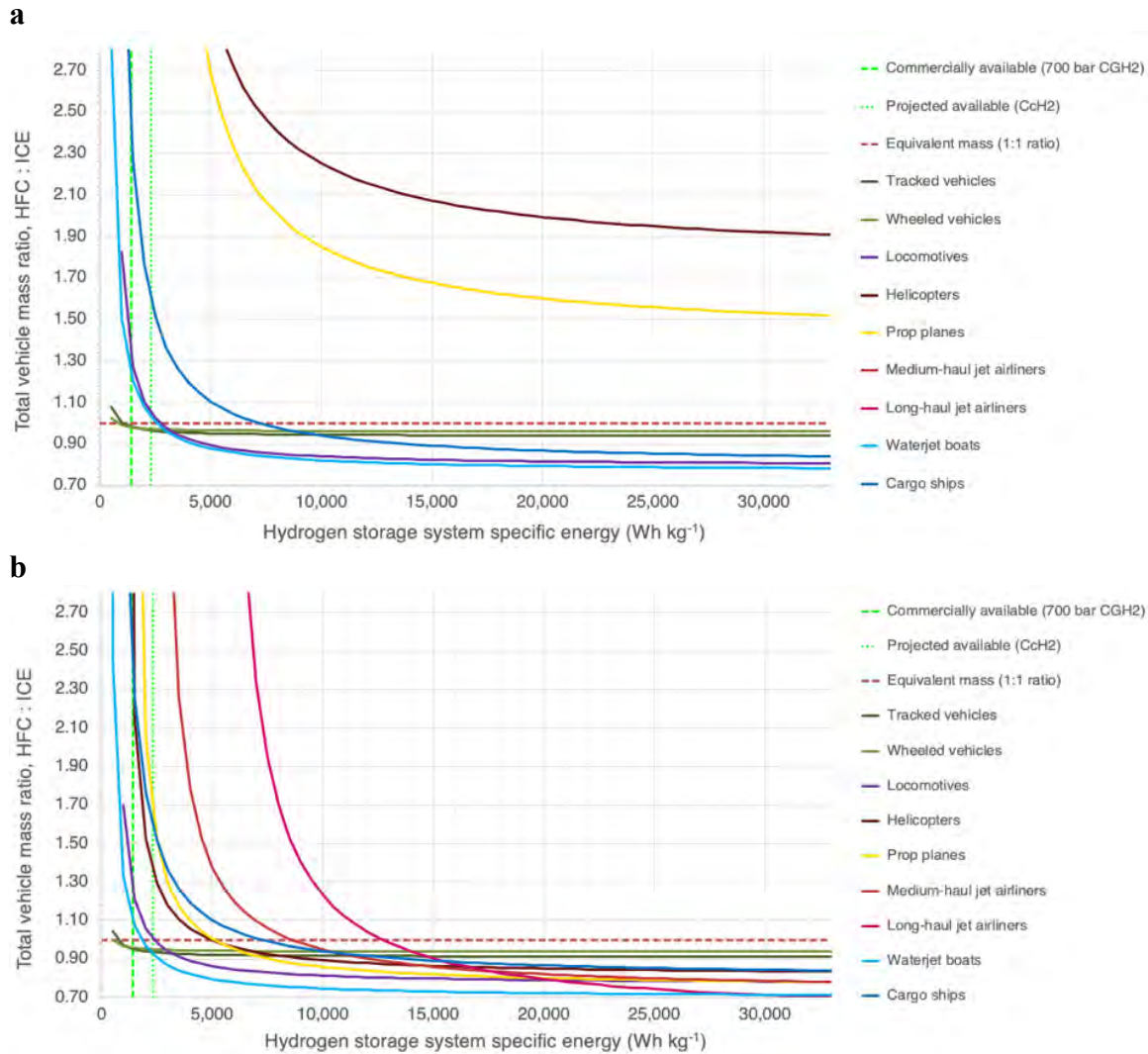


**Fig. S.98. Impact of hydrogen storage system specific energy on total vehicle mass using an electric motor PWR and fuel cell stack specific power of  $3 \text{ kW kg}^{-1}$  and  $659 \text{ W kg}^{-1}$  (a) and  $15 \text{ kW kg}^{-1}$  and  $8 \text{ kW kg}^{-1}$  (b), respectively.**

Calculations are based on the requirement for HFC variants to have the same PWR (or TWR) and range as existing ICE vehicles. Commercially available 700 bar compressed gas hydrogen system specific energy is shown by the vertical green dashed line. Projected available cryogenic-compressed hydrogen system specific energy is shown by the vertical green dotted line. A 1:1 mass ratio between HFC and ICE vehicles is shown by the horizontal red dashed line. Where each vehicle platform's line crosses the red dashed line indicates the technological tipping point at which the HFC variant will have the same mass as the existing ICE vehicle. A vertical line drawn at any hydrogen storage system specific energy value will indicate the percent increase or decrease in total vehicle mass achieved upon conversion at that technology level. Since onboard useful energy storage is only one component of a vehicle platform, the effect upon total vehicle mass decreases as specific energy increases. Not all vehicle platforms have solutions due to technology levels selected.



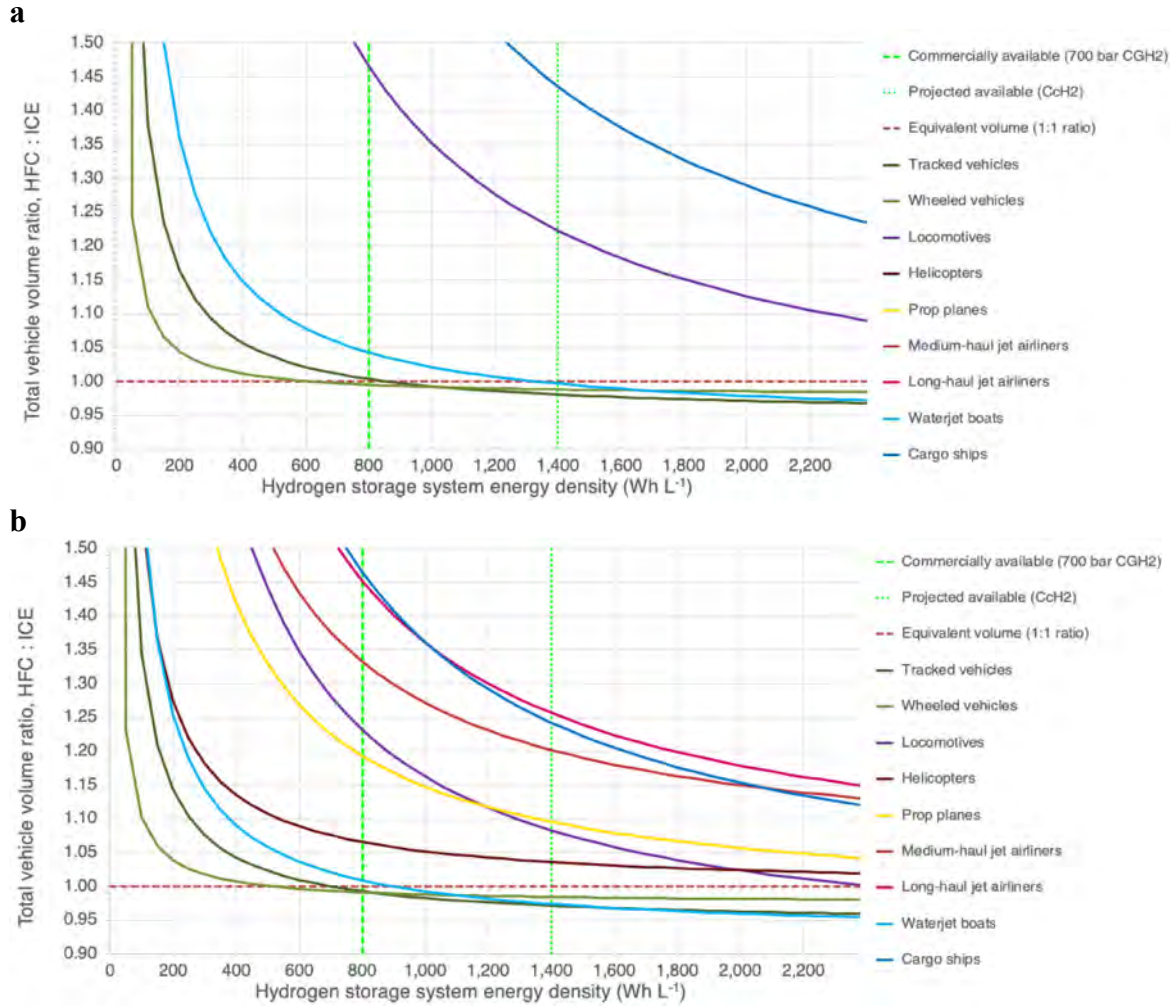


**Fig. S.99. Impact of hydrogen storage system energy density on total vehicle volume using an electric motor PWR, hydrogen storage system specific energy, fuel cell stack specific power, and fuel cell stack power density of 3 kW kg<sup>-1</sup>, 1,465 Wh kg<sup>-1</sup>, 659 W kg<sup>-1</sup>, and 640 W L<sup>-1</sup> (a) and 15 kW kg<sup>-1</sup>, 21,000 Wh kg<sup>-1</sup>, 8 kW kg<sup>-1</sup>, and 850 W L<sup>-1</sup> (b), respectively.**

Calculations are based on the requirement for HFC variants to have the same PWR (or TWR) and range as existing ICE vehicles. Commercially available 700 bar compressed gas hydrogen system energy density is shown by the vertical green dashed line. Projected available cryogenic-compressed hydrogen system energy density is shown by the vertical green dotted line. A 1:1 volume ratio between HFC and ICE vehicles is shown by the horizontal red dashed line. Where each vehicle platform's line crosses the red dashed line indicates the technological tipping point at which the HFC variant will have the same volume as the existing ICE vehicle. A vertical line drawn at any hydrogen storage system energy density value will indicate the percent increase or decrease in total vehicle volume achieved upon conversion at that technology level. Since onboard useful energy storage is only one component of a vehicle platform, the effect upon total vehicle volume decreases as specific energy increases. Not all vehicle platforms have solutions due to technology levels selected.

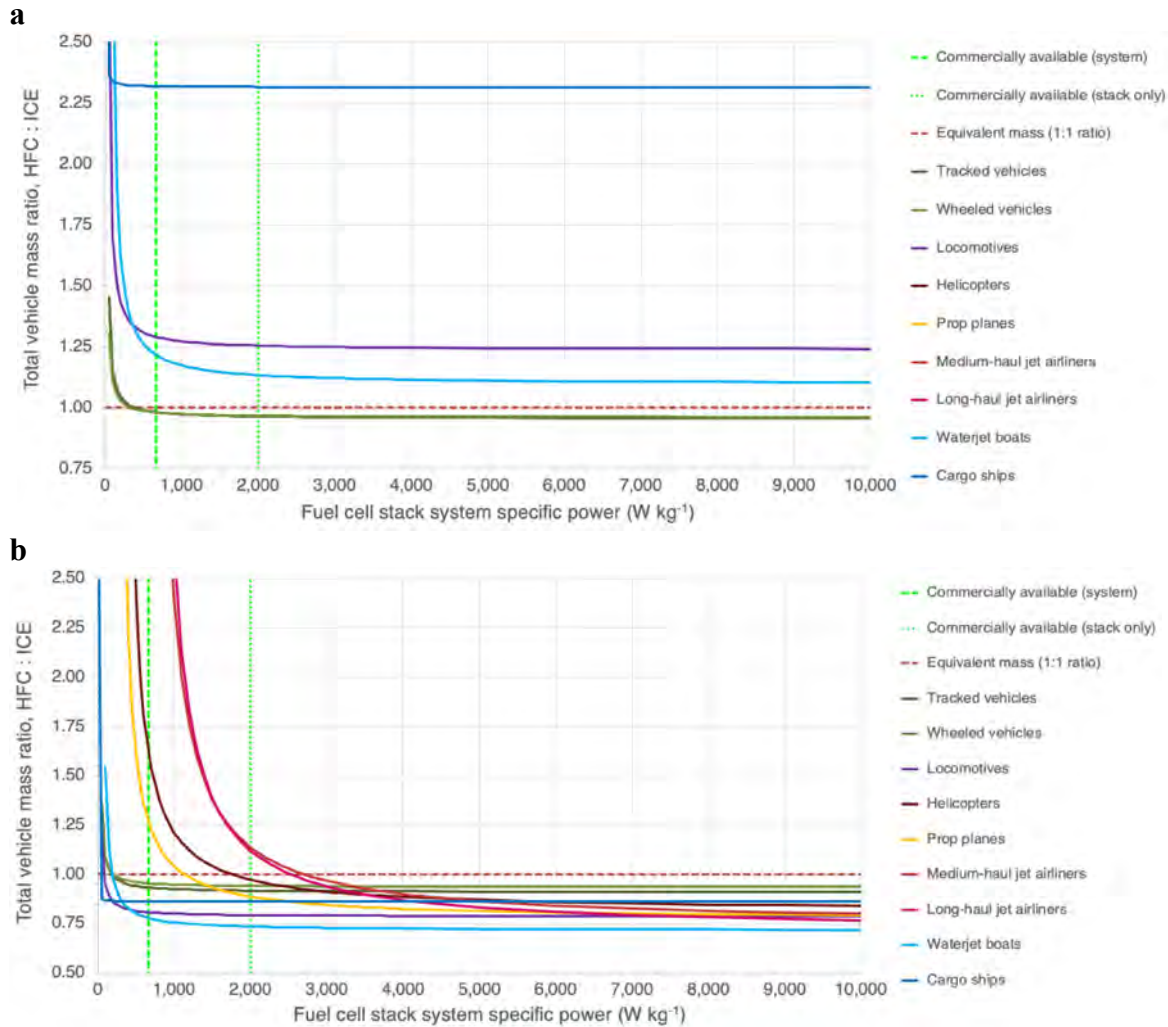


**Fig. S.100. Impact of fuel cell stack system specific power on total vehicle mass using an electric motor PWR and hydrogen storage system specific energy of 3 kW kg<sup>-1</sup> and 1,465 Wh kg<sup>-1</sup> (a) and 15 kW kg<sup>-1</sup> and 21,000 Wh kg<sup>-1</sup> (b), respectively.**

Calculations are based on the requirement for HFC variants to have the same PWR (or TWR) and range as existing ICE vehicles. Commercially available integrated fuel cell stack system (with balance of plant components) specific power is shown by the vertical green dashed line. Commercially available fuel cell (stack only) specific power is shown by the vertical green dotted line. A 1:1 mass ratio between HFC and ICE vehicles is shown by the horizontal red dashed line. Where each vehicle platform's line crosses the red dashed line indicates the technological tipping point at which the HFC variant will have the same mass as the existing ICE vehicle. A vertical line drawn at any fuel cell stack system specific power value will indicate the percent increase or decrease in total vehicle mass achieved upon conversion at that technology level. Not all vehicle platforms have solutions due to the value selected for hydrogen storage system specific energy.

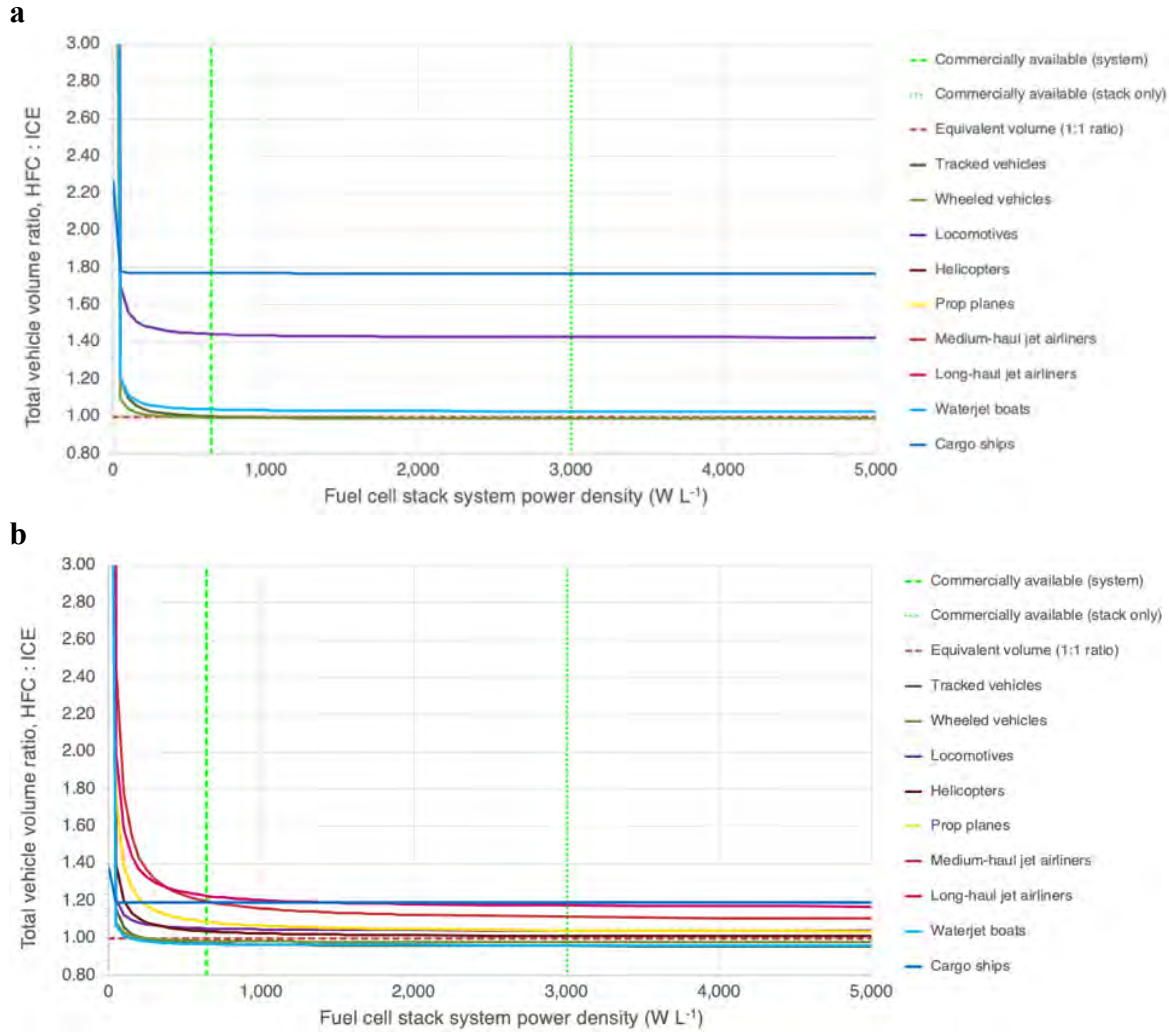


**Fig. S.101. Impact of fuel cell stack system power density on total vehicle volume using an electric motor PWR, hydrogen storage system specific energy, hydrogen storage system energy density, and fuel cell stack specific power of  $3 \text{ kW kg}^{-1}$ ,  $1,465 \text{ Wh kg}^{-1}$ ,  $833 \text{ Wh L}^{-1}$ , and  $659 \text{ W kg}^{-1}$  (a) and  $15 \text{ kW kg}^{-1}$ ,  $21,000 \text{ kWh kg}^{-1}$ ,  $1.7 \text{ kWh L}^{-1}$ , and  $8 \text{ kW kg}^{-1}$  (b), respectively.**

Calculations are based on the requirement for HFC variants to have the same PWR (or TWR) and range as existing ICE vehicles. Commercially available integrated fuel cell stack system (with balance of plant components) power density is shown by the vertical green dashed line. Commercially available fuel cell (stack only) power density is shown by the vertical green dotted line. A 1:1 volume ratio between HFC and ICE vehicles is shown by the horizontal red dashed line. Where each vehicle platform's line crosses the red dashed line indicates the technological tipping point at which the HFC variant will have the same volume as the existing ICE vehicle. A vertical line drawn at any fuel cell stack system power density value will indicate the percent increase or decrease in total vehicle volume achieved upon conversion at that technology level. Not all vehicle platforms have solutions due to technology levels selected.

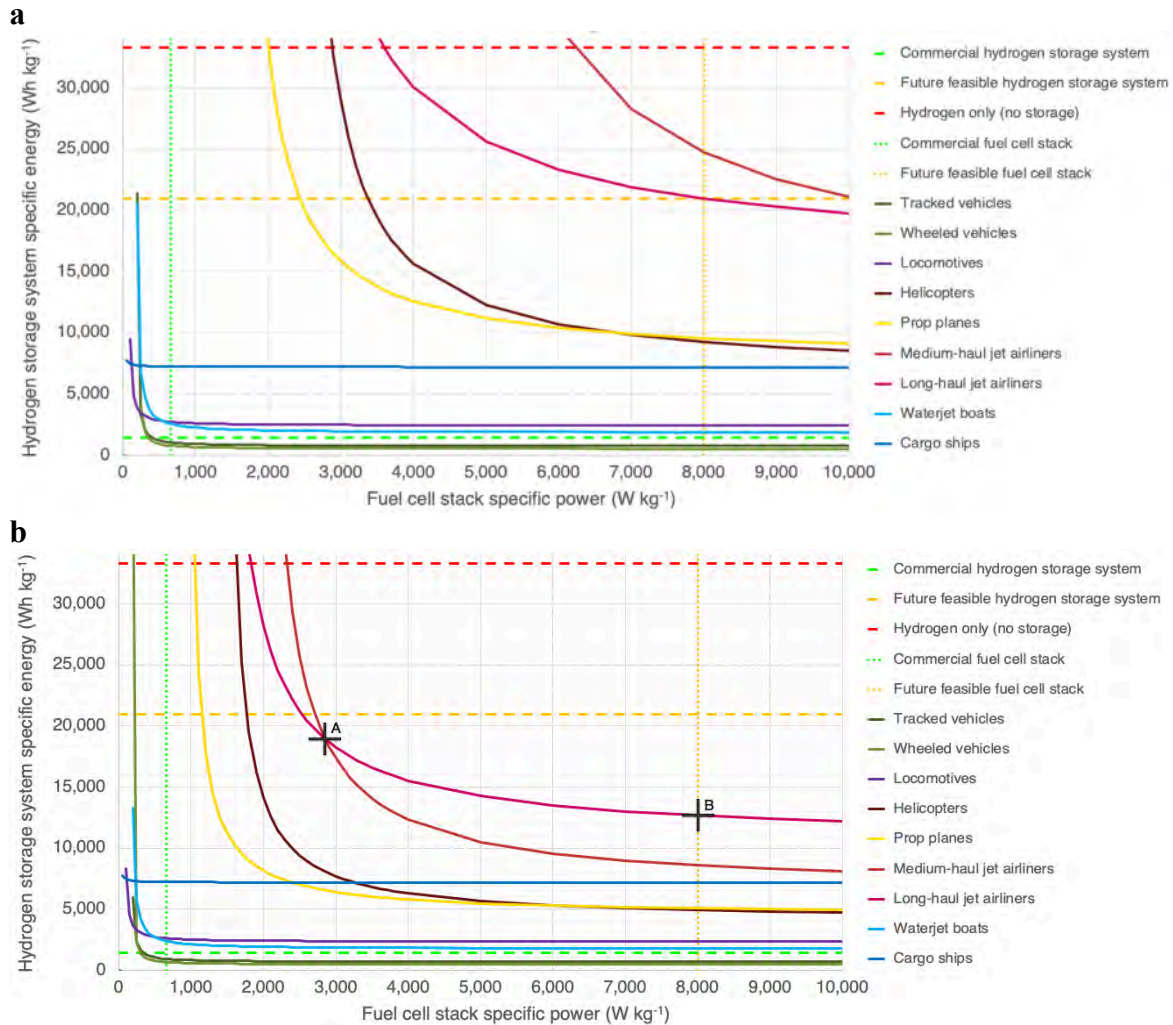


**Fig. S.102. Competition between hydrogen storage system specific energy and fuel cell stack specific power requirements for a 1:1 mass ratio (equivalent mass) between HFC and ICE variants for each individual vehicle platform using an electric motor PWR of 3 kW kg<sup>-1</sup> (a) and 15 kW kg<sup>-1</sup> (b).**

Calculations are based on the requirement for HFC variants to have the same PWR (or TWR) and range as existing ICE vehicles. Specific power values for commercially-available integrated fuel cell stack system (with balance of plant components) and future feasible fuel cell stacks are shown by the vertical green and amber dotted lines, respectively. Specific energy values for commercially-available 700-bar hydrogen storage systems, future feasible liquid hydrogen storage tanks (no balance of plant components), and hydrogen alone (no tank or storage balance of plant components) are shown by the horizontal green, amber, and red dashed lines, respectively. A 1:1 mass ratio between HFC and ICE variants is shown by each vehicle platform's line. Points A and B show two possible combinations of technology levels that would enable all HFC variants to have equivalent or improved characteristics for PWR (or TWR), range, and mass compared to existing ICE vehicles. (b) is the same as Fig. 6(a).

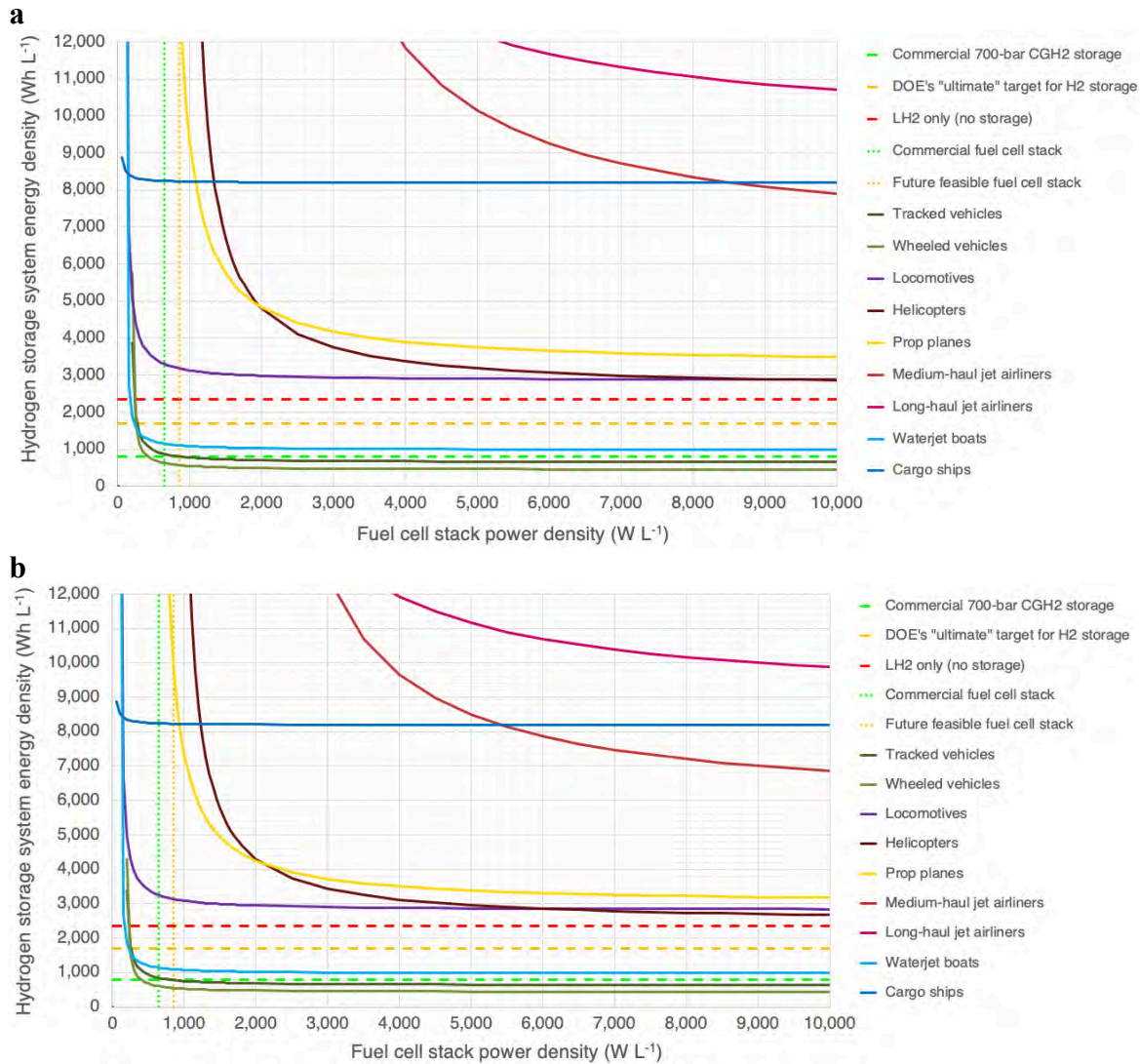


**Fig. S.103. Competition between hydrogen storage system energy density and fuel cell stack power density requirements for a 1:1 volume ratio (equivalent volume) between HFC and ICE variants for each individual vehicle platform using an electric motor PWR of 3 kW kg<sup>-1</sup> (a) and 15 kW kg<sup>-1</sup> (b).**

Calculations are based on the requirement for HFC variants to have the same PWR (or TWR) and range as existing ICE vehicles. Power density values for commercially-available integrated fuel cell stack system (with balance of plant components) and future feasible fuel cell stacks are shown by the vertical green and amber dotted lines, respectively. Energy density values for commercially-available 700-bar hydrogen storage systems, the DOE's "ultimate" target for electric vehicle hydrogen storage, and liquid hydrogen alone (no tank or storage balance of plant components) are shown by the horizontal green, amber, and red dashed lines, respectively. A 1:1 volume ratio between HFC and ICE variants is shown by each vehicle platform's line. Note that using just the volume budget for each vehicle platform defined by stripping out the existing fossil fuel system components, all aircraft, the locomotive, and cargo ships must become larger if converted to HFC variants. (b) is the same as Fig. 6(b).

## **2.C. Additional factors for transitioning FF/ICE vehicles to BE and HFC variants**

### **2.C.1. Vehicle platforms considered**

#### **2.C.1.A. Ground combat vehicles**

The Army classifies its vehicles as either “ground combat vehicles” or “non-tactical vehicles” (NTVs). All ground combat vehicles considered in this analysis are medium or heavy-duty by commercial standards (above 10,000 pounds GVW), whereas NTVs are classified as passenger, light trucks, medium trucks, trucks, or other [8]. In 2012, the Army had a total of ~300,000 ground combat vehicles and ~200,000 NTVs [8]. In recent years, the Army has made significant advancements in adopting measures to reduce fossil fuel consumption in its NTV fleet through its Vehicle Allocation Methodology/Vehicle Utilization Review Board process [385]. Under Executive Order 13693: Planning for Federal Sustainability in the Next Decade, the mandated FY 2025 cumulative goal for NTV fossil fuel reduction was 30%, and the Army had already achieved nearly 40% by FY 2017 [386–388]. Reducing fossil fuel consumption in the Army’s tactical vehicle fleet, however, has proved to be more difficult and related initiatives dominated the top five Operational Energy programs for FY 2018 [389]. The Army conducts combat vehicle modernization efforts to “solve the ‘combat vehicle challenge;’ that is, designing combat vehicles that protect Soldiers against threats and deliver precision lethality, while providing both tactical mobility and global responsiveness within the limitations of vehicle cost and weight” [390].

#### **2.C.1.B. Freight locomotive**

Railways are used to transport military vehicles from installations to port where they are shipped worldwide for deployments. House Resolution 3671, introduced in September 2017, calls for 80% of train rail lines and train engines to be electrified by 2027 and 100% by 2035 [391]. Still, BE locomotives are nothing new. The first known battery locomotive was built by Robert Davidson of Aberdeen, United Kingdom in 1837 [392]. Through the years, battery electric locomotives have been used in applications where exhaust from diesel is a problem, such as in underground mines or other enclosed spaces [393]. However, their widespread use was never adopted due to higher costs, heavier platforms, shorter range, and the need for recharging stations. As battery technology improves and becomes more mainstream through the manufacture of other battery electric platforms like automobiles, it is likely that these challenges will be overcome. Our analysis considered the General Electric (GE) ET44AC model locomotive designed to meet the EPA’s Tier 4 emissions standards. The naming convention stands for Evolution Series Tier 4, 4400 HP, AC traction [61].

#### **2.C.1.C. Aircraft**

The Army has both rotary- and fixed-wing aircraft. In 2007, the Congressional Budget Office reported that the United States would spend approximately \$3.3 billion annually through 2030 to modernize its rotary-wing fleet of over 3,500 aircraft [394]. In 2014, the Army’s fixed-wing fleet consisted of ~340 aircraft of 16 different designs and 35 variants [395].

### **2.C.1.D. Watercraft**

In World War II, the US Army had a total of over 127,800 watercraft – more than the US Navy [396]. Since then, that number has decreased significantly, but the Army still maintains numerous watercraft ranging from inflatable Zodiacs with outboard motors to the General Frank S. Besson class Logistics Support Vessel (LSV) with over 4,200 tons displacement [397]. In 2011, the Army had 76 large, named vessels to include six floating cranes, 16 small tugs, 11 large tugs, 35 Landing Craft Utility (LCU), and eight LSVs [398]. Consequently, watercraft are still an important part of the overall Army vehicular fleet.

### **2.C.2. Longevity**

The expected useful life of a vehicle is an important factor when considering the management of vehicle fleets. The Army, via appropriated funding from Congress, continuously embarks upon a fleet modernization program that introduces new capabilities by either replacing or significantly upgrading identified vehicle platforms [394]. Electric motors are very durable, however, and can outlast traditional ICEs as well as other components of all-electric variants. For BE variants, the batteries themselves become the new limiting factor. Batteries can last 1,500 to 3,000 cycles before losing 20% of their capacity with 5,000 to >10,000 cycles expected by 2030; thus, researchers conclude that a BE vehicle with a range of 450 km can have a useful life of ~450,000 to 1,350,000 km [399]. If batteries are made to be swappable as technology continues to improve, this could significantly extend the useful life of vehicles, keeping them in use longer and significantly reducing the time they are removed from the field for upgrades or repairs.

Some vehicle platforms included in this study are completely new, fully replacing former platforms. Others have been in use for decades and continue to receive upgrades. The average date of entry for the baseline vehicle type included in this study is 1985, illustrating that the Army tends to make incremental improvements and upgrades to its fleet rather than frequently adopt completely new platforms.

### **2.C.3. Fleet modernization**

The Army requires a modern fleet of combat vehicles capable of being deployed worldwide, maneuvered across a wide variety of terrain, and sustained with a ready and reliable source of fuel. Modernized vehicles should have improved capabilities, and the logistics required to maintain and operate new vehicles should be less burdensome than today. The Defense Advanced Research Projects Agency “envisions tomorrow’s land vehicle as one with a 50% reduction in weight, 50% reduction in crew requirements, 100% increase in speed, and a reduced vehicle signature. The vehicle would also be able to maneuver in 95% of terrain” [400]. The Next-Generation Combat Vehicle and Future Vertical Lift are two modernization programs currently underway in the Army [401].

### **2.C.4. Safety**

Tactical vehicle rollovers are a concern in the Army, especially as they are used in rough, off-road terrain. To help prevent rollovers, the center of gravity can be lowered, which has already been done by manufacturers of commercial BE cars by placing batteries low to the ground. We recommend research into the safety of batteries, to include potential blast

attenuation and fire retardation by their cooling structure, as battery placement within ground combat vehicles may be able to help protect occupants.

Critics of hydrogen claim that material handling safety is an unknown, but over 100 hydrogen-powered forklifts have been in use in Defense Logistics Agency distribution warehouses since 2009 [402]. Their success, along with over 700 forklifts cost-shared through the Department of Energy's Program Record #17003, led to more than 15,800 additional hydrogen-fueled forklift orders from industry [403]. In a period of just three years, between 2009 and 2012, the DOE-sponsored forklifts alone logged 1.25 million hours of operation using 140,000 kg of hydrogen dispensed over nearly 200,000 safe refueling occurrences [404]. Furthermore, studies have shown that punctures to fuel tanks are safer on HFC variants than traditional FF/ICE vehicles. One study compared an HFC vehicle and a gasoline vehicle; the HFC vehicle leaked 3.4 pounds of hydrogen (~175,000 BTU) and the gasoline vehicle leaked five pints of gas (~70,000 BTU) before both were ignited [405]. Because hydrogen is much lighter than the surrounding atmosphere, the flame shot straight up, and the vehicle itself was not damaged. The gasoline, however, spread, and the car was consumed.

### **2.C.5. Vehicle size and weight**

Whereas, in the clean energy economy, it may be acceptable for BE or HFC vehicles to be heavier than FF/ICE vehicles, adding mass to ground combat vehicles is more complicated. We already discussed NATO's MLC system of standards for classifying safe loads on roads and bridges (see Section 1.C.1.A.1.A). Army vehicles have a wide range of weights, from ~1 to ~70 tons [406,407]. Adding mass to ground combat vehicles reduces capability because it limits the terrain, roadways, and bridges that vehicles can traverse, to include combat bridges within the Army's own inventory. Similarly, adding either mass or volume to ground combat vehicles reduces their worldwide deployability. Increasing the volume of ground combat vehicles makes maneuverability more difficult (especially in urban terrain) and decreases the capability for deployment worldwide by reducing the loading capacity per sea vessel, aircraft, or truck trailer.

Vehicle mass and volume are also important to the other vehicle types. Freight locomotive design is constrained by railway infrastructure, like tunnel size, track separation, and track ballast maintenance requirements. Heavier airplanes may cause quicker degradation of airfields, and larger airplanes may not fit within tight passenger terminal areas. Making watercraft heavier displaces more water, which increases the wetted surface area of the hull and increases the force required to propel the vessel through the water. Additionally, if the vessel becomes heavier than the weight of the volume of water it displaces, it will sink.

### **2.C.6. Energy storage limitations**

A significant benefit of FF is its ability to conform to the shape of its container. When transitioning to BE or HFC vehicles, energy storage may have further challenges. For example, HFC airplanes will likely need to use cylindrical or spherical tanks in order to maximize storage density efficiency, but this may preclude storing fuel in the wings. Efficient hydrogen storage would likely require a large tank that extends along the length of the fuselage or several tanks fore and aft of the cabin [408]. Energy storage limitations for BE airplanes is also challenging, so designers are staying focused on short- to medium-distance flights with few passengers. Alice, by Eviation, is designed to carry nine passengers with a range up to 1,000 km using a 900 kWh lithium-ion battery pack [409]. Zunum Aero (backed by Boeing and Jet Blue) promise to deliver a 12-passenger, 700-mile range plane by 2022 using ducted electric fans and batteries



followed by a 50-passenger, 1,000-mile aircraft, with 40% reduction in runway length, 75% reduction in noise, and 80% reduction in emissions [221].

Another example of current challenges with energy storage is with large watercraft and long-distance transport. China has already launched a 2,000 metric ton BE ship (albeit to haul coal along the Pearl River), but it is limited to 80 km of travel after two hours of charging [410,411]. Japan plans to launch a zero-emission BE tanker by mid 2021, but its use will be for coastal operations within Tokyo Bay [412]. HFC ships are also of interest. Viking Cruises announced in 2017 that it plans to build the world's first cruise ship fueled by liquid hydrogen and fuel cells [413]. The German Navy built a submarine using PEMFCs that has an underwater range of 12,000 nm over 50 days at 10 knots [414].

### **2.C.7. Other vehicle energy requirements**

Our analysis focuses on the main purpose of these transportation platforms – physical movement. However, many other onboard systems require power, such as night vision devices, radios, weapon systems, and other ancillary gear. The Army is already investigating the use of HFCs as an energy source for ground combat vehicles due to their relatively low operating temperature of ~70°C, silent operation, and relatively high overall system efficiency of near 50% [415]. In fact, fuel cells have recently been investigated to allow for operations in “silent watch” where the vehicle engine is off and all ancillary equipment is powered through the fuel cell [416]. Low operating temperatures and noise reduction help not just with efficient operation but also reduce an adversary's ability to locate, track, target, and destroy vehicles. Additionally, future vehicle-to-grid possibilities may prove especially useful for forward operating bases and may influence BE and/or HFC designs.

### **2.C.8. Cost**

Fueling the Army's tactical vehicles is costly, especially when considering the “fully burdened cost” of fuel, which is defined in 10 U.S.C. § 2922h as “the commodity price of the fuel plus the total cost of all personnel and assets required to move and, when necessary, protect the fuel from the point at which the fuel is received from the commercial supplier to the point of use” [417].

### **2.C.9. Energy infrastructure**

Interest is growing for a new energy infrastructure built upon sources of renewable energy. This is due to a variety of reasons, ranging from achieving energy security to building the economy to reducing carbon emissions. Today, there are multiple proposed resolutions and bills in Congress calling for a transition to some variation of 100% renewable energy within specified timelines. Variations are defined by key words. For example, “clean” excludes polluting renewables to include the burning of biofuels, and “renewable” excludes two types of “zero-carbon emission” technologies – nuclear power and the burning of fossil fuels with carbon capture. The requirement for clean, renewable energy is the most restrictive of portfolio goals currently being considered by legislative bodies; consequently, this study considers vehicle systems that could support a 100% clean, renewable energy infrastructure.

## 2.C.10. Quantifying environmental improvements from potential greenhouse gas emission reductions

U.S. Army vehicle emissions result from both combat vehicles and non-tactical vehicles (NTVs). Combat vehicles include all types of vehicles used for operational missions or training purposes. They include tracked and wheeled ground vehicles, rotary- and fixed-wing aircraft, and both cargo ships and smaller boats. NTVs are used in and around the U.S. Army's permanent bases for day-to-day business and include all sedans; passenger vans; sport-utility vehicles (SUVs); light-, medium-, and heavy-trucks; ambulances; buses; and other vehicles. In order to estimate the magnitude of U.S. Army vehicle tailpipe emissions and its impact on climate, we use mobile combustion emissions factors published by the U.S. Environmental Protection Agency (EPA) and The Climate Registry, focusing on the three major greenhouse gases from emissions: carbon dioxide, CO<sub>2</sub>; methane, CH<sub>4</sub>; and nitrous oxide, N<sub>2</sub>O [21,22,418].

### 2.C.10.A. Combat vehicles

Due to the lack of available data on operational fuel consumption in the military, several assumptions are necessary to conduct this analysis. We explain these assumptions, why they are necessary, and why our assumed values are reasonable.

First, there is a lack of published data on the specific end-use consumption of operational energy fuels for the Department of Defense (DOD). This analysis uses the DOD's Annual Operational Energy Reports to the U.S. Congress from 2007 to 2019, in which the number of millions of barrels of fuel are reported by service branch [23]. As can be seen in Table S.40, the annual consumption of fuel is highly dependent upon operational requirements and can fluctuate significantly.

**Table S.40. Annual “barrels of fuel” consumed for U.S. Army operational energy.**

<b>Fiscal Year</b>	<b>Barrels Fuel (millions)</b>
2019	9.0
2018	9.2
2017	7.6
2016	7.1
2015	7.3
2014	10.1
2013	12.7
2012	16.1
2011	20.2
2010	19.0
2009	18.7
2008	19.9
2007	17.9

Data from DOD [23].

Second, the breakdown for how this operational fuel is consumed is not reported beyond the service branch divisions (i.e., to levels below the Department of the Army, Department of the Air Force, or the Department of the Navy). However, in 2008, a *Report of the Defense Science*

*Board Task Force on DOD Energy Strategy: “More Fight – Less Fuel”* reported operational energy fuel use specific to the U.S. Army for various vehicle categories under both “Peacetime OPTEMPO” and “Wartime OPTEMPO,” where OPTEMPO is the abbreviation for “Operations Tempo” [419]. The U.S. Army has experienced continuous deployments from 2001 to 2021, but, as reflected in Table S.40, there can be significant differences in DOD fuel consumption from year to year as the level of wartime activity fluctuates. Because we cannot predict whether future years will see higher or lower level of U.S. Army operations worldwide, we use this data to calculate an average operational fuel consumption by domain, as shown in Table S.41, taking a simple average between the wartime and peacetime OPTEMPOs. Because the Defense Science Board Task Force did not fully define their vehicle categories such as “combat vehicles” and “tactical vehicles,” we make a necessary assumption to estimate the percentage of fuel that goes to watercraft, which includes large cargo ships used to transport equipment across oceans. We use this average breakdown in our analysis of the past 13 years’ worth of data, electing not to arbitrarily declare definitions for wartime or peacetime OPTEMPOs. After conducting a sensitivity analysis of our results, we believe this is an adequate assumption. The resulting 20- and 100-year Global Warming Potential (GWP) of emissions using wartime and peacetime OPTEMPO percentages is just ~0.1% higher and ~0.1% lower, respectively, than results using averaged percentages.

**Table S.41. Approximate breakdown of operational vehicle fuel use by domain with an average between Peacetime and Wartime OPTEMPOs**

<b>Domain</b>	<b>Peacetime OPTEMPO</b>	<b>Wartime OPTEMPO</b>	<b>Average</b>
Land	31%	47%	39%
Air	65%	48%	57%
Sea	4%	5%	4%

Third, the actual fuel used by vehicle platforms may differ. The U.S. Army uses a single-fuel standard in order to simplify resupply logistics on the battlefield, and the vast majority of diesel engines use JP-8, which is a lighter distillate mix than diesel and is similar to kerosene. For CO<sub>2</sub> emissions, the EPA publishes values for both “kerosene-type jet fuel” and diesel fuel. Although most U.S. Army ground vehicle engines can burn either JP-8 or diesel, we elect to use the lower CO<sub>2</sub> emissions values for kerosene-type jet fuel in order to have a more conservative result than what diesel emission factors would produce. For CH<sub>4</sub> and N<sub>2</sub>O, the EPA publishes values for ground vehicles using gasoline, diesel, methanol, ethanol, compressed natural gas (CNG), liquefied petroleum gas (LPG), and biodiesel, but not kerosene or jet fuel; therefore, we use the EPA’s diesel emission factors for these two greenhouse gases for all ground vehicles. The EPA does publish CH<sub>4</sub> and N<sub>2</sub>O emissions factors for turbine-engine aircraft using jet fuel, which we use for both rotary- and fixed-wing aircraft. For cargo ships, we assume the use of marine residual fuel oil; for smaller boats, we assume the use of diesel. We further assume a 50-50 split in fuel requirements between those two types of watercraft (the Army uses many types of smaller boats, to include those used to support the emplacement of floating bridges over rivers and lakes). Until such divisions in fuel use are measured and recorded in more detail, these assumptions remain necessary to complete this analysis.

Using these assumptions, we can take our estimates for operational fuel use across the land, air, and sea domains and apply published emissions factors from the EPA and The Climate

Registry to calculate vehicle emissions of CO<sub>2</sub>, CH<sub>4</sub>, and N<sub>2</sub>O by-year and quantify the total amount of operational vehicle greenhouse gas emissions.

The first step is to take the barrels of fuel used by the U.S. Army each year and subtract out the estimated percentage of fuel that went to powering diesel generators at contingency bases to produce electricity. According to the Defense Science Board Task Force on DOD Energy Strategy, the average between Peacetime and Wartime OPTEMPOs suggests about 23% of total operational fuel consumption was by generators, with the remaining 77% going to combat vehicles of all types [419].

Then, we take the fuel used by all combat vehicles each year and, using the averages from Table S.41, calculate the barrels of fuel used by each major category of combat vehicles: ground vehicles, aircraft, and watercraft.

Next, for each major category of combat vehicles, we calculate the annual emissions of each greenhouse gas (GHG) (i.e., CO<sub>2</sub>, CH<sub>4</sub>, and N<sub>2</sub>O) according to the general formula shown by Eq. (S.597). Afterwards, we take the summation of each type of greenhouse gas emission across all vehicle categories by year.

**Eq. (S.597)**

$$\text{Emissions}_{\text{GHG, yr, vehicle category}} \left[ \frac{\text{tonne}}{\text{yr}} \right] = \text{Fuel Consumption}_{\text{yr, vehicle category}} \left[ \frac{\text{barrels}}{\text{yr}} \right] \cdot \left[ \frac{42 \text{ gal}}{\text{barrel}} \right] \cdot \text{Emission Factor}_{\text{fuel type, GHG}} \left[ \frac{\text{kg}}{\text{gal}} \right] \cdot \left[ \frac{10^{-6} \text{ tonne}}{\text{g}} \right] \cdot \left[ \frac{1,000 \text{ g}}{\text{kg}} \right]$$

**2.C.10.B. Non-tactical vehicles**

Data for fuel consumption from U.S. Army non-tactical vehicles are largely from the General Services Administration’s (GSA’s) annual Federal Fleet Report [24]. We recorded data from 2011 to 2019 Federal Fleet Reports from Tab 2-1 (Worldwide Number of Vehicles), Tab 4-1 (Worldwide Number of Miles), and Tab 5-1 (Worldwide Fuel Consumption). The GSA publishes these data with subdivisions by vehicle type and fuel type. One note: the GSA subdivides the U.S. Army’s vehicles into “Department of Army” and “Corps of Engineers, Civil Works” vehicles, which must be summed in order to get the total annual data for all Department of the Army NTVs.

The analysis for NTVs also requires several assumptions. First, we neglect data for low speed electric vehicles (LSEVs) and electric vehicles (EVs). We assume that, if the U.S. Army were to use clean, renewable energy, then there would already be zero greenhouse gas emissions from these vehicle types. Second, the EPA publishes emissions factors for CH<sub>4</sub> and N<sub>2</sub>O from on-road vehicles by fuel type and vehicle year with lower emissions from newer vehicles. We assume that all vehicles used by the U.S. Army in a year are that model year’s vehicles (i.e., we assume a completely new fleet of vehicles each year, which therefore underestimates total emissions). Third, we calculate an estimate for biodiesel (B20) emissions by using weighted EPA values for B100 (20%) and diesel (80%). Forth, we assume all hydrogen is used in fuel cells (as opposed to being combusted), so has zero emissions, and that the hydrogen is produced using electrolysis powered by clean, renewable electricity. Fifth, we can use EPA values to calculate CO<sub>2</sub> emissions directly from the total emissions by fuel type from the Federal Fleet

Report (Eq. (S.598)), but to use the EPA’s emission factors for CH<sub>4</sub> and N<sub>2</sub>O requires knowledge of both the fuel and vehicle type. Since this relationship is unknown, we must assume a breakdown for gasoline and diesel fuels across vehicle types and use weighted averages along with Eq. (S.599) to find the total emissions for CH<sub>4</sub> and N<sub>2</sub>O. Across the total U.S. Army NTV fleet, we assume that sedans, passenger vans, SUVs, and light trucks use gasoline; heavy trucks and buses use diesel; medium truck miles are 50% from gasoline and 50% from diesel; and ambulance miles are 25% gasoline and 75% diesel. Although different fuel types result in different emissions (e.g., using CNG results in higher CH<sub>4</sub> emissions and lower N<sub>2</sub>O emissions than gasoline or diesel) the impact is very small in this analysis. In fact, summing all gasoline gallon equivalent fuel consumption from B100, CNG, LNG, and LPG results in, on average over all years considered, one-hundredth of one percent of all annual U.S. Army gasoline gallon equivalent fuel consumption. Furthermore, all “alternative” fuels, which include biodiesel (B20 and B100), compressed natural gas, electricity, ethanol (E-85), liquefied natural gas, and hydrogen, are still just 3% to 5% of total gasoline gallon equivalent fuel consumption. Even after applying their higher global warming potentials, the combined effect of CH<sub>4</sub> and N<sub>2</sub>O is still less than 1% of the overall GWP in terms of CO<sub>2</sub>e for U.S. Army NTV greenhouse gas emissions. Consequently, we believe these assumptions are necessary, reasonable, and, likely, result in a conservative estimate for overall greenhouse gas emissions.

**Eq. (S.598)**

$$\text{CO}_2 \text{ Emissions}_{\text{yr}} \left[ \frac{\text{tonne}}{\text{yr}} \right] = \text{Worldwide Fuel Consumption}_{\text{yr, fuel type}} \left[ \frac{\text{gal}}{\text{yr}} \right] \\ \cdot \text{Emission Factor}_{\text{fuel type}} \left[ \frac{\text{kg CO}_2}{\text{gal}} \right] \cdot \left[ \frac{10^{-6} \text{tonne}}{\text{g}} \right] \cdot \left[ \frac{1,000\text{g}}{\text{kg}} \right]$$

**Eq. (S.599)**

$$\text{Emissions (CH}_4 \text{ or N}_2\text{O)}_{\text{yr, fuel type}} \left[ \frac{\text{tonne}}{\text{yr}} \right] = \text{Worldwide Miles}_{\text{yr, vehicle type}} \left[ \frac{\text{miles}}{\text{yr}} \right] \\ \cdot \text{Emission Factor (CH}_4 \text{ or N}_2\text{O)}_{\text{yr, fuel type}} \left[ \frac{\text{g}}{\text{mile}} \right] \cdot \left[ \frac{10^{-6} \text{tonne}}{\text{g}} \right]$$

### **2.C.10.C. Total U.S. Army vehicle greenhouse gas emissions**

At this point, we have estimated the total combat vehicle emissions and total NTV vehicle emissions, in tonnes/yr of CO<sub>2</sub>, CH<sub>4</sub>, and N<sub>2</sub>O. We next sum these numbers to find the total U.S. Army vehicle emissions. We further calculate the 20- and 100-yr global warning potentials with and without, climate-carbon feedback (see Table S.42) [25].

**Table S.42. 20- and 100-yr GWPs to derive CO<sub>2</sub>e**

Greenhouse Gas		Global Warming Potential			
		20-yr		100-yr	
		No cc fb	With cc fb	No cc fb	With cc fb
Carbon Dioxide	CO <sub>2</sub>	1	1	1	1
Methane	CH <sub>4</sub>	84	86	28	34
Nitrous Oxide	N <sub>2</sub> O	264	268	265	298

Data from UNFCCC [25]; cc fb is “climate-carbon feedback.”

The generalized equation for calculating annual global warming potential (GWP) in terms of CO<sub>2</sub>e is given by Eq. (S.600).

**Eq. (S.600)**

$$\begin{aligned}
 \text{Total GWP}_{\text{yr}} & \left[ \frac{\text{megatonne CO}_2\text{e}}{\text{yr}} \right] \\
 & = \left[ \frac{10^{-6} \text{ megatonne}}{\text{tonne}} \right] \\
 & \cdot \left( \text{CO}_2 \text{ Emissions}_{\text{yr}} \left[ \frac{\text{tonne}}{\text{yr}} \right] \cdot \text{GWP} \left[ \frac{\text{unit CO}_2\text{e}}{\text{unit CO}_2} \right] + \text{CH}_4 \text{ Emissions}_{\text{yr}} \left[ \frac{\text{tonne}}{\text{yr}} \right] \right. \\
 & \left. \cdot \text{GWP} \left[ \frac{\text{unit CO}_2\text{e}}{\text{unit CH}_4} \right] + \text{N}_2\text{O Emissions}_{\text{yr}} \left[ \frac{\text{tonne}}{\text{yr}} \right] \cdot \text{GWP} \left[ \frac{\text{unit CO}_2\text{e}}{\text{unit N}_2\text{O}} \right] \right)
 \end{aligned}$$

If all U.S. Army vehicles are transitioned to either battery electric or hydrogen fuel cell technology, then all of these calculated tailpipe greenhouse gas emissions can be eliminated. To put such results into relative terms for comparison, we use the EPA’s published value of 4.6 tonne/yr CO<sub>2</sub>e for typical passenger car emissions in the U.S.[26] Dividing results from Eq. (S.600) by this value reveals the impact of such a transition in equivalent terms of the number of typical passenger cars taken off the road in a year (Eq. (S.601)).

**Eq. (S.601)**

$$\begin{aligned}
 \text{Equivalent U. S. Passenger Cars Taken Off the Road} & \left[ \frac{\text{cars}}{\text{yr}} \right] \\
 & = \frac{\text{Total GWP}_{\text{yr}} \left[ \frac{\text{megatonne CO}_2\text{e}}{\text{yr}} \right]}{4.6 \left[ \frac{\text{tonne CO}_2\text{e}}{\text{car}} \right] \cdot \left[ \frac{10^{-6} \text{ megatonne}}{\text{tonne}} \right]}
 \end{aligned}$$

## REFERENCES

- [1] Vavrin J. Power and Energy Considerations at Forward Operating Bases (FOBs). Champaign, IL: USACE, ERDC, CERL; 2010.
- [2] Nicholson M, Stepp M. Lean, Mean, and Clean II: Assessing DOD Investments in Clean Energy Innovation 2012.
- [3] Jones-Bonbrest N. Army to Deliver Fuel-Efficient Generators to Afghanistan. US Army 2012.  
[https://www.army.mil/article/81578/army\\_to\\_deliver\\_fuel\\_efficient\\_generators\\_to\\_afghanistan](https://www.army.mil/article/81578/army_to_deliver_fuel_efficient_generators_to_afghanistan) (accessed August 20, 2018).
- [4] Davis SJ, Lewis NS, Shaner M, Aggarwal S, Arent D, Azevedo IL, et al. Net-Zero Emissions Energy Systems. *Science* (80- ) 2018;360.  
<https://doi.org/10.1126/science.aas9793>.
- [5] Earl T, Mathieu L, Cornelis S, Kenny S, Ambel CC, Nix J. Analysis of Long Haul Battery Electric Trucks in EU. *Eur Fed Transp Environ* 2018.
- [6] Marcinkoski J, Vijayagopal R, Kast J, Duran A. Driving an Industry: Medium and Heavy Duty Fuel Cell Electric Truck Component Sizing. *World Electr Veh J* 2016;8:78–89.
- [7] Lovins AB, Lovins LH, Hawken P. A Road Map for Natural Capitalism. *Harv Bus Rev* 1999;May-June.
- [8] Gerth R. US Army Sustainability Needs - NCMS Sustainability Conference. Ann Arbor, MI: 2012.
- [9] Winnefeld C, Kadyk T, Bensmann B, Krewer U, Hanke-Rauschenbach R. Modelling and Designing Cryogenic Hydrogen Tanks for Future Aircraft Applications. *Energies* 2018;11:1–23. <https://doi.org/10.3390/en11010105>.
- [10] Kadyk T, Winnefeld C, Hanke-Rauschenbach R, Krewer U. Analysis and Design of Fuel Cell Systems for Aviation. *Energies* 2018;11:375. <https://doi.org/10.3390/en11020375>.
- [11] Ozpineci B. Annual Progress Report for the Electric Drive Technologies Program. Oak Ridge, TN: 2016.
- [12] Proterra. Proterra to Power North America’s First Electric Double Deck Transit Bus 2018. <https://www.proterra.com/press-release/global-double-deck-bus-market-leader-alexander-dennis-selects-proterra-to-power-north-americas-first-electric-double-deck-transit-bus/> (accessed August 23, 2018).
- [13] Department of Energy. US DRIVE Hydrogen Storage Technical Team Roadmap. 2017.
- [14] Department of Energy. US DRIVE Fuel Cell Technical Team Roadmap. 2017.
- [15] Department of Energy. US DRIVE Fuel Cell Technical Team Roadmap. 2013.
- [16] Moreels D, Leijnen P. High Efficiency Axial Flux Machines 2018.
- [17] Department of Energy. US DRIVE - Electrochemical Energy Storage Technical Team Roadmap. 2017.
- [18] United States Advanced Battery Consortium. Goals for Advanced Batteries for EVs - CY 2020 Commercialization. USCAR Website Energy Storage Syst Goals 2018.  
[http://www.uscar.org/commands/files\\_download.php?files\\_id=364](http://www.uscar.org/commands/files_download.php?files_id=364) (accessed August 23, 2018).
- [19] Department of Energy. Technical Targets for Fuel Cell Systems and Stacks for Transportation Applications 2019. <https://www.energy.gov/eere/fuelcells/doe-technical-targets-fuel-cell-systems-and-stacks-transportation-applications> (accessed May 3, 2019).
- [20] Kane M. Sion Power – Production of Breakthrough 500 Wh/kg Cell Starts this Year. *InsideEVs* 2018. <https://insideevs.com/sion-power-says-itll-start-production-of->

- breakthrough-500-whkg-cell-later-this-year/ (accessed April 18, 2019).
- [21] Environmental Protection Agency. Emission Factors for Greenhouse Gas Inventories 2020.
- [22] Environmental Protection Agency. Greenhouse Gas Inventory Guidance: Direct Emissions from Mobile Combustion Sources 2016.
- [23] Department of Defense. Annual Operational Energy Reports. Off Assist Secr Def Sustain 2020. [https://www.acq.osd.mil/eie/OE/OE\\_library.html](https://www.acq.osd.mil/eie/OE/OE_library.html) (accessed February 28, 2021).
- [24] General Services Administration. Vehicle Management Library. Fed Fleet Reports 2019. <https://www.gsa.gov/policy-regulations/policy/vehicle-management-policy/vehicle-management-library> (accessed February 28, 2021).
- [25] Myhre G, Shindell D, Bréon F-M, Collins W, Fuglestedt J, Huang J, et al. Anthropogenic and Natural Radiative Forcing. In: Stocker TF, Qin D, Plattner G-K, Tignor M, Allen SK, Boschung J, et al., editors. *Clim. Chang. 2013 Phys. Sci. Basis Contrib. Work. Gr. I to Fifth Assess. Rep. Intergov. Panel Clim. Chang.*, Cambridge, UK: Cambridge University Press; 2013.
- [26] Environmental Protection Agency. Greenhouse Gas Emissions from a Typical Passenger Vehicle 2018. <https://www.epa.gov/greenvehicles/greenhouse-gas-emissions-typical-passenger-vehicle> (accessed February 28, 2021).
- [27] Magnax. Breakthrough Motor Technology for Electric Vehicles 2019. <https://www.magnax.com> (accessed May 1, 2019).
- [28] Faïd S. A Highly Efficient Two Speed Transmission for Electric Vehicles. EVS28 Int Electr Veh Symp Exhib 2015.
- [29] Chavdar B. Multi-Speed Transmission for Commercial Delivery Medium Duty Plug-In Electric Drive Vehicles. Eaton Corporation; 2016.
- [30] Eaton. Electric Vehicle 2-Speed Transmission 2016.
- [31] Janek J, Zeier WG. A Solid Future for Battery Development. *Nat Energy* 2016;1:16141. <https://doi.org/10.1038/nenergy.2016.141>.
- [32] SolidEnergy. Hermes™ High Energy Rechargeable Metal Cells for Space 2017. [http://assets.solidenergysystems.com/wp-content/uploads/2017/09/08171937/Hermes\\_Spec\\_Sheet1.pdf](http://assets.solidenergysystems.com/wp-content/uploads/2017/09/08171937/Hermes_Spec_Sheet1.pdf) (accessed April 18, 2019).
- [33] Solid Power. The Promise and Challenge of Scaling Lithium Metal Batteries 2019. <http://solidpowerbattery.com/solid-state-101/CONTACT> (accessed April 18, 2019).
- [34] Fan Y, Chen X, Legut D, Zhang Q. Modeling and Theoretical Design of Next-Generation Lithium Metal Batteries. *Energy Storage Mater* 2019;16:169–93. <https://doi.org/10.1016/j.ensm.2018.05.007>.
- [35] Weinrich H, Come J, Tempel H, Kungl H, Eichel R, Balke N. Nano Energy Understanding the Nanoscale Redox-Behavior of Iron-Anodes for Rechargeable Iron-Air Batteries. *Nano Energy* 2017;41:706–16. <https://doi.org/10.1016/j.nanoen.2017.10.023>.
- [36] Julich F. Iron-Air Batteries Promise Higher Energy Density Than Lithium-Ion Batteries. *SciTechDaily* 2019. <https://scitechdaily.com/iron-air-batteries-promise-higher-energy-density-than-lithium-ion-batteries/> (accessed February 6, 2019).
- [37] Department of Energy. US DRIVE - Target Explanation Document: Onboard Hydrogen Storage for Light-Duty Fuel Cell Vehicles. 2017.
- [38] Thirkell A, Chen R, Harrington I. A Fuel Cell System Sizing Tool Based on Current Production Aircraft. SAE Aerosp Congr Exhib 2017 2017. <https://doi.org/10.4271/2017-01-2135>.



- [39] National Fuel Cell Research Center. Hybrid Fuel Cell / Gas Turbine Systems Proton Exchange Membrane Fuel Cell (PEMFC) 2004.
- [40] Toyota. 2018 Mirai 2018. [https://ssl.toyota.com/mirai/assets/modules/carpagewhatworks/Docs/MY18\\_Mirai\\_eBrochure\\_FuelCellTech.pdf](https://ssl.toyota.com/mirai/assets/modules/carpagewhatworks/Docs/MY18_Mirai_eBrochure_FuelCellTech.pdf) (accessed September 13, 2018).
- [41] REN21. Global Status Report 2019 2019. [https://www.ren21.net/gsr-2019/tables/table\\_06/table\\_06/](https://www.ren21.net/gsr-2019/tables/table_06/table_06/) (accessed August 13, 2019).
- [42] RE100. 164 companies have made a commitment to go “100% renewable” 2019. <http://there100.org/companies> (accessed February 18, 2019).
- [43] Sierra Club. 100% Commitments in Cities, Counties, and States 2020. <https://www.sierraclub.org/ready-for-100/commitments> (accessed April 22, 2020).
- [44] 114th United States Congress. H. Res. 540 - House Simple Resolution. United States of America: 2015.
- [45] 114th United States Congress. S. Res. 632 - Senate Simple Resolution. United States of America: 2016.
- [46] 115th United States Congress. S. 987 - Senate Bill - “100 by '50 Act.” United States of America: 2017.
- [47] 115th United States Congress. H.R. 3314 - House Bill - “100 by '50 Act.” United States of America: 2017.
- [48] 115th United States Congress. H.R. 3671 - House Bill - “Off Fossil Fuels for a Better Future Act.” United States of America: 2017.
- [49] 116th United States Congress. H.R.330 - House Bill - “Climate Solutions Act of 2019.” United States of America: 2019.
- [50] 116th United States Congress. H. Res. 109 - House Simple Resolution - “Green New Deal.” United States of America: 2019.
- [51] 116th United States Congress. S. Res. 59 - Senate Simple Resolution - “Green New Deal.” United States of America: 2019.
- [52] 116th United States Congress. S.J. Res. 8 - Senate Joint Resolution - “Green New Deal.” United States of America: 2019.
- [53] Hoffrichter A, Miller AR, Hillmansen S, Roberts C. Well-to-Wheel Analysis for Electric, Diesel and Hydrogen Traction for Railways. *Transp Res Part D Transp Environ* 2012;17:28–34. <https://doi.org/10.1016/j.trd.2011.09.002>.
- [54] Datta A, Johnson W. Requirements for a Hydrogen Powered All-Electric Manned Helicopter. 12th AIAA Aviat Technol Integr Oper Conf 14th AIAA/ISSMO Multidiscip Anal Optim Conf 2012:1–28. <https://doi.org/10.2514/6.2012-5405>.
- [55] Brelje BJ, Martins JRRA. Electric, Hybrid, and Turboelectric Fixed-Wing Aircraft: A Review of Concepts, Models, and Design Approaches. *Prog Aerosp Sci* 2018:1–19. <https://doi.org/10.1016/j.paerosci.2018.06.004>.
- [56] Hepperle M. Electric Flight–Potential and Limitations. *Ger Aerosp Cent* 2012. <https://doi.org/10.14339/STO-MP-AVT-209>.
- [57] Brown G V., Kascak AF, Ebihara B, Johnson D, Choi BB, Siebert M, et al. NASA Glenn Research Center Program in High Power Density Motors for Aeropropulsion 2005:1–28. <https://doi.org/NASA/TM—2005-213800>.
- [58] Postiglione CS, Collier DAF, Dupczak BS, Heldwein ML, Perin AJ. Propulsion System for an All Electric Passenger Boat Employing Permanent Magnet Synchronous Motors and Modern Power Electronics. *Electr Syst Aircraft, Railw Sh Propulsion, ESARS* 2012.

- <https://doi.org/10.1109/ESARS.2012.6387441>.
- [59] van Biert L, Godjevac M, Visser K, Aravind P V. A Review of Fuel Cell Systems for Maritime Applications. *J Power Sources* 2016;327:345–64.  
<https://doi.org/10.1016/j.jpowsour.2016.07.007>.
- [60] Department of the Army. Technical Manuals (1987 - 2018) 2018.
- [61] General Electric. GE Transportation - Locomotive Brochure.pdf 2016.
- [62] Haddock J. CE563: Airport Design - Aircraft Performance 2014.
- [63] Boeing. Airplane Characteristics for Airport Planning - 747. Chicago, Illinois: 2012.  
<https://doi.org/10.2307/2230120>.
- [64] United States Army Corps of Engineers. TI 850-02: Technical Instructions - Railroad Design and Rehabilitation 2000.
- [65] Martland CD. Introduction of Heavy Axle Loads by the North American Rail Industry. *Transp Res Forum* 2013;52:103–25.
- [66] Flugzeug. Boeing 737-700 2017.  
[http://www.flugzeuginfo.net/acdata\\_php/acdata\\_7377\\_en.php](http://www.flugzeuginfo.net/acdata_php/acdata_7377_en.php) (accessed March 27, 2019).
- [67] Boeing. Boeing 737: Airplane Characteristics for Airport Planning. Boeing Commercial Airplanes; 2005.
- [68] Bachand J-D. General Electric ES44AC. Diesel Shop 2007.  
<http://www.thedieselshop.us/Data/ES44AC.HTML> (accessed September 18, 2018).
- [69] Department of the Army. Army Regulation 70-12 - Fuels and Lubricants Standardization Policy for Equipment Design, Operation, and Logistics Support 2015.
- [70] Schmitigal J, Bramer J. JP-8 and Other Military Fuels (2014 Update) 2014.
- [71] Department of Defense. MIL-DTL-83133E: Detail Specification - Turbine Fuels, Aviation, Kerosene Types NATO F-34 (JP-8), NATO F-35, and JP-8+100 1999.
- [72] Energy Information Administration. Distillate Fuel Oil 2018.  
[https://www.eia.gov/tools/glossary/index.php?id=distillate fuel oil](https://www.eia.gov/tools/glossary/index.php?id=distillate%20fuel%20oil) (accessed September 19, 2018).
- [73] ExxonMobil. Jet A/ Jet A-1. Aviat Fuels 2018.  
<https://www.exxonmobil.com/en/aviation/products-and-services/products/jet-a-jet-a-1> (accessed December 3, 2018).
- [74] Burel F, Taccani R, Zuliani N. Improving Sustainability of Maritime Transport Through Utilization of Liquefied Natural Gas (LNG) for Propulsion. *Energy* 2013;57:412–20.  
<https://doi.org/10.1016/j.energy.2013.05.002>.
- [75] Bacha J, Freel J, Gibbs A, Gibbs L, Hemighaus G, Hoekman K, et al. Diesel Fuels Technical Review. 2007. <https://doi.org/10.1063/1.3575169>.
- [76] Environment Canada. Marine Diesel Fuel Oil 2018.
- [77] Department of Defense. SD-15: Guide for Performance Specifications 2009.
- [78] Lawicki D. Jet Fuel Characteristics 2002.
- [79] Wu P, Bucknall R. Marine Propulsion Using Battery Power. London, UK: 2016.
- [80] The Engineering Toolbox. Fuels - Higher and Lower Calorific Values 2003.  
[https://www.engineeringtoolbox.com/fuels-higher-calorific-values-d\\_169.html](https://www.engineeringtoolbox.com/fuels-higher-calorific-values-d_169.html) (accessed October 4, 2018).
- [81] Verstraete D. The Potential of Liquid Hydrogen for Long Range Aircraft Propulsion. Cranfield University, 2009.
- [82] McCormick S, Motzenbecker P, Clauson M. Passive Fuel Tank Inerting Systems for Ground Combat Vehicles. Warren, MI: 1988.

- [83] Alvarado PJ. Steel vs. Plastics: The Competition for Light-Vehicle Fuel Tanks. *JOM J Miner Met Mater Soc* 1996;48:22–5. <https://doi.org/10.1007/BF03222990>.
- [84] Aero Tech Laboratories. *ATL BallistiCoat Fuel Tanks* 2016. <http://atline.com/pdfs/Ballistic/balllit.pdf> (accessed August 29, 2018).
- [85] Kyle Bates. *Advances in Self-Sealing Fuel Tank Technology*. Def Syst Inf Anal Cent 2016. <https://www.dsiac.org/resources/journals/dsiac/summer-2016-volume-3-number-3/advances-self-sealing-fuel-tank-technology> (accessed August 29, 2018).
- [86] Kokkins S, Kwok P, Punwani SK, Tom Tsai N. Evaluating Locomotive Fuel Tank Safety And Crash Worthiness. *Am Soc Mech Eng Rail Transp Div RTD* 2002;22:1–12. <https://doi.org/10.1115/IMECE2002-33255>.
- [87] Gilissen B. Where is Fuel in a Passenger Aircraft Stored and What is the Typical Capacity? *Quora* 2015. <https://www.quora.com/Where-is-fuel-in-a-passenger-aircraft-stored-and-what-is-the-typical-capacity> (accessed October 19, 2018).
- [88] Defense Logistics Agency. *MIL-T-46786 - General Requirements for Tanks, Fuel, Engine* 2016.
- [89] British Plastics Federation. *High Density Polyethylene (HDPE)* 2018. <http://www.bpf.co.uk/plastipedia/polymers/HDPE.aspx> (accessed August 28, 2018).
- [90] ARM-R-COAT. *Self-Sealing Fuel Tank Coating* 2018. <https://fuelsafe.com/media/downloadable/ARM-R-COAT-White-Paper.pdf> (accessed August 29, 2018).
- [91] United States Congress. *United States Code of Federal Regulations (CRF), Title 49 – Transportation, Subtitle B – Other Regulations Relating to Transportation, Chapter II – Federal Railroad Administration, Department of Transportation, Part 238 – Passenger Equipment Safety Standards*. United States of America: 2002.
- [92] American Public Transportation Association. *APTA PR-CS-S-007-98, Rev. 1: Standard for Fuel Tank Integrity on Non Passenger Carrying Locomotives* 2001. <https://www.apta.com/resources/standards/Documents/APTA-PR-CS-S-007-98.pdf>.
- [93] The Engineering Toolbox. *Metals and Alloys - Densities* 2014. [https://www.engineeringtoolbox.com/metal-alloys-densities-d\\_50.html](https://www.engineeringtoolbox.com/metal-alloys-densities-d_50.html) (accessed September 19, 2018).
- [94] D’Antonio S. *Diesel Fuel Tank Design*. PassageMaker 2012. <https://www.passagemaker.com/technical/diesel-fuel-tank-design> (accessed July 30, 2018).
- [95] AZO Materials. *Aluminium Alloys - Aluminium 5083 Properties, Fabrication and Applications* 2005. <https://www.azom.com/article.aspx?ArticleID=2804> (accessed October 4, 2018).
- [96] General Electric. *GEJ-6915 Operating Manual: GEVO Evolution Series Diesel-Electric Locomotive ES44* 2018.
- [97] Spectrum. *The New General Electric GEVO-Engine for Tier2-Locomotive Application*. Spectrum 2004.
- [98] Safran. *CFM56 Technical Characteristics* 2019. <http://www.safran-aircraft-engines.com/commercial-engines/single-aisle-commercial-jets/cfm56/cfm56-5b> (accessed March 27, 2019).
- [99] Boeing. *Boeing 747-8* 2018. <https://www.boeing.com/commercial/747/> (accessed October 19, 2018).
- [100] General Electric Aviation. *GENx High Bypass Turbofan Engines* 2004.

- [101] European Aviation Safety Agency. Type-Certificate Data Sheet for GENx Engines 2018.
- [102] Barrington S. Detroit Diesel 8v92 Manuals and Specifications. Barringt Diesel Club 2018. <https://barringtondieselclub.co.za/detroit/8v92-detroit-diesel.html> (accessed August 30, 2018).
- [103] Caterpillar. C7 ACERT Industrial Engine Specifications 2012.
- [104] Oshkosh. FMTV Cargo 4x4 / 6x6 Brochure 2015.
- [105] Capital 135. CAT C7 Specs and Engine History 2017. <http://capitalremanexchange.com/cat-c7-specs-and-engine-history/> (accessed August 30, 2018).
- [106] Caterpillar. C7 300-350 2004.
- [107] Cummins. ISL9 450hp Engine 2009.
- [108] Cummins. QSL9 Engine Specifications 2015.
- [109] Cummins. ISL e Engines 2010.
- [110] Honeywell. T55 Turboshift Engine 2016.
- [111] General Electric Aviation. T700-701D 2014.
- [112] Pratt & Whitney. PT6A 2018. <https://www.pwc.ca/en/products-and-services/products/general-aviation-engines/pt6a> (accessed October 29, 2018).
- [113] MTU Aero Engines. GENx Turbofan Engine 2014.
- [114] Cummins. QSB6.7/QSB7 for Marine 2018. <https://www.cummins.com/engines/qs67qs7> (accessed October 2, 2018).
- [115] Progress Rail. EMD 710 Series Engines 2018.
- [116] Honeywell Aerospace. T55 Turboshift Engine 2005.
- [117] Tebbe P, Minnesota State University - Mankato. Military Tanks. Engag Thermodyn 2015. [http://cset.mnsu.edu/engagethermo/systems\\_tank.html](http://cset.mnsu.edu/engagethermo/systems_tank.html) (accessed August 29, 2018).
- [118] Thompson J. Amphibious Assault Vehicle - Military Power. Truck Trend 2009. <http://www.trucktrend.com/cool-trucks/0911dp-amphibious-assault-vehicle/> (accessed August 29, 2018).
- [119] WBPARTS. NSN 2815-01-290-1290 VTA-903T Technical Data 2016.
- [120] Army Guide. 6V53 Engine Specifications 2015. <http://www.army-guide.com/eng/product160.html> (accessed August 29, 2018).
- [121] General Services Administration. A-A-52624A - Commercial Item Description: Antifreeze, Multi-Engine Type 1997.
- [122] United States Army Tank Automotive Research Development and Engineering Center. POL Products Guide 2010.
- [123] Engine Factory. 350 Chevy Engine Dimensions 2018. <http://www.enginefactory.com/chevdimensions.htm> (accessed July 29, 2018).
- [124] General Motors - Electro-Motive Division. 645E3 Turbocharged Engine Maintenance Manual 1979.
- [125] Federal Aviation Administration. Type Certificate Data Sheet E00078NE: GENx-2B Engine 2016.
- [126] European Aviation Safety Agency. Type-Certificate Data Sheet for Pratt & Whitney PT6A Engines 2016.
- [127] Honeywell Aerospace. T55 Turboshift Engine 2018. <https://aerospace.honeywell.com/en/products/engines/t55-turboshift-engine> (accessed August 29, 2018).
- [128] Fehrm B. Fundamentals of Airliner Performance, Part 6; The Engine. Leeham News 2018.

- <https://leehamnews.com/2015/01/19/fundamentals-of-airliner-performance-part-6-the-engine/> (accessed October 19, 2018).
- [129] Raymer DP. Aircraft Design: A Conceptual Approach. Fourth. Reston, VA: American Institute of Aeronautics and Astronautics; 2006.
- [130] Wilkinson S. Do The Locomotion: 207 Tons and 4,400 hp. Pop Sci 2004.
- [131] Gibbon A. James Watt and the Revolution of Horsepower. Chron Horse 2011.
- [132] Noria Corporation. How to Choose the Right Engine Oil. Mach Lubr 2018. <https://www.machinerylubrication.com/Read/30197/choose-engine-oil> (accessed December 11, 2018).
- [133] Total. Oil Grades. Lubricants 2018. <https://www.lubricants.total.com/what-are-oil-grades> (accessed December 11, 2018).
- [134] Department of Defense. MIL-PRF-2104H: Performance Specification: Lubricating Oil, Internal Combustion Engine, Combat/Tactical Service 2004.
- [135] Department of Defense. MIL-PRF-23699F - Performance Specification: Lubricating Oil, Aircraft Turbine Engine, Synthetic Base 1997.
- [136] Canada Environmental Technology Centre. Lubricating Oil (Engine, Diesel Locomotive). 2001.
- [137] General Electric Aviation. GEnx Technical Manual Index 2018.
- [138] Safety-Kleen. Safety Data Sheet - MIL-PRF-2104G,H,J 15W-40 Oil 2015.
- [139] ExxonMobil. Mobil Jet Oil II 2017. <https://www.exxonmobil.com/english-US/Aviation/pds/GLXXMobil-Jet-Oil-II> (accessed December 11, 2018).
- [140] Shell. AeroShell Turbine Oil 500 Material Safety Data Sheet 2016.
- [141] Engineering ToolBox. Water - Density, Specific Weight and Thermal Expansion Coefficient. Eng ToolBox 2003. [https://www.engineeringtoolbox.com/water-density-specific-weight-d\\_595.html](https://www.engineeringtoolbox.com/water-density-specific-weight-d_595.html) (accessed August 29, 2018).
- [142] United States Geological Service. Water Density 2018. <http://water.usgs.gov/edu/density.html> (accessed September 19, 2018).
- [143] General Motors - Electro-Motive Division. Locomotive Instruction Manual 254: 5400 HP Diesel Freight Locomotive 1944.
- [144] San Juan International Inc. Material Safety Data Sheet: Antifreeze, Ethylene Glycol, Inhibited Coolant, CID A-A-52624 2018.
- [145] Army Guide. HMPT-500HP Transmission 2015. <http://www.army-guide.com/eng/product258.html> (accessed December 11, 2018).
- [146] Allison Transmission. Allison HT 740 Transmission Specification 2009. [http://www.messb.com.my/allison\\_HT740-HT750.html](http://www.messb.com.my/allison_HT740-HT750.html) (accessed August 31, 2018).
- [147] Allison Transmission. International Series 3700 2013. [https://www.allisontransmission.com/docs/default-source/specification-sheets/int3700\\_sa5343\(201306\)blk.pdf?sfvrsn=2](https://www.allisontransmission.com/docs/default-source/specification-sheets/int3700_sa5343(201306)blk.pdf?sfvrsn=2) (accessed August 31, 2018).
- [148] Allison Transmission. Allison 5th Gen Vocational Model Guide 2017 2017. [https://www.allisontransmission.com/docs/default-source/marketing-materials/sa7943en\\_-2017-vocational-model-guide\\_-vmg-lr9af07359281567eeb272ff0000a566aa.pdf?sfvrsn=13](https://www.allisontransmission.com/docs/default-source/marketing-materials/sa7943en_-2017-vocational-model-guide_-vmg-lr9af07359281567eeb272ff0000a566aa.pdf?sfvrsn=13) (accessed August 31, 2018).
- [149] TCI Auto. Automatic Transmission Dimensions - 4L80E 2012. <http://www.tciauto.com/tc/trans-dim/> (accessed August 31, 2018).
- [150] Melton Industries. MSS Reman HMMWV 4L80E Transmission, 2520-01-489-0849 2014. <https://www.meltons.com/product/mss-reman-hmmwv-4l80e-transmission/> (accessed

- August 31, 2018).
- [151] Allison Transmission. International Series 3000/3200 Transmission 2013.  
[https://www.allisontransmission.com/docs/default-source/specification-sheets/int3000\\_sa5341\(201306\)blk.pdf?sfvrsn=847fbf1c\\_2](https://www.allisontransmission.com/docs/default-source/specification-sheets/int3000_sa5341(201306)blk.pdf?sfvrsn=847fbf1c_2) (accessed August 9, 2018).
  - [152] Masson Marine. MM W20200 NR Reduction Gearbox 2018.
  - [153] Trans Atlantic Diesels Inc. Marine Propulsion Systems ZF 280-1 Transmission 2012.
  - [154] Allison Transmission. Allison X1100-3B Transmission 2013.  
[https://www.allisontransmission.com/docs/default-source/defense/11568\\_atm\\_sales\\_sheets\\_x1100-3b.pdf?sfvrsn=2](https://www.allisontransmission.com/docs/default-source/defense/11568_atm_sales_sheets_x1100-3b.pdf?sfvrsn=2) (accessed August 9, 2018).
  - [155] L3 Combat Propulsion Systems. HMPT 500/600HP Transmission 2018.  
[https://www2.l3t.com/cps/cps/hmpt\\_500\\_600hp.htm](https://www2.l3t.com/cps/cps/hmpt_500_600hp.htm) (accessed August 31, 2018).
  - [156] Mobil. Mobil 1 Synthetic Automatic Transmission Fluid 2017.
  - [157] Total. Data Sheet - ATF Dexron III 2012.
  - [158] Pennzoil. DEXRON® -III MERCON® Automatic Transmission Fluid 2001.
  - [159] Penrite. ATF DX-III (Mineral) 2018.
  - [160] Department of Defense. MIL-L-2104F Military Specification - Lubricating Oil, Internal Combustion Engine, Combat/Tactical Service 1992.
  - [161] Roshfrans. Product Data Sheet - Automotive Division - Transmission and Torque Fluids - Automatic Transmission Fluid Type DEXRON® II 2015.
  - [162] Engineering ToolBox. SAE Multigrade Oils - Viscosities and Densities. Eng ToolBox 2008. [https://www.engineeringtoolbox.com/sae-grade-oil-d\\_1208.html](https://www.engineeringtoolbox.com/sae-grade-oil-d_1208.html) (accessed December 11, 2018).
  - [163] Allison Transmission. Safety Data Sheet - Allison TES-295 Fluid 2017.
  - [164] Hayes JG, Goodarzi GA. Electric Powertrain: Energy Systems, Power Electronics and Drives for Hybrid, Electric and Fuel Cell Vehicles. Hoboken, NJ: Wiley; 2018.  
<https://doi.org/10.1002/9781119063681>.
  - [165] An F, Santini D. Assessing Tank-to-Wheel Efficiencies of Advanced Technology Vehicles. SAE Tech Pap Ser 2003. <https://doi.org/10.4271/2003-01-0412>.
  - [166] Brinkman N, Wang M, Weber T, Darlington T. Well-to-Wheels Analysis of Advanced Fuel/Vehicle Systems — A North American Study of Energy Use, Greenhouse Gas Emissions, and Criteria Pollutant Emissions. 2005.
  - [167] Ahlawat R, Bredenbeck J, Ichige T. Estimation of Road Load Parameters via On-Road Vehicle Testing Energy Loss in Vehicles 2013:1–44.
  - [168] United States Army Tank Automotive Research Development and Engineering Center. FED Alpha Revealed. Accelerate 2010.  
<https://apps.dtic.mil/dtic/tr/fulltext/u2/a560314.pdf> (accessed May 12, 2020).
  - [169] Department of Energy. Diesel Engine 2003.  
[https://www1.eere.energy.gov/vehiclesandfuels/pdfs/basics/jtb\\_diesel\\_engine.pdf](https://www1.eere.energy.gov/vehiclesandfuels/pdfs/basics/jtb_diesel_engine.pdf) (accessed August 22, 2018).
  - [170] Manahan SE. Fundamentals of Environmental Chemistry. 3rd ed. Boca Raton, Florida: CRC Press; 2008.
  - [171] Miller AR, Hess KS, Barnes DL, Erickson TL. System Design of a Large Fuel Cell Hybrid Locomotive. J Power Sources 2007;173:935–42.  
<https://doi.org/10.1016/j.jpowsour.2007.08.045>.
  - [172] Miste GA, Benini E. Performance of a Turboshift Engine for Helicopter Applications

- Operating at Variable Shaft Speed. Proc ASME 2012 Gas Turbine India Conf 2012:1–15.
- [173] Leishman JG. Principles of Helicopter Aerodynamics. 2nd Editio. Cambridge, UK: Cambridge University Press; 2006.
- [174] Cunha FS. Momentum Theory in Hover 2018.
- [175] Johnson W. Helicopter Theory. New York, NY: Dover Publications, Inc.; 1994.
- [176] Helicopters & Aircrafts. Helicopters & Aircrafts 2016. <http://heli-air.net/2016/02/20/figure-of-merit-3/> (accessed October 24, 2018).
- [177] The National Academies of Science Engineering and Medicine. Commercial Aircraft Propulsion and Energy Systems Research: Reducing Global Carbon Emissions. 2016.
- [178] Jessica Barnes. A Look at Propeller Efficiency. Can Owners Pilot Assoc 2016. <https://copanational.org/en/2016/12/08/a-look-at-propeller-efficiency/> (accessed October 24, 2018).
- [179] Rogers DF. Propeller Efficiency Rule of Thumb. Am Bonanza Soc 2010. [http://www.nar-associates.com/technical-flying/propeller/cruise\\_propeller\\_efficiency\\_screen.pdf](http://www.nar-associates.com/technical-flying/propeller/cruise_propeller_efficiency_screen.pdf) (accessed October 24, 2018).
- [180] Spakovszky ZS. Trends in Thermal and Propulsive Efficiency. MIT Turbines 2002;2:16–9. <http://web.mit.edu/16.unified/www/FALL/thermodynamics/notes/node84.html> (accessed August 15, 2018).
- [181] Waitz IA. Unified Lecture #2: The Breguet Range Equation 2008.
- [182] Epstein AH. Aeropropulsion for Commercial Aviation in the Twenty-First Century and Research Directions Needed. AIAA J 2014;52:901–11. <https://doi.org/10.2514/1.J052713>.
- [183] Wenger U. Rolls-Royce Technology for Future Aircraft Engines RAeS Hamburg 2014.
- [184] Hathaway MD, Del Rosario R, Madavan N. NASA Fixed Wing Project Propulsion Research and Technology Development Activities to Reduce Specific Energy Consumption. Moffett Field, CA: 2013. <https://doi.org/10.2514/6.2013-3605>.
- [185] Benvenuto G, Campora U, Trucco A. Comparison of Ship Plant Layouts for Power and Propulsion Systems with Energy Recovery. J Mar Eng Technol 2014;13:3–15. <https://doi.org/10.1080/20464177.2014.11658117>.
- [186] MAN Diesel & Turbo. Basic Principles of Ship Propulsion 2011.
- [187] Ghadimi P, Shademani R, Fard MY. Performance Assessment of the Waterjet Propulsion System Through a Combined Analytical and Numerical Approach. Int J Phys 2013;1:22–7. <https://doi.org/10.12691/ijp-1-2-1>.
- [188] Bulten NWH. Numerical Analysis of a Waterjet Propulsion System. Eindhoven University of Technology, 2006.
- [189] Altosole M, Benvenuto G, Figari M, Campora U. Dimensionless Numerical Approaches for the Performance Prediction of Marine Waterjet Propulsion Units. Int J Rotating Mach 2012;2012. <https://doi.org/10.1155/2012/321306>.
- [190] Theotokatos G, Tzelepis V. A Computational Study on the Performance and Emission Parameters Mapping of a Ship Propulsion System. Proc. Inst. Mech. Eng. Part M J. Eng. Marit. Environ., vol. 229, Glasgow, Scotland: Department of Naval Architecture and Marine Engineering, University of Strathclyde Glasgow; 2013.
- [191] MAN Diesel & Turbo. Propulsion Trends in Tankers 2013.
- [192] United States Naval Academy. Resistance and Powering of Ships 2018.
- [193] Flugzeug. Boeing 747-8 Airliner Technical Data 2017. [http://www.flugzeuginfo.net/acdata\\_php/acdata\\_boeing\\_7478\\_en.php](http://www.flugzeuginfo.net/acdata_php/acdata_boeing_7478_en.php) (accessed October 19, 2018).

- [194] Luskin P. A Systems Engineering Methodology for Fuel Efficiency and its Application to a Tactical Wheeled Vehicle Demonstrator. Massachusetts Institute of Technology, 2010.
- [195] Kleinberg R. Tactical Wheeled Vehicle Fuel Economy Improvement Breakeven Analysis. 2012 SCEA/ISPA Jt. Annu. Conf. Train. Work., TACOM Soldier and Ground Systems Life Cycle Management Command; 2012.
- [196] Gerth R. Weight Analysis of a Combat Vehicle 2015.
- [197] Griffin K. Here's What a Power-to-Weight Ratio Means for Car Buyers. Motor1Com 2015. <https://www.motor1.com/news/76305/heres-what-a-power-to-weight-ratio-means-for-car-buyers/> (accessed December 13, 2018).
- [198] International Organization for Standardization. International Standard - Road Vehicles - Road Load - ISO 10521-1:2006(E). Geneva, Switzerland: 2006.
- [199] Environmental Protection Agency. Determination and Use of Vehicle Road-Load Force and Dynamometer Settings 2015.
- [200] Ehsani M, Gao Y, Gay SE, Emadi A. Modern Electric, Hybrid Electric, and Fuel Cell Vehicles: Fundamentals, Theory, and Design. Boca Raton, Florida: CRC Press; 2005.
- [201] Kadijk G, Ligterink N. Road Load Determination of Passenger Cars. Delft, Netherlands: 2012.
- [202] Browand F. Reducing Aerodynamic Drag and Fuel Consumption. Work Adv Transp 2005.
- [203] The Car Tech. Road Loads 2017. [http://www.thecartech.com/subjects/auto\\_eng/Road\\_loads.htm](http://www.thecartech.com/subjects/auto_eng/Road_loads.htm) (accessed October 9, 2018).
- [204] Sebeck K, Mange J, MacLennan J, Rizzo D. Characterization of Army Ground Vehicle Drive Cycles. 2017 NDIA Gr. Veh. Syst. Eng. Technol. Symp., Novi, MI: U.S. Army Tank Automotive Research Development and Engineering Center (TARDEC); 2017.
- [205] HPWizard. Tire Friction and Rolling Resistance Coefficients 2018. <http://hpwizard.com/tire-friction-coefficient.html> (accessed October 10, 2018).
- [206] Creedy AP. Skid Steering of Wheeled and Tracked Vehicles - Analysis with Coulomb Friction Assumptions. Victoria, Australia: 1984.
- [207] Baladi GY, Rohani B. Analysis of Steerability of Tracked Vehicles: Theoretical Predictions versus Field Measurements. Vicksburg, MS: 1981.
- [208] Republic Locomotive. AC Traction vs DC Traction 2016. <http://www.republiclocomotive.com/ac-traction-vs-dc-traction.html> (accessed September 18, 2018).
- [209] Hess KS, Miller AR, Erickson TL, Dippo JL. Demonstration of a Hydrogen Fuel-Cell Locomotive. Rail Conf 2010:1–6.
- [210] Republic Locomotive. Locomotive Tractive Effort and Power Calculations 2016. <http://www.republiclocomotive.com/locomotive-power-calculations.html> (accessed September 17, 2018).
- [211] CSX. Fuel Efficiency 2015. <https://www.csx.com/index.cfm/about-us/the-csx-advantage/fuel-efficiency/?mobileFormat=true> (accessed December 20, 2018).
- [212] Jackson D. Helicopter Overtorque. Aerosp Web 2001. <http://www.aerospaceweb.org/question/helicopters/q0019.shtml> (accessed January 11, 2019).
- [213] Leishman JG. The Helicopter: Thinking Forward, Looking Back. College Park, MD: College Park Press; 2007.



- [214] Lombardi F. Understanding Helicopter Power Requirements: The Power Struggle. Rotor Wing Int 2017. <https://www.rotorandwing.com/2017/10/10/understanding-helicopter-power-requirements-power-struggle/> (accessed January 11, 2019).
- [215] Cunha F. Helicopters 2018.
- [216] Helicopter Forum. Vertical Reference Helicopter. What Is Up Limit Heavy-Lift Helicopters? 2015. <http://helicopterforum.verticalreference.com/topic/19325-what-is-the-upper-limit-for-heavy-lift-helicopters/> (accessed January 10, 2019).
- [217] Johnson W. NDARC - NASA Design and Analysis of Rotorcraft Validation and Demonstration. Am. Helicopter Soc. Aeromechanics Spec. Conf., San Francisco, CA: NASA; 2010.
- [218] Garavello A, Benini E. Preliminary Study on a Wide-Speed-Range Helicopter Rotor/Turboshaft System. J Aircr 2012;49:1032–8. <https://doi.org/10.2514/1.C031526>.
- [219] Heli-Chair. Aerodynamics 101 - How Much Can a Rotor Lift, How Much Can a Propeller Pull? 2018. [http://www.heli-chair.com/aerodynamics\\_101.html](http://www.heli-chair.com/aerodynamics_101.html) (accessed December 21, 2018).
- [220] Federal Aviation Administration. FAA-H-8083-21A: Helicopter Flying Handbook. Oklahoma City, OK: U.S. Department of Transportation, Federal Aviation Administration, Flight Standards Service; 2012.
- [221] Liebreich M. Planes, Trains and Automobiles – the Electric Remake. Bloom NEF 2018. <https://about.bnef.com/blog/planes-trains-automobiles-electric-remake/>.
- [222] National Aeronautics and Space Administration. Part II: The Jet Age, Chapter 10: Technology of the Jet Airplane. Quest Perform. Evol. Mod. Aircr., 2018.
- [223] National Aeronautics and Space Administration. Turbofan Thrust 2016;4:3–5. <https://www.grc.nasa.gov/www/k-12/airplane/turbofan.html> (accessed October 19, 2018).
- [224] Moran MJ, Shapiro HN, Boettner DD, Bailey MB. Fundamentals of Engineering Thermodynamics. Eighth. Wiley; 2014.
- [225] National Aeronautics and Space Administration. General Thrust Equation. Glenn Res Cent 2016. <https://www.grc.nasa.gov/www/k-12/airplane/thrsteq.html> (accessed December 5, 2018).
- [226] Hunecke K. Jet Engines: Fundamentals of Theory, Design and Operation. Osceola, WI: Motorbooks International; 1997.
- [227] El-sayed AF, Emeara MS, El-habet MA. Performance Analysis of High Bypass Ratio Turbofan Aeroengine. Int J Dev Res 2016;06:8382–98.
- [228] Fielding JP. Introduction to Aircraft Design. Cambridge, UK: Cambridge University Press; 1999. <https://doi.org/10.1017/CBO9780511808906>.
- [229] National Aeronautics and Space Administration. Thrust to Weight Ratio 2014. [https://www.grc.nasa.gov/www/k-12/BGP/Donna/t\\_w\\_ratio\\_answers.htm](https://www.grc.nasa.gov/www/k-12/BGP/Donna/t_w_ratio_answers.htm) (accessed October 19, 2018).
- [230] Isikveren AT, Seitz A, Vratny PC, Pernet C, Plötner K, Hornung M. Conceptual Studies of Universally-Electric Systems Architectures Suitable for Transport Aircraft. Dtsch Luft-Und Raumfahrtkongress 2012 2012:Document-ID: 281368.
- [231] Vratny PC, Forsbach P, Seitz A, Hornung M. Investigation of Universally Electric Propulsion Systems for Transport Aircraft, St. Petersburg, Russia: 2014.
- [232] Flack RD. Fundamentals of Jet Propulsion with Applications. New York, NY: Cambridge University Press; 2005.
- [233] Kundu AK. Aircraft Design. New York, NY: Cambridge University Press; 2010.

- [234] Colozza A. High Altitude Propeller Design and Analysis Overview. Cleveland, OH: 1998.
- [235] National Aeronautics and Space Administration. NASA Armstrong Fact Sheet: Helios Prototype 2014. <https://www.nasa.gov/centers/armstrong/news/FactSheets/FS-068-DFRC.html> (accessed December 6, 2018).
- [236] Nagpurwala QH. Ducted Propellers and Fans 2018.
- [237] Gaj E. The Electric Aircraft is Taking Off. TechCrunch 2018. <https://techcrunch.com/2018/07/08/the-electric-aircraft-is-taking-off/> (accessed October 16, 2018).
- [238] Kuhn H, Seitz A, Lorenz L, Isikveren A, Sizmann A. Progress and Perspectives of Electric Air Transport. 28th Congr Int Counc Aeronaut Sci 2012, ICAS 2012 2012;6:4886–99. <https://doi.org/10.13140/RG.2.1.4833.4889>.
- [239] Aerospace Technology. E-Fan Electric Aircraft 2018. <https://www.aerospace-technology.com/projects/e-fan-electric-aircraft/> (accessed October 25, 2018).
- [240] Nygren CKP, Schulz MRR. Breguet's Formulas for Aircraft Range & Endurance An Application of Integral Calculus. ASEE Annu Conf Proc Fig 1 Typ US Air Force Airpl 1996;Session 12:5.
- [241] Draijf. Jet Breguet Range 2016. <https://www.youtube.com/watch?v=XTfYTZLxxDI> (accessed November 5, 2018).
- [242] Aviation Stack Exchange. Boeing 747-8 Engines 2015. <https://aviation.stackexchange.com/questions/20696/are-the-boeing-747-8-engines-more-efficient-than-the-747-400-engines> (accessed October 19, 2018).
- [243] Jenkinson LR, Simpkin P, Rhodes D. Civil Jet Aircraft Design. Elsevier Limited; 1999.
- [244] Lutze FH. Range and Endurance 2018.
- [245] Raymer DP, Wilson J, Perkins HD, Puentes AR. Advanced Technology Subsonic Transport Study N+3 Technologies and Design Concepts. NASA/TM—2011-217130 2011:1–51.
- [246] Filippone A. Data and Performances of Selected Aircraft and Rotorcraft. Prog Aerosp Sci 2000;36:629–54. [https://doi.org/10.1016/S0376-0421\(00\)00011-7](https://doi.org/10.1016/S0376-0421(00)00011-7).
- [247] Aerodynamic Database. Lift-to-Drag Ratios 2012. <https://web.archive.org/web/20080328133906/http://aerodyn.org/HighLift/ld-tables.html> (accessed November 4, 2018).
- [248] Sadraey M. Preliminary Design. Aircr. Des. A Syst. Eng. Approach, Wiley; 2012.
- [249] Ventura M. Estimation Methods for Basic Ship Design 2018.
- [250] Baier LA. Principles of Towing-Tank Research. Proc. Second Hydraul. Conf., Iowa City, IA: State University of Iowa; 1942, p. 51–70.
- [251] BoatDesign.Net. Wetted Surface Area - Approximate Formulas 2002. <https://www.boatdesign.net/threads/wetted-surface-area-approximate-formulas.930/> (accessed October 9, 2018).
- [252] Schneekluth H, Bertram V. Ship Design for Efficiency and Economy. 2nd ed. Elsevier; 1998.
- [253] Yang L, Zhu P, Qin Z. Numerical Analysis of Ship Hull Resistance Considered Trims. Proc Twenty-Fourth Int Ocean Polar Eng Conf Busan, Korea 2014:782–6.
- [254] Schultz MP. Effects of Coating Roughness and Biofouling on Ship Resistance and Powering. Biofouling 2007;23:331–41. <https://doi.org/10.1080/08927010701461974>.
- [255] Molland AF, Turnock SR, Hudson DA. Ship Resistance and Propulsion: Practical Estimation of Ship Propulsive Power. 2nd ed. Cambridge, UK: Cambridge University

- Press; 2017. <https://doi.org/10.1017/9781316494196.005>.
- [256] Engineers Edge. Kinematic Viscosity Table Chart of Liquids 2018. [https://www.engineersedge.com/fluid\\_flow/kinematic-viscosity-table.htm](https://www.engineersedge.com/fluid_flow/kinematic-viscosity-table.htm) (accessed January 7, 2019).
- [257] Engineering ToolBox. Water - Dynamic and Kinematic Viscosity 2004. [https://www.engineeringtoolbox.com/water-dynamic-kinematic-viscosity-d\\_596.html](https://www.engineeringtoolbox.com/water-dynamic-kinematic-viscosity-d_596.html) (accessed January 7, 2019).
- [258] Waide P, Brunner CU. Energy-Efficiency Policy Opportunities for Electric Motor-Driven Systems. Paris, France: 2011. <https://doi.org/10.1787/5kgg52gb9gjd-en>.
- [259] Hashernia N, Asaei B. Comparative Study of Using Different Electric Motors in the Electric Vehicles. Int Conf Electr Mach 2008.
- [260] Chan CC, Chau KT. An Overview of Power Electronics in Electric Vehicles. IEEE Trans Ind Electron 1997;44:3–13.
- [261] Daware K. Difference Between Synchronous Motor and Induction Motor. Electr Easy 2016. <https://www.electriceasy.com/2015/06/difference-between-synchronous-and-induction-motor.html> (accessed December 14, 2018).
- [262] Daware K. Working Principle and Types of an Induction Motor. Electr Easy 2016. <http://www.electriceasy.com/2014/02/working-principle-and-types-of.html> (accessed December 14, 2018).
- [263] Tesla Motors. Model S Owner’s Manual 2018.
- [264] Daware K. Synchronous Motor - Construction and Working. Electr Easy 2016. <https://www.electriceasy.com/2014/02/synchronous-motor-construction-working.html> (accessed December 14, 2018).
- [265] Moreels D. Axial-Flux Motors and Generators Shrink Size, Weight. Power Electron 2018. <https://www.powerelectronics.com/automotive/axial-flux-motors-and-generators-shrink-size-weight> (accessed September 5, 2018).
- [266] Toll M. New Axial Flux Electric Motors Pack More EV Power in a Smaller Package. Electrek 2018. <https://electrek.co/2018/05/03/axial-flux-electric-motors-more-ev-power-smaller-package/> (accessed September 4, 2018).
- [267] Magnax. Next-Gen Axial Flux Motor / Generator Compact and Lightweight Direct-Drive 2018. <https://www.magnax.com/product> (accessed September 4, 2018).
- [268] Magnax. Electric Transport 2018. <https://www.magnax.com/electric-transport> (accessed September 4, 2018).
- [269] Emrax. EMRAX 268 / 268 VHML Technical Data Table (Dynamometer Test Data). Kamnik, Slovenia: 2018.
- [270] Emrax. User’s Manual for Advanced Axial Flux Synchronous Motors and Generators EMRAX 348 Technical Data Table 2018.
- [271] Morris C. Elon Musk: Cooling, Not Power-to-Weight Ratio, is the Challenge with AC Induction Motors. Charg - Electr Veh Mag 2014. <https://chargedevs.com/newswire/elon-musk-cooling-not-power-to-weight-ratio-is-the-challenge-with-ac-induction-motors/> (accessed August 23, 2018).
- [272] Remy International Inc. HVH250 Series Electric Motors 2009.
- [273] Remy International Inc. Remy HVH250 Series Electric Motors 2010.
- [274] BorgWarner. HVH Series Electric Motors 2018. <https://www.borgwarner.com/technologies/electric-drive-motors/hvh-series-electric-motor> (accessed September 4, 2018).

- [275] BorgWarner. HVH250-090 Electric Motor. Pendleton, IN: BorgWarner; 2016.
- [276] BorgWarner. HVH250-115 Electric Motor. Pendleton, IN: BorgWarner; 2016.
- [277] BorgWarner. HVH410-075 Electric Motor. Pendleton, IN: BorgWarner; 2016.
- [278] BorgWarner. HVH410-150 Electric Motor. Pendleton, IN: BorgWarner; 2016.
- [279] YASA. YASA 750R E-Motor 2018.
- [280] Schiferl R, Flory A, Livoti WC, Umans SD. High-Temperature Superconducting Synchronous Motors: Economic Issues for Industrial Applications. *IEEE Trans Ind Appl* 2008;44:1376–84. <https://doi.org/10.1109/TIA.2008.2002219>.
- [281] Blain L. Magnax Prepares to Manufacture Radically High-Powered, Compact Axial Flux Electric Motor. Magnax 2018. <https://www.magnax.com/magnax-blog/magnax-prepares-to-manufacture-radically-high-powered-compact-axial-flux-electric-motor> (accessed September 5, 2018).
- [282] Department of Energy. US DRIVE - Electrical and Electronics Technical Team Roadmap. 2017.
- [283] Drives and Automation. NEMA Insulation Classes 2018. <http://www.drivesandautomation.co.uk/useful-information/nema-insulation-classes/> (accessed December 14, 2018).
- [284] TECO-Westinghouse Motor Company. Standard Motor Catalogue. Round Rock, TX: 2014.
- [285] Chavdar B, Deng Y, Naghshtabrizi P, Genise T. Modular Multi-Speed Transmission for MD-EV. CTI Symp China, Automot Transm HEV EV Drives 2016;5th Intern.
- [286] Sorokanich B. Why Don't Electric Cars Have Multi-Gear Transmissions? *Road Track* 2017. <https://www.roadandtrack.com/new-cars/car-technology/a12019034/why-dont-electric-cars-have-multi-gear-transmissions/> (accessed September 6, 2018).
- [287] Straubel J. An Engineering Update on Powertrain 1.5. *Tesla Mot* 2008. <http://www.teslamotors.com/blog4/?p=67> (accessed September 6, 2018).
- [288] Motor Vehicle Maintenance & Repair Stack Exchange. Motor Vehicle Maintenance & Repair. *Stack Exch* 2015. <https://mechanics.stackexchange.com/questions/5574/why-do-engines-have-so-much-unused-horsepower> (accessed December 14, 2018).
- [289] UnitConverters.net. Convert Pferdestarke (PS) to Horsepower 2018. <https://www.unitconverters.net/power/pferdestarke-ps-to-horsepower.htm> (accessed December 17, 2018).
- [290] Oshkosh Defense. Family of Independent Suspension Systems 2015.
- [291] Goodyear. Tire Size 2018. <https://www.goodyearautoservice.com/en-US/tire-basics/tire-size> (accessed December 14, 2018).
- [292] Eberhard M, Tarpenning M. The 21st Century Electric Car 2006.
- [293] Dow J. Tesla's Next-Gen Roadster. *Electrek* 2017. <https://electrek.co/2017/11/20/teslas-next-gen-roadster-technical-analysis/> (accessed December 14, 2018).
- [294] Wang Y, Lü E, Lu H, Zhang N, Zhou X. Comprehensive Design and Optimization of an Electric Vehicle Powertrain Equipped with a Two-Speed Dual-Clutch Transmission. *Adv Mech Eng* 2017;9:1–13. <https://doi.org/10.1177/1687814016683144>.
- [295] Eaton. 2-Speed EV Transmission Specifications 2018. <http://www.eaton.com/us/en-us/catalog/emobility/2-speed-ev.specifications.html> (accessed September 6, 2018).
- [296] Proterra. Proterra ProDrive and DuoPower Drivetrains 2016. <https://www.proterra.com/technology/drivetrain/> (accessed September 6, 2018).
- [297] Jensen S. Performance and Power Exceeding a Diesel Engine. *OEM Off-Highw* 2018.

- <https://www.oemoffhighway.com/drivetrains/article/20985885/drivetrain-electrification> (accessed September 6, 2018).
- [298] Urlacher J-M. Electric Circuits - First Look - Pipistrel WATTsUP. Pilot 2015. [https://www.pipistrel.si/en/file/download/683\\_f177bc091f05/2015-01-15 Article Alpha Trainer in Pilot HQ.pdf](https://www.pipistrel.si/en/file/download/683_f177bc091f05/2015-01-15%20Article%20Alpha%20Trainer%20in%20Pilot%20HQ.pdf) (accessed October 30, 2018).
- [299] Torqeedo. Deep Blue Operating Manual. Oper Man 2018.
- [300] Eaton. Transmission Lubricant Data Sheet 2013.
- [301] xTrac. P1166 Integrated Lightweight Electric Vehicle (ILEV) Transmission 2018. <http://www.xtrac.com/sectors/automotive-engineering/dedicated-hybrid-transmissions/product/161> (accessed September 6, 2018).
- [302] GETRAG. 1eDT200 – Electrical Drive Train 2018. [http://www.getrag.com/en/products/edrive\\_1/1edt200/1edt200\\_1.html](http://www.getrag.com/en/products/edrive_1/1edt200/1edt200_1.html) (accessed September 6, 2018).
- [303] xTrac. P1227 Integrated Lightweight Electric Vehicle (ILEV) Transmission 2018. <http://www.xtrac.com/sectors/automotive-engineering/dedicated-hybrid-transmissions/product/145> (accessed September 6, 2018).
- [304] GETRAG. 2eDT200 – Electrical Drive Train 2018. [http://www.getrag.com/en/products/edrive\\_1/2edt200/2edt200.html](http://www.getrag.com/en/products/edrive_1/2edt200/2edt200.html) (accessed September 6, 2018).
- [305] GETRAG. 1eDT350 – Electrical Drive Train 2018. [http://www.getrag.com/en/products/edrive\\_1/1edt350/1edt350.html](http://www.getrag.com/en/products/edrive_1/1edt350/1edt350.html) (accessed September 6, 2018).
- [306] Punch PowerTrain. TwinSpeed Spec Sheet 2018.
- [307] GETRAG. 1eDT330 - Electric Single--Speed Transmission 2018:1–2. [http://www.getrag.com/en/products/edrive\\_1/1edt330/1edt330\\_1.html](http://www.getrag.com/en/products/edrive_1/1edt330/1edt330_1.html) (accessed August 15, 2018).
- [308] GETRAG. 1eDT330 – Electrical Drive Train 2018. [http://www.getrag.com/en/products/edrive\\_1/1edt330/1edt330\\_1.html](http://www.getrag.com/en/products/edrive_1/1edt330/1edt330_1.html) (accessed September 6, 2018).
- [309] Sivaram V, Dabiri J, Hart D. The Need for Continued Innovation in Solar, Wind, and Energy Storage. *Joule* 2018;2.
- [310] Torqeedo. High Capacity Deep Blue Batteries with BMW i Technology 2018. <https://www.torqeedo.com/us/en-us/technology-and-environment/battery-technology.html> (accessed October 4, 2018).
- [311] Xia C, Kwok CY, Nazar LF. A high-energy-density lithium-oxygen battery based on a reversible four-electron conversion to lithium oxide. *Science* (80- ) 2018;361:777–81. <https://doi.org/10.1126/science.aas9343>.
- [312] Eftekhari A. On the Theoretical Capacity/Energy of Lithium Batteries and Their Counterparts. *ACS Sustain Chem Eng* 2018:acssuschemeng.7b04330. <https://doi.org/10.1021/acssuschemeng.7b04330>.
- [313] Environmental Protection Agency. 2018 Tesla Model S 75 Certification Summary Information Report 2018.
- [314] Petersen J. Tesla’s First Decade of Battery Pack Progress - Much Ado About Nothing. *Seek Alpha* 2017. <https://seekingalpha.com/article/4101993-teslas-first-decade-battery-pack-progress-much-ado-nothing> (accessed August 23, 2018).
- [315] Environmental Protection Agency. 2018 Tesla Model 3 Long Range Certification

- Summary Information Report 2017.
- [316] Environmental Protection Agency. 2018 Tesla Model X P100D, 100D, and 75D Certification Summary Information Report 2017.
  - [317] Field K. Proterra and LG Chem Announce New Battery Cell With Higher Energy Density. Gas 2 2017. <http://gas2.org/2017/09/19/proterra-lg-chem-announce-new-battery-cell-higher-energy-density/> (accessed August 23, 2018).
  - [318] Green Car Congress. Proterra and LG Chem Co-Develop New Battery Cell for Heavy-Duty Market; Proterra Sets Electric Distance Record 2017. <http://www.greencarcongress.com/2017/09/20170919-proterra.html> (accessed August 23, 2018).
  - [319] Berjoza D, Jurgena I. Effects of Change in the Weight of Electric Vehicles on Their Performance Characteristics. *Agron Res* 2017;15:952–63.
  - [320] Ali I. Battery Expert: Tesla Model 3 Has “Most Advanced Large Scale Lithium Battery Ever Produced.” Evannex 2018.
  - [321] Bower G. Tesla Model 3 2170 Energy Density Compared To Bolt, Model S P100D. InsideEVs 2019. <https://insideevs.com/news/342679/tesla-model-3-2170-energy-density-compared-to-bolt-model-s-p100d/> (accessed April 18, 2019).
  - [322] Thielmann A, Sauer A, Isenmann R, Wietschel M. Technology Roadmap Energy Storage for Electric Mobility 2030. Karlsruhe, Germany: 2012.
  - [323] Lambert F. BMW i3 Gets a 100 kWh Battery Pack for 435 Miles of Range as a Proof-of-Concept by Lion Smart. Electrek 2018. <https://electrek.co/2018/09/07/bmw-i3-100-kwh-battery-pack-lion-smart/> (accessed October 4, 2018).
  - [324] C4V. C4V Solid State Battery 2018. <http://chargeccv.com/updates/detail/18>.
  - [325] Noon C. Leading The Charge: Locomotives Will Be Pushing US Freight Related Stories. GE Reports 2018. <https://www.ge.com/reports/leading-charge-battery-electric-locomotives-pushing-us-freight-trains/> (accessed January 14, 2019).
  - [326] Kokam. Powered by Kokam’s Ultra High Energy NMC Batteries , Solar Impulse 2 Completes First Flight Around the World by a Zero-Fuel Solar Airplane. PR News Wire 2016. <https://www.prnewswire.com/news-releases/powered-by-kokams-ultra-high-energy-nmc-batteries-solar-impulse-2-completes-first-flight-around-the-world-by-a-zero-fuel-solar-airplane-300313150.html> (accessed October 22, 2018).
  - [327] Kokam. Kokam Li-ion / Polymer Cell More Than 16 Years of Battery Technology Experience. Kokam 2015. <http://kokam.com/cell/> (accessed January 14, 2019).
  - [328] Timothy J. Haugan. Development of Superconducting and Cryogenic Power Systems and Impact for Aircraft Propulsion. *Energy Mater. Appl.*, Orlando, FL: Air Force Research Laboratory; 2013.
  - [329] Pipistrel. Taurus Electro 2018. <https://www.pipistrel.si/plane/taurus-electro/faq> (accessed October 22, 2018).
  - [330] Zart N. The Pipistrel Alpha Electro, An Awesome 2-Seat Electric Trainer. Clean Tech 2017. <https://cleantechnica.com/2017/11/13/pipistrel-alpha-electro-awesome-2-seat-electric-trainer/> (accessed October 22, 2018).
  - [331] Pipistrel. Pipistrel Alpha Electro 2017.
  - [332] National Aeronautics and Space Administration. NASA Armstrong Fact Sheet: NASA X-57 Maxwell 2018.
  - [333] Cigarette Racing. Cigarette AMG Electric Drive 2018. [http://www.cigaretteracing.com/eng/SP\\_amgelec.php](http://www.cigaretteracing.com/eng/SP_amgelec.php) (accessed January 14, 2019).

- [334] Lambert F. New Electric Boat Powered by BMW i3 Battery Packs. Electrek 2017. <https://electrek.co/2017/07/05/electric-boat-torqueedo-bmw-i3-battery-packs/> (accessed July 30, 2018).
- [335] Schewel F, Hockgeiger E. The High Voltage Batteries of the BMW i3 and BMW i8. Adv Automot Batter Conf 2014.
- [336] Markowitz M. Wells to Wheels: Electric Car Efficiency. WordPress 2013. <https://matter2energy.wordpress.com/2013/02/22/wells-to-wheels-electric-car-efficiency/> (accessed August 22, 2018).
- [337] Apostolaki-Iosifidou E, Codani P, Kempton W. Measurement of Power Loss During Electric Vehicle Charging and Discharging. *Energy* 2017;127:730–42. <https://doi.org/10.1016/j.energy.2017.03.015>.
- [338] Battery University. BU-808c: Coulombic and Energy Efficiency with the Battery 2017. [https://batteryuniversity.com/learn/article/bu\\_808c\\_coulombic\\_and\\_energy\\_efficiency\\_with\\_the\\_battery](https://batteryuniversity.com/learn/article/bu_808c_coulombic_and_energy_efficiency_with_the_battery) (accessed January 16, 2019).
- [339] Lu L, Han X, Li J, Hua J, Ouyang M. A Review on the Key Issues for Lithium-Ion Battery Management in Electric Vehicles. *J Power Sources* 2013;226:272–88. <https://doi.org/10.1016/j.jpowsour.2012.10.060>.
- [340] Trancossi M, Madonia M. The Efficiency of an Electric Turbofan vs. Inlet Area: A Simple Mathematical Model and CFD Simulations. *SAE Int* 2012. <https://doi.org/10.4271/2012-01-2217>.
- [341] Gohardani AS, Doulgeris G, Singh R. Challenges of Future Aircraft Propulsion: A Review of Distributed Propulsion Technology and its Potential Application for the All Electric Commercial Aircraft. *Prog Aerosp Sci* 2011;47:369–91. <https://doi.org/10.1016/j.paerosci.2010.09.001>.
- [342] Dippold III V, Hosder S, Schetz JA. Analysis of Jet-Wing Distributed Propulsion from Thick Wing Trailing Edges. *AIAA Pap* 2004:7938–50. <https://doi.org/10.2514/6.2004-1205>.
- [343] Torqeedo. Torqeedo Performance and Efficiency 2018. <https://www.torqueedo.com/us/en-us/technology-and-environment/performance-and-efficiency.html> (accessed August 15, 2018).
- [344] Lin Z, Ou S, Elgowainy A, Reddi K, Veenstra M, Verduzco L. A Method for Determining the Optimal Delivered Hydrogen Pressure for Fuel Cell Electric Vehicles. *Appl Energy* 2018;216:183–94. <https://doi.org/10.1016/j.apenergy.2018.02.041>.
- [345] Curtin S, Gangi J. Fuel Cell Technologies Market Report 2016. Washington DC: 2017.
- [346] BMW. BMW Hydrogen 7. BMW Media Inf 2006. [https://www.wired.com/images\\_blogs/autopia/files/bmw\\_hydrogen\\_7.pdf](https://www.wired.com/images_blogs/autopia/files/bmw_hydrogen_7.pdf) (accessed October 26, 2018).
- [347] Law K, Rosenfeld J, Han V, Chan M, Chiang H, Leonard J. US Department of Energy Hydrogen Storage Cost Analysis 2013. <https://doi.org/10.1103/PhysRevLett.111.237404>.
- [348] Züttel A. Materials for Hydrogen Storage. *Mater Today* 2003;6:24–33. [https://doi.org/10.1016/S1369-7021\(03\)00922-2](https://doi.org/10.1016/S1369-7021(03)00922-2).
- [349] Niaz S, Manzoor T, Pandith AH. Hydrogen Storage: Materials, Methods and Perspectives. *Renew Sustain Energy Rev* 2015;50:457–69. <https://doi.org/10.1016/j.rser.2015.05.011>.
- [350] Krewitt W, Schmid S. Fuel Cell Technologies and Hydrogen Production/Distribution Options. Bonn, Germany: 2005.
- [351] Bouza A, Petrovic J, Read C, Satapal S, Milliken J. The “National Hydrogen Storage

- Project.” Am Chem Soc Div Fuel Chem 2004;49.
- [352] Ahluwalia RK, Peng JK, Roh HS, Hua TQ, Houchins C, James BD. Supercritical Cryo-Compressed Hydrogen Storage for Fuel Cell Electric Buses. *Int J Hydrogen Energy* 2018;43:10215–31. <https://doi.org/10.1016/j.ijhydene.2018.04.113>.
- [353] Ahluwalia RK, Hua TQ, Peng J-K, Roh HS. System Level Analysis of Hydrogen Storage Options 2017.
- [354] Aceves SM, Espinosa-Loza F, Ledesma-Orozco E, Ross TO, Weisberg AH, Brunner TC, et al. High-Density Automotive Hydrogen Storage with Cryogenic Capable Pressure Vessels. *Int J Hydrogen Energy* 2010;35:1219–26. <https://doi.org/10.1016/j.ijhydene.2009.11.069>.
- [355] Department of Energy. Lower and Higher Heating Values of Gas, Liquid, and Solid Fuels. Oak Ridge, TN: 2011.
- [356] Burke A, Gardiner M. Hydrogen Storage Options: Technologies and Comparisons for Light-Duty Vehicle Applications. 2005.
- [357] Tech-Etch. Photoetched Fuel Cell Plates, Frames, Support Screens & End Caps 2018. <https://www.tech-etch.com/photoetch/fuelcell.html> (accessed January 17, 2018).
- [358] ElringKlinger. PEMFC 2019. <https://www.elringklinger.de/en/products-technologies/electromobility/fuel-cells#ui-id-3> (accessed January 17, 2019).
- [359] Ballard Power Systems Inc. FCveloCity - MD 2016. [http://www.ballard.com/docs/default-source/motive-modules-documents/fcvelocity\\_md\\_low\\_res.pdf](http://www.ballard.com/docs/default-source/motive-modules-documents/fcvelocity_md_low_res.pdf) (accessed January 17, 2019).
- [360] Ballard Power Systems Inc. FCveloCity - HD 2016. [http://www.ballard.com/docs/default-source/motive-modules-documents/fcvelocity\\_hd\\_family\\_of\\_products\\_low\\_res.pdf](http://www.ballard.com/docs/default-source/motive-modules-documents/fcvelocity_hd_family_of_products_low_res.pdf) (accessed January 17, 2019).
- [361] ElringKlinger. PEM Fuel Cells 2017.
- [362] HES. Aerostak Ultra-Light Fuel Cells 2018. <https://doi.org/10.15713/ins.mmj.3>.
- [363] Hydrogenics. HyPM-HD Power Modules 2018.
- [364] Intelligent Energy Ltd. AC64 Stack Data Sheet 2018.
- [365] Intelligent Energy Ltd. AC64 Lightweight Stack 2018.
- [366] Intelligent Energy Ltd. Ultra Lightweight Fuel Cell Systems - UAV Application Guide 2016.
- [367] Re-Fire. CAVEN Series Fuel Cells 2018. <http://www.re-fire.com/en/#products> (accessed January 17, 2019).
- [368] Environmental Protection Agency. 2018 Toyota Mirai Certification Summary Information Report. Washington DC: 2017.
- [369] Department of Energy. DOE Technical Targets for Fuel Cell Systems and Stacks for Transportation Applications 2018. <https://www.energy.gov/eere/fuelcells/doe-technical-targets-fuel-cell-systems-and-stacks-transportation-applications> (accessed September 13, 2018).
- [370] Meteorology Training. U.S. Standard Atmosphere Heights and Temperatures 2019. [http://meteorologytraining.tpub.com/14269/css/14269\\_75.htm](http://meteorologytraining.tpub.com/14269/css/14269_75.htm) (accessed January 18, 2019).
- [371] Brunner T. Hydrogen & Fuel Cell Technology 2013.
- [372] Volute. Conformable Hydrogen Tanks 2018. <http://voluteinc.com> (accessed September 17, 2018).
- [373] Demirdöven N, Deutch J. Hybrid Cars Now, Fuel Cell Cars Later. *Science* (80- )



- 2004;305:974–6. <https://doi.org/10.1126/science.1093965>.
- [374] Siemens. SINAVY PEM Fuel Cell for Submarines 2013.
- [375] Sattler G. Fuel Cells Going On-Board. *J Power Sources* 2000;86:61–7. [https://doi.org/10.1016/S0378-7753\(99\)00414-0](https://doi.org/10.1016/S0378-7753(99)00414-0).
- [376] Greig A. Fuel Cells and Issues for Their Use in Warships. *J Mar Des Oper* 2003;B3:9–18.
- [377] Alkaner S, Zhou P. A Comparative Study on Life Cycle Analysis of Molten Carbon Fuel Cells and Diesel Engines for Marine Application. *J Power Sources* 2006;158:188–99. <https://doi.org/10.1016/j.jpowsour.2005.07.076>.
- [378] Tronstad T, Astrand HH, Haugom GP, Langfeldt L. Study on the Use of Fuel Cells in Shipping. Hamburg, Germany: 2017.
- [379] Sigler D. Magnax Motor Claim Impressive Power-to-Weight Ratios. *Sustain Ski* 2018. <http://sustainableskies.org/magnax-motor-claim-impressive-power-to-weight-ratios/> (accessed February 14, 2019).
- [380] Brelje B. Deriving the Modified Breguet Range Equation for a Hybrid-Turboelectric Aircraft 2017. <http://www.brelje.net/blog/deriving-modified-breguet-range-equation-hybrid-turboelectric-aircraft/> (accessed November 4, 2018).
- [381] Ferrier L. Electric Jet V1.1 2015. <https://lochief.files.wordpress.com/2015/11/electric-aircraft-v1point1.pdf> (accessed November 5, 2018).
- [382] Ferrier L. Math on the Musk Electric Jet 2015. <https://lochief.wordpress.com/2015/08/04/how-the-musk-electric-jet-works/> (accessed November 4, 2018).
- [383] Singiresu S. Rao. *Engineering Optimization*. 4th ed. Hoboken, New Jersey: John Wiley & Sons, Inc.; 2009.
- [384] Young C. Excel Solver: Which Solving Method Should I Choose? *EngineerExcel* 2018. <http://www.engineerexcel.com/excel-solver-solving-method-choose/> (accessed July 24, 2019).
- [385] Department of Defense. *Annual Energy Management and Resilience Report - Fiscal Year 2016*. Washington DC: 2017.
- [386] Department of the Army. *FY17 Annual Energy Management & Resilience (AEMR) Report*. Washington DC: 2018.
- [387] Department of the Army. *Energy Security & Sustainability (ES2) Strategy* 2015.
- [388] United States Government. Executive Order 13693: Planning for Federal Sustainability in the Next Decade. vol. 80. United States of America: 2015. [https://doi.org/EO\\_13693](https://doi.org/EO_13693).
- [389] Department of the Army. *Army Operational Energy* 2018. <http://www.asaie.army.mil/Public/ES/operationalenergy.html> (accessed August 10, 2018).
- [390] Department of the Army. *The US Army Combat Vehicle Modernization Strategy* 2015. [http://www.arcic.army.mil/app\\_Documents/CVMS\\_SEP\\_Master.pdf](http://www.arcic.army.mil/app_Documents/CVMS_SEP_Master.pdf) (accessed August 15, 2018).
- [391] 115th United States Congress. H.R.3671 - House Bill - “Off Fossil Fuels for a Better Future Act.” United States of America: 2017.
- [392] Reid DJS (University of A. Robert Davidson – Pioneer Electrician. *Nat Philos Museum, Univ Aberdeen* 2007:1–2. <https://homepages.abdn.ac.uk/npmuseum/Scitour/Davidson.pdf>.
- [393] Polnik B, Budzynski Z, Miedzinski B. Effective Control of a Battery Supplied Mine Locomotive Unit. *Elektron IR Electroteh* 2014;20:39–43.
- [394] Congressional Budget Office. *Modernizing the Army’s Rotary-Wing Aviation Fleet*. Washington DC: 2007.

- [395] United States Army. Army Fixed Wing Aircraft. United States Army 2014. [https://www.army.mil/article/137612/army\\_fixed\\_wing\\_aircraft](https://www.army.mil/article/137612/army_fixed_wing_aircraft) (accessed August 21, 2018).
- [396] Grover DH. U.S. Army Ships and Watercraft of World War II. Annapolis, Maryland: Naval Institute Press; 1987.
- [397] Rogoway T. Meet The Biggest And Baddest Ships In the US Army. The Drive 2016. <http://www.thedrive.com/the-war-zone/6149/meet-the-biggest-and-baddest-ships-in-the-us-army> (accessed August 21, 2018).
- [398] Office of the Chief of Transportation. Registry of Army Vessel Names 2011.
- [399] Hoekstra A. The Underestimated Potential of Battery Electric Vehicles to Reduce Emissions. *Joule* 2019;3:1412–4. <https://doi.org/10.1016/j.joule.2019.06.002>.
- [400] Dodgson L. Greener, Cleaner & Less Explosive: The Rise of Military Electric Vehicles. *Army Technol* 2016. <https://www.army-technology.com/features/featuregreener-cleaner-less-explosive-the-rise-of-military-electric-vehicles-4809219/> (accessed August 28, 2018).
- [401] Dubik JM. A Dual Approach to Military Innovation. *Assoc United States Army* 2019. <https://www.ausa.org/articles/dual-approach-military-innovation> (accessed January 31, 2019).
- [402] Satyapal S. Hydrogen and Fuel Cells Overview 2017.
- [403] Department of Energy. DOE Hydrogen and Fuel Cells Program. *Progr Rec # 17003* 2017.
- [404] Ramsden T. An Evaluation of the Total Cost of Ownership of Fuel Cell- Powered Material Handling Equipment. Golden, Colorado: 2013.
- [405] Swain MR. Fuel Leak Simulation. 2001 DOE Hydrog. *Progr. Rev. NREL/CP-570-30535*, Coral Gables, FL: Department of Energy; 2001.
- [406] Gouré D. The US Army’s All-But Forgotten Vehicle Fleet. *RealClear Def* 2017:1–6. [https://www.realcleardefense.com/articles/2017/08/22/the\\_us\\_armys\\_all-but\\_forgotten\\_vehicle\\_fleet\\_112116.html](https://www.realcleardefense.com/articles/2017/08/22/the_us_armys_all-but_forgotten_vehicle_fleet_112116.html) (accessed August 15, 2018).
- [407] Special Operations Forces Warrior. Family of Special Operations Vehicles 2015.
- [408] Westenberger A. Hydrogen Fueled Aircraft. *AIAA Int Air Sp Symp Expo Next 100 Years* 2003:1–11. <https://doi.org/10.2514/6.2003-2880>.
- [409] Schmidt B. This Cheap, Clean, Electric Airplane Could Reshape Regional Air Travel. *The Driven* 2018. <https://thedriven.io/2018/11/12/this-cheap-clean-electric-airplane-could-reshape-australian-regional-air-plane-travel/> (accessed November 26, 2018).
- [410] Quanlin Q. Fully Electric Cargo Ship Launched in Guangzhou. *China Dly* 2017. [http://www.chinadaily.com.cn/business/2017-11/14/content\\_34511312.htm](http://www.chinadaily.com.cn/business/2017-11/14/content_34511312.htm) (accessed December 3, 2018).
- [411] Leary K. China Has Launched the World’s First All-Electric Cargo Ship. *Futurism* 2017. <https://futurism.com/china-launched-worlds-first-all-electric-cargo-ship/> (accessed July 23, 2018).
- [412] Mitsubishi Corporation. Asahi Tanker, Exeno Yamamizu, MOL and MC Agree on Strategic Partnership To Develop Zero-emission Fully Electric Vessels 2019. <https://www.mitsubishicorp.com/jp/en/pr/archive/2019/html/0000038028.html> (accessed August 10, 2019).
- [413] MAREX. World’s First Hydrogen-Powered Cruise Ship Scheduled. *Marit Exec* 2017. <https://www.maritime-executive.com/article/worlds-first-hydrogen-powered-cruise-ship-scheduled> (accessed August 22, 2018).
- [414] Han J, Charpentier JF, Tang T. State of the Art of Fuel Cells for Ship Applications. *IEEE*

- Int Symp Ind Electron 2012:1456–61. <https://doi.org/10.1109/ISIE.2012.6237306>.
- [415] Siegel JB, Stefanopoulou AG, Rizzo D, Prakash N. Cooling Parasitic Considerations for Optimal Sizing and Power Split Strategy for Military Robot Powered by Hydrogen Fuel Cells. SAE Tech Pap 2018;2018-April:1–8. <https://doi.org/10.4271/2018-01-0798>.
- [416] Conover J, Husted H, Macbain J, Mckee H. Logistics and Capability Implications of a Bradley Fighting Vehicle with a Fuel Cell Auxiliary Power Unit. SAE World Congr 2004. <https://doi.org/10.4271/2004-01-1586>.
- [417] United States Congress. 10 USC 2292h - Limitation on procurement of drop-in fuels. United States of America: 2018.
- [418] The Climate Registry. Default Emission Factors 2018.
- [419] Department of Defense. Report of the Defense Science Board Task Force on DoD Energy Strategy: “More Fight – Less Fuel” 2008.